Geology and Mineral Resources of the East Mojave National Scenic Area, San Bernardino County, California

Ted G. Theodore, Editor

U.S. Geological Survey Bulletin 2160

Encompasses almost all of the Mojave National Preserve and its 22 included Wilderness Areas that were created in 1994. These desert conservation areas, administered by the National Park Service, replaced the East Mojave National Scenic Area

Photograph showing dark basaltic lava flows and cinder cone on skyline at Cima volcanic field, East Mojave National Scenic Area, California. Tongue-like lava flow in central field of view spilled out onto light-colored Mesozoic granitic rocks.

U.S. Department of the Interior
U.S. Geological Survey

U.S. Department of the Interior
Gale A. Norton, Secretary

U.S. Geological Survey
Charles G. Groat, Director

U.S. Geological Survey: 2007

Additional USGS publications can be found at
http://geology.usgs.gov/products.html

For more information about the USGS and its products:

Telephone: 1–888–ASK–USGS (1–888–275–8747)
World Wide Web: http://www.usgs.gov/

Published in the Western Region, Menlo Park, California
Manuscript approved for publication, September 11, 1996
Text and figures edited by Taryn A. Lindquist, Julia A. Thomas, and Jan L. Zigler
Production and design by Sara Boore, Susan Mayfield, and Stephen L. Scott

Contents

Tables

Illustrations

Abstract

The rocks of the East Mojave National Scenic Area (EMNSA) record a history of dynamic geologic events that span more than 1,800 million years (m.y.). These geologic events contributed significantly to development of the spectacular vistas and panoramas present in the area today. The oldest rocks underlie much of the northern part of the EMNSA. These rocks were subjected to extreme pressures and temperatures deep in the Earth's crust about 1,700 million years ago (Ma). They were subsequently intruded by granitic magmas from about 1,695 to 1,650 Ma, by additional granitic magmas at about 1,400 Ma and, later, at about 1,100 Ma, by iron-rich magmas that crystallized to form dark igneous rocks termed diabase. Unusual potassium- and magnesium-rich rocks, emplaced at about 1,400 Ma, crop out in a few places within and near the EMNSA. Their distinctive composition results from very small degrees of partial melting of mantle peridotite that was highly enriched in incompatible trace elements. At Mountain Pass, just outside the northeast boundary of the EMNSA, the potassium- and magnesium-rich rocks are accompanied by a rare type of carbonatite, an igneous rock composed of carbonate minerals, that contains high-grade rare earth element mineralization.

Subsequent to these igneous-dominated events, sedimentary strata began to be deposited at about 1,000 Ma; mostly sandstone and shale were deposited initially in marine and, less commonly, in continental environments along the west edge of the core of the North American continent. Sedimentation eventually culminated in the widespread deposition of thick marine limestones from about 400 to about 245 Ma. These limestones represent a continental-shelf environment where shallow-water limestone formed to the east and deeper water limestone formed to the west. The end of the formation of these sedimentary deposits probably was caused by uplift of the shelf, which marked the beginning of a long period of tectonic upheaval.

At about 170 Ma, widespread emplacement of coarse-grained granitic magmas began again in the region; some of these magmas also erupted as volcanic rocks. Additional episodes of magmatism took place at about 100 Ma and at 75 Ma. Most of the metallic-mineral occurrences in the EMNSA are associated with the igneous rocks that range in age from 170 to 75 Ma. During each of these magmatic events, the previously deposited sedimentary strata were buckled and broken as the entire region, part of a continental-scale fold and thrust belt, underwent crustal shortening and compression.

A period of tectonic quiescence characterized the region from about 65 Ma to about 20 Ma. The quiet period ended abruptly with widespread volcanism along the southern and eastern parts of the EMNSA. The major gold deposits in the Castle Mountains are associated with this episode of volcanism. During this volcanic outburst, the crust extended laterally in several areas that border the EMNSA: along the lower Colorado River 65 km to the east, in the Kingston Range 20 km to the north, and in the central Mojave Desert 75 km to the southwest. This extensional deformation is characterized by the superposition of upper-crustal rocks over midcrustal rocks along large flat-lying faults, several of which project beneath rocks now exposed at the surface in the EMNSA. The near-surface rocks of the EMNSA, however, apparently escaped much of this intense extensional deformation. High-angle faults, which cut several of the mountain ranges, possibly have undergone several periods of movement, which date back to approximately 70 to 100 Ma. Some faults are of local importance to the physiographic development of the mountain ranges and intervening basins, and, in places, the faults seem to have localized various kinds of ore bodies and mineral occurrences.

Volcanism and extensional deformation waned from 14 to 11 Ma. By approximately 10 Ma, widespread erosion had produced broad erosional dome-shaped mountains in the northwestern part of the EMNSA; study of these classic examples has led to many of the modern concepts of desert erosion. Basaltic volcanism accompanied further development of these dome-shaped mountains over the last 10 m.y.

Large areas of the EMNSA contain indications of various types of metallic mineralization at the ground surface. These metallic indications can be classified into approximately 20 specific types of metallic occurrences that are known to show extremely wide ranging concentrations of metals in variably sized accumulations. Among the metallic occurrences recognized are lead-zinc-silver-gold polymetallic vein; low-sulfide gold-quartz vein; lead-zinc-silver polymetallic replacement; gold breccia pipe; gold-silver quartz-pyrite vein; copper-lead-zinc-silver polymetallic fault and skarn; copper, zinc-lead, tungsten, tin-tungsten, and iron skarn; porphyry molybdenum-copper; and low-temperature quartz-adularia (alunite) gold. Of the 20 types of

mineral occurrence, only ten provide enough geologic information to make highly qualified estimates about the number of additional mineral deposits that remain to be discovered in the EMNSA. Nonetheless, economically significant concentrations of some metals may well remain to be discovered in the EMNSA, and some known occurrences may become economic in the future. Most of the approximately 700 known individual mineral occurrences have been extensively prospected for more than a century, and at least 15 percent of them have been credited with some production, mostly of minor quantities of metals. In recent years, gold ore bodies at three relatively large mineralized systems in the EMNSA (Castle Mountain, Colosseum, and Morning Star) have been brought into production, and, at another occurrence (Golden Quail), additional resources have been discovered. Each of the former three is present in a different geologic environment and, thus, is assigned to a specific mineral-occurrence model. The Golden Quail deposit is similar to the Morning Star. The gold production from these four deposits since 1985, combined with the gold reserves remaining in them as of 1993, is much greater than that of all preceding gold discoveries in the EMNSA, partly owing to the present availability of low-cost heap-leaching extraction methods.

The Providence Mountains, the Clark Mountain Range, the Ivanpah Mountains, and the New York Mountains have large numbers of metallic occurrences and show geochemical anomalies in various types of samples. In addition, although the general area of Hackberry Mountain lacks abundant metallic-mineral occurrences, we have included it in a tract of land judged to be favorable for the discovery of additional gold deposits similar to those in the Castle Mountains because the geology of Hackberry Mountain is similar to that of the Castle Mountains. These five mountainous regions make up a broad, roughly north-south-trending region in the central part of the EMNSA. Much less endowed with known occurrences of all types of deposits considered above are the Granite Mountains, the central parts of the Piute Range, the Fenner Valley area, the general area of Cima Dome, Old Dad Mountain and areas west to Soda Lake, and the Cima volcanic field. These areas lie in the eastern and western parts of the EMNSA.

We have made some judgments about the geology underlying the gravel-covered areas in the EMNSA, which include the extent of shallow bedrock apparently covered only by thin veneers of gravel. These areas are prime targets for exploration because many known ores that were exposed at one time in the mountain ranges have been found during earlier periods of exploration, but few data are available to us for most of these covered areas. The presence of mineralized rocks, the type of mineral occurrence, and the extent and intensity of mineralization in the covered areas are essentially unknown. Most covered mineral deposits do not respond to the standard aeromagnetic geophysical methods evaluated in this study, particularly at the broad spacing of our data-collection flight lines.

The restriction of estimates of undiscovered metal resources in the EMNSA to only currently known types of occurrences would, at reasonable levels of probability, yield small estimates for volumes of many metals, particularly base and ferrous metals, that might be exploited at some future date. However, this statement is true only if the size of most previously discovered deposits in the EMNSA is indicative of the size of deposits still to be discovered there. In our opinion, metals from any newly discovered copper, lead, and zinc deposit of the types presently known in the EMNSA probably would be insignificant from the standpoint of national needs.

Some parts of the EMNSA appear to represent geologic settings capable of hosting significant undiscovered gold and silver resources, primarily on the basis of geologic environments of recently discovered large deposits of gold in the EMNSA. In addition, the widespread distribution in many parts of the EMNSA of geochemically anomalous samples and numerous mineral occurrences, many of which are associated with introduction of igneous rock, indicates the presence of metal-bearing environments in those parts of the EMNSA that may be sites of additional future discoveries of new types of mineral deposits.

The study of the EMNSA by the U.S. Geological Survey has involved a team of more than 15 scientists who have expertise in geology, geochemistry, geophysics, mineral deposits, and resource analysis. Some main points of this report regarding mineralization follow:

1. Large areas of the EMNSA contain abundant direct and indirect indications of metallic mineralization.
2. Only partial estimates of the entire undiscovered metallic mineral endowment of the EMNSA are possible. Of the approximately 20 metallic-occurrence types known to be present in the EMNSA,

estimates are possible only for those ten types for which adequate geologic information is available, including knowledge of size and metal concentrations of similar occurrences elsewhere.

3. Of the ten specific mineral-deposit types that can be estimated, lead-zinc-silver-gold polymetallic vein and copper skarn are the most common deposits and, therefore, are the most likely to be discovered in the future.

4. Of the metal commodities estimated, those with the most important economic potential in 1993 appear to be gold, and, to considerably lesser degrees, copper, zinc, and lead.

5. The Mountain Pass deposit, just outside the northeast boundary of the EMNSA, is a world-class source of rare earth elements such as lanthanum, cerium, neodymium, samarium, europium, and gadolinium.

6. It was not possible to make numerical estimates for any of the nonmetallic industrial minerals. Nonetheless, vast resources of limestone and dolomite appear to be present in many of the mountain ranges in the EMNSA, some of which are composed almost entirely of limestone and dolomite.

7. Much of the EMNSA is covered by geologically young unconsolidated deposits of sand and gravel in broad valleys between the mountain ranges. These deposits of sand and gravel are younger than the age of introduction of metals into the rocks of the EMNSA. Although some potential for presence of undiscovered metal deposits of various types in these covered areas exists, it is essentially unknown because of a lack of data.

Introduction

By Carroll Ann Hodges and Ted G. Theodore

The East Mojave National Scenic Area (EMNSA), designated on January 13, 1981 (46 Federal Register 3994) by the Secretary of Interior and modified on August 9, 1983 (48 Federal Register 36,210), encompasses approximately 1.5 million acres of federal, state, and private land in the Mojave Desert of southern California. The lands are in northeastern San Bernardino County, adjacent to the Nevada border about halfway between Barstow and Las Vegas (fig. 1).

Under the California Desert Protection Act, first introduced in 1986 and signed into law on October 31, 1994, most lands of the EMNSA were incorporated into the Mojave National Preserve under the administration of the National Park Service. General differences in areal extents of the EMNSA and the Mojave National Preserve (MNP) are shown at small scale on figure 2, and the borders of the two areas also are included at 1: 125,000 scale on plates 1–6 for comparative purposes. The major difference between the two is the exclusion of (1) an approximately 3–km-wide corridor along Interstate 15 in the general area of the north boundary of the MNP, south of the Clark Mountain Range, (2) an irregularly shaped area of approximately 100 km^2 in the general area of Castle Mountains, and (3) a large number of small parcels of land in the Lanfair Valley area, in aggregate approximately 160 km^2 (not shown separately on the plates). The impending withdrawal of all these lands for protection in the late 1980s and early 1990s prompted a series of investigations by the U.S. Bureau of Mines and the U.S. Geological Survey to assess the nature and extent of mineral resources in the area under consideration. The present report is an updated version of previous studies by the U.S. Geological Survey (U.S. Geological Survey, 1991; Hodges and Ludington, 1991; Miller and others, 1991).

The legislative history that culminated in elevation of the EMNSA (the name is retained for the area studied in this report) to National Preserve status began in 1976 with creation of the California Desert Conservation Area (CDCA), which comprised about 25 million acres total in separate tracts in southern California. Established by Congress under Section 601 of the Federal Land Policy and Management Act, about half of the Conservation Area was public land administered by the Bureau of Land Management (BLM), which completed a comprehensive plan for multiple use of the entire area in 1980. Numerous sites considered by BLM to be Areas of Critical Environmental Concern are scattered throughout the conservation area, and several are within the EMNSA.

In 1986 the California Desert Protection Act was introduced in Congress by California Senator Alan Cranston and Representative Mel Levine. Under that proposed Act, which was reintroduced in 1991, approximately 4.5 million acres of the CDCA, including the EMNSA, were to be transferred to the National Park Service and granted National Park status. In January 1993 as the 103d Congress began, the California Desert Protection Act was again introduced, as Senate Bill 21, by Senator Diane Feinstein of California; this Bill was cosponsored by Senator Barbara Boxer, also of California, and 21 other Senators. The companion House Resolution H.R. 518 was also introduced in January 1993 by Congressmen Richard Lehman and George Miller of California and cosponsored by 15 other Representatives. In both of these bills, the EMNSA was to be abolished: Senate Bill 21 created Mojave National Park, whereas the House version created Mojave National Monument, in place of the EMNSA. In July 1991, President George H.W. Bush countered the above protection acts with a proposal that approximately 2.24 million acres in 62 individual units, most of them in the southern California desert, be added to the National Wilderness Protection System under the California Public Lands Wilderness Act; six of these units (CDCA–239, –250, –256, –262, –263, and –266) were in the EMNSA.

In order that the available mineral-resource database be as complete as possible while these bills were before Congress, an evaluation of known and undiscovered, metallic mineral resources of the EMNSA was undertaken by the U.S. Geological Survey as a successor to investigations by the U.S. Bureau of Land Management (1980, 1982) and recently completed studies by the U.S. Bureau of Mines (1990a; Schantz and others, 1990; Wetzel and others, 1992). A few parts of the California Desert Conservation Area, generally outside the EMNSA, are among the most highly mineralized regions in the nation (Weldin, 1991).

The EMNSA includes the following units of the California Desert Conservation Area, all of which were initially designated BLM Wilderness Study Areas (WSA), but only eight of which were found suitable for wilderness designation by BLM:

CDCA–227	Clark Mountain
CDCA–235A	Shadow Valley
CDCA–237	Magee-Atkins
CDCA–237A	Deer Spring
CDCA–237B	Valley View
CDCA–238A	Teutonia Peak
CDCA–238B	Cima Dome
CDCA–239	Cinder Cones
CDCA–243	Old Dad Mountain
CDCA–244	Rainbow Wells
CDCA–245	Eight-Mile Tank
CDCA–249	Kelso Mountains
CDCA–250 (part)	Kelso Dunes
CDCA–256 (part)	Bristol-Granite Mountains
CDCA–262	South Providence Mountains
CDCA–263	Providence Mountains
CDCA–264	Mid Hills
CDCA–265	New York Mountains
CDCA–266	Castle Peaks
CDCA–267	Fort Piute
CDCA–270	Table Mountain
CDCA–271	Woods Mountains
CDCA–272	Signal Hill

After preliminary examination of these lands with respect to the extent of their existing use and state of degradation, BLM recommended the following eight units for wilderness designation: CDCA–237A, –239, –250 (part), –256 (part), –262, –263, –266, and –267. Of these, only the six listed earlier were included in the proposed Wilderness Act of July 1991. However, the Mojave National Preserve as finally enacted into law as part of the California Desert Protection Act includes 22 Wilderness Areas (Frank Bono, written commun., 1995), most of which were on the original list of WSAs proposed by BLM. Nonetheless, some substantive changes were made involving the following units:

Cima Dome (formerly the Deer Spring, Teutonia, and Cima Dome WSAs)

Shadow Valley (formerly the Shadow Valley and Valley View WSAs)

Joshua Forest (formerly the Magee-Atkins WSA)

Rainbow Wells North (part of the Rainbow Wells WSA north of Mojave Road)

Rainbow Wells South (part of the Rainbow Wells WSA south of Mojave Road)

Marl Mountains (not previously designated as a WSA by BLM)

Old Dad Mountain (previously designated as a single area, parts of which are now (1995) included in two areas under one name)

Devil's Playground (formerly part of the Old Dad Mountain WSA)

Soda Lake (not previously designated as a WSA by BLM)

Thus, the only two units that did not become Wilderness Areas when the Mojave National Preserve was created are Signal Hill and Eight Mile Tank, which BLM had originally designated as WSAs but did not recommend for wilderness status.

The known mineral resources of the eight units formerly recommended as WSAs by BLM, as well as of all others recommended for wilderness designation within the California Desert Conservation Area, were examined by the U.S. Geological Survey and the U.S. Bureau of Mines. A Mineral Summary was prepared as

Background Data for the California Desert Protection Act of 1987 (Calzia and others, 1979; U.S. Bureau of Land Management, 1988). These studies were, necessarily, cursory and recommended additional investigations before any land-use decisions were made, particularly where substantial mineral resources were identified.

The present report contains an assessment of the potential for discovery of new metallic mineral resources specifically within the EMNSA, that partly updates earlier studies (U.S. Geological Survey, 1991; Hodges and Ludington, 1991), and it includes data derived from limited field examinations specifically for this report by some of the authors of the various sections below. This report also includes syntheses from the ongoing detailed investigations of many geologists. These geologic investigations are aimed primarily toward assembling a modern geologic framework for the region but also include study of the mineral resources of many individual areas considered for wilderness designation within the EMNSA.

Known mineral occurrences are classified by deposit type insofar as possible, and tracts of ground that are permissive geologically for additional discoveries of such deposits are outlined, with discussion of deposit-type characteristics; degree of favorability for discovery is included where adequate information exists on which to base such evaluations. A previously published report presents estimates of the numbers of undiscovered deposits for approximately 10 of the 20 types of metallic deposits known to be present in the EMNSA (Hodges and Ludington, 1991). The section below entitled "Evaluation of Metallic Mineral Resources" includes definitions of many terms used throughout this report.

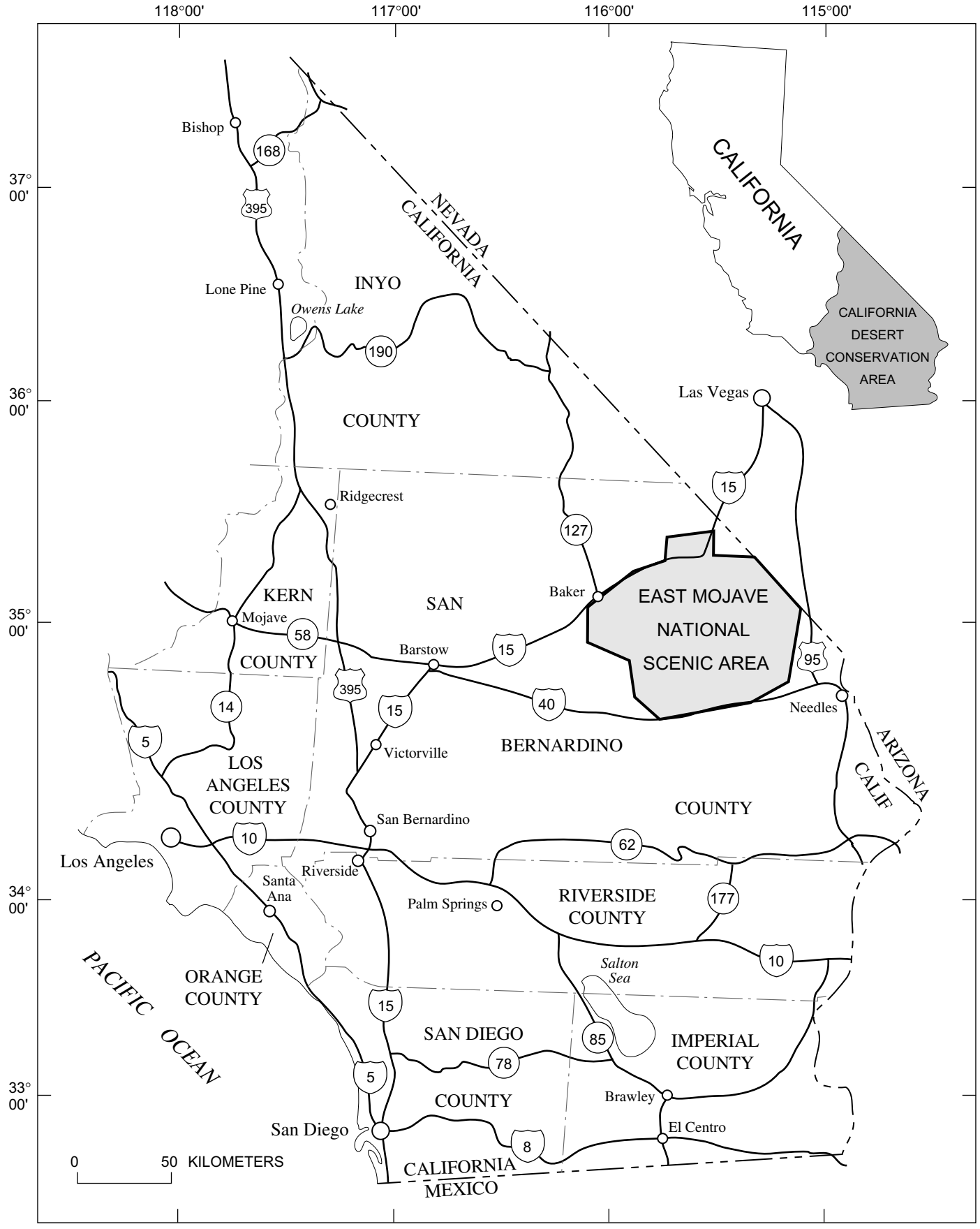

Figure 1. Location map showing East Mojave National Scenic Area, San Bernardino County, California.

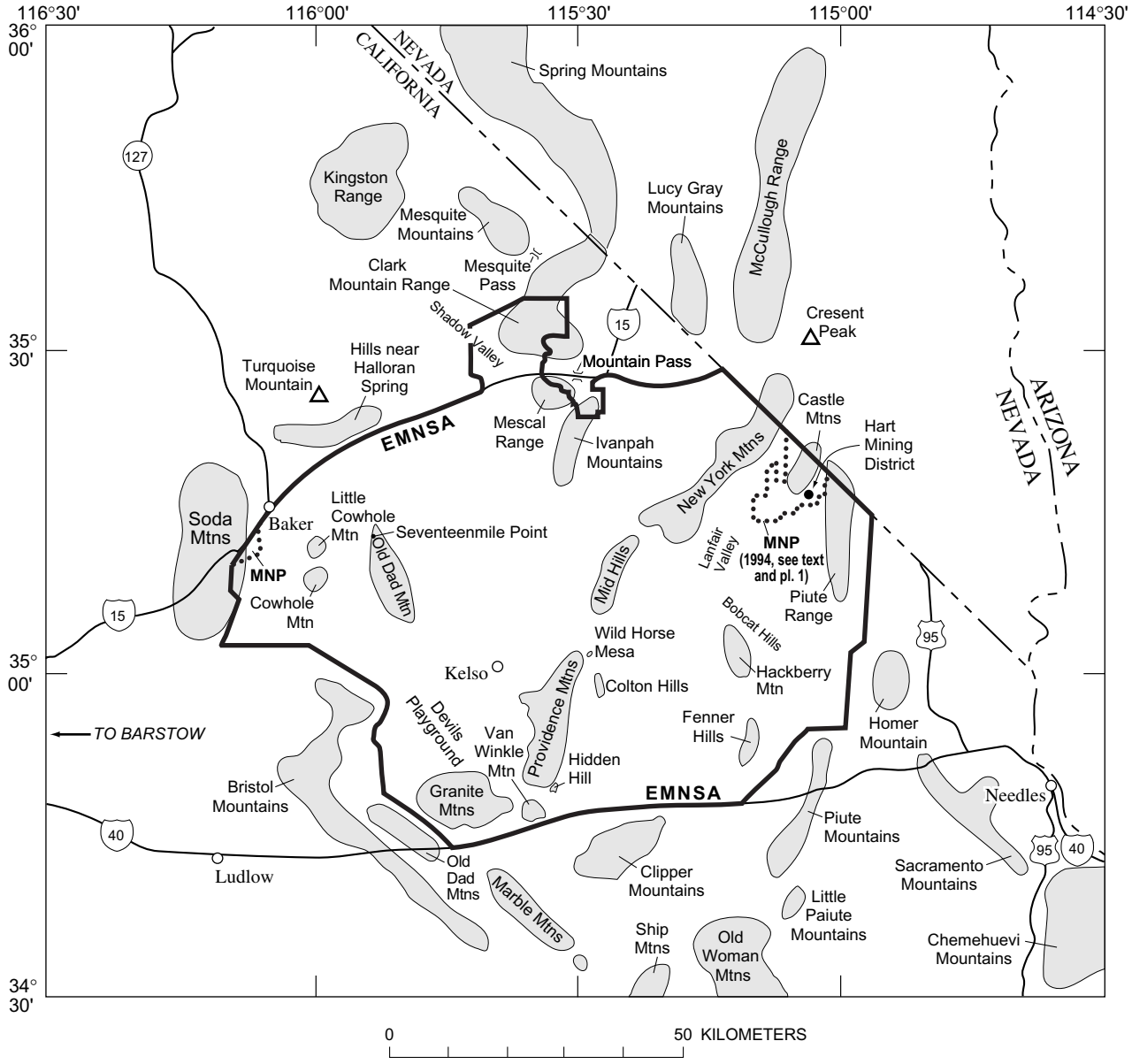

Figure 2. Index map of the East Mojave National Scenic Area (EMNSA, heavy solid line), Mojave National Preserve (MNP, heavy dotted line), and locations of major mountain ranges in California and Nevada. Congressional intent is to exclude all private land in the Lanfair Valley area from inclusion in the MNP.

Acknowledgments

This report was assembled under the Southern California Mineral-Resource Framework and Assessment Project, supervised by Richard M. Tosdal of the Menlo Park, California, Branch of Western Mineral Resources, in response to a request from the National Mineral Resource Assessment Program (NAMRAP), then (1993) chaired by Joseph A. Briskey, Jr., Reston, Va. In addition to contributions by each of the authors of the sections and subsections cited below, specific indispensible contributions to the report also include the following: (1) computer-generated plots of mineral deposits and files of geochemical data by Kenneth R. Bishop; (2) inferred isopachs showing depths to basement rocks in the valley-fill areas by Robert C. Jachens; (3) computer-generated geologic map of the EMNSA (pl. 1) compiled by David M. Miller, Robert J. Miller, Jane E. Nielson, Howard G. Wilshire, Keith A. Howard, and Paul Stone; (4) computer-generated isostatic residual gravity and aeromagnetic maps of the EMNSA (pls. 4 and 5, respectively) by Robert J. Miller; (4) timely preparation of many of the illustrations by Diana L. Mangan; and (5) extraordinarily comprehensive editorial reviews initially by Taryn A. Lindquist and finally by Jan L. Zigler. All contributors responded admirably and punctually to schedule requirements of this report, as well as to the preliminary report (U.S. Geological Survey, 1991) that preceded it. The U.S. Geological Survey wishes to express its appreciation to personnel of the U.S. Bureau of Mines for providing copies of its field examinations in the EMNSA (U.S. Bureau of Mines, 1990a; Schantz and others, 1990) and its economic analysis (Wetzel and others, 1992) as soon as these documents became available. In particular, we wish to thank Linda R. Gray of the Western Field Operations Center, Spokane, Wash., of the U.S. Bureau of Mines for providing us with computer-readable files and paper copies of the above reports, and Nicholas Wetzel, also of the Spokane office of the U.S. Bureau of Mines, for confirming our locations of some mineral occurrences in the EMNSA.

General Geologic Setting

By Richard M. Tosdal

The East Mojave National Scenic Area (EMNSA), located in southeastern California (figs. 1, 2), lies in the northeastern Mojave Desert (fig. 3), a large physiographic province whose extent is defined by its Neogene geologic history. The desert physiography consists of ranges that are separated by basins either filled by alluvial materials or underlain at shallow depths by pediments. In the EMNSA several ranges attain greater than 7,000-ft (2,133-m) elevations, some 5,000 ft (1,524 m) above the alluvial valley floors; extensive range-fringing pediments are present and some spectacular pediment domes are developed.

The diverse geologic history of the EMNSA spans more than 1,760 million years (m.y.). The oldest rocks, which underlie much of the northern part of the area, are Early Proterozoic gneisses that underwent regional metamorphism at high metamorphic grades about 1,700 million years ago (Ma). These rocks were subsequently intruded by granitic rocks from about 1,695 to 1,650 Ma, again by granitic rocks at about 1,400 Ma, and by diabase at about 1,100 Ma. Unique carbonatites and alkaline igneous rocks compose part of the 1,400-Ma intrusive episode. Latest Proterozoic, Paleozoic, and early Mesozoic sedimentary strata were deposited unconformably across the Proterozoic gneissic and granitic rocks. These sedimentary rocks formed in marine and, less commonly, continental environments along the west edge of the North America craton and represent the transition from the cratonal sedimentary sequence in the southeast to a miogeoclinal sequence in the northwest.

Beginning in the Mesozoic, widespread magmatism affected the region. Triassic volcanic rocks, locally present in several ranges in the western part of the EMNSA, represent the oldest products of this magmatism. Jurassic volcanism and plutonism produced rocks with slight alkalic affinities that lie along the east edge of the magmatic arc of that age. Subsequent plutonism in the Cretaceous is characterized by rocks of calc-alkaline affinities, typical of batholithic rocks within the cores of continental magmatic arcs. During the middle to late Mesozoic, the interior of the cordillera underwent shortening along a fold and thrust belt. Thrust slices within this belt in the EMNSA involve the cratonal Proterozoic basement and, locally, some of the Mesozoic plutonic rocks.

A period of tectonic quiescence characterized the region in the early Cenozoic. In the Miocene, volcanism became widespread along the south and east margins of the EMNSA and possibly elsewhere. Significant extensional deformation occurred in metamorphic core complexes during the Miocene both in northern parts and in areas largely just outside of the EMNSA, as well as along the lower Colorado River to the east and in the central Mojave Desert to the southwest (lightly shaded areas, fig. 3). This deformation is characterized by the structural superposition of intensely faulted, upper-crustal rocks over midcrustal rocks along regionally subhorizontal detachment faults, several of which project underneath rocks now exposed in the EMNSA. The near-surface rocks of the EMNSA, however, apparently escaped much of this intense extensional deformation. High-angle faults cut several ranges, and many faults possibly have undergone several periods of movement, which date back to Mesozoic time. Some faults are of local importance to the physiographic development of the ranges and basins and, in places, seem to have controlled formation of various kinds of ore bodies and mineral occurrences.

In the late Miocene, extensive erosion produced broad pediment domes in the northwestern part of the area. Alkali-basaltic volcanism followed pediment formation in the late Miocene and Pliocene (frontispiece). Erosion during the Quaternary has continued to degrade the pediment domes and mountain ranges and to supply sediments to adjacent valleys.

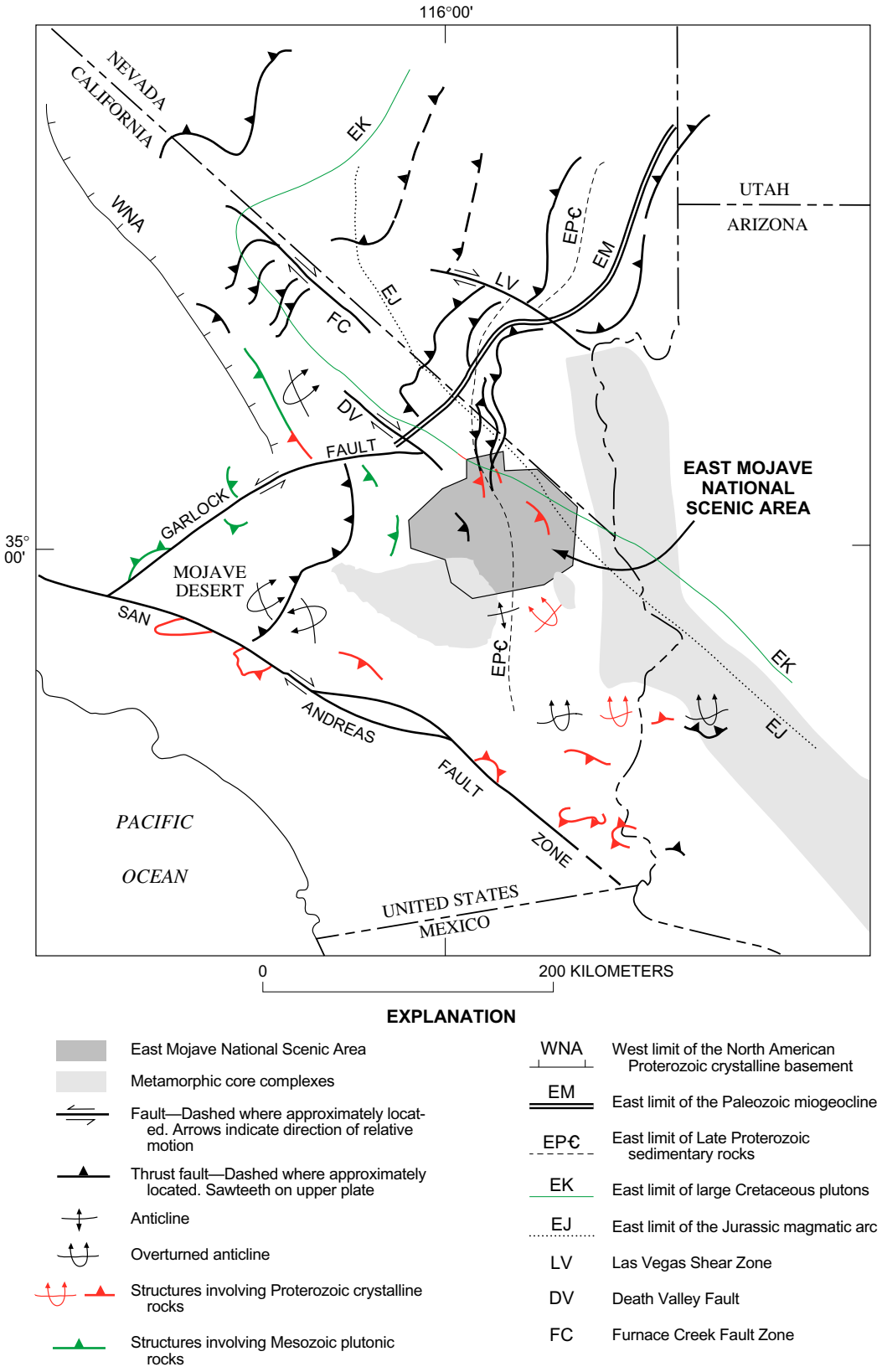

Figure 3. Schematic tectonic map of southeastern California and adjoining regions, showing relations among major structural and paleogeographic elements. Vergence of major overturned folds also shown. Modified from Burchfiel and Davis (1981, 1988) and Brown (1986).

Proterozoic Rocks and Their Mineralization

By David M. Miller, Joseph L. Wooden, and Clay M. Conway

Early Proterozoic Rocks

Early Proterozoic rocks constitute one-third or more of the area of bedrock exposure in the East Mojave National Scenic Area (EMNSA) (pl. 1; see also fig. 4). These rocks received very little attention until the past few years. Earliest studies were part of regional mapping investigations by Hewett (1956), who distinguished two Proterozoic rock units: (1) gneiss and granite, and (2) syenite and shonkinite. The former unit is now known to be Early Proterozoic in age. The latter unit encompasses Middle Proterozoic intrusions at Mountain Pass. Reconnaissance geochronologic studies (Wasserburg and others, 1959; Silver and others, 1961; Lanphere, 1964) established that the crystalline Proterozoic rocks in the Death Valley (25 km northwest of the EMNSA) and eastern Mojave Desert regions are approximately 1.7 to 1.6 billion years old (Ga). Mapping studies of the area through the 1970s (Providence Mountains, Hazzard (1954); Mountain Pass area, Olson and others (1954); Clark Mountain Range, Clary (1967); Clark Mountain Range and Ivanpah Mountains, Burchfiel and Davis (1971); McCullough Range, Bingler and Bonham (1972); Old Dad Mountain, Dunne (1977)) generally showed one or only a few map units designated as Early Proterozoic in age and gave sketchy lithologic and petrographic descriptions for them. As a consequence, reviews of the eastern Mojave Desert region (Miller, 1946; McCulloh, 1954; Burchfiel and Davis, 1981) emphasized the paucity of data on the Early Proterozoic rocks and the need for additional research.

Geologic mapping and geochronologic, isotopic, and petrologic studies during the 1980s have led to major advances in understanding the Early Proterozoic crustal evolution of the region. Geologic mapping in and near the EMNSA (hills near Halloran Spring, DeWitt and others (1984); New York Mountains, Miller and others (1986) and Miller and Wooden (1993); Providence Mountains, Goldfarb and others (1988); McCullough Range (10 km north in southern Nevada), Anderson and others (1985)) locally has resulted in extensive subdivision of the Early Proterozoic rocks. Wooden and Miller (1990) and Miller and Wooden (1993) summarized the Proterozoic evolution of this part of the Mojave Desert and presented most of the new data that form the basis for this review.

The Early Proterozoic history of the northeastern part of the Mojave Desert is primarily one of plutonism and metamorphism. DeWitt and others (1984) dated gneissic granites in the hills near Halloran Spring as about 1.71 Ga, setting the stage for the ensuing documentation of a 1.705-Ga granulite-facies metamorphic event (the Ivanpah orogeny), as well as pre-, syn-, and post-metamorphic granitoids (Wooden and Miller, 1990). Metaplutonic and plutonic rocks that range in age from 1.76 to 1.66 Ga are now documented, and some of their wallrocks contain zircons that are 700 m.y. older than the oldest granitoids. The emerging picture is one of a 1.8-Ga sedimentary and volcanic province that, in part, received detritus from much older sources (1.9, 2.3, and 2.5 Ga) and was probably built upon a 2.5-Ga basement. These older rocks were intruded, and perhaps deformed and metamorphosed, at 1.76 and 1.73 Ga; the magmas were mafic and metaluminous in some cases and potassium rich in others. Between 1.71 and 1.695 Ga, a major orogenic event, the Ivanpah orogeny, thoroughly migmatized older rocks, as well as synkinematic potassium-rich granitoids. The hallmark of the event is widespread migmatite, which in many places is characterized by abundant leucocratic-granitoid layers and by ubiquitous garnet. Metamorphism was at low-pressure granulite facies (Thomas and others, 1988; Young, 1989; Young and others, 1989) in this region. Following the Ivanpah orogeny, granitoids were emplaced in a north-south-trending zone in the New York Mountains and McCullough Range as two intrusive suites, the first at about 1.695 to 1.675 Ga and the second at about 1.8 to 1.66 Ga. Although these two suites of granitoids apparently overlap in age, the suites can be separated by differences in chemistry and style of intrusion; the younger of the two is calc-alkaline and compositionally expanded. Groups of plutons emplaced during these plutonic events are of batholithic dimensions and display an evolution from peraluminous potassium-rich magmas to metaluminous calc-alkaline magmas. Events that followed the youngest Early Proterozoic magmatism at about 1.66 Ga are sketchy, but they include the following: (1) formation of mylonite belts, perhaps during prolonged cooling through the Early and Middle Proterozoic; (2) anorogenic magmatism at

about 1.4 Ga, including emplacement of carbonatite at Mountain Pass, to be described below; and (3) diabase-sheet intrusion at about 1.1 Ga.

Protoliths for the supracrustal gneisses are variable and include a variety of sedimentary and volcanic rock types (Hewett, 1956; DeWitt and others, 1984, 1989; Anderson and others, 1985; Miller and others, 1986; Wooden and Miller, 1990). Inferred sedimentary rock types are fine-grained aluminous and quartz-rich rocks such as shale and siltstone, immature sandstone, volcaniclastic sandstone, and quartzite, the latter of which is restricted mostly to the hills near Halloran Spring. Volcanic protoliths are most commonly of felsic compositions, such as dacite and rhyodacite. In some places, distinguishing between intrusive and extrusive origins is difficult because the rocks have undergone granulite-facies metamorphism. For example, in the Providence Mountains and Mid Hills, a bimodal suite of felsic and mafic gneisses may represent either volcanic or intrusive rocks (Wooden and Miller, 1990). Contact relations and textures best support an intrusive origin (Miller and Wooden, 1993). Minimum ages for the supracrustal rocks range from 1.7 to about 2.0 Ga on the basis of $^{207}Pb/^{206}Pb$ ages determined by conventional U-Pb zircon geochronology (Wooden and Miller, 1990). Spot ion-probe analyses of single zircon grains yield clusters of ages at about 2.5 Ga, 2.3 Ga, 1.9 Ga, and 1.8 Ga (Miller and Wooden, 1994). The simplest interpretation of these ages is that they represent ages of igneous zircons from several source terranes; and so, the older zircons were redeposited with the youngest group of syndepositional volcanic and sedimentary rock strata at about 1.8 Ga. A minimum age for these rocks is 1.76 Ga, the age of the oldest dated plutonic suite that intrudes the supracrustal gneiss.

The EMNSA and nearby areas in southeastern California, southern Nevada, and northwestern Arizona are underlain by Early Proterozoic crust (Mojave crustal province of Wooden and Miller, 1990) that is isotopically and chronologically anomalous compared to other Early Proterozoic crust throughout the rest of the western United States. Neodymium-model ages for crust formation are 2.3 to 2.0 Ga in the Mojave crustal province, which suggests that this terrane formed from the mantle at 2.3 to 2.0 Ga or that the terrane formed at approximately 1.9 to 1.65 Ga and incorporated a significant component of Archean crust (Bennett and DePaolo, 1984, 1987). Because of the general lack of crust in the 2.3- to 2.0-Ga age range in the United States, Bennett and DePaolo (1987) preferred the latter interpretation and, furthermore, suggested that this terrane was transported on a left-lateral fault at least 400 km from the north where it both formed against and incorporated Archean crust. Lead-isotope characteristics (Wooden and others, 1988; Wooden and Miller, 1990) require that the Mojave crustal province incorporated lead from an Archean reservoir; lead in1.7-Ga-rocks is more radiogenic than would be expected if it were derived directly from the mantle. The Nd-model ages coupled with U-Pb detrital-zircon data suggest 2.2 to 1.8 Ga as the likely age for an event in which Archean clastic materials, possibly from the Wyoming Province, were deposited along with synorogenic deposits. Similar deposits may have been subducted, which allowed the addition of radiogenic lead into the mantle from which the Mojave crustal province was derived (Wooden and Miller, 1990).

Middle Proterozoic Granite

Several areas adjacent to the north-central part of the EMNSA are underlain by distinctive intrusive rocks whose age is approximately 1.4 Ga. The rocks principally consist of syenite, shonkinite, carbonatite, and granite; they crop out in the vicinity of Mountain Pass just outside the EMNSA (pl. 1). Although the mafic and alkalic rocks of this group are unusual, the granites are similar to others of this age that are widespread in southern California, in central and southern Arizona, and in southern Nevada (Anderson and Bender, 1989; Anderson, 1989). These rocks are commonly called “anorogenic,” as their emplacement is generally not associated with regional or, commonly, even local deformation. They are generally coarse grained and characterized by large, conspicuous phenocrysts of K-feldspar. Most plutons are granite, although some are granodiorite, quartz monzodiorite, and quartz monzonite. Common accessory and minor minerals include biotite, hornblende or muscovite, fluorapatite, zircon, and magnetite. Highly evolved members of the 1.4-Ga granitoid suite are enriched in Rb, Th, and U, and depleted in Ba and Sr.

Middle Proterozoic igneous rocks of the Mountain Pass area are described more fully in the section below entitled “Ultrapotassic Rocks, Carbonatite, and Rare Earth Element Deposit, Mountain Pass, Southern California.” Middle(?) Proterozoic porphyritic granite in the eastern Vontrigger Hills is grouped with other

granitoids on the geologic map (pl. 1). These rocks are coarse-grained biotite granite that contains megacrysts of K-feldspar and are undated.

Middle Proterozoic Diabase

Middle Proterozoic diabase dikes are known in the northeastern part of the EMNSA (Miller and Wooden, 1994) and are likely present as sparse small dikes in other parts of the study area. The dikes are generally less than 2 m thick; typically altered, mostly deuterically; and a few tens of meters in length, too small to show at the scale of the geologic map (pl. 1). They are part of a diabase suite emplaced at about1.1 Ga throughout the southwestern United States (Hammond, 1990; Howard, 1991; Conway and others, 1993; Conway, 1994). Widespread large dikes and sills are present in the southern Death Valley and Kingston Range region, about 25 km north-northwest of the EMNSA (Wright, 1968; Wright and others, 1976). Dikes and sheets are present in mountain ranges of the Mojave Desert south of the EMNSA (Howard, 1991) and are widespread in northwestern Arizona (Albin and Karlstrom, 1991; Bryant, 1992a,b; Conway, 1994; Conway and others, 1993; Conway, unpub. data, 1995). Diabase has been dated at numerous places in the Southwest at between 1.07 and 1.10 Ga, in the Death Valley area at 1,087±3 and 1,069±3 Ma (Heaman and Grotzinger, 1992), and in northwestern Arizona at 1.08 Ga (Shastri and others, 1991).

Examination of diabase dikes at numerous localities throughout the Southwest, including most of the radiometrically dated localities, indicates that 1.1-Ga diabase has a distinctive ophitic texture that in most cases clearly distinguishes it from mafic dikes of any other age. There is little doubt that the diabase dikes in the EMNSA are of the regional Middle Proterozoic diabase suite, although no systematic isotopic work has yet been done on the diabase dikes in the EMNSA.

Proterozoic Mineralization

Hewett (1956) noted that, although many mineral occurrences are hosted by Early Proterozoic gneiss in the eastern Mojave Desert region, the major periods of ore deposition were the Mesozoic and the late Tertiary. He furthermore concluded that no clear evidence exists for widespread Early Proterozoic mineralization in the area. However, limited evidence does exist for some minor mineralization of Proterozoic age, in addition to the rare earth element deposits associated with the 1,400-Ma carbonatite at Mountain Pass (see section below entitled "Ultrapotassic Rocks, Carbonatite, and Rare Earth Element Deposit, Mountain Pass, Southern California").

Minor amounts of rare earth elements and thorium have been mined from pegmatite in the New York Mountains (Miller and others, 1986). Similar pegmatites are common within the Early Proterozoic gneiss terrane throughout the EMNSA and have been interpreted to be the source of most of the anomalous concentrations of these elements in stream-sediment geochemical data (see section below entitled "Geochemistry"; see also Miller and others, 1986). Volborth (1962) suggested that these allanite-bearing pegmatites are related genetically to Mountain Pass-type syenite-carbonatite, but the field evidence of Miller and others (1986) indicated that the pegmatites are older, presumably Early Proterozoic, and therefore unrelated to a Middle Proterozoic carbonatite system.

Some suggestion of minor amounts of Proterozoic mineralization exists in the Ivanpah Mountains. At Mineral Spring, in the northern Ivanpah Mountains southeast of Mineral Hill, intensely fractured Early Proterozoic migmatite and granitoid gneiss (unit Xg_1, pl. 1) is cut by numerous quartz-galena-chalcopyrite veins. Most quartz is milky white and generally shows variable amounts of staining by secondary copper minerals. Most of the mineralized rock seems to be concentrated along a 1- to 2-m-wide fault zone that contains abundant gossan along its trace, which strikes N. 10° E. and dips 25° W. These veins are foliated and concordant with the fabric of the surrounding gneisses. Some veins have highly deformed, schistose selvages of brown carbonate-rich material along their margins; in places, some formerly clay rich zones are now recrystallized to white mica. The presence of jasperoidal-appearing material along the structure and its subsequent brecciation and neomineralization suggest that multiple episodes of mineralization have occurred in the general area. Mesozoic breccia development and sericitization are common in Nevada adjacent to the EMNSA (Miller and Wooden, 1994). We tentatively assign the deformed quartz-galena-chalcopyrite veins to a

Middle Proterozoic mineralization event related to magmatic rocks of this age in the immediately surrounding area (see section below entitled "Geochemistry"). However, some or all veins in the general area of Mineral Spring also could be Mesozoic in age.

Some mineral occurrences are associated with diabase dikes and sills examined in the northernmost New York Mountains. Several closely spaced, 2- to 4-m-wide diabase dikes strike N. 60° to 70° W. and dip 60° to 70° NE. approximately 1 to 2 km east of the Albermarle Mine (Miller and others, 1986; U.S. Bureau of Mines, 1990a, map no. 216). They intrude brecciated gray to white massive quartz and underlying mylonitized leucocratic granitoid gneiss; foliation in the granitoid gneiss and predominant shear surfaces in the breccia dip about 25° to 30° SW. Two shafts and numerous excavations are present in this area, many of which explore gossaniferous polymetallic quartz-sulfide veins as much as 1 m wide that are present as selvages to diabase sills. The diabase dikes and sills and their associated veins are undeformed; both clearly postdate deformation of the vein quartz and granitoid gneiss. The diabase also is locally altered in the vicinity of the veins. Systematic juxtaposition of dikes and quartz-sulfide veins suggests a genetic relation.

Similar diabase dikes and quartz-vein deposits were described elsewhere in the Southwest (Hewitt, 1959; Beard, 1987; Silberman and Wenrich, 1993; Wenrich and Silberman, 1993). Vein-type mineralization related to the emplacement of 1.1-Ga diabase dikes in Early Proterozoic crystalline rocks in the EMNSA may be more widespread than recognized previously.

Diabase dikes intruding the southern Death Valley area formed talc deposits by contact metamorphism of a carbonate member of the Middle Proterozoic Crystal Spring Formation of the Middle and Late Proterozoic Pahrump Group (Wright, 1968). The region between the southern Panamint Range, 35 km northwest of the EMNSA, and the Kingston Range contains 29 deposits that produced 1.09 million tonnes of talc ore. Talc and clay mines are present within a few kilometers of the north boundary of the EMNSA in the hills near Halloran Spring; whether these mines are associated with diabase is unknown. Additionally, asbestos, iron, and uranium deposits in the Middle Proterozoic Apache Group in central Arizona were formed by processes related to emplacement of large diabase sills (Wrucke and others, 1986).

The locations of many mineral deposits in both the Death Valley and central Arizona regions are controlled by the nature of the intruded sedimentary rocks. Host rocks suitable to the formation of such ore deposits, notably the Pahrump Group, are virtually absent in the EMNSA. Absence of host rocks and the scarcity of diabase sills suggests that little, if any, potential exists for talc, asbestos, iron, and uranium deposits associated with diabase in the study area.

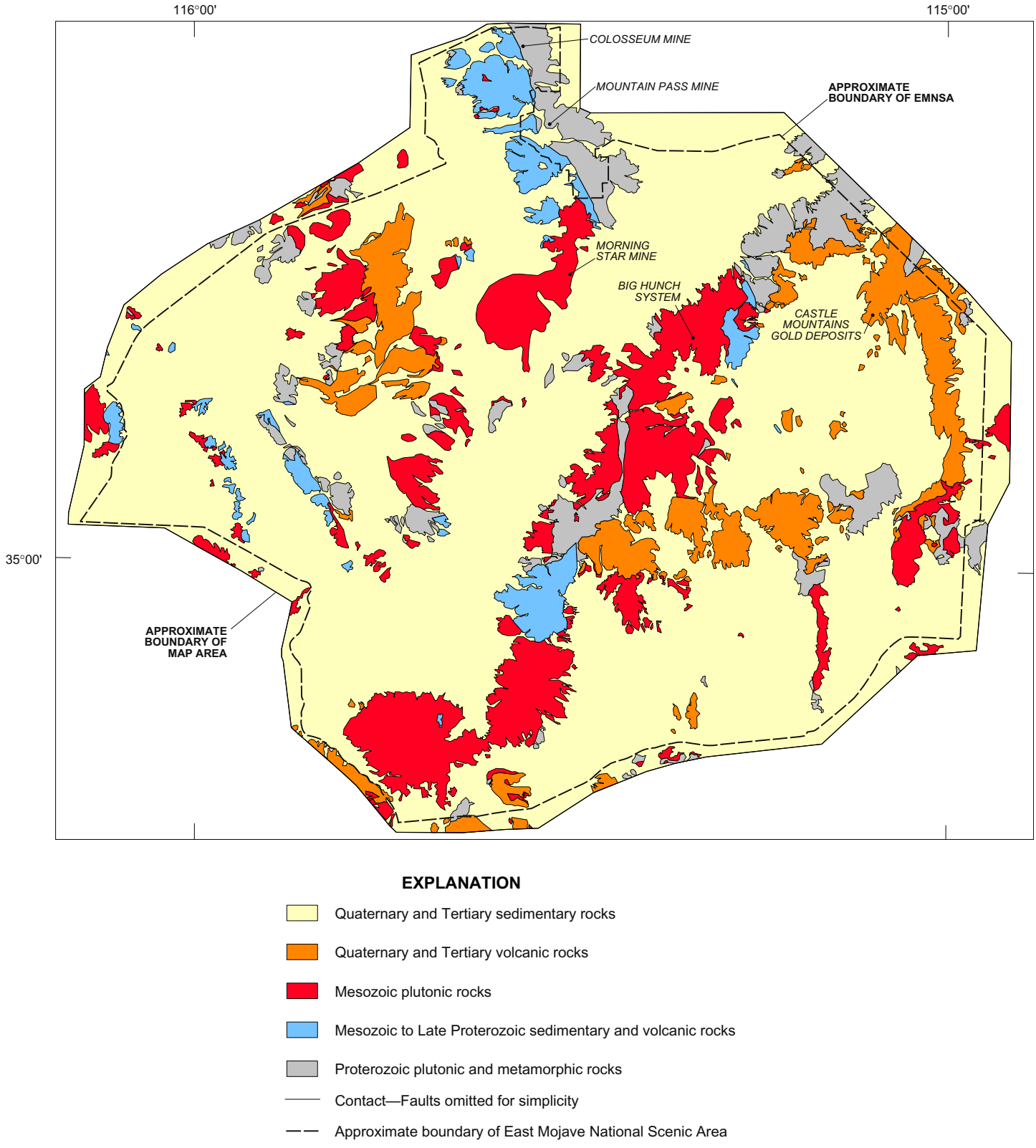

Figure 4. Generalized geologic map of East Mojave National Scenic Area (EMNSA), California, showing locations of major mineral occurrences. Simplified from plate 1.

Ultrapotassic Rocks, Carbonatite, and Rare Earth Element Deposit, Mountain Pass, Southern California

By Gordon B. Haxel

Introduction

The Mountain Pass area of southeastern California, just outside the irregular northeast boundary of the East Mojave National Scenic Area (EMNSA) (fig. 4), is notable for three extraordinary geologic phenomena: a geochemically unique carbonatite intrusion, a world-class rare earth element deposit hosted by the carbonatite, and a suite of mafic to silicic ultrapotassic plutonic rocks that are coeval with and presumably genetically related to the carbonatite. Olson and others (1954) described comprehensively the geology, petrography, and mineralogy of the Mountain Pass area and the rare earth element deposit; their work has been summarized in several succeeding articles (Olson and Pray, 1954; Heinrich, 1966; Woyski, 1980; Möller, 1989). Subsequently, rocks at Mountain Pass have been studied by Watson and others (1974), Crow (1984), DeWitt and colleagues (DeWitt, 1987; DeWitt and others, 1987), and Castor (1990, 1991). Despite the considerable petrologic and economic significance of the alkaline rocks at Mountain Pass, no comprehensive geochemical and petrogenetic study has been published to this date (1993).

In this chapter, a brief summary of the geologic setting, physical configuration, and petrography of the ultrapotassic rocks and carbonatite at Mountain Pass is followed by a more detailed examination of the petrochemistry of the ultrapotassic rocks. The limited chemical data available permit descriptive characterization and provisional comparison with other ultrapotassic igneous suites. Primitive ultrapotassic rocks at Mountain Pass contain remarkably high abundances of many incompatible elements. A simple numerical model supports the hypothesis that these igneous rocks were produced by very small degrees of partial melting of highly enriched lithospheric-mantle peridotite. Finally, the geology, geochemistry, and significance of the Mountain Pass rare earth element deposit are summarized.

Geologic Setting

The Middle Proterozoic ultrapotassic rocks and carbonatite of the Mountain Pass area (unit Yg, pl. 1) crop out within an elongate block of crystalline rocks approximately 60 km long that extends from east of Kokoweef Peak, in the northeastern Ivanpah Mountains, north-northwestward to Mesquite Pass, about 4 km north of the EMNSA boundary (fig. 2; see also Hewitt, 1956). This block is composed largely of Early Proterozoic gneisses and pegmatites (Xg), about 1,700 Ma (see section above entitled "Proterozoic Rocks and Their Mineralization;" see also, DeWitt, 1987; Wooden and Miller, 1990). These rocks are intruded by, but unrelated to, the Middle Proterozoic ultrapotassic rocks and carbonatite. This block of Proterozoic rocks is autochthonous, bounded on the west by a thrust fault and a high-angle fault within the Ivanpah Mountains-Clark Mountain area, and on the east by an inferred high-angle fault beneath the western Ivanpah Valley (Hewitt, 1956; Burchfiel and Davis, 1971, 1981). The Proterozoic rocks are cut by Tertiary(?) andesite and rhyolite dikes.

The ultrapotassic rocks and carbonatite are restricted to an area extending from approximately 2 km northwest of the Mountain Pass deposit to approximately 9 to 13 km southeast of the deposit. This outcrop belt of ultrapotassic rocks and carbonatite is truncated on the north by a northwest-striking high-angle transverse fault (Olson and others, 1954, pl. 1). To the southeast, the abundance of ultrapotassic rocks and carbonatite decreases gradually toward Mineral Spring.

Configuration, Distribution, and Age Relations of Intrusions

The ultrapotassic silicate igneous rocks at Mountain Pass include shonkinite (melanosyenite), minette (phlogopite lamprophyre), syenite, and granite. These rocks form several hundred thin dikes and seven larger intrusive bodies. The dikes are approximately 0.3 to 10 m wide and as much as 1,100 m long. Most of the larger dikes dip moderately to steeply southwestward. The larger intrusive bodies are ovoid to irregular in map

view and range from 200 to 1,800 m in largest exposed dimension. The largest of these bodies crops out north of the Mountain Pass deposit.

Carbonatite forms about 200 small dikes and one large intrusive body. Most of the carbonatite dikes are approximately 0.3 to 2 m thick and rather variable in orientation. The dikes intrude both Early Proterozoic gneiss and the Middle Proterozoic shonkinite, syenite, and granite. A few of these tabular carbonate bodies could be veins rather than dikes.

The single largest carbonatite body, called the Sulfide Queen carbonatite body (pl. 1), strikes approximately north-south, has a strike length of approximately 700 m, dips about 40° W., and is roughly 70 m thick (Barnum, 1989). Its principal map dimensions are approximately 700 by 200 m. The carbonatite intrusion is irregular, having apophyses extending into the enclosing Early Proterozoic gneiss, satellitic carbonatite intrusions as much as 60 m long along its margin, and inclusions of gneiss and shonkinite as much as 50 m long within the marginal parts of the intrusion.

Carbonatite is considerably less widespread than the ultrapotassic rocks. Most of the carbonatite dikes crop out within a belt that extends approximately 2 km north from the south end of the Sulfide Queen carbonatite body. Only a few small, scattered carbonatite dikes crop out south of Mountain Pass and Interstate 15; most of these dikes are in close proximity to the smaller (nondike) shonkinite intrusions, and some of them parallel shonkinite dikes.

The general intrusive sequence of rock types in the Mountain Pass area is, from oldest to youngest, (1) the main shonkinite bodies, (2) mesosyenite, (3) syenite, (4) quartz syenite, (5) potassic granite, (6) late minette (or shonkinite) dikes, and (7) carbonatite intrusions, including dikes and the Sulfide Queen body. However, at least one late shonkinite dike appears to cut a carbonatite dike (Olson and others, 1954, p. 16; see also DeWitt and others, 1987).

Geochronology and Isotopic Compositions

Lanphere (1964) obtained K-Ar and Rb-Sr ages of 1,380 to 1,440 Ma for biotite from shonkinite at Mountain Pass and calculated a $^{208}Pb/^{232}Th$ monazite age of 1,436±71 Ma using data from Jaffe (1955) and Gottfried and others (1959). DeWitt and others (1987) conducted a comprehensive U-Th-Pb and $^{40}Ar/^{39}Ar$ geochronologic study: apatite from the shonkinite has a U-Pb age of 1,410±2 Ma; phlogopite from the shonkinite and arfvedsonite from the syenite have $^{40}Ar/^{39}Ar$ plateau ages of 1,400±8 and 1,403±7 Ma, respectively; and monazites from the carbonatite have Th-Pb ages of 1,375±7 Ma. Bastnaesite and parisite from the carbonatite have complex isotopic systematics that suggest postintrusion migration of Pb. Collectively, these data indicate that the ultrapotassic rocks at Mountain Pass are approximately 1,410 to 1,400 Ma and that the related carbonatite probably was emplaced some 15 to 25 m.y. later.

Unfortunately, the single determination each of Sr and Nd isotopic composition from Mountain Pass are for two different rock types. The carbonatite has a $^{87}Sr/^{86}Sr$ ratio of 0.7044 (Powell and others, 1966); presumably this is the initial ratio as the carbonatite has very high Sr content and very low Rb/Sr ratio (<0.001; table 1). ε_{Nd} for shonkinite from Mountain Pass is –3.5 (for age of 1,400 Ma) (DePaolo and Wasserburg, 1976). Lead and sulfur isotopic compositions of rocks and minerals from Mountain Pass are discussed by Mitchell (1973), Mitchell and Krouse (1971, 1975), DeWitt and others (1987), and Deines (1989). The "extinct" nuclide ^{244}Pu has been reported at a concentration on the order of 10^{-18} g/g in bastnaesite from Mountain Pass (Hoffman and others, 1971).

Petrography

The following summary of the petrography of the ultrapotassic rocks and carbonatite at Mountain Pass is derived mostly from the detailed descriptions provided by Olson and others (1954). The modal progression from shonkinite to syenite involves decrease in color index and concomitant increase in feldspar content; the granites have markedly lower color index and higher quartz content (fig. 5). Given the Mg-rich character of many of the ultrapotassic rocks at Mountain Pass, much of the dark mica probably is phlogopite. In this summary, the general term biotite is used except where phlogopite was specified in the original descriptions.

Shonkinite

The main shonkinite bodies typically consist of medium- to coarse-grained, equigranular, mesocratic to melanocratic shonkinite composed of subequal proportions of grayish-red microcline, green augite, black biotite, and subordinate amphibole. Microperthitic albite is common within the microcline, but separate grains of plagioclase typically constitute only 1 to 3 volume percent of the shonkinite. Other accessory minerals include various combinations of apatite (typically, 2 to 4 volume percent), iron-titanium oxides, sphene, zircon, epidote, olivine, and, rarely, pseudoleucite(?). Quartz is absent. The pyroxenes are augite and aegirine-augite. Amphiboles are hornblende and (or) sodic amphibole; commonly, both are present. The sodic amphibole is riebeckite and (or) arfvedsonite. Textures are hypidiomorphic-granular or poikilitic, with microcline enclosing biotite, augite, apatite, and other minerals.

Minette Dikes

The late dikes at Mountain Pass are mafic and fine grained, have phlogopite phenocrysts, and can be classified as either shonkinites or minettes (Olson and others, 1954). The latter term is used here to distinguish these late dikes from the main shonkinites, which are earliest in the intrusive sequence. The minettes consist of K-feldspar, phlogopite, augite or aegirine-augite, and hornblende; accessory minerals are quartz (fig. 5), apatite, sphene, iron-titanium oxides, calcite, and fluorite. Phlogopite, the dominant mafic mineral, is present both as phenocrysts and in the groundmass. Some rocks also contain phenocrysts of pyroxene and (or) hornblende. Biotite-rich melanocratic dikes composed largely of phlogopite and aegirine and subordinate or minor feldspar and calcite crop out in one area north of the Mountain Pass rare earth element deposit.

Syenite and Granite

With decreasing pyroxene and biotite content and increasing feldspar and quartz content, shonkinite grades into syenite (fig. 5). Typical syenite contains approximately 80 to 85 volume percent alkali feldspar (orthoclase and (or) microcline, commonly perthitic); less than 10 volume percent each of plagioclase and quartz; and 10 to 15 volume percent each of biotite, amphibole, and, less commonly, augite or aegirine-augite. Common accessory minerals include hematite, apatite, sphene, zircon, rutile, and allanite. Much of the syenite is coarse grained and equigranular; some contains orthoclase phenocrysts. Textures are hypidiomorphic-granular. Mafic, augite- and biotite-rich syenites generally have mafic phenocrysts. In leucosyenite, biotite is the sole mafic mineral. Some syenites contain hornblende; others, sodic amphibole. Late crocidolite (fibrous or asbestiform sodic amphibole) replaces other mafic minerals and also forms veinlets. Quartz syenite, gradational in character between syenite and granite, is petrographically similar to syenite but contains more quartz.

The granites of the Mountain Pass area are fine to coarse grained and commonly have pinkish alkali-feldspar phenocrysts. Most have modal compositions of quartz-poor syenogranite (fig. 5). The plagioclase is quite sodic (An_6). Color index is typically 10 percent or less, distinctly lower than that of the syenite and shonkinite. Mafic minerals are biotite, hornblende, and sodic amphibole. Accessory minerals include iron-titanium oxides, zircon, apatite, sphene, monazite, metamict thorite(?), allanite, epidote, and fluorite.

Carbonatite

Although Olson and others (1954, p. 59–63) recognized the igneous character and origin of the carbonatite at Mountain Pass from regional, field, petrologic, and geochemical evidence, they conservatively referred to it as "carbonate rock." All subsequent workers have simply treated the carbonatite as an intrusive igneous rock.

One large mass (the Sulfide Queen intrusive body), a number of smaller masses, and many dikes of carbonatite crop out in the Mountain Pass area. The following summary focuses on the Sulfide Queen carbonatite body, which Olson and others (1954; see also, Heinrich, 1966; Woolley and Kempe, 1989) divided into the following three map units (oldest to youngest): ferruginous dolomite carbonatite (beforsite), barite-calcite carbonatite (sövite), and silicified carbonatite. These three types are mutually intergradational, and each has several textural and compositional variants. The following paragraphs describe the principal compositional types.

The dolomite carbonatite is fine grained and consists of dolomite, barite, and monazite, as well as accessory calcite, magnetite, and pyrite. Some rocks also contain the rare earth fluorocarbonate minerals bastnaesite and parisite (table 2). Local additional accessory minerals include thorite(?), apatite, aegirine, and phlogopite.

Barite-calcite carbonatite is the most abundant rock type within the Sulfide Queen body. This sövite consists of 40 to 75 volume percent calcite, 15 to 50 volume percent barite, and 5 to 15 volume percent bastnaesite and (or) parisite. Common accessory minerals include crocidolite, chlorite, phlogopite, apatite, thorite(?), allanite, zircon, galena, hematite, magnetite, and pyrite. The rock typically has a fine-grained groundmass surrounding blocky, subhedral barite phenocrysts 1 to 4 cm wide.

The silicified carbonatite is texturally similar to the barite-calcite carbonatite but has abundant quartz and correspondingly lower calcite content. The silicified carbonatite consists of bastnaesite, barite, and quartz, as well as subordinate or accessory calcite, monazite, hematite and goethite, sericite, galena, and pseudomorphs of hematite after pyrite. Bastnaesite content is as much as 60 volume percent. Quartz forms both euhedral crystals and late chalcedonic veins or layers.

All three types of carbonatite within the Sulfide Queen body are cut by fractures, veins, and shear zones that are coated or filled with crocidolite, chlorite, iron oxides, or other minerals. Supergene minerals include iron oxides, lead or copper carbonate minerals, quartz, and wulfenite.

Fenitization

Fenitization (alkali metasomatism; Heinrich, 1966, chapter 3; McKie, 1966) is widespread in and around the ultrapotassic rocks and carbonatite. Alteration minerals include microcline, albite, riebeckite (including crocidolite), aegirine, chlorite, phlogopite, barite, calcite, iron oxides, sericite, and quartz. Some, perhaps much, of the fenitization is associated with carbonatite intrusions.

Petrochemistry of Ultrapotassic Rocks

Analytical Data

Whole-rock geochemical data for the ultrapotassic rocks and carbonatite at Mountain Pass are limited in quantity and quality. Published and unpublished data from Olson and others (1954), Crow (1984), Lister and Cogger (1986), and J.P. Calzia (written commun., 1992), as well as new data obtained by the author provide a total of 32 analyses. However, both major- and trace-element data are available for only 15 of these samples, and only the four new analyses reported in table 1 include all of the petrologically important trace elements. The previous analyses include reasonably complete and precise data for only four trace elements, Cr, Rb, Ba, and Sr. Most samples have data for Zr or Hf but not both, as well as Nb or Ta but not both. For several geochemical plots, missing values have been estimated on the basis of the assumption that the ratios of Zr/Hf approximately equal to 37 and Nb/Ta approximately equal to 17, which are observed in common types of chondritic, terrestrial, and lunar mafic igneous rocks (Jochum and others, 1986), apply as well to the silicate ultrapotassic suite at Mountain Pass. Given these limitations, petrochemical interpretations of the ultrapotassic rocks at Mountain Pass are necessarily provisional. Petrochemistry of the carbonatite at Mountain Pass is briefly discussed in a later section.

Watson and others (1974) presented, in an abstract, partial mean compositions for 95 major-element analyses of six rock types from Mountain Pass but reported no trace-element data.

Geochemical data for samples from Mountain Pass have been determined by gravimetric wet-chemical methods and wavelength-dispersive X-ray fluorescence spectrometry for major elements and, for trace elements, by energy-dispersive X-ray fluorescence spectrometry, instrumental neutron-activation analysis (INAA), and inductively coupled plasma-atomic emission spectrometry (ICPES) (Crow, 1984; Baedecker, 1987).

The paucity of complete analyses necessitates the use of two complementary indices of fractionation or evolution: Cr content and *mg* number (*mg*, the molar MgO/(MgO+FeO) ratio, calculated with weight percent Fe_2O_3/(Fe_2O_3+FeO) ratio set to 0.2 (Hughes and Hussey, 1976)). Several common acronyms are used in the ensuing discussions of petrology and mineral resources: REE, rare earth elements; LREE, light rare earth elements (La, Ce, Pr, and Nd); HREE, heavy rare earth elements (Tb through Lu); LILE, large-ion-lithophile

elements (K, Ba, Rb, and Cs); and HFSE, high-field-strength elements (Nb, Ta, Zr, Hf, and Ti). Y is commonly included with the HREE. Though not strictly large-ion-lithophile elements, Th and U frequently behave similarly to, and so are generally included with, the LILE. The subscript "cn" designates chondritic-normalized abundances or ratios (normalizing abundances from Nakamura, 1974).

Major-Element Compositions

Normative compositions calculated for the shonkinites and minettes at Mountain Pass frequently contain nepheline or leucite. However modal nepheline has not been reported; Olson and others (1954) found only a single sample possibly containing pseudoleucite; and Crow (1984) found no nepheline or leucite. The shonkinites lack quartz, but the minettes do contain small amounts of quartz, as much as 3 volume percent. The shonkinites and minettes evidently are silica saturated to marginally oversaturated. The normative nepheline and leucite apparently are artifacts of a formalism ill suited to rocks containing 20 to 40 volume percent biotite. Biotite contains both essential Mg and Fe and essential K, whereas the normative calculation scheme inappropriately allocates Mg-Fe and K to separate minerals.

In their molar proportions of alumina and alkalis, the shonkinites, minettes, syenites, and granites at Mountain Pass vary from marginally metaluminous to weakly peralkaline and from potassic to ultrapotassic (fig. 6). Most samples have unusually high molar K_2O/Al_2O_3 ratios, equal to or greater than 0.6; in contrast, common igneous rocks have molar K_2O/Al_2O_3 ratios less than or equal to 0.3. One sample from Mountain Pass, a syenite, is marginally perpotassic.

Ultrapotassic igneous rocks are generally defined as those that have weight percent contents of MgO greater than 3 and K_2O greater than 3, as well as weight percent K_2O/Na_2O ratios greater than 2.5 or 3 (Bergman, 1987; Peccerillo, 1992). According to these criteria, all or nearly all shonkinites, minettes, and syenites at Mountain Pass, which have K_2O/Na_2O ratios of 2.6 to 16, are ultrapotassic. In the standard classification of igneous rocks by silica and total alkali contents (Le Bas and others, 1986), the shonkinites and minettes plot chiefly in the phonotephrite and tephriphonolite fields.

The granites at Mountain Pass are less unusual compositionally than the more mafic rocks. Most of the granites are merely potassic, having K_2O/Na_2O ratios of 1.4 to 3.0. Two samples of altered granite that have excessively high K_2O/Na_2O ratios, greater than 35, are discussed separately below (these samples are omitted from all geochemical diagrams except fig. 9).

The succession from shonkinite through syenite to granite is marked by increase in SiO_2 content from 47 to 71 weight percent, decrease in MgO content from 11 or 12 weight percent to 1 weight percent or less, and decline of *mg* from about 0.8 to about 0.25 (fig. 7). Using the decline in *mg* as an index of progressive evolution, contents of TiO_2, P_2O_5 (fig. 8*A*,*B*), FeO* (total Fe as FeO), and CaO decrease sharply; Na_2O increases markedly; Al_2O_3 increases moderately; and K_2O content is unsystematic. The K_2O/Na_2O ratio decreases sharply with declining *mg* (fig. 8*C*).

Effects of Fenitization

Most shonkinites, minettes, syenites, and granites at Mountain Pass have weight percent K_2O/Na_2O ratios of about 2 to 11 (fig. 8*C*). Two granite samples (not plotted on fig. 8*C*) have very high K_2O/Na_2O ratios, 37 and 45. Such extreme values are not primary but rather a product of subsolidus fenitization. As might be expected, the fenitized granites are moderately enriched in K_2O and strongly depleted in Na_2O relative to unfenitized granites (fig. 9); Fe, Mg, Ca, P, and Mn are moderately depleted; Si, Al, and Ti are little affected. Surprisingly, Ba is not enriched in the fenites. An additional sample, which has a K_2O/Na_2O ratio of about 66, is so strongly fenitized that its prealteration composition and identity are uncertain.

Shonkinites and Minettes as Primary Magmas

Primary, mantle-derived mafic magmas are considered to have *mg* from about 0.65 to 0.80 (Rock, 1991, p. 131–132), although ultrapotassic primary melts may have somewhat higher or lower *mg* (Foley, 1992). Primary magmas also have moderately high Cr (200–500 ppm), Co (25–80 ppm), and Ni (90–700 ppm) contents. The more Mg-rich shonkinites and minettes at Mountain Pass have *mg* equal to 0.72 to 0.82, Cr contents equal to

400 to 700 ppm, Co contents of about 30 to 40 ppm, and Ni contents greater than or equal to 200 ppm, thus equaling or exceeding common criteria for primary magmas.

The shonkinites and minettes that have the highest *mg* and highest Cr and Ni contents may be partially accumulative. As the main shonkinites are, in general, medium-grained plutonic rocks, they probably do not represent strictly liquid compositions but rather were emplaced in the upper crust as mixtures of magma and crystals. The fine-grained minette dikes, which have *mg* of about 0.72, may more closely approximate liquid compositions. Recognition of rocks that have accumulated mafic minerals is problematic in the absence of detailed petrographic information for the analyzed samples. Comparison with a suite of Scottish lamprophyres (Rock and others, 1986) suggests that some shonkinites at Mountain Pass are primary and some, those that have *mg* greater than 0.75, are accumulative (fig. 10).

Abundances of Lithophile Trace Elements

Abundances of Rb, Ba, Sr, and REE are generally greatest in the shonkinites and minettes, where they are generally enriched over MUCC (abundance in mean upper continental crust; Taylor and McLennan, 1985) by factors of 4 to 20. Overall, Ba is the most highly enriched, averaging 6,700 ppm (12×MUCC) in the shonkinites and minettes. Data for Th are available for only four samples (table 1); three of these, a shonkinite, a syenite, and a granite, have extraordinarily high abundances of Th (160–300 ppm, 15–28×MUCC; these elevated Th values, determined by INAA methods, were confirmed by ICPES methods). The shonkinite also has extraordinarily high F content, 1.4 weight percent (table 1).

All of the ultrapotassic rocks have high abundances of LREE but unexceptional abundances of HREE. In the shonkinites and minettes, mean abundances of La and Ce are about 290 and 670 ppm, respectively; both are about 10×MUCC. In contrast, Yb abundances in the shonkinites and minettes are less than 2×MUCC. The shonkinites, minettes, and syenites all have very steep chondrite-normalized REE spectra, typically having La_{cn} contents equal to 600 to 1800, Yb_{cn} contents of about 17, and $(La/Yb)_{cn}$ ratios of about 30 to 60 (fig. 11). Most samples show small negative Eu anomalies, having Eu/Eu* ratios of about 0.8 (Eu* is obtained by logarithmic interpolation between Sm and Tb: $Eu^*=10^{(\frac{2}{3}\log(Sm)+\frac{1}{3}\log(Tb))}$). The granites typically have somewhat lower abundances of all REE; steeper REE spectra, having $(La/Yb)_{cn}$ ratios equal to 60 to 80; and shallower negative Eu anomalies, having mean Eu/Eu* ratios of about 0.9.

Fractional Crystallization of Shonkinite and Syenite

Abundances of Cr decrease from about 400 ppm or more in the primitive, probably primary, shonkinites and minettes at Mountain Pass to as low as about 50 ppm in the syenites (fig. 12). Other highly compatible elements—Co, Ni, and Sc—show comparable progressive depletion. Precipitous decline of highly compatible elements strongly suggests fractional crystallization. For example, if the cumulates are rich in biotite, augite, and iron-titanium oxides, then the bulk distribution coefficient for Cr might be in the range of 5 to 10. Approximately 20 to 40 percent perfect fractional crystallization (Arth, 1976) would then explain the observed decrease in Cr from shonkinite to syenite. Whether or not fractional crystallization of the shonkinite-syenite sequence was accompanied by assimilation of continental crust cannot be determined from the limited trace-element and isotopic data presently available.

Several lithophile trace elements that are incompatible or highly incompatible during fractional crystallization in most igneous suites act compatibly in the ultrapotassic rocks at Mountain Pass, owing to the unusual assemblage of fractionating minerals. For those trace elements that show systematic behavior, most trends can be qualitatively explained in terms of fractionation of minerals present in the rocks. During progressive fractional crystallization (as indicated by declining *mg* and Cr content), Ba and Sr contents decrease (fig. 13) as do P and Ti contents (fig. 8). Progressive depletion of Ba can be explained by fractionation of alkali feldspar and biotite; depletion of Sr, by precipitation of alkali feldspar and apatite. Although Sr depletion is commonly interpreted as evidence of plagioclase fractionation, alkali feldspar also can have a large partition coefficient for Sr (Villemant and others, 1981). Depletion of Ti presumably was caused by fractionation of some combination of biotite, augite, and iron-titanium oxides. Decrease of P indicates apatite fractionation, and the strong correlation between P and Ce (fig. 14*A*) suggests control of the LREE by apatite crystallization. The

abundance of Rb shows no systematic change with progressive evolution; a preponderance of alkali feldspar and biotite in the fractionating mineral assemblage(s) apparently prevented Rb from behaving incompatibly.

Lithophile trace elements other than those just discussed exhibit less systematic behavior (possibly in part owing to analytical imprecision). Many pairs of trace elements either do not correlate or show weak correlations that are of uncertain significance, given the limitations of the data. Some of these trace elements probably are controlled or affected by several different fractionating minerals. For example, significant amounts of Yb could be hosted by augite, biotite, apatite, sphene, and zircon. Roughly constant Yb contents in the shonkinites, minettes, and syenites (fig. 14*B*) suggest a bulk distribution coefficient near unity.

Close similarity in the incompatible-element patterns of representative samples of shonkinite and syenite from Mountain Pass clearly evinces their consanguinity (fig. 15). Relative to the parental shonkinite, the derivative syenite shows only slight depletions of Cs, Ba, Th, Sr, and P, all readily attributable to fractionation of observed minerals.

Crow (1984) used major-element and REE data to model the production of syenite from shonkinite by fractional crystallization of an assemblage of aegirine-augite, biotite, apatite, zircon, and minor plagioclase, K-feldspar, quartz, and amphibole. The very small proportion of alkali feldspar in the model precipitate seems to conflict with both the much greater abundance of this mineral in the rocks and the observed depletion of Sr and Ba, which were not considered in the model.

Origin of the Granite

On several trace-element variation diagrams, the granites plot in a separate cluster or trend, distinct from the cluster or trend defined by the shonkinites, minettes, and syenites (for example, figs. 12, 14). This distinction is particularly apparent on plots involving Zr or Yb. Depletion of Zr and HREE in the granites could be explained by the onset of zircon fractionation. However, the shonkinites, syenites, and granites all contain abundant zircon. The presence of discontinuities in several variation diagrams suggests that the granites may not be cogenetic with the shonkinites and syenites. In addition to the possibility of production of the granite by fractional crystallization of syenite or by a separate melting event (Crow, 1984; see also Crow, oral commun., 1987, *quoted by* DeWitt, 1987, p. 54), formation of the granite by assimilation of continental crust during fractional crystallization of the shonkinite-syenite sequence should also be considered.

Whatever their origin, the granites at Mountain Pass are not highly evolved. Highly evolved (highly differentiated) granites are strongly or extremely depleted in the feldspar-compatible elements Sr, Ba, and Eu, having Eu/Eu* ratios of about 0.4 to less than 0.1 (see for example, Mittlefehldt and Miller, 1983). In contrast, the granites at Mountain Pass all have high and roughly similar Sr and Ba abundances, and the mean and least values of Eu/Eu* ratio are only 0.9 and 0.7, respectively.

Shonkinite and Minette: Comparison With Other Ultrapotassic Rocks

The shonkinites and minettes at Mountain Pass have compositions comparable to the most strongly ultrapotassic of terrestrial igneous rocks (fig. 16). All common igneous rock types have weight percent K_2O/Na_2O ratios less than 2. Ultrapotassic rocks, that is rocks that have K_2O/Na_2O ratios greater than 2.5 or 3, make up less than one percent of all igneous rocks; nonetheless, they have received much attention from petrologists. Three widespread petrologic groups of ultrapotassic rocks are recognized: lamproites, kamafugites, and plagioleucitites (Bergman, 1987; Foley and others, 1987; Mitchell and Bergman, 1991; Foley, 1992; Peccerillo, 1992). (Kamafugites are strongly silica undersaturated, K- and Ca-rich ultramafic rocks that typically contain kalsilite or melilite. The plagioleucitite group includes such rocks as leucite tephrites, leucitites, and leucite phonolites.) Some minettes also are ultrapotassic (Rock, 1987, 1991). Petrologic relations between lamproites and minettes are controversial (Bergman, 1987; Mitchell and Bergman, 1991, p. 405; Rock and others, 1992).

The shonkinites at Mountain Pass differ sharply in major-element composition from both kamafugites and plagioleucitites. In particular, the shonkinites have decisively lower CaO and higher SiO_2 contents than kamafugites, as well as decisively lower Al_2O_3 and higher MgO contents than plagioleucitites (fig. 17). On the other hand, the shonkinites are compositionally similar to the lamproite group. Important similarities, in addition to ultrapotassic character, include low Al_2O_3, CaO, and Na_2O contents and high to very high

abundances of Ba, Zr, LREE, Th, and F. Of the two general types of lamproites, olivine lamproites and phlogopite lamproites, the shonkinites at Mountain Pass have chemical affinities to the latter (fig. 18).

Despite the numerous similarities of the shonkinites at Mountain Pass to lamproites, several significant differences also exist. The shonkinites contain less Ti and Zr than many lamproites and consequently lack the unusual Ti- and Zr-bearing accessory minerals characteristic of lamproites from such classic localities as Leucite Hills, Wyoming, and West Kimberley, Australia. Some shonkinites at Mountain Pass contain small amounts of plagioclase, which is by definition absent from lamproites in the strict sense. Though their LREE contents are similar to those of lamproites, the shonkinites have greater HREE abundances, and, therefore, lower La/Yb ratios than most lamproites. Furthermore, a shonkinite from Mountain Pass has initial $\varepsilon_{Nd} = -3.5$ (DePaolo and Wasserburg, 1976), whereas lamproites typically are significantly less radiogenic, having initial $\varepsilon_{Nd} = -7.4$ to -26 (Mitchell and Bergman, 1991). (The parameter ε_{Nd} is defined as

$$\varepsilon_{Nd}(t) = [(^{143}Nd/^{144}Nd)_{sample}(t)/(^{143}Nd/^{144}Nd)_{CHUR}(t) - 1]\times 10^4,$$

where CHUR stands for "chondritic uniform reservoir" and t represents time.)

In figure 19, the shonkinites at Mountain Pass are compared with compositional fields for lamproites and minettes or, more generally, calcalkaline lamprophyres. In their K_2O contents and K_2O/Al_2O_3 ratios, the shonkinites overlap with the high-K part of the calcalkaline lamprophyre field but are more typical of lamproites (figs. 19*A*–*C*). Plots of Sr versus Ba contents and Sm content versus La/Yb ratio discriminate particularly well between minettes and lamproites (figs. 19*D*, 19*E)*. Abundances of Ba in the shonkinites are in the highest part of the minette range, but typical of lamproites. The La/Yb ratio is within the lowest part of the range of lamproites and typical of minettes. However, the shonkinites contain substantially more Sm than either typical minettes or most lamproites.

Chondrite-normalized incompatible-element spectra (fig. 20*A*) further illustrate differences between a representative shonkinite from Mountain Pass and some typical lamproites. Although both rock types share the elevated abundances of LILE that are characteristic of ultrapotassic suites, their patterns show three significant contrasts: (1) In the LILE, the lamproite and shonkinite patterns are antithetical. The lamproites are typically enriched in Ba relative to Cs and Rb and depleted in Th and U relative to Rb and K, whereas the shonkinite is depleted in Ba relative to Cs and Rb and strongly enriched in Th and U relative to all other LILE. Furthermore, the shonkinite has extraordinarily high Th and Cs abundances, approximately an order of magnitude greater than those of the lamproite averages. (2) The shonkinite has lower normalized abundances of all the HFSE than the lamproites. The prominent troughs at Nb-Ta and Ti in the shonkinite pattern are subdued or absent in the lamproite patterns, and the lamproites contain somewhat more Zr and Hf. (3) The shonkinites have considerably higher HREE and Sm contents than the lamproites. Possible genetic significance of some of these contrasts is discussed in the next section.

In summary, among ultrapotassic rocks the shonkinites at Mountain Pass are more similar to lamproites than to minettes. However, a few significant differences indicate that the shonkinites are best not classified as lamproites. In general, relations between lamproites, which occur as volcanic and subvolcanic rocks, and plutonic ultrapotassic rocks such as shonkinites are poorly understood (Mitchell and Bergman, 1991, p. 17).

Petrogenesis of Shonkinite

"… kimberlite and potassium-rich magmas. Despite their small volume, such melts are of enormous importance." —*D. McKenzie, 1985*

According to current petrogenetic concepts, the extraordinary composition of the shonkinites at Mountain Pass can be explained only by partial melting of enriched subcontinental lithospheric mantle (Bergman, 1987; Wilson, 1989, chap. 12; Peccerillo, 1992). The primitive, ultrapotassic, strongly LILE- and LREE-enriched character of the shonkinites could not be produced by crustal contamination of basaltic magma. In general, the genesis of mantle-derived alkaline igneous rocks probably involves interaction of both lithospheric and asthenospheric components (Menzies, 1987). However, the distinctively high LILE/HFSE ratios of the

shonkinites, even in comparison with other lithosphere-derived ultrapotassic rocks (for example, fig. 20*A*), indicates a predominantly or completely lithospheric source.

The shonkinites at Mountain Pass share a key major-element characteristic with the lamproite suite: distinctively lower contents of Al, Ca, and Na than other primitive mafic rocks. This indicates derivation from infertile, refractory, magnesian, harzburgitic peridotite that has been previously depleted in Al, Ca, and Na by extraction of basaltic magma (Mitchell and Bergman, 1991, chap. 10). On the other hand, the very high abundances of incompatible elements in lamproites and in the shonkinites at Mountain Pass requires that their mantle sources were enriched or reenriched in incompatible elements. Such enrichment, or metasomatism, of lithospheric mantle is a global phenomena and apparently can be caused by migration or infiltration of either silicate magmas or volatile-rich fluids (Menzies and others, 1987). Depleted but reenriched peridotite evidently constitutes much of the continental lithospheric mantle.

Thus, analogy with the much more thoroughly studied lamproite clan suggests a three-stage history for the origin of the shonkinites at Mountain Pass: depletion of the mantle source, then reenrichment of the source, and, finally, partial melting to generate the shonkinites (compare with Tainton and McKenzie, 1994). With the limited elemental and isotopic data presently available, only the partial melting stage can be elucidated further. Thus, the high to extreme incompatible-element contents of the shonkinites at Mountain Pass must be caused by some combination of source enrichment and small degrees of partial melting. The relative importance of these two factors can be explored by means of a simple numerical model for partial melting.

Batch Partial Melting Model

The batch partial melting model assumes that the liquid is in chemical equilibrium with the melting solid and remains at the site of melting until it escapes or is removed as a "batch" of magma. The behavior of a trace element is idealized as

$$c_1(f) = c_s \frac{1}{D + f(1-P)},$$

where c_S and c_1 are the concentrations of a trace element in the source and derivative liquid, respectively; f, the mass fraction of melt (degree of partial melting); and D and P, the bulk distribution coefficients in the whole rock and the melting assemblage, respectively (Arth, 1976; Wilson, 1989, chap. 3). For each trace element,

$$D = \sum_i x_i^s k_i \text{ and } P = \sum_i x_i^m k_i,$$

where k_i is the solid-liquid partition coefficient for the ith mineral; x_i^s, the mass fraction of the ith mineral in the source rock; and x_i^m, its fraction in the melting assemblage.

I have implemented this model as an interactive, graphic spreadsheet in Microsoft Excel®. Input parameters are the mineral-melt partition coefficients and the composition of the mantle source. The input variables, which can be adjusted to optimize the model, are (1) the mass fractions of the source minerals and the melting minerals and (2) the degree of melting. The model (see fig. 21; table 3) is evaluated by comparison with the best characterized sample of the shonkinite at Mountain Pass (sample EM–1, table 1).

Mineralogy and Composition of the Mantle Source

I have assumed, following the evidence and arguments summarized above, that the shonkinites at Mountain Pass were indeed produced by small degrees of partial melting of highly metasomatized and enriched harzburgite. The metasomatic phases considered are those most commonly found as reservoirs of incompatible elements in xenolithic or xenocrystic samples of enriched mantle peridotite: phlogopite, amphiboles (such as potassian richterite, kaersutite, and pargasite), clinopyroxene, rutile, ilmenite, apatite, and garnet (Menzies and Hawkesworth, 1987). Similar but less familiar minerals, such as potassium-barium titanites, also could be involved (Mitchell and others, 1987; Guo and Green, 1990).

Most analyses of mantle xenoliths, including those from the Southwest, lack data for one or more of the elements, notably Th, that are important in the shonkinites. Therefore, I have used as the model source

composition the geometric mean of analyses of eight highly enriched xenolithic peridotites and pyroxenites from South Africa, Yemen, and Germany (table 3; data from Menzies and others, 1987).

Partition Coefficients

Although most published partition coefficients for Ba in biotite or phlogopite are between 1 and 7, Guo and Green (1990) obtained $k_{\text{phlog}}^{\text{Ba}}$ of about 0.2 to 0.8 for a lamproite composition at upper mantle temperature and pressures; I have used a value of 0.29 (Guo and Green, 1990, p. 91). In turn, the value I selected for $k_{\text{phlog}}^{\text{Rb}}$ is based on the expectation that the smaller and more highly charged Ba^{2+} ion is favored over Rb^{1+} for incorporation into K sites (Henderson, 1982, p. 125).

The pronounced depletion of Nb, Ta, and Ti relative to adjacent elements in the incompatible-element spectrum of the shonkinite (fig. 15*A*) can be generated from a source lacking these depletions only in the presence of a titanium-bearing phase, probably ilmenite or rutile (Foley and Wheller, 1990). Partition coefficients for Ta in ilmenite, approximately 0.3 to 2, are too low to allow successful modeling of Ta in the shonkinite. I have therefore assumed that the titanium-bearing phase is rutile and so have used $k_{\text{rutile}}^{\text{Ta}}$ and $k_{\text{rutile}}^{\text{Hf}}$ values from Jenner and others (1994). For other elements, few partition coefficients for rutile are available in the literature, so I have used averages (geometric means) of published values for ilmenite, magnetite-ilmenite, iron-titanium oxide, and titanium-magnetite. In reality, the source could contain both rutile and ilmenite.

Other partition coefficients were taken from numerous published sources (see table 3 footnotes). Several poorly known but probably small partition coefficients were set to zero. Partition coefficients for olivine and orthopyroxene were assumed to be zero for all the incompatible elements modeled.

Results: Model Magma

For small degrees of melting (f <1 percent), the composition of the model magma is much more sensitive to the fractions of minerals in the source rock (x_i^{s}) than to the degree of melting (f) or to the mineral fractions in the melting assemblage (x_i^{m}). Variations in the mineral fractions in the melting assemblage proved to be quantitatively insignificant, so I have simply assumed that the melting assemblage is entirely phlogopite. Abundances of most elements in the model magma are controlled largely by the mass fractions of phlogopite and amphibole in the source. These two variables are not independent, as the phlogopite and amphibole together must account for the K content of the source rock: $\left[K_2O\right]_{\text{source}} = x_{\text{phlog}}^{\text{s}}\left[K_2O\right]_{\text{phlog}} + x_{\text{amph}}^{\text{s}}\left[K_2O\right]_{\text{amph}}$ (see table 3 footnotes).

The model magma that best matches the shonkinites at Mountain Pass (fig. 21) is generated by approximately 0.01 percent melting of enriched harzburgite that contains 4.9 percent amphibole, 3.4 percent phlogopite, approximately 5 (±5) percent clinopyroxene, and traces of rutile and apatite (table 3). Clinopyroxene slightly improves the fit for Yb and Sr but is not required. For this optimum source mineralogy, model magmas are quantitatively similar for f values ranging from nearly zero to approximately 0.2 percent; for f values greater than or equal to 0.20 percent, the required high abundances of Th can not be generated from the assumed mantle source material. As the observed and modeled chondrite-normalized abundances in figure 21 vary over nearly four orders of magnitude, agreement between the model magma and shonkinite within a factor of two is satisfactory. The optimum model produces satisfactory results for all elements except Sr and Sm (fig. 21).

The high abundances of Th, Rb, Ba, LREE, and Sm in the shonkinites at Mountain Pass can, as expected, readily be modeled as a consequence of combined source enrichment and very low degree of partial melting. The model further demonstrates that depletion of Ti, Ta, and Nb in the shonkinites could be a result of residual rutile. However, these depletions could equally well be an inherited characteristic of the lithospheric-mantle source without the need for a residual titanium phase.

Depletion of Sr relative to adjacent elements (figs. 15, 21) in the shonkinites cannot be modeled sucessfully. If the amount of amphibole or apatite in the source is increased sufficiently to match the Sr depletion in the shonkinites, abundances of LREE and Sm become much too low. Increasing the partition coefficient for Sr in individual minerals to the maximum reasonable value reduces but does not eliminate the problem. Thus, the melting model suggests that Sr depletion in the shonkinites is inherited from their source.

Moderate underabundance of Nd, Sm, and Tb in the model magma reflects retention of these elements, primarily, by amphibole and, secondarily, by apatite and clinopyroxene. Increasing the ratio of phlogopite to amphibole in the source improves the fit for the Nd, Sm, and Tb but ruins the fit for LILE, La, and Ce. The abundance of Tb and Yb (representing HREE) in the shonkinites at Mountain Pass can be satisfactorily modeled with amphibole and clinopyroxene in the source without need for garnet. If garnet rather than amphibole plus clinopyroxene controls Yb and Tb, then no reasonable fit can be achieved for LILE.

Conclusions

The simple batch partial melting model can explain most of the important incompatible-element characteristics of the shonkinites at Mountain Pass but only for a tightly restricted set of input parameters and variables. Thus, the model makes three specific predictions concerning the origin of the shonkinites; (1) the mantle-peridotite source was strongly enriched in highly incompatible elements, having abundances approximately 10 to 40 times greater than chondritic or primitive mantle values (fig. 21; fig. 15 caption); (2) the source peridotite contained residual phlogopite, amphibole, clinopyroxene, rutile, and apatite (or, possibly, similar but less familiar minerals) but not garnet; and (3) the degree of partial melting was low, less than 0.2 percent.

Mantle xenoliths from the Southwest (Wilshire and others, 1988) generally are insufficiently enriched to generate the shonkinites at Mountain Pass even at very low degrees of partial melting. However, the probability that the mantle source for the shonkinites is represented in xenolith collections is slight. The shonkinites at Mountain Pass are regionally unique rocks, very small in volume, that must have originated from rare, anomalously enriched mantle. Such material probably constitutes only a tiny fraction of the lithospheric mantle and, therefore, is unlikely to be sampled by xenolith entrainment. The source enrichment in LILE and LREE inferred from the melting model is consistent with regional geochemical evidence (described in the following section), suggesting that the Mojave lithosphere as a whole is anomalously enriched in Th and LREE.

The preferred melting model, having more amphibole than phlogopite (table 3) and no garnet in the source, also rationalizes some of the differences between the shonkinites at Mountain Pass and the lamproite suite (fig. 20*A*). Phlogopite is probably more important than amphibole in lamproite genesis (Guo and Green, 1990; Mitchell and Bergman, 1991, chap. 10). Mantle phlogopites apparently have somewhat higher Ba/K ratios than mantle amphiboles (Irving and Frey, 1984). This may partially explain the differing LILE systematics of the shonkinites and lamproites. The optimum melting model for the shonkinites does not require garnet in the source, whereas several comparable melting models for lamproites or similar rocks (for example, Cullers and others, 1985) do invoke garnet. This difference is consistent with the markedly higher Yb content and lower La/Yb ratios (figs. 19*E*, 20*A*) of the shonkinites.

As expected, the degree of melting required to generate the shonkinites at Mountain Pass is quite small. The optimum value, f equal to 0.01 percent, is not particularly significant as all values of f less than 0.2 percent yield similar model melts. These results are consistent with the hypothesis that low-viscosity, K-rich melt fractions as small as approximately 0.001 percent will separate from their mantle source (McKenzie, 1985). Such magmas will seldom become voluminous enough to rise to upper-crustal or surface levels, which partially explains the scarcity of ultrapotassic and related rocks.

Thus, the shonkinites at Mountain Pass are rare rocks because their genesis (and perhaps that of the associated carbonatite?) requires the conjunction of two unlikely events: melting of unusually highly enriched lithospheric mantle and ascent of the magma into the upper crust.

Regional Setting and Related Ultrapotassic Rocks Elsewhere in the Mojave Desert

Ultrapotassic to potassic intrusive rocks that are known or presumed to be approximately 1.4 Ga in age are present at six localities in a discontinuous chain about 130 km long in southeastern California (Castor and Gleason, 1989; Castor, 1991). Mountain Pass lies near the north end of this discontinuous chain. The only locality other than Mountain Pass that has been described in any detail lies near the south end of this chain: the Barrel Spring pluton, located in the southwestern Piute Mountains 10 to 15 km south of the EMNSA and about

90 km south-southeast of Mountain Pass. This small pluton, about 5 km in largest map dimension, consists of shonkinite, syenite, and alkali granite (Gleason, 1988; Gleason and others, 1988). These rocks are potassic to ultrapotassic and generally have high abundances of LILE and, to a lesser extent, HFSE.

Compared with the ultrapotassic suite at Mountain Pass, the Barrel Spring pluton contains a lesser proportion of shonkinitic or melanocratic rocks and a greater proportion of silicic rocks, namely, quartz syenite and K-feldspar porphyry. The Barrel Spring rocks are less strongly potassic: more than 90 percent of the Mountain Pass samples, but only about 40 percent of the Barrel Spring samples, have weight percent K_2O/Na_2O ratios greater than or equal to 2.5 (fig. 22).

Several authors (DeWitt and others, 1987; Gleason, 1988; Castor and Gleason, 1989; Castor, 1991) have pointed out that the Middle Proterozoic ultrapotassic to potassic rocks in southeastern California and the carbonatite at Mountain Pass are coeval with and lie within a 1.4- to 1.5-Ga granitic terrane that encompasses much of the Southwest (Anderson and Bender, 1989). These granitic rocks are characterized by moderate enrichment in a number of lithophile elements, but they generally lack the strong to extreme enrichment in LREE, Ba, Sr, and Th found in the Mountain Pass and Barrel Spring suites. The ultrapotassic rocks in southeastern California and the carbonatite at Mountain Pass presumably are genetically related to the larger 1.4-Ga granitic terrane, but the nature of this relation has not been elucidated.

The Th- and LREE-rich character of the ultrapotassic suite and carbonatite at Mountain Pass and similar or related igneous rocks elsewhere in southeastern California apparently reflects the nature of the Mojave crustal province and its underlying lithospheric mantle. Lead-isotopic data show that the Mojave province has anomalously high time-integrated Th/U ratios, averaging about 7 and ranging as high as 15 for many samples, as opposed to the normal or average crustal value of approximately 4 (Wooden and others, 1988; Wooden and DeWitt, 1991). This elevated Th/U ratio evidently was inherited by the shonkinites and syenites at Mountain Pass, for which Th/U ratio is about 11 (table 1). A further tendency toward enrichment in LREE is suggested by an unusual frequency of occurrences of LREE minerals in the Mojave Desert region of southeastern California, southern Nevada, and northwestern Arizona (Jahns, 1952; Heinrich, 1960; Volborth, 1962; Evans, 1964; Otton and others, 1980; DeWitt and others, 1987; Castor, 1991). The most common of these LREE occurrences is allanite in Early or Early(?) Proterozic pegmatites.

Among the occurrences of 1.4-Ga ultrapotassic to potassic rocks in southeastern California, associated carbonatite is known only at Mountain Pass. Furthermore, the carbonatite body at Mountain Pass is the only one known in California, and none are known in Nevada or Arizona (Woolley, 1987). The only carbonatites known in Utah are a few small dikes associated with a minette-breccia diatreme in the southeast corner of the state (McGetchin and Nikhanj, 1973). Except for these minor dikes, the known carbonatites nearest to Mountain Pass are several in Colorado and New Mexico. Isotopic dates of these carbonatites are less than 800 Ma, suggesting that they are unrelated to the Middle Proterozoic carbonatite at Mountain Pass.

Carbonatite

Composition

Both its field relations and its extraordinary composition leave no doubt as to the igneous nature of the carbonatite at Mountain Pass. This is corroborated by experiments conducted by Jones and Wyllie (1983, p. 1,723): "The results from our synthetic rare earth carbonate mixture indicate that the addition of H_2O is all that is required to permit the analogous carbonatite at Mountain Pass, California to exist as a liquid magma at a low pressure and at a temperature near 650° C." Additional experiments support a magmatic origin for the bastnaesite in the carbonatite at Mountain Pass (Wyllie, 1989).

The only published analysis of the carbonatite at Mountain Pass was determined for use as an international geochemical reference (table 1). The material analyzed was mill-feed ore (crushed carbonatite) comprising bastnaesite with "… considerable baryte-celestine, quartz and/or silicates, iron minerals and various carbonates." (Lister and Cogger, 1986). The carbonatite at Mountain Pass shares several key compositional characteristics of the associated shonkinites and minettes: high *mg* (0.75), K_2O/Na_2O ratio (10.7), K_2O/Al_2O_3 ratio (0.61), and Th content (200 ppm). Abundances of Ba, Sr, and LREE are one to two orders of magnitude

greater in the carbonatite than in the shonkinites and minettes. Other differences include much lower Rb contents and Th/U ratios in the carbonatite. Despite its high K_2O/Na_2O ratio, the carbonatite is not strictly an ultrapotassic rock as it contains only 1.3 weight percent K_2O.

The REE spectrum of the carbonatite shows extraordinary LREE enrichment and LREE-HREE fractionation, having La_{cn} content of about 60,000 and $(La/Yb)_{cn}$ ratio of about 3,000 (fig. 11*D*). The irregularities in the pattern for REE that have a higher atomic number than Gd probably represent analytical errors (Lister and Cogger, 1986); some other published carbonatite REE spectra show similar, though less pronounced, irregularities.

Comparison With Other Carbonatites

The carbonatite at Mountain Pass is "one of the most unusual of all carbonatites…" (Heinrich, 1966). A number of characteristics distinguish it from most or all other carbonatites (Möller, 1989; Mariano, 1989a,b):

1. Association with potassic rather than sodic silicate igneous rocks.
2. Absence of feldspathoids in associated silicate rocks (most carbonatites are genetically associated with sodic, silica-undersaturated rocks such as nephelinite and ijolite).
3. Absence of volcanic or subvolcanic rocks.
4. Absence of concentric or ring structure.
5. Low abundance of apatite and magnetite.
6. Absence of Ca-silicate minerals (such as garnet or monticellite).
7. Absence of titanium-niobium minerals (such as pyrochlore or perovskite).
8. Extreme abundance of barite and bastnaesite.
9. Bastnaesite and parisite as primary igneous minerals that cocrystallized with calcite, barite, and dolomite (in other carbonatites, bastnaesite is hydrothermal).
10. Extremely high concentration of LREE (fig. 11*D*).
11. Lack of enrichment in Nb and Ta.

Several unique compositional characteristics of the carbonatite at Mountain Pass are illustrated by comparison with global averages for carbonatites (Woolley and Kempe, 1989) (fig. 20*B*). The carbonatite at Mountain Pass is relatively enriched in LREE, Ba, and U by factors of 10 to 30 and depleted in Nb by a factor of 5 to 10. This relative depletion in Nb is further emphasized by interelement ratios:

	Nb/Th	Nb/La	Nb/Ti
Carbonatite at Mountain Pass	0.50	0.0049	0.13
Average calcio-carbonatite	23.	2.0	1.8
Average magnesio-carbonatite	6.1	0.75	0.40

Among all terrestrial igneous rocks, carbonatites have the greatest abundances of LREE and the strongest LREE-HREE fractionation, typically having La_{cn} contents of about 1,000 to 10,000 and $(La/Yb)_{cn}$ ratios of about 100 to 1,000 (Cullers and Graf, 1984; Woolley and Kempe, 1989). Thus, even when compared with other carbonatites, the LREE enrichment and REE fractionation of the carbonatite at Mountain Pass are remarkable: La_{cn} content is about 60,000, and $(La/Yb)_{cn}$ ratio is about 3,000 (fig. 11*D*).

Constraints on the Origin of the Carbonatite at Mountain Pass

Although the geochemical, mineralogical, and physical uniqueness of the carbonatite at Mountain Pass is well established, the genetic significance of these unique characteristics has not been explored. The origin of the carbonatite at Mountain Pass cannot be determined until more petrologic data are available.

In general, the origin of carbonatites is controversial (Le Bas, 1987; Twyman and Gittins, 1987; Hall, 1987; Gittins, 1989; Kjarsgaard and Hamilton, 1989; Hamilton and others, 1989). Among the key facts to be explained are the frequent association of carbonatites with nephelinitic rocks and the very high concentrations of certain incompatible elements, notably LREE and Nb, in most carbonatites. Three possibilities are commonly entertained (Gittins, 1989): (1) fractionation of mantle-derived "carbonated nephelinite" to produce carbonatite; (2) immiscible

separation of a carbonatitic liquid and a nephelinitic or phonolitic silicate liquid from a mantle-derived parent; and (3) direct melting of carbonate-metasomatised mantle peridotite to produce separate carbonatitic and silicate magmas. The first possibility is implausible, as "carbonated nephelinite" magma apparently does not exist in nature, and it is unlikely that fractional crystallization could generate the high to extreme REE and Nb abundances that generally characterize carbonatites. Applicability of either of the remaining hypotheses to the carbonatite at Mountain Pass is problematic. A valid model for the origin of the carbonatite at Mountain Pass presumably will be exceptional, as the association of this carbonatite with potassic rather than sodic silicate rocks, extraordinarily high content of LREE, and pronounced paucity of Nb are exceptional.

The spatial association of the Sulfide Queen carbonatite intrusion with the largest of the shonkinite-syenite intrusions, as well as the spatial association of some smaller shonkinite and carbonatite intrusions, certainly suggests a genetic link. The association is temporal as well: shonkinite magma evidently was present both before and after carbonatite intrusion, and the two rock types yield similar U-Th-Pb ages (DeWitt and others, 1987). A close genetic link could be compatible with the separation of the carbonatite and shonkinite by liquid immiscibility or with separate but related genesis of the carbonatitic and shonkinitic magmas in the lithospheric mantle, followed by ascent of the two magmas through the same mantle and crustal passages.

The Mountain Pass Rare Earth Element Deposit

Mineralogy and Composition of Ore

Production of REE at the Mountain Pass deposit is from the Sulfide Queen carbonatite body. Textural relations indicate that REE mineralization is dominantly primary or magmatic; only a small portion is hydrothermal (Mariano, 1989a). Bastnaesite and parisite are the chief ore minerals. Subordinate to rare REE minerals (table 2) in the deposit include allanite, ancylite, cerite (Glass and others, 1958), florencite, hydroxl-bastnaesite, monazite, sahamalite (Jaffe and others, 1953), and synchisite (Castor, 1990).

The single published major-element analysis of bastnaesite from Mountain Pass (table 4) is of a mineral separate containing about 5 volume percent quartz and minor barite and carbonate minerals. These impurities presumably account for most or all of the reported Si, Ba, S, Ca, and Mg. The composition of the bastnaesite alone can be estimated by recalculating the analysis after allocating Si to quartz, Ca and Mg to their carbonates, and Ba to barite and carbonate. The resulting composition, $(Ce,La,Pr,Nd)_{1.09}(CO_3)_{1.00}F_{0.93}$, differs only slightly from the ideal formula of bastnaesite. This slight deviation could be real or it could, in part, reflect analytical error and (or) incorrect assumptions in the recalculation. Specifically, some Ca in the analysis could occupy Ce sites in bastnaesite, and several minor constituents that are probably present in significant amounts in the bastnaesite and (or) in the impurities, notably Sr and OH^{1-} or H_2O (compare with Evans, 1966, p. 31), were not reported in the analysis.

Bastnaesite from Mountain Pass has extraordinary LREE enrichment and LREE–HREE fractionation: La_{cn} content of about 7×10^5, Yb_{cn} content of about 20, and $(La/Yb)_{cn}$ ratio of about 35,000 (fig. 23). Thus, Yb is enriched over average upper continental crust by a factor of only about 2, whereas La is enriched by a factor of nearly 10^4. Chondrite normalization, commonly used to display REE data (see for example, figs. 11, 23*A*), deliberately obscures the even-odd alternation of REE abundances. The actual concentration of REE in bastnaesite from Mountain Pass (fig. 23*B*) reflects the superposition of two effects: the solar system and terrestrial abundances of REE that have even atomic numbers (such as Ce, Nd) that are higher than those that have odd atomic number (La, Pr) and the extreme LREE enrichment of the bastnaesite.

Typical REE ore from Mountain Pass contains approximately 40 volume percent calcite, 25 volume percent barite and (or) celestite, 10 volume percent strontianite, and 12 volume percent bastnaesite (Barnum, 1989). The proportions of individual REE in average ore is such that Ce alone makes up about one-half of the total REE content, and the four lightest REE elements together constitute about 99 percent (table 5).

Reserves, Grade, and Pricing

Estimates of proven and probable reserves and grade for ore from Mountain Pass are about 28 million tonnes and 8 to 9 weight percent REE oxides, respectively (table 6). Prices of REE produced from Mountain

Pass range from $16/kg for the abundant LREE oxides Ce_2O_3 and Nd_2O_3 at relatively low purity (96 percent) to more than $1,800/kg for highly purified Eu_2O_3 (table 7). Europium, which constitutes only about 0.1 percent of the ore, is much more costly than any of the other REE produced at Mountain Pass.

Processing

Processing of ore at the Mountain Pass Mine is described by Shaw (1959), Kruesi and Duker (1965), Evans (1966), Johnson (1966), Harrah (1967), Warhol (1980), and Neary and Highley (1984). The entire process emphasizes efficient recovery of Eu, the most valuable of the REE (Barnum, 1989). The carbonatite ore, mined by blasting in an open pit, is crushed to free the REE-bearing mineral grains. Following preflotation treatment by heating, agitation, and conditioning agents, the ore and gangue are separated by froth flotation. Initial flotation concentrates contain about 60 weight percent REE oxides. Additional flotation with an HCl leachant removes Ca and Sr carbonate gangue and liberates CO_2 from the bastnaesite and similar minerals, producing a mixture of REE oxides and fluorides that have grades of 70 to 90 weight percent REE oxide. Some of these intermediate or final REE concentrates produced by flotation are dried and packaged; others undergo further processing to partially or fully separate the individual REE.

The initial step in REE separation is leaching with HCl to convert the trivalent REE to soluble chlorides. The only tetravalent REE, Ce, precipitates as CeO_2. Separation of the remaining REE is accomplished by solvent extraction, an ion-exchange process involving partitioning of individual REE between two immiscible or only partially miscible liquid phases, the aqueous feed solution of trivalent REE chlorides and an organic solvent that preferentially extracts the heavier REE. The first stage of solvent extraction produces principally high purity La, precipitated and packaged as $La_2(CO_3)_3$, and La-rich LREE concentrate, precipitated and packaged as carbonate phases. A second stage of solvent extraction separates, purifies, and recovers oxides of Eu and others of the middle and heavy REE. Some products of solvent extraction at Mountain Pass are shipped to other plants for further purification.

Applications of the Rare Earth Elements: Summary

Designation of the lanthanides as "rare" earth elements relates more to unfamiliarity than to true scarcity (Muecke and Möller, 1988). Actually, REE are more abundant in the Earth's upper crust than many familiar elements. The two most abundant REE, La and Ce, are comparable in upper-crustal concentration to the common metals Ni, Cu, Zn, and Pb. Even the least common REE are about 10 to 100 times more abundant than Ag and Au.

Most applications of REE fall into two broad categories: high-volume industrial uses chiefly as catalysts, in metallurgy, and in the manufacture of glass and ceramics and low-volume "high technology" uses, such as in phosphors, magnets, and special glasses and ceramics (Neary and Highley, 1984; O'Driscoll, 1988; Preinfalk and Morteani, 1989; Vijayan and others, 1989). The first category uses principally LREE in the form of multielement concentrates and compounds; the second uses mostly HREE, and some LREE, as highly purified separate elements.

Most metallurgical applications of REE employ either mischmetal, a Ce-rich mixture of LREE, or LREE silicides (silicides are binary compounds, commonly nonstoichiometric, of metals and Si; for example, $CeSi_{\approx 0.5}$, Ce_3Si_2, CeSi, $CeSi_{\approx 1.3}$, $CeSi_{1.7-2.0}$ (Aronsson and others, 1965)). Mischmetal is used in several types of steel, in ductile cast iron, and in some nonferrous alloys, particularly those of Mg and Al. The other major application of mischmetal is in pyrophoric alloys, such as those used to make lighter flints. The two principal catalytic applications of REE are in LREE mixtures used in petroleum-cracking catalysts and as Ce used with Pt, Pd, and Rh in catalytic converters for vehicular-exhaust emission control.

Powders of Ce-rich LREE oxide are widely used for polishing glass. High-purity oxides of several REE have applications in glass manufacture, for decolorizing, as coloring agents, and as ingredients in optical glass to affect or control refractive index, dispersion, optical transmissivity, or ultraviolet absorption. Various REE are used to color ceramic dyes or glazes and to produce ceramics for specialized electronic and refractory applications. In addition, REE-bearing phosphors are used in cathode-ray tubes, X-ray screens, fluorescent lamps, and lasers. One of the most economically important high-technology applications of the REE is the use

of Eu and Y in the red phosphors for color televisions and computer monitors (McColl and Palilla, 1981). "The most important invention in the evolution of Mountain Pass was the commercialization of color television in the mid-1960s." (Barnum, 1989). Permanent magnets utilizing Sm-Co or Nd-Fe-B compounds or alloys have high field strength and resistance to demagnetization and are stronger and lighter than those made of other materials (Herbst, 1993). These REE-bearing permanent magnets are used chiefly in electrical and electronic assemblies and products, including powerful, light-weight electric motors.

Other, minor techological applications of REE are described by O'Driscoll (1988) and Preinfalk and Morteani (1989). Although technical and industrial innovation over the past three decades has generally increased demand for REE, the opposite can also occur. For example, increasing use of plastic and polycarbonate for eyeglass lenses has reduced the use of Ce as a polishing agent.

Possible future major applications of REE include high-temperature superconductivity and safe storage of hydrogen for use as an energy source (Greenwood and Earnshaw, 1984, p. 46). Hydrogen can be reversibly stored at ambient temperatures and modest pressure as lanthanum-nickel hydride. A potential advantage of REE is their relatively low toxicity (Brown and others, 1990) compared with some other industrial metals. In the future, rechargeable batteries using Ni and Cd, which are highly toxic, may be replaced or supplanted by lanthanum-nickel rechargeable batteries (O'Driscoll, 1990). The REE may also have certain agricultural applications (Brown and others, 1990).

In summary, for some applications a single or a few individual REE are the material of choice despite high cost. This situation is exemplified by Eu as a phosphor in cathode-ray tubes or by Sm and Nd as constituents of permanent magnets. In many other applications, the relatively costly REE compete with less desirable but less expensive alternatives or substitutes. For example, recent innovations have reduced the need for REE in some aspects of ferrous metallurgy (Neary and Highley, 1984).

Mineral Resource Significance of the Mountain Pass Deposit

Until recently, the Mountain Pass deposit was the world's principal source of LREE. Its reported reserves are approximately 28 million tonnes of REE oxide ore. However, the recently developed Bayan Obo, Mongolia Fe-Nb-REE deposit, which has estimated reserves of 48 million tonnes of ore at grades of 6 percent REE oxides, is now the largest known REE deposit (O'Driscoll, 1988; Mariano, 1989b; Drew and others, 1990). The Bayan Obo deposit is advantageous in its comparatively high contents of Eu and Sm, two of the less abundant but more valuable REE (compare with table 7). In 1986, production of REE from the United States, largely from Mountain Pass, and from China were approximately equal. In 1993, U.S. production was 18,000 tonnes of REE oxide derived from bastnaesite, presumably largely from Mountain Pass; total Chinese production was 22,000 tonnes (Hedrick, 1995). (For comparison, total world production of REE oxides in 1993 was 58,000 tonnes.) Thus, Mountain Pass will no longer solely dominate the world's LREE supply (unless supply from China were to be disrupted or restricted). Nonetheless, Mountain Pass will continue to be a major source of the light and middle REE for the foreseeable future. [The mineral resource significance of Mountain pass has changed significantly since this report was written, in the early 1990s; for current information see Haxel and others (2002)].

Status of the Mountain Pass Deposit in Mineral-Deposit Models

Numerous unusual geological and geochemical characteristics of the REE deposit at Mountain Pass, summarized above, indicate that it is unique among Earth's REE deposits. Mountain Pass is apparently the only ore deposit, and certainly the only large deposit, mined solely for its REE content (O'Driscoll, 1988; Castor, 1990). With respect to mineral resources, the most significant features of Mountain Pass are its combination of large reserves and high REE grade (fig. 24) and its absence of Nb enrichment or mineralization. Many or most carbonatite REE deposits contain either accessory Nb minerals, such as pyrochlore or columbite, or major Ti minerals, commonly perovskite or sphene, that bear substantial amounts of Nb (Mariano, 1989a). Except for minor sphene, none of these Nb-bearing minerals have been found in the carbonatite at Mountain Pass. The single analysis of carbonatite from Mountain Pass (Lister and Cogger, 1986) indicates only 100 ppm Nb, whereas typical carbonatite Nb deposits contain 1,400 to 21,000 ppm Nb (Cox and Singer, 1986; Mariano, 1989a). Nb has never been produced from the Mountain Pass deposit.

Until the genesis of the carbonatite at Mountain Pass and its extraordinary LREE mineralization have been elucidated, it cannot be assumed that they have the same origin as other carbonatites. Mountain Pass provisionally should be considered a member, presently the only known member, of a separate mineral-deposit model for LREE-rich, Nb-poor carbonatite having primary bastnaesite mineralization. Inclusion of the Mountain Pass REE deposit in the same model with other carbonatite REE deposits (Cox and Singer, 1986) may distort the mineral resource significance of both types of deposits.

In contrast to the Nb-poor carbonatite, the ultrapotassic rocks at Mountain Pass are moderately enriched in Nb and Ta. However, the limitations of the petrochemical data preclude a detailed assessment. Taking the data at face value, some of the ultrapotassic rocks have 100 to 250 ppm Nb, 4 to 10 times average upper crustal abundance. Niobium contents are greatest in the syenites and granites. Exploration for Nb and (or) Ta presumably would focus on pegmatites or greisen zones associated with granitic plutons (Pollard, 1989a) or on granites that are highly evolved, as indicated by strong depletion in the feldspar-compatible elements Ca, Sr, Ba, and Eu (Pollard, 1989b). All granite bodies of the ultrapotassic suite at Mountain Pass are smaller than about 0.5 km in largest map dimension. Though simple pegmatites are common in the Mountain Pass area, these are Early Proterozoic rocks more than 300 m.y. older than and, therefore, unrelated to the Middle Proterozoic ultrapotassic suite. Olson and others (1954) mention only patches or streaks, a few centimeters to a few meters in size, of Middle Proterozoic pegmatite at a single locality, and they describe no greisenlike alteration. None of the analyzed granites from Mountain Pass is highly evolved geochemically. Thus, none of the available data suggests that the Mountain Pass area is favorable for economically significant Nb and (or) Ta mineralization.

Acknowledgments

Thanks to Ted G. Theodore, David M. Miller, Jenny L. Bronk, Caron S. Jones, Chester T. Wrucke, Clay M. Conway, Paul J. Lamothe, James P. Calzia, James H. Wittke, Ardyth M. Simmons, and Donald A. Singer for assistance with various aspects of this report. Edmund Barnum and John Landreth of Molycorp provided grade and pricing infomation for the Mountain Pass rare earth deposit. The manuscript was improved by reviews and comments from David A. John, James E. Conrad, and Taryn A. Lindquist.

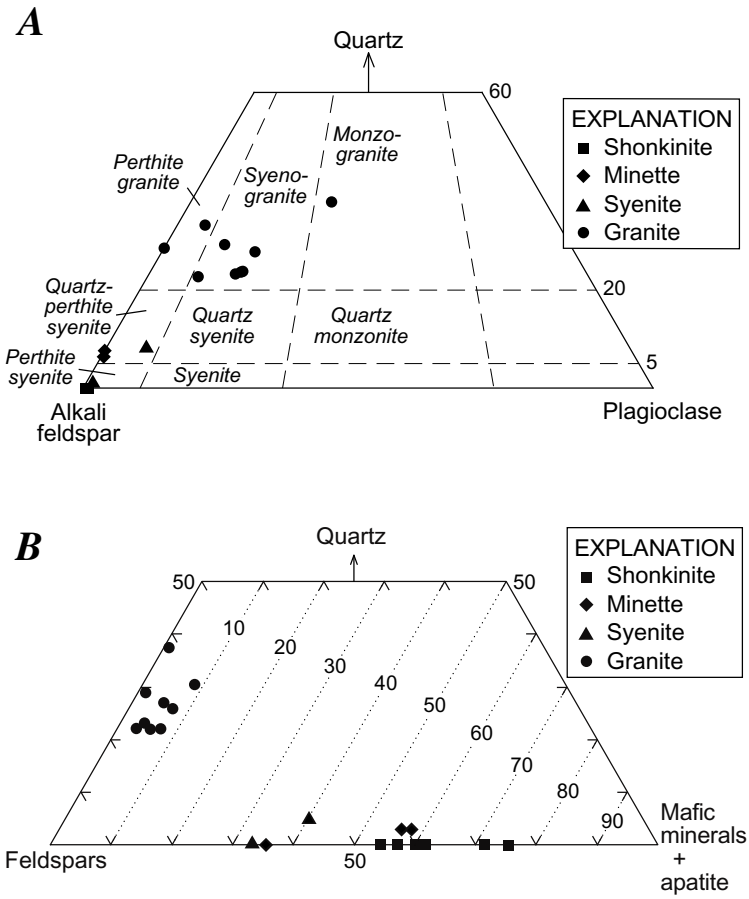

Figure 5. Ternary diagrams of modal composition of ultrapotassic and potassic silicate igneous rocks at Mountain Pass, California (fig. 2). *A*,quartz, alkali feldspar (including perthite), and plagioclase. Seven shonkinite samples and one minette sample plot at or very near the alkali-feldspar apex. Field names and boundaries from Streckeisen (1976). *B*, quartz, feldspars, and total mafic minerals plus apatite; mafic minerals include biotite, augite, amphibole, Fe-Ti oxides, and olivine. Dotted lines show approximate color-index values.

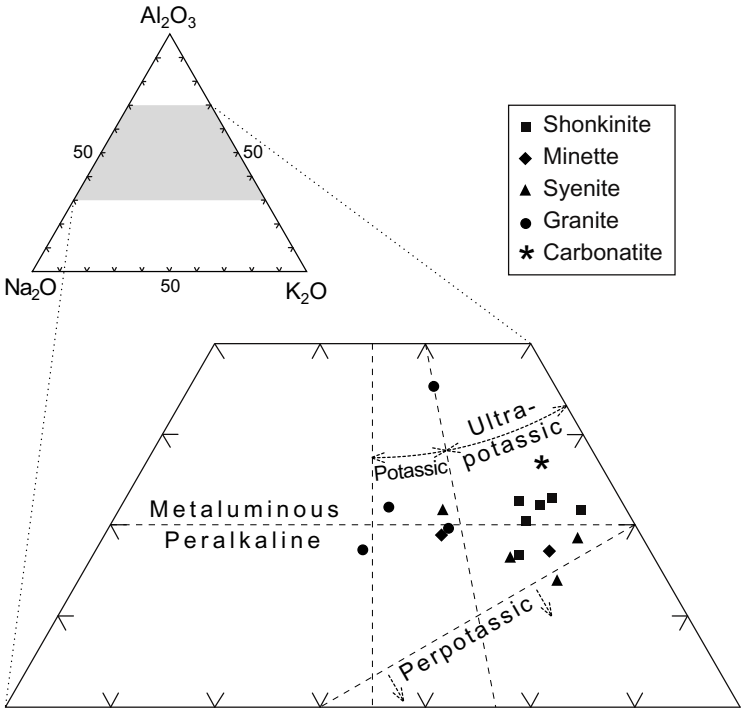

Figure 6. Ternary diagram of molar alumina and alkali content of ultrapotassic and potassic igneous rocks at Mountain Pass, California (fig. 2). Dashed lines distinguish overlapping compositional fields based on the following molar ratios: metaluminous, $(Na_2O+K_2O)/Al_2O_3 < 1$; peralkaline, $(Na_2O+K_2O)/Al_2O_3 > 1$; perpotassic, $K_2O/Al_2O_3 > 1$; potassic, $1 < K_2O/Na_2O < 2$; and ultrapotassic, $K_2O/Na_2O \geq 2$ (equivalent to weight percent $K_2O/Na_2O \geq 3$, the definition of ultrapotassic given by Bergman, 1987).

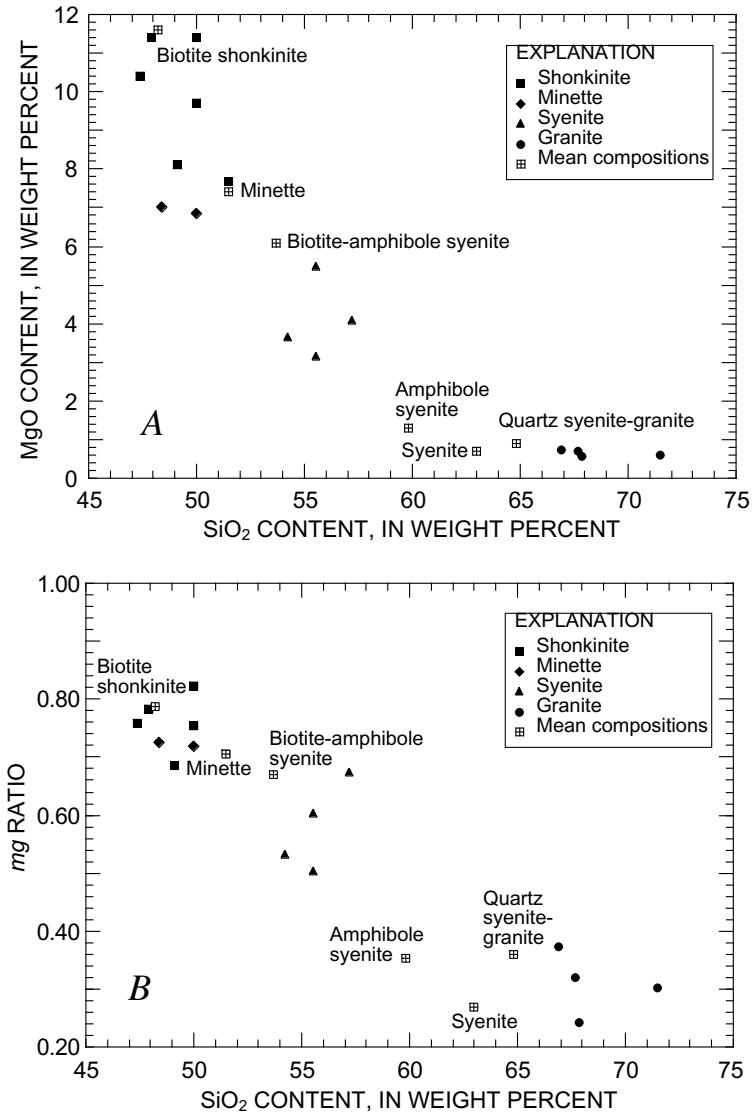

Figure 7. Chemical variation diagrams for ultrapotassic and potassic silicate igneous rocks at Mountain Pass, California (fig. 2). Data for individual samples from table 1, Olson and others (1954), and Crow (1984); mean compositions (labeled with rock type) from Watson and others (1974). *A*, MgO versus SiO_2. *B*, *mg* versus SiO_2; *mg* is molar MgO/(MgO+FeO), assuming weight percent $Fe_2O_3/(Fe_2O_3+FeO) = 0.2$ (Hughes and Hussey, 1976).

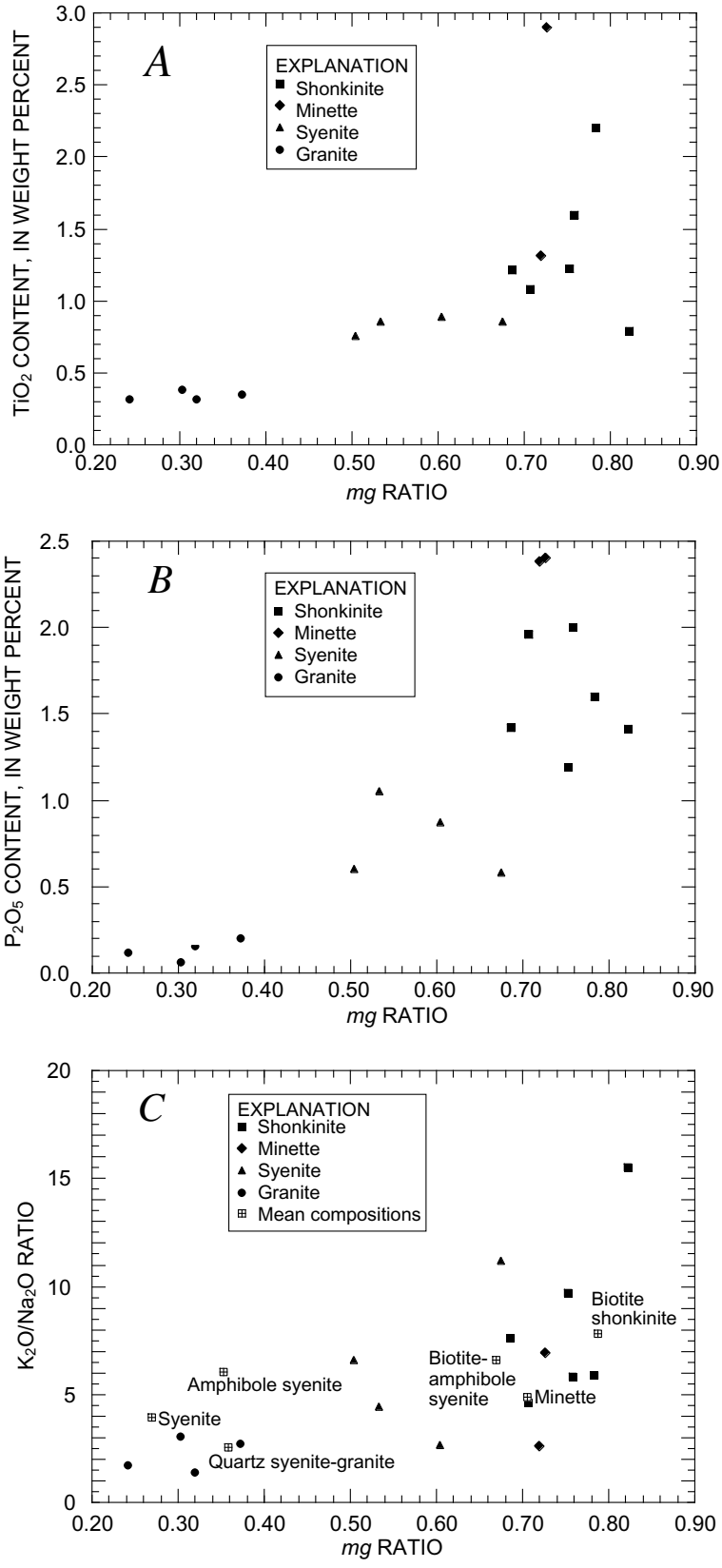

Figure 8. Chemical variation diagrams for ultrapotassic and potassic silicate igneous rocks at Mountain Pass, California (fig. 2), showing decline of TiO_2 and P_2O_5 and K_2O/Na_2O with decreasing *mg* (molar MgO/(MgO+FeO), assuming weight percent $Fe_2O_3/(Fe_2O_3+FeO) = 0.2$). Data for individual samples from table 1, Olson and others (1954), and Crow (1984). *A*, TiO_2 versus *mg*. *B*, P_2O_5 versus *mg*. *C*, K_2O/Na_2O versus *mg*; mean compositions (labeled with rock type) from Watson and others (1974).

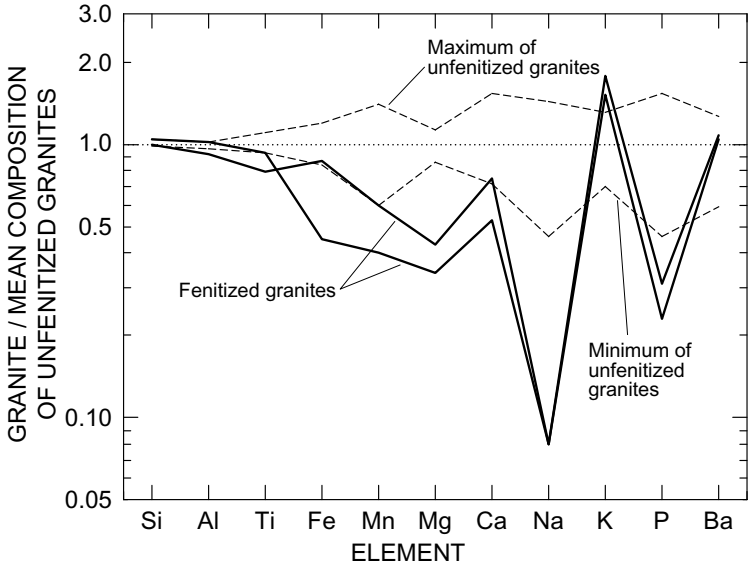

Figure 9. Plot showing major elements and Ba in two fenitized granites (heavy lines) compared with maximum and minimum in four unfenitized granites (dashed lines) from the Mountain Pass area, California (fig. 2). Plotted values are normalized to the mean composition (horizontal dotted line) of the four unfenitized granites.

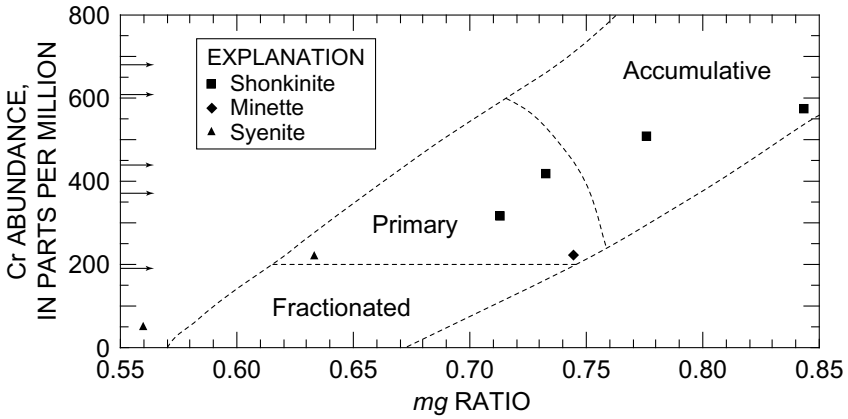

Figure 10. Plot showing Cr versus *mg* in shonkinites, minettes, and two syenites from Mountain Pass, California (fig. 2), compared with the fields of "approximately primary", accumulative, and fractionated calcalkaline lamprophyres from southern Scotland (diagram from Rock and others, 1986, based on 108 analyzed samples). The lower boundary of the primary field is placed at 200 ppm Cr (Rock, 1991). Arrows along the vertical axis represent Cr content of two shonkinite and three minette samples from Mountain Pass for which major element data are lacking. For this diagram only, *mg* (molar MgO/(MgO+FeO) is calculated with $Fe_2O_3/(Fe_2O_3+FeO) = 0.3$, for consistency with Rock and others (1986). All syenite samples except the two plotted on this diagram have $mg < 0.55$.

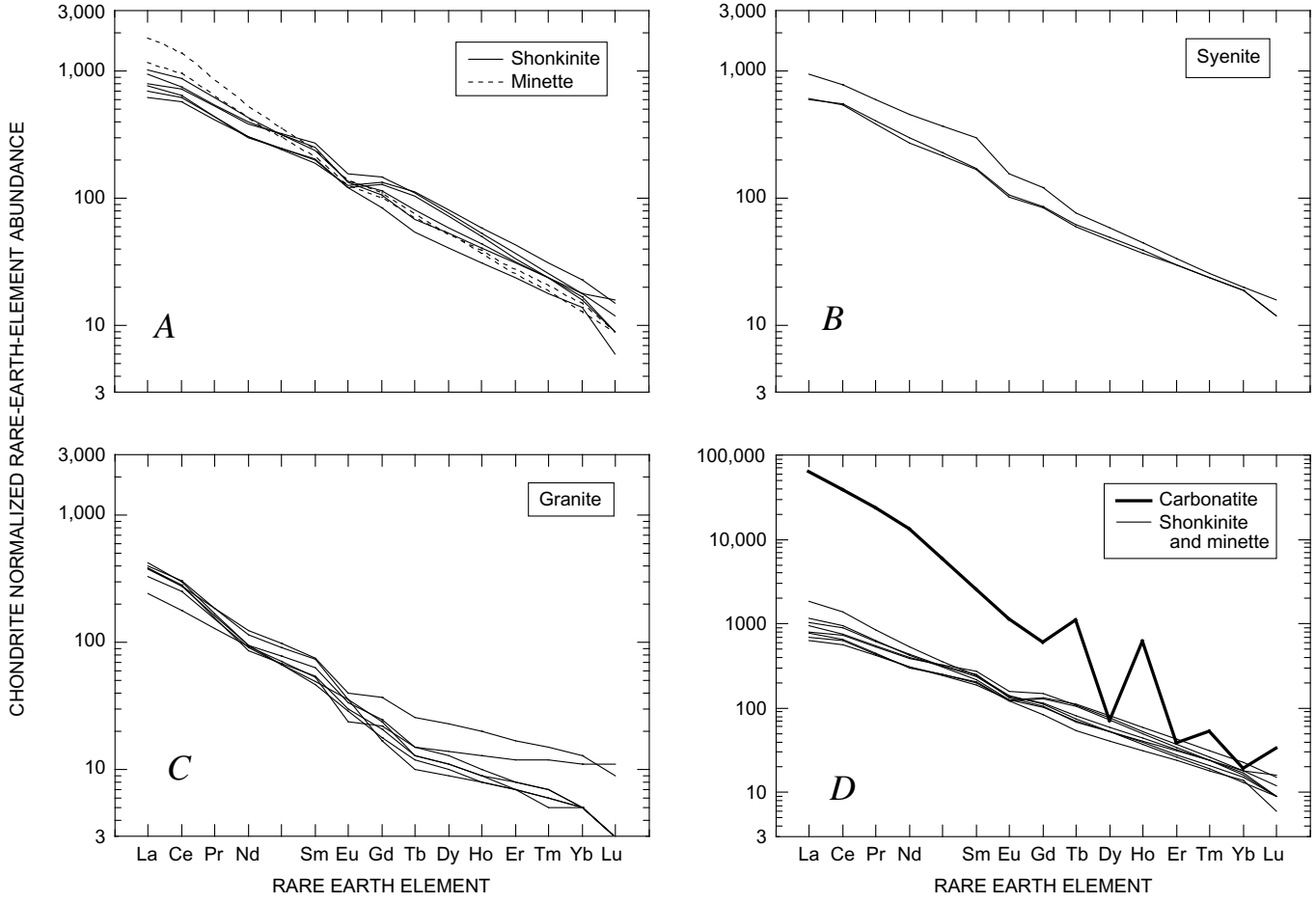

Figure 11. Plots showing chondrite-normalized rare-earth-element (REE) spectra for ultrapotassic and potassic igneous rocks at Mountain Pass, California (fig. 2). Data from table 1, Crow (1984), and Lister and Cogger (1986); normalizing abundances from Nakamura (1974). For 11*A*, 11*B*, and 11*C*, abundances were determined for La, Ce, Nd, Sm, Eu, Tb, Yb, and Lu only; other plotted REE values are interpolated. For 11*D*, all REE were determined, but values for REE with atomic number greater than Gd may be affected by large analytical errors (see text). *A*, Shonkinite and minette. *B*, Syenite. *C*, Granite. *D*, Carbonatite; REE spectra of shonkinite and minette (from 11*A*) are repeated for comparison.

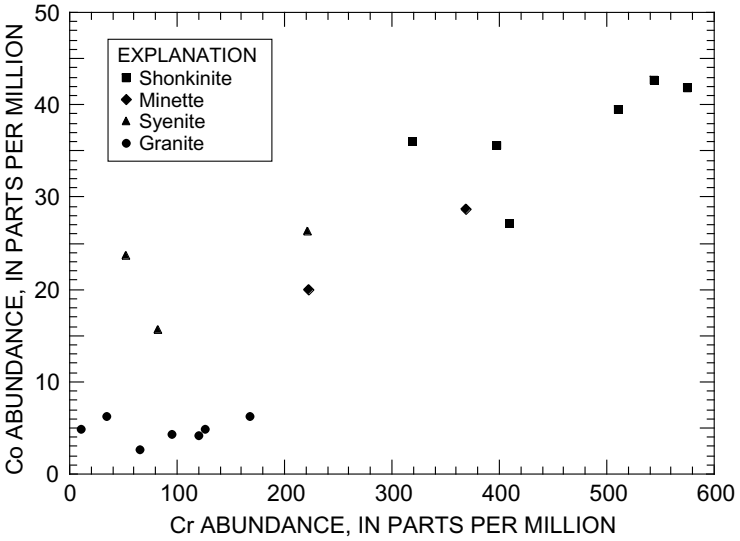

Figure 12. Plot showing covariation of Co and Cr abundances for ultrapotassic and potassic silicate igneous rocks at Mountain Pass, California (fig. 2).

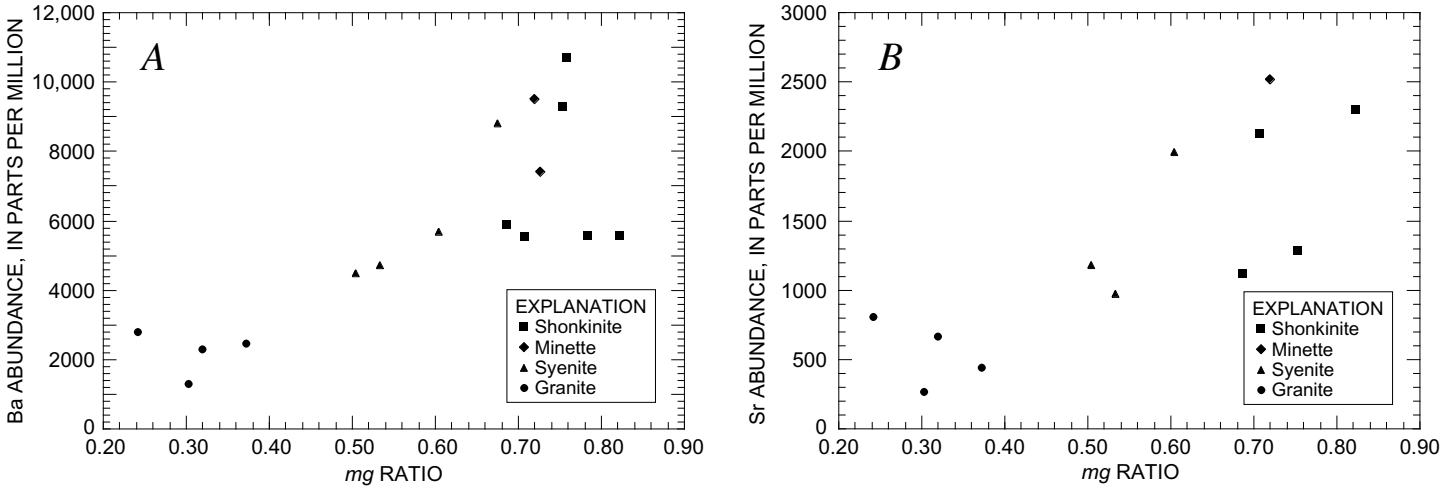

Figure 13. Chemical variation diagrams for ultrapotassic and potassic silicate igneous rocks at Mountain Pass, California (fig. 2), showing the behavior of Ba and Sr during progressive evolution as indexed by the decline of *mg* (molar MgO/(MgO+FeO), assuming weight percent $Fe_2O_3/(Fe_2O_3+FeO) = 0.2$). *A*, Ba versus *mg*. *B*, Sr versus *mg*.

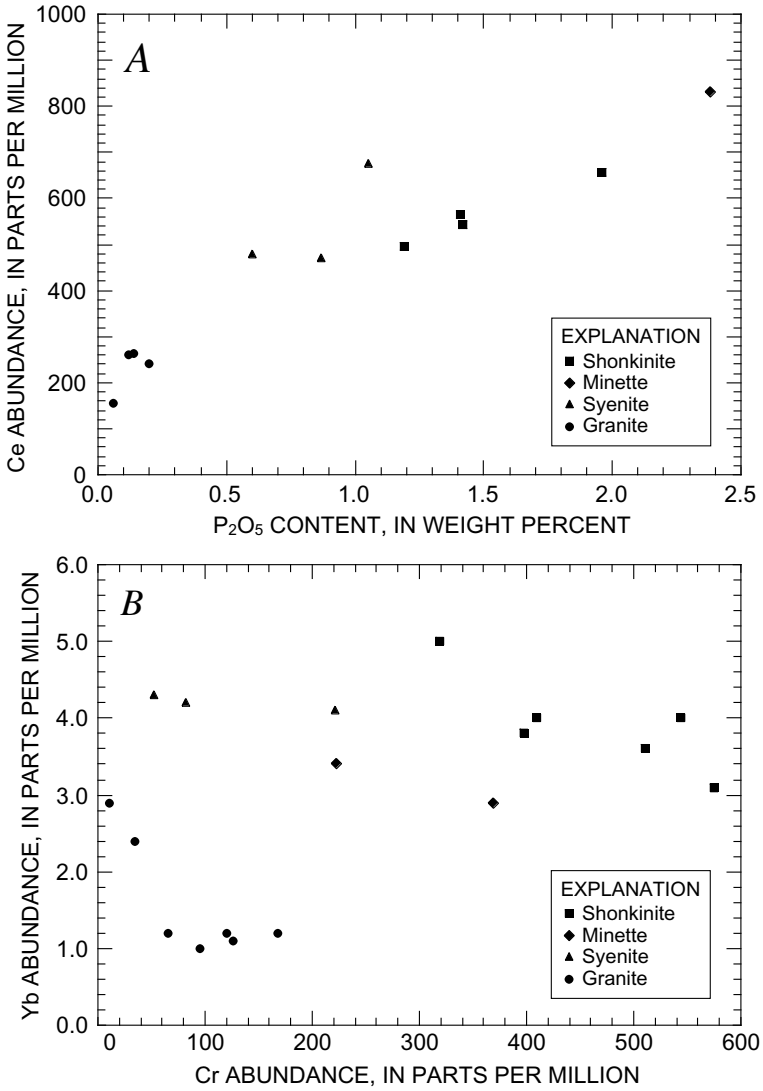

Figure 14. Chemical variation diagrams for ultrapotassic and potassic silicate igneous rocks at Mountain Pass, California (fig. 2). *A*, Ce versus P_2O_5. *B*, Yb versus Cr.

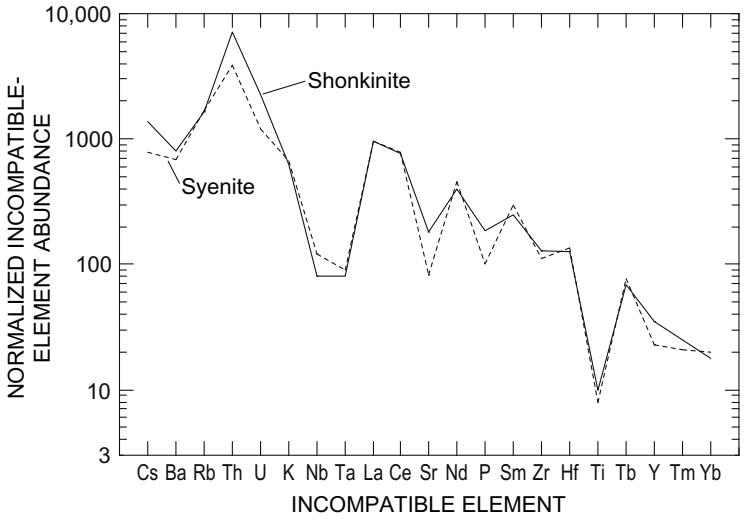

Figure 15. Normalized incompatible-element spectra of two respresentative ultrapotassic rocks from Mountain Pass, California (fig. 2). The shonkinite (EM–1, table 1) has *mg* = 0.71 and 410 ppm Cr; the syenite (EM–3, table 1) has *mg* = 0.53 and 52 ppm Cr. Normalizing values (R.N. Thompson, 1982a) are chondritic except that values for Cs, Rb, K, and P are estimates for primordial or undepleted terrestrial mantle (Sun, 1980). Normalizing value for U (0.012 ppm) is calculated from the chondritic abundance of Th used by R.N. Thompson (1982a) and the chondritic Th/U ratio of 3.6 (Sun and McDonough, 1989).

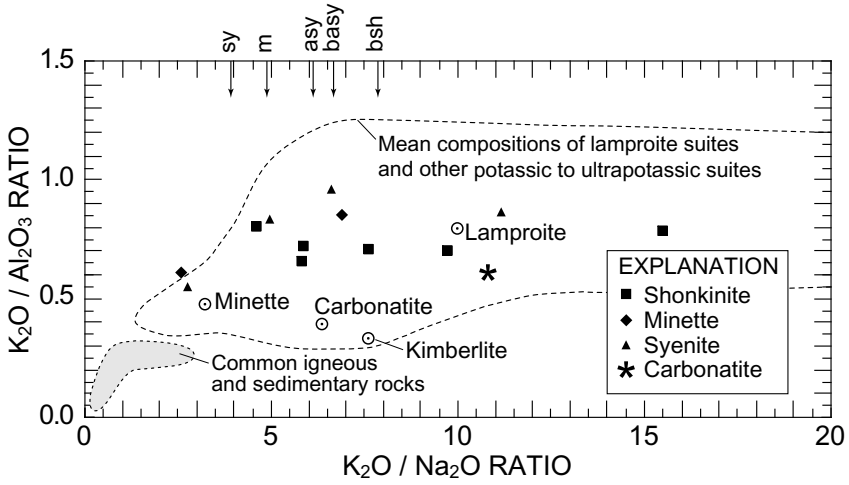

Figure 16. Plot showing weight percent K_2O/Na_2O and K_2O/Al_2O_3 ratios of shonkinite, minette, syenite, and carbonatite at Mountain Pass, California (fig. 2), compared with the field (dashed line) of worldwide mean compositions of lamproite suites and other potassic to ultrapotassic suites (Bergman, 1987). This field extends beyond the right side of the diagram to values of K_2O/Na_2O as large as 50. The global mean compositions of lamproite, minette, carbonatite, and kimberlite are marked by encircled dots. Most Earth materials plot within the small shaded field near the origin. Arrows at the top of the diagram show K_2O/Na_2O for mean compositions of rocks from Mountain Pass (Watson and others, 1974) for which Al_2O_3 content is not given (rock abbreviations: asy, amphibole syenite; basy, biotite-amphibole syenite; bsh, biotite shonkinite; m, minette; sy, syenite).

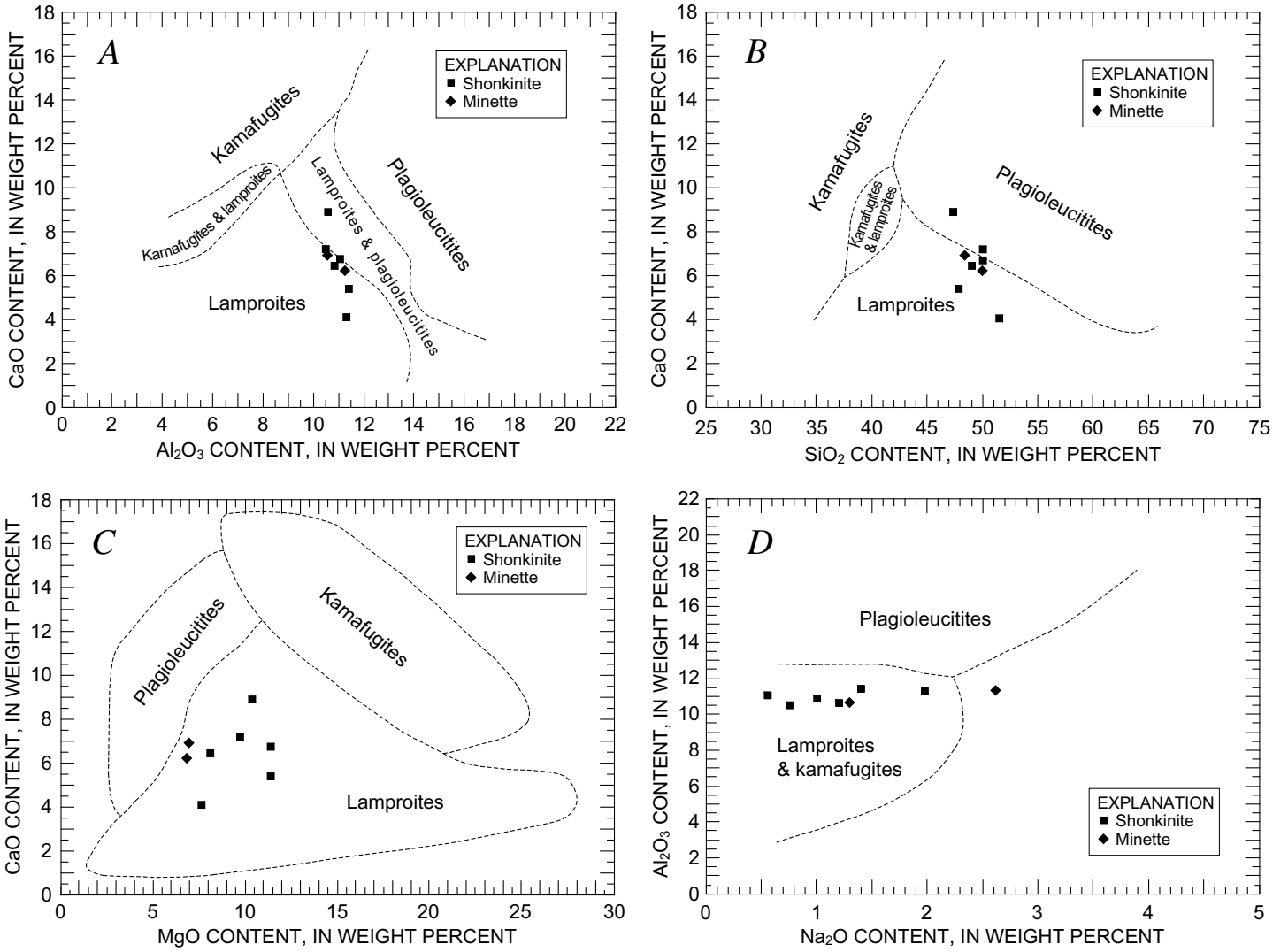

Figure 17. Plots showing abundances of five major oxides in shonkinites and minettes at Mountain Pass, California (fig. 2), compared with generalized compositional fields (dashed lines) of the three major groups of ultrapotassic rocks (after Foley and others, 1987). *A*, CaO versus Al_2O_3. *B*, CaO versus SiO_2. *C*, CaO versus MgO. *D*, Al_2O_3 versus Na_2O.

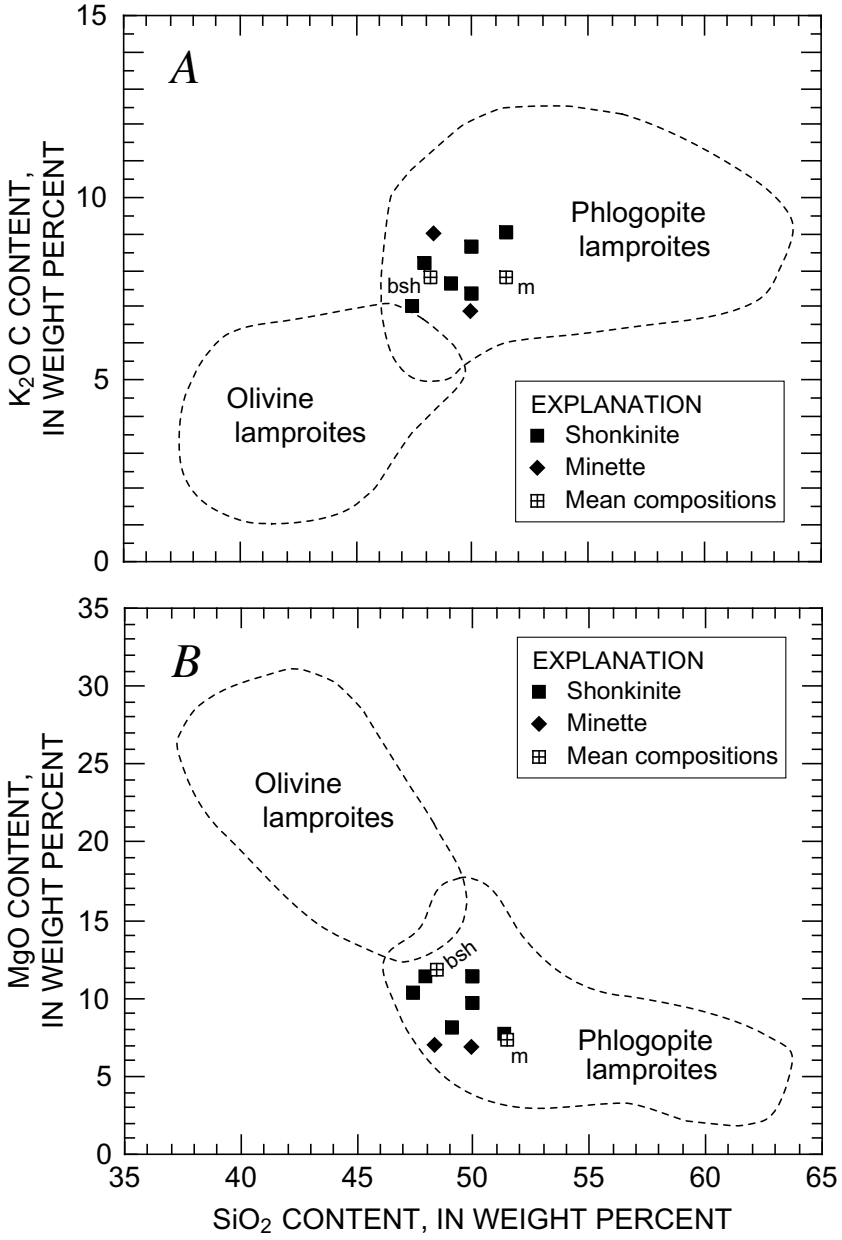

Figure 18. Plots showing SiO_2, MgO, and K_2O (weight percent) in shonkinites and minettes at Mountain Pass, California (fig. 2), compared with compositional fields (dashed lines) of olivine lamproites and phlogopite lamproites from West Kimberley, Australia (from Mitchell and Bergman, 1991, fig. 7.5). Mean compositions of biotite shonkinites (bsh) and minettes (m) at Mountain Pass from Watson and others (1974). *A*, K_2O versus SiO_2. *B*, MgO versus SiO_2.

bs

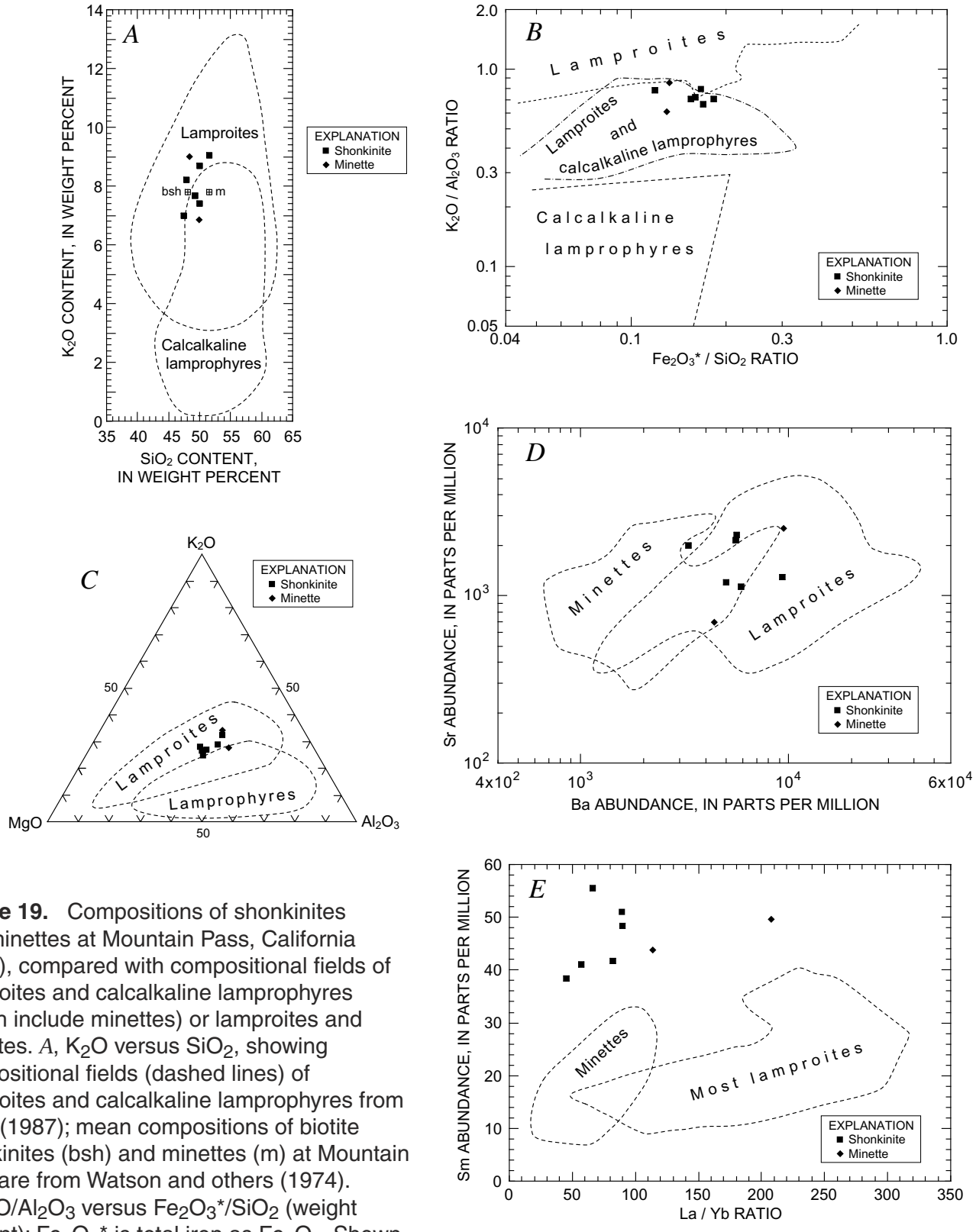

Figure 19. Compositions of shonkinites and minettes at Mountain Pass, California (fig. 2), compared with compositional fields of lamproites and calcalkaline lamprophyres (which include minettes) or lamproites and minettes. *A*, K_2O versus SiO_2, showing compositional fields (dashed lines) of lamproites and calcalkaline lamprophyres from Rock (1987); mean compositions of biotite shonkinites (bsh) and minettes (m) at Mountain Pass are from Watson and others (1974). *B*, K_2O/Al_2O_3 versus Fe_2O_3*/SiO_2 (weight percent); Fe_2O_3* is total iron as Fe_2O_3. Shown are compositional fields (dashed lines) that are diagnostic of lamproites and calcalkaline lamprophyres from Rock (1991, fig. 5.4). Also shown is the field of overlap of lamproite and calcalkaline lamprophyre (dash-dot lines); among hundreds of analyses plotted by Rock (1991), all calcalkaline lamprophyres plot below the upper dash-dot line, and all lamproites plot above the lower dash-dot line. *C*, Ternary diagram of K_2O, MgO, and Al_2O_3 (weight percent) compared with compositional fields (dashed lines) of lamproites and lamprophyres from Bergman (1987). *D*, Sr versus Ba, compared with compositional fields (dashed lines) of minettes and lamproites from Mitchell and Bergman (1991). *E*, Sm versus La/Yb, compared with compositional fields (dashed lines) of minettes and lamproites from Mitchell and Bergman (1991).

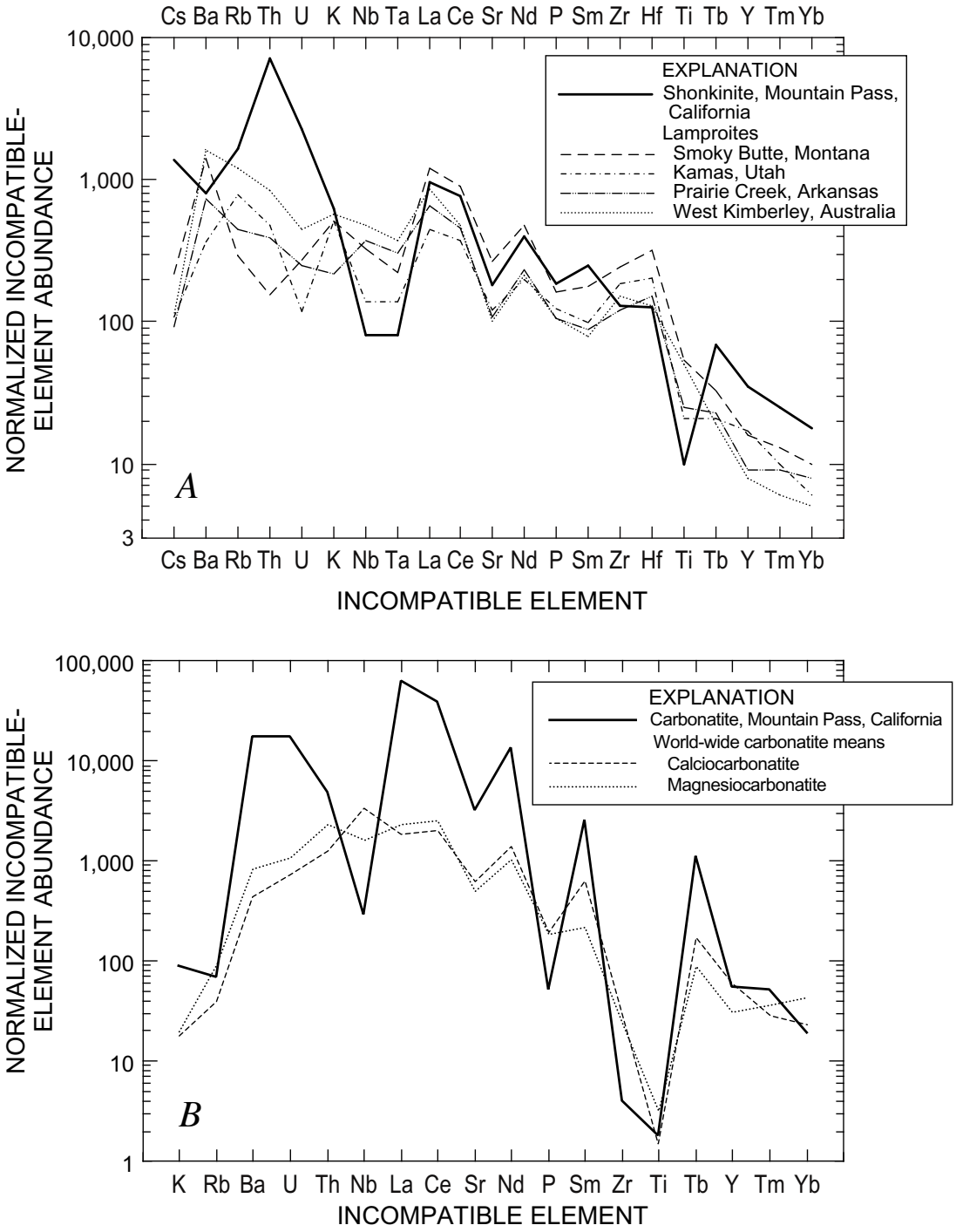

Figure 20. Normalized incompatible-element spectra of two representative alkaline rocks from Mountain Pass, California (fig. 2). Normalizing values (R.N. Thompson, 1982a) are chondritic except that values for Cs, Rb, K, and P are estimates for primordial or undepleted terrestrial mantle (Sun, 1980). Normalizing value for U (0.012 ppm) is calculated from the chondritic abundance of Th used by R.N. Thompson (1982a) and the chondritic Th/U ratio of 3.6 (Sun and McDonough, 1989). *A*, Spectrum of shonkinite (EM–1, table 1) compared with mean compositions of four lamproite suites (Bergman, 1987, table 6; Mitchell and Bergman, 1991, p. 340, 342). *B*, Spectrum of carbonatite (IGS–40, table 1; from Lister and Cogger, 1986), compared with average compositions of calciocarbonatites and magnesiocarbonatites (Woolley and Kempe, 1989, table 1.1). Abundance of Zr in the carbonatite sample, which was not reported by Lister and Cogger (1986), was estimated from Olson and others (1954, table 5).

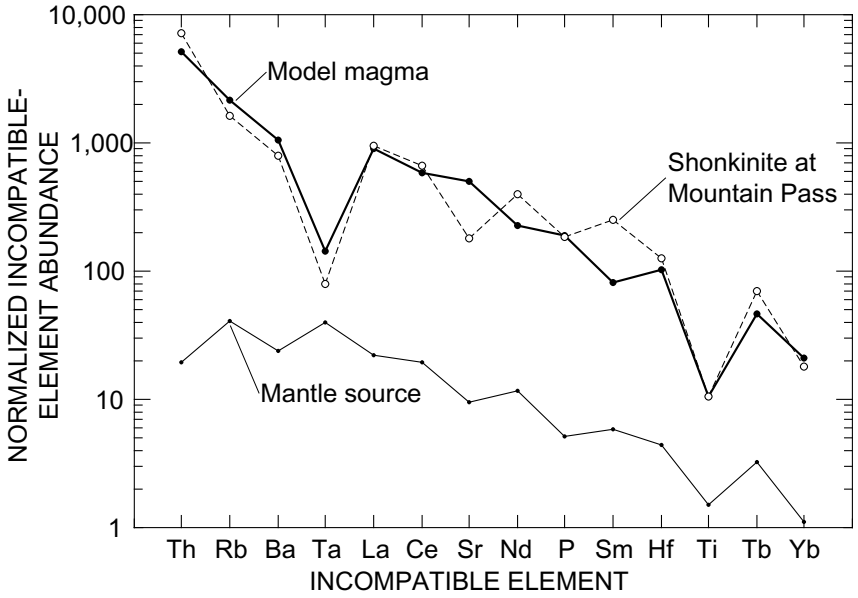

Figure 21. Normalized incompatible-element spectra of assumed mantle source and model magma for preferred batch partial melting model (table 3). Spectrum of shonkinite at Mountain Pass, California (fig. 2; EM–1, table 1), is shown for comparison with the model magma. Normalizing values (R.N. Thompson, 1982a) are chondritic except that values for Rb and P are estimates for primordial or undepleted terrestrial mantle.

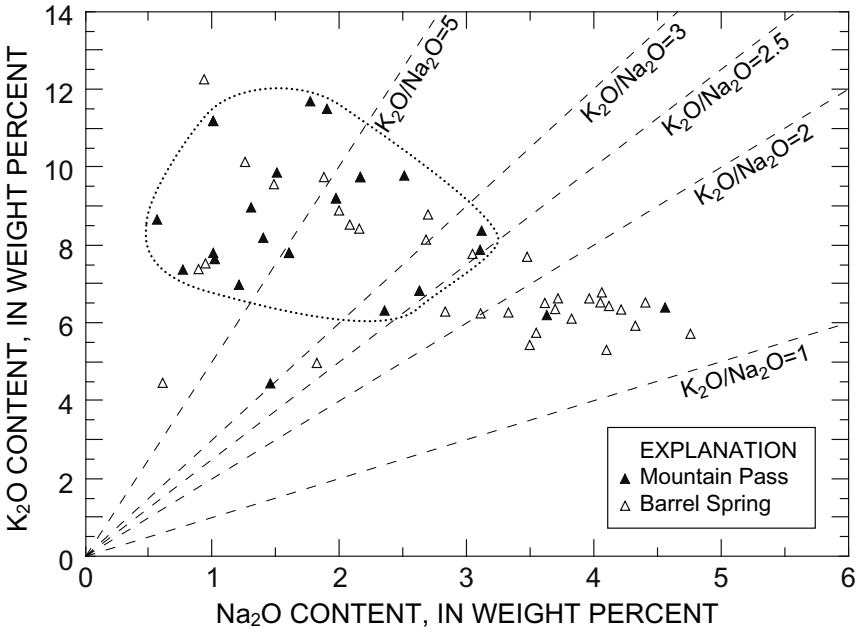

Figure 22. Plot comparing K_2O and Na_2O in ultrapotassic and potassic rocks at Mountain Pass, California, and from the Barrel Spring pluton, Piute Mountains, California, (fig. 2; Gleason, 1988). Data for Mountain Pass includes both individual samples (data from table 1; Olson and others, 1954; and Crow, 1984) and mean compositions reported by Watson and others (1974). Dotted line encloses compositional field for 86 percent of the Mountain Pass samples and means; three granite samples plot outside this field.

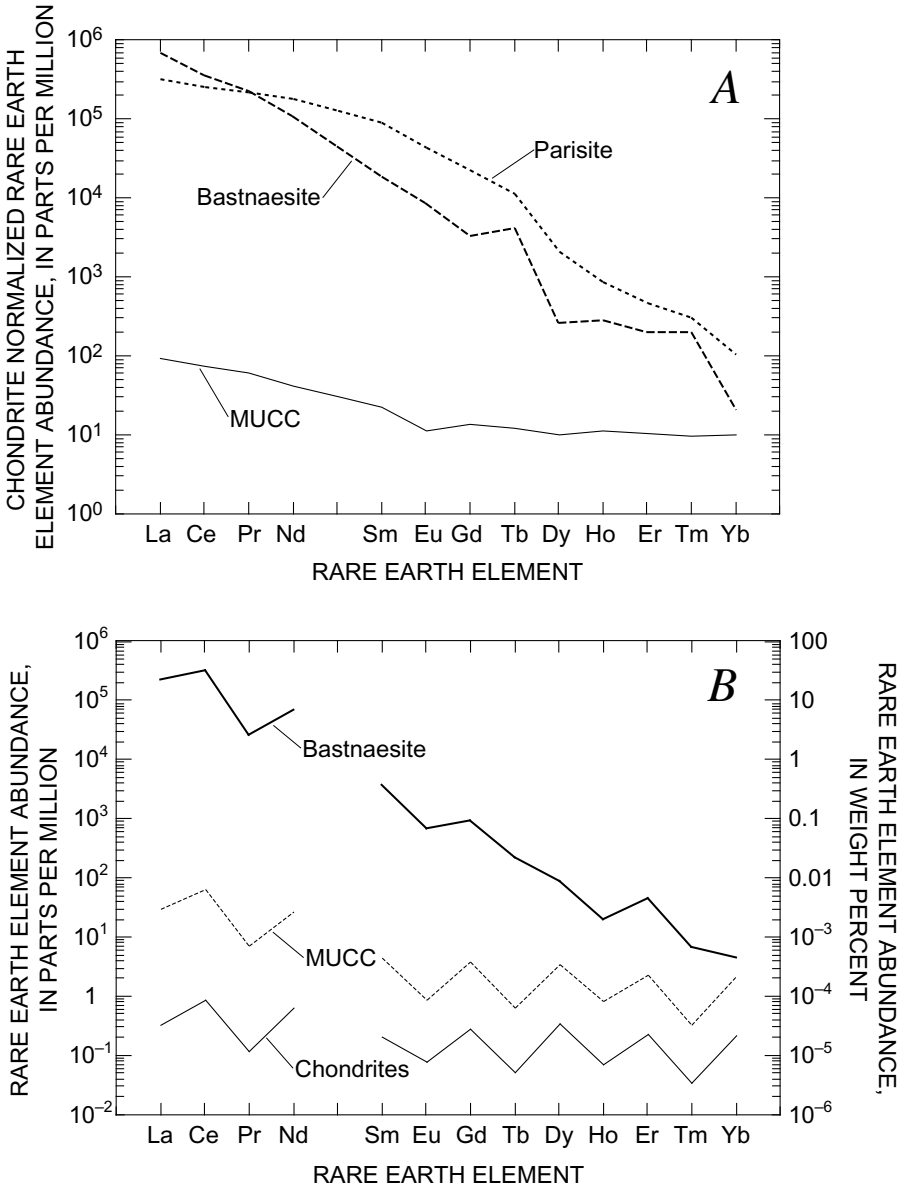

Figure 23. Rare-earth-element (REE) spectra for bastnaesite and parisite from carbonatite at Mountain Pass, California (fig. 2). *A*, Chondrite-normalized REE spectra of bastnaesite from the Mountain Pass REE deposit and parisite from a carbonatite dike south of the deposit (from Mariano, 1989b; source of chondritic normalizing abundances not specified) compared with Ree spectra of average upper continental crust (MUCC) (Taylor and McLennan, 1985). *B*, Plot showing REE content, in both parts per million and weight percent, of bastnaesite from the Mountain Pass REE deposit, compared with that of MUCC and CI chondrites (Nakamura, 1974).

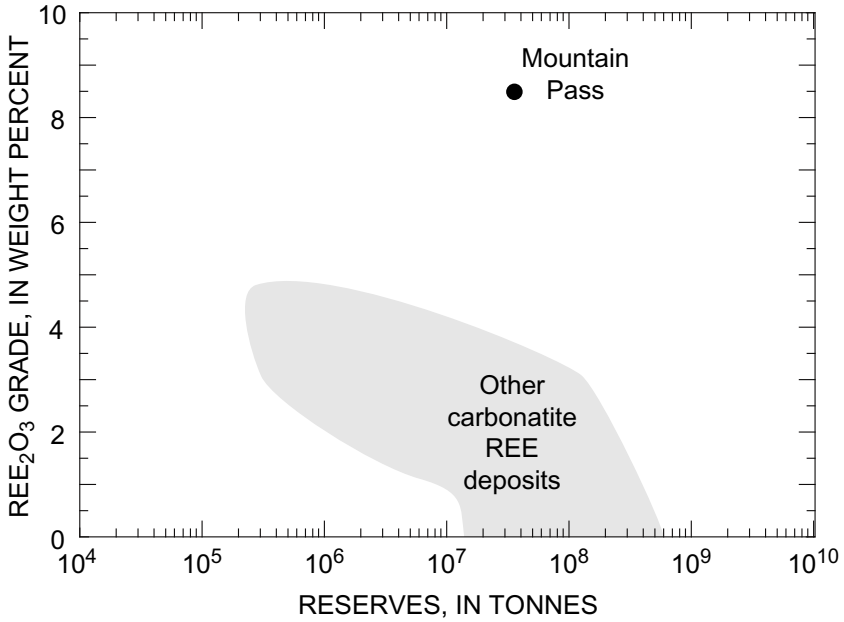

Figure 24. Rare-earth-element (REE) grade and tonnage of the REE deposit at Mountain Pass, California (fig. 2; table 6), compared with 11 other carbonatite REE deposits (D.A. Singer, written commun., 1992).

Table 1. Representative compositions of ultrapotassic rocks and carbonatite, Mountain Pass, California.

[LOI, loss on ignition; --, not reported or not determined]

Lithology	Shonkinite			Minette	Syenite	Granite		Carbonatite
Sample No.[1]	C–8	OSPS–A	EM–1	OSPS–C	EM–3	EM–2	EM–4	IGS–40
Major-element chemistry (weight percent)								
SiO_2	50.0	47.4	51.5	48.4	54.2	66.9	71.5	16.59
Al_2O_3	11.05	10.6	11.3	10.6	12.1	13.8	13.5	2.1
Fe_2O_3	[2]5.95	2.9	3.08	3.4	5.27	2.25	1.97	[2]3.28
FeO	--	4.6	4.19	2.7	2.27	.66	1.24	--
MgO	11.4	10.4	7.67	7.	3.67	.73	.6	4.02
CaO	6.72	8.9	4.07	6.9	3.71	1.16	1.30	16.99
Na_2O	.56	1.2	1.98	1.3	2.16	3.09	1.45	.12
K_2O	8.68	7.	9.06	9.	9.63	8.32	4.42	1.28
TiO_2	.79	1.6	1.08	2.9	.86	.35	.38	.185
P_2O_5	1.41	2.	1.96	2.4	1.05	.2	.06	.54
MnO	.09	.18	.14	.08	.11	.06	.07	.4
H_2O	--	--	.69	--	.45	.27	1.39	--
CO_2	--	--	.05	--	1.94	.62	.83	18.
F	--	--	1.36	--	.41	.11	.09	.61
LOI	.56	1.1	--	3.2	--	--	--	--
Total[3]	98.4	99.6	[4]99.3	99.	[4]99.	[4]99.1	[4]99.2	[5]99.5
mg[6]	.82	.76	.71	.73	.53	.37	.30	.75
K_2O/Na_2O	15.5	5.8	4.6	6.9	4.5	2.7	3.	10.7
Trace-element chemistry (parts per million)								
Cr	575	--	410	--	52.0	11	34.7	--
Ni	--	--	130	--	78	<27	<24	48
Co	--	--	27.2	--	23.7	4.8	6.2	--
Sc	--	--	22.8	--	18.7	5	10.6	--
Cs	--	--	16.7	--	9.33	4.91	4.94	--
Rb	722	--	572	--	592	439	152	24
Ba	5,600	10,700	5,540	7,400	4,730	2,450	1,300	121,000
Sr	2,300	--	2,130	--	971	440	270	37,200
Th	--	--	302	--	163	183	38.7	202
U	--	--	27	--	14.6	17.5	1.7	210
Zr	--	--	870	--	750	740	190	--
Hf	4.2	--	25.2	--	26.8	18.7	7.35	--
Nb	--	--	28	--	42	40	--	102
Ta	--	--	1.6	--	1.8	2.95	0.23	--
La	255	--	315	--	313	127	79.5	20,700
Ce	564	--	657	--	675	241	155	33,800
Nd	190	--	250	--	290	79	59	8,316
Sm	41.7	--	51	--	60.5	15.5	10.8	517
Eu	9.4	--	10.3	--	12.0	3.05	1.81	86
Tb	2.8	--	3.61	--	4.02	1.35	0.76	[7]57
Yb	3.1	--	4.0	--	4.3	2.9	2.4	[7]4.1
Lu	.2	--	.53	--	.53	.31	.37	[7,8]1.1
Y	--	--	70	--	45	44	26	110
Eu/Eu*[9]	.93	--	.82	--	.82	.74	.68	.91
Cl	--	--	120	--	120	240	70	4,000
S	--	--	100	--	1,900	200	<100	34,500

[1]Sources of analytical data: C, Crow (1984); IGS, Lister and Cogger (1986); OSPS, Olson and others (1954). All other samples (EM–1 through EM–4) are newly reported; analysts: P.A. Baedecker, D.L. Fey, J. Kent, J.S. Mee, M. Motooka, S.T. Pribble, and D.F. Siems.

[2]Total iron as Fe_2O_3.

[3]Totals include oxides of Ba, Sr, Rb, La, Ce, Nd, Cr, and Zr, for samples in which these elements were reported.

[4]Totals for samples EM–1 through EM–4 include F and S with correction for equivalent O.

[5]Total for IGS–40 includes Cl and F with correction for equivalent O; SO_3; and oxides of Ba, Sr, Th, Pb, La, Ce, Pr, Nd, Sm, Eu, Gd, and Y.

[6]*mg* = molar MgO/(MgO+FeO), where weight percent $Fe_2O_3/(Fe_2O_3+FeO) = 0.2$.

[7]Value is not well determined.

[8]Value is estimated; published value (129 ppm Lu_2O_3) is presumably a misprint.

[9]$Eu^* = 10^{(2/3\log(Sm)+1/3\log(Tb))}$.

Table 2. Ideal formulae of unusual rare earth minerals in carbonatite at Mountain Pass, California.

Mineral	Formula[1]
Ancylite	$SrCe(CO_3)_2OH \bullet H_2O$
Bastnaesite	$(Ce,La)(CO_3)F$
Cerite	$(Ce,Ca)_9(Mg,Fe^{2+})Si_7(O,OH,F)_{28}$
Florencite	$CeAl_3(PO_4)_2(OH)_6$
Hydroxl-bastnaesite	$(Ce,La)(CO_3)(OH,F)$
Parisite	$(Ce,La)_2Ca(CO_3)_3F_2$
Sahamalite[2]	$(Mg,Fe)(Ce,La)_2(CO_3)_4$
Synchisite	$(Ce,La)Ca(CO_3)_2F$

[1]From Clark (1984).
[2]First discovered at Mountain Pass (Jaffe and others, 1953).

Table 3. Batch partial-melting model for incompatible elements in shonkinites at Mountain Pass, California. Melt fraction is 0.01 percent.

	Amphibole[1]	Phlogopite[2,3]	Clinopyroxene[1]	Rutile[2,4]	Apatite[2]	D
Th	0.04	0.01	0	0.02	1.4	0.0036
Rb	.20	.25	0.01	0	.01	.0188
Ba	.25	.29	.01	0	.01	.023
Ta	.44	.1	.05	99.5	.03	.276
La	.17	.03	.05	.01	14	.0245
Ce	.26	.03	.1	.01	16	.0332
Sr	.12	.21	.07	0	3	.0192
Nd	.44	.03	.21	.01	20	.0512
P	0	0	0	0	30	.0275
Sm	.76	.03	.26	.01	21	.0703
Hf	.44	.25	.02	4.8	.05	.0432
Ti	.69	.09	.1	30	0	.144
Tb	.83	.04	.27	.02	15	.0692
Yb	.59	.04	.28	.07	9	.0527

Mass fraction of minerals in source rock (percent)

Amphibole[5]	Phlogopite[5]	Clinopyroxene	Rutile	Apatite	Total[6]
4.92	3.40	5.00	0.25	0.09	13.7

Abundance, chondrite normalized[7]

	Mantle source[8]	Model magma	Skonkinite[9]	Abundance ratio, model magma/shonkinite
Th	19.3	5200	7167	0.73
Rb	40.7	2150	1634	1.32
Ba	24.2	1050	803	1.3
Ta	39.5	143	80	1.79
La	22.2	900	957	.94
Ce	19.7	591	657	.9
Sr	9.62	498	181	2.76
Nd	11.6	226	397	.57
P	5.2	189	187	1.01
Sm	5.78	82.1	251	.33
Hf	4.44	103	126	.81
Ti	1.51	10.4	10.5	.99
Tb	3.26	47.0	69.4	.68
Yb	1.12	21.2	18.2	1.16
$(La/Yb)_{cn}$[10]	20	42	53	.81

[1]From Irving and Frey (1984), McKenzie and O'Nions (1991), and Hawkesworth and others (1993).
[2]Selected or averaged from numerous published sources, using geometric means and medians rather than arithmetic means.
[3]Value for Ba from Guo and Green (1990). Regarding Ba and Rb, see text.
[4]Values for Ta and Hf in rutile from Jenner and others (1994). Other values are for ilmenite; see text.
[5]These two variables are related: $[K_2O]_{source} = x^s_{phlog}[K_2O]_{phlog} + x^s_{amph}[K_2O]_{amph}$, where the concentration of K_2O in the source rock, in phlogopite, and in amphibole are taken as 0.39, 9.3, and 1.5 percent, respectively (averages from Irving and Frey, 1984; Menzies and others, 1987).
[6]The remaining 86.3 percent of the source rock comprises harzburgitic olivine and orthopyroxene; see text.
[7]Normalizing values (R.N. Thompson, 1982a) are chondritic except that values for Rb and P are estimates for primordial or undepleted terrestrial mantle (Sun, 1980).
[8]Geometric means of compositions of eight xenolithic enriched peridotites and pyroxenites, RS1 to RS7 (inclusive), and RS9; RS8, a glimmerite, is excluded (Menzies and others, 1987). Mean K_2O for these samples is 0.39 weight percent.
[9]Sample EM–1 (table 1, figs. 15*A*, 20*A*).
[10]Chondrite normalized.

Table 4. Analyses of bastnaesite at Mountain Pass, California.

[--, not applicable or not calculated]

	Reported[1]	Recalculated, impurity free[2]	Ideal bastnaesite[3]
Abundances, in weight percent			
	Attributed to bastnaesite		
Ce	27.7	--	--
La+Pr+Nd	31.3	--	--
Ce+La+Pr+Nd	[4]59.1	65.35	64.0
CO_3	25.	[5]25.76	27.4
F	6.88	7.61	8.67
	Attributed to impurities		
SiO_2	4.42	--	--
Ba	1.97	--	--
SO_4	.74	--	--
Ca	.5	--	--
Mg	.22	--	--
Na+K	.08	.09	--
H_2O^-	.22	.24	--
Total	99.1	99.1	100
Abundances, in parts per million[6]			
Rb	<10	--	--
Sr	3200	--	--
Zr	<10	--	--
Nb	<10	--	--
Y	>200	--	--

[1]Calculated from analysis of impure bastnaesite separate that contains about 5 volume percent quartz and minor amounts of barite and carbonate minerals (Olson and others, 1954, table 7).

[2]Recalculated free of SiO_2, $BaSO_4$, $CaCO_3$, $MgCO_3$, and $BaCO_3$.

[3]Assuming same proportions of La, Ce, Pr, and Nd as bastnaesite samples in table 4; ideal formula is $(Ce,La,Nd,Pr)(CO_3)F$.

[4]Value is a subtotal.

[5]Value is reduced by amount of CO_3 needed to form $CaCO_3$ and $MgCO_3$, as well as to form $BaCO_3$ from Ba in excess of that required for $BaSO_4$.

[6]Analyses by energy-dispersive X-ray fluorescence spectrometry; analyst, J. Kent. Sample number 91TT100.

Table 5. Proportions of rare earth elements (REE) and Y in bastnaesite concentrate and average ore from Mountain Pass, California.

[All values in weight percent except values in italic, which are in parts per million; --, not reported]

	Proportion of REE	
	Bastnaesite concentrate[1]	Average ore[2]
La	34	33
Ce	48	49
Pr	4.3	4
Nd	12.4	13
Sm	.81	.5
Eu	.11	.1
Gd	.18	.2
Tb	*160*	--
Dy	*330*	--
Ho	*52*	--
Er	*37*	--
Tm	*8*	--
Yb	*14*	--
Lu	*1*	--
Y	*850*	--
Tb+Y	--	.1
Other HREE[3]	--	.2
Total	100.0	100.1

[1]Recalculated from Neary and Highley (1984).
[2]From Barnum (1989).
[3]Heavy rare earth elements.

Table 6. Estimates of proven and probable reserves and grade for the Mountain Pass rare earth element (REE) deposit, California.

[--, not reported]

Reserves (10^6 tonnes)	[1]REE_2O_3 grade (weight percent)	Year of estimate	Cut off grade (weight percent)	Reference
28	9	--	5	Barnum, 1989
36	7.67	End 1986	--	Mariano, 1989a
28	8.86	--	--	Mariano, 1989b
29	8.9	1987	5	Castor, 1990, 1991
24.5	--	End 1990	--	J. Landreth, written commun., 1992

[1]Rare earth element oxide.

Table 7. Prices of rare earth element oxides from the Mountain Pass deposit, California

[From Molycorp, Inc. Price Schedule, June 1, 1992 (E. Barnum, written commun., 1992)]

Oxide	Purity (weight percent)	Price ($/kg)
La_2O_3	[1]99.99	21
CeO_2	96.0	16
CeO_2	99.0	23
Pr_6O_{11}	96.0	39
Nd_2O_3	96.0	16
Nd_2O_3	99.9	99
Sm_2O_3	96.0	132
Eu_2O_3	99.99	1,819
Gd_2O_3	[1]99.99	132
Tb_4O_7	99.9	882
Dy_2O_3	96.0	143
Dy_2O_3	99.0	187
Er_2O_3	98.0	154
Y_2O_3	99.99	121

[1]Also available at 99.995% purity.

Latest Proterozoic and Paleozoic Strata

By Gordon B. Haxel

Overview

Latest Proterozoic and Paleozoic strata in the East Mojave National Scenic Area (EMNSA) were deposited upon a substrate consisting of Early Proterozoic gneissic and granitoid rocks (Wooden and Miller, 1990) and Middle Proterozoic granite (Anderson and Bender, 1989) as described in the section above entitled "General Geologic Setting." These strata are exposed in small areas of several ranges in the EMNSA: Clark Mountain Range, Ivanpah Mountains, Providence Mountains, New York Mountains, Little Cowhole Mountains, Kelso Mountains, and Old Dad Mountain (pl. 1). The uncomformity between latest Proterozoic or Cambrian quartz-pebble quartzite and underlying Early Proterozoic rocks is well exposed at some localities in the EMNSA (fig. 25*A*). A few small bodies of metasedimentary rocks, most commonly marble or calc-silicate hornfels, of probable Paleozoic age are scattered throughout the EMNSA (see for example, DeWitt and others, 1984; Miller and others, 1985; Howard and others, 1987). These small bodies typically are roof pendants in Jurassic or Cretaceous plutons or slivers within fault zones (pl. 1).

Two northeast-trending boundaries or transitions between the Late Proterozoic to Paleozoic miogeocline on the west and the North American craton on the east pass through the central part of the Mojave Desert (fig. 3). The boundary that is defined by the presence of Late Proterozoic clastic rocks passes through the EMNSA, and the boundary defined by the presence of Paleozoic carbonate shelf rocks of Ordovician and Silurian age passes to the west of the EMNSA (Stewart and Poole, 1975; Burchfiel and Davis, 1981). Thus, the latest Proterozoic to Paleozoic strata in the EMNSA are mostly cratonal and relatively thin. Latest Proterozoic strata in the Clark Mountain Range, the Providence Mountains, and Old Dad Mountain are transitional to the miogeocline, but they are overlain by cratonal early Paleozoic strata. The autochthonous latest Proterozoic rocks in the Clark Mountain Range and the Ivanpah Mountains, thrust to the east by several tens of kilometers, are miogeoclinal (Burchfiel and Davis, 1981). The paleogeographic position of the late Paleozoic rocks is obscured by generally incomplete preservation or exposure (Burchfiel and Davis, 1981).

Summary of Rock Sequences

The most complete and best preserved sequences of the latest Proterozoic and Paleozoic rocks are in the Providence Mountains (Hazzard, 1954). These rocks are only locally metamorphosed, notably where they are intruded by Mesozoic plutons. The section, which rests unconformably on Early Proterozoic gneiss, is approximately 2,700 m thick (Hazzard, 1954). The lower part of the section consists of latest Proterozoic to Late Cambrian quartzite, dolomite, limestone, siltstone, and shale. The upper part comprises Devonian to Permian units that contain limestone and subordinate chert, sandstone, and shale. Ordovician and Silurian strata are absent, making this section similar to those defined as cratonal in the Southwest. Latest Proterozoic and Paleozoic stratigraphic units in the Providence Mountains (fig. 25*B*) have been correlated with units both in the Death Valley region 35 km to the north and in the western Grand Canyon region 75 km to the east (Stewart, 1970; Stone and others, 1983; Goldfarb and others, 1988).

At Old Dad Mountain and in the Cowhole Mountains, Paleozoic rocks and conformably underlying latest Proterozoic strata are strongly disrupted structurally but are not highly metamorphosed. The section is generally similar to that in the Providence Mountains (Dunne, 1977). Similar rocks also crop out in the Kelso Mountains but do not form a complete section there.

Paleozoic rocks in the central New York Mountains are preserved as wallrocks to a batholith of Cretaceous granitic rocks. Most strata have been converted to marbles, calc-silicate hornfels, or pelitic hornfels. They also have been affected by multiple episodes of Mesozoic folding and faulting. Despite the metamorphism and deformation these rocks have undergone, a stratigraphic section generally similar to that in the Providence Mountains can be reconstructed (Burchfiel and Davis, 1977). The chief difference is that latest Proterozoic strata are absent; the lowest Cambrian unit rests unconformably on Early Proterozoic gneiss.

In the area of the Clark Mountain Range, miogeoclinal stratigraphic sequences were thrust eastward over a cratonal sequence (Burchfiel and Davis, 1971). The autochthonous and parautochthonous Paleozoic strata are cratonal, whereas the overlying thrust sheets carry latest Proterozoic and Paleozoic rocks of transitional to miogeoclinal facies. Low-grade metamorphism is locally developed in the south, close to the extensive, informally named, Jurassic Ivanpah granite of Beckerman and others (1982).

Latest Proterozoic and Paleozoic strata in the central part of the Ivanpah Mountains are included in the generalized regional descriptions given by Hewett (1956), and subsequent detailed information shows that they are similar to and continuous with rocks in the Clark Mountain Range and the Mescal Range (Burchfiel and Davis, 1971).

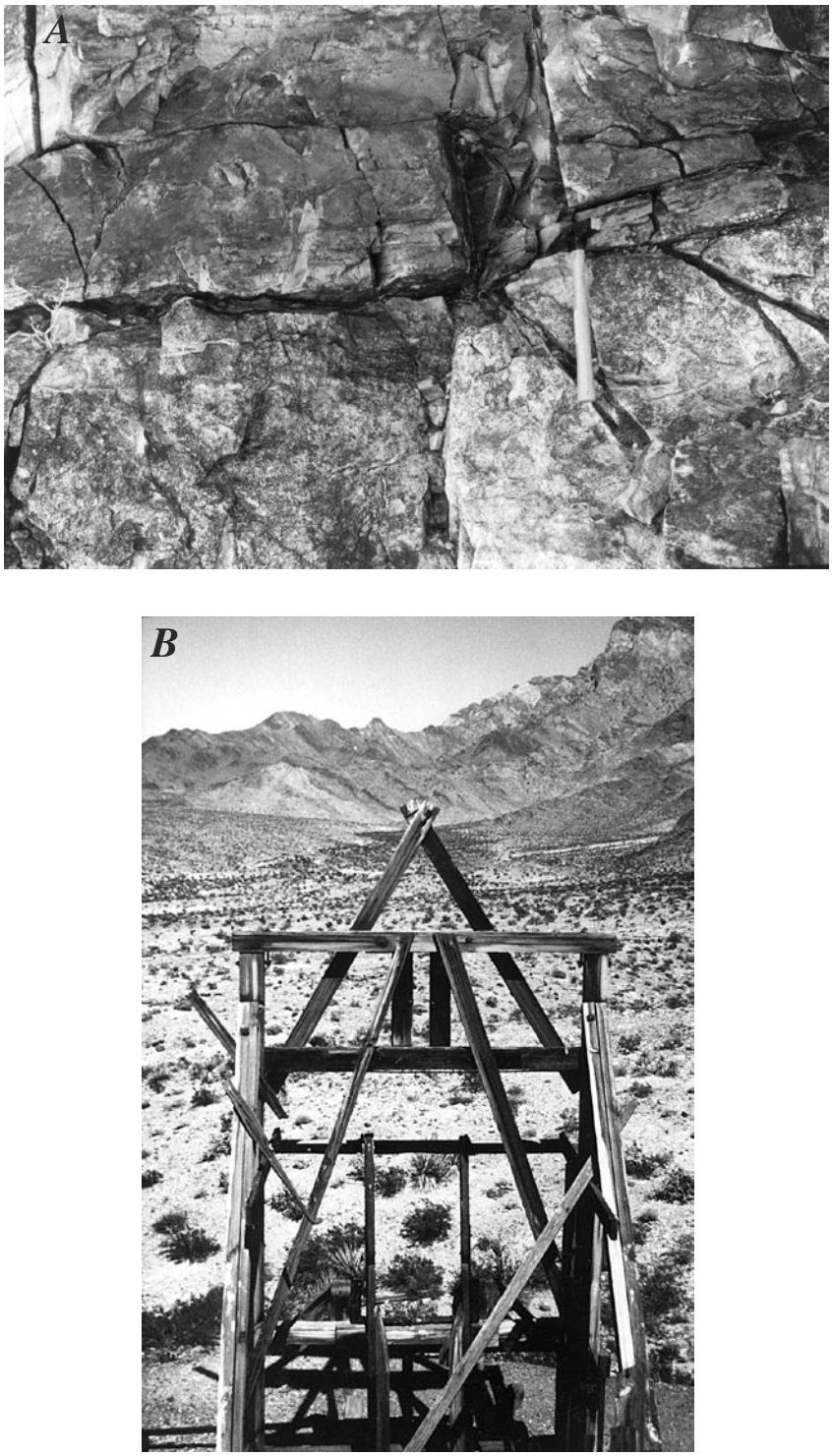

Figure 25. Paleozoic strata in the East Mojave National Scenic Area, California. *A*, Latest Proterozoic or Cambrian, undeformed quartz-pebble quartzite in depositional contact (hammer point on contact with underlying, ductilely deformed Proterozoic metaquartzite near Brannigan Mine, approximately 3 km south of Seventeenmile Point). *B*, Light-colored, rugged slopes of eastern Providence Mountains (fig. 2) are underlain by Paleozoic strata, mostly limestone and dolomite. Low slopes below skyline are underlain by Jurassic and Early Proterozoic granitoids. View to northwest from headframe at Bonanza King Mine.

Mesozoic Rocks

By Gordon B. Haxel and David M. Miller

Mesozoic rocks in the East Mojave National Scenic Area (EMNSA) consist of minor Triassic plutons and sedimentary rocks, some volcanic and volcaniclastic Triassic and (or) Jurassic rocks, and Jurassic and Cretaceous plutonic rocks. The Cretaceous plutonic rocks are the most widespread of the Mesozoic rocks in the EMNSA.

Triassic Plutons

Triassic plutonic rocks are widely scattered in regions mostly west and southwest of the EMNSA (Barth and others, 1990; Miller, 1978) and have not yet (1993) been documented in the EMNSA. In the Clark Mountain area, several small dioritic stocks intrude Paleozoic strata, and one of these bodies has yielded K-Ar hornblende ages of 190 and 200 Ma (Burchfiel and Davis, 1971; Mueller and others, 1979). However, preliminary U-Pb zircon ages for these bodies are Late Jurassic (J.D. Walker, oral commun., 1993). Evidently, the hornblende contained excess argon, resulting in ages spuriously old. No Triassic U-Pb ages have been reported for plutons in the EMNSA, but few of the plutons of possible Triassic age have yet been dated by U-Pb methods. A dioritic orthogneiss unit in the Granite Mountains, assigned a probable Triassic age by Howard and others (1987), is now known to be Jurassic (Young and others, 1992). Small bodies of hornblende monzonite, commonly present between the Teutonia batholith and septa of Paleozoic marble in the western New York Mountains (fig. 26), is similar to Triassic monzonites known in the western Mojave Desert. This hornblende monzonite is younger than Paleozoic rocks and older than the informally named, Cretaceous Mid Hills adamellite of Beckerman and others (1982).

Triassic Sedimentary Rocks

In most of the ranges of the EMNSA that contain latest Proterozoic and Paleozoic sequences (see previous section entitled "Latest Proterozoic and Paleozoic Strata"), these strata are conformably overlain by reddish sandstone, limestone, and shaley limestone or by their metamorphosed equivalents. These rocks are correlated with the Early Triassic Moenkopi Formation (unit Ṯrm, pl. 1) according to Burchfiel and Davis (1971, 1977) and Walker (1987). In the Providence Mountains, this unit is approximately 300 m thick and contains Early Triassic fossils. In many ranges, these rocks are metamorphosed to distinctive calc-silicate rock (Stone and others, 1983).

In the Mescal Range, a unit of sandstone, shale, and limestone stratigraphically above the Moenkopi Formation and below a Jurassic sandstone unit was correlated with the Late Triassic Chinle Formation by Hewett (1956). This correlation was questioned by Marzolf (1983), who considered several Jurassic units to lie directly on the Moenkopi. Possible Chinle-correlative rocks have not been reported elsewhere in the EMNSA.

Mesozoic Volcanic and Hypabyssal Rocks

Several ranges within the EMNSA contain volcanic and volcaniclastic rocks, intercalated sedimentary rocks, and related hypabyssal rocks of Triassic and (or) Jurassic age. Stratigraphic sequences, in varying degrees of preservation, are exposed in four areas: the Mescal Range, the Old Dad Mountain-Cowhole Mountain-Soda Mountains area (the latter mountains are 1 to 5 km west of the EMNSA; see fig. 2), the New York Mountains, and the Providence Mountains. In a few other areas, metamorphosed or hydrothermally altered Triassic and (or) Jurassic volcanic, hypabyssal, and sedimentary rocks are present as roof rocks or pendants in Jurassic plutons or as slivers in fault zones. Among these small relicts, Jurassic rocks are probably more common than Triassic rocks. Owing to common metamorphism or alteration, as well as to lack of study, little is known about the petrology and geochemistry of Triassic and Jurassic volcanic rocks in the EMNSA.

A sequence of diverse volcanic and sedimentary rocks more than 3 km thick in Old Dad Mountain and the Cowhole Mountains consists of interbedded intermediate-composition to silicic lava flows and flow breccias, quartzarenite, sandstone and siltstone, sedimentary breccia and megabreccia, silicic ignimbrite, and other minor

rock types (Marzolf, 1983, 1988, 1991; Busby-Spera, 1988; Busby-Spera and others, 1989). Zircon U-Pb ages of some of the volcanic rocks indicate that the age of this sequence is approximately 170 Ma, which is Middle Jurassic according to the geologic time scale of Harland and others (1989). A generally similar sequence of rocks is present in the Soda Mountains (Grose, 1959).

The quartzarenite units in the Mescal Range, the Cowhole Mountains, and Old Dad Mountain are, in part, eolian. Until recently, these quartzarenites were generally correlated with the Early Jurassic (Peterson and Pipiringos, 1979) eolian Aztec Sandstone of the southern Great Basin and Navajo Sandstone of the Colorado Plateau. However, the U-Pb ages cited above indicate that the Jurassic quartzarenites in these ranges, and probably others in the EMNSA, may correlate with the Middle Jurassic Carmel Formation or Entrada Sandstone of the Colorado Plateau. Poor age constraints for the Colorado Plateau units permit either correlation.

In the Mescal Range, a unit of crossbedded arenitic sandstone approximately 250 m thick contains dinosaur tracks, the only dinosaur tracks known in California (Reynolds, 1983). This unit probably correlates with the Carmel Formation or Entrada Sandstone (included in unit Ja, pl. 1) in the Cowhole Mountains. The crossbedded arenaceous sandstone is overlain by a sequence, approximately 200 m thick, of basaltic, dacitic, and rhyolitic flow breccias and lava flows (Hewett, 1956; Fleck and others, 1994). These volcanic rocks have not been studied in detail, but they have been dated by K-Ar and Rb-Sr methods as Early Cretaceous, about 117 Ma (Fleck and others, 1994), and, therefore, differ in age as well as in composition from Jurassic volcanic sequences in other parts of the EMNSA.

In the New York Mountains, a sequence of metamorphosed volcanic rocks approximately 250 m thick overlies the Moenkopi Formation and is, in turn, overlain by a metasedimentary unit approximately 70 m thick (Burchfiel and Davis, 1977). The volcanic rocks are silicic in composition, include breccia or agglomerate, and contain subordinate intercalated metasiltstone and, near the base of the unit, metaconglomerate. The metasedimentary unit comprises siltstone, conglomerate, and tuffaceous sandstone and siltstone. The conglomerate beds contain clasts derived from the underlying volcanic unit. These two units could be either Triassic or Jurassic in age; the latter is more likely. The metavolcanic rocks are generally schistose or have fabrics that appear mylonitic; however, some of this fabric probably is partly inherited from original welded-tuff textures. Metasedimentary lithologies vary from argillite to schist. Both the volcanic and sedimentary units in the New York Mountains contain metamorphic biotite.

In the Providence Mountains, intermediate-composition to silicic volcanic and volcaniclastic rocks have been mapped by Hazzard (1954) and Goldfarb and others (1988). These igneous rocks, in part, overlie the Moenkopi Formation and are probably Triassic and (or) Jurassic in age (Walker, 1987). In some places, the volcanic rocks contain intercalated conglomerate and siltstone. Farther south in the Providence Mountains, hypabyssal rocks and probable volcanic rocks are present as roof rocks or septa adjacent to Jurassic plutons (Miller and others, 1985). These rocks are intensely altered, but some have granitic textures.

Jurassic and Cretaceous Plutonic Rocks

Introduction

Plutons known to be of Jurassic or Cretaceous age, on the basis of U-Pb geochronology, are common in the EMNSA (pl.1). Other plutons are definitely or almost certainly Mesozoic in age, but it is uncertain whether they are Jurassic or Cretaceous. The Jurassic and Cretaceous plutons, as well as the ranges in which they crop out within the EMNSA, are too numerous to list or describe individually. Rather, the descriptions below focus on typical or relatively well studied plutons and on features of special interest.

The Jurassic and the Cretaceous plutons within the EMNSA are small remnants or parts of larger magmatic belts that extend throughout much of the southern part of the North American Cordillera. The Jurassic and Cretaceous magmatic belts are oblique to each other (Tosdal and others, 1989; Miller and Barton, 1990; Fox and Miller, 1990). The northeast margin of the composite magmatic belt lies in the central parts of the Ivanpah and New York Mountains.

Known Jurassic plutons and Cretaceous plutons in the EMNSA region generally differ in petrology and geochemistry. Miller and others (1982, 1985), Howard and others (1987), and Fox and Miller (1990) have

summarized the characteristics of Jurassic and Cretaceous plutonic rocks in the Granite Mountains, southern Providence Mountains, and Colton Hills, all in the southern part of the EMNSA. The Cretaceous granitoids are characterized by relatively low color index, white- to buff- or flesh-colored feldspars, and absence of clots of mafic minerals. In contrast, the Jurassic granitoids commonly are more heterogeneous, contain less quartz, more commonly are conspicuously sphene bearing, are more potassic, have higher color index, and contain lavender, gray, or pinkish alkali feldspar and clots of mafic minerals. In some places, Jurassic plutons are associated with magnetite-skarn deposits or zones of extensive albitization, neither of which has been documented for Cretaceous plutons. Thus, for some Mesozoic plutons for which U-Pb ages have not been determined, a reasonable inference for a Jurassic or a Cretaceous age can be made from the overall petrology or composition of the plutons. Such estimates are probably most applicable to granodiorite and typical granite compositions and have a lower probability of being correct for either high-silica granite or dioritic or gabbroic rocks. In this report, we follow the IUGS classification scheme (Streckeisen, 1976) for plutonic igneous rocks.

Geochronologic data, much of it unpublished, for plutons in the EMNSA hint at multiple intrusive episodes for each of the Jurassic and Cretaceous groups of plutons. Many Jurassic plutons appear to be 170 to 160 Ma in age, but some plutons and dikes are as young as 150 to 145 Ma. Most of the Cretaceous plutons appear to belong to either a late Early to early Late Cretaceous intrusive event, from 100 to 90 Ma, or a late Late Cretaceous event, from 75 to 70 Ma. General distingushing characteristics of Jurassic and Cretaceous plutons are maintained despite episodic occurrence within the two groups.

Jurassic Plutonic Rocks

Widespread emplacement of Jurassic plutons followed by approximately 50 m.y. the emplacement of scattered Triassic plutons in the Mojave Desert region (Tosdal and others, 1989; Anderson and others, 1992). The most thoroughly studied Jurassic plutonic rocks in the region of the EMNSA are those in the area of the southern Bristol Mountains (10 km south of the EMNSA; see fig. 2), southern Providence Mountains, and Colton Hills (Miller and others, 1985; Fox and Miller, 1990); Granite Mountains (Young and others, 1992); and Clipper Mountains (10 km south of the EMNSA) (Gerber and others, 1991). Three types of Jurassic plutonic rocks are common: mafic rocks; intermediate-composition to silicic, mixed or heterogeneous rocks; and leucocratic monzogranite (pl. 1). These plutons are difficult to date precisely but appear to be largely 170 to 160 Ma in age. Except in the Granite Mountains where Late Jurassic diorite is known (Young and others, 1992), the mafic rocks are generally the oldest, and the leucocratic rocks, the youngest. Other plutons possibly in the 170- to 160-Ma age group are in the Old Dad Mountain and Devils Playground areas.

The mafic rocks include fine- to coarse-grained gabbro, diorite, and monzodiorite; common mafic minerals include clinopyroxene, hornblende, and biotite. In general, the mafic rocks have SiO_2 contents of 49 to 55 weight percent and are subalkaline and metaluminous. They also have relatively high abundances of large-ion lithophile elements (LILE), for example, commonly as much as about 3 weight percent K_2O and about 1,000 ppm Ba. Young and others (1992) concluded from geochemical modeling that diorite evolved from parental magma that was derived from hydrous, subcontinental lithosphere enriched in rare earth elements (REE) and that was contaminated by mafic granulite in the lower crust as it ascended to the upper crust.

The mixed intrusive rocks are by far the most abundant. They are markedly heterogeneous, varying from fine-grained equigranular to coarsely porphyritic and from quartz monzodiorite to syenogranite and syenite. A number of phases or subgroups are present, typically bounded by gradational contacts. The mixed intrusive rocks have a wide range of SiO_2 contents, from 50 to 74 weight percent; they are subalkaline to, less commonly, alkaline and metaluminous to weakly peraluminous. Some rocks are potassic, having K_2O/Na_2O ratios as great as 2. Abundances of Ba are as great as 2,000 to 4,000 ppm in some of the mafic and intermediate-composition rocks.

The leucocratic monzogranite is the most homogeneous of the three rock types. Whereas other plutonic phases grade complexly into one another, in general the monzogranite cleanly crosscuts as the youngest phase. In the Colton Hills, it consists of medium- to coarse-grained, porphyritic leucocratic biotite monzogranite, locally containing minor muscovite. It is subalkaline and generally moderately peraluminous. Trace-element abundances are unremarkable.

Many of the Jurassic plutonic rocks in the EMNSA are strongly altered. In the southern Providence Mountains and the southern Bristol Mountains, the rocks have undergone widespread albitization, characterized by the replacement of K-feldspar by albite and the continued stability of intermediate-composition plagioclase (Miller and others, 1985; Fox, 1989; Fox and Miller, 1990). This alteration is comparable to sodic-calcic alteration reported in some deep-seated porphyry-copper systems (see for example, Battles, 1991). Intense albitization is present as white zones in otherwise normally mesotype rocks; less intense albitization produces mottled patches or spots. Albitization is characterized by the doubling of Na_2O content and the nearly complete loss of K_2O: typically, K_2O decreases from 6 weight percent to less than 1 weight percent. Accompanying changes in Fe, Mg, and Ca abundances depend on the extent of chloritization of mafic phases. During alteration, Al, Ti, Zr, Y, and REE are generally immobile on a hand-specimen scale. Alteration was probably caused mainly by repeated intrusion of magma into the shallow crust, which generated large, long-lived hydrothermal systems.

Late Jurassic plutons in the EMNSA are recognized in the Granite and Ivanpah Mountains and may be more widely present. Diorite in the Granite Mountains is about 155 Ma in age on the basis of U-Pb zircon ages (Young and others, 1992). Other than its younger age, the diorite is similar to diorite in the Providence and Bristol Mountains. The informally named Ivanpah granite of Beckerman and others (1982) (unit Ji, pl. 1) is 150 to 145 Ma in age, also on the basis of U-Pb zircon ages (J.D. Walker, oral commun., 1992). It consists of biotite monzogranite that is strongly porphyritic. The pluton is moderately peraluminous and potassic. A similar peraluminous pluton in the Providence Mountains near Tough Nut Spring is less porphyritic but is possibly related to the Ivanpah pluton (Goldfarb and others, 1988).

Late Jurassic Dikes

In the southern Providence Mountains, swarms of Middle to Late Jurassic intermediate-composition to silicic dikes intrude Jurassic plutons (Miller and others, 1985). The dikes vary from dacite porphyry to aphanitic rhyodacite to aplite. Similar intermediate-composition dikes in the Colton Hills are intruded by Cretaceous plutons (Fox and Miller, 1990). Dikes in the Colton Hills have a minimum age of 146 Ma by K-Ar methods on biotite (D.M. Miller, unpub. data, 1984). Similar dikes are known in a few other places within the EMNSA, such as the Cowhole Mountains. Possibly related swarms of Late Jurassic mafic or intermediate-composition to silicic dikes are widespread in eastern California and southwestern Arizona (Chen and Moore, 1979; Powell, 1981; Karish and others, 1987; Hopson, 1988; Haxel and others, 1988; Tosdal and others, 1989). Some Jurassic dikes that crop out in the Providence Mountains were correlated by James (1989) with the approximately 150-Ma Independence dike swarm of eastern California. James (1989) suggested that the more than 500-km-long dike swarm may be related to either continental-scale arc-normal extension, changes in plate motions, or oblique subduction combined with left-lateral shear. The similar age of the informally named Ivanpah granite of Beckerman and others (1982) raises the possibility that plutons were also emplaced at the time of dike intrusion.

Cretaceous Plutonic Rocks

Most Cretaceous plutonic rocks in the EMNSA belong to the Early and Late Cretaceous Teutonia batholith (Beckerman and others, 1982). Beckerman and others (1982) considered the Teutonia batholith to be Jurassic and Cretaceous in age, chiefly on the basis of K-Ar cooling ages that provide minimum emplacement ages. They divided the batholith into seven informally named plutons; a large area of granitic rocks in the hills near Halloran Spring (DeWitt and others, 1984) remains undivided and undescribed (fig. 26). One pluton is Jurassic in age, the informally named Ivanpah granite of Beckerman and others (1982) (pl. 1). The other six plutons, which constitute most of the eastern part of the batholith, are Cretaceous in age. Preliminary U-Pb zircon ages for major plutons of the batholith range from 93 to 100 Ma (E. DeWitt, oral commun., 1990). Thus, the Teutonia batholith is hereby redefined to exclude the coincidentally spatially associated, Jurassic Ivanpah granite; this revised usage is followed in the summary below.

The six major plutons that constitute the eastern Teutonia batholith crop out chiefly in the New York Mountains, the Mid Hills, and the Cima Dome-Wildcat Butte-Marl Mountains area (fig. 26; pl. 1). Five of the six

plutons are fairly large, having exposed areas of about 50 to 200 km^2. These plutons are intermediate to felsic in composition; in places, they form craggy exposures and also include volumetrically minor dikes (fig. 27). The sixth pluton is of mafic composition and forms a subcircular outcrop area about 2 km in diameter; bodies of correlative composition are smaller. Similar mafic to felsic rock units have been noted in the hills near Halloran Spring (E. DeWitt and H.G. Wilshire, oral commun., 1992).

The five relatively large plutons of the Teutonia batholith mostly vary in composition from quartz monzodiorite to syenogranite; granodiorite and monzogranite are the principal compositional types; monzodiorite is a minor phase of one pluton. Despite this compositional range, granite constitutes most of the exposed rocks. Quartz-poor modal compositions (quartz monzodiorite, quartz monzonite, and quartz syenite) are present only in the Rock Spring monzodiorite of Beckerman and others (1982) (unit Krs, pl. 1). Other rocks are medium to coarse grained; some plutons or facies within plutons are equigranular, whereas others have alkali-feldspar phenocrysts. Biotite is ubiquitous; hornblende is common to absent. The Kessler Springs pluton locally contains minor primary muscovite. Three of the five plutons are leucocratic, having color indices less than 5: the Teutonia adamellite (Kt), Mid Hills adamellite (Kmh), and Kessler Springs adamellite of Beckerman and others (1982) (Kks).

The mafic pluton (Black Canyon hornblende gabbro of Beckerman and others (1982) (Kbc), which is presumably associated with the Teutonia batholith, comprises compositionally and texturally variable, hornblende-rich mesotype to melanocratic gabbro. Magnetite content is high: average is 6.5 volume percent. This phase of the batholith is intruded by two of the more widespread granitic phases of the Teutonia batholith, the Mid Hills adamellite and the Rock Spring monzodiorite. Probable correlative bodies include one in Cedar Canyon and another, not shown on plate 1, near Wildcat Butte on Cima Dome.

The six plutons of the Teutonia batholith form a broadly calc-alkaline series (Beckerman and others, 1982). The hornblende gabbro contains 43 to 49 weight percent SiO_2; the other five plutons range from 68 to 77 weight percent SiO_2. The granitoid plutons generally straddle the boundary between metaluminous and peraluminous compositions. Moderately or strongly peraluminous granites are absent. Abundances of Ba, Sr, and Rb (the only trace elements analyzed) are generally normal and unremarkable for granitic rocks.

Geobarometric data indicate that the Rock Spring monzodiorite of Beckerman and others (1982) was emplaced at pressures of from less than 1 to 3 kb (Anderson and others, 1988, 1992), corresponding to upper-crustal depths of approximately less than 3 to 10 km. According to J.L. Anderson (oral commun., 1990), present exposures provide a tilted view of the batholith: the shallowest plutons, emplaced at pressures of approximately 0.5 kb, are to the north, and the deepest plutons, emplaced at approximately 3 kb, are to the south. However, these pressure data conflict with geologic evidence that the roof of the batholith is exposed in the south (Goldfarb and others, 1988) as a shallowly south dipping surface in the Providence and Marl Mountains; therefore, the south should be the shallowest part of the batholith. The Teutonia batholith is among the shallowest of the Mesozoic plutonic complexes in the Mojave Desert region (Anderson and others, 1988, 1991); pressure estimates for ten other complexes range from 2 to 9 kb.

Small, shallow-level stocks northeast of the Teutonia batholith appear to represent outliers of the magmatic belt formed in earliest Late Cretaceous time. Magmatic alteration, intrusive breccia, and felsite dikes in the Colosseum Mine area of the Clark Mountain Range (described in subsection below entitled "Breccia Pipe and Related Deposits") are about 100 Ma in age (Sharp, 1984). Similar alteration and breccia, as well as small hypabyssal bodies of biotite granodiorite, lie about 5 km northeast of the EMNSA in the New York Mountains, near Crescent Peak (Miller and Wooden, 1993). This granodiorite yielded a K-Ar biotite age of 94.4±2.4 Ma.

Latest Cretaceous plutons in the EMNSA range from 75 to 70 Ma in age (Howard and others, 1987; J.L. Wooden, oral commun., 1987, *quoted in* Fox and Miller, 1990). Late Cretaceous plutons, known to be approximately 70 Ma, crop out in the Granite Mountains and at Homer Mountain (5 km east of the EMNSA); probable Late Cretaceous plutons crop out in the Fenner Hills and near Bobcat Hill. In the Granite Mountains, a suite of Cretaceous igneous rocks includes a granodiorite pluton and a larger, compositionally zoned pluton, as well as granite, aplite, and pegmatite dikes (Howard and others, 1987). The granodiorite pluton makes up most of the western Granite Mountains (pl. 1); the zoned pluton makes up the southeastern part of the Granite Mountains (Howard and others, 1987) and part of the adjacent Providence Mountains (Miller and others, 1985).

Magmatic biotite from the zoned pluton yielded K-Ar dates, possibly emplacement ages, of 74.5 to 70.9 Ma (Miller and others, 1985; Howard and others, 1987). In general, latest Cretaceous plutonic rocks are silicic, weakly to strongly peraluminous granites.

Mesozoic Deformation

Mesozoic deformational features of regional extent crop out in the western and north-central parts of the EMNSA. These deformational features are reflections of crustal shortening, as shown by brittle-style deformation of thrust plates, which have developed in the foreland of the Cordilleran thrust belt (Burchfiel and Davis, 1971, 1977, 1981; Snoke and Miller, 1988). Ductile-style nappes in southeastern California and Arizona extend to the south border of the EMNSA (Howard and others, 1980; Miller and Barton, 1990).

Generally east directed thrust faults, present in the Cowhole Mountains and Clark Mountain Range areas, may be Middle Triassic(?) through Early Jurassic in age (Burchfiel and Davis, 1981). Burchfiel and Davis (1981) interpreted metamorphosed Paleozoic rocks in the Cowhole Mountains as having been thrust eastward and then overlapped unconformably by the Early Jurassic Aztec Sandstone (unit Ja, pl. 1). However, Busby-Spera (1988) and Busby-Spera and others (1989) presented evidence that the sandstone is Middle Jurassic in age and may have accumulated in an intra-arc graben. In the Clark Mountain Range, some east-directed thrust faults are cut by small dioritic plutons, which were originally dated at 200 to 190 Ma by K-Ar methods (Burchfiel and Davis, 1981) but are now known to be Late Jurassic in age. Latest Early Cretaceous thrusting placed Paleozoic strata over Early Cretaceous volcanic rocks. This thrust was then intruded by plutons of the mid-Cretaceous Teutonia batholith (Burchfiel and Davis, 1971, 1981; Fleck and others, 1994). A similar sequence of faulting, although not as well chronologically constrained, is present in the New York Mountains.

Contrasting with the thrust faults and folds that represent horizontal shortening are complexes of normal faults, in places accompanied by stratal tilting, that represent horizontal extension. The best-documented period of extension is of Middle Jurassic age in the Cowhole Mountains and probably of a similar age in the Providence Mountains. In the former location, normal faults are interpreted by Busby-Spera (1988) and Busby-Spera and others (1989) as being active during extension of Middle Jurassic lava flows. In the Providence Mountains, Hazzard (1954) mapped four sets of normal faults, all but the youngest of which are cut by rhyolite dikes dated as Jurassic (J.D. Walker, oral commun., 1993). For both the Cowhole Mountains and Providence Mountains, most normal faults strike north, suggesting east-west extension.

In summary, Mesozoic deformation is incompletely understood. Available evidence points to Middle Jurassic or older thrusting, Middle Jurassic localized extension, and Late Jurassic to Early Cretaceous thrusting.

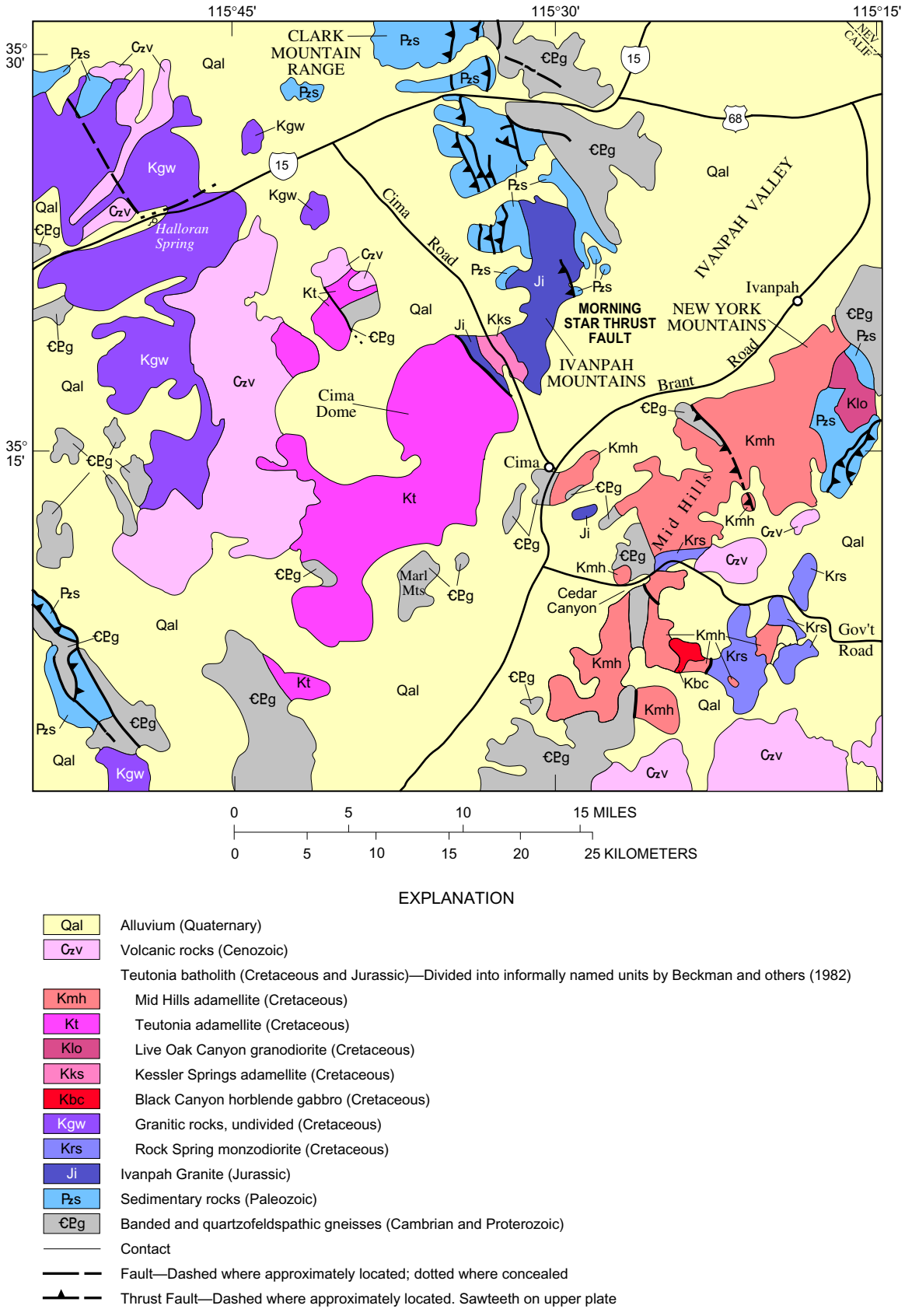

Figure 26. Geologic map of north-central part of East Mojave National Scenic Area, California, showing distribution of various phases of Teutonia batholith. Modified from Beckerman and others (1982).

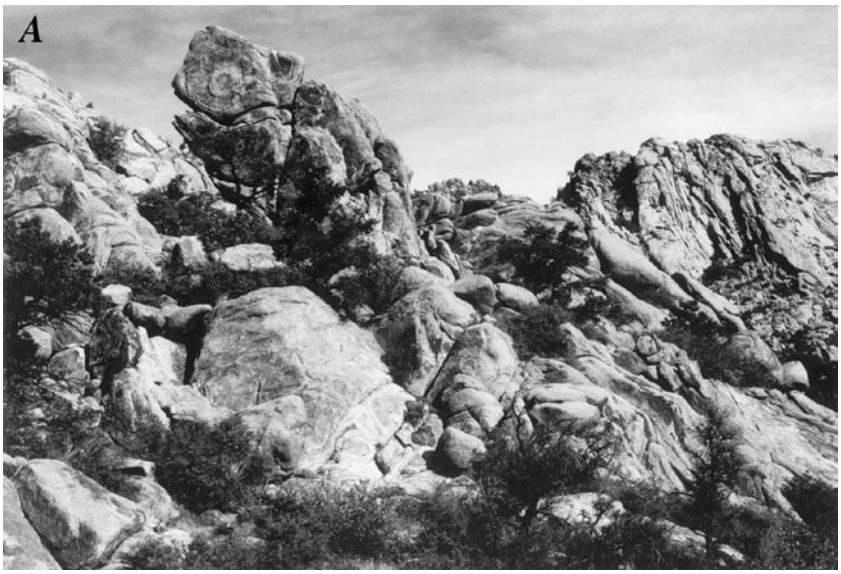

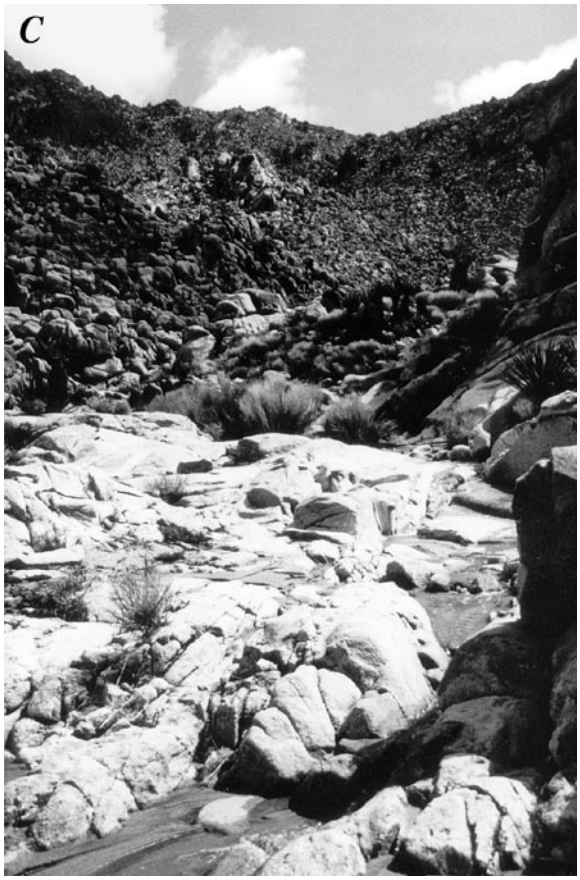

Figure 27. Typical exposures of two plutonic phases of Teutonia batholith, East Mojave National Scenic Area, California. *A*, Informally named Mid Hills adamellite of Beckerman and others (1982) (unit Kmh, pl. 1) near Giant Ledge Mine. View to east. Bold exposures in left-center of field of view are approximately 40 m high. *B*, Coarsely crystalline phase of informally named Teutonia adamellite of Beckerman and others (1982) (unit Kt, pl. 1) to left, cut by narrow hornblende quartz diorite dike (qd), in center, in northern part of Cima Dome (fig. 26). Width of dike is approximately 10 m. *C*, Latest Cretaceous granite in southern Providence Mountains (fig. 2) forms white, bouldery-appearing outcrops. Top of ridge is underlain by Jurassic granitoids.

Tertiary Rocks

By Robert J. Miller and James J. Rytuba

Introduction

Following the period of crustal shortening and plutonism during the Late Cretaceous, a quiescent period ensued that lasted until about the early Miocene. Very little tectonic or magmatic activity has been documented for the Mojave Desert region during this quiescent period. The early to middle Miocene, however, was a period of intense volcanism and extensional faulting throughout much of the Mojave and Sonoran Desert regions. Volcanism in the East Mojave National Scenic Area (EMNSA) during the Tertiary, in part, reflects continental-scale retreat of calc-alkaline intermediate-composition magmatism from the southeast to the northwest along a narrow magmatic arc (Eaton, 1984). Eaton (1984) envisioned this region as a back arc developed in a predominantly continental crustal environment. Much of the eastern part of the EMNSA represents a tectonic block that retained relative structural stability when extensional movement on low-angle normal faults resulted in significant rotation and disruption of supracrustal sequences in many of the mountain ranges to the north, southwest, and east of the EMNSA (Spencer, 1985; McCurry and Hensel, 1988; Reynolds and Nance, 1988; Burchfiel and Davis, 1988; Wilshire, 1988; Hileman and others, 1990). However, Miocene extensional deformation was described by Burchfiel and Davis (1988) in the Clark Mountain Range, as well as in the Mesquite Mountains and in the Kingston Range to the north and northwest of the EMNSA (see fig. 2). Sedimentary and tectonic deposits also accumulated in a Miocene extensional basin that underlies part of the Shadow Valley area (Reynolds and Nance, 1988; Wilshire, 1988). Multiple detachment faults exposed on Homer Mountain (Spencer, 1985), immediately east of the EMNSA, roughly coincide with the west edge of the north-trending Colorado River extensional corridor, which has been well documented in many of the reports cited above. The west edge probably lies east of the Piute Range, but the extensional corridor also may encompass the northern Piute Range and the Castle Mountains. The region immediately to the south of the EMNSA, including the Old Woman, Piute, Little Piute, and Ship Mountains (see fig. 2), underwent moderate extension during the Miocene (Hileman and others, 1990); the central Mojave, from Barstow to near Baker, may have been extended greatly in the early Miocene (Glazner and others, 1989). Glazner and O'Neil (1989) determined a smooth eastward increase in initial whole-rock $^{87}Sr/^{86}Sr$ ratios for silicic volcanic rocks in the Mojave Desert region of southern California; they reported ratios for these types of rocks in the Castle Mountains that range from 0.70526 to 0.70990. Glazner and O'Neil (1989) interpreted the smoothness and lack of discontinuities in the eastward increase in initial whole-rock $^{87}Sr/^{86}Sr$ ratios to reflect the absence of any broad zones of pre-Tertiary rifting or major faulting. The increase in these ratios must be due to an eastward increase in the amount of crustal material incorporated into the magmas. Broad areas in the northern parts of the EMNSA also were subjected to moderate amounts of extension from the late Miocene into the Holocene in association with the development of pediment domes (see section below entitled "Development of Pediment Domes")

Overall basal stratigraphic sequences of both Tertiary rocks and Tertiary and Quaternary alluvial deposits are similar in the Piute Range, Castle Mountains, and the hills near Halloran Spring (fig. 2; Nielson and Nakata, 1993; Nielson and others, 1993; Reynolds, 1993). In each of these three areas, a Miocene sanidine- and sphene-bearing ash-flow tuff, the approximately 19–Ma Peach Springs Tuff of Young and Brennan (1974) (unit Tps, pl. 1), is present near the base of the Miocene section where it rests on arkosic sandstone and conglomerate that, in turn, rest unconformably on a basement of Proterozoic and Mesozoic metamorphic and igneous rocks. Volcanic rocks stratigraphically above the Peach Springs Tuff in the Piute Range include basalt to rhyodacite lava flows, volcaniclastic breccia, and air-fall tuff (Nielson and Nakata, 1993). In the Castle Mountains, andesitic-basaltic flows, minor basalt dikes, and volcanic breccias, all of which are interbedded with sedimentary rocks derived from andesitic-basaltic protoliths (Nielson and others, 1993), overlie the Peach Springs Tuff. Rhyolite plugs, flows, and sills, as well as rhyodacite ash-flow tuffs, all of which are associated with the gold deposits in the Castle Mountains, are younger than the intermediate-composition volcanic rocks. In the hills near Halloran Spring, fine-grained lacustrine rocks, which are in places interbedded with arkosic fanglomerate deposits, are present above an ash-flow tuff that is similar in age and lithology to the Peach Springs Tuff (Reynolds, 1993).

Van Winkle Mountain and Vicinity

The oldest Tertiary volcanic and sedimentary rocks in the region of the EMNSA are exposed in Van Winkle Mountain, northernmost Clipper Mountains (see fig. 2), and Old Dad Mountains (pl. 1). In Van Winkle Mountain, the sequence consists of tuff breccia, rhyodacite lava flows, and air-fall and ash-flow tuff that are capped conformably by olivine basalt flows (fig. 28*A*). These rock types are correlative with sequences of rock exposed to the west in the Bristol Mountains (see fig. 2) (Miller and others, 1985). The distinctive sanidine-bearing rhyolite tuff present near the top of this sequence has been correlated with the Peach Springs Tuff of Young and Brennan (1974) by Glazner and others (1986). Its presence at the top of the Tertiary sequence is in marked contrast to the presence of the Peach Springs Tuff near the base of the section in the northern part of the EMNSA. Thus, stratigraphy of Tertiary rocks and deposits comprises two geographically distinct sequences on the basis of the presence of the Peach Springs Tuff in two different places in the stratigraphic succession. This regionally extensive ash-flow tuff also has been used as a chronostratigraphic marker in many other mountain ranges in the eastern Mojave Desert of California and in western Arizona (Glazner and others, 1986). Published ages for the tuff range from 22 to 16 Ma. However, Nielson and others (1990) established an age of 18.5±0.2 Ma for the emplacement of the unit; they attributed the older reported ages to contamination by pre-Tertiary rocks and the younger ages to alteration or incomplete argon extraction during the dating process. The Peach Springs Tuff is exposed in discontinous patches in the Piute Range, Castle Mountains, Mid Hills, New York Mountains, Bristol Mountains, and Clipper Mountains and on the east side of the Providence Mountains (pl. 1).

Hackberry Mountain, Woods Mountains, and Wild Horse Mesa

The Hackberry Mountain and Woods Mountains areas are underlain by volcanic and sedimentary rocks predominantly of middle Miocene age (pl. 1). These rocks rest unconformably on an erosional surface of pre-Tertiary crystalline basement that locally includes paleotopographic relief in excess of 300 m (Bonura, 1984). Flat-lying mesas in the western Woods Mountains and eastern Providence Mountains are capped by a prominent ash-flow tuff. The rocks that make up the tuff originally were informally termed the Hole-in-the-Wall tuff by McCurry (1985) but later were renamed the Wild Horse Mesa Tuff by McCurry (1988) (unit Tw, pl. 1; see also fig. 28*B*). The tuff represents approximately 80 km^3 of metaluminous to weakly peralkaline magma erupted at 15.8 Ma (McCurry, 1988). This eruption apparently produced a shallow trap-door caldera roughly 10 km in diameter centered in the eastern Woods Mountains (see section below entitled "Geophysics"). Resurgent doming and eruption of rhyolitic flows and tuff largely filled the caldera; one flow has been dated isotopically at 14.8 Ma. The final eruptions in the area of Woods Mountains were basalt, basaltic andesite, and basanite flows, one of which has a whole-rock K-Ar age of 10.3 Ma. Minor lacustrine and alluvial sedimentary rocks are intercalated in the upper part of the volcanic sequences exposed there, but some lacustrine deposits are also present stratigraphically below the Wild Horse Mesa Tuff and above the Peach Springs Tuff of Young and Brennan (1974). Large-magnitude aeromagnetic and gravity anomalies coincide with the caldera (see section below entitled "Geophysics"). On the basis of geophysical modeling, McCurry and Hensel (1988) suggested that the anomalies are probably due to a buried pluton. Rhyolite flows and domes, breccias, and tuffs on the east side of Hackberry Mountain and in the Vontrigger Hills have not been dated isotopically, and the Tertiary rocks in this area are less well understood than those in the western Woods Mountains. A lacustrine unit composed of limestone, dolomite, and minor sandstone at the top of the Tertiary sequence at Hackberry Mountain overlies the silicic volcanic rocks and contains vertebrate fossils of Barstovian to Clarendonian age (McCurry, 1985). At Hackberry Mountain, the silicic rocks are made up of a high-K, trachyte-trachydacite-rhyolite association (McCurry, 1988). However, lacustrine rocks are also present near the base of the Tertiary sequence in the area of Wild Horse Mesa where their presence in areas of the thickest accumulations of the Wild Horse Mesa Tuff was used as evidence for the presence of a pretuff basin into which the tuff was deposited (McCurry, 1988).

Piute Range, Castle Mountains, and Castle Peaks

The sequences of Cenozoic rocks exposed in the Piute Range are similar to those in the Castle Peaks area, and they have been correlated by Nielson and others (1987, 1993) and Nielson and Nakata (1993). The rocks

in the Castle Mountains, although contemporaneous with rocks in the adjoining ranges, are dominated by rocks from a silicic volcanic center (fig. 29). These rocks thin rapidly to the east and west and apparently are not present in the Piute Range. Nielson and others (1987) divided the rocks of the Piute Range, which generally yield a smooth-sloped topography along much of the range (fig. 30), into two units. The lower unit consists of arkose and conglomerate that contain clasts derived from underlying pre-Tertiary basement in the Piute Range and possibly also from pre-Tertiary basement rocks exposed in the New York Mountains; basaltic andesite flows and breccias and some remnants of the Peach Springs Tuff of Young and Brennan (1974) are intercalated with the sedimentary rocks at the north end of the range. The upper unit consists of mafic lava flows and breccias, rhyolitic lava flows and tuffs, and interbedded alluvial sediments; a white tuff in the middle of the upper unit may be correlative with a similar tuff, which was first described by Miller and others (1986) in the general area of Castle Peaks but which is now known as the Wild Horse Mesa Tuff (Gusa and others, 1987).

The lower part of the exposed sequences of Tertiary rocks in the Castle Mountains comprises predominantly andesite underlain by what is probably the Peach Springs Tuff, thereby allowing correlation of these sequences with those in the Piute Range. Capps and Moore (1991), however, considered the basal tuff to be older than the Peach Springs Tuff, on the basis of the results of K-Ar ages of approximately 22 Ma that were obtained from the unit. The lower unit in the Castle Mountains has been folded into a broad, northeast-trending anticline (Turner and others, 1983; Turner, 1985). As much as 350 m of rhyolite flows, tuffs, and associated domes overlie the folded unit. The tuffs and rhyolites of this silicic volcanic center host most of the known mineralization in the Hart Mining District (see section below entitled “Tertiary Deposits”). The aggregate thickness of these silicic rocks apparently decreases rapidly to the south, west, and east, and they were not considered by Nielson and others (1987) to underlie the volcanic rocks of the Piute Range as Turner (1985) suggested. Geochronologic data reported by Turner (1985), Nielson and others (1987), Linder (1988), Ausburn (1988, 1991), and Capps and Moore (1991) are somewhat inconsistent but generally define a period of rhyolite, latite, and basalt volcanism that occurred from about 17 Ma to about 13 to 12 Ma in the Castle Mountains. The mineralization probably accompanied rhyolite-dome formation at about 15.5 Ma (Capps and Moore, 1991). An age of about 8 Ma (Nielson and others, 1987) on basalt from the Piute Range is the youngest age reported from the eastern part of the EMNSA.

Cima Volcanic Field

The volcanic rocks of the Cima volcanic field consist of more than 50 basalt cinder cones and numerous associated lava flows that overlie as much as 300 m of variably tilted Tertiary sedimentary rocks (pl. 1). The sedimentary materials were deposited nonconformably on, and are derived from, Cretaceous and older crystalline rocks (Wilshire and others, 1987). Eruptions of basalt in the area west of Cima Dome began as volcanism was waning elsewhere in the EMNSA. The majority of the flows associated with the Cima volcanic (basalt) field erupted between 7.6 Ma and the present, although an eruptive hiatus occurred between 3 and 1 Ma (Wilshire, 1988). The timing of the youngest flow has been estimated to be between 120,000 and 400 yr B.P. (H.G. Wilshire, written commun., 1991). All basalts in the field are alkalic, hypersthene- or nepheline-normative hawaiites or basanites (Wilshire, 1987). Study of Nd, Sr, and Pb isotopic compositions of hawaiites less than 1 Ma in age from the Cima volcanic field suggested that they were derived from a mantle source (Farmer and others, 1991). Wilshire and others (1988) discussed the possible origins of various types of xenoliths found in the Cima volcanic field.

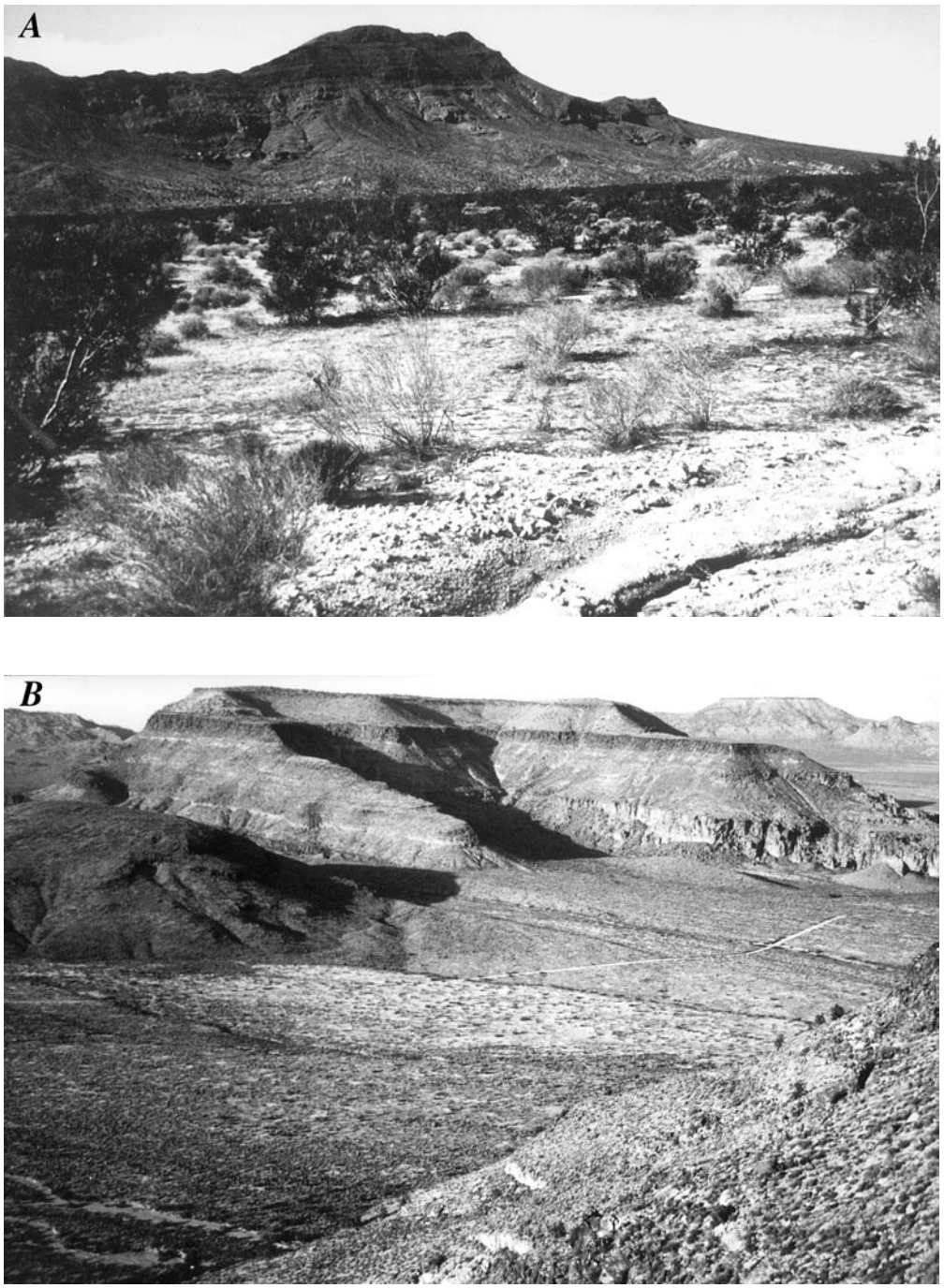

Figure 28. Tertiary volcanic sequences in East Mojave National Scenic Area, California. *A*, Volcanic sequence at Van Winkle Mountain (fig. 2). Light-colored tuffaceous rocks are capped by dark basalt lava flows. *B*, Wild Horse Mesa Tuff of McCurry (1988) in spectacular Wild Horse Mesa (fig. 2) with steep, eroded flanks. Hole-in-the-Wall lies to right of, and just beyond, mesa in upper right part of view.

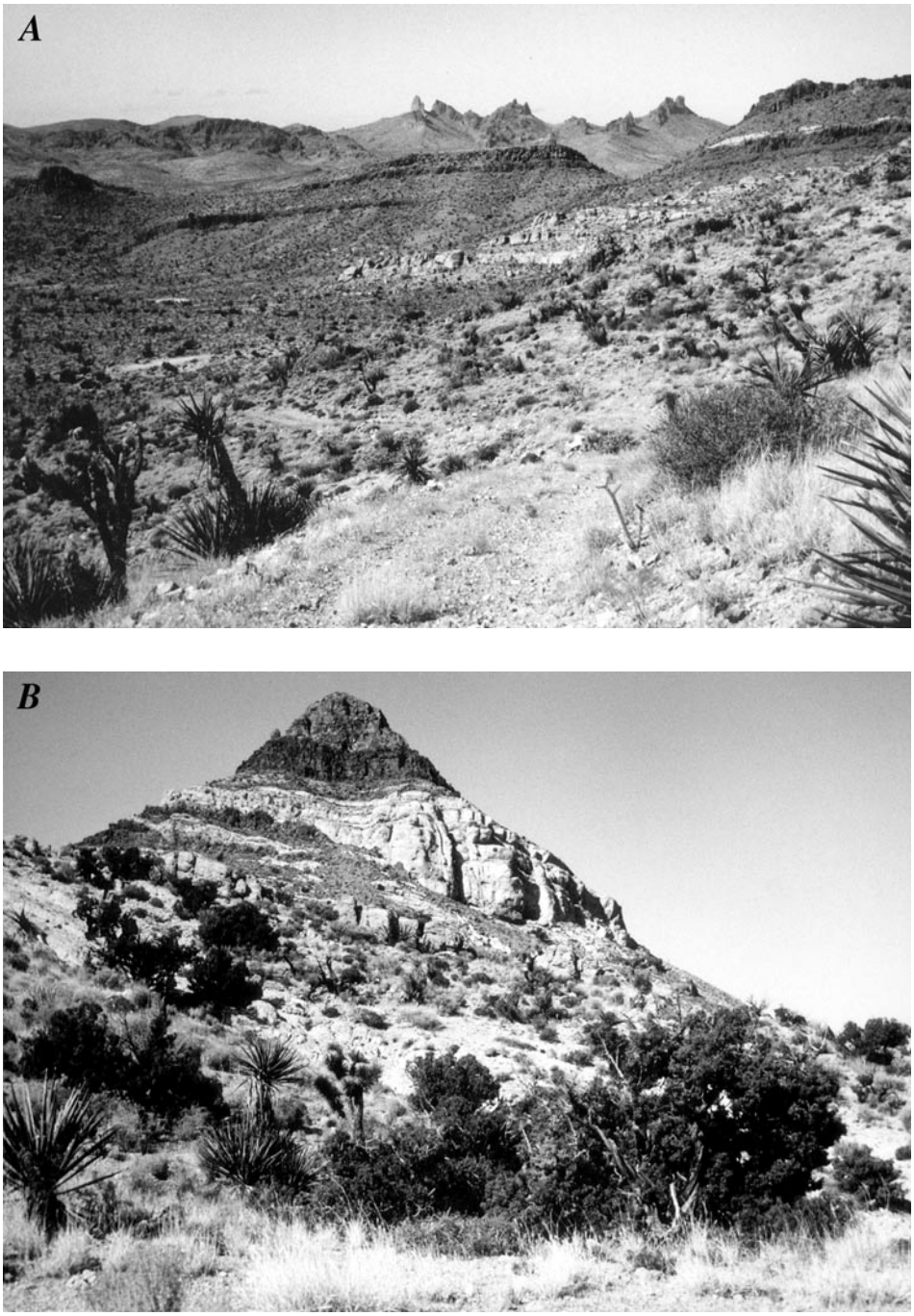

Figure 29. Silicic volcanic rocks in Castle Mountains (fig. 2), near northeast margin of East Mojave National Scenic Area, California. *A*, In foreground, light-colored ash-flow tuff approximately 13–12 Ma; slightly older rhyolitic rocks at Castle Peaks on skyline. *B*, Prominent peak capped by ash-flow tuff and underlain by dark basal vitrophere just below triangular top of peak. Sample collected at top of peak yielded 14 Ma date.

Figure 30. Smooth, rounded slopes of east-dipping Miocene andesite in Piute Range, East Mojave National Scenic Area, California.

Tertiary and Quaternary Deposits

By John C. Dohrenwend

Deposits of Tertiary and Quaternary age in the East Mojave National Scenic Area (EMNSA) include landslide and sedimentary-breccia deposits, gravel, playa and pluvial-lake deposits, and basaltic lava flows, cinder cones, cinder deposits, and vent basalt (pl. 1). Quaternary deposits include eolian sand, alluvial fan deposits, playa and pluvial-lake deposits, basaltic lava flows, cinder cones, and cinder deposits.

General compositions of piedmont deposits in the EMNSA are delineated on plate 3, as are source areas for many alluvial fan deposits. This map was prepared from analysis of geometrically rectified Landsat Thematic Mapper (TM) image data, which was processed by R.G. Blom and R.E. Crippen of the Jet Propulsion Laboratory, Pasadena, California, using the following data: (1) Landsat 5, Path 39, Row 36, Quads 1 and 2 (acquired 12/12/84), and (2) Landsat 5, Path 39, Row 35, Quad 3 (acquired 1/10/85). Midwinter, low-sun-angle scenes were used to maximize topographic expression. Individual spectral bands were adjusted for path (atmospheric) radiance and sensor calibration. These data were then ratioed (bands 3:1 to emphasize ferric-iron variations, bands 5:4 to emphasize ferrous-iron variations, and bands 5:7 to emphasize hydroxyl-carbonate variations), and the resulting band-ratioed images were scaled for approximately 1 percent saturation at range extremes. The achromatic component of the TM data was computed by averaging bands 3, 4, 5, and 7, edge enhancing with a high pass 5×5 box filter, and then merging by component multiplication with each of the three band-ratioed images. Ratioed bands were combined as false-color composites where 5:7 is displayed as red, 5:4 is displayed as green, and 3:1 is displayed as blue. The resulting false-color composite images maximize compositional discrimination while at the same time retaining topographic and structural information within the merged achromatic component.

Compositional boundaries in piedmont areas were delineated on the basis of abrupt changes in color and texture on 1:100,000-scale Landsat TM images (pl. 3). Drainage divides within the ranges were mapped from 1:100,000-scale, 50-m contour maps. Compositional information was inferred from mapped bedrock lithologies exposed in these source areas (pl. 1). The most extensively exposed bedrock lithologies within a given upland source area were inferred to make up the predominant lithologic component of surface deposits on the associated piedmont surface; these dominant lithologies are shown in red boldface type on plate 3. The false-color composite image of the Providence Mountains (fig. 31*A*) shows notable contrasts in the lithologic components of alluvial deposits on the flanking piedmont surfaces. This particular figure illustrates well the spatial distribution of uniform color responses within the band-ratioed images that were used to delineate the compositional boundaries (compare fig. 31*A* with fig. 31*B*, the geologic map of the same area).

Pediments and areas of thin late Tertiary and Quaternary alluvial cover within the EMNSA also are shown on plate 3—alluvial deposits exceeding approximately 300 m in thickness are on the hachured side of a red boundary line. Contacts between range front and piedmont contacts were delineated on the basis of abrupt transitions between areas of little shadow and smooth texture (piedmonts) and areas of abundant shadow and coarse texture (uplands). These interpretations were supplemented by stereoscopic-photogeologic observations made from high-altitude U-2 Color IR photography. Areas of pediments and thin alluvial deposits were estimated from interpretation of the distribution of planar areas of exposed bedrock (including some areas of deformed Tertiary sedimentary rocks), small residual bedrock knobs, and inselbergs (as inferred from analysis of enhanced TM imagery, aerial photography, and available geologic mapping). These features are particularly abundant in the following areas (from north to south): intermontane valleys and piedmonts adjacent to the hills near Halloran Spring; piedmont areas within and surrounding the Cima volcanic field and Cima Dome; the north margin of Lanfair Valley; intermontane valleys and piedmonts along the east flank of the Mid Hills; the piedmonts adjacent to the east and south flanks of the Piute Range; the piedmonts surrounding the Woods Mountains, Hackberry Mountain, the Vontrigger Hills, and Homer Mountain (approximately 5 km east of the EMNSA); and the southern piedmont of the Granite Mountains. Extensive areas of thick basin-filling deposits are apparently limited to parts of Ivanpah Valley, Fenner Valley, and the valley occupied by Kelso Wash (the area of the Devils Playground).

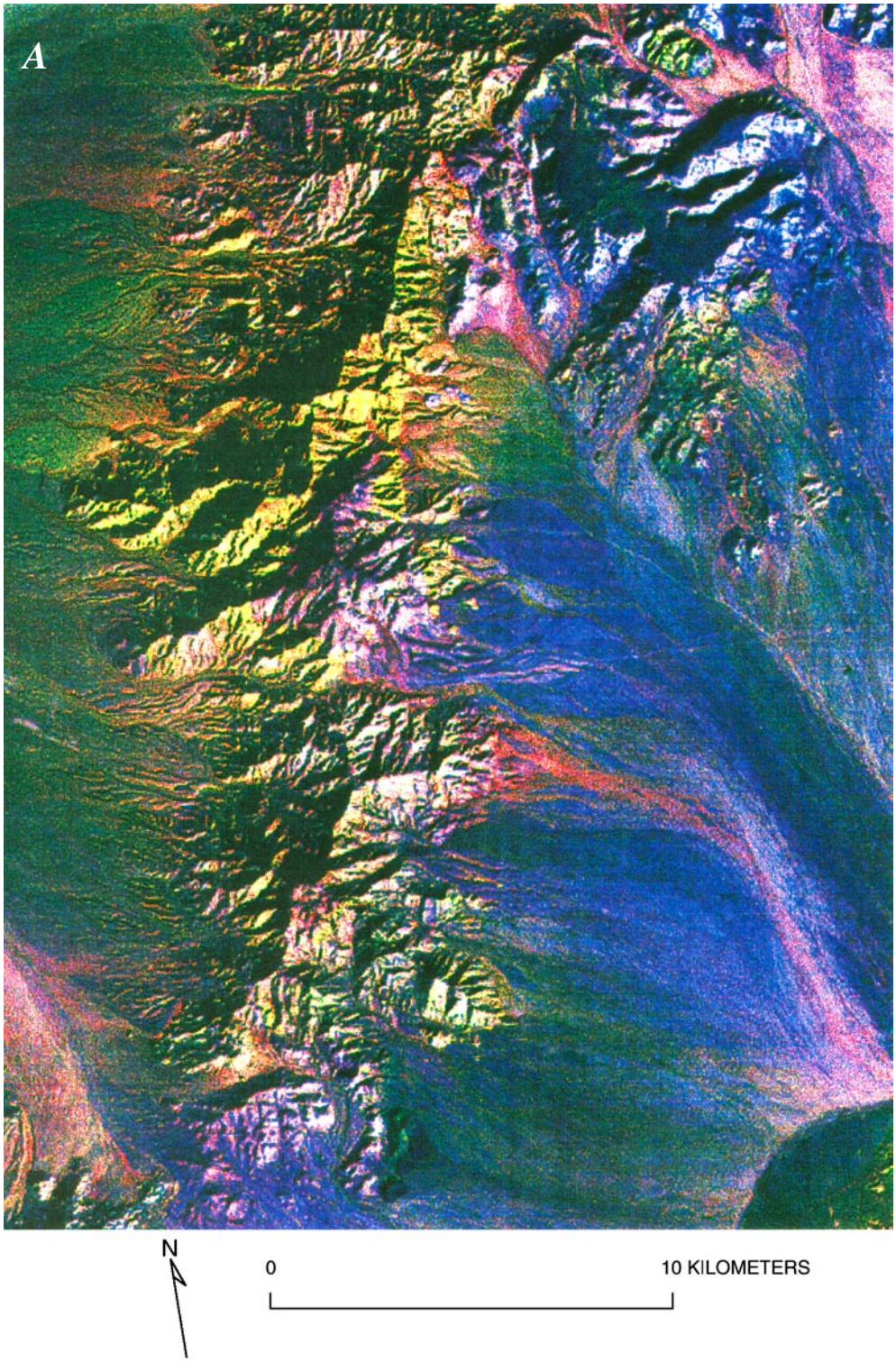

Figure 31. Compositional domains on piedmonts adjoining Providence Mountains (fig. 2), East Mojave National Scenic Area, California. *A*, Satellite image of Providence Mountains and adjacent piedmonts (from Landsat 4 Thematic Mapper, Scene 40149–17441, Path 39, Row 36; acquired 12/12/84). Image enhanced to emphasize lithologic compositions of piedmont deposits and source areas from which they were derived. Individual spectral bands were corrected for atmospheric absorption and scattering, as well as for variations in scanner sensitivity. Differences between spectral bands were then calculated and presented as false-color composite image, using following ratios: red, band 5:7; green, band 5:4; and blue, band 3:1. *B*, Geologic map of same area as 31*A*, showing geology of bedrock areas and predominant composition of piedmont deposits.

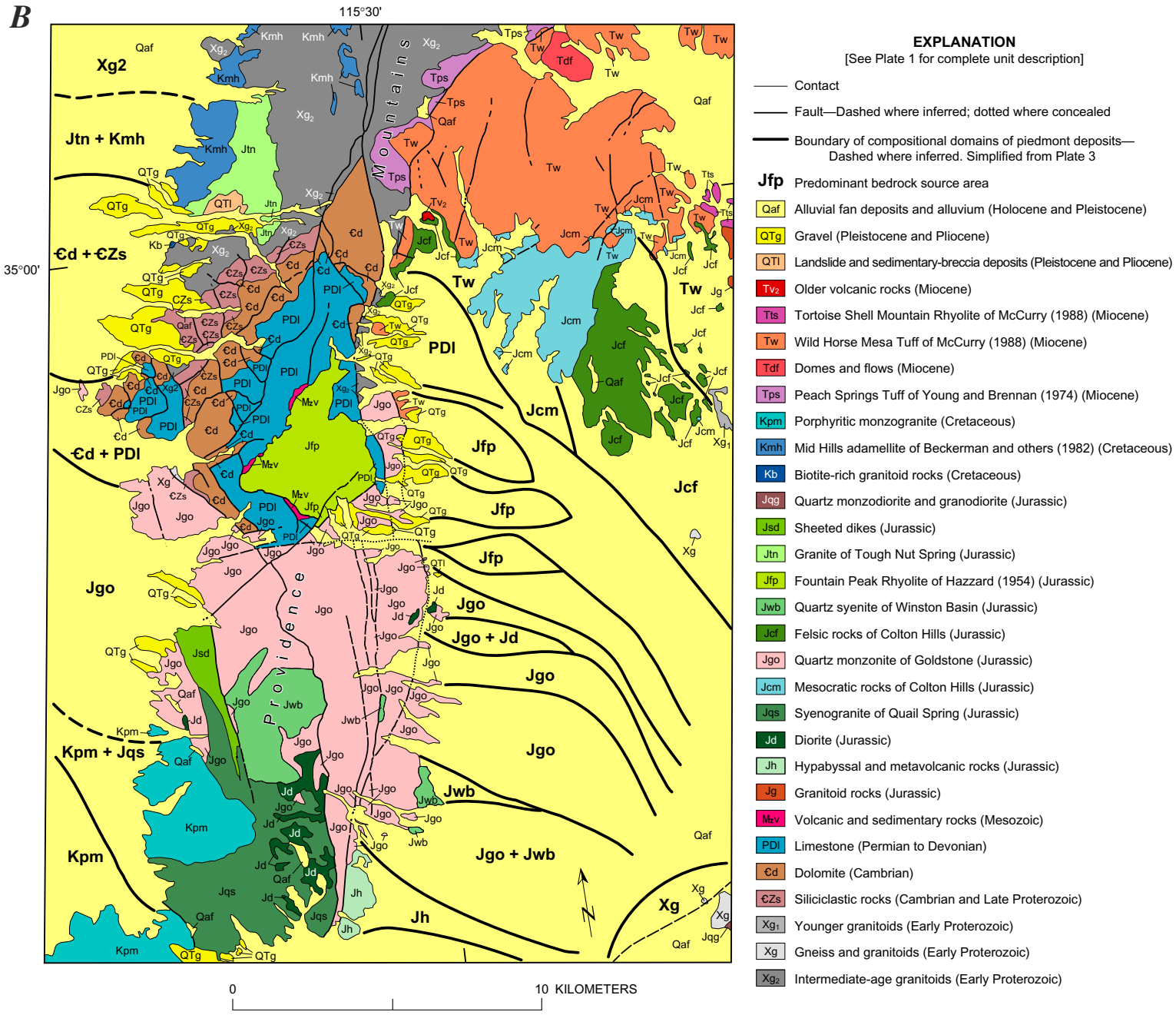

Figure 31. Compositional domains on piedmonts adjoining Providence Mountains (fig. 2), East Mojave National Scenic Area, California. *A*, Satellite image of Providence Mountains and adjacent piedmonts (from Landsat 4 Thematic Mapper, Scene 40149–17441, Path 39, Row 36; acquired 12/12/84). Image enhanced to emphasize lithologic compositions of piedmont deposits and source areas from which they were derived. Individual spectral bands were corrected for atmospheric absorption and scattering, as well as for variations in scanner sensitivity. Differences between spectral bands were then calculated and presented as false-color composite image, using following ratios: red, band 5:7; green, band 5:4; and blue, band 3:1. *B*, Geologic map of same area as 31*A*, showing geology of bedrock areas and predominant composition of piedmont deposits—Continued.

Development of Pediment Domes

By John C. Dohrenwend

Large, well-developed bedrock domes form the crest of the Ivanpah Upland of Hewett (1956), a broad irregular highland that forms the south and west flanks of Shadow Valley in the north-central part of the East Mojave National Scenic Area (EMNSA) (fig. 32; see also Dohrenwend, 1988). More than 60 late Cenozoic lava flows of the Cima volcanic field, which cover large areas on the crests and flanks of these domes, record a 7.5-m.y. history of pediment-dome evolution in this area. Comparison of the relative positions of lava-flow-covered pediment remnants and modern pediment surfaces indicates the following: (1) downwearing has been the dominant mode of dome modification since at least latest Miocene time; (2) downwearing rates have been highest in crestal areas, have progressively decreased downslope, and have been significantly influenced by general base-level differences; and (3) the general form of the domes has changed little during the last 5 to 7.5 m.y. The ages of the youngest rock units that are truncated by these domes and of the oldest lava flows that overlie them indicate that they formed rapidly during a 3.5-m.y. interval of the late Miocene and have been a conspicuous landscape element in the general area of Shadow Valley since that time. No apparent mineralization is associated temporally with bedrock domes in the EMNSA.

Eleven bedrock domes have been more or less continuously evolving in the Ivanpah Upland over the past several million years, and the remnants of at least three other domes have been partly buried and preserved by lava flows of the Cima volcanic field (fig. 32). Although termed "domes," these landforms are more conical than domelike in cross section (Sharp, 1957), having slopes that typically vary by less than ±0.75° along any radial profile. The domes are low (0.1–0.4 km high), broad (5–16 km across), and, therefore, gently sloping (1.5° to 4.5°) (fig. 33). Although in places interrupted by inselbergs, surfaces are generally smooth and regular, and local relief is commonly less than 5 m. Locally, networks of shallow drainageways have incised these surfaces into irregular patchworks of dissected and undissected areas. Undissected areas are mostly flat, having anastomosing drainageways and indistinct interfluves; dissected areas are scored by shallow, subparallel valleys separated by low, rounded interfluves.

These pediments have been the subject of several geomorphic analyses (Davis, 1933; Sharp, 1957; Warnke, 1969; Oberlander, 1974; and Dohrenwend and others, 1987). Davis (1933) speculated that Cima Dome, the largest of these domes (fig. 32), was formed primarily by the backwasting of bounding scarps on an upfaulted terrain of low relief. Sharp (1957) explained Cima Dome and adjacent domes as the product of upwarping of an ancient erosion surface combined with subsequent erosional modification and regrading. Warnke (1969) argued that downcutting followed by lateral corrosion and backwasting were the most important processes of pediment formation and concluded that the combined presence of suitable rock types, specifically granitic rocks and their sedimentary derivatives, and a temporary local base level is the principal determinant of pediment formation in this area. Oberlander (1974) interpreted the present pediment domes as relict forms produced by erosional stripping of deeply weathered terrains developed during periods of greater effective moisture. Dohrenwend and others (1987) documented a latest Tertiary and Quaternary history of essentially continuous downwearing. Rates of downwearing have been greatest in crestal areas and have progressively decreased downslope to midflank areas, which have remained in a state of approximate topographic equilibrium.

As all these workers have observed, the distribution of pediments in the Ivanpah Upland is largely controlled by lithology. Most pediment surfaces cut indiscriminantly across both Mesozoic granitic rocks of the Teutonia batholith (pl. 1) and Tertiary terrigenous clastic rocks, whereas inselbergs of Proterozoic metamorphic rocks stand as much as 180 m above these surfaces. At least three separate Cretaceous plutons probably are present within the area of the Cima volcanic field, and these rocks are intruded by swarms of Tertiary dikes (Wilshire, 1988). The plutonic rocks are typically deeply weathered; low-energy seismic measurements indicate pervasive subsurface weathering to depths in excess of 40 m (K.D. Mahrer, written commun., 1985; see also Dohrenwend and others, 1987) . The Tertiary sedimentary rocks vary in composition from clastic materials derived mainly from Teutonia granitic sources to those derived mainly from Proterozoic metamorphic sources, including gneisses and carbonate, and granitic and volcanic rocks. These rocks consist of gravel, fine-grained

sandstone, siltstone, and claystone; generally near the base, coarse avalanche breccias and extremely coarse debris-flow deposits; and, in places, gravity-slide blocks (as much as 0.5 km across) of various breccias, including abundant clasts of dolomite. These materials were deposited in several steep-sided basins. Locally, they are significantly deformed, having dips as steep as 70° NE. to SSE. Relief on their contact with the Cretaceous granitic rocks locally exceeds 150 m (Sharp, 1957; Wilshire and others, 1987). Lithologic, biostratigraphic, and paleomagnetic correlations suggest an 18.5- to 9-Ma age for these rocks (Reynolds and Nance, 1988).

Available K-Ar ages indicate three principal periods of late Cenozoic volcanic activity in the Cima volcanic field (Dohrenwend and others, 1984; Turrin and others, 1984, 1985). The earliest period, dated at between 7.5±0.2 and 6.5±0.2 Ma, is represented by one small, deeply eroded vent-and-flow complex in the southeast corner of the field. Lavas of the latest period, which spans the last 1.1 m.y. of Quaternary time, were confined to the southern part of the field and flowed generally west and southwest toward Soda Lake Valley. An intermediate period, dated at between 5.1±0.2 and 3.3±0.1 Ma, was the longest and most volumetric. Flows of this period form the northern part of the field and are the most significant lavas in the present discussion.

Flows of the intermediate period form mesa caprocks that preserve remnants of the pediment surfaces that flanked the west side of Shadow Valley in latest Miocene and early Pliocene time. North of Interstate 15, flows were erupted between 5.1±0.2 and 4.2±0.2 Ma from several vents. At least five flows moved southwest down shallow valleys toward Soda Lake valley and northeast toward Shadow Valley. South of Interstate 15, more voluminous flows were erupted between 4.8±0.2 and 3.3±0.1 Ma from at least 16 vents. These flows, including several overlapping and superimposed lava sheets, were erupted near the crest of a large bedrock dome. The lava sheets spread east and northeast across the dome's east flank toward Shadow Valley and south to southeast toward what is now the Quaternary part of the Cima volcanic field. In addition, several smaller flows extended west and southwest toward Soda Lake valley down valleys between several small pediment domes along the west edge of the field (pl. 1).

Comparing differences in height between the late Tertiary erosional surfaces buried by these lava flows and adjacent modern pediment surfaces enables the reconstruction of a detailed 5-m.y. history of pediment evolution in the Ivanpah Upland. Topographic relations demonstrate that the Cima lava flows have been erupted into a continually downwearing, erosional environment that has been active since before inception of the volcanism. Progressively younger flows have buried progressively lower surfaces so that each caprock-protected pediment remnant now stands above the modern surfaces at a height that is directly related to the age of its overlying basalt flow (Dohrenwend and others, 1987).

Average downwearing rates, determined from the height differences between lava-flow-covered and modern surfaces, have been strongly influenced by distance from dome crests and general base-level elevations. On pediments sloping toward Soda Lake Valley, where the basin floor elevation is about 280 m, average downwearing rates have ranged between 1.2 and 2.8 cm/10^3 yr on upper flanks and between 0.0 and 0.4 cm/10^3 yr in midflank areas. Lower flanks have probably aggraded to some extent (Dohrenwend and others, 1987). On pediments sloping towards Shadow Valley, where the axial elevation is 1,100 to 1,200 m, average downwearing rates have ranged between 0.5 and 0.9 cm/10^3 yr on upper flanks and between 0.0 and 0.3 cm/10^3 yr in midflank areas. Thus, downwearing has been greatest in crestal and upper-flank areas and has progressively decreased downslope so that overall pediment degradation, in areas unprotected by resistant caprocks, has followed a general pattern of crestal lowering, upper-slope decline, and midslope stability. Also, as might be expected, average downwearing rates have been substantially greater on those pediments that drain westward to the relatively low basin floor of Soda Lake Valley than on those that drain eastward toward the much higher level of Shadow Valley. However, even the most rapid of these rates indicate relatively little landscape change during the past 5 m.y., no more than 50 m of downwearing in crestal and upper-slope areas and little to no change in midslope areas.

Relations among the pediment surfaces of the Ivanpah Upland, the rock units truncated by these surfaces, and the lava flows that overlie them indicate that these surfaces formed rapidly during the late Miocene and have been a conspicuous landscape element in the Shadow Valley area since that time. The oldest basalt flows that cap an extensive pediment surface have been dated by K-Ar methods at 5.1±0.2 Ma (Turrin and others, 1985), and the age of the truncated terrigenous clastic rocks has been estimated on the basis of biostratigraphic and

paleomagnetic correlations at approximately 11 Ma (Reynolds and Nance, 1988). Therefore, dome formation occurred between 11 and 5 Ma. Moreover, limited occurrences of lava flows as old as 7.5±0.2 Ma that lie at or very close to the levels of both modern and remnant latest Miocene pediment surfaces suggest that these surfaces may have been in existence before 7.5 Ma. Thus, the bedrock domes of the Ivanpah Upland likely formed within a period of less than 3.5 m.y.

For those few instances in the Basin and Range Province where field relations have permitted estimates of average long-term rates of range-front retreat and pediment formation, estimates reach a maximum of 1 km/10^6 yr (Wallace, 1978; Menges and McFadden, 1981; Saunders and Young, 1983; Dohrenwend, 1987). However, formation of the large bedrock domes of the Ivanpah Upland in the EMNSA by slope retreat would appear to require rates of at least 1.5 to perhaps as much as 3.5 km/10^6 yr. Thus, it would appear that either general slope retreat proceeded at a significantly faster rate in this area than elsewhere in the Basin and Range Province or that some other process, or combination of processes, was responsible for the formation of these bedrock domes.

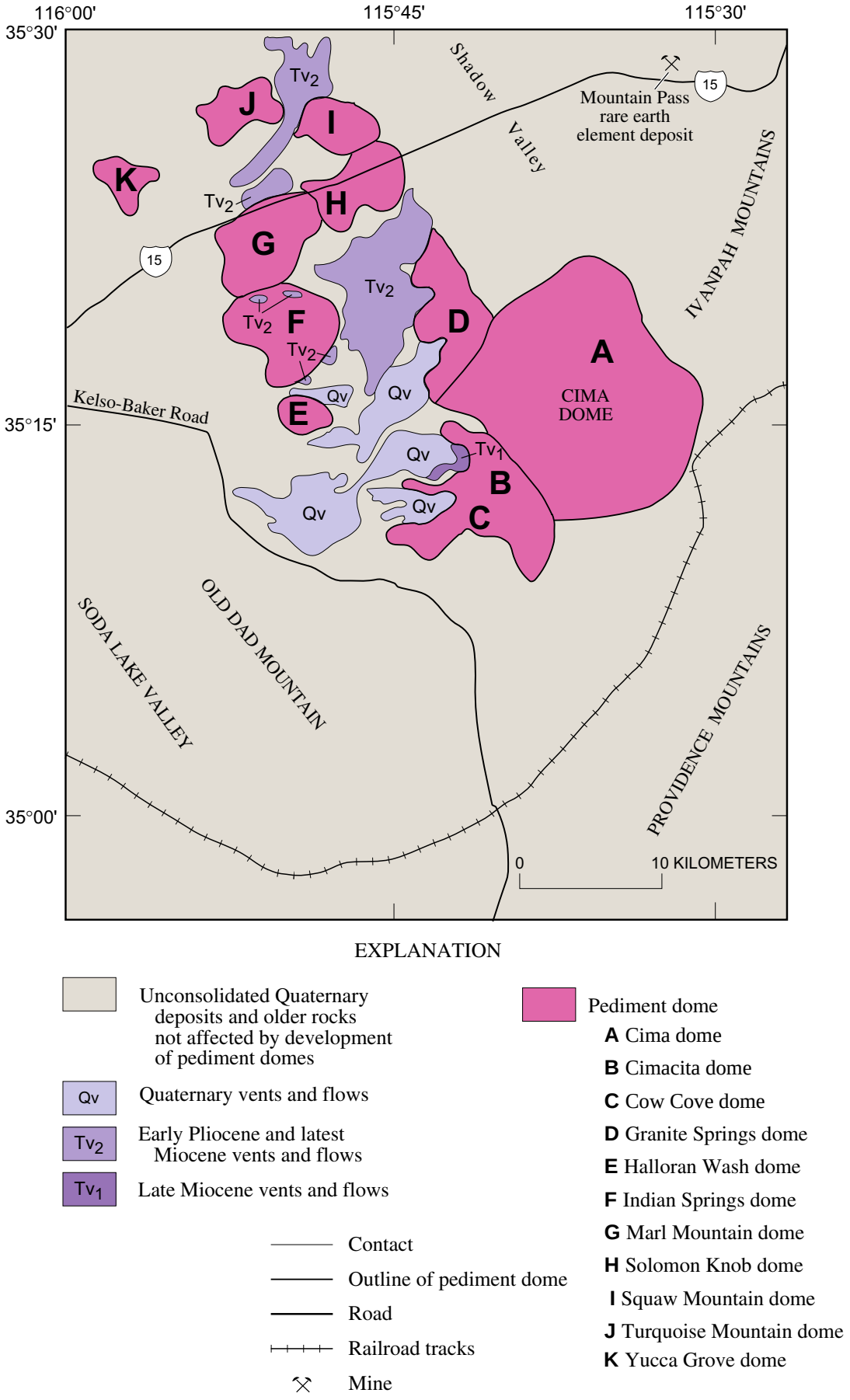

Figure 32. Generalized geologic map of Cima volcanic field, East Mojave National Scenic Area, California, showing locations of major bedrock domes and pediment domes (from Dohrenwend, 1988).

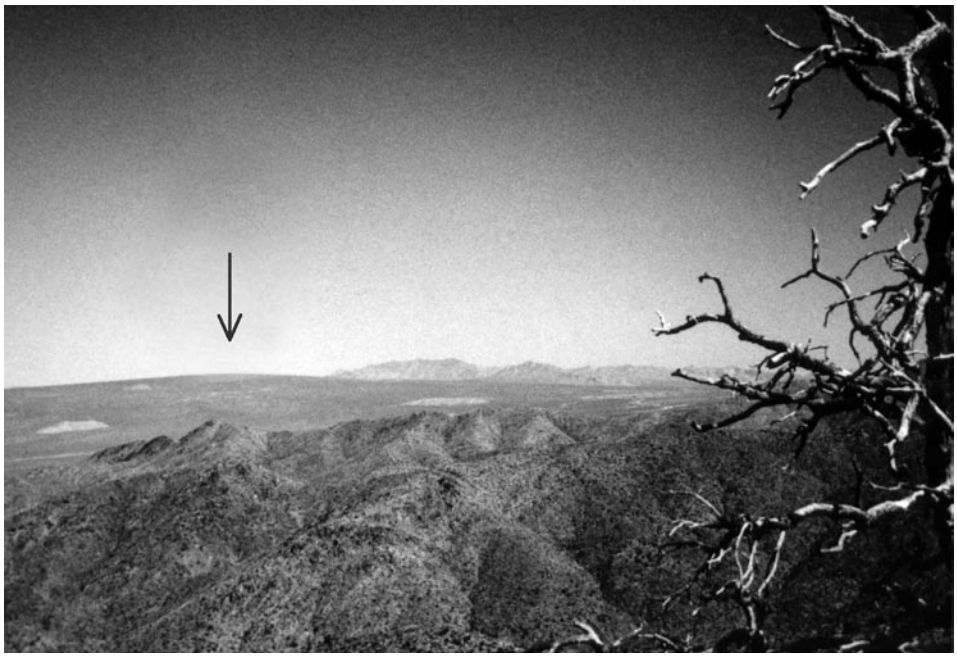

Figure 33. Cima Dome (at head of arrow), East Mojave National Scenic Area, California. Ivanpah Mountains form skyline on right. View to west from New York Mountains (fig. 2).

Geophysics

By John D. Hendricks

Geophysical studies conducted within the East Mojave National Scenic Area (EMNSA) include gravity and aeromagnetic surveys on a regional scale, local electrical (induced polarization, telluric, and audio magnetotelluric) traverses, a limited number of heat-flow measurements, and airborne radiometric measurements. Each of these methods has a particular application in assessing the mineral potential of the area.

In general, gravity anomalies, when analyzed for regions the size of the study area, will yield information about (1) the rock-density distribution within the crust, (2) the isostatic state of the region, and (3), when combined with other geophysical data, the nature of the lower crust and upper mantle. Although the isostatic state and nature of the lower crust and upper mantle are important in understanding the genesis of mineral deposits in a region, they do not have a direct application to the resource potential in the upper crust. In order to eliminate the gravitational effects arising from deep sources, the isostatic anomaly (Jachens and Griscom, 1982) will be used in describing gravity anomalies in the EMNSA.

In contrast to gravity anomalies, magnetic anomalies arise strictly from sources in the upper crust and, in this part of the Basin and Range Province, represent susceptibility contrasts of less than about 15 km in depth. Magnetic variations result primarily from differences in magnetite content and in the inherent or remanant magnetization of a particular rock body. Analysis of the magnetic patterns in the study area are helpful in delineating buried contacts between varying rock units, the location and attitude of fault zones, the depth to basement beneath sedimentary cover, and, at least in one case, the presence of substantial iron and iron-related deposits.

Electrical traverses have been conducted in the Providence Mountains (Miller and others, 1985; Goldfarb and others, 1988) to delineate the extent of alteration and sulfide mineralization along the East Providence and Bighorn fault systems (pl. 1).

Heat-flow measurements obtained within the EMNSA are part of a broad regional survey of the southern Basin and Range Province (J.H. Sass and others, unpub. data, 1990). When viewed over a large area, the EMNSA shows values in the range of about 80 to 100 mW/m^2 (milliwatts per square meter), which are fairly typical of the region. Heat-flow measurements are important to an understanding of the thermal history of the region. However, currently available spacing of the individual measurements does not allow us to make direct comparisons with individual geologic features.

Airborne radiometric measurements were conducted throughout the region as part of the National Uranium Resource Evaluation Program (NURE). These measurements are sensitive to concentrations of U, K, and Th. Results of this survey are discussed in the subsection below entitled "Aerial Gamma-Ray Surveys."

Gravity Survey

Gravity data for the EMNSA and surrounding areas were obtained from Snyder and others (1982), Miller and others (1986), and Mariano and others (1986). The observed gravity data were reduced to the free-air anomaly. Bouguer, curvature, and terrain corrections, using a density of 2.67 g/cm^3, were added to obtain the complete Bouguer anomaly. To eliminate that part of the Bouguer field that arises from deep sources, a regional field was subtracted from the Bouguer anomaly using the method described by Jachens and Griscom (1982). The resulting isostatic anomaly (pl. 4) will be used below in the description of specific gravity features.

A relatively straightforward relation exists between the isostatic anomaly and rock types mapped within the study area (pl. 4). In general, isostatic "highs" are present in areas consisting predominantly of Proterozoic metamorphic rocks and Jurassic granitoids; intermediate values, in regions of Cretaceous plutonic rocks; and "lows," in areas of thick deposits of Tertiary volcanic rocks and Tertiary and Quaternary surficial deposits. Density measurements presented by Miller and others (1986) and Wilshire and others (1987) indicate, from samples collected in the New York Mountains and Cinder Cone lava beds area, that Proterozoic schist and gneiss average 2.674±0.07 g/cm^3; Mesozoic intrusive rocks (adamellite or monzogranite and granite), 2.60 ±0.02 g/cm^3; and unspecified Tertiary volcanic rocks, a wide range that averages 2.456±0.40 g/cm^3. In addition, two samples of Proterozoic amphibolite have densities of 2.96 and 3.10 g/cm^3.

Magnetic Survey

Data used to produce the aeromagnetic map (pl. 5) were collected during three separate surveys: in California, (1) the Kingman-Trona area (U.S. Geological Survey, 1983) and (2) the Needles 1° × 2° quadrangle (U.S. Geological Survey, 1981); and in Nevada, (3) part of the Kingman 1° × 2° quadrangle (Oliver and others, 1986). In all of these surveys, a flight height of 1,000 ft (304 m) above average terrain was employed. Because of the irregularity of the local topography, however, the actual height above ground varied from about 400 ft (122 m) to 2,500 ft (762 m) (Miller and others, 1986). In the California surveys, flight-line spacing was 0.5 mi (0.8 km), whereas spacing averaged 1.0 mi (1.6 km) in Nevada. The California and Nevada surveys have been merged to eliminate any effects caused by the differing survey parameters. The standard (uniform) Earth's magnetic field has been subtracted from the observed measurements to yield the residual-magnetic field.

Within the EMNSA, regions show diverse residual-magnetic characteristics (pl. 5). These regions generally fall into three types of magnetic patterns: (1) low-amplitude (>200 nanoTesla (nT)), low-gradient highs and lows, (2) intermediate- to large-amplitude (200–500 nT), intermediate-gradient highs and lows, and (3) intermediate-amplitude (100–300 nT), steep-gradient complex anomalies. In general, these three anomaly patterns can be related to rock type or geologic environment. Type-1 patterns correspond to alluvium-filled valleys and areas of predominantly Cretaceous granite; type-2 anomalies correlate with exposures of Proterozoic metamorphic rocks and Jurassic granitoids; and type-3 anomalies are present in areas that comprise mostly Tertiary and Quaternary, mafic to silicic lava flows, vents, and pyroclastic materials. The magnetic signature of a region not only depends on the magnetic character of the rocks but also the depth to the source. For example, in a deep basin the basement rocks may be quite magnetic, but, because of the increased distance between sensor and source and the nonmagnetic character of the intervening basin fill, the amplitudes and gradients of anomalies will be reduced and the magnetic signature may be quite different from areas where similar source rocks are near the surface. Two isolated magnetic anomalies of particular note in the EMNSA are associated with the Vulcan iron-skarn deposit and the Woods Mountains caldera (McCurry, 1988).

Discussion of Gravity and Magnetic Anomalies

Interpretation of the gravity and magnetic maps (pls. 4 and 5, respectively) are summarized from a series of relatively recent U.S. Geological Survey Wilderness Bulletins and Miscellaneous Field Studies Maps. Interpretations included in four additional geologic and geophysical studies pertaining to the region also contributed significantly to this report (Carlisle and others, 1980; Beckerman and others, 1982; DeWitt and others, 1984; McCurry, 1988). Although these studies are for the most part not adjoining, they do cover a large part of the area, and so the geophysical interpretations can be projected across intervening regions. In addition to this summary of previous work, a brief discussion of the gravity and magnetic characteristics of the southern Clark Mountain Range and Woods Mountains caldera is presented.

Ivanpah Valley and New York Mountains

Isostatic-gravity values range from a high of about –12 mGal over the central New York Mountains to a low of –40 mGal in the Ivanpah Valley (pl. 4). The highest values are associated with outcrops of Proterozoic schist and gneiss, whereas the lowest values are present over unconsolidated basin-fill materials in Ivanpah Valley. The thickness of alluvium in Ivanpah Valley is in excess of 1,980 m, as shown by cuttings and drill-hole logs from the Ivanpah Partnership "Ivanpah 13" drill hole (Hodgson, 1980). On the basis of detailed gravity, magnetic, and seismic surveys (Carlisle and others, 1980), the maximum sediment thickness is about 2,440 m on the east side of the valley. The north-northwest-striking Ivanpah fault cuts across the valley from the vicinity of Mountain Pass to the general area of the Vanderbilt Mine (pl. 2). Seismic information provided by Carlisle and others (1980) suggested that vertical offset is approximately 366 m in the center of the valley near the Morningstar Road (pl. 1). The series of northwest-striking faults in the area of the Vanderbilt Mine generally correspond to a change in the type of basement rocks from Proterozoic schist and gneiss on the northeast to the informally named, Cretaceous Mid Hills adamellite of Beckerman and others (1982) (unit Kmh, pl. 1) on the southwest. This change is marked by a steep gravity gradient, decreasing to the southwest, that has

a variation of about 20 mGal. Gravity values also decrease toward the south and southeast from the northern New York Mountains, attributed to a southward-thickening wedge of volcanic rocks, gravel, and alluvium that cumulatively attain a thickness of a few thousand feet in Lanfair Valley (Miller and others, 1986). A gravity decrease that is present between the north-central part of the New York Mountains and the town of Nipton cannot be explained by examination of surface exposures. This decrease is probably due to an unexposed felsic intrusion of unknown age or perhaps thrust faults or detachment faults that penetrate Proterozoic basement and juxtapose Proterozoic rocks over Tertiary basin fill (Miller and others, 1986). However, Proterozoic rocks are not known to be thrust over Tertiary rocks in any of the mountain ranges of the EMNSA.

Magnetic-anomaly values in this area range from highs of slightly more than +200 nT to lows in excess of –200 nT. Anomalies over Proterozoic rocks are broad, having amplitudes of about 100 nT. Three such positive anomalies are present in the Ivanpah Valley. Two of them, in the southwestern and southeastern part of the valley, are roughly circular; Carlisle and others (1980) suggested that the tops of the sources are approximately 975 m below the surface, which would place these tops beneath the interface between basement and sedimentary deposits. The third is a positive ridge that trends north along the west side of the valley. Depth-to-source estimate for this anomaly is 1,738 m (Carlisle and others, 1980). The magnetic signature in areas of exposed Proterozoic rocks suggests that metamorphism or hydrothermal alteration has affected the magnetite content of the rocks (Miller and others, 1986). The positive anomalies in Ivanpah Valley may, therefore, represent relatively unaltered Proterozoic basement sources. Volcanic rocks exposed along the southeast margin of the New York Mountains near Barnwell (pl. 1) produce high-amplitude, short-wavelength anomalies, which indicate strongly the magnetic character of the rocks. In the New York Mountains, a change from Proterozoic schist and gneiss on the northeast to Cretaceous adamellite on the southwest corresponds to a down-to-the-northeast magnetic gradient. This change in magnetic intensity corresponds, but is opposite in sense, to the gravity gradient discussed earlier, which would imply that the Mid Hills adamellite is less dense, but more magnetic, than the adjacent Proterozoic metamorphic rocks. The reduced magnetic character of the Proterozoic rocks may reflect extensive alteration of magnetite in these rocks. However, the reduced magnetic character could also result from either metamorphism under low-oxygen-fugacity or reducing conditions or, perhaps, high-sulfur-fugacity conditions such that most of the iron is tied up in iron-magnesium silicates or pyrite rather than magnetite (D.A. John, written commun., 1993).

Lanfair Valley and Piute Range

The Lanfair Valley and Piute Range area is characterized by large magnetic anomalies and a relatively flat isostatic-gravity field. A northeast-trending belt of positive magnetic anomalies extends from Fenner Valley on the southwest through the Vontrigger Hills and southern Piute Range, terminating some 6 mi (10 km) east of the central Piute Range. An apparent westerly oriented arm of this pattern connects the Grotto Hills and Lanfair Buttes region to the central part of the northeast-trending belt of positive anomalies. These positive anomalies correlate well with outcrops of Proterozoic crystalline rocks. Southeast of this magnetic ridge is an area consisting primarily of Mesozoic granitic rocks in the Signal Hill and Homer Mountain areas. The region here is characterized by a series of magnetic lows. The contact between these two units is largely concealed beneath volcanic and alluvial deposits of the southern Lanfair Valley and may correspond to the abrupt magnetic change between the magnetically high and low areas (Nielson and others, 1987). The northern Piute Range and Castle Mountains contain extensive volcanic vents and associated rocks, and the magnetic field shows a number of sharp, large-amplitude highs and lows. In the vicinity of Hart Mining District (pl. 2), near the northeast corner of the EMNSA, the magnetic field is fairly subdued, although this area also contains extensive volcanic materials similar to those exposed in the Piute Range. The relatively smooth magnetic field here may represent a topographic effect because the area is lower and not as rugged as the Piute Range; this results in a more constant survey height. Alternatively, highly magnetic volcanic vents may possibly be absent in the immediate vicinity.

The isostatic-gravity field in this region is relatively smooth, showing a general decrease into Lanfair Valley. On the basis of one station, low closure of about 5 mGal over the Lanfair Buttes probably represents a sequence of alluvial and volcanic materials as much as 1 km thick. A similar anomaly is present near the junction of Ivanpah and Hart Mine roads (pls. 4 and 5). Small gravity highs are present over the Vontrigger Hills and south

of the Grotto Hills. These anomalies probably represent the thinning or absence of Cenozoic sedimentary or volcanic cover.

Mid Hills, Providence Mountains, and Southern Providence Mountains

In the New York Mountains and northern Mid Hills, gravity and magnetic anomalies are relatively smooth and flat (pls. 4, 5), thereby highlighting the overall uniform character of the informally named Mid Hills adamellite of Beckerman and others (1982). South of Cedar Canyon, however, both gravity and aeromagnetic maps show large changes and numerous closures, reflecting the mixture of Proterozoic metamorphic rocks, Mesozoic intrusions, Tertiary volcanic rocks, and Tertiary sedimentary rocks. A large (–400 nT), arcuate magnetic low extends from the Grotto Hills to the Cedar Canyon fault in the Mid Hills (pl. 5). This feature probably results from both a thickened Tertiary and Quaternary volcanic and (or) sedimentary sequence and dipolar lows associated with positive anomalies to the south. A circular area, some 15 km in diameter, of relatively high magnetic values lies to the south of the large, arcuate low. This area is characterized by outcrops of both Proterozoic and Mesozoic crystalline rocks, and the high magnetic anomaly reflects the presence of these rocks at the surface. The westernmost peak in this area of high magnetic values is present over the informally named Black Canyon hornblende gabbro of Beckerman and others (1982) (unit Kbc, pl. 1), which is a circular plug of Cretaceous hornblende gabbro enclosed by the Mid Hills adamellite, some 2 km in diameter. The gabbro here contains as much as 6.5 volume percent opaque minerals, primarily magnetite (Beckerman and others, 1982), resulting in the observed magnetic anomaly. A 5- to 10-mGal gravity anomaly corresponds to the large, magnetically high area. Gravity values in the central and northern Providence Mountains show a general decrease towards the northwest. This gradient probably reflects the general change in the types of rock in the basement from relatively dense Jurassic granitoids in the southeast to the less dense Cretaceous Mid Hills adamellite in the northwest (pl. 1).

The central and southern Providence Mountains are characterized by several large positive magnetic anomalies. The largest of these is associated with the Vulcan iron-skarn deposit. This anomaly (3,500 nT) suggests a possible continuation of the ore body to the east (Goldfarb and others, 1988). Another large magnetic anomaly (~2,000 nT) some 6 mi (10 km) to the northeast may represent the presence of an iron skarn and (or) a highly magnetic Jurassic granitoid body. Positive anomalies present in the southern part of the Woods Mountains suggest that the nonmagnetic tuff that makes up the surfical exposures overlies magnetic basement of probable Jurassic age.

The East Providence fault strikes north along the east side of the range (pl. 1). In general, a series of magnetic lows correspond to the surface trace of the fault. Some lows are present over exposures of apparently nonmagnetic Paleozoic sedimentary rocks, whereas others, present in areas of Proterozoic or Jurassic crystalline rocks, may result from hydrothermal alteration of magnetic minerals along the fault. Steep down-to-the-west gravity and magnetic gradients are present 1 to 2 mi (1.6–3.2 km) into Kelso Wash along the west side of the Providence Mountains, suggesting that the east side of the valley is a pediment surface.

Granite Mountains

Isostatic-gravity values in this region range from a high of about –10 mGal to a low of –25 mGal (pl. 4). Areally corresponding magnetic values range from greater than 200 to less than –100 nT (pl. 5). In general, the northern part of the range is characterized by a magnetic low and a positive gravity closure. The southern part of the range shows a gravity minimum and a variable, but generally high, magnetic anomaly. The division between these two geophysically distinct regions is marked by the concave-to-the-southeast Bull Canyon fault (pl. 4). Gravity and magnetic features of the region have been discussed by Howard and others (1987) and are, therefore, only summarized briefly here. The magnetic trough in the northern part of the range corresponds to the Bull Canyon fault and probably reflects topographic effects, low magnetic susceptibility of the unaltered plutonic rocks, and possibly alteration along the fault zone. Gravity anomalies indicate that the predominantly Jurassic basement rocks north of the fault are denser than the mostly Cretaceous granites that crop out to the south of the fault.

The west margin of the Granite Mountains is marked geomorphologically by Budweiser Wash and the corresponding Bristol Mountains fault (pl. 1). Steep gravity gradients here indicate that this fault is a major

structure that juxtaposes less dense Tertiary volcanic rocks of the Old Dad Mountains (2 to 3 km southwest of the EMNSA; see fig. 2) and some sedimentary rocks to the west against Mesozoic crystalline rocks of the Granite Mountains.

North and northwest of the Granite Mountains in the alluvial plain of the Devils Playground, gravity values suggest that the thickness of sedimentary deposits is not greater than about 1,000 ft (305 m), and basement rocks here are probably Mesozoic granitoids. In the western part of this valley, a northwest-trending, 300-nT magnetic ridge is present along the southwest margin of the northern Bristol Mountains (approximately 5 km southwest of the EMNSA; see fig. 2). This anomaly also roughly corresponds to the projection of the Bristol Mountains fault farther to the southeast. The anomaly is fairly broad and has subdued gradients, suggesting that the source lies at some depth below the surface, possibly as much as about 1 mi (1.6 km). The source of this anomaly is not evident from surface observations, and no conspicuous associated gravity anomaly exists. Two possibilities for a source are extensive iron mineralization or intrusion of Tertiary igneous rocks along the fault zone.

Old Dad Mountain and Kelso Mountains

Exposed in the Old Dad Mountain and Kelso Mountains area are a wide variety of rock types that include Proterozoic schist and gneiss, Paleozoic sedimentary rocks, Mesozoic granitoids, Tertiary volcanic rocks, and unconsolidated sediments (pl. 1). The gravity and magnetic patterns are equally complex. The northwest-trending Old Dad Mountain is characterized by both gravity and magnetic highs of as much as 10 mGal and 400 nT, respectively (pls. 4, 5). Along the southwest margin of this mountain, the magnetic gradient is typical of a steeply dipping fault, although some of the gradient probably results from topographic differences. Both the gravity and magnetic anomalies appear to wrap around the south end of Old Dad Mountain and the Kelso Mountains before dying out in Kelso Wash. A prominent arcuate magnetic and gravity trough is present over the Kelso Mountains, which separates the gravity and magnetic highs of Old Dad Mountain from an area of positive anomalies centered north of Kelso Peak. The northwest limb of the trough appears to continue for as much as 30 km, and the northeast limb some 10 km, before merging with lows of Kelso Wash. Because the area of the trough is, for the most part, covered by alluvial deposits, the source of the anomaly is not evident. If these features represent a fault or series of faults, extensive hydrothermal alteration may have taken place along the fault zones, and the area of the trough might have been downdropped; if the anomalies reflect an intrusive contact, alteration may have occurred along this contact, and the rocks underlying the trough are less dense than the surrounding terrane.

Trending due north from Old Dad Mountain and the Kelso Mountains is a very conspicuous linear isostatic-gravity feature (pl. 4). Relief across this feature is about 10 mGal, decreasing to the east. A somewhat similar north-northwest-trending gradient is noted along the northeast side of Shadow Valley. These two conspicuous anomalies intersect at the north end of Shadow Valley. The magnetic pattern is quite similar to the gravity lineation, although the area of the western gravity gradient is represented by a series of sharp magnetic highs and lows that reflect surficial Tertiary basaltic vents and associated volcanic rocks. The gravity gradient along the northeast edge of Shadow Valley has a corresponding magnetic gradient, although the sense of relief is opposite (in other words, a down-to-the-northeast magnetic anomaly). The southern part of the area of the gravity low defined by these two linear anomalies includes extensive exposures of Cretaceous granite. One interpretation is that the granite extends northward beneath sedimentary cover and forms the floor of Shadow Valley. The gravity low, therefore, represents the combined effect of low-density alluvial valley fill and relatively low density basement rocks. Small outcrops of pre-Tertiary rocks have been noted in Shadow Valley (DeWitt and others, 1984). These have no corresponding gravity anomaly, suggesting that the alluvial fill is relatively thin. The magnetic pattern within the valley shows little relief but is a relative high when compared to immediately adjacent terranes; this would be consistent with the above interpretation. A northwest-trending magnetic gradient crosses the valley in the vicinity of Interstate 15. This linear feature may mark either a lithologic change in the Cretaceous granitoid suite or a subsurface fault with down-to-the-northeast displacement.

Clark Mountain Range

Lying between the Ivanpah and Shadow Valleys, the Clark Mountain Range is a structurally and lithologically complex block that consists of Early Proterozoic metamorphic rocks, Middle Proterozoic igneous

intrusions, and Paleozoic to Mesozoic sedimentary units (pl. 1). The east side of the range is characterized by a structurally complex, diverse assemblage of Proterozoic metamorphic and igneous rocks, while the western part of the range is characterized by a relatively thick section of Phanerozoic sedimentary rocks that has been thrust over the basement complex. Both gravity and magnetic anomalies indicate that the Proterozoic rocks continue to the east at shallow depths nearly to the center of Ivanpah Valley (pls. 4, 5). The trend of the anomalies in the western part of Ivanpah Valley is north-south, which is at an angle of approximately 20° to the north-northwest structural grain of the surrounding region. In the western Clark Mountain Range, geophysical anomalies follow the regional structural trends.

Isostatic-gravity values in this region range from lows of about –40 mGal in the Ivanpah and Shadow Valleys to a high of approximately –10 mGal over the eastern range front near the intersection of Interstate 15 and the Ivanpah Road. Gravity values show a gentle decrease westward across the range until sharp gradients associated with Shadow Valley are encountered. The apparent smoothness of the isostatic anomaly is due, in part, to the relatively wide spacing of gravity stations within the range. Small features, such as igneous dikes and plugs in the general area of Mountain Pass, cannot be detected with the available survey, even though large density contrasts may exist between rock units. Lower gravity values in the western part of the Clark Mountain Range are due, in part, to the presence of a sequence of Paleozoic sedimentary rocks that may have a total thickness of as much as 2.5 km.

The residual-magnetic anomaly shows a large amount of relief within the Clark Mountain Range in contrast to the isostatic gravity. Although some magnetic variation may result from topographic effects, a series of highs and lows in the southern part of the range cannot be accounted for by the varying distance between the aircraft and ground surface. Traversing from east to west across the southern part of the mountains, the broad magnetic high in western Ivanpah Valley probably represents a magnetite or pyrrhotite component of the Proterozoic basement there. This anomaly continues from the southern Ivanpah Valley northward, generally conforming to the shape of the margins of the valley. Immediately to the west of this high, an elongate magnetic low closure of about –80 nT, which shows gradients similar to the above high, is present. This low corresponds to the subsurface projection of the Ivanpah fault (Burchfiel and Davis, 1971) and may indicate the presence of hydrothermal alteration along the fault zone. A magnetic high extends from immediately northwest of Mountain Pass some 10 km to the south-southeast. Gradients associated with this anomaly suggest a shallow source, and the anomaly appears to be related to a series of Middle Proterozoic ultrapotassic rocks and carbonatite exposed in the area. These rocks are the host for the rare earth element deposits of Mountain Pass. To the west of this magnetic ridge, a northwest-oriented low of about –100 nT is present. The location and trend of this anomaly appear to correspond to a series of thrust faults that are exposed in the western Clark Mountain Range and Ivanpah Mountains, and the low may represent a thrust stacking of Paleozoic sedimentary rocks on Proterozoic basement. A +200–nT magnetic anomaly is present in the southwestern Clark Mountain Range, Mescal Range, and Striped Mountain areas. The source of this anomaly is not obvious from surface exposures; gradients, however, indicate that the top of the causative body cannot be much more than 1.6 km below the surface and is probably at the top of the Proterozoic basement. Several small outcrops of Mesozoic granitoids are present in this area (pl. 1). When combined, the above anomalies indicate a complex distribution of lithologies and magnetic properties in the southern Clark Mountain Range and northern Ivanpah Mountains. In contrast, the northern Clark Mountain Range is typified by gentle gravity and magnetic gradients, although the region is structurally complex. The gravity anomaly in the northern Clark Mountain Range consists of a gradient that extends southwestward from a high in the southern Spring Mountains (20 km north of the EMNSA; see fig. 2) to the low in Shadow Valley. A northwest-trending magnetic gradient in this area is present between positive anomalies in the western Ivanpah Valley and a series of lows along the west flank of the Clark Mountain Range.

Woods Mountains Caldera

Two conspicuous features shown on plates 4 and 5 are the negative gravity and magnetic anomalies associated with the late Tertiary Woods Mountains caldera (McCurry, 1988; see also pl. 1). Both anomalies are large-amplitude, circular features that have very steep gradients. These features are in sharp contrast to the

surrounding gravity and magnetic fields. The gravity anomaly is approximately –30 mGal and some 14 km in diameter, while the magnetic anomaly is about –600 nT and about 9 km in diameter. Both features appear to be related to a caldera and (or) an underlying pluton. The presence of sparse Jurassic granitoids within the boundaries of the gravity low at its south margin, the fact that the anomalies are of differing lateral extent, and the fact that centers of the lows do not coincide (the magnetic center is offset some 3 km to the southwest), all indicate that the anomalies do not result strictly from a caldera infilling of low-density and low-susceptibility, low-remanent-magnetization pyroclastic materials. Most granitoids on the west and north sides of the anomalies are Cretaceous in age. Thus, the negative magnetic anomaly may represent the true size and geometry of the actual caldera, which, as was shown by McCurry (1988, figs. 1, 2), is a "trap door" feature that has the western and south-western parts downdropped more than the eastern parts, which results, therefore, in a west-dipping, relatively smooth caldera floor. Structural relief along the west caldera margin may be somewhat in excess of 1 km, although the size of this relief is relatively small when compared to the relief at other well-exposed calderas (D.A. John, written commun., 1993).

The associated gravity anomaly of the Woods Mountains caldera extends well beyond the surficial bounds of this feature (pl. 4). This indicates that a negative density contrast, which occupies an area larger than the surface expression, must be present in the subsurface. Positive magnetic anomalies are present peripheral to the magnetic low but are within the area of the negative gravity anomaly.

The gravity low probably represents intrusion of a relatively low density granitic stock into Jurassic and Cretaceous granitoids combined with caldera formation and infilling with low-density pyroclastic materials and rhyolite. The silicic stock in this case would be circular, about 14 km in diameter, and have steeply dipping sides. The magnetic low probably results from filling of the caldera by pyroclastic materials and by nonmagnetic silicic lava. Positive magnetic anomalies peripheral to the magnetic low but within the gravity anomaly would reflect the presence of magnetic Jurassic and Cretaceous granitoids left above the intrusion. These granitoids may have been remagnetized during the Tertiary magmatic event.

Aerial Gamma-Ray Surveys

By Joseph S. Duval

Aerial gamma-ray surveys measure the gamma-ray flux produced by the radioactive decay of the naturally occurring elements potassium (^{40}K), uranium (^{238}U), and thorium (^{232}Th) in the top few inches of rock or soil (Duval and others, 1971). If the gamma-ray system is properly calibrated (see for example, Grasty and Darnley, 1971), the data can be expressed in terms of the estimated concentrations of the radioactive elements. Data for potassium are usually expressed as concentrations in units of percent potassium (percent K); thorium as parts per million equivalent thorium (ppm eTh); and uranium as parts per million equivalent uranium (ppm eU). The term equivalent is used because the technique actually measures the gamma-ray flux from the decay of thallium (^{208}Tl) and bismuth (^{214}Bi), which are decay products of ^{232}Th and ^{238}U, respectively, and also because the possibility of radioactive disequilibrium exists in the thorium and uranium decay series.

During the period from 1975 to 1983, the U.S. Department of Energy carried out the National Uranium Resource Evaluation (NURE) Program, which included aerial gamma-ray surveys of most of the conterminous United States. Figure 34 shows the $1° \times 2°$ National Topographic Map Series quadrangles from which data (U.S. Department of Energy, 1979a,b,c, 1980) were taken for this study. Although many airborne gamma-ray systems used to make these surveys were calibrated, many early surveys were done without calibration and were not converted to the concentrations of the radioactive elements. Detailed examinations of the digital data available on magnetic tape also showed that many "calibrated" surveys do not match the data from "calibrated" surveys of adjacent areas. For these reasons, the data must be corrected to obtain a consistent database. Duval and others (1989, 1990) discussed the types of corrections applied to the data and provided index maps that indicate the specific kinds of corrections applied to the data sets used in this work.

The NURE aerial gamma-ray data were collected by several private contractors using "high-sensitivity" gamma-ray systems. These systems used sodium-iodide detector crystals that have detector volumes of 2,000–3,300 in^3 (33,000–54,000 cm^3). All systems included electronic navigation equipment, radar altimeters, magnetometers, and "upward-looking" gamma-ray detectors. The upward-looking detectors were partially shielded from radiation coming from the ground by either placing them on top of the other detectors or by using

lead. The upward-looking detectors measure the amount of radiation from ^{214}Bi in the atmosphere, which is used to correct the estimated ground concentrations of ^{238}U. The data were corrected by the contractors for background radiation due to aircraft contamination and cosmic rays, Compton scattering effects, altitude variations, and airborne ^{214}Bi. The gamma-ray surveys were flown at a nominal altitude of 122 m above the ground. The gamma-ray systems were calibrated using the calibration pads at Grand Junction, Colo. (Ward, 1978), and the dynamic test strip at Lake Mead, Ariz. (Geodata International, Inc., 1977). The nominal flight-line spacings for the surveys were 1.6 to 4.8 km and included tie lines flown approximately perpendicular to the flight lines at intervals of 25 to 29 km. Contoured plots of K, eTh, and eU for the EMNSA and its surrounding area are shown in figure 35.

Table 8 lists the estimated average concentrations of potassium, uranium, and thorium for some of the geologic units that crop out in the EMNSA. The values listed in table 8 were determined by inspection of gamma-ray profiles (fig. 35) overlain on the geologic map (pl. 1), but not all geologic units found in the study area are included in table 8 because of little or inadequate data over some units. Average potassium concentrations range from 0.5 to 3.5 percent K. The highest values (>2.9 percent K) are present in the following map units (pl. 1): Jurassic quartz monzonite of Goldstone (Jgo); informally named, Jurassic Ivanpah granite of Beckerman and others (1982) (Ji); informally named, Cretaceous Mid Hills adamellite of Beckerman and others (1982) (Kmh); younger Tertiary volcanic rocks (Tv_1); Tertiary Wild Horse Mesa Tuff of McCurry (1988) (Tw); Tertiary Tortoise Shell Mountain Rhyolite of McCurry (1988) (Tts); and Early Proterozoic intermediate-age granitoids (Xg_2). As pointed out by Beckerman and others (1982), the K_2O contents determined for the Mid Hills adamellite and Ivanpah granite commonly range from 3.5 to 4.8 and 5.0 to 9.0 weight percent, respectively, and seem to corroborate the potassium concentrations sensed remotely by the aerial gamma-ray surveys. The lowest average potassium concentration (0.5 weight percent K) coincides with Cambrian dolomite (Cd). Average uranium concentrations range from 1.5 to 4.4 ppm eU. The highest values (>3.5 ppm eU) are present in the following units: Quaternary eolian sand deposits (Qes); Quaternary playa deposits (Qp); younger Tertiary volcanic rocks (Tv_1); Tertiary dacite and rhyolite (Tdr); Tertiary Tortoise Shell Mountain Rhyolite (Tts); and Mesozoic volcanic and sedimentary rocks (Mzv). The lowest average uranium values (<2 ppm eU) are present in Jurassic felsic rocks of Colton Hills (Jcf), Cambrian dolomite (Cd), and Late Proterozoic and Cambrian siliciclastic rocks (CZs). Average thorium concentrations range from 3.0 to 31.0 ppm eTh. The highest values (>17 ppm eTh) are present in Quaternary eolian sand deposits (Qes); Quaternary playa deposits (Qp); Tertiary dacite and rhyolite (Tdr); informally named, Cretaceous Teutonia adamellite of Beckerman and others (1982) (Kt); Jurassic Ivanpah granite of Beckerman and others (1982) (Ji); and Early Proterozoic migmatite (Xm). The lowest average thorium values (<7 ppm eTh) are present in Quaternary eolian sand deposits (Qes); Jurassic(?) Sands Granite (Js); Cambrian dolomite (Cd); and Late Proterozoic and Cambrian siliciclastic rocks (CZs).

Anomalously high thorium concentrations also are present at two locations that were not listed in table 8 because the flight lines pass near the contacts between different geologic units and the data could not be positively assigned to a particular unit. The first of these locations has a maximum value of 42 ppm eTh; the flight line passes near an outcrop of Middle Proterozoic granitic rocks, located approximately at lat 35°29′ N. and long 115°32′ W. This same location has high uranium values, greater than 7 ppm eU, and some potassium values greater than 4 percent K. The second area of anomalously high thorium values is present near a patch of Jurassic Ivanpah granite (Ji), located approximately at lat 35°22′ N. and long 115°30′ W. Another anomalously high potassium value of greater than 5 percent K is present in a small mass of Jurassic quartz monzonite of Goldstone (Jgo) near lat 34°56′ N. and long 115°32′ W.

The ratios of K/eTh, eU/K, and eU/eTh were examined for anomalies that can indicate a relative enrichment of one or more elements. Enrichment of potassium and (or) uranium can be indicative of alteration processes that are associated with various types of mineralization. Enrichment of thorium can be indicative of the presence of the heavy mineral monazite, which may contain rare earth elements.

An anomalous K/eTh ratio of 0.72, indicative of a relatively enriched potassium content, is present in Early Proterozoic younger granitoids (Xg_1) near lat 35°4′ N. and long 115°7′30″ W. This anomaly is located in the vicinity of an occurrence of polymetallic veins. Similarly anomalous K/eTh ratios ranging from 0.3 to 0.5 are also present over parts of the informally named, Cretaceous Live Oak Canyon granodiorite of Beckerman

and others (1982) (Klo). One outcrop near lat 35°17′ N. and long 115°16′ W. is known to have a tungsten-skarn deposit (pl. 2). Limited amounts of data over a large mass of Jurassic quartz monzonite of Goldstone (Jgo) in the vicinity of lat 34°52′ N. and long 115°34′ W. have anomalous K/eTh ratios that range from 0.3 to 0.5. This mass of Jurassic quartz monzonite of Goldstone is known to host numerous mineral occurrences of various types (pl. 2). Other apparently anomalous K/eTh ratios ranging from 0.3 to 0.7 are present in Quaternary eolian sands (Qes) near lat 34°55′ N. and long 115°44′ W. The high ratios are caused by the low thorium concentration (about 4.4 ppm eTh) of the eolian sands.

Various eU/K and eU/eTh ratio anomalies also are present in the EMNSA. One eU/K ratio anomaly that has values of 4.5 to 5.9 is present approximately at lat 36°54′ N. and long 115°36′ W. This anomaly is apparently associated with Tertiary gravel (Tg), but its significance is unknown. Approximately at lat 34°56′ N. and long 135°34′ W., a similar eU/K ratio anomaly is present in Devonian to Permian limestone (PDl). At this location, the uranium concentration is a moderate value of about 2 ppm eU, which suggests that the apparently anomalous concentration is likely to be characteristic of the limestone. Near lat 35°4′ N. and long 115°11′ W., anomalies of eU/K ratio of 4.4 and eU/eTh ratio of 0.8 are present in Tertiary younger volcanic rocks (Tv$_1$). The radioelement concentrations at the anomaly location are 1.5 percent K, 7 ppm eU, and 8 ppm eTh. The potassium and thorium values can be considered as moderate, but the uranium value is relatively high and should be considered anomalous. Other high eU/K ratios ranging from 2.5 to 4.8 are present along a section of a north-south flight line, at long 115°32′ W. from lat 35°25′ N. to lat 35°29′ N.; eU/eTh ratios are as high as 1.4 at some places along the same section of flight line. This section of flight line crosses various rock types.

In conclusion, the NURE gamma-ray data available for the study area provide limited measurements of the potassium, uranium, and thorium concentrations of the various geologic units present on the surface. Some concentrations of potassium are consistent with measured potassium contents of exposed plutonic rocks. The most prominent thorium anomalies are likely to be associated with the carbonatite-related, rare earth element deposits at Mountain Pass, just outside the EMNSA. The ratio data also show a number of interesting anomalies, and some of them may be related to mineral occurrences. A more detailed gamma-ray survey would provide more site-specific information that could then be more closely related to the geology and mineral occurrences.

Landsat Thematic Mapper Surveys

By Marguerite J. Kingston, Shirley L. Simpson, and Martha S. Power

One-quarter of a Landsat Thematic Mapper (TM) scene was processed to be used as a guide for mapping various lithologic units in the EMNSA and to highlight the general distribution of possible areas of hydrothermal alteration. For the preliminary results described in this section, a color-ratio-composite image was produced by digital image processing and interpreted by inspection (fig. 36).

A TM scene, recorded June 6, 1986, was selected for the study because the sun angle is highest at the time of the summer solstice, and so shadowing in this area of high topographic relief is minimized. Landsat TM imagery has 30-m spatial resolution. Data are recorded in six spectral bands or channels in the visible and near infrared; they have excellent radiometric and geometric characteristics. The wavelength coverage of each TM band is as follows:

TM Bands	*Wavelength coverage (in micrometers)*
1	0.45–0.52
2	0.52–0.60
3	0.63–0.69
4	0.76–0.90
5	1.55–1.75
6	(Thermal infrared, not used in this study)
7	2.08–2.35

Color composite images display color variations that indicate differences in spectral radiance recorded by the Landsat TM from surface materials. Ratioing of selected bands minimizes the influence of topography and enhances spectral differences. Color compositing of three stretched ratios to form color-ratio-composite (CRC) images of TM data allows the detection of specific minerals, which show up as unique colors on the color image. Rocks and soils that are mineralogically and spectrally similar possibly may not be discriminated.

The CRC image of the EMNSA (fig. 36) was produced by combining ratios of TM bands 5:7 (red), 3:1 (green), and 3:4 (blue) according to the techniques of Knepper and Simpson (1992). The resulting colors, used for identification of minerals or mineral groups that may be associated with hydrothermal alteration, are summarized in table 9.

A working copy of a color print was prepared of the CRC image at a scale of 1:100,000, so that it could be overlaid on various geophysical and geologic maps of the EMNSA. Unfortunately, nuances of color and tonal differences were lost in the color paper copy, necessitating referal to the original color transparency to better interpret the CRC image.

In the CRC image, a contribution by a color filter indicates a high ratio value relative to other materials in the scene; thus, red is due to high TM 5:7 ratio values and represents vegetation, which has a strong H_2O absorption in the region of band 7. The TM 3:4 ratio expresses the increase in reflectance from the chlorophyll-absorption band in TM 3 to the near-infrared reflectance plateau in TM band 4, so that the blue color component is very low for vegetated areas. Carbonate minerals and hydroxyl-bearing minerals such as muscovite, kaolinite, or jarosite, which may be associated with hydrothermal alteration, should result in a magenta color owing to the combination of a high value for TM 5:7 ratio (red) and a moderate value for TM 3:4 ratio (blue). However, most hydrothermally altered rocks that contain hydroxyl-bearing minerals are also limonitic, so that the magenta color usually designates only carbonate-mineral-bearing units. The TM 3:1 ratio is coded green and defines rocks and soil that contain ferric iron (limonite). Yellow, the result of combining red and green, appears where TM 5:7 ratio value (red) is high owing to the presence of carbonate or hydroxyl-bearing minerals, as well as where TM 3:1 ratio value (green) is high owing to ferric-iron-bearing minerals such as limonite. White areas indicate a high value in all three component ratios, which is most indicative of the presence of many alteration minerals, especially jarosite, which strongly contributes to the overall radiance.

The detection of limonite traditionally has been important to remote sensing for hydrothermal alteration. As defined by Blanchard (1968), limonite is a general term for hydrous ferric-iron oxides and hydroxides. These minerals absorb strongly in the visible region near TM bands 1 and 4. Limonite may be associated with hydrothermally altered rocks as a result of weathering of pyrite or hematite or other iron-bearing minerals. Gossans typically have an intense ferric-iron absorption. However, some limonite may also be disseminated in sedimentary, volcanic, or metamorphic rocks, unrelated to any epigenetic hydrothermal alteration. Field evaluation is needed to absolutely distinguish hydrothermally altered rocks from those that may only include some limonitic materials from weathering of syngenetic iron-bearing minerals. For example, weathering of biotite and other mafic minerals in granite or metamorphic rocks may produce hematite on some outcrops.

Laboratory spectral-reflectance measurements of representative rock samples collected from the EMNSA were made using a Beckman UV5240 spectrophotometer, using a 100 percent reflectance standard. Four to six representative rock samples were collected from outcrop for the laboratory measurements. Two or three spectral-reflectance measurements were made on the weathered surface of each sample to assure that recorded measurements were consistent, and then the spectral curves were averaged for plotting. Some of these plots of data, which measure spectral reflectance from 400 nm to 2,500 nm to encompass the wavelength range of the TM bands, are reproduced in figures 37 through 48. Note that many unaltered igneous rock samples are spectrally flat, and so they will not show a distinctive color in the image. Also, the red color response of overlying vegetation masks these rocks and any derived soils. The altered samples display deep absorption bands between 2,200 nm and 2,350 nm, which correspond to TM band 7. Carbonate samples typically display absorption features from 2,331 nm to 2,335 nm, which also correspond to band 7.

The most obvious area of alteration in the EMNSA, as defined by the CRC-image color assignments, is in the Castle Mountains, which includes the Hart Mining District (fig. 36; see also pl. 2). Clusters of white pixels are surrounded by yellow and green pixels. Similar areas of alteration represented by the white-to-

yellow clusters of pixels may be in the area of the southeastern Providence Mountains, in the general area of Hidden Hill (fig. 36). Some areas correspond to workings at the Hidden Hill Mine, near the southern tip of the Providence Mountains; others have not been field checked. From the yellow-to-white colors on the CRC image, some areas of alteration appear to be within south-central Hackberry Mountain (fig. 36), where Proterozoic granitoids are in contact with Tertiary volcanic rocks (pl. 1). Some groups of yellow-white pixels correspond with the northern part of Hackberry Mountain, where field checking has confirmed alteration of the volcanic rocks. Another grouping of small numbers of alteration-related pixels is present in the Ivanpah Mountains, where yellow-to-white pixels are displayed in the image on the south and east slopes. This region includes the Morning Star Mine, which was active in 1990 (fig. 36; see also pl. 2). Also, small skarn deposits of various types (pl. 2) are located at the contact of carbonate rocks with quartz monzonite on the west slopes of the Ivanpah Mountains and Mescal Range, and these correspond to pixels showing the yellow and white colors.

Small clusters of yellow pixels are spread throughout the alluvial areas. Many may correspond to areas of exposed soil where cattle have frequented wells; others seem to correspond to mine workings, as in the Tungsten Flat area (fig. 36) of the Signal Hill Mining District (pl. 2). However, no widespread exposure of apparently altered rocks exists at these localities.

The magenta color in the CRC image in the area of the northeast slope of the New York Mountains corresponds to outcrops of carbonate rocks that are intruded by granite (fig. 36). This area has also been the site of some skarn-type mineralization.

Granite outcrops in the Granite Mountains, present at low elevations as boulders and unvegetated talus, appear blue in the image. The fracture pattern typical for granite can be seen in the CRC image, both at low and high elevations, but lichen cover at high elevations causes a red color response in the image (fig. 36).

Additional areas in the EMNSA that show a yellow-to-white color on the CRC image need to be field checked to determine presence or absence of hydrothermal alteration. Other causes of the color responses in the CRC image may exist. Further processing of the TM data might reveal a more direct correspondence with hydrothermal alteration on the ground, as well as allow a better discrimination of the various rock types that crop out over the EMNSA.

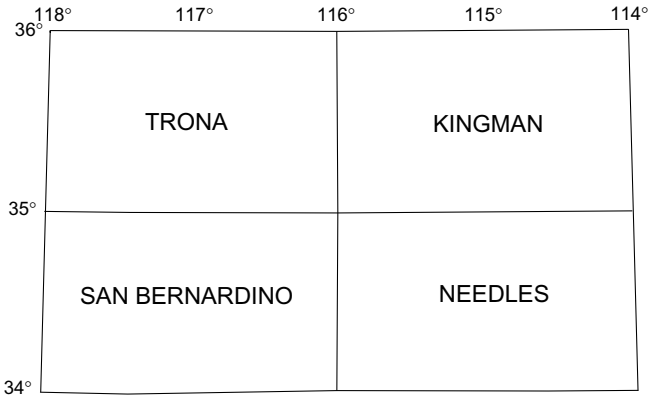

Figure 34. Index map showing 1° x 2° quadrangles from which National Uranium Resource Evaluation Program (NURE) aerial gamma-ray data were taken for study of East Mojave National Scenic Area, California. Data for Trona, Kingman, Needles, and San Bernardino quadrangles are from U.S. Department of Energy (1979a,b,c, and 1980, respectively).

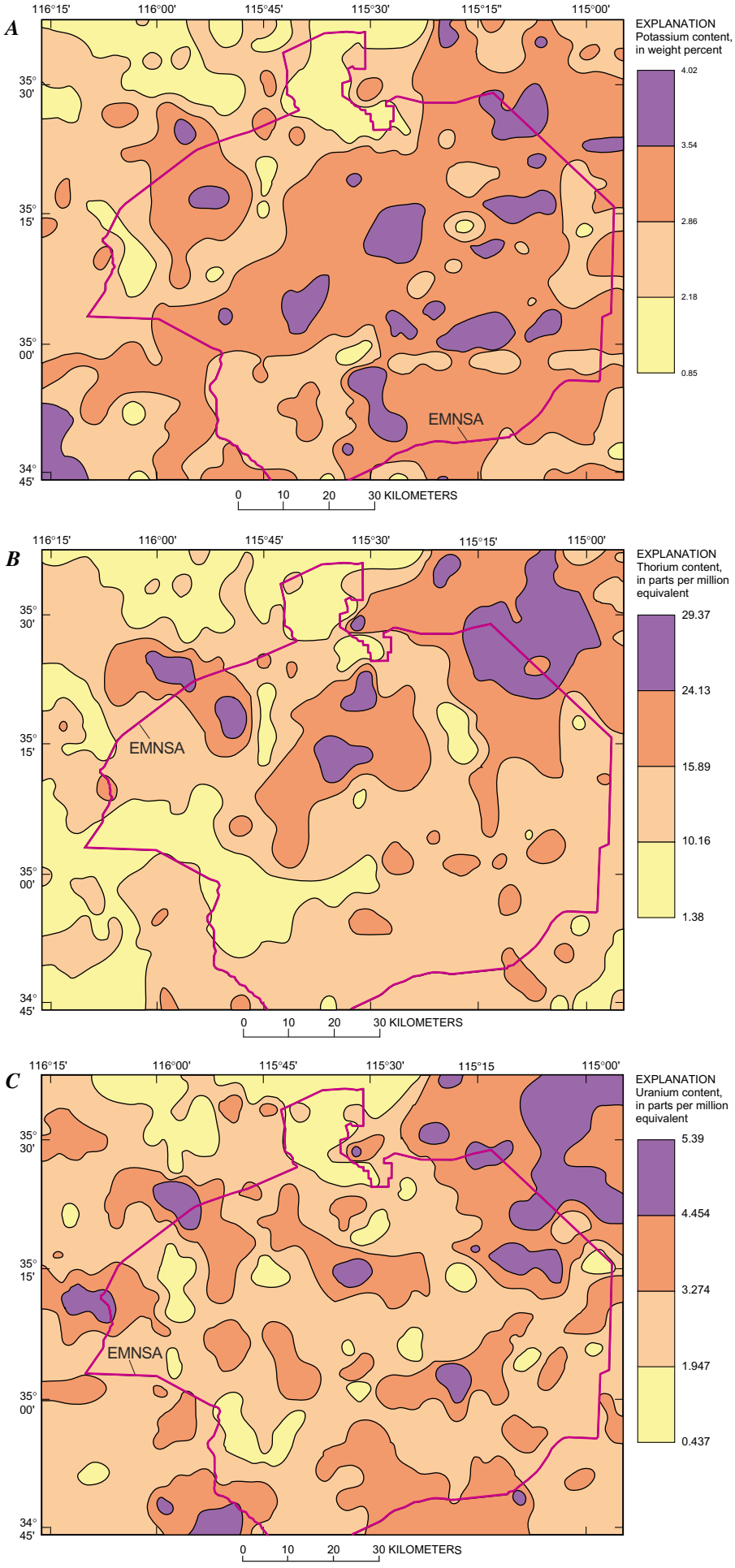

Figure 35. Contoured chemical-composition values, derived from aerial gamma-ray surveys, of rocks in area of East Mojave National Scenic Area (EMNSA, outlined); representative data given in table 8. *A*, Potassium, in weight percent. *B*, Thorium, in parts per million equivalent. *C*, Uranium, in parts per million equivalent.

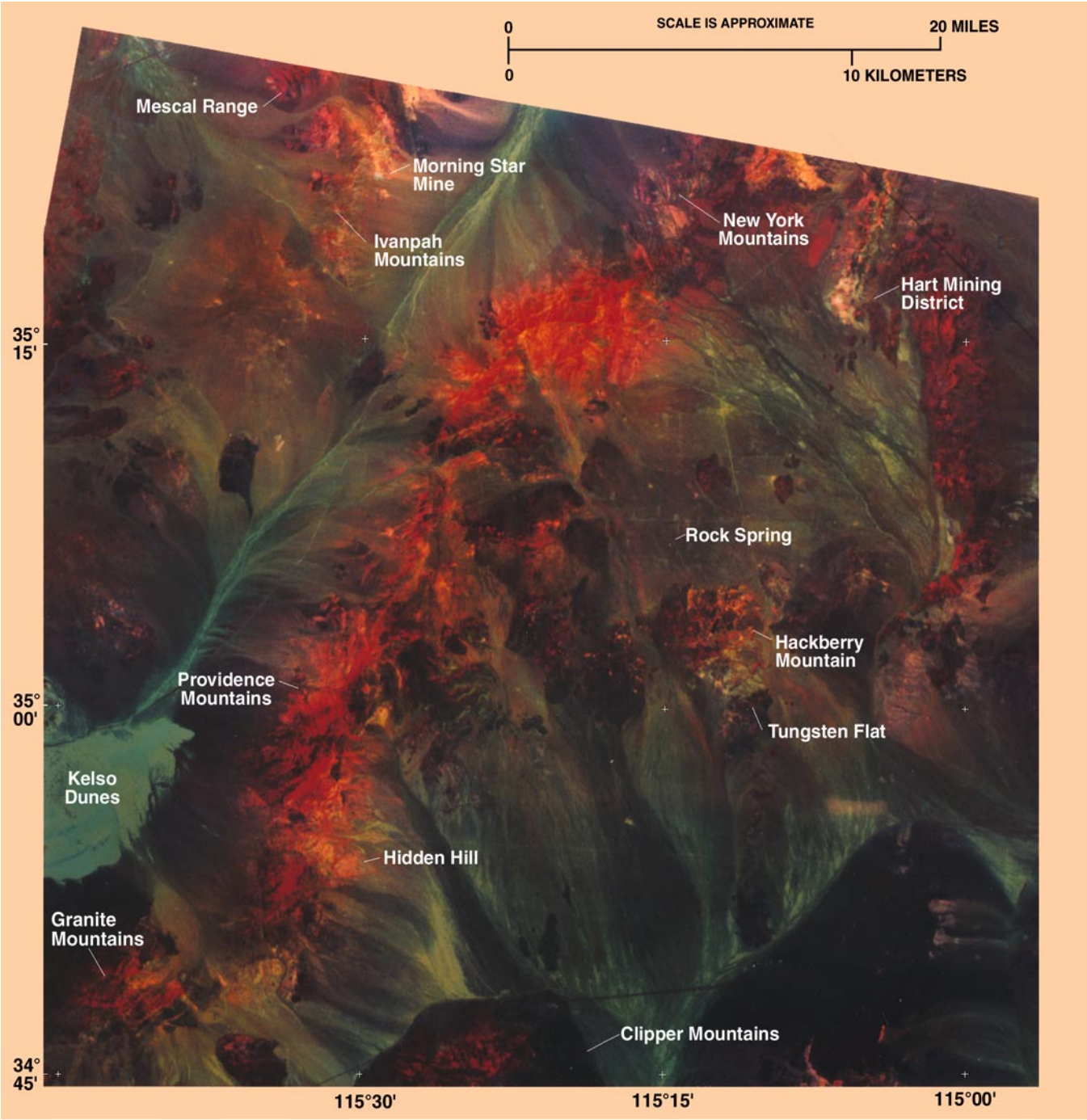

Figure 36. Color-ratio-composite (CRC) image of part of East Mojave National Scenic Area, California, showing significant alteration (white areas) in area of Hart Mining District (CRC image produced by digital image processing of one-quarter of Landsat Thematic Mapper scene 50 8271 73 95). Other areas of alteration appear to be located at Hidden Hill, at Hackberry Mountain, and near Morning Star Mine.

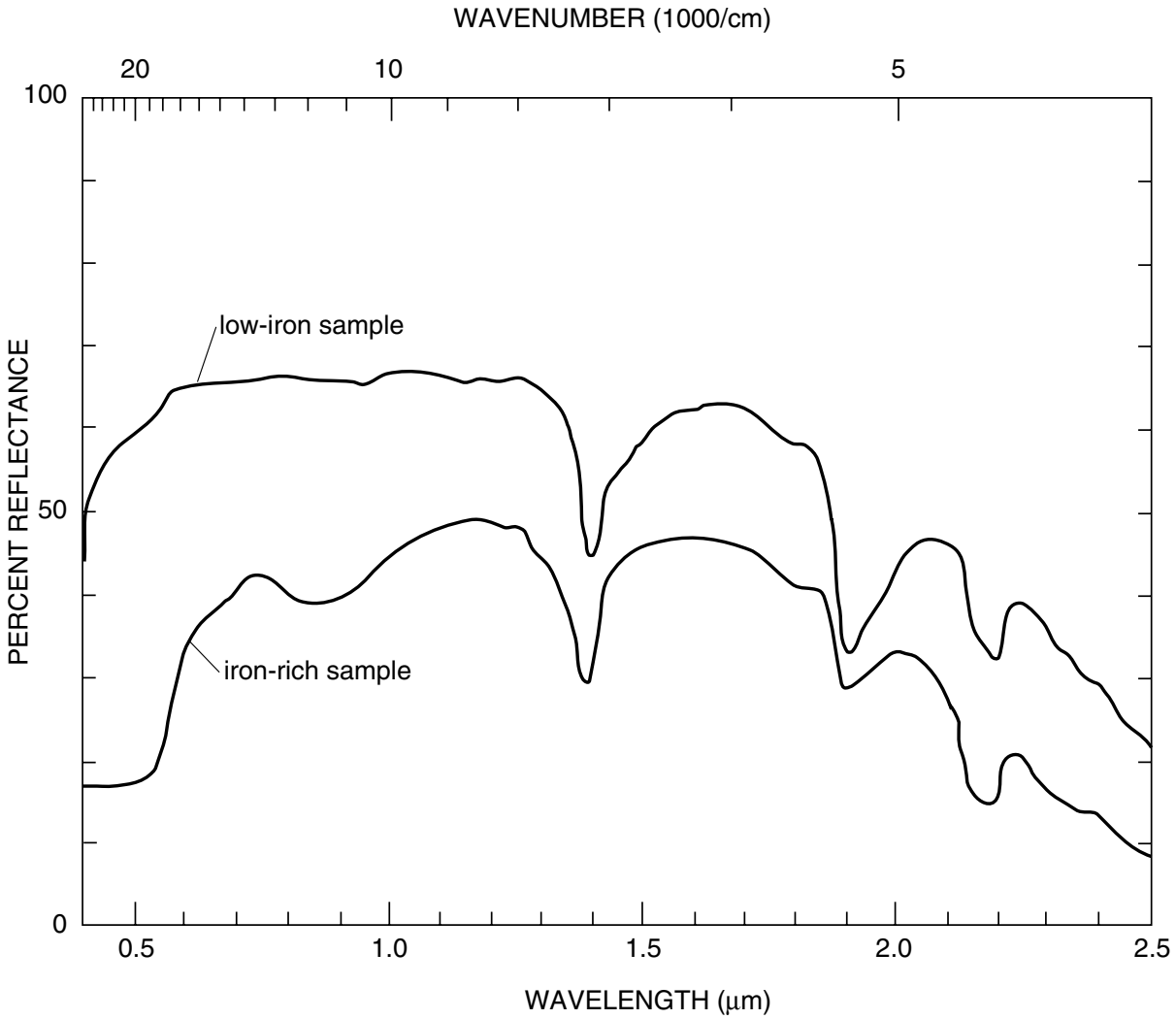

Figure 37. Spectral reflectance of two highly altered dacite-rhyolite samples collected at Castle Mountains gold deposit, Hart Mining District (fig. 2; unit Tdr, pl. 1), East Mojave National Scenic Area, California. For both samples, Thematic Mapper (TM) band 7 will have a low value, resulting in high TM 5:7 ratio value (red). Value of TM 3:1 ratio (green) will be high for iron-rich sample, moderate for low-iron sample; TM 3:4 ratio (blue) value will be low to moderate for the iron-rich sample, low for low-iron sample. Sum of TM ratio values will produce white-to-yellow color-ratio-composite image (fig. 36).

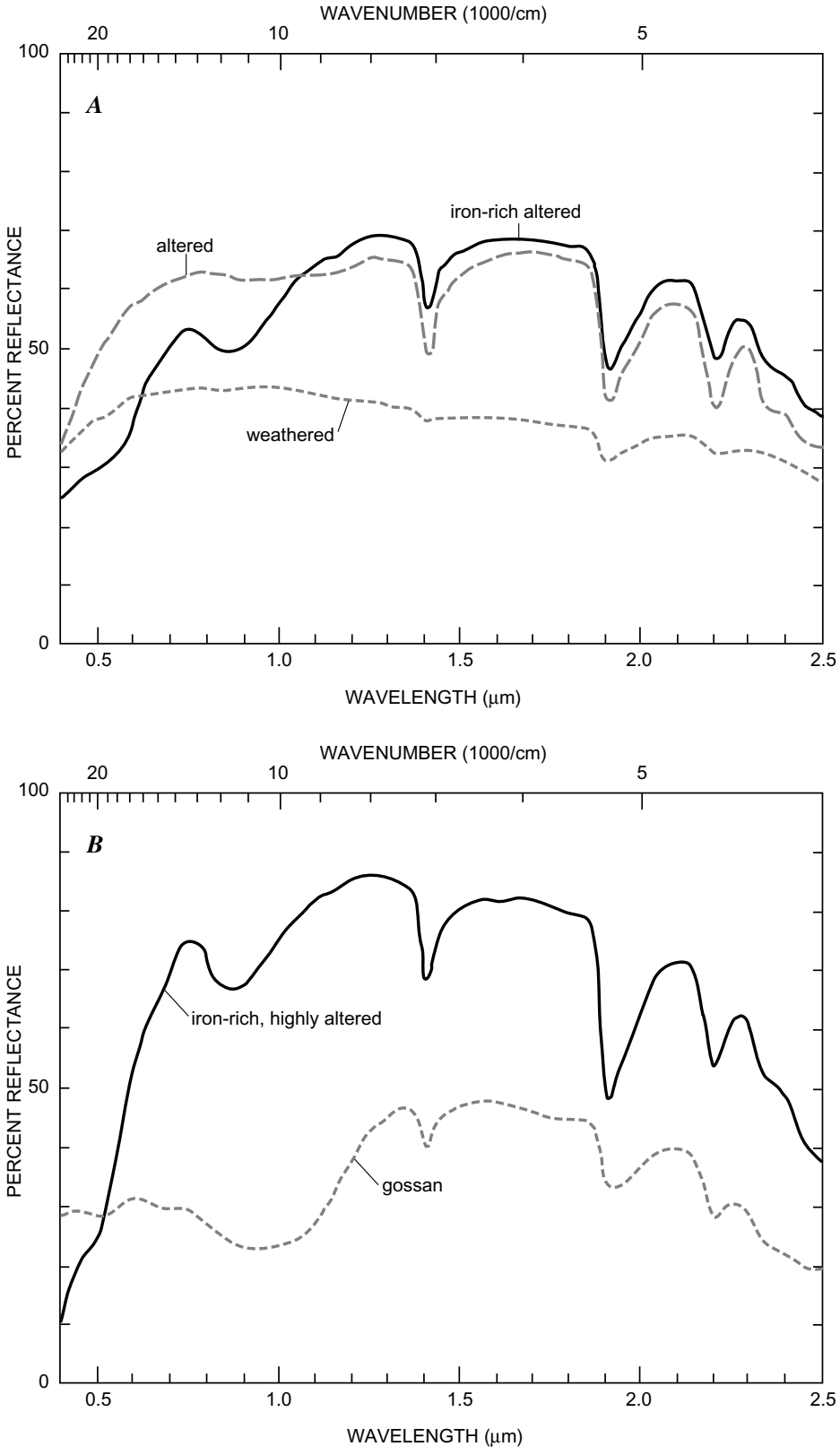

Figure 38. Spectral reflectance of samples at Hidden Hill Mine, East Mojave National Scenic Area, California. *A*, Spectral reflectance of weathered sample of quartz monzonite (unit Jgo, pl. 1), of altered sample of quartz monzonite, and of altered, iron-rich sample of quartz monzonite. Color response on color-ratio-composite (CRC) image of weathered rocks will be blue to slight magenta. *B*, Spectral reflectance of highly altered, iron-rich sample of quartz monzonite and of gossan. Altered rocks will produce yellow-to-white color on CRC image similar to white areas present at Hart Mining District (fig. 36). Value for Thematic Mapper (TM) 3:1 ratio will not be as high for gossan sample, reducing green component on CRC image.

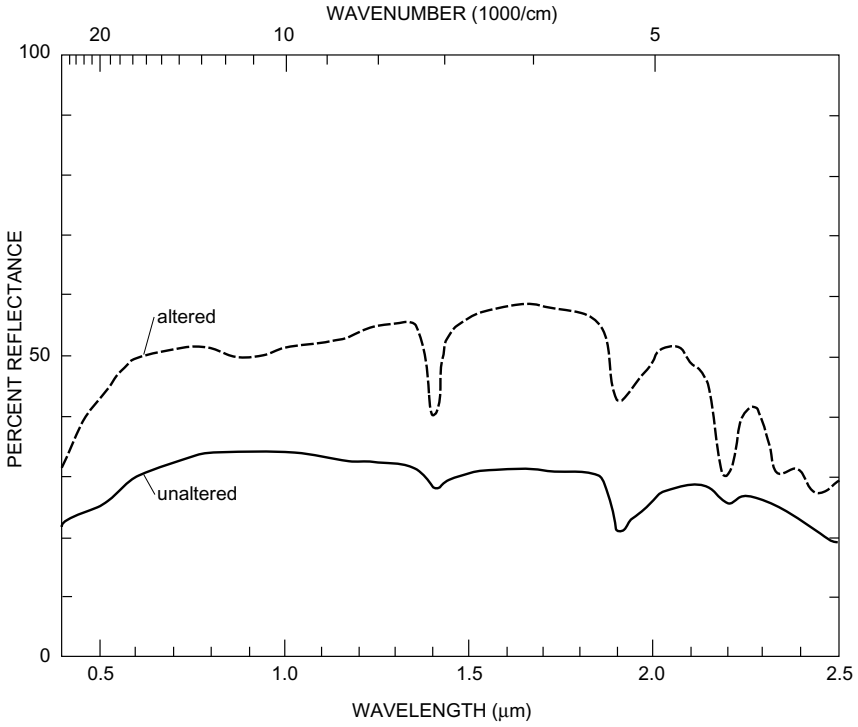

Figure 39. Spectral reflectance of altered and unaltered samples of monzogranite (unit Kg_1, pl. 1) collected at open shaft in general area of Tungsten Flat, East Mojave National Scenic Area, California Color response of altered sample will be white on color-ratio-composite image (fig. 36); unaltered sample, blue to slight red.

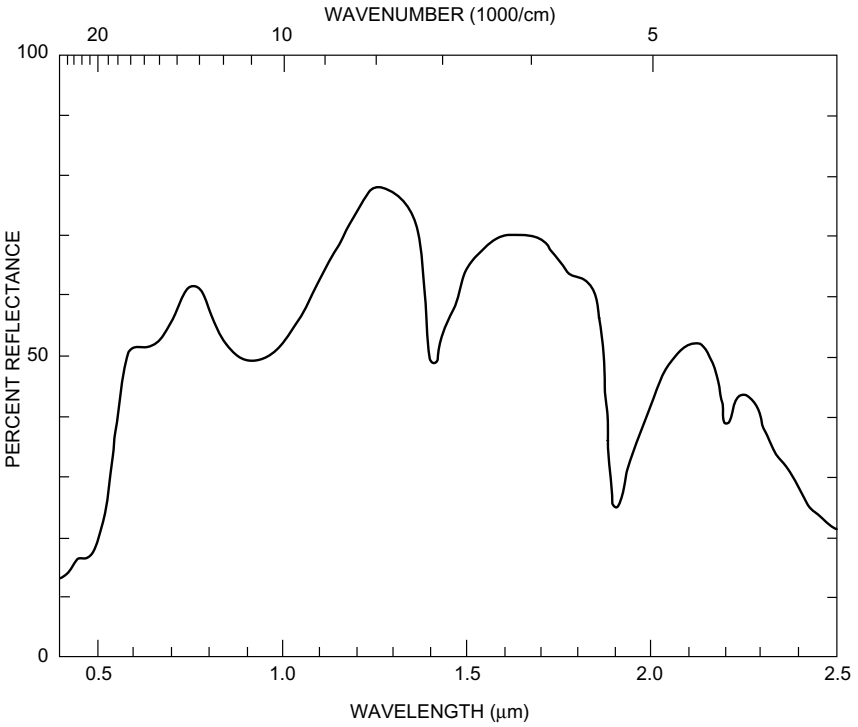

Figure 40. Spectral reflectance of sample of highly altered, informally named Rock Spring monzodiorite of Beckerman and others (1982) (unit Krs, pl. 1), East Mojave National Scenic Area, California. Mafic minerals have been altered to nontronite, which dominates spectrum. Color response will be white on color-ratio-composite image (fig. 36).

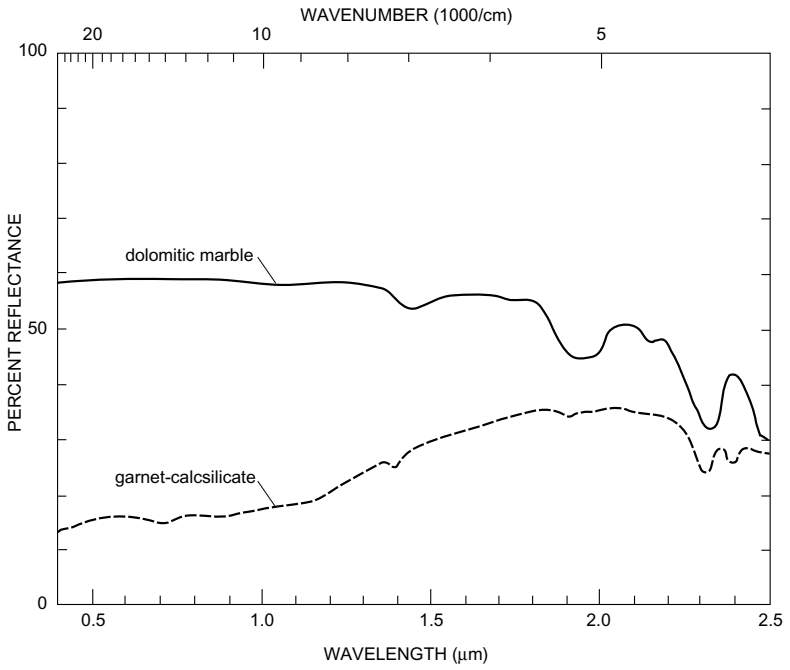

Figure 41. Spectral reflectance of samples of dolomitic marble (altered dolomite(?) of Bird Spring Formation; part of unit PDl, pl. 1) and of garnet-calc-silicate rocks derived from Moenkopi Formation (unit Rm, pl. 1), both collected near skarn deposit in East Mojave National Scenic Area, California. Value for Thematic Mapper (TM) 5/7 ratio (red) for marble will be high, less so for calc-silicate rocks. Color response of TM 3:1 (green) and 3:4 (blue) ratio values will be low for both samples. Resultant colors on color-ratio-composite image (fig. 36) are similar but show deeper red response for carbonate-bearing rocks.

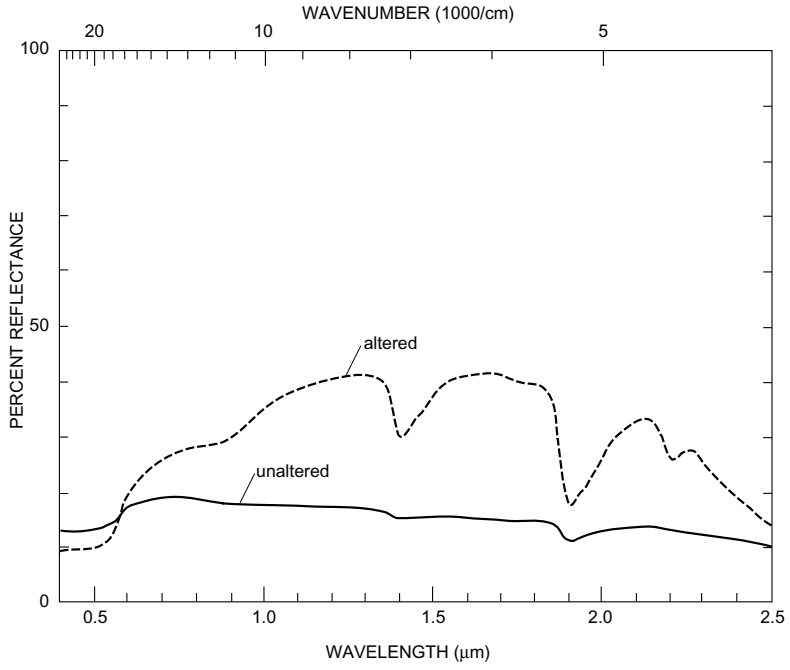

Figure 42. Spectral reflectance of altered and unaltered samples of monzogranite (unit Kg_1, pl. 1) (adamellite?), collected from road cut (old railroad grade) in New York Mountains, East Mojave National Scenic Area, California (fig. 36). Color response for altered rocks will be white on color-ratio-composite (CRC) image. Value for Thematic Mapper (TM) 3:1 ratio will be high owing to ferric-iron absorption of monzogranite, so otherwise-flat spectrum will result in slight cyan color on CRC image.

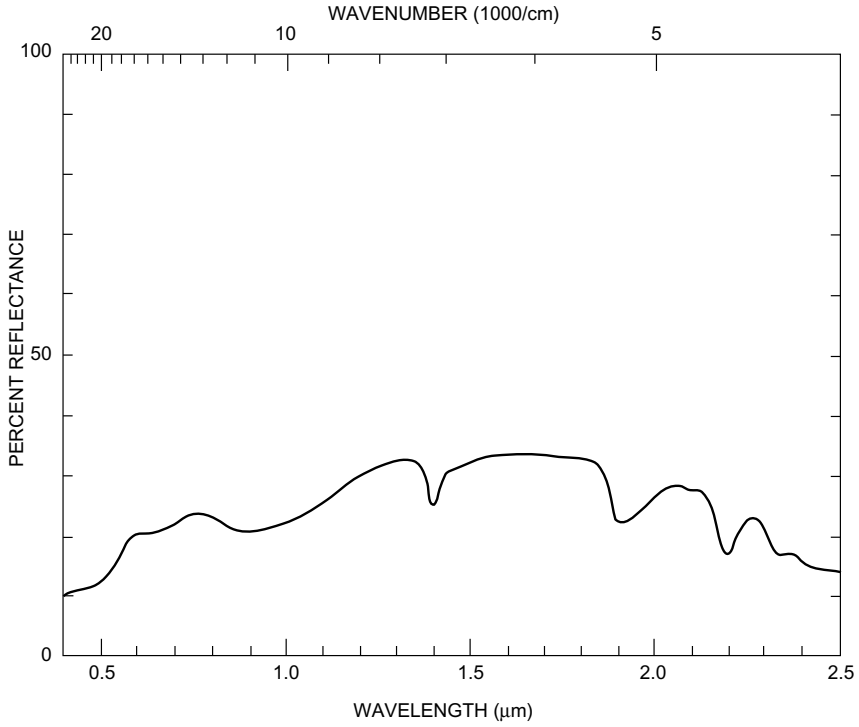

Figure 43. Spectral reflectance of sample of altered quartz monzonite (unit Jgo, pl. 1), collected at Bighorn Mine, East Mojave National Scenic Area, California. Resultant color on the color-ratio-composite image will be white to yellow but, as spectral reflectance is low relative to spectra exhibited on figure 36, these rocks would not be as bright on image.

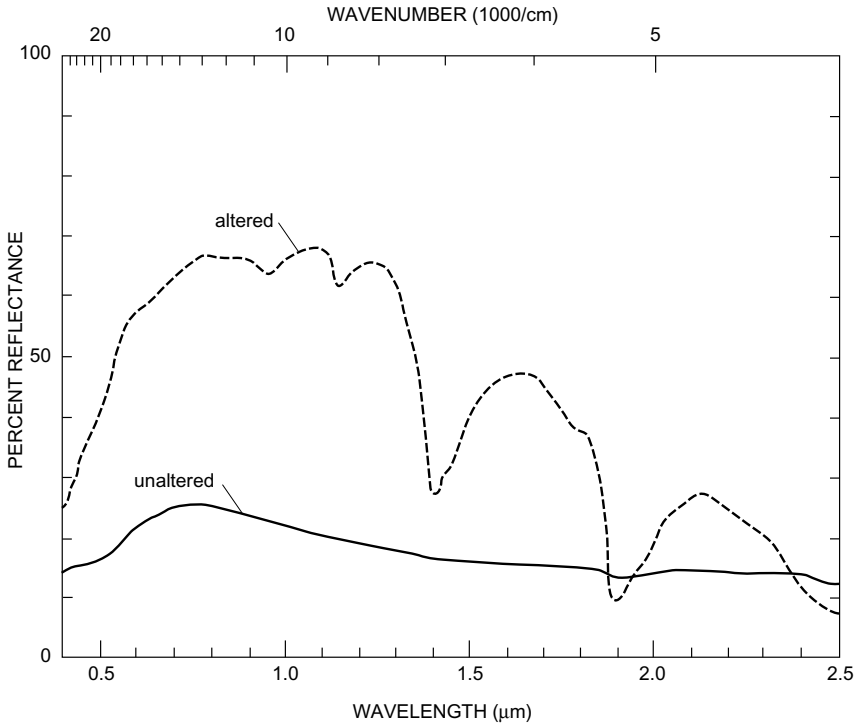

Figure 44. Spectral reflectance of altered and unaltered samples of Tertiary volcanic rocks (Peach Springs(?) Tuff of Young and Brennan (1974); unit Tps, pl. 1), East Mojave National Scenic Area, California. Altered sample collected north of Hackberry Mountain. Altered volcanic rocks should be very bright white but actually appear yellow on color-ratio-composite (CRC) image, possibly because of thin cover of vegetation. Unaltered volcanic rocks are blue to slight magenta on CRC image.

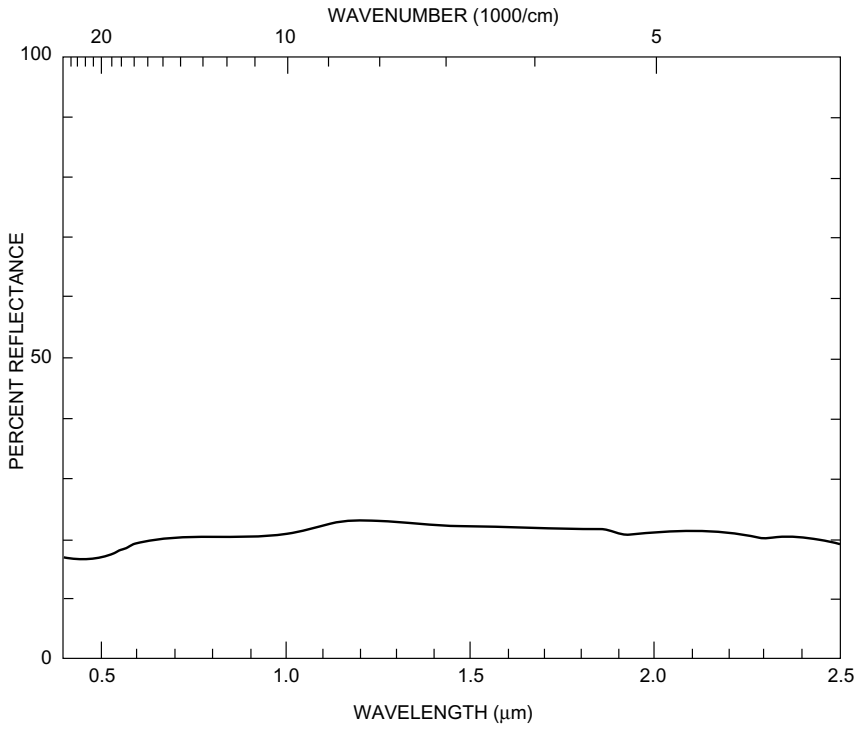

Figure 45. Spectral reflectance of altered and unaltered dacite flow rock (unit Td, pl. 1), collected in Piute Hills, near old Mohave road, East Mojave National Scenic Area, California. Flat spectrum produces blue color in color-ratio-composite image.

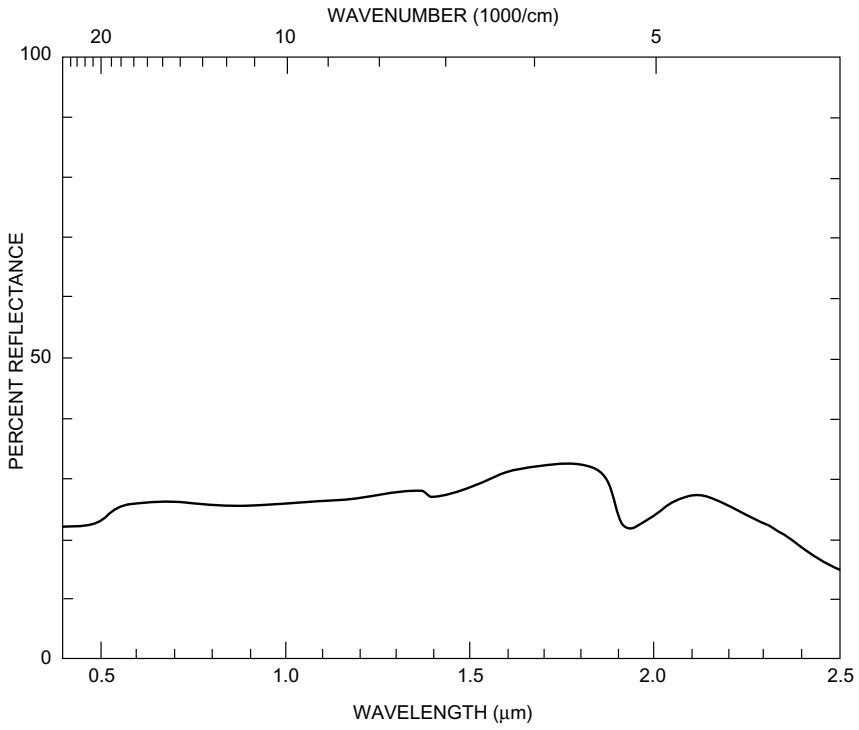

Figure 46. Spectral reflectance of sample of weathered surface of Early Proterozoic quartz diorite (unit Xg_1, pl. 1), collected near True Blue Mine. Sample does not appear to be altered. Spectrum is flat except for slight absorption in short wavelengths (Thematic Mapper (TM) band 1) owing to ferric iron on weathered surface. Color response will be blue with very slight green component on color-ratio-composite image.

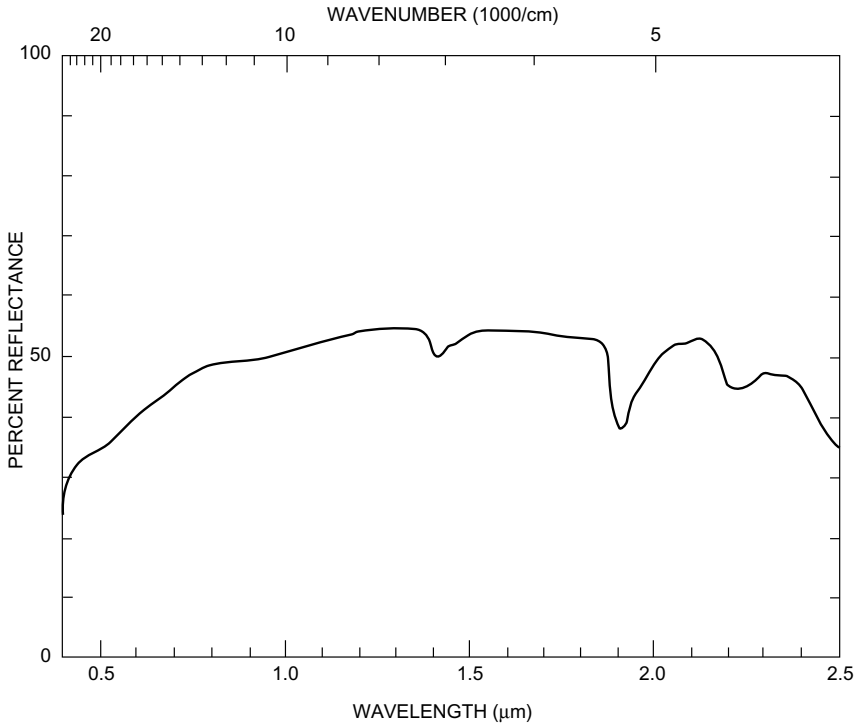

Figure 47. Spectral reflectance of sample of light-colored rhyolite ash-flow tuff (White Horse Mesa Tuff of McCurry (1988); unit Tw, pl. 1), which appears to be slightly altered; collected near Hole-in-the-Wall campground, East Mojave National Scenic Area, California. Spectrum of this very bright tuff displays an absorption band near 2.2 μm, resulting in high Thematic Mapper (TM) 5:7 ratio value (red), as well as moderately high TM 3:1 and 3:4 ratio values (green and blue, respectively). Unaltered rocks can be confused with altered rocks because of resulting white-to-yellow color response on color-ratio-composite image.

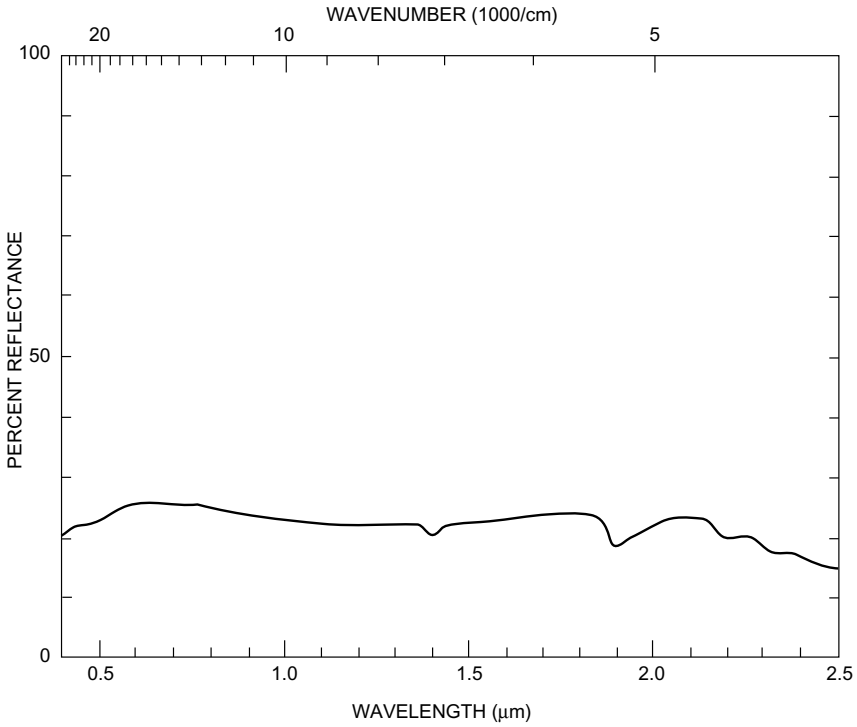

Figure 48. Spectral reflectance of sample of syenogranite (unit Jqs, pl. 1), collected at Granite Pass, East Mojave National Scenic Area, California. Because of 2.2-μm and 2.34-μm absorption, which is due to micaceous minerals, Thematic Mapper (TM) 5:7 ratio value (red) will be high. Weathering of biotite results in ferric-iron absorption (high TM 3:1 ratio value) and should produce green component in color-ratio-composite image. Ferric-iron band is relatively weak for most of exposed syenogranite in CRC image, resulting in blue color.

Table 8. Estimated average concentrations of potassium, uranium, and thorium, derived from aerial gamma-ray surveys, for various geologic units in the East Mojave National Scenic Area, California.

[Contoured data shown on fig. 35; see plate 1 for description of map units]

Map unit	Estimated Concentration Values		
	Potassium (percent K)	Uranium (ppm eU)	Thorium (ppm eTh)
Qaf	2.9	3.2	13.0
Qes	2.2	2.4	0.4
Qes	2.9	3.9	18.5
Qp	2.4	4.2	18.5
QTbl	1.6	2.5	8.0
QTg	2.6	2.7	8.3
Td	2.2	3.0	10.9
Tdr	2.1	3.9	19.5
Tg	2.7	2.4	13.0
Tts	3.5	4.4	15.4
Tv_1	3.0	3.9	14.3
Tw	3.0	3.5	15.0
Kg_1	2.4	2.4	10.1
Klo	2.7	2.9	7.3
Kmh	3.0	2.4	13.3
Kpm	2.0	3.4	12.0
Krs	2.3	2.6	12.0
Kt	2.8	3.4	18.9
KJg	2.4	3.4	14.5
Jd	2.3	2.5	9.5
Jcf	2.6	1.9	12.0
Jg	2.1	3.1	11.5
Jgo	3.0	2.9	11.5
Ji	3.2	3.4	31.0
Jcm	1.9	2.8	9.0
Js	2.8	2.1	6.5
Mzv	2.3	4.0	11.3
€Zs	1.9	1.6	6.5
€d	0.5	1.5	3.0
Xg	2.5	2.8	15.2
Xg_1	2.4	2.5	12.4
Xg_2	3.2	3.4	14.0
Xm	2.0	2.1	17.5

Table 9. Summary of resultant colors of alteration minerals and vegetation on a color-ratio-composite image prepared from Landsat Thematic Mapper satellite image.

[Primary colors calculated using the following ratios: red, band 5:7; green, 3:1; blue, 3:4. Resultant color is sum of primary colors. From Knepper and Simpson, unpub. data, 1991]

Material	Primary color			Resultant color
	Red	Green	Blue	
Carbonate and hydroxyl-bearing minerals	High	Low	Moderate to low	Magenta
Limonite (hematite, goethite)	Low	High	Moderate to high	Green to cyan
Limonite (jarosite)	High	High	Moderate to high	Yellow to white
Carbonate minerals, hydroxyl-bearing minerals, and limonite	High	High	Moderate to high	Yellow to white
Vegetation	High	Low	Very low	Red

Geochemistry

By Gary A. Nowlan and Ted G. Theodore

This section of the report includes two parts. In the first part, the Rock Analysis Storage System (RASS), the geochemical database of the United States (PLUTO), and National Uranium Resource Evaluation (NURE) computerized databases of the U.S. Geological Survey are examined, largely on the basis of regional geochemistry. In addition, descriptions of a number of mineral occurrences obtained during our investigation are included. Table 10 lists sources of data that have been released, and tables 11 and 12, respectively, list geochemical data and sample descriptions from selected rocks collected from a small number of mineralized systems in the East Mojave National Scenic Area (EMNSA). In the second part, the implications of data obtained from analyses of 1,050 rocks by the U.S. Bureau of Mines (1990a) from various sites within the EMNSA are examined; these samples are mostly mineralized or altered samples from mines and prospects.

RASS, PLUTO, and NURE Databases

The objective of the examination of RASS, PLUTO, and NURE data is to recognize geochemical patterns that might be related to mineralization. Application of the principles of mineral-deposit models (Cox and Singer, 1986) includes the recognition of characteristic geochemical signatures for each model. The regional geochemistry addresses geochemical signatures in terms of possible mineral deposits without regard to the size or grade of the deposits. The discussion of the geochemistry of each area includes some descriptions of known mineral occurrences and classifies them in terms of mineral-deposit models.

Analytical data for the EMNSA that are stored in the RASS, PLUTO, and NURE databases were retrieved and examined using the Statistical Package (STATPAC) system (VanTrump and Miesch, 1977) of the U.S. Geological Survey. The RASS and PLUTO databases contain data for rock, stream-sediment, heavy-mineral-concentrate, and soil samples, as well as other types of geologic samples collected by the U.S. Geological Survey and other sample types such as water and vegetation. The NURE database contains data for samples collected during the National Uranium Resource Evaluation Program of the U.S. Department of Energy (Cook and Fay, 1982).

The RASS and PLUTO databases were designed and managed by the Branches of Exploration Geochemistry and Analytical Laboratories, respectively, of the U.S. Geological Survey before their merger into the Branch of Geochemistry in 1987. The two databases are similar in content and characteristics, but major differences in their operation have hindered their merger into a single database; in addition, the logistical problem of merging two large databases is a major obstacle during a time of limited budgets. Since merger of the two branches into the Branch of Geochemistry in 1987, most new data have gone into the PLUTO database; however, most data for the EMNSA were obtained before 1987 and, therefore, are resident in both RASS and PLUTO databases. Before the merger of the branches, RASS data tended to be from large mineral-resource evaluations of public lands or other large projects, whereas the PLUTO database tended to receive data from more specialized projects and from a wider variety of types of projects.

The data for selected elements useful in mineral-resource evaluations were studied and, from them, map plots were produced. The data in the RASS, PLUTO, and NURE databases are available to the public, but most data have not been released as either published or open-file reports; table 9 lists sources of data that have been released.

Sample Types

Sieved stream-sediment samples, heavy-mineral-concentrate samples (in most cases, panned from stream sediments), and rock samples from the RASS and PLUTO databases were considered because they were the most widely sampled media in the study area and also are the standard sample media for mineral-resource evaluations by the U.S. Geological Survey. The PLUTO database contained some samples that have very approximate coordinates (rounded to one-half minute or more of latitude or longitude); these samples were not considered in this study.

Standard coding in the RASS and PLUTO databases does not always specify the size fraction analyzed for the stream-sediment samples. Examination of the original requests for analysis or consultation with the original investigators confirmed that the minus-80-mesh (<0.177 mm) fraction of each stream-sediment sample was the fraction analyzed.

Heavy-mineral-concentrate samples from the RASS database are the nonmagnetic heavy fraction of stream sediments, except for 15 samples from the west side of the Ivanpah Mountains that were panned from mine-dump material. The RASS concentrate samples were prepared by subjecting panned samples to a series of magnetic and heavy-liquid separations, resulting in samples consisting of nonmagnetic ore minerals and accessory heavy minerals such as sphene and zircon. The PLUTO heavy-mineral-concentrate samples were all derived from stream sediments; after panning, the highly magnetic minerals (mostly magnetite) were removed with a hand magnet, and the less-magnetic fraction was ground and analyzed (Jean Juilland, oral commun., 1991). Because of the major difference in the processing of RASS and PLUTO heavy-mineral-concentrate samples, they were treated as different sample media in the data analysis; drastic differences in concentrations of common elements such as Fe, Ca, and Mn confirmed that the RASS and PLUTO concentrate samples should be treated as different sample media.

Of the 944 RASS and PLUTO rock samples, about 700 are specified by coding or by notes to be samples of mineralized or altered rocks or from faults. These 700 samples may be thought of as samples of the channels where mineralizing fluids passed. Coding for about 140 of the 944 samples does not indicate whether they are of economic significance; for most elements in these approximately 140 samples, the range of concentrations varies from 1 to 2 orders of magnitude, and the maximum concentrations indicate that some samples may be mineralized. In any case, concentrations significantly above expected regional background are of interest, especially if several elements have anomalously high concentrations in the same samples or same areas. For mineralized rocks, the geochemical signature is more important than absolute concentrations because, typically, no way exists to determine the exact nature of the sample or the intent of the sampler. For example, the sample may be from a highly mineralized vein, may be a composite of dump samples, or may be a sample of altered but not obviously mineralized rock. For this mineral-resource evaluation, data from all 944 rock samples were combined for data analysis and considered to be mineralized.

The NURE data consist of analyses of the 35- to 18-mesh (0.5-1.0 mm) fraction of stream sediments from the Kingman 1:250,000-scale quadrangle and of the minus-100-mesh (<0.149 mm) fraction of stream sediments and soils from the Needles, San Bernardino, and Trona 1:250,000-scale quadrangles. The data also contain 13 playa-sediment samples. Comparison of the minus-100-mesh stream-sediment and soil data showed that the two media could be combined into one data set, and so this was done. Comparison of data from the Kingman quadrangle (35-18 mesh) with data from the Needles-San Bernardino-Trona quadrangles (minus-100 mesh) showed biases in the means of the concentrations of as much as two to one for the nine elements (Ce, Dy, Eu, La, Lu, Sm, Th, U, and Yb) included in this report. However, the bias was high for Ce, Dy, Eu, and Lu in Kingman samples and high for La, Sm, Th, U, and Yb in Needles-San Bernardino-Trona samples; therefore, the biases in the means are difficult to attribute to differences in sample grain size and may represent either geologic differences or analytical biases.

Evaluation of Data

The standard method of analysis for RASS and PLUTO samples was semiquantitative, direct-current arc-emission spectrography (Myers and others, 1961; Grimes and Marranzino, 1968); RASS samples were usually analyzed for 31 elements by this method, while PLUTO samples were analyzed for those 31 elements plus about 15 more, mostly rare earth elements (REE). RASS and PLUTO samples from specific areas in the EMNSA were analyzed by atomic absorption and other methods; these additional analyses were examined, but their usefulness is limited because of poor areal coverage.

Concentrations of elements determined by the emission-spectrographic method are usually reported as one of six steps per order of magnitude; the steps represent intervals of some power of 10 times 1.2 to 1.8, 1.8 to 2.6, 2.6 to 3.8, 3.8 to 5.6, 5.6 to 8.3, and 8.3 to 12 (Motooka and Grimes, 1976). For most samples in this report, those intervals are represented by the values (steps) 1.5, 2, 3, 5, 7, and 10, respectively (or powers of 10 of these

numbers). For some samples, the reported values are somewhat different but still represent approximately the same intervals. Upper and lower limits of determination (table 13) varied somewhat with method and with time during the approximately 6-year period when the samples were analyzed. This is reflected in table 13 by variations in lower determination limits and by some maximum concentrations greater than the customary upper determination limits listed. The precision of the emission-spectrographic method is approximately plus or minus one reporting interval at the 83 percent confidence level and plus or minus two reporting intervals at the 96 percent confidence level (Motooka and Grimes, 1976).

In the NURE program, stream-sediment and soil samples were routinely analyzed by neutron-activation analysis for approximately 17 elements (Cook and Fay, 1982). These routine procedures did not include most of the elements that are generally of interest in mineral-resource evaluations. The NURE program made extensive use of a supplemental package of analyses that includes most elements of interest in the search for hydrothermal ore deposits, but those supplemental analyses were performed only on samples from the Kingman quadrangle. In addition, certain ambiguities exist between the digital NURE database and the published reports. For example, it is not clear whether a reported value of zero means that an analysis was not performed or that an analysis was performed but the concentration was less than the lower limit of determination. Therefore, the NURE database is of limited usefulness for evaluations of elements that might be indicative of hydrothermal processes, but it is useful for evaluating the presence of U, Th, and rare earth elements (REE). Coefficients of variation for three NURE stream-sediment or soil samples that were each analyzed from 16 to 297 times by neutron-activation analysis for various elements ranged from 5.0 to 47.8 percent (Cook and Fay, 1982, table 2).

The RASS and PLUTO 31-element emission-spectrographic data for stream-sediment samples appeared to be compatible, and so the two databases were merged into one data set for statistical evaluation and map plotting. The RASS and PLUTO 31-element emission-spectrographic data for rocks also appeared to be compatible, and they were also merged into a single data set. The additional elements, mostly REE, analyzed by emission spectrography for PLUTO stream-sediment samples and rock were treated as separate data sets. Data for RASS and PLUTO concentrate samples were treated as separate data sets because differences in sample preparation led to incompatible geochemical results.

Data Coverage

Figure 49 shows geographic areas covered by the geochemical data sets in and along the border of the EMNSA. This map is used as a base map for other figures in this section of the report. Sampling localities for the various sample media are shown in figures 50 to 53. Stream-sediment samples (fig. 50) were collected in almost all areas outlined on figure 49; sampling density is quite sparse except in areas in the Clark Mountain Range, the Ivanpah Mountains, and the Providence Mountains. PLUTO concentrate samples (fig. 51) are quite evenly but sparsely distributed throughout the area. RASS concentrate samples (fig. 51) are limited to several areas, and sampling density is fairly adequate for geochemically characterizing those areas; the Providence Mountains were heavily sampled, allowing an excellent geochemical characterization of that area. Distribution of sampling sites of rocks (fig. 52) is spotty, dominated by heavy sampling in the Providence Mountains. NURE samples (fig. 53) are distributed fairly uniformly, although somewhat sparsely.

Geochemical Evaluation

Symbol plots of selected elements in the various sample media were prepared in order to show geochemical trends in the EMNSA and adjacent areas. The selected elements were the possibly ore-related elements Ag, As, Au, B, Ba, Be, Bi, Co, Cu, Mn, Mo, Nb, Pb, Sb, Sn, Th, U, W, and Zn; also included because of the proximity of the Mountain Pass REE deposit were the rare earth elements Ce, Dy, Eu, La, Lu, Nd, Sm, Tb, and Yb.

Table 13 lists statistics for the selected elements that are based on samples from the EMNSA and the surrounding area from lat 34°30′ N. to lat 35°45′ N. and from long 114°45′ W. to long 116°15′ W. Threshold concentrations, defined as highest background concentrations, were selected by visual and statistical examination of the data, by observation of elemental concentrations near known mineralized areas, and by reference to published reports of specific geochemical studies of various wilderness-study areas within the EMNSA. The threshold concentrations listed in table 13 for the EMNSA are regional thresholds and do not take into account

any variations in bedrock or other factors. Table 13 includes published threshold concentrations established for two wilderness-study areas within the EMNSA (Miller and others, 1985, tables 1, 2; Goldfarb and others, 1988, table 3), which are included for reference and to illustrate how threshold concentrations vary with scale of study, degree of local bedrock mineralization, and judgment of the individual investigator.

Selected percentiles are listed in table 13 and also in the captions of figures 54 to 73. First, the computer program ranks concentration values from lowest to highest, then it lists the concentration values at selected percentiles. Concentration values qualified by "N" (not detected at lower limit of determination) are ranked lowest; those qualified by "L" (detected below lower limit of determination) or "<" (less than lower limit of determination) are ranked next to the lowest; and those qualified by "G" or ">" (both signify concentration values greater than upper limit of determination) are ranked highest. Unqualified values are ranked in the middle according to their magnitude. Concentration values listed in percentile columns in table 13 for RASS and PLUTO samples are rounded to the emission-spectrographic steps mentioned above (1.5, 2, 3, 5, 7, or 10, or powers of 10 of these numbers); those listed for NURE samples are rounded to two significant figures.

Because lower limits of determination for emission-spectrographic techniques are high relative to average crustal abundances for some elements (Ag, As, Au, Bi, Sb, Th, W), almost all detectable concentrations for these elements are anomalous, depending on sample type; some of the rare earth elements also fall in this category (Dy, Tb). For elements that have a wide range of detectable concentrations, a "high" category is plotted on figures 54 to 73 showing distribution of anomalous and high concentrations of various elements. Because some subjectivity is involved in establishing threshold concentrations, inclusion of a "high" category shows the appearances of geochemical patterns if lower thresholds are chosen.

The high proportion of samples that have anomalous concentrations of Ag, Ba, Cu, Mo, Pb, and Zn in rock and heavy-mineral-concentrate samples (table 13) is the result of the large number of samples collected in highly mineralized parts of the Providence Mountains.

Figures 54 through 73 show map distributions of anomalous and high concentrations of elements in the various sample media. Each figure plots no more than four elements; these are grouped by common elemental association and are represented by vertical, horizontal, and diagonal lines. Anomalous concentrations and high concentrations are shown as lines of longer and shorter length, respectively.

Any geochemical evaluation of a geologic terrane has to deal with the issue of determining which elemental concentrations are background and which are anomalous. This issue becomes more difficult when a wide range of rock types is present. For example, average Co concentration in mafic rocks is 48 ppm (parts per million), but, in granites, average Co concentration is 1 ppm (Rose and others, 1979, p. 554). If high Co concentrations are accompanied by high concentrations of other common constituents of mafic rocks such as Ni and Cr, high Co concentrations might be due to the presence of mafic rocks and, therefore, will probably not be anomalous. On the other hand, if high Co concentrations are accompanied by high concentrations of base metals but not by Ni and Cr, then hydrothermal activity may be the reason for the high concentrations; Co is part of the geochemical signature for a number of mineral-deposit types (porphyry copper, for example) that are not associated with mafic rocks (Cox and Singer, 1986). Therefore, the recognition of geochemical signatures is an important part of this geochemical evaluation of the EMNSA in view of the wide range of bedrock types. The following suggestions for permissive mineral-deposit types in each of the areas discussed are based on both the general types of bedrock in a given area and the geochemical signature for the area.

A special problem in the identification of geochemical signatures in the EMNSA is that of the recognition of REE signatures, inasmuch as the rare earth elements tend to be present together (Levinson, 1980, p. 868), whether in accessory minerals, such as apatite or monazite, or in economic deposits, such as at the Mountain Pass Mine. Also, REE tend to be present in high concentrations in Proterozoic and Jurassic granites of the EMNSA (D.M. Miller, written commun., 1991), especially in syenite, a fairly common rock type in the EMNSA. Thresholds for REE listed in table 13 were established on the basis of concentrations in RASS-PLUTO stream-sediment and NURE sediment-soil samples collected within about 0.8 km of the Mountain Pass Mine and also downstream from it, 3.2 to 4.8 km away. These samples showed an association of REE, Ba, and Sr, all components of the ore in the Mountain Pass Mine (see subsection above entitled "Ultrapotassic Rocks, Carbonatite, and Rare Earth Element Deposit, Mountain Pass, Southern California").

On the basis of mineral-deposit occurrences and geologic studies of the EMNSA and surrounding areas, the EMNSA has potential for many types of mineral deposits, which include porphyry copper-molybdenum deposits, precious and base metals (polymetallic) in veins or replacement bodies, gold deposits of several types (for example, breccia-pipe gold and volcanic-hosted gold), various types of mineralized skarn, and U-Th-Nb-REE-bearing carbonatites or pegmatites. Table 14 summarizes the geochemical results on an area-by-area basis. The listing of elements for each area in table 14 is based only on samples from within the specific areas shown on figure 49. Therefore, the listings differ slightly from those reported in table 7 of U.S. Geological Survey (1991, p. 182–183), which also included some samples near but outside the areas. The combined RASS and PLUTO stream-sediment data sets are referred to as stream-sediment samples, whereas the combined NURE stream-sediment and soil samples are referred to simply as NURE samples.

The following discussions of areas apply the qualitative terms "not," "weakly," "mildly," "moderately," or "highly" anomalous to each of the areas as a whole. These qualitative terms are based on the number and proportion of samples that have anomalous concentrations, the number of elements present in anomalous concentrations, the intensity of the anomalous concentrations in individual samples, and the number of sample media that have anomalous concentrations. A preponderance of high but not necessarily anomalous concentrations is the basis for regarding some areas as at least weakly anomalous (table 14) in terms of a given element. The rationale is that a mineralizing system at depth might result in what appears to be a high background; the geochemical signature then determines where the area falls on the scale between "not anomalous" and "highly anomalous." As always, the mineral-resource potential of each area is determined by its geochemistry in conjunction with geologic, geophysical, and mineral-deposit studies, as well as other data. As stated before, the geochemical signatures for each area are defined without regard to possible grade or tonnage of any possibly included mineralized system.

Bedrock types in the following sections are listed according to relative abundance in each area. Elements are listed in the general order of (1) those associated with various sulfide deposits, (2) those associated with late-stage magmatic differentiates, and (3) those elements that are part of the REE association; obviously, considerable overlap of these three associations exists.

Soda Mountains

Bedrock of that part of the Soda Mountains that lies on the west border of the EMNSA (fig. 49) consists of Jurassic and Cretaceous granitoid rocks and Mesozoic volcanic and sedimentary rocks (pl. 1). Some stream-sediment samples from the Soda Mountains have anomalous concentrations of Zn, B, Mo, and Sn. Concentrate samples contain anomalous concentrations of Cu, Ag, Zn, Mn, Pb, Au, Ba, Co, Bi, B, Sn, Mo, Be, Th, Nb, La, Ce, Tb, Yb, and Dy. No rock samples were collected in the area. NURE samples have anomalous concentrations of Eu. The area is overall mildly anomalous geochemically. Possible deposit types include porphyry copper-molybdenum, polymetallic veins and replacement bodies, copper or lead-zinc skarns, and Th-Nb-REE-bearing pegmatite or carbonatite. The anomalous values of the Nb-REE elements in concentrate samples may have been derived from small outcrops of Proterozoic rocks too small to show at the scale of our geologic map (pl. 1). Inasmuch as most of the Soda Mountains are outside the EMNSA, types of deposit are not shown on the compilation of the types of mineral deposits (pl. 2).

Little Cowhole Mountain

Cambrian dolomite and Jurassic and (or) Cretaceous granitoid rocks of Cowhole Mountains and Cambrian dolomite are present in approximately equal amounts in the area of Little Cowhole Mountain (pl. 1). The granitoid rocks of Cowhole Mountains in places are cut by epidote-chlorite veins plus or minus quartz and pyrite, especially near their southwesternmost exposure in Little Cowhole Mountain. Stream-sediment samples do not contain anomalous concentrations of any of the elements analyzed. Concentrate samples contain anomalous concentrations of Cu, Bi, Sn, Mo, Be, Th, and Tb. No rock samples were collected. The area is geochemically mildly anomalous. From the available geochemistry, possible deposit types include copper and tin skarns and Th-Be-REE-bearing pegmatites. Known deposits at Little Cowhole Mountain include the copper skarns at the Anthony prospects and at the El Lobo Mine (pl. 2). At the Anthony prospects (U.S. Bureau

of Mines, 1990a, map no. 338, pl. 1), copper skarn is seemingly zoned mineralogically from dense, steeply dipping, locally well bedded, light-green pyroxene skarn to olive-green to olive-brown compact masses of approximately 100 percent andradite that contains secondary copper minerals replacing chalcopyrite. Along the easternmost skarn at this locality, skarn is developed variably at least 500 m along the contact between the granitoid rocks of Cowhole Mountains (unit KJcm, pl. 1) and dolomite. The highest concentration of secondary copper minerals is associated directly with the most intense retrograde alteration of andradite to epidote. In detail, the contact between the granitoid rocks of Cowhole Mountains and wallrock is quite irregular, and the most continuously exposed pod of skarn has a width of approximately 100 to 150 m. In all, some skarn is exposed for more than 800 m along the contact. At the El Lobo Mine (U.S. Bureau of Mines, 1990a, map no. 339, pl. 1), extensive banded, brown-black garnet-pyroxene skarn in places is mantled by early-stage calc-silicate hornfels and cut by K-feldspar- and chalcedonic-quartz-bearing veins that include diffuse boundaries that fade into the surrounding groundmass of calc-silicate hornfels. Medial parts of the millimeter- to centimeter-sized veins are occupied by irregular concentrations of apple-green epidote. In places, ovoid pods of garnet-pyroxene skarn are approximately 100 m wide. The bulk of the sulfide minerals, mostly chalcopyrite, apparently is associated with epidote-altered garnet-pyroxene skarn. In addition, some coarsely crystalline sphalerite, in masses approximately 0.5 cm wide, is intergrown with epidote. The granitoid rocks of Cowhole Mountains, in the area immediately adjacent to the El Lobo Mine, mostly consist of partially chloritized hornblende diorite that includes less than 1 volume percent dispersed cubes of iron oxide replacing pyrite. One prospect pit at the El Lobo Mine shows intense development of siderite that is controlled strongly by minor structures striking north-south and dipping approximately 40° W. Some open spaces in brecciated siderite along these structures are filled by quartz (fig. 74). Nonetheless, the overall concentration of secondary copper minerals in the general area is relatively weak.

Cowhole Mountain

Bedrock of Cowhole Mountain consists of Jurassic and (or) Cretaceous granitoid rocks, Jurassic quartzarenite, Mesozoic volcanic and sedimentary rocks, Cambrian dolomite, Devonian to Permian limestone, and Early Proterozoic gneiss and granitoid rocks (pl. 1). The only element present in anomalous concentrations in samples from the Cowhole Mountain area is Mo in one concentrate sample. No rock samples were collected. The area is not geochemically anomalous, on the basis of RASS and PLUTO stream-sediment data sets and NURE samples. In addition to the polymetallic and iron skarn shown on plate 2 in the northern part of Cowhole Mountain (U.S. Bureau of Mines, 1990a, map nos. 343–344, pl. 1), the polymetallic skarn at the Mosaic Queen Mine (map no. 344) is the proximal occurrence of a fairly continuous zone of genetically related mineralized rocks that extend along a strike length of about 0.5 km in a northwest-southeast direction (fig. 75). At its southeasternmost end, unprospected mineralized rock, in places as much as 30 m wide, is dominated by massive replacement of Cambrian dolomite and Devonian to Permian limestone by specularite associated with epidote. Some coarsely crystalline specularite crystals are as much as 1 cm wide, and the specularite-replacement bodies show very sharp contacts with fractured and altered limestone. The iron-mineralized rock becomes dominated by a magnetite-garnet-pyroxene skarn alteration somewhat to the south of the Mosaic Queen, and some pendants of limestone have been converted almost entirely to massive epidote that includes some disseminated, fine-grained crystals of specularite. At the Mosaic Queen, sucrosic, gray-white marble that weathers pinkish tan includes less than 5 volume percent calc-silicate minerals. Immediately above the major prospect pit there, magnetite-hematite is intergrown with olive-green to olive-brown massive garnet. Magnetite definitely predominates over specularite. Samples analyzed by the U.S. Bureau of Mines (1990a) from this locality include as much as 3,900 ppm Zn, as much as 2,600 ppm Cu, and greater than 10,000 ppm Pb.

Cinder Cone Area

Approximately equal map areas of Cretaceous adamellite and Pliocene and Pleistocene basalt lava flows dominate the Cinder Cone area, located due east of Baker in the northwestern part of the EMNSA (pl. 1). Lesser amounts of Early Proterozoic gneiss and granitoid rocks, at and east of Seventeenmile Point, and Pliocene and Pleistocene basalt cinder deposits also are present. All sample media are represented in the samples collected in the

Cinder Cone area. Many elements are present in anomalous concentrations in all sample media. Stream-sediment samples contain anomalous concentrations of Zn, Mo, and Co. Concentrate samples have anomalous concentrations of Cu, Mn, Ag, Zn, Co, Bi, Sn, Mo, Be, Th, Nb, Tb, and Yb. Rock samples have anomalous concentrations of Cu, Pb, Ag, Zn, As, Sb, Mn, Bi, B, Sn, Mo, and W. NURE samples contain anomalous concentrations of Th, Ce, and Eu. Possible deposit types, which are based on geochemistry, include porphyry copper-molybdenum, polymetallic veins and replacement bodies, a variety of types of mineralized skarn, and Th-Nb-REE-bearing carbonatite and pegmatite. This large area is moderately anomalous, on the basis of the large number of elements present in anomalous concentrations even though the concentrations tend to be only weakly to moderately anomalous.

Types of deposits known in this general area include gold-silver quartz-pyrite veins, polymetallic veins, polymetallic fault, and polymetallic and tungsten skarn (pl. 2). Occurrences of polymetallic fault essentially are oxidized, base- and precious-metal-mineralized fault zones that include mostly brittle-style fault gouge and breccia and lack high concentrations of quartz and carbonate minerals as gangue. Most mineral occurrences are in the general area of Seventeenmile Point and the Paymaster and Oro Fino Mines; these epigenetic occurrences are hosted by Early Proterozoic rocks. Some likelihood exists that these areas may be parts of large slide blocks (H.G. Wilshire and J.E. Nielson, written commun., 1991). Approximately 50 percent of the occurrences have been classified as gold-silver quartz-pyrite veins. In general, widely spaced fractures that show northwesterly directed strikes are filled by brick-red iron oxides that locally include approximately 0.3-m-wide brecciated vein quartz. The attitudes of such mineralized fractures and veins are at very high angles to the ductile-style metamorphic foliation in the enclosing gneiss and granitoid. At the main workings of the Paymaster Mine (U.S. Bureau of Mines, 1990a, map no. 353, pl. 1), a 1- to 2-m-wide zone of brecciated gneiss and granitoid is densely veined by quartz (fig. 76). Some nearby veins pinch and swell, also at high angles to the metamorphic fabrics. At the Paymaster No. 3 Mine, mineralized gold-silver quartz-pyrite zones are as much as 2 to 3 m wide, have a strike of N. 10° W., and dip to the northeast. At the surface, these zones extend as much as 50 m from the main portal.

Exposures in the pediment area approximately 0.8 km due west of the Paymaster Mine contain epidotized granodiorite that may be the locus of emplacement of a widespread mineralized system that shows the general area of the gold-silver quartz-pyrite veins at the Paymaster Mine as a distal manifestation. In the pediment area, away from the major exposures of bedrock, small pods of 1- to 2-m-wide heavily epidotized granodiorite and, possibly, some dark-green, pyroxene-bearing calcic exoskarn are present where the epidotized granodiorite is in contact with marble.

Gold-silver quartz-pyrite veins also appear to be the predominant type of occurrence in the general area of the Oro Fino Mine (this particular mine is designated incorrectly as the Brannigan Mine on the Old Dad Mountain 15′ quadrangle). Such veins have been emplaced along a west-northwest-striking fault that includes recrystallized, well-bedded marble and brecciated limestone in the hanging wall. The fault zone is at least 2 to 3 m wide and shows evidence in outcrop of a brittle style of deformation; its dip is approximately 35° to 40° N. The brecciated-limestone body is terminated on the east by another north-northeast-striking fault that seems to have hosted most of the mineralization explored in the workings. Near the headframe at these workings, very steeply dipping and shattered rocks crop out for distances of as much as 5 to 6 m and have been explored by at least two shafts.

Some of the most intensely mineralized rock in this area is in the immediate vicinity of the Oro Fino Mine and its nearby workings (U.S. Bureau of Mines, 1990a, map no. 356, pl. 1). At the Oro Fino Mine, a west-northwest-striking mineralized fault includes recrystallized, well-bedded limestone and brecciated limestone in its hanging wall. Brecciated limestone, possibly indicative of some type of collapse, is fairly widespread in this area and is present also in some relatively thick sequences of rock exposed nearby (fig. 77). These rocks presumably are part of the Paleozoic sequence of rocks in the EMNSA, but they have not been mapped separately on the geologic map (pl. 1) because of limitations of scale. The mineralized fault zone is 2 to 3 m wide, dips 35° to 40° N., and includes gold-silver quartz-pyrite-type veins along it. On the east, the limestone megabreccia in the hanging wall is bounded by a north-northeast-striking mineralized structure that apparently hosted some of the most productive ore shoots at the mine and was explored by a major shaft and auxiliary

levels. Heavily iron-oxide-stained quartz-pyrite veins show maroon- to brick-red colors that grade into ochre-dominated colors. In the area of the main headframe, very steeply dipping, shattered mineralized rocks along the north-northeast-striking mineralized structure are as much as 5 to 6 m wide and are explored by at least two shafts.

The workings of the Brannigan Mine are actually located close to the southeast corner of sec. 26, T. 13 N., R. 10 E. (U.S. Bureau of Mines, 1990a, map no. 362, pl. 1). Near these workings, some well-bedded quartzite includes a thin quartz-pebble conglomerate at its base, which in turn lies unconformably on gneissic metaquartzite that presumably is Proterozoic in age (fig. 25*A*). The quartzite is probably Late Proterozoic and Cambrian in age and has been included with the Early Proterozoic gneiss and granitoids (Xg) unit on the geologic map (pl. 1) because of its limited areal extent. At the main workings of the Brannigan Mine (termed the Brannigan East Mine by the U.S. Bureau of Mines (1990a) and subsequently restaked as the Rachele claim group), quartz-sulfide (pyrite) veins plus or minus chalcopyrite and tremolite and (or) actinolite appear to have been the ore worked in the past. Some veins show altered wallrocks that contain a coarsely crystalline, dark-green, possibly hedenbergitic, pyroxene. Such zones of alteration and mineralization closely follow bands of dolomite in the Paleozoic rocks. A sample analyzed by the U.S. Bureau of Mines (1990a) from this locality included 8.75 ppm Au and 160 ppm Ag, which is consistent with the high Ag/Au ratio that is characteristic of many polymetallic veins in the EMNSA.

In the Turquoise Mountain Mining District in the hills near Halloran Spring, 5 km northwest of the EMNSA, copper-molybdenum mineralization is related apparently to shallow-seated porphyritic intrusions (Hall, 1972). Little known mineralization exists in Proterozoic rocks of this area. Mineralization at the Telegraph Mine (U.S. Bureau of Mines, 1990a, map no. 121, pl. 1), near the southeast end of the hills near Halloran Spring, includes low-sulfide, vug-filling, gold- and silver-bearing quartz veins that were emplaced at approximately 10 Ma (Lange, 1988). These veins, which cut the informally named, Cretaceous Teutonia adamellite of Beckerman and others (1982) (Kt), are classified as gold-silver quartz-pyrite veins that are epithermal and related to wrench faulting. Early Proterozoic rocks in southeastern parts of the hills near Halloran Spring lie within the Cinder Cones Wilderness Study Area, where Wilshire and others (1987) found no evidence of mineralization. Wilshire and others (1987) assigned a low potential for gold and silver to areas underlain by Early Proterozoic rocks primarily because of their proximity to Cretaceous plutonic rocks, thought elsewhere in the region to be associated genetically with mineralization in Proterozoic wallrocks (Hewett, 1956). However, neither indications of mineralization in the vicinity of those contacts nor signs of prospecting were found by Wilshire and others (1987).

Marl Mountains

Bedrock geology of the Marl Mountains, approximately 6 km northeast of Kelso Peak, is dominated by Cretaceous adamellite (pl. 1). Early Proterozoic gneiss and granitoid rocks also are present. Stream-sediment samples from the Marl Mountains have anomalous concentrations of Pb, Ag, Zn, and Mo. Concentrate samples have anomalous concentrations of Cu, Ag, Zn, Au, Bi, Mo, Th, La, Ce, Nd, Sm, Tb, Yb, and Dy. No rock samples from the Marl Mountains are available. NURE samples have anomalous concentrations of Th and Dy. The area is moderately anomalous geochemically. Deposit types possible from these data include porphyry copper-molybdenum, polymetallic veins and replacement bodies, and REE-Th-bearing carbonatite and pegmatite. Cretaceous adamellite in the Marl Mountains is known to include four polymetallic-vein, one polymetallic-fault, and five gold-silver quartz-pyrite vein occurrences (pl. 2). We use the designation of polymetallic fault to refer to brittle-type fault zones, almost all heavily oxidized, that are mineralized by base and precious metals and lack silicate and carbonate veins.

Old Dad Mountain

No single rock type dominates Old Dad Mountain and its surrounding area (pl. 1). The promontory at Old Dad Mountain itself is underlain by a resistant knob of limestone that is part of the Devonian to Permian limestone (PDl, pl. 1) unit. Other lithic units present are Early Proterozoic gneiss and granitoid rocks (Xg), Jurassic Aztec Sandstone (Ja), Mesozoic volcanic and sedimentary rocks (Mzv), Late Proterozoic and Cambrian

siliciclastic rocks (ЄZs), and Tertiary volcanic rocks (Tv_1). Dunne (1972, 1977) mapped the Old Dad Mountain area but did not subdivide the Proterozoic rocks. Hewett (1956) reported the presence of granite, schist, and quartzite intruded by syenite dikes in the Proterozoic rocks in this general area.

Stream-sediment samples from Old Dad Mountain do not have anomalous concentrations of any of the elements considered. Concentrates have anomalous concentrations of Cu, Pb, Ag, Bi, Sn, Th, and Tb. Rocks have anomalous concentrations of Cu, Pb, Zn, Ag, Au, Co, Mo, Bi, B, and Be. The area is mildly anomalous geochemically. Porphyry copper-molybdenum deposits, polymetallic vein or replacement bodies, mineralized skarn, pegmatites, or carbonatites may be present on the basis of the elemental concentrations above. The area in the vicinity of Old Dad Mountain under discussion here extends approximately 16 km in a northwest-southeast direction from south of Seventeenmile Point to south of the Kelso Mountains (pl. 1). From northwest to southeast, the types of deposits in the vicinity of Old Dad Mountain include polymetallic faults at the Sweet (Reviella) claim group (U.S. Bureau of Mines, 1990a, map no. 366, pl. 1) and Lucky (ODM) claim group (U.S. Bureau Mines, 1990a, map no. 368, pl. 1), some polymetallic veins also at the Lucky (ODM) claim group, and iron skarn at the Old Dad Mountain iron deposit (U.S. Bureau Mines, 1990a, map no. 369, pl. 1) that also shows some minor amounts of polymetallic vein (fig. 78*A*). In addition, copper- and zinc-bearing magnetite skarn is present at the Golden M Mine (U.S. Bureau Mines, 1990a, map no. 372, pl. 1), located approximately 3 km southeast of the main promontory at Old Dad Mountain itself (pl. 2), that we classify as polymetallic skarn because of high concentrations of base metals at the occurrence.

Although these four mineralized occurrences extend almost across the entire length of the Old Dad Mountain area, surface indications of alteration are confined to the general areas of the mineralized occurrences. However, alteration is well exposed and widespread at one of the occurrences. At the Lucky (ODM) claim group, a zone of chloritic alteration as much as 150 m thick and containing abundant iron oxides (presumably after iron sulfide minerals of some type) is present in Late Proterozoic and Cambrian siliciclastic rocks (ЄZs), which as mapped includes shattered and chloritized granodiorite. Some of this granodiorite contains fault zones filled by 0.3-m-wide ochre gossan. Recrystallized limestone, presumably part of the Devonian to Permian limestone (PDl) and seemingly in tectonic contact with the siliciclastic rocks, overlies the siliciclastic rocks and, in places, is laced with iron-oxide-stained fractures. Shattered siliciclastic rocks below the contact show fairly abundant secondary copper minerals on their weathered surfaces together with some glassy-appearing vein-type quartz. The exposed width of the shattered and mineralized rocks at this particular locality is as much as 150 m and the strike length is approximately 3.5 to 4 km. Some narrow, sulfide-impregnated, clay-altered rhyolite or rhyodacite dikes, which contain 5 to 15 volume percent phenocrystic quartz, have been emplaced into the shattered siliciclastic rocks and apparently are related genetically to the surrounding alteration (fig. 78*B*). A sample analyzed by the U.S. Bureau of Mines (1990a) from this locality included about 500 ppb Au. In many gold-rich porphyry-type systems, 500 ppb is the Au concentration in many ore zones (Sillitoe, 1979), and this Au value in samples is considered by many exploration geologists to constitute a threshold that warrants additional investigation. As a comparison, geochemical studies of the Kalamazoo porphyry copper deposit, located in Arizona, show that the ore there, not known particularly for its Au content, contains as much as 800 ppb Au along some extended intercepts of drill core (Chaffee, 1976). However, alteration in the general area of the Lucky (ODM) claim group suggests that other types of occurrences may be present, including porphyry gold and polymetallic replacement, in addition to those already listed above.

At the Old Dad Mountain iron deposit, massive magnetite-hematite replacement bodies show knife-edge contacts with the surrounding coarsely crystalline, brecciated white marble. The U.S. Bureau of Mines (1990a) estimated approximately 363,000 to 454,000 tonnes of magnetite-hematite-rich rocks remain in place at this locality. Much of the magnetite is intergrown with actinolite and seems to be related genetically to a highly schistose, chloritized granodiorite (not shown on plate 1 because of its relatively small size) that is cut by magnetite-actinolite-epidote veins. Blades of actinolite commonly are present in clusters as much as 2 to 4 cm wide. In addition, the schistose granodiorite shows development of some early-stage gray-green pyroxene hornfels in adjoining limestone. The apparently richest pods of magnetite-bearing rocks formed in limestone that crop out as much as 5 to 10 m away from the actual contact with schistose granodiorite. Overall, the mineralization at this locality is associated with a low-sulfur-bearing environment, although minor amounts of

secondary copper minerals, probably chrysocolla, are present in some pods of magnetite as alteration products of chalcopyrite.

At the Golden M polymetallic-skarn occurrence, most mineralization is confined to an approximately 1-m-wide minor fault zone that strikes about N. 40° E., dips 80° to 90° S., and separates Devonian to Permian limestone (PDl) from a small mass of Proterozoic gneiss, which has been included with Mesozoic volcanic and sedimentary rocks (Mzv). The fault zone is at a high angle to foliation in the gneiss. Secondary copper minerals are present in most masses of magnetite-epidote, which form highly irregular replacement pods along a strike length of about 150 to 300 m. Some olive-green to brown garnet skarn is cut by reticulated, millimeter-sized veinlets of magnetite. In addition, much of the limestone close to the workings (two adits and an incline) is heavily stained by orange iron oxide minerals, suggestive of disseminated iron sulfide minerals. One sample analyzed by the U.S. Bureau of Mines (1990a) from this locality included more than 500 ppb Au.

Kelso Mountains

Bedrock of the Kelso Mountains includes Early Proterozoic gneiss and granitoid rocks (unit Xg, pl. 1), Late Proterozoic and Cambrian siliciclastic rocks (€Zs), and Cretaceous granitoid rocks, the latter of which includes fairly wide expanses of the informally named Teutonia adamellite of Beckerman and others (1982) (Kt) and some relatively small occurrences of biotite-rich granitoid (Kb). Concentrate samples have anomalous concentrations of Cu, Ag, Au, Sn, W, La, Ce, Nd, Sm, Tb, and Dy. NURE samples contain anomalous concentrations of La and Dy. No rock samples from the area are in the databases. The area is geochemically mildly anomalous overall. Mineralized skarns and REE-bearing pegmatite and carbonatite are possible deposit types. The Kelso Mountains are characterized by a REE geochemical signature, although the presence of Cu, Ag, and Au may be indicative of the presence of polymetallic veins. Types of mineral occurrences known in the general area of the Kelso Mountains include polymetallic fault, gold-silver quartz-pyrite vein, and polymetallic vein (pl. 2). Most of these occurrences, 12 in all, are associated spatially with Late Proterozoic and Cambrian siliciclastic rocks that crop out in the southeastern part of the Kelso Mountains (pl. 1). The two gold-silver quartz-pyrite veins known here crop out in areas underlain by Early Proterozoic gneiss and granitoid rocks. These spatial associations between mineral occurrence and host rock suggest derivation of some of the Au and Ag from Early Proterozoic gneiss and granitoid rocks. The known mineralization in the general area of the Kelso Mountains is presumed to be related to Mesozoic magmatism. However, Jurassic and Cretaceous granitoid rocks (pl. 1) that crop out in the southern part of the Kelso Mountains area are not known to host any metallic-mineral occurrences. Analyses of mineralized rocks from the area of the Kelso Mountains further suggest that overall intensity of precious-metal mineralization here is less than that found elsewhere in the EMNSA (U.S. Bureau of Mines, 1990a). Only two analyzed samples of mineralized rocks contain more than 500 ppb Au at the 12 sites.

Bristol Mountains

Bedrock of the Bristol Mountains, located northwest of the Granite Mountains just outside of the EMNSA near its southwest corner, consists of Jurassic granitoid rocks. Stream-sediment samples in the Bristol Mountains contain anomalous concentrations of Mn, Pb, Zn, Sn, Mo, and B. Concentrate samples contain anomalous concentrations of Cu, Mn, Ag, Zn, Mo, Sn, Be, Nb, La, Nd, Sm, Eu, Yb, and Dy. NURE samples have anomalous Eu concentrations. The databases contain no rock data. The area geochemically is mildly to moderately anomalous overall. Skarn, polymetallic vein, or replacement bodies and REE-bearing carbonatite or pegmatite are possible deposit types. We have not classified or shown the distribution of the types of mineral occurrences present in the Bristol Mountains because all of the bedrock in the mountains is outside of the EMNSA.

Clark Mountain Range

Bedrock of the Clark Mountain Range includes Early Proterozoic gneiss and granitoid rocks (unit Xg, pl. 1), Late Proterozoic and Cambrian siliciclastic rocks (€Zs), Cambrian dolomite (€d), and Devonian to Permian limestone (PDl). The Clark Mountain Range is moderately to highly anomalous geochemically. Many

elements are present in anomalous concentrations in all sample media (table 13). Present and past mining activities emphasize the anomalous geochemistry of the area. The presence of the carbonatite-hosted REE deposit at Mountain Pass is reflected by anomalous concentrations of REE in concentrate and NURE samples. Other possible deposit types in the Clark Mountain Range include porphyry copper-molybdenum, polymetallic vein and replacement bodies, skarn, and pegmatite, on the basis of anomalous metal concentrations. Types of mineral occurrences and deposits in the Clark Mountain Range include the following: (1) silver-copper veins in brecciated dolostone; (2) polymetallic veins; (3) gold breccia pipe at the Colosseum Mine; (4) tungsten veins; (5) barite veins; (6) polymetallic replacement; (7) copper skarn at the Copper World Mine (fig. 79*A*); (8) zinc-lead skarn; (9) gold-silver quartz-pyrite vein; (10) placer gold and platinum-group elements; and (11) polymetallic skarn (pl. 2). As described in the sections that follow, many deposits and mineral occurrences apparently are linked genetically, as exemplified by many occurrences that surround the gold breccia pipe at the Colosseum Mine (Sharp, 1984). Silver-copper brecciated dolostone, tungsten veins, and barite veins apparently are related to emplacement of the gold breccia pipe at the Colosseum Mine during the Cretaceous. All tungsten vein occurrences are present on the east side of the range and are hosted by Early Proterozoic younger granitoids (Xg_1). In addition, on the west side of the range, some polymetallic replacement deposits and occurrences are present in another areally extensive mineralized environment where they are distal to polymetallic, copper, and zinc-lead deposits and occurrences associated with emplacement of Cretaceous granitoid rocks (Kg_2). Also, mineralization at the Conquistador No. 2 Mine (U.S. Bureau of Mines, 1990a, map no. 70, pl. 1) apparently is related to development of the metamorphic fabric in the enclosing Late Proterozoic and Cambrian siliciclastic rocks (pl. 1). At this locality, a series of shafts and approximately 15 trenches and shallow prospects explore a vein that strikes N. 35° E. and dips 35° to 45° N. This vein system is exposed discontinuously along a strike length of about 300 m. Where well exposed in the shafts, individual veins commonly are as much as 1 m wide and show bleaching of the surrounding siliciclastic rocks for distances of about 3 m on either side of the trace of the vein segments. Quartz in the veins is milky white and typically includes some iron oxide minerals that replace pyrite, which at one time constituted probably as much as 2 volume percent of the vein. The fabric of the vein quartz parallels the schistosity in the surrounding siliciclastic rock. Elsewhere in the general area of the Conquistador No. 2 Mine, wispy, apparently deformed stringers of vein quartz cut across the well-developed slaty cleavage in the siliciclastic rocks. The occurrences at the Conquistador No. 2 Mine are one of the few places in the EMNSA where mineralization seems to be associated with the metamorphic deformation. Nonetheless, cursory examination of exposures of the siliciclastic rock in the general area of the Conquistador No. 2 Mine suggests that this type or style of mineralization is fairly isolated. No widespread development exists of a pervasive low-sulfide gold-quartz type of vein mineralization, as we classify the Conquistador No. 2 Mine following the criteria of Berger (1986a) for these types of deposit. The geologic environment and overall extent of mineralization at the Conquistador No. 2 Mine may be more analogous to low-sulfide gold-quartz veins of the Chugach, Alaska, type (Bliss, 1992b), which are restricted to nonbatholithic terranes, than to those reported previously by Berger (1986a).

Mescal Range

Bedrock of the Mescal Range includes Cambrian dolomite (unit $\mathcal{C}d$, pl. 1), Late Proterozoic and Cambrian siliciclastic rocks ($\mathcal{C}Zs$), Jurassic sandstone (Ja), Devonian to Permian limestone (PDl), and Jurassic Ivanpah granite of Beckerman and others (1982) (Ji). Concentrations of Pb, Zn, and Tb are anomalous in concentrate samples. The databases have no rock samples from the area shown as the Mescal Range on figure 49. Polymetallic veins or replacements are the most likely deposit types in the area because Early Proterozoic rocks hosting REE-bearing pegmatite and carbonatite do not crop out in this area. Known deposits and occurrences in the general area of the Mescal Range are predominantly zinc and lead bearing. They include zinc and lead skarn (exemplified by the Mohawk Mine), polymetallic skarn, polymetallic replacement, and polymetallic vein, and they are concentrated in the general area of several small bodies of Cretaceous monzogranite that crop out near the west end of Mohawk Hill in the northwestern part of the area of the Mescal Range (pl. 2). Lead-zinc-mineralized garnet-pyroxene skarn in direct contact with clay-altered biotite monzodiorite is well exposed near the main headframe at the Mohawk Mine (fig. 79*B*). In addition, a small number of gold-silver quartz-

pyrite veins is present, as well as one placer-gold occurrence present in gravels near the Mohawk Mine. The widespread presence of zinc-lead-bearing types of deposit here contrasts markedly with the copper-bearing types, classified mostly as copper skarn (pl. 2), just to the north of Mohawk Hill in the general area of the Copper World Mine. However, the predominance of zinc-lead types of occurrences here does not exclude the possibility of significant precious-metal deposits being present. Some fairly widespread exposures of coarse-grained monzogranite porphyry that is intensely propylitically and argillically altered in association with emplacement of pyrite-bearing quartz veins and stockworks are present in the southern part of the Mescal Range. These exposures of altered monzogranite, shown as unit Kg_1 on plate 1, are in the general area of the Iron Horse (Bonanza), Lead Lady, and Blue Buzzard Mines (U.S. Bureau of Mines, 1990a, map nos. 144–146, pl. 1). The mostly polymetallic-replacement-type mineralization at these three deposits appears to be related to the altered monzogranite. However, analyses by the U.S. Bureau of Mines (1990a) of mineralized rock samples from these three deposits all show Au concentrations of less than 500 ppb (pl. 6). Nonetheless, many jasperoids in the general area of these deposits include Au concentrations in excess of 1,000 ppb, and related targets were being drilled during 1991 by the exploration group of Phelps Dodge Mining Co. (John D. Forrester, oral commun., 1991). Additional discussion concerning genetic linkages among types of deposits is included in the section below entitled "Evaluation of Metallic Mineral Resources."

Ivanpah Mountains

Bedrock of the Ivanpah Mountains includes Jurassic granite (unit Ji, pl. 1); Early Proterozoic granitoid rocks, gneiss, and migmatite (Xm); Devonian to Permian limestone (PDl); Late Proterozoic and Cambrian siliciclastic rocks (ЄZs); and Cambrian dolomite (Cd). Thick sequences of thin-bedded Paleozoic carbonate rocks are exposed conspicuously in the Striped Mountain block of the Ivanpah Mountains area (fig. 80; pl. 1). Stream-sediment samples from the Ivanpah Mountains contain anomalous concentrations of Cu, Ag, Zn, Mo, Sn, and W. Other sample media contain anomalous concentrations of many elements that suggest the presence of polymetallic veins or replacement bodies, porphyry copper-molybdenum deposits, skarns, and carbonatites or pegmatites containing deposits of REE or Th. Concentrate samples have anomalous concentrations of Cu, Mn, Pb, Ag, Au, Co, Bi, Sb, Mo, W, Sn, Be, Th, La, Ce, Nd, Sm, Tb, and Dy. Rock samples have anomalous concentrations of Cu, Zn, Co, Mn, Pb, Ag, As, Bi, W, Sn, Mo, Be, and B. NURE samples contain anomalous concentrations of La, Ce, Lu, Sm, Eu, Tb, Yb, and Dy. Overall, the Ivanpah Mountains geochemically are moderately to highly anomalous.

Known deposit types in this area include tungsten skarn, polymetallic fault, polymetallic vein, copper skarn (pl. 2), and one unnamed occurrence of low-sulfide gold-quartz vein in the Late Proterozoic and Cambrian siliciclastic rocks (U.S. Bureau of Mines, 1990a, map no. 16, pl. 1). At the gold-quartz-vein locality, shattered rocks approximately 1 m wide show local emplacement of quartz-pyrite-minor chalcopyrite veins at a high angle to the regional attitude of foliation in the surrounding siliciclastic rock. However, the vein quartz is itself deformed and shows a foliated fabric that includes lineated margins in its selvages. Approximate attitude of the veins is a N. 40° W. strike and a 55° S. dip. Massive epidote skarn is present at the Silverado-Tungstite Mine at the east end of Striped Mountain (fig. 79*C*), from which a small tonnage of silver ore was shipped prior to 1900 (U.S. Bureau of Mines, 1990a). Mineralization at this locality is probably associated with the adjoining Jurassic Striped Mountain pluton (Jsm), which is present as a narrow intrusion of hornblende diorite along the west side of the Ivanpah Mountains (pl. 1). Silver mineralization at the Silverado-Tungstite Mine may be associated with retrograde quartz, which fills open spaces and cuts prograde garnet skarn (fig. 79*D*). In addition, some endoskarn is well developed near the Silverado-Tungstite Mine as diffuse epidote skarn that shows relict igneous textures. Jasperoid along a 2- to 3-m-wide, steeply dipping fault that strikes N. 35° W. at the Express Mine (U.S. Bureau of Mines, 1990a, map no. 171, pl. 1) has been explored by a 10- to 12-m-wide open cut and is classified by us as a polymetallic fault (pl. 2). In addition, the area of Striped Mountain contains a vast resource of limestone (U.S. Bureau of Mines, 1990a).

The bulk of the mineralization in terms of numbers of occurrences in this part of the EMNSA is present in Jurassic granitoid rocks as polymetallic veins, gold-silver quartz-pyrite veins, polymetallic faults, zinc-lead skarns in pendants too small to show at the scale of the geologic map, and one fluorite vein (pl. 2). The gold-

silver quartz-pyrite veins show no apparent lateral zonation relative to the distribution of polymetallic veins in this general area. The tin (tungsten) skarn mineralization at the Evening Star Mine (U.S. Bureau of Mines, 1990a, map no. 193, pl. 1) apparently is related to emplacement of Jurassic granitoid rocks, although the main mass of the Jurassic granitoid rocks crops out approximately 1 to 5 km east of the workings at the Evening Star Mine (pl. 1). Narrow dikes at the Evening Star Mine and at the nearby Standard Mine No. 2 are similar lithologically to Jurassic granitoid rocks east of these two occurrences. At the Evening Star Mine, chalcopyrite-bearing tremolite hornfels is present near the outer limits of skarn development and is mantled by a zone of recrystallized limestone that includes fine-grained crystals of magnetite and (or) pyrite. In places, the marble has been dolomitized as much as 10 m away from some zones of heavily sulfidized, structurally controlled skarn. South-southwest of the Evening Star Mine, Jurassic granitoid rocks have been converted to an epidote endoskarn that shows relict outlines of plagioclase. Magnetite is abundant in many pods of skarn at the Evening Star Mine, and the magnetite seems to be one of the earliest postsilicate phases to crystallize in the open-space environment of the skarns.

Cima Dome

Bedrock of the Cima Dome area includes two bodies of Cretaceous adamellite, the Teutonia adamellite and the Kessler Springs adamellite, both of which are informally named units of Beckerman and others (1982), and an elongate, northwest-trending body of Jurassic granite (pl. 1). Geochemical samples in the area of Cima Dome are represented by only one sample, a rock that contains an anomalous concentration of Tb. The only known mineral occurrence in the area of Cima Dome is present at the Teutonia Mine (pl. 2; see also U.S. Bureau of Mines, 1990a, map no. 210, pl. 1).

At the Teutonia Mine, polymetallic-vein mineralization is concentrated along a zone that strikes N. 60° W. in the Kessler Springs adamellite. Alteration in the area of the mine extends approximately 20 to 30 m from some of the major strands of vein exposed by several currently inaccessible shafts. Alteration consists mainly of conversion of plagioclase to clay minerals, possibly including some halloysite. Some 4- to 5-cm-wide, greasy-appearing, gray veins of quartz show early-stage sulfide minerals, now oxidized to ochre-brown iron oxide minerals, primarily along the walls of the veins, but some late-stage sulfide minerals also are present along the medial parts of the veins. A sample of ore obtained from a dump at the Teutonia Mine was examined using the scanning electron microscope. Silver-bearing minerals identified include galena, argentite, and tetrahedrite. Contents of silver in galena are highly variable even at the scale of the several-hundred-micron-wide domains examined. Some silver-bearing galena, as narrow, 5-µm-wide rims that discontinuously surround much larger crystals of sphalerite, is confined to short segments of the rims; the remaining galena is apparently free of any detectable silver. Some tetrahedrite detected is argentiferous, and it seems to be paragenetically intermediate between early-stage sphalerite and late-stage, notably non-silver-bearing galena. Other minerals detected during the scanning-electron-microscope study are aurichalcite (ideally, $2(Zn,Cu)CO_2 \cdot 3(Zn,Cu)OH_2$), barite, possibly specular hematite, covellite, and argentite. Argentite is present as feathery 2- to 3-mm-long crystals on the borders of irregularly shaped crystals of galena. The argentite is mantled by covellite in places. Overall, the locality shows relatively sparse concentrations of secondary copper minerals, including both malachite and chrysocolla. Although some veins also include iron-carbonate minerals, overall the veins still retain a high quartz-carbonate-mineral ratio. No carbonate minerals were noted in the walls of the veins. In places, vein material is coxcombed, brecciated, and filled by jasperoidal material. We have classified the mineralization at the Teutonia Mine as a silver-rich variety of polymetallic vein (pl. 2). Production from the Teutonia Mine includes approximately 46.9 kg Ag during 1880 (U.S. Bureau of Mines, 1990a).

New York Mountains

Bedrock of the New York Mountains includes extensive areas of Cretaceous adamellite (namely, the informally named Mid Hills adamellite of Beckerman and others (1982) (unit Kmh, pl. 1) and Early Proterozoic migmatite and granitoid rocks (Xm), as well as lesser amounts of Tertiary andesite and basalt (Tab), Devonian to Permian limestone (PDl), Cretaceous granodiorite (Klo), Tertiary dacite flows (Td), Mesozoic volcanic and sedimentary rocks (Mzv), Triassic sedimentary rocks (Trm), Cambrian dolomite (Cd), and Miocene

rhyolite ash-flow tuff (Tw). Numerous elements are present in anomalous concentrations in all sample media from the New York Mountains. The area is one of the most highly anomalous geochemically in the EMNSA. Stream-sediment samples contain anomalous concentrations of Cu, Mn, Pb, Ag, Zn, Mo, W, Co, B, and Be. Concentrate samples have anomalous concentrations of Cu, Mn, Pb, Ag, Zn, Co, Ba, Bi, Sn, Mo, W, Be, B, Th, La, Ce, Nd, Sm, Eu, Tb, Yb, and Dy. Rock samples have anomalous concentrations of Cu, Pb, Ag, Zn, Au, As, Co, Sb, Ba, Bi, La, Mo, and B. NURE samples have anomalous concentrations of Th, Ce, Dy, Lu, Eu, and Yb. Possible deposit types include porphyry copper-molybdenum, polymetallic vein and replacement bodies, disseminated gold, skarn of all types, and U-Th-Nb-bearing carbonatite and pegmatite.

A number of different types of mineralized systems are present in the New York Mountains. The Mid Hills adamellite hosts the Big Hunch stockwork molybdenum system (Ntiamoah-Agyakwa, 1987; U.S. Bureau of Mines, 1990a, map no. 290, pl. 1) that shows intensely developed quartz stockworks cropping out across an area of approximately 5 km^2 near the southwest edge of the New York Mountains (pl. 2). This system initially was thought to contain as much as approximately 363,000,000 kg Mo in about 1.6 billion tonnes of rock (U.S. Bureau of Land Management, 1980). However, subsequent investigations have shown that this amount of Mo should be revised substantially and that a content of approximately 21,000,000 kg Mo probably is a more reasonable estimate on the basis of results of drilling to date (Wetzel and others, 1992). In addition, the New York Mountains include the following other types of deposit: (1) polymetallic fault, gold-silver quartz-pyrite vein, and polymetallic vein in Early Proterozoic migmatite; (2) copper skarn and polymetallic skarn in Devonian to Permian limestone; and (3) polymetallic vein, polymetallic fault, gold-silver quartz pyrite vein, and tungsten vein in the Mid Hills adamellite. The polymetallic veins at the Golden Quail Mine near the southeast edge of the New York Mountains (pl. 2; see also U.S. Bureau of Mines, 1990a, map no. 417, pl. 1) were known to include an identified resource of 12,500 kg Au in 1992 (Wetzel and others, 1992). Elsewhere in the New York Mountains, the most intense concentration of mineral occurrences and deposits is present in Early Proterozoic migmatite. Analyses of mineralized rock samples from a cluster of these occurrences and deposits, in an area of about 20 km^2 near the site of Vanderbilt, show Au concentrations higher than 500 ppb (pl. 6).

Mid Hills

The Cretaceous Mid Hills adamellite (unit Kmh; pl. 1) and Rock Springs monzodiorite (Krs), both informally named units of Beckerman and others (1982), and Early Proterozoic granitoid rocks (Xg_2) are the predominant rock types in the Mid Hills. Tertiary tuffs (Tw) also are present. Stream-sediment samples from the Mid Hills contain anomalous concentrations of Zn, Mo, and B. Concentrate samples contain anomalous concentrations of Mn, Ag, Ba, Bi, Mo, W, Nb, La, Ce, Eu, and Nd. Rock samples contain anomalous concentrations of Zn, Mn, Pb, Ag, and Bi. NURE samples contain anomalous concentrations of Ce. Possible deposit types include porphyry copper-molybdenum, polymetallic vein and replacement bodies, skarns, and REE-Th-Nb-bearing pegmatites and carbonatites (pl. 2). The area is mildly to moderately anomalous geochemically overall.

The Mid Hills area includes some polymetallic vein; gold-silver quartz-pyrite vein; and polymetallic fault types of occurrences and deposits, together with a small number of polymetallic-skarn and copper-skarn occurrences hosted by pendants of Devonian to Permian limestone enclosed within the Mid Hills adamellite. Most occurrences are present near the mapped outer intrusive margin of the Mid Hills adamellite. Analyses of mineralized rock samples from several polymetallic-vein and polymetallic-fault occurrences in the general area of the Gold Valley Mine (U.S. Bureau of Mines, 1990a, map no. 570, pl. 1) show Au concentrations in excess of 500 ppb (pl. 6). Although the Mid Hills adamellite in places shows intense mineralization at the surface, large areas of this pluton in the Mid Hills are unaltered.

Providence Mountains

The geology of the Providence Mountains is complicated by the presence of major faults that bound many of the map units (pl. 1). The area is dominated by Devonian to Permian limestone (unit PDl; pl. 1); Cambrian dolomite (Cd); Jurassic granitoid rocks, which include the quartz monzonite of Goldstone (Jgo) and the quartz syenite of Winston Basin (Jwb); Early Proterozoic granitoid rocks (Xg_2); and Miocene rhyolite ash-flow tuff

(Tw). Significant amounts of Cretaceous porphyritic monzogranite (Kmh), Late Proterozoic and Cambrian siliciclastic rocks (€Zs), and Jurassic hypabyssal and metavolcanic rocks (Jh) and diorite (Jd) also are present. The Providence Mountains are geochemically the most highly anomalous area in the EMNSA (figs. 50–73) and have been heavily sampled. All sample media contain anomalous concentrations of many elements. Stream-sediment samples contain anomalous concentrations of Cu, Mn, Pb, Ag, Zn, Co, Sn, Mo, Ba, and W. Concentrate samples have anomalous concentrations of Cu, Mn, Pb, Ag, Zn, Au, Ba, As, Co, Sb, Bi, Sn, Mo, W, Be, B, Th, Nb, La, Ce, Nd, Sm, Eu, and Tb. Rock samples contain anomalous concentrations of Cu, Mn, Pb, Ag, Zn, Au, Ba, Co, Sb, As, Bi, Sn, Mo, W, Be, B, Th, Nb, Nd, Eu, and La. NURE samples contain anomalous concentrations of Th, La, Lu, Eu, Yb, and Dy. Possible deposit types in the Providence Mountains include porphyry copper-molybdenum, polymetallic veins and replacement bodies, mineralized skarn of all types, disseminated gold, and REE-U-Th-Nb-bearing carbonatite and pegmatite.

Plate 2 shows the density and overall distribution of types of mineral occurrences in the Providence Mountains. The Providence Mountains contain the largest occurrence of known iron skarn in the EMNSA at the Vulcan Iron Mine (fig. 81*A*; pl. 2). Iron skarn formed here at the now-faulted contact (fig. 81*B*) between Jurassic albitized diorite and Cambrian dolomite (unit €d, pl. 1; see also Goldfarb and others, 1988). Approximately 3 million tonnes of magnetite-rich skarn is still present in the ground at this locality (Goldfarb and others, 1988). That part of the northern Providence Mountains underlain by Early Proterozoic granitoids, mostly augen gneiss of granite and granodiorite composition, includes the densest concentration of metallic-mineral occurrences in the EMNSA. In this area, the metallic-mineral occurrences seem to be preferentially concentrated in a broadly elongate, north-northeast-trending zone centered along the trace of the East Providence fault (pl. 1). Polymetallic-vein, polymetallic-fault, and gold-silver-quartz-pyrite-vein occurrences are predominant (pl. 2). Near the center of this intensely mineralized area, two occurrences of possible low-fluorine stockwork-molybdenum systems also are present. These two possible stockwork-molybdenum systems are in and near Cretaceous intrusive breccia (part of unit Kmh) at Globe Wash (Goldfarb and others, 1988). Goldfarb and others (1988) describe these molybdenum occurrences as, in upper Globe Wash, massive felsic dikes or sills and irregularly shaped, silica-cemented breccias that are altered to quartz and sericite; widespread propylitic alteration in Proterozoic gneiss that becomes more pervasive and intense near mineralized zones; and sericitic alteration of wallrock that is common along quartz veins. The SS No. 17 prospect contains visible grains of molybdenite (one sample yielded 250 ppm Mo) along with large pyrite crystals and mostly native sulfur apparently after pyrite, in massive, white radial and ring quartz veins (fig. 82*A*) surrounding a felsic intrusive breccia. Another sample of gossan from a minor fault in the general area of the SS No. 17 prospect includes approximately 600 ppm Mo (table 11, analysis no. 46). The development of breccia in this general area may reflect explosive release of vapor concomitant with transition from a single phase to a two-phase fluid regime. Several companies have explored this area since 1970 on the basis of evidence that suggests a stockwork-molybdenum system at depth. The highest Mo concentrations were detected in chip samples collected near the SS Nos. 20–22 and 27–29 Mines and the South (Star?) Mine, which are near the center of the area of molybdenum exploration. Goldfarb and others (1988) further suggest that there is unknown potential for a molybdenum-porphyry system in upper Globe Wash. The brecciated, porphyritic, leucocratic, informally named, Cretaceous Mid Hills adamellite of Beckerman and others (1982), which intrudes Proterozoic gneiss to the west of the East Providence fault zone, shows extensive propylitic and argillic alteration; local sericitic alteration and pyritization are common near silicified breccia zones (fig. 82*B*). One prospect pit contains molybdenite rosettes in white quartz veins of both ring and radial geometry; the veins have anomalous F, Pb, and Zn concentrations.

Although the age of mineralization of the polymetallic veins and other occurrences hosted by the Early Proterozoic (intermediate-age) granitoids has not been established, they may be related to, and zoned around, a large Cretaceous porphyry-type system centered on the molybdenite occurrences at Globe Wash described above. However, the lateral extent of the quartz stockworks at Globe Wash at the inferred center of the system is quite small compared to the areal size and intensity of quartz stockworks known in many other similar stockwork-molybdenum systems (Theodore and Menzie, 1984; Theodore and others, 1992). In fact, at Globe Wash, brecciated fragments of sericitically altered leucogranite have been flooded secondarily by quartz and

some molybdenite (Goldfarb and others, 1988) across only a relatively small area in the bottom of Globe Wash. The vein quartz is not coextensive with the mapped Cretaceous granite there (Kmh). Therefore, we questionably designate these occurrences of molybdenite as part of a stockwork-molybdenum system and, further, suggest that if this is the central part of a very large porphyry system, then the most heavily molybdenum- and (or) copper-mineralized parts would be at approximately 4 to 5 km depths below the surface.

Granite Mountains

Bedrock of the Granite Mountains is dominated by Cretaceous granitoid rocks (units Kpm, Kgd, pl. 1), mostly 70 to 75 Ma in age. Lesser amounts of Jurassic diorite and granitoid rocks (Jd, Jqd) are also present. Concentrate and rock samples have anomalous concentrations of many elements: Cu, Pb, Ag, Zn, Co, Ba, Bi, Sn, Mo, W, Be, Th, La, La, Ce, Nd, Tb, and Yb are present in anomalous concentrations in concentrate samples; rock samples have anomalous concentrations of Cu, Mn, Ag, As, Pb, Co, Sn, Zn, Ba, Bi, Mo, B, Nb, Nd, Tb, Yb, Ce, and Dy. NURE samples contain anomalous concentrations of La and Eu. The area is only mildly to moderately anomalous geochemically because, although many elements are present in anomalous concentrations, they are generally weakly anomalous or only a small proportion of samples from the area have anomalous concentrations of a given element. Porphyry copper-molybdenum, polymetallic veins and replacements, and REE-Th-Nb-bearing pegmatites are possible deposit types on the basis of available geochemistry. Only a small number of mineral occurrences are present in the Granite Mountains area (pl. 2). These include two polymetallic veins, one iron skarn, and one gold-silver quartz-pyrite vein, all widely separated from one another and not showing any apparent zonal relations. Moreover, most exposed granitoid rocks in the Granite Mountains area are not altered visibly at the surface.

Van Winkle Mountain

Van Winkle Mountain, near the south-central edge of the EMNSA, is largely made up of Miocene air-fall tuff and lava flows (unit Tal, pl. 1). Miocene tuff breccia (Ttb) and Cretaceous monzogranite (Kpm) make up small parts of the area. The only sample from the area shown as Van Winkle Mountain on figure 49 is a NURE sample. The only element present in an anomalous concentration is La. The area is weakly anomalous geochemically, on the basis of limited information. Three mineral occurrences are known in the area of Van Winkle Mountain (pl. 2). Only one of these has sufficient data available upon which to make a deposit-type classification, and that one occurrence has been classified as a polymetallic fault that cuts Miocene air-fall tuff and lava flows.

Grotto Hills

Most of the Grotto Hills is composed of Miocene shallow-intrusive rocks (unit Ti, pl. 1) and rhyolite, basalt, and dacite (Tv_1) that crop out in an area of about 6 km^2. The smaller, western hills are composed of Cambrian dolomite (Cd) and Devonian to Permian limestone (PDl), which cover an area of about 0.5 km^2. Stream-sediment samples from the Grotto Hills contain anomalous concentrations of Ag, Zn, and Mo. Concentrate samples contain anomalous concentrations of Cu, Mn, Zn, Co, and Mo. No rock samples were collected in the Grotto Hills. NURE samples from the area do not have anomalous concentrations of any element. Possible types of occurrences include polymetallic veins and replacements. The area is geochemically weakly anomalous. No known mineral occurrences are present in the Grotto Hills (pl. 2).

Pinto Mountain

Pinto Mountain is underlain mainly by Miocene rhyolite ash-flow tuff (fig. 83), but a small area underlain by the informally named Cretaceous Mid Hills adamellite of Beckerman and others (1982) also is present (pl. 1). The only elements present in anomalous concentrations near Pinto Mountain are Mo in concentrate samples and Eu in NURE samples. Molybdenum in the concentrate samples may be derived from the general area of the Big Hunch stockwork-molybdenum system, which is directly upstream from the Pinto Mountain area (pl. 2). No rock samples in the RASS and PLUTO databases were collected from the area. The area is not geochemically anomalous. No mineral occurrences are known in the immediate area of Pinto Mountain.

Table Mountain

Most of the Table Mountain area is underlain by Cretaceous granitoid rocks (units Krs, Kmh, pl. 1); small areas are underlain by Early Proterozoic granitoid rocks (Xg_1) and Tertiary tuff (Tw). Stream-sediment samples from Table Mountain contain anomalous concentrations of Zn and Mo. Concentrate samples contain anomalous concentrations of Ag. Rock samples contain anomalous concentrations of Cu, Pb, Ag, Sb, Sn, Mo, and Eu. NURE samples contain anomalous concentrations of Th, La, Ce, and Dy. The area is geochemically mildly anomalous. Possible deposit types suggested by the geochemical results include polymetallic veins and REE-Th-bearing pegmatites. Three mineral occurrences are present in the area of Table Mountain, and they consist of two polymetallic vein systems and one polymetallic fault (pl. 2). A rock sample collected at one of these occurrences contains more than 500 ppb Au (pl. 6; see also U.S. Bureau of Mines, 1990a).

Woods Mountains

Bedrock of the Woods Mountains is dominated by Miocene rhyolite ash flows and domes (unit Tts, pl. 1). Lesser areas of bedrock are composed of Miocene rhyolite ash-flow tuff (Tw) and basalt flows (Tb). No rock samples from the Woods Mountains are in the data sets examined. The only anomalous element concentrations are Ag and La in concentrate samples and Dy in NURE samples. The area is weakly anomalous geochemically. No metallic mineral occurrences are known in the Woods Mountains area (pl. 2; see also U.S. Bureau of Mines, 1990a).

Hackberry Mountain

Bedrock of Hackberry Mountain is mostly Miocene volcanic rocks of trachyte, trachydacite, and rhyolite (unit Ths, pl. 1); rhyolite ash-flow tuff (Tw); and rhyolite lava flows and ash flows, tuffaceous sedimentary rocks, tuff breccia, basalt flows, and andesite flows (Tv_2). A small area of Early Proterozoic gneiss and granitoid rocks (Xg) also is present. Stream-sediment samples from Hackberry Mountain contain anomalous concentrations of Ba. Concentrate samples have anomalous concentrations of Mn, Ag, Zn, Ba, and Mo. NURE samples contain anomalous concentrations of Ce, Eu, Yb, and Dy. No rock samples were collected. The area is geochemically mildly anomalous. Possible deposit types include polymetallic vein, polymetallic fault, and REE-bearing pegmatite. Seven of 16 mineral occurrences known in the area of Hackberry Mountain (pl. 2) have been classified as polymetallic fault, although the base-metal-enriched signatures of these occurrences may be reflections of a Creede-type quartz-adularia precious-metal system at depth (Mosier and others, 1986). Most of these seven polymetallic faults are concentrated in a northeast-trending zone along the southeast flank of Hackberry Mountain. Analyses of mineralized rock samples from the seven polymetallic faults all contain less than 500 ppb Au (pl. 6; see also U.S. Bureau of Mines, 1990a). One sample from a locality classified as a polymetallic vein (U.S. Bureau of Mines, 1990a, map no. 600, pl. 1), however, does contain more than 500 ppb Au. This particular locality is well south of the locus of most recent exploration activities by private industry (Gottlieb and Friberg, 1984). These exploration activities center on widely dispersed silicification in the general area of the seven occurrences of polymetallic faults described above. In addition, these seven occurrences coincide with (1) a magnetic low (pl. 5), suggesting demagnetization resulting from hydrothermal alteration, and (2) an anomaly of limonitic and argillic alteration, as well as silicification, detected by our analysis of the Landsat Thematic Mapper image (fig. 36).

Our field examinations noted abundant silicification along the southeast flank of Hackberry Mountain, but none of this silicification appears to be comparable to the intensity of the pervasive silicification and stockwork veining described below in the general area of the Hart Mining District. Most silicification at Hackberry Mountain is present in rhyolite flows or densely welded ash-flow tuffs. In addition, pervasive bleaching of these rocks is found in association with the argillic alteration, which is confined mostly to a northeast-trending zone on the southeast flank of Hackberry Mountain where the polymetallic faults are present. These mineralized faults at Hackberry Mountain contain elevated abundances of Pb, As, Sb, and some Zn. Production of approximately 1,730 kg Pb is credited to the Dewey Mine, one of the seven occurrences classified as a

polymetallic fault (U.S. Bureau of Mines, 1990a). Furthermore, Gottlieb and Friberg (1984) describe results of exploration activities as follows:

> The Hackberry Mountain prospect is a late Tertiary disseminated precious metal deposit hosted by rhyolites and ash-flow tuffs. Geochemical and lithologic logging of four drill holes down to 900 ft [274 m] show an upper [essentially] unaltered zone down to 200 ft [61 m] with occasional native Au in hematite-replaced sanidine. An altered zone extends to 800 ft [244 m], and an unaltered zone extends from 800 to 900 ft [244 to 274 m]. The altered zone is mainly ash-flows and the unaltered zones are mainly rhyolite lava flows.
>
> Surface and drill hole samples [in the Hackberry Mountain prospect] show varying degrees of alteration and mineralization. The ore consists of fine grained native Au surrounded by bladed stibnite, chalcedony and hematite. Argillic alteration is dominant, with lesser amounts of silicification. In the argillically altered rock the phenocrysts are altered to clay minerals, and the groundmass, which had devitrified to quartz and potassium feldspar prior to alteration, remains fresh. Silicified rocks are altered to quartz plus Fe and Mn oxides. Major element chemistry indicates Si and Mn increase in altered rocks, Al, Fe, and K remain constant, and Mg, Ti, Na, and Ca decrease. Ca is the best indicator of alteration. Minor element chemistry shows that Zn increases with alteration, Ba, Cr, and V remain constant, and Sr decreases. Sr, believed to be contained in plagioclase, is an accurate indication of alteration whereas Ba, contained in the more stable sanidine was not mobilized. Trace elements La, Y, and Yb remain constant with respect to alteration. Au varies from 0.001 to 0.088 oz/ton [0.03 to 2.75 g/t].

Vontrigger Hills

Bedrock of the Vontrigger Hills is mostly Early Proterozoic granitoid rocks (unit Xg_1, pl. 1), dated between 1,660 and 1,695 Ma, and migmatite (Xm). Small areas of Miocene volcanic rocks (Tv_1) and Cretaceous granitoid rocks (Kpg) are found mainly in the western part of the area. Stream-sediment samples from the Vontrigger Hills do not contain anomalous concentrations of any elements. However, concentrate samples have anomalous concentrations of Ag and Ba, and rock samples have anomalous concentrations of Cu, Mn, Pb, Zn, Ag, As, Bi, Mo, Be, B, and Nb. The area is geochemically moderately anomalous overall. Possible deposit types include porphyry copper-molybdenum, polymetallic veins and replacement bodies, and REE-Nb-bearing pegmatites.

Six mineral occurrences in the Vontrigger Hills include three polymetallic veins, two low-sulfide gold-quartz veins, and one polymetallic fault (pl. 2). All occurrences are far removed from the Cretaceous granitoid that crops out near the southwest end of the Vontrigger Hills (pl. 1), and all the occurrences are hosted by Early Proterozoic younger granitoid rocks. Mineralization is extremely widespread at some localities (pl. 2), such as in the general area of the Rattlesnake Mine (U.S. Bureau of Mines, 1990a, map no. 592, pl. 1), where numerous prospect pits, shafts, and a partially reclaimed open cut approximately 100 m wide follow favorable indications of gold mineralization of various attitudes and types in an area of about 3 km^2. Much of the gold mineralization initially exploited at the Rattlesnake Mine, classified as polymetallic vein, is along a 10-m-wide zone of intensely silicified and highly fractured, foliated Early Proterozoic younger granitoid rocks. This mineralized zone has a strike of about N. 70° W. and is present at the north edge of a porphyritic monzogranite of undetermined size (not shown on pl. 1). Numerous unmineralized porphyritic granite dikes containing K-feldspar phenocrysts cut the Early Proterozoic younger granitoid rocks.

At the True Blue Mine (U.S. Bureau of Mines, 1990a, map no. 588, pl. 1), discontinuous, narrow stringers of vein quartz in places partly fill open cavities developed in Early Proterozoic younger granitoid rocks and elsewhere. The open cavities are lined by chrysocolla, azurite, and iron oxide minerals that replace pyrite. These veins typically are 1 to 2 cm wide and approximately 10 to 16 cm long; they cut the foliation in the surrounding Early Proterozoic younger granitoid rocks at high angles.

Piute Range

The southern part of the Piute Range is dominated by Cretaceous granitoid rocks (unit Kpg, pl. 1) but also contains substantial areas of Early Proterozoic younger granitoid rocks (Xg_1) and Miocene basalt flows (Tb). The middle and northern parts of the range are almost exclusively Miocene dacite to andesite flows, domes, and breccias (Td) but also contain small areas of underlying Early Proterozoic granitoid rocks (Xg), Miocene welded ash-flow tuff (Tps), and Early Proterozoic younger granitoid rocks (Xg_1). Stream-sediment samples from the

southern and middle parts of the Piute Range contain anomalous concentrations of Pb, Zn, Mn, Co, Mo, and B. Stream-sediment samples from the northern part of the range do not have anomalous concentrations of any element. Concentrate samples from the southern and middle parts of the range have anomalous concentrations of Cu, Pb, Zn, Ag, Ba, B, Bi, Sn, W, Be, Mo, La, Sm, and Tb. Rock samples from the southern part of the range contain anomalous concentrations of Cu, Pb, Ag, Zn, Au, Sb, Bi, Mo, and W. NURE samples from the southern part of the range have anomalous concentrations of Th. Rock and concentrate samples from the northern part of the range contain anomalous concentrations of Be. Concentrate samples from the northern part of the range also have anomalous concentrations of Sn. NURE samples from the northern part of the range contain anomalous concentrations of Ce, Lu, Sm, Eu, Yb, and Dy. Overall, the Piute Range is geochemically moderately to highly anomalous. Possible deposit types include porphyry copper-molybdenum, polymetallic veins and replacement bodies, disseminated gold, and REE-bearing carbonatite or pegmatite.

No mineral occurrences were reported by the U.S. Bureau of Mines (1990a) in the northern and central part of the Piute Range. Much of this part of the range includes relatively thick sequences of Miocene dacite to andesite flows, domes, and breccias (pl. 1). However, numerous prospects and previously mined areas are present in the southern part of the range, particularly to the west-northwest of Signal Hill and to the east-northeast of Billie Mountain (pl. 2). This area, known as Tungsten Flat and coinciding with the Signal Hill Mining District, includes several polymetallic-vein localities but only a small number (U.S. Bureau of Mines, 1990a) of the actual tungsten-vein localities are present. However, prospects and other workings of various types are extensively developed in an area of about 6 to 7 km^2 at Tungsten Flat that contains widespread exposure of Cretaceous granitoid rocks. Wolframite-bearing quartz veins typically are 1 to 2 m wide, strike N. 20° W., and dip steeply to the northeast; these veins are concentrated mostly in the northern part of the district. They are generally discontinous and have been extensively explored by shallow prospect pits and underground workings as much as 100 m long along strike. Secondary copper minerals are common in many of the workings. Intense clay alteration is confined to rocks generally within 5 to 7 m of the veins. The Leiser Ray Mine, near the south end of the mining district, shows elevated abundances of galena and chalcopyrite relative to occurrences at the north end of the district. The Leiser Ray Mine is a polymetallic-vein occurrence that has a past production of 6,877 kg Cu, 755 kg Pb, 36.8 kg Ag, and 0.8 kg Au (U.S. Bureau of Mines, 1990a). The main vein at the Leiser Ray Mine probably was discovered before 1891 (Hewett, 1956). The metal zonation in the Tungsten Flat Mining District seems to show silver-bearing polymetallic veins on the south, distal to tungsten veins on the north. Mineralization in the Tungsten Flat Mining District lies astride the projected east-northeast trend of the hinge line of the Piute Anticline (Hewett, 1956).

Castle Mountains

Bedrock of the Castle Mountains is mainly Miocene dacite and rhyolite shallow intrusions and extrusive domes, flows, and breccia (unit Tdr, pl. 1). Smaller areas of bedrock are composed of Early Proterozoic migmatite (Xm) and Miocene basalt and andesite lava flows (Tab) and rhyolite ash-flow tuffs (Tps). Stream-sediment samples from the Castle Mountains contain anomalous concentrations of Mn, Pb, Zn, Co, B, and Mo. Concentrate samples have anomalous concentrations of Cu, Mn, Zn, Ba, Co, Bi, Mo, B, Th, La, Ce, Nd, Sm, Eu, Yb, and Dy. Rock samples contain anomalous concentrations of Mn, Ag, Sb, Pb, Ba, Mo, B, Nb, Eu, and Tb. NURE samples contain anomalous concentrations of Dy and Eu. The Castle Mountains geochemically are moderately to highly anomalous. Possible deposit types include porphyry copper-molybdenum, polymetallic vein and replacement bodies, epithermal gold, and REE-Th-Nb-bearing carbonatite and pegmatite. The Castle Mountains include the economically significant epithermal quartz-alunite quartz-adularia gold deposits at the Castle Mountains Mine, hosted by Tertiary volcanic rocks that show a diagnostic vuggy silica, acid-sulfate-type alteration (fig. 84; pls. 1, 2). These deposits constitute one of the largest economic reserves of minable gold known in 1995 in southern California.

Homer Mountain

Bedrock of Homer Mountain, located outside the east edge of the EMNSA, is composed of Early Proterozoic granitoid rocks (unit Xg_1, pl. 1). Stream-sediment samples from Homer Mountain contain

anomalous concentrations of Ag and Mo. Concentrate samples have anomalous concentrations of Mn. NURE samples have anomalous concentrations of Eu and Dy. The area is geochemically weakly anomalous. Possible deposit types include polymetallic vein and REE-Nb-bearing pegmatite. Inasmuch as the area of Homer Mountain is outside the EMNSA, we have not included herein a discussion of its mineral occurrences.

U.S. Bureau of Mines Database

Assembly of Database

In this section of this report, we examine some of the metallic-mineral-resource implications of geochemical data obtained by the U.S. Bureau of Mines (1990a, tables 2*A*,*B*) on 1,050 rocks analyzed from the EMNSA. Most rock samples are from mineralized occurrences known within the EMNSA; approximately 98 percent of the rock samples can be assigned to the mineralized sites, or their immediate vicinity, that are classified by us as belonging to a particular type of deposit model (table 15). As such, the analyses that make up this database provide sampling across the EMNSA of many of the various types of mineral deposits that are known to be present there. These samples yield data that can be used to determine local geochemical thresholds to be expected for various metals and suites of metals present in various systems, to determine zonal relations of metals among genetically linked types of deposits, and to determine metal associations in variously grouped samples of the database.

Rock samples are classified as chip, random chip, grab, and select by the U.S. Bureau of Mines (1990a, table A–1). The chip samples, which consist of small rock chips taken in a regular series continuously along a line across a mineralized zone or other exposure, contain the most information for determination of the presence or absence of metal concentrations in a volume of rock. Select samples are generally judged to be most representative of the best mineralized parts of a mineralized vein or exposure and are typically used to help determine the presence or absence of a particular minor metal or metals in a mineralized system (for example, gold in a sample of sulfidized skarn).

Most samples that make up the database are from the mesothermal environment, which is widespread in the EMNSA. Only seven samples of the 1,050 in the database are from sites that have been assigned by us as belonging to an epithermal, quartz-alunite or quartz-adularia, gold-type system that is volcanic hosted and Tertiary in age. The overwhelming bulk of the samples are associated with Mesozoic metallogenic environments. However, the database does not include any samples from the Providence Mountains in the south-central part of the EMNSA (pl. 6), because the number of elements per sample analyzed from this area is much less than the number of analyzed elements in the rest of the database. The distribution of the sampling sites is an important point that must be kept in mind during the discussion below of various subsets of the database. The Providence Mountains contain some of the most widely distributed and intensely concentrated mineral occurrences, both mined and unmined (U.S. Bureau of Mines, 1990a), in the EMNSA. In the Providence Mountains, approximately 200 mineralized sites have been examined and described by the U.S. Bureau of Mines (1990a; see also Moyle and others, 1986) and by the U.S. Geological Survey and the U.S. Bureau of Mines (Goldfarb and others, 1988) in an area of about 250 km^2. Most mineralized sites are polymetallic veins (pl. 2). In the Providence Mountains Wilderness Study Area, past production has been recorded from 13 nonferrous-metallic lode deposits, the largest production coming from the Bonanza King Mine from 1901 to 1960 (Goldfarb and others, 1988, table 1). The Bonanza King Mine yielded 4,811 or more tonnes of ore that included 1.8 kg Au, 2,571 kg Ag, 415 kg Cu, 31,489 kg Pb, and 1,051 kg Zn. Production recorded from the remaining 12 mines is minimal. The Vulcan Iron Mine produced 2.4 million tonnes iron ore from an iron skarn from 1942 to 1947 (Moyle and others, 1986; Goldfarb and others, 1988).

Although the report by the U.S. Bureau of Mines (1990a) includes analyses for 33 elements, we have selected 20 elements (Ag, As, Au, Ba, Ce, Co, Cr, Cs, Fe, La, Mo, Ni, Sb, Sc, Sm, Ta, Th, U, W, and Zn) upon which to base our statistical calculations described below. These studies are primarily an attempt to determine elemental associations in the sampled mineral deposits and mineral occurrences. One cannot make any inference about sizes of known or unknown deposits from the presence of a particular element, regardless of its concentration and its association with other elements, if one has only a small number of samples from a

site. As noted by Barton (1986), "the presence of a given element seldom if ever proves the existence of an ore deposit." As indicated in table 16, many of the 20 elements selected include large numbers of undetermined concentrations; primarily, the undetermined values of elemental concentration are less than some threshold. In fact, detection thresholds for individual elements vary highly among the samples for many of the reported analyses. For example, 56 different detection thresholds exist for Au in the less than 0.002 to less than 4.9 ppm range. However, 158 of 253 samples reported as containing Au concentrations at less-than-detection thresholds actually have a detection threshold of 2 ppb. To study elemental interrelations in the 20-element-by-1,050-rock matrix, as well as to maximize the number of samples for which supposedly valid values are available, we substituted a concentration that is 50 percent of the value of the most sensitive detection level for the entire data-base (that is, 0.001 ppm for Au) for each concentration reported as "less than" a particular value. A completely filled matrix is required for sampling adequacy by some of the correlation techniques that use principal-components factor analysis that we describe below in the subsection entitled "Nonparametric Correlations." Following these outlined procedures for elemental substitutions, we were able to assemble a completely filled composite 20-element-by-1,050-sample geochemical matrix. Only one "greater than" value was substituted from the raw data reported by the U.S. Bureau of Mines (1990a). This reported concentration, greater than 10,000 ppm As, was substituted with a value of 10,000 ppm As in the geochemical matrix, although values much higher than this are present in many of the other samples.

Some elements that are important to an analysis of economic resources, such as Cu and Pb, are present in a wide variety of geologic environments in the EMNSA but are judged not to be suitably represented in the raw-data matrix. Such a judgment reflects primarily the large number of samples for which unreported concentrations for these elements exist. Among the 1,050 rock samples, Cu concentrations are not available for 485 samples (U.S. Bureau of Mines, 1990a), and another 113 samples show Cu concentrations in excess of the uppermost reporting limit (10,000 ppm). In addition, 563 samples show no reported values for Pb, and 76 samples contain Pb concentrations higher than the uppermost reporting limit (10,000 ppm). Therefore, we do not examine Cu or Pb relations to the 20 elements listed above.

Some elements we chose to include in the matrix, nonetheless, do show a high percentage of values below detection relative to the 1,050 rock samples analyzed. Included among these are the following seven elements (the number of values below detection are shown paranthetically after each element): Ag (481), Ce (402), Co (642), Cs (549), Ni (801), Ta (687), and Zn (477). However, a very high percentage of the reported concentrations below detection in the raw-geochemical-data matrix (U.S. Bureau of Mines, 1990a, tables 2*A*,*B*) for each of the seven elements are at the most sensitive detection threshold. For example, detection thresholds are 2 ppm Ag for 468 of the 481 analyses shown on table 16 as having a value below detection in the raw-data matrix. Therefore, a replacement value of 1 ppm Ag for each of the 481 analyses should not distort the resulting matrix significantly. In addition, the presence of Co, a metal which in 1993 is considered to have some strategic importance, in highly anomalous concentrations at several localities in the EMNSA (U.S. Bureau of Mines, 1990a) is considered by us to be important geochemically, and so we chose to examine its relations to other elements and to type of deposit in the EMNSA even though concentrations below detection are more than 60 percent of the total number of Co concentrations reported (table 16; see also U.S. Bureau of Mines, 1990a). The most sensitive detection threshold for Co was 5 ppm, and 609 of the 642 values below detection are reported to be less than 5 ppm (U.S. Bureau of Mines, 1990a).

Frequency Distributions of Elements

Frequency distributions of the untransformed geochemical data obtained by the U.S. Bureau of Mines (1990a, tables 2*A*, *B*) are strongly skewed positively; that is, the most frequently occurring values are in the lowermost ranges of the reported concentrations and show long "tails" in the distribution of elemental concentrations toward high values. They are thus strongly nonnormal in overall distribution. To perform standard statistical calculations, the geochemical data in the composited 20-element-by-1,050-sample matrix were transformed by common logarithms to thereby approximate a closer fit to lognormality. Figure 85 shows frequency diagrams for the transformed data of the 20 elements. We should emphasize again that these data represent samples obtained from a wide variety of geologic environments and types of deposits in the EMNSA

but outside the general area of the Providence Mountains. Somewhat more deposit-type-specific relations among elemental suites are included below in the descriptions of several deposits present in the EMNSA. Tests of kurtosis and skewness values (table 16), frequently used measures of goodness of fit for normality, at the 95 percent confidence level show that all 20 elemental distributions tested in the log-transformed data set deviate from lognormality. Positive values of skewness indicate that the right "tail" of the distribution is longer than the left "tail," which also is readily apparent in the plotted histograms (fig. 85). Kurtosis refers to relations among the peak, the center, and the tails of a distribution (for example, a deviation from normality that might be due to an extremely flat peak with relatively flat tails). A zero value of both kurtosis and skewness indicates a normal distribution. Among the 20 elements tested, visual inspection of the log-transformed distributions for Fe and U show them to have the closest approaches to normality; Sb also approaches a normal distribution (fig. 85). The fact that the original data represent a compositing of geochemical information from a wide variety of deposit types that show a wide range of concentrations of elements, coupled with a censoring of the data for many elements because thresholds of detection are higher than the actual distribution, have certainly contributed to yield the elemental distributions found. Nonetheless, distribution of Au values in the geochemical-data matrix shows that approximately 200 of the 1,050 rocks analyzed from the EMNSA by the U.S. Bureau of Mines (1990a) include concentrations of Au higher than, or equal to, 500 ppb, a value considered by many exploration geologists as suggestive for pursuing evaluations in mesothermal geologic environments. Similar conclusions were reached by the U.S. Bureau of Mines (1990a). In light of questions that might be raised concerning correlation calculations that employ statistical methods requiring normal distributions in the sampled population, nonparametric Spearman correlations were calculated below for the 20 elements transformed by logarithms to the base 10 (table 17).

The distribution of concentrations of Ag, As, Au, and Sb in the 20-element-by-1,050-rock matrix by deposit type for 12 of the 20 types of deposit we recognize in the EMNSA is shown graphically on figure 86. Most samples that show elevated concentrations of Au are from mineralized occurrences classified as polymetallic vein, polymetallic fault, and gold-silver quartz-pyrite vein (fig. 86*A*). The number of samples analyzed for each of these three types of deposits are 286, 75, and 97, respectively. Silver is especially enriched in the silver-copper brecciated-dolostone type of vein occurrence that is distal, and related genetically, to emplacement of the gold breccia pipes at the Colosseum Mine (fig. 86*B*; see also Sharp, 1984). Arsenic apparently is most strongly concentrated in polymetallic veins and, to a somewhat lesser degree, in the polymetallic-replacement deposits (fig. 86*C*). High concentrations of Sb are common in silver-copper brecciated dolostone, polymetallic vein, and, to a lesser degree, lead-zinc skarn (fig. 86*D*). However, only seven analyses are available from the lead-zinc-skarn environment.

If values of Mo were shown on a similar distribution plot, high values would be present in polymetallic veins, polymetallic replacement, and in two of the three samples analyzed from the known Big Hunch stockwork-molybdenum system in the EMNSA. Additional analyses of rock from the Big Hunch system are reported below in the section entitled "Low-Fluorine Porphyry-Molybdenum Deposits." Furthermore, as already noted, the U.S. Bureau of Mines (1990a) database to which we refer does not include samples from the Providence Mountains, which have been demonstrated to show some elevated abundances of Mo at Globe Wash (Moyle and others, 1986). Lastly, if concentrations of Zn were shown on a similar plot, they would be fairly common throughout the range of values reported in figure 86 in those samples obtained from the polymetallic-replacement occurrences, polymetallic veins, and copper skarns.

Nonparametric Correlations

A nonparametric correlation statistic for all trace-element pairs available for the 20-element data set was calculated as Spearman correlation coefficient r (Davis, 1986), where $r=1-[6\Sigma(RX-RY)^2/(n(n^2-1)]$, RX and RY are the two sets of rankings, and n is the number of trace-element pairs (table 16). Each value is ranked, and corrections are made for tied observations.

Scatter plots for Ag and Fe versus Au are given in figures 87*A–B*. Gold shows the strongest positive Spearman correlation coefficients for Ag and Fe, 0.323 and 0.319, respectively, in the 1,050-sample database. Such relatively reduced values of Spearman correlation coefficients for Au to other elements in the data

set are probably a result of the presence of Au in a large number of types of deposits in the EMNSA, such as polymetallic vein, low-sulfide gold-quartz vein, polymetallic replacement, distal disseminated gold-silver, gold breccia pipe, silver-copper brecciated dolostone, gold-silver quartz-pyrite vein, polymetallic fault, polymetallic skarn, tungsten skarn, tin (tungsten) skarn, and copper skarn (table 15). Gold shows a somewhat enhanced association for Ag, having an r value of 0.4 in a 97-sample subset composited from 47 localities of gold-silver quartz-pyrite vein occurrences in the EMNSA. A stepwise-regression analysis (Davis, 1986) shows that only about 10 percent of the variance in the log values of Au can be predicted from the log values of Fe alone in the 1,050–sample database. Similarly, stepwise regression analysis, which includes log values for Ag, Ba, Cr, Fe, Sb, Sc, Ta, and U, accounts for about 31 percent of the variance of the log values of Au in the 1,050-sample database, reflecting primarily the geologic inhomogeniety of the data. Plots showing strong, positive associations between element pairs in the data set are exemplified by Sm-La (r=0.896), Sb-Ag (r=0.552), and Fe-Co (r=0.691) (figs. 87*C*-*E*; see also table 17). Finally, a plot of Ba versus U (fig. 87*F*) provides an example of an elemental association that is extremely weak (r=0.001; table 17). In all of these plots, most samples for which we substituted values at the detection threshold are readily apparent.

Associations Using Factor Analysis

Principal-components factor analysis, another multivariate statistical approach (Klovan, 1968; Davis, 1986), was used in an attempt to detect additional geologically significant elemental associations that may not have been resolved through the use of correlation coefficients. Our preliminary tests involved utilization of various other standard manipulations of the 20-element-by-1,050-sample data set (table 16). On the basis of our knowledge of the geologic environments sampled in the EMNSA, we conclude that the data set should primarily reflect contributions from the Proterozoic environment and the Mesozoic mesothermal environment. A simple factor analysis using two factors provides the following high loadings, which are measures of the degree of intercorrelation among the grouped elements (Klovan, 1968), for the geochemical data:

Factor 1: Ce, Th, Sc, Sm, Cs, Ta, Ba

Factor 2: Fe, Co, Zn, U

Factor 2 in this simple model also includes some moderate loadings for Au, As, Mo, and Ni. Therefore, in an attempt to resolve further the elemental associations masked by the simple two-factor model, we examined the data set using more than two factors. Of the options attempted, a relatively complex factor analysis using eight factors provides a geologically reasonable discrimination of the variances among the geochemical data. The R-mode principal components analysis, which emphasizes interrelations among elements under consideration (Krumbein and Graybill, 1965), reveals, using an orthogonal-transformation solution, the following high, positive loadings among elements in the eight-factor model (listed in order of decreasing loadings; notably lower elemental loadings in each factor are shown in parentheses):

Factor 1: La, Sm, Th, Ce, Sc, Ta, Ba, Cs

Factor 2: Co, Fe, (Sc)

Factor 3. Sb, As, Ag, Zn, (Mo)

Factor 4: Au, Ag

Factor 5: W, (Cs)

Factor 6: Ni

Factor 7: U, (Ta)

Factor 8: Cr, Mo, Ba

These loadings are considered to be firmly established statistically because total matrix-sampling adequacy has a value of 0.868 and, thus, meets minimum mathematical expectations of partial correlations that tend toward zero (Kaiser, 1970). For the eight-factor model adopted, calculated communalities suggest that anywhere from

approximately 62 percent (for Cs) to approximately 93 percent (for W) of any elemental variance in the 20-element-by-1,050-sample data set is predictable from the remaining 19 other elements.

Elemental associations in the eight-factor model suggest dominance in their loadings by the following geologic processes or environments:

Factor 1: Proterozoic and Jurassic igneous rocks

Factor 2: Selected skarns and polymetallic veins

Factor 3: Gold breccia pipe and distal occurrences, selected skarns, and polymetallic veins and replacements

Factor 4: All deposit types in Mesozoic mesothermal environment

Factor 5: Tungsten vein and tungsten skarn

Factor 6: Iron skarn and polymetallic vein

Factor 7: Mesozoic polymetallic veins and skarns and Jurassic igneous rocks

Factor 8: Polymetallic vein, fluorite veins, and stockwork-molybdenum occurrences

As pointed out in the subsection above entitled "Evaluation of Data," the EMNSA resides in a broad geologic province that apparently contains widespread elevated abundances of rare earth elements in rocks of highly diverse ages. As shown, many unaltered samples of Proterozoic and Jurassic granites are modestly enriched in La, Ce, Nd, Sn, Th, and several other elements (D.M. Miller, written commun., 1991). Therefore, the high loadings of many of these elements in Factor 1 must reflect their elevated abundances in Proterozoic and Jurassic granites in the EMNSA. In addition, the high loading of U and, to somewhat lesser degree, Ta in Factor 7 must also be at least a partial reflection of their modest but persistent elevated presence in Jurassic granites. Uranium is present in some unaltered samples of Jurassic granite in concentrations of as much as 20 ppm.

From the 1,050-sample database, we assembled a smaller one (89 samples) that included all samples showing Co concentrations greater than or equal to 50 ppm. We then examined elemental relations in it to establish deposit types associated with high loadings of Co and its associated elements (Factor 2). Sixty-four samples in this smaller database are from a geologic environment dominated by development of skarn (copper skarn, polymetallic skarn, iron skarn, tin-tungsten skarn, tungsten skarn, or zinc-lead skarn) and polymetallic-vein types of deposits. The highest concentration of Co detected is 859 ppm (U.S. Bureau of Mines, 1990a). Other types of deposit that include high concentrations of Co are gold-silver quartz-pyrite veins (two samples contain 799 and 460 ppm Co); polymetallic faults; vein barite; polymetallic replacement; and, finally, four samples from localities that cannot be classified into types of deposit on the basis of information available. Furthermore, Co in the 89-sample database shows relatively weak overall Spearman correlation coefficients for other metals, the three highest being for Ni, Cs, and U, which range from 0.22 to 0.27. On the basis of these relations, mesothermal environments in the EMNSA that include the above-listed types of deposits can be considered to be permissive hosts for significant concentrations of Co. The known occurrences of these types of deposit in the EMNSA are shown on plate 2, and additional discussion of the types of deposits and their permissive areas and favorable tracts is included in the section below entitled "Evaluation of Metallic Mineral Resources."

A 131-sample database, including all samples that contain more than 200 ppm Sb from the U.S. Bureau of Mines (1990a), also was prepared to evaluate Factor 3 loadings listed previously. Of the 131 samples, 55 are from vein occurrences distal to the Colosseum gold breccia pipe and genetically related to it (Sharp, 1984); 42 of these Sb-enriched samples are from sites included by us with the silver-copper brecciated-dolostone type of vein occurrence. In addition, some deposits of skarn, polymetallic vein, and polymetallic replacement also show abundances of Sb greater than 200 ppm elsewhere in the EMNSA (fig. 86*D*). In the 131 samples, Sb shows the highest positive correlation coefficients with Ag, As, and Au; figure 88 is a plot of Sb versus As for the 131 samples. Although we are not able to evaluate statistically the relations of Cu and Pb because of the large number of qualified values for these elements in the database, Cu and Pb in the silver-copper brecciated dolostones that are marginal to the gold-bearing breccia pipes at the Colosseum Mine are uniformly high (U.S. Bureau of Mines, 1990a). If data were available for Cu and Pb, these elements undoubtedly would make up a

strong component of Factor 3. The presence of elevated concentrations of Sb, As, and some Au in silver-copper brecciated dolostones in the Clark Mountain Range might be used as a favorable geochemical signature for gold-bearing breccia pipes at depth. In addition, the Ag/Au ratio in silver-copper brecciated dolostone distal to the Colosseum Mine is typically higher than 1,000, as is described in the subsection below entitled "Breccia Pipe and Related Deposits."

Factor 4 shows high loading for Au and Ag. Our evaluation of the 197 samples in the database that contain abundances of Au in excess of 500 ppb indicates that no type of metallic-mineral deposit appears to exist in the Mesozoic mesothermal environment of the EMNSA which does not contain significant Au (pl. 6). By far, the most abundant deposit type whose samples contain Au in excess of 500 ppb is polymetallic vein, reflecting its predominance in the EMNSA (table 15). A select sample from the polymetallic veins at the Bighorn Mine near the south end of the Providence Mountains includes 22,000 ppb Au (table 11, analysis no. 15). In addition, skarns of all types show some analyses carrying at least 500 ppb Au or, corroborating the conclusions of Theodore and others (1991), that all types of skarns are, at a minimum, permissive sites of enhanced Au deposition.

Although Factor 6 shows a high loading only for Ni, the number of samples containing elevated concentrations of Ni is quite low. Only 31 of the 1,050 samples analyzed by the U.S. Bureau of Mines (1990a) contain higher than 100 ppm Ni, and only two of these are in excess of 500 ppm. These two samples are from mineralized sites classified as polymetallic vein (U.S. Bureau of Mines, 1990a, map no. 282) and iron skarn at the Old Dad Mountain deposit (U.S. Bureau of Mines, 1990a, map no. 369). Eleven of the 31 analyzed samples shown to contain more than 100 ppm Ni are from polymetallic veins. In addition, three of the silver-copper brecciated-dolostone occurrences that are distal, in a petrogenetic sense, to the gold breccia pipes at the Colosseum Mine also contain some rocks whose Ni contents are greater than 100 ppm.

Factor 7 shows a high loading for U and a moderate loading for Ta. Only 18 samples analyzed by the U.S. Bureau of Mines (1990a) contain in excess of 50 ppm U, and eight of these are from mineralized sites classified as some type of metallized skarn, of which four are iron skarn. The highest content of U found (1,590 ppm) in the EMNSA is from the general area of the REE-bearing carbonatites at the Esperanza group of claims in the northern part of the Ivanpah Mountains (U.S. Bureau of Mines, 1990a, map no. 156, pl. 1). Some polymetallic veins elsewhere in the EMNSA also contain high concentrations of U.

The high loading of Cr, Mo, and Ba in Factor 8, presumably reflecting polymetallic-vein, fluorite-vein, and stockwork-molybdenum occurrences in the EMNSA, may be an indication of interaction of fluids, which are associated with these types of occurrences, with mafic igneous rocks of the Proterozoic basement.

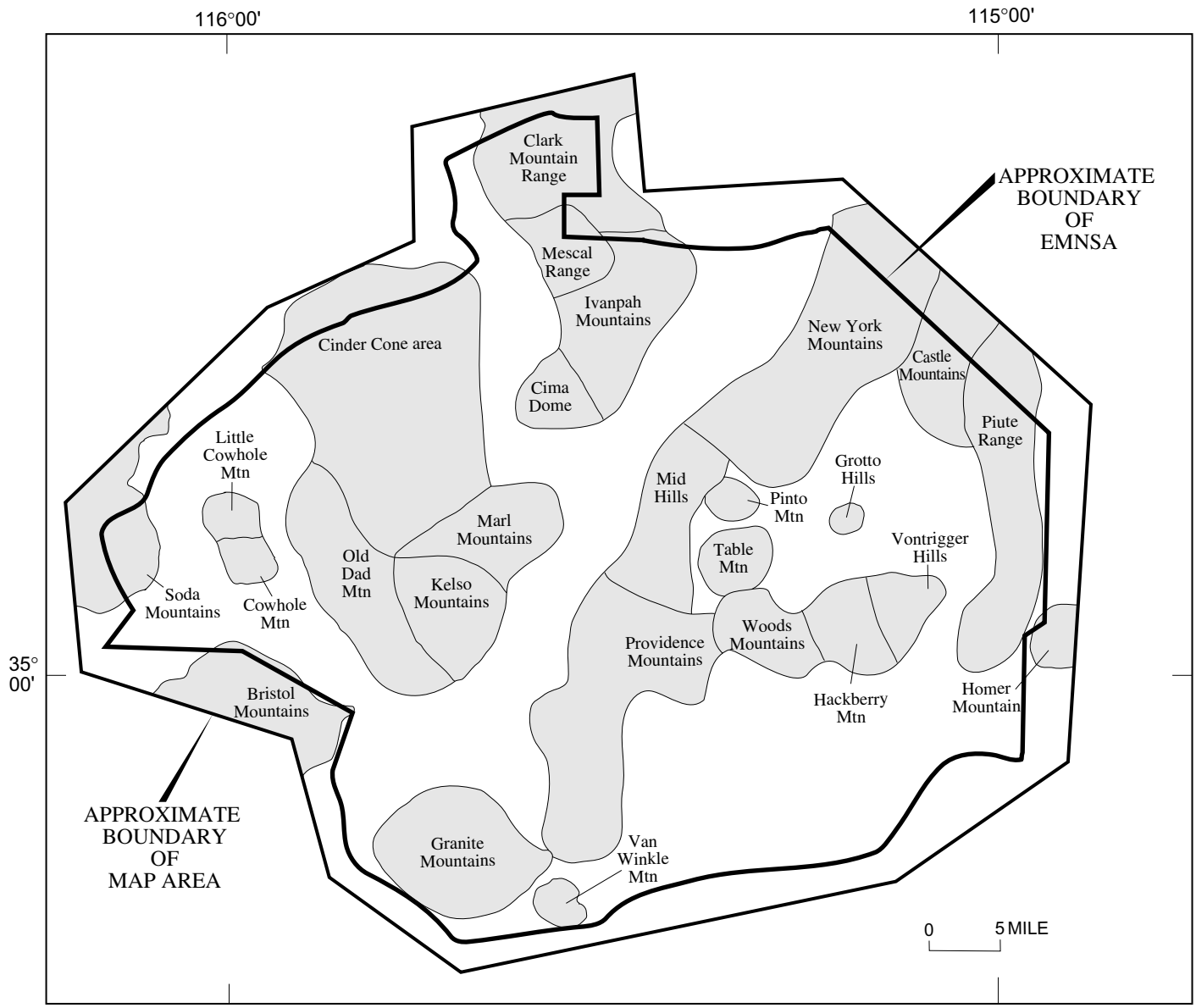

Figure 49. Map of East Mojave National Scenic Area (EMNSA), California, showing geographic areas (shaded) that were geochemically evaluated using data from Rock Analysis Storage System (RASS), geochemical database for the United States (PLUTO), and National Uranium Resource Evaluation (NURE) databases. Statistical data given in table 13; summary of geochemical anomalies given in table 14; sample localities shown on figures 50 to 53; data plotted on figures 54 to 73.

Figure 50. Sampling sites for Rock Analysis Storage System (RASS) and geochemical database for the United States (PLUTO) stream-sediment samples from East Mojave National Scenic Area (EMNSA), California, and surrounding area. General outlines of geochemically evaluated areas (shaded) shown for reference; see figure 49 for location names. Statistical data given in table 13; summary of geochemical anomalies given in table 14; data plotted on figures 54 to 73.

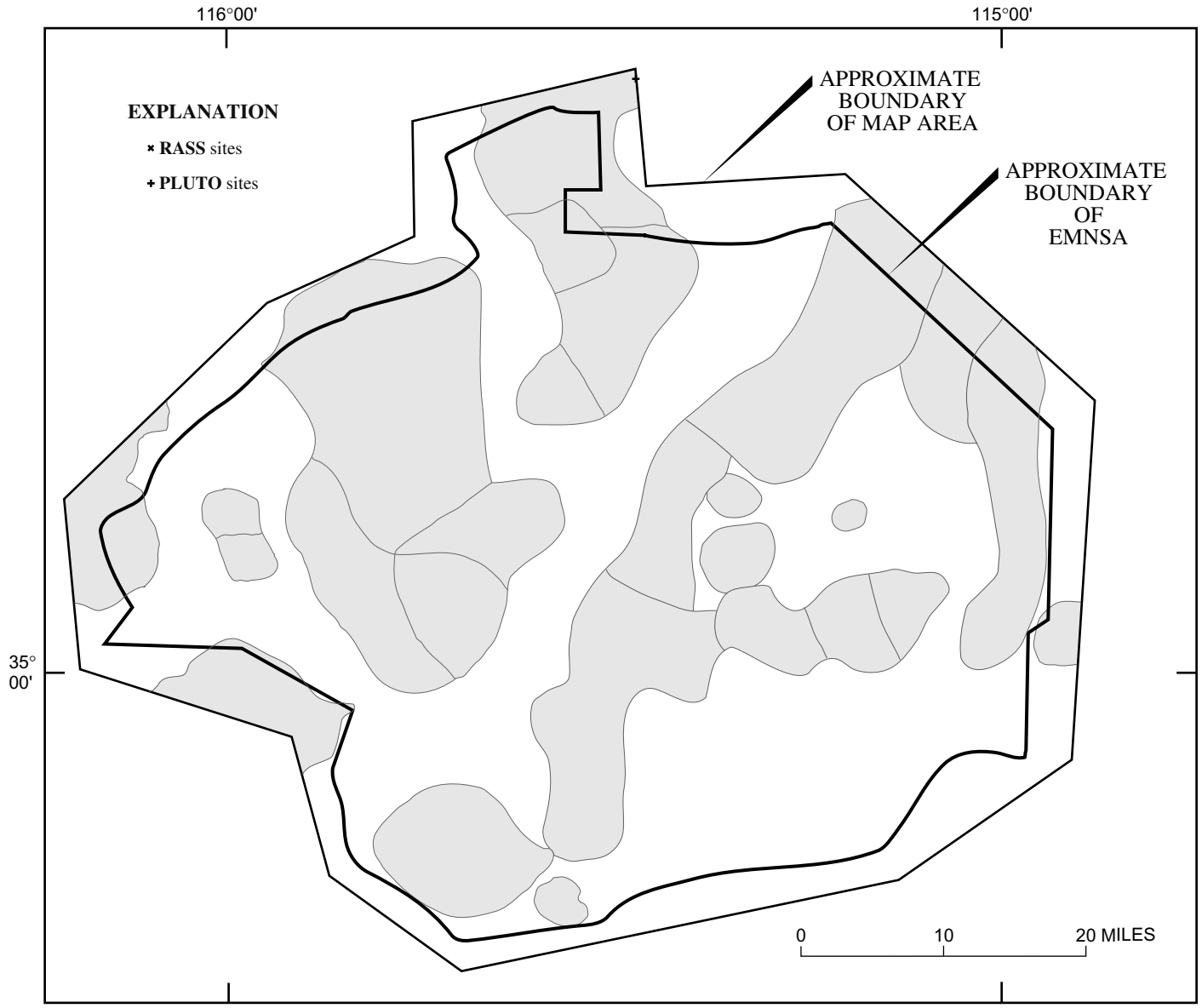

Figure 51. Sampling sites for Rock Analysis Storage System (RASS) and geochemical database for the United States (PLUTO) heavy-mineral-concentrate samples from East Mojave National Scenic Area (EMNSA), California, and surrounding area. General outlines of geochemically evaluated areas (shaded) shown for reference; see figure 49 for location names. Statistical data given in table 13; summary of geochemical anomalies given in table 14; data plotted on figures 54 to 73.

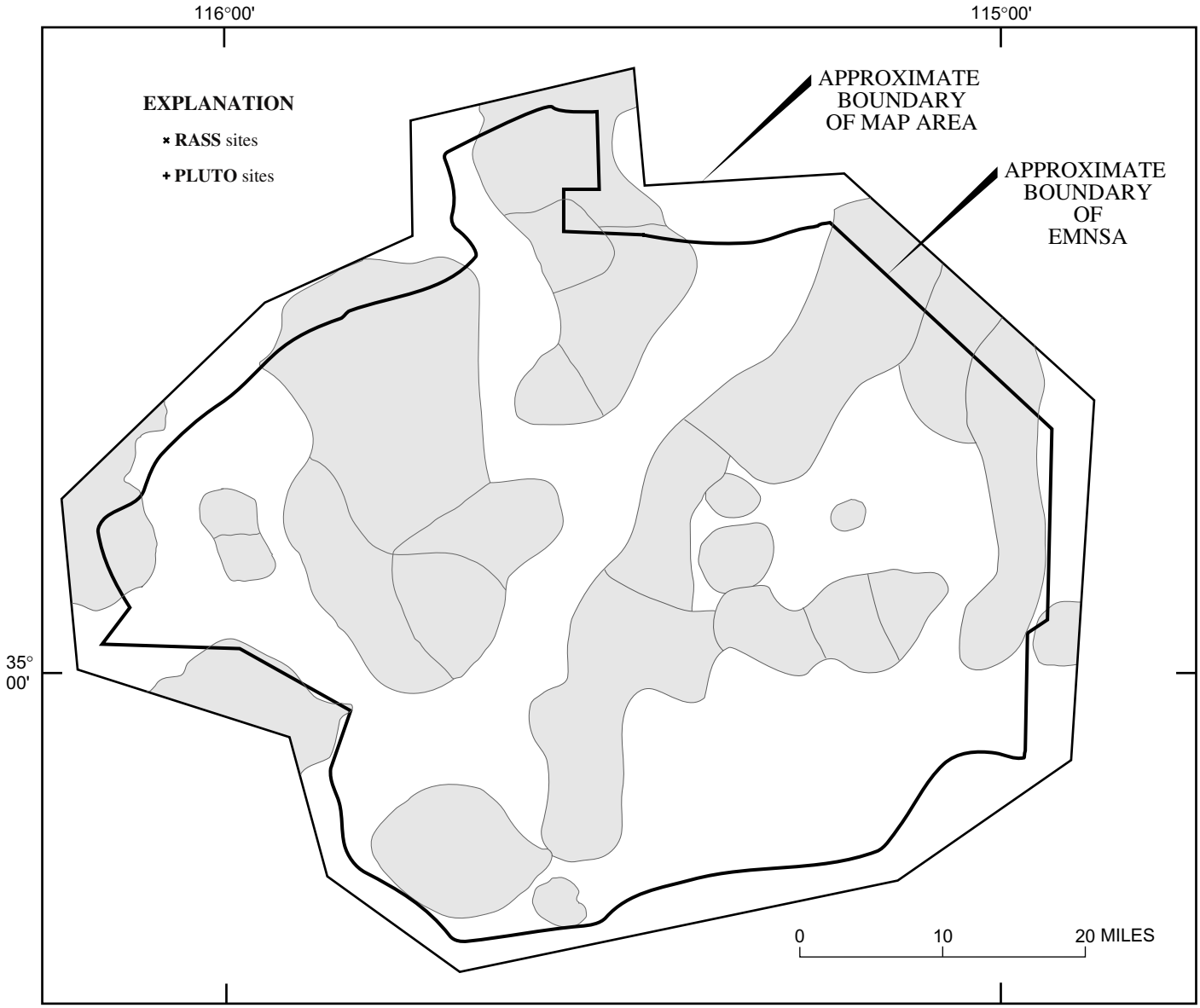

Figure 52. Sampling sites for Rock Analysis Storage System (RASS) and geochemical database for the United States (PLUTO) rock samples from East Mojave National Scenic Area (EMNSA), California, and surrounding area. General outlines of geochemically evaluated areas (shaded) shown for reference; see figure 49 for location names. Statistical data given in table 13; summary of geochemical anomalies given in table 14; data plotted on figures 54 to 73.

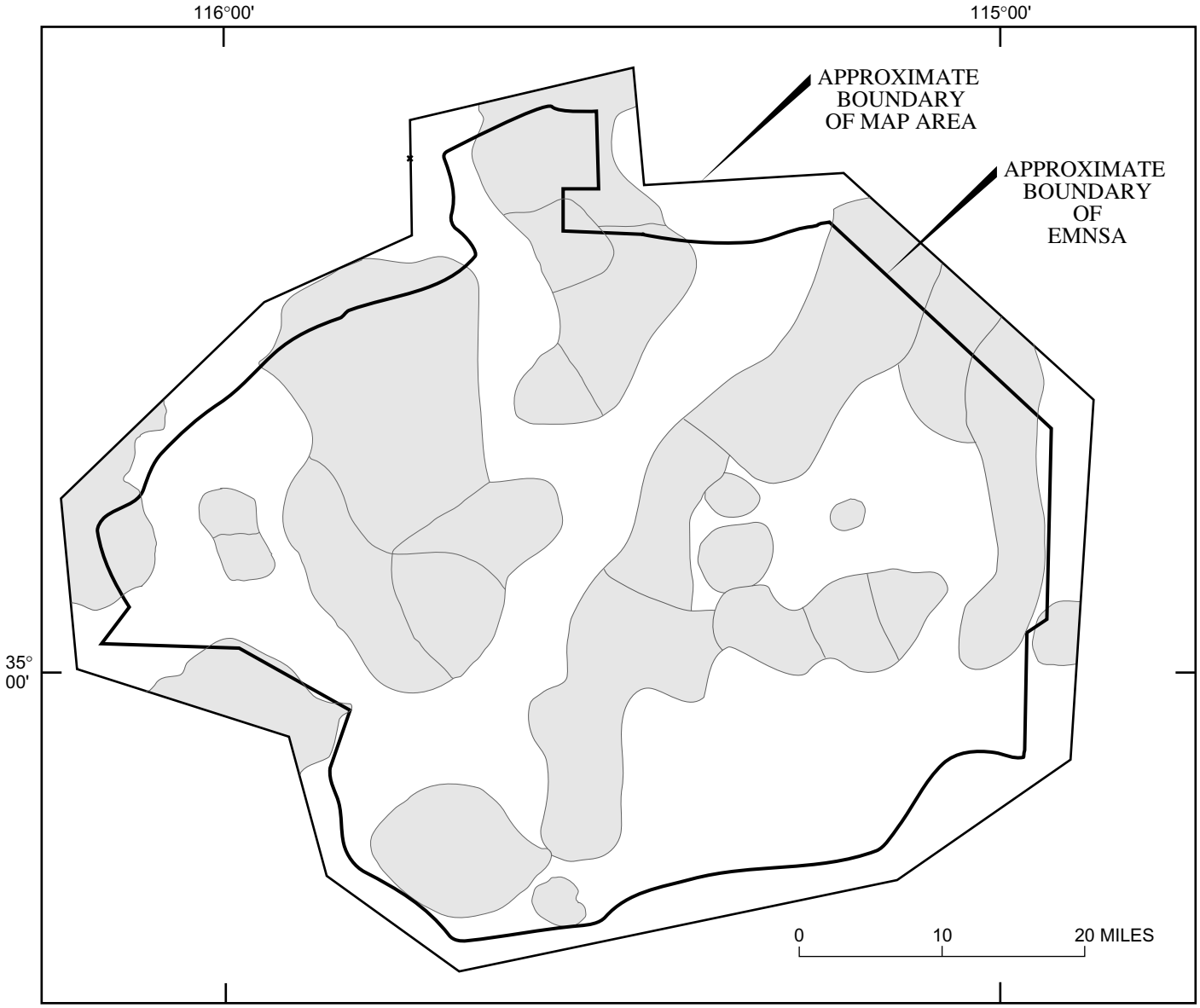

Figure 53. Sampling sites for National Uranium Resource Evaluation (NURE) stream-sediment and soil samples from East Mojave National Scenic Area (EMNSA), California, and surrounding area. General outlines of geochemically evaluated areas (shaded) shown for reference; see figure 49 for location names. Statistical data given in table 13; summary of geochemical anomalies given in table 14; data plotted on figures 54 to 73.

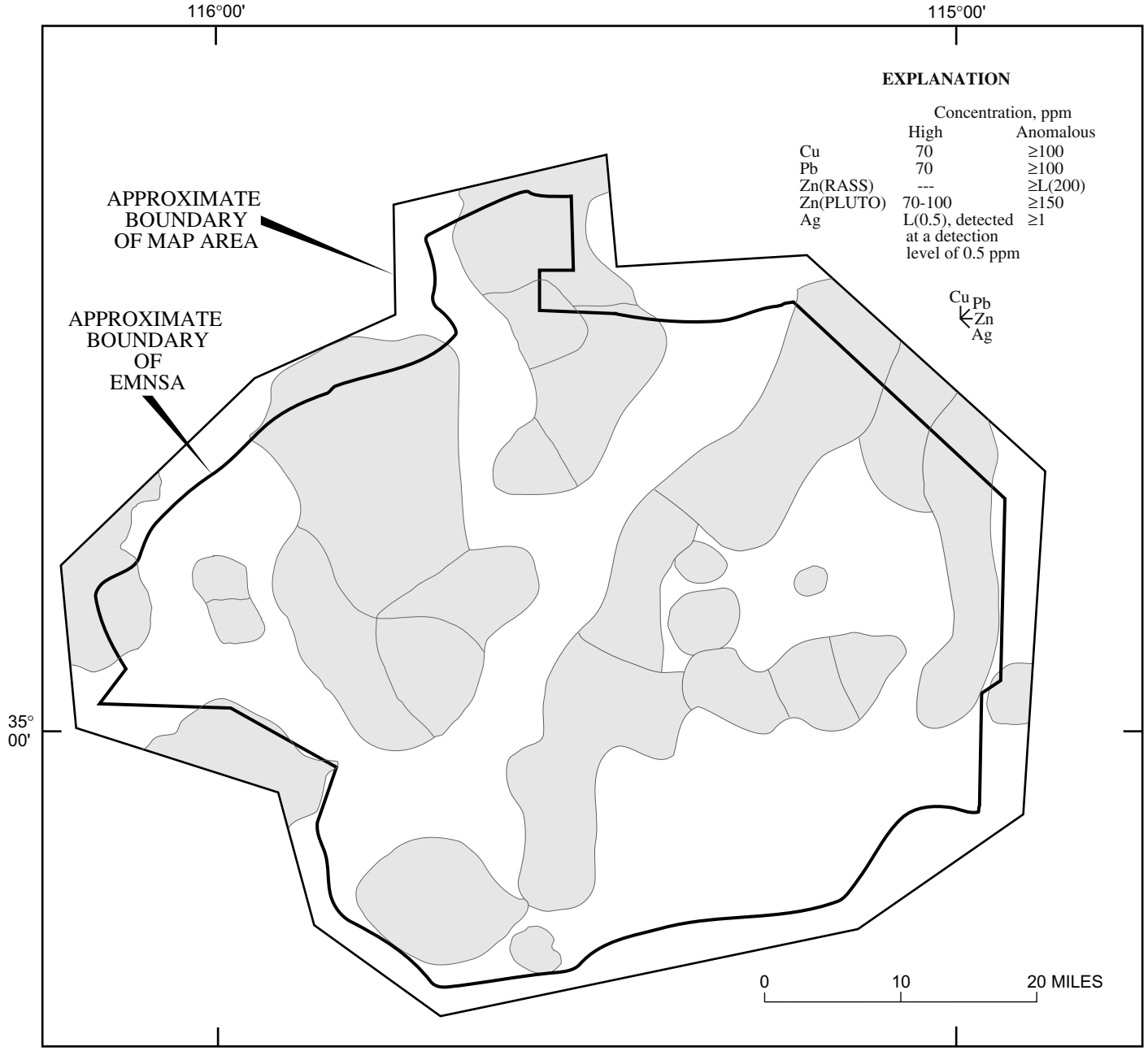

Figure 54. Distribution of anomalous and high concentrations, in parts per million, of Cu, Pb, Zn, and Ag in Rock Analysis Storage System (RASS) and geochemical database for the United States (PLUTO) stream-sediment samples from East Mojave National Scenic Area (EMNSA), California, and surrounding area. For each locality, elements are shown by either vertical, horizontal, or diagonal lines emanating from a common locality point (overlapping lines represent more than one locality). Longer lines indicate anomalous concentrations; shorter lines, high concentrations. Concentration values shown are defined as follows: anomalous, above threshold values given in table 13; high, selected ranges that include threshold values as upper limits; L, detected below lower limit of determination (given in parentheses); ---, no value (any detectable concentration is anomalous). Percentiles for high concentrations are as follows: Cu, 90 to 95; Pb, 89 to 94; Zn, 67 to 79; Ag, 88 to 94. General outlines of geochemically evaluated areas (shaded) shown for reference; see figure 49 for location names. Statistical data given in table 13; summary of geochemical anomalies given in table 14; sample localities plotted on figure 50.

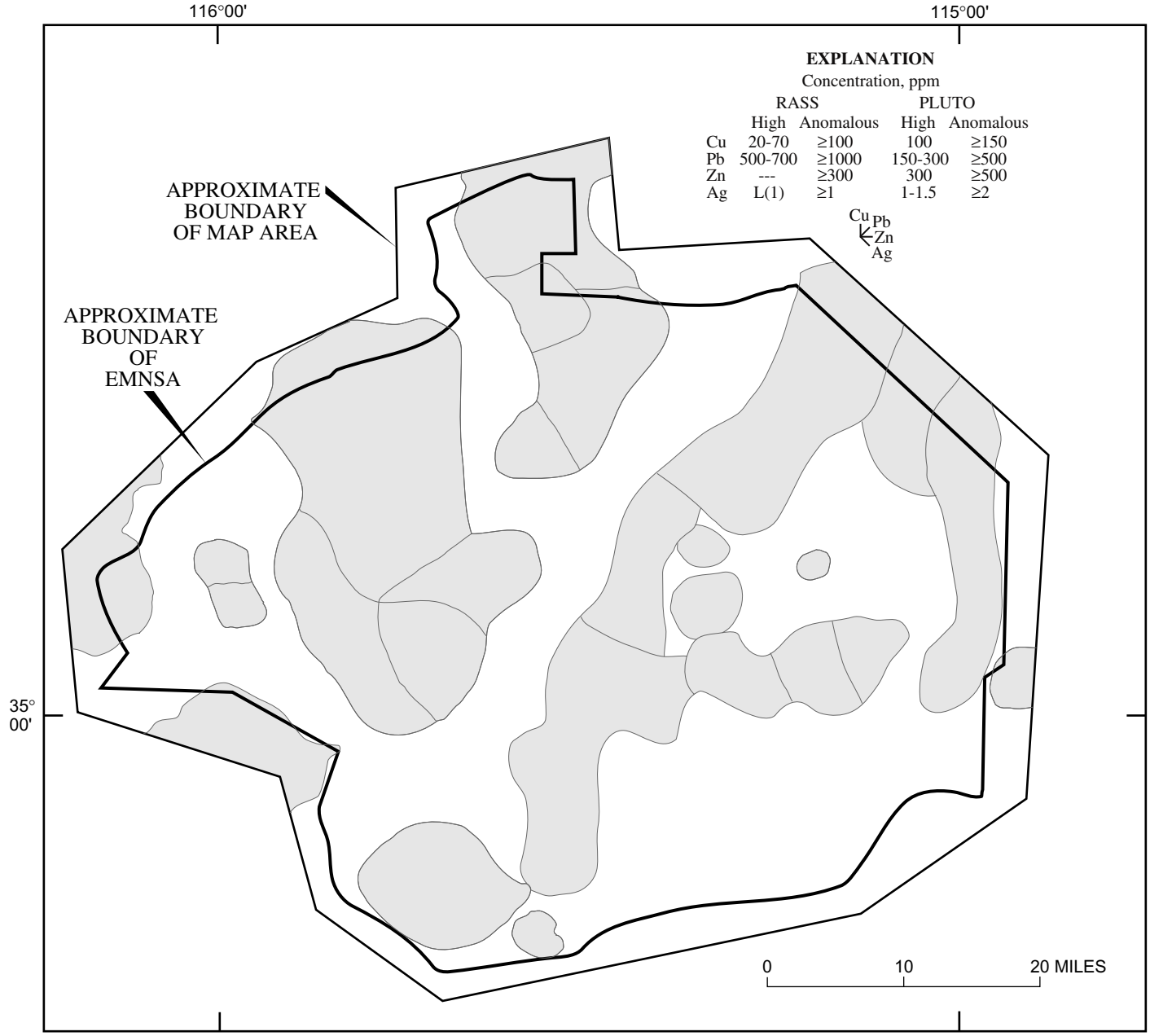

Figure 55. Distribution of anomalous and high concentrations, in parts per million, of Cu, Pb, Zn, and Ag in Rock Analysis Storage System (RASS) and geochemical database for the United States (PLUTO) heavy-mineral-concentrate samples from East Mojave National Scenic Area (EMNSA), California, and surrounding area. For each locality, elements are shown by either vertical, horizontal, or diagonal lines emanating from a common locality point (overlapping lines represent more than one locality). Longer lines indicate anomalous concentrations; shorter lines, high concentrations. Concentration values shown are defined as follows: anomalous, above threshold values given in table 13; high, selected ranges that include threshold values as upper limits; L, detected below lower limit of determination (given in parentheses); ---, no value (any detectable concentration is anomalous). Percentiles for high concentrations in PLUTO samples are as follows: Cu, 77 to 92; Pb, 77 to 81; Ag, 81 to 86. Percentiles for high concentrations in PLUTO samples are as follows: Cu, 60 to 79; Pb, 74 to 97; Zn, 65 to 79; Ag, 54 to 77. General outlines of geochemically evaluated areas (shaded areas) shown for reference; see figure 49 for location names. Statistical data given in table 13; summary of geochemical anomalies given in table 14; sample localities plotted on figure 51.

Figure 56. Distribution of anomalous and high concentrations, in parts per million, of Cu, Pb, Zn, and Ag in Rock Analysis Storage System (RASS) and geochemical database for the United States (PLUTO) rock samples from East Mojave National Scenic Area (EMNSA), California, and surrounding area. For each locality, elements are shown by either vertical, horizontal, or diagonal lines emanating from a common locality point (overlapping lines represent more than one locality). Longer lines indicate anomalous concentrations; shorter lines, high concentrations. Concentration values shown are defined as follows: anomalous, above threshold values given in table 13; high, selected ranges that include threshold values as upper limits; L, detected below lower limit of determination (given in parentheses); ---, no value (any detectable concentration is anomalous). Percentiles for high concentrations are as follows: Cu, 71 to 78; Pb, 61 to 75; Zn, 80 to 81; Ag, 65 to 73. General outlines of geochemically evaluated areas (shaded) shown for reference; see figure 49 for location names. Statistical data given in table 13; summary of geochemical anomalies given in table 14; sample localities plotted on figure 52.

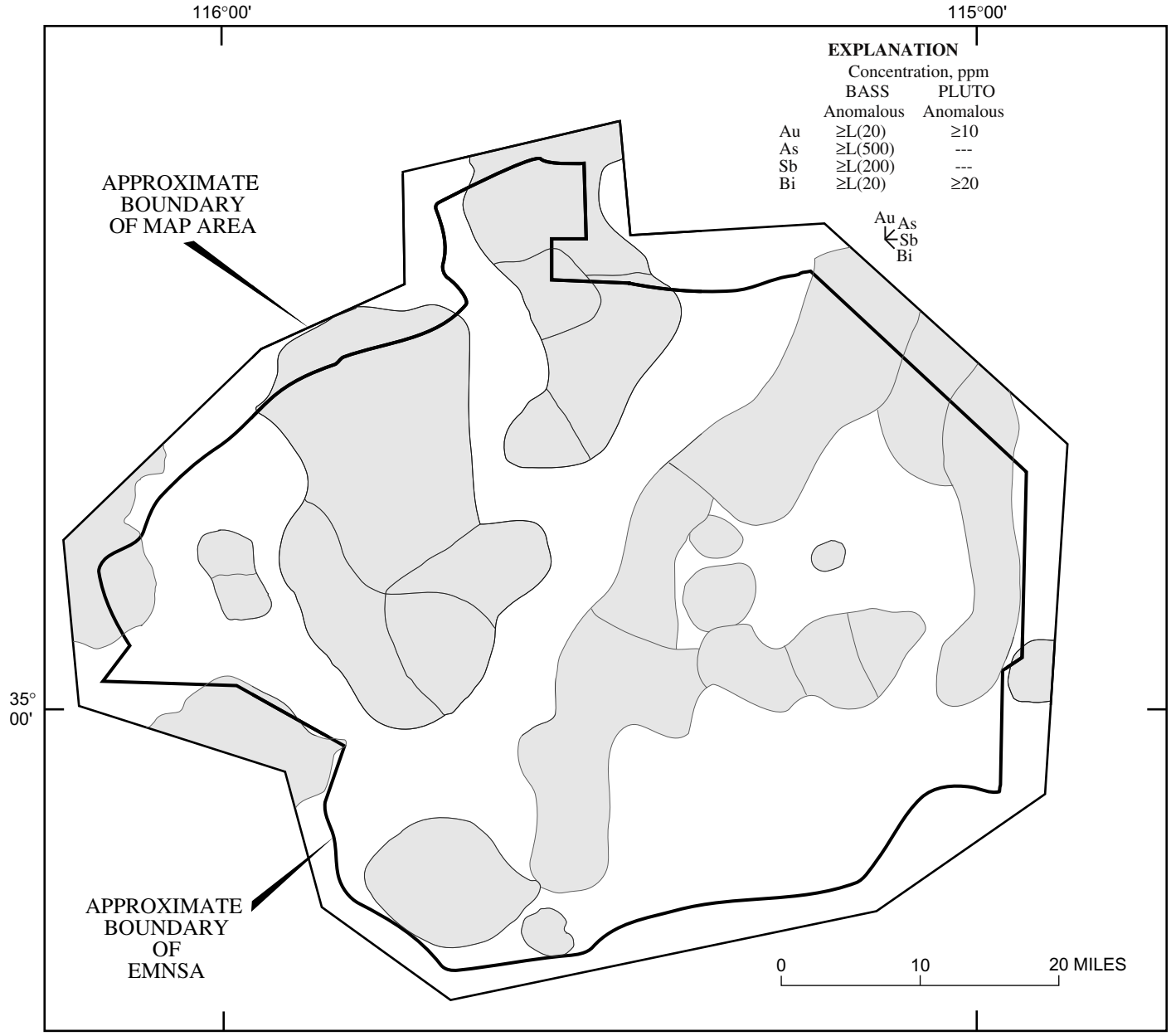

Figure 57. Distribution of anomalous concentrations, in parts per million, of Au, As, Sb, and Bi in Rock Analysis Storage System (RASS) and geochemical database for the United States (PLUTO) heavy-mineral-concentrate samples from East Mojave National Scenic Area (EMNSA), California, and surrounding area. For each locality, elements are shown by either vertical, horizontal, or diagonal lines emanating from a common locality point (overlapping lines represent more than one locality). Anomalous concentration values shown are defined as those above threshold values given in table 13; L, detected below lower limit of determination (given in parentheses); ---, no data (As was not determined and Sb was not detected in PLUTO samples). General outlines of geochemically evaluated areas (shaded) shown for reference; see figure 49 for location names. Statistical data given in table 13; summary of geochemical anomalies given in table 14; sample localities plotted on figure 51.

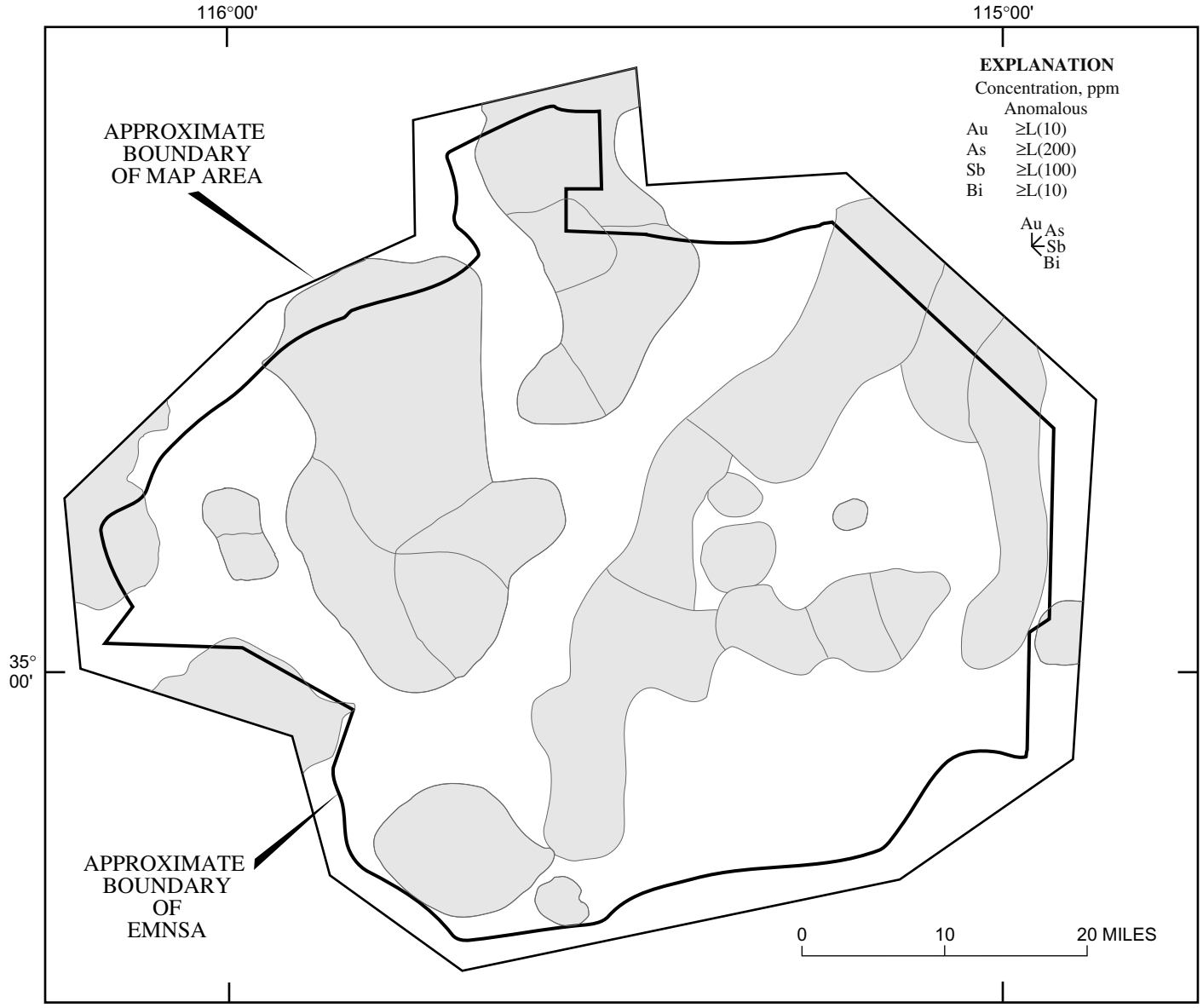

Figure 58. Distribution of anomalous concentrations, in parts per million, of Au, As, Sb, and Bi in Rock Analysis Storage System (RASS) and geochemical database for the United States (PLUTO) rock samples from East Mojave National Scenic Area (EMNSA), California, and surrounding area. For each locality, elements are shown by either vertical, horizontal, or diagonal lines emanating from a common locality point (overlapping lines represent more than one locality). Anomalous concentration values shown are defined as those above threshold values given in table 13; L, detected below lower limit of determination (given in parentheses). General outlines of geochemically evaluated areas (shaded) shown for reference; see figure 49 for location names. Statistical data given in table 13; summary of geochemical anomalies given in table 14; sample localities plotted on figure 52.

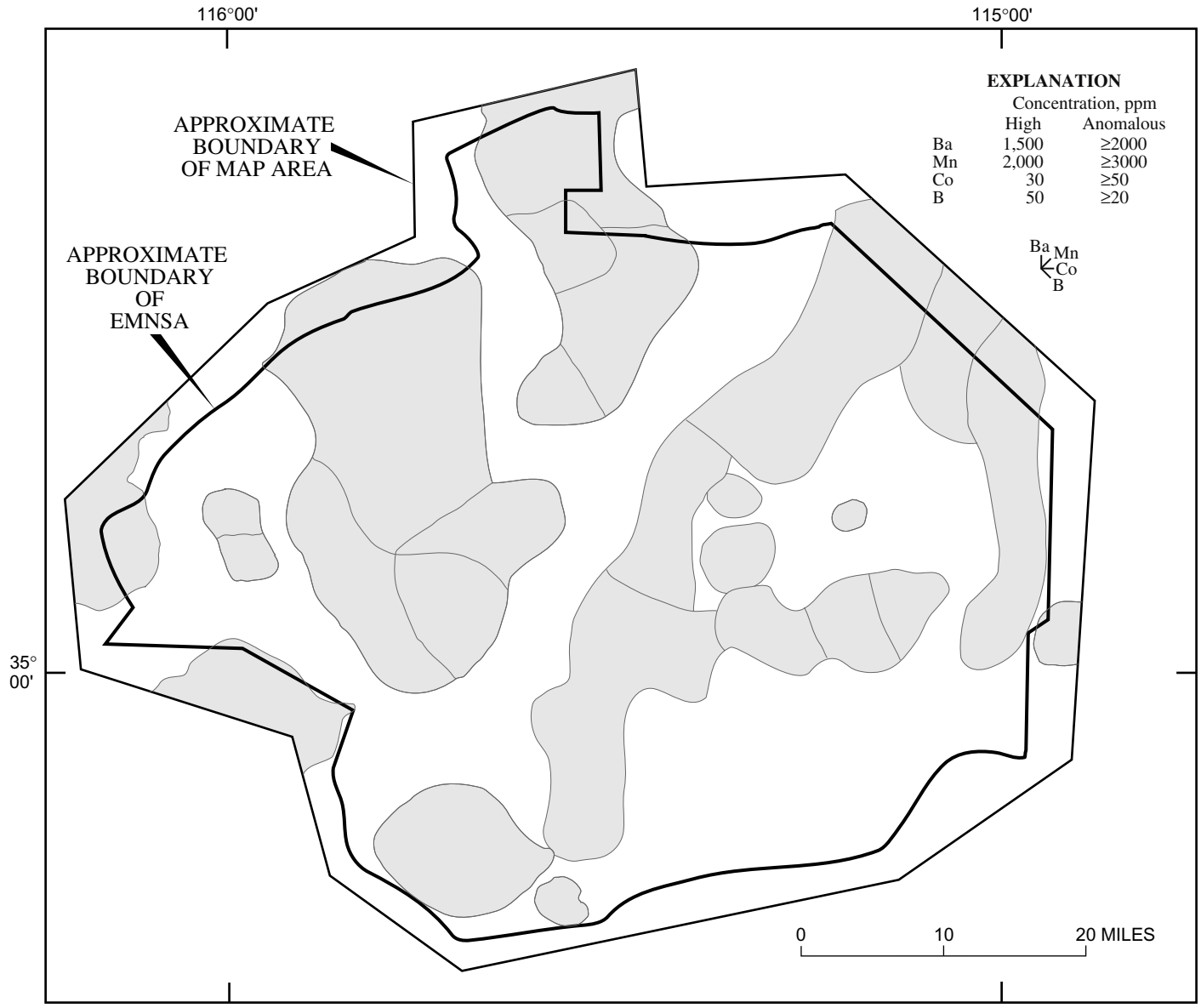

Figure 59. Distribution of anomalous and high concentrations, in parts per million, of Ba, Mn, Co, and B in Rock Analysis Storage System (RASS) and geochemical database for the United States (PLUTO) stream-sediment samples from East Mojave National Scenic Area (EMNSA), California, and surrounding area. For each locality, elements are shown by either vertical, horizontal, or diagonal lines emanating from a common locality point (overlapping lines represent more than one locality). Longer lines indicate anomalous concentrations; shorter lines, high concentrations. Concentration values shown are defined as follows: anomalous, above threshold values given in table 13; high, selected ranges that include threshold values as upper limits. Percentiles for high concentrations are as follows: Ba, 95 to 97; Mn, 90 to 95; Co, 81 to 92; B, 90 to 95. General outlines of geochemically evaluated areas (shaded areas) shown for reference; see figure 49 for location names. Statistical data given in table 13; summary of geochemical anomalies given in table 14; sample localities plotted on figure 50.

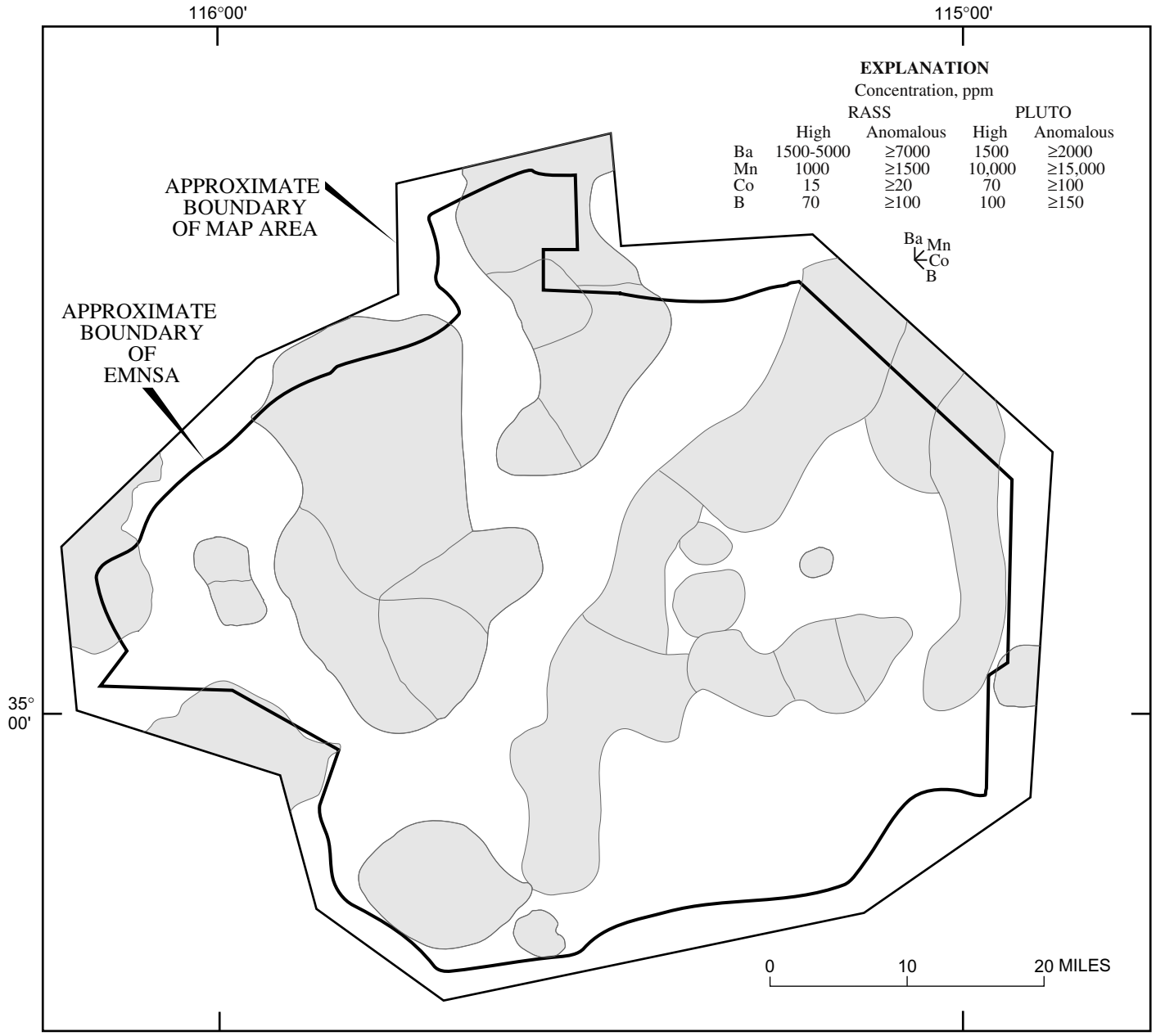

Figure 60. Distribution of anomalous and high concentrations, in parts per million, of Ba, Mn, Co, and B in Rock Analysis Storage System (RASS) and geochemical database for the United States (PLUTO) heavy-mineral-concentrate samples from East Mojave National Scenic Area (EMNSA), California, and surrounding area. For each locality, elements are shown by either vertical, horizontal, or diagonal lines emanating from a common locality point (overlapping lines represent more than one locality). Longer lines indicate anomalous concentrations; shorter lines, high concentrations. Concentration values shown are defined as follows: anomalous, above threshold values given in table 13; high, selected ranges that include threshold values as upper limits. Percentiles for high concentrations in RASS samples are as follows: Ba, 58 to 79; Mn, 72 to 90; Co, 91 to 92; B, 92 to 94. Percentiles for high concentrations in PLUTO samples are as follows: Ba, 87 to 90; Mn, 74 to 94; Co, 77 to 87; B, 78 to 93. General outlines of geochemically evaluated areas (shaded) shown for reference; see figure 49 for location names. Statistical data given in table 13; summary of geochemical anomalies given in table 14; sample localities plotted on figure 51.

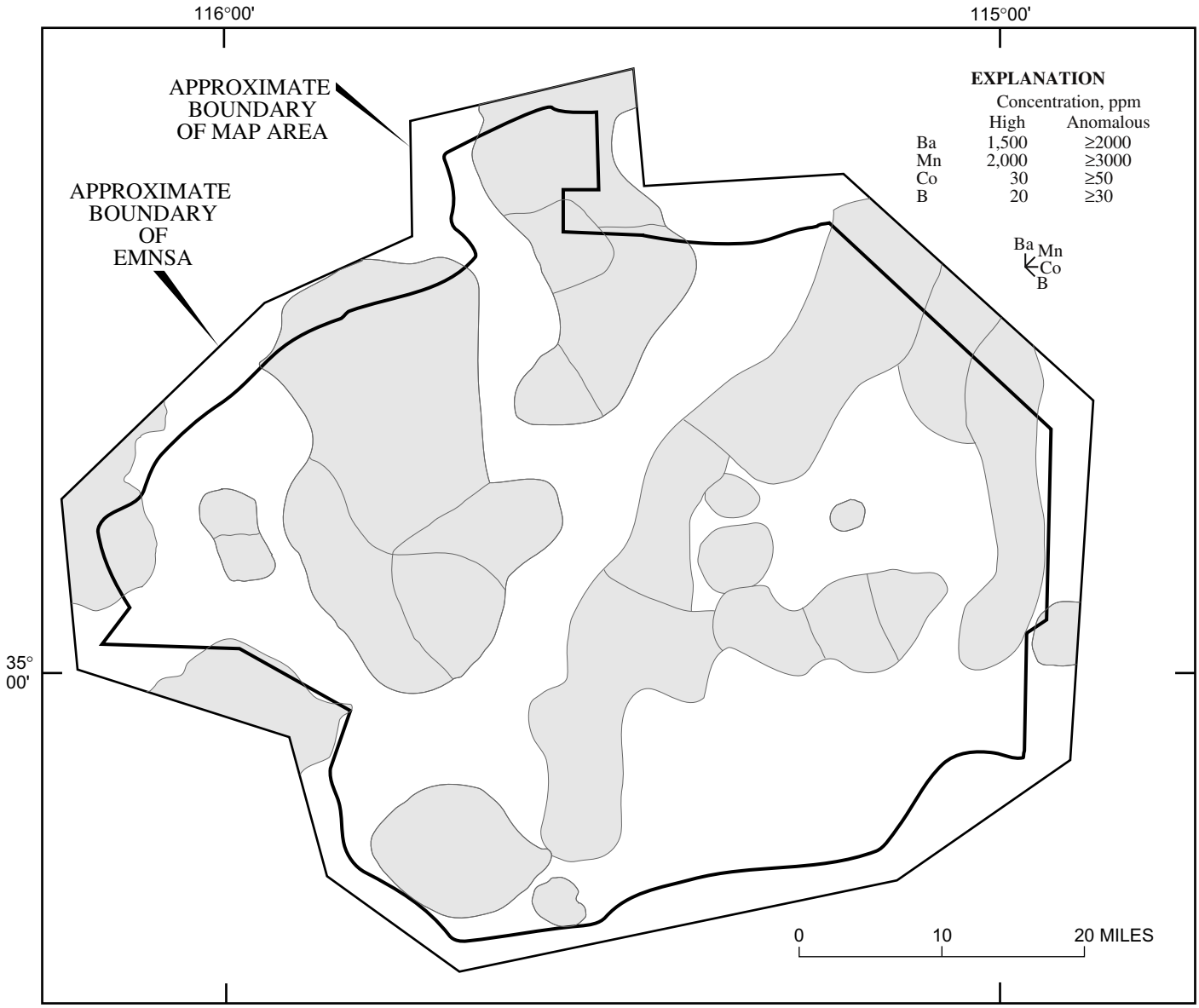

Figure 61. Distribution of anomalous and high concentrations, in parts per million, of Ba, Mn, Co, and B in Rock Analysis Storage system (RASS) and geochemical database for the United States (PLUTO) rock samples from East Mojave National Scenic Area (EMNSA), California, and surrounding area. For each locality, elements are shown by either vertical, horizontal, or diagonal lines emanating from a common locality point (overlapping lines represent more than one locality). Longer lines indicate anomalous concentrations; shorter lines, high concentrations. Concentration values shown are defined as follows: anomalous, above threshold values given in table 13; high, selected ranges that include threshold values as upper limits. Percentiles for high concentrations are as follows: Ba, 83 to 92; Mn, 93 to 94; Co, 87 to 90; B, 83 to 88. General outlines of geochemically evaluated areas (shaded) shown for reference; see figure 49 for location names. Statistical data given in table 13; summary of geochemical anomalies given in table 14; sample localities plotted on figure 52.

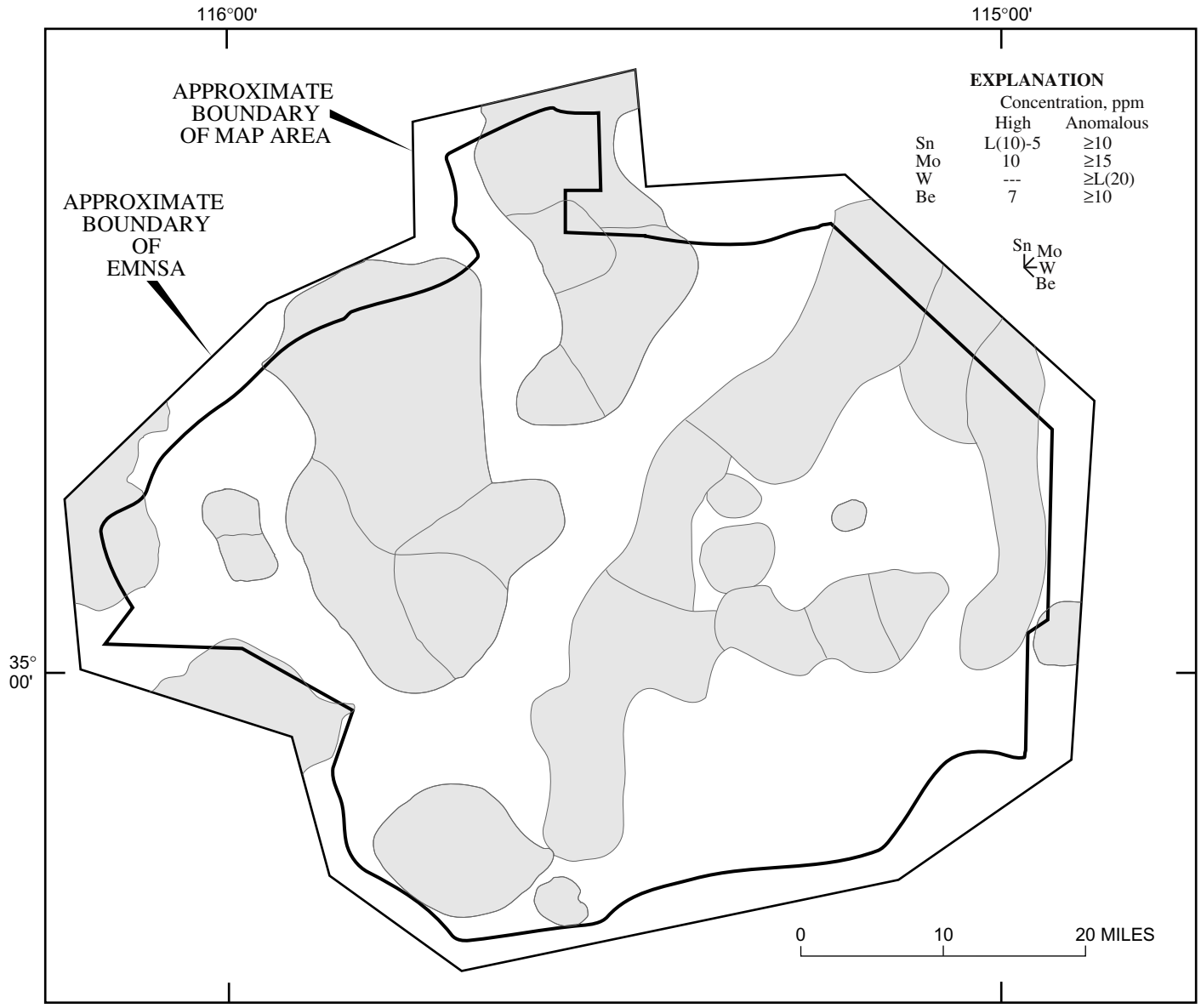

Figure 62. Distribution of anomalous and high concentrations, in parts per million, of Sn, Mo, W, and Be in Rock Analysis Storage System (RASS) and geochemical database for the United States (PLUTO) stream-sediment samples from East Mojave National Scenic Area (EMNSA), California, and surrounding area. For each locality, elements are shown by either vertical, horizontal, or diagonal lines emanating from a common locality point (overlapping lines represent more than one locality). Longer lines indicate anomalous concentrations; shorter lines, high concentrations. Concentration values shown are defined as follows: anomalous, above threshold values given in table 13; high, selected ranges that include threshold ; L, detected below lower limit of determination (given in parentheses); ---, no value (any detectable concentration is anomalous). Percentiles for high concentrations are as follows: Sn, 96; Mo, 77 to 85; Be, 94 to 98. General outlines of geochemically evaluated areas (shaded) shown for reference; see figure 49 for location names. Statistical data given in table 13; summary of geochemical anomalies given in table 14; sample localities plotted on figure 50.

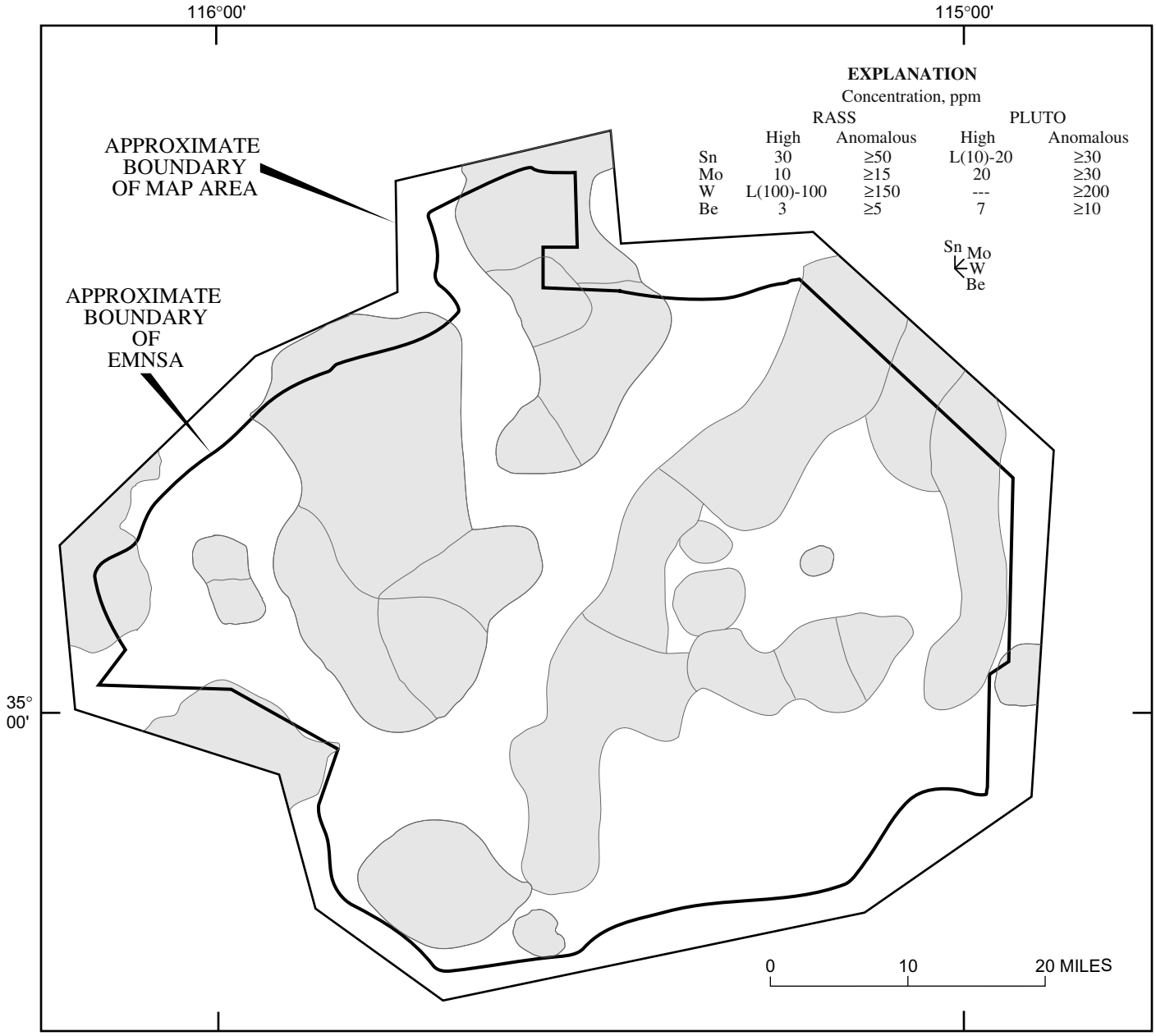

Figure 63. Distribution of anomalous and high concentrations, in parts per million, of Sn, Mo, W, and Be in Rock Analysis (RASS) and geochemical database for the United States (PLUTO) heavy-mineral-concentrate samples from East Mojave National Scenic Area (EMNSA), California, and surrounding area. For each locality, elements are shown by either vertical, horizontal, or diagonal lines emanating from a common locality point (overlapping lines represent more than one locality). Longer lines indicate anomalous concentrations; shorter lines, high concentrations. Concentration values shown are defined as follows: anomalous, above threshold values given in table 13; high, selected ranges that include threshold values as upper limits; L, detected below lower limit of determination (given in parentheses); ---, no value (any detectable concentration is anomalous). Percentiles for high concentrations in RASS samples are as follows: Sn, 79; Mo, 84; W, 74 to 83; Be, 90 to 95. Percentiles for high concentrations in PLUTO samples are as follows: Sn, 50 to 85; Mo, 62 to 76; Be, 71 to 94. General outlines of geochemically evaluated areas (shaded) shown for reference; see figure 49 for location names. Statistical data given in table 13; summary of geochemical anomalies given in table 14; sample localities plotted on figure 51.

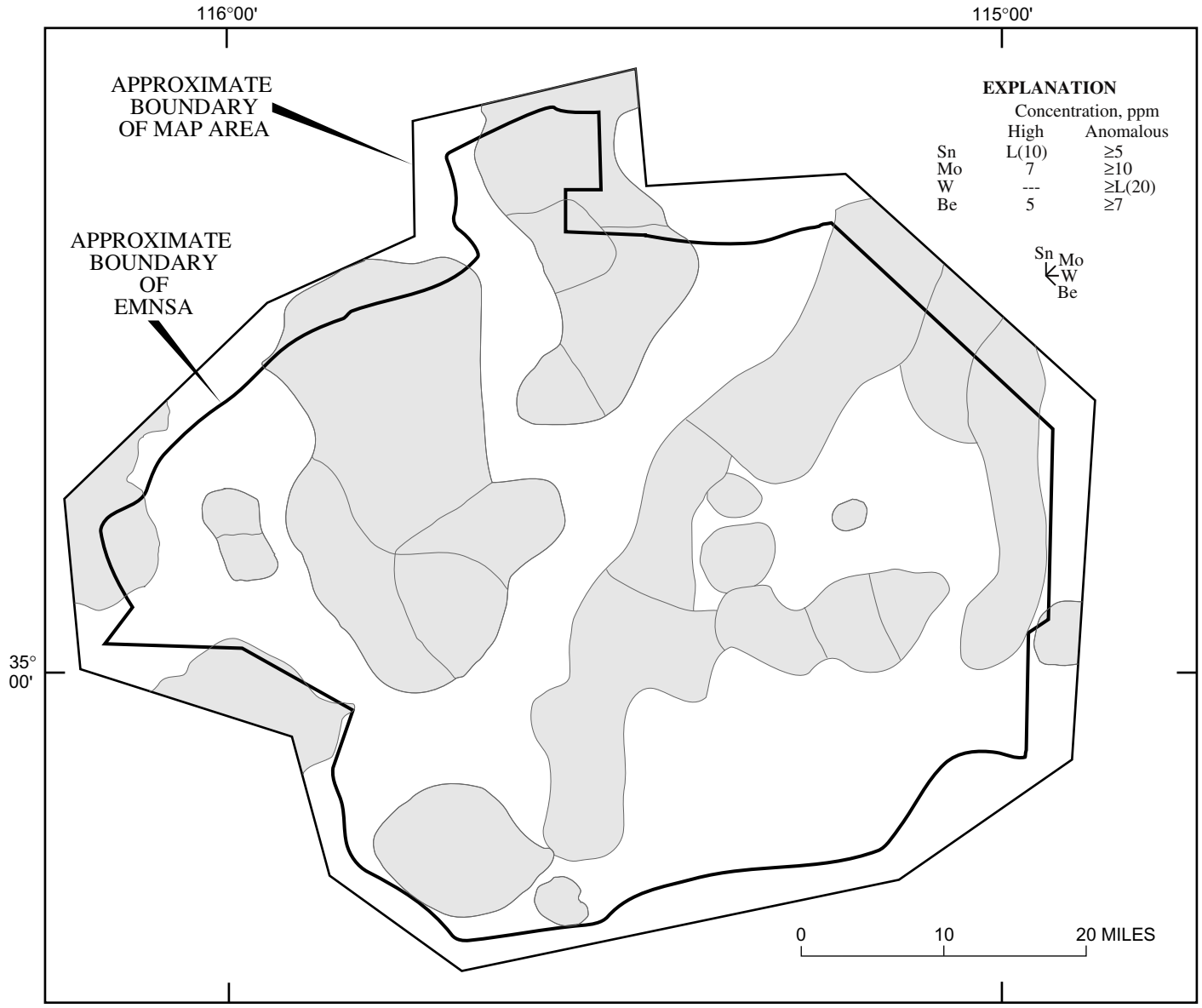

Figure 64. Distribution of anomalous and high concentrations, in parts per million, of Sn, Mo, W, and Be in Rock Analysis Storage System (RASS) and geochemical database for the United States (PLUTO) rock samples from East Mojave National Scenic Area (EMNSA), California, and surrounding area. For each locality, elements are shown by either vertical, horizontal, or diagonal lines emanating from a common locality point (overlapping lines represent more than one locality). Longer lines indicate anomalous concentrations; shorter lines, high concentrations. Concentration values shown are defined as follows: anomalous, above threshold values given in table 13; high, selected ranges that include threshold values as upper limits; L, detected below lower limit of determination (given in parentheses); ---, no value (any detectable concentration is anomalous). Percentiles for high concentrations are as follows: Sn, 95 to 96; Mo, 82 to 86; Be, 95 to 97. General outlines of geochemically evaluated areas (shaded) shown for reference; see figure 49 for location names. Statistical data given in table 13; summary of geochemical anomalies given in table 14; sample localities plotted on figure 52.

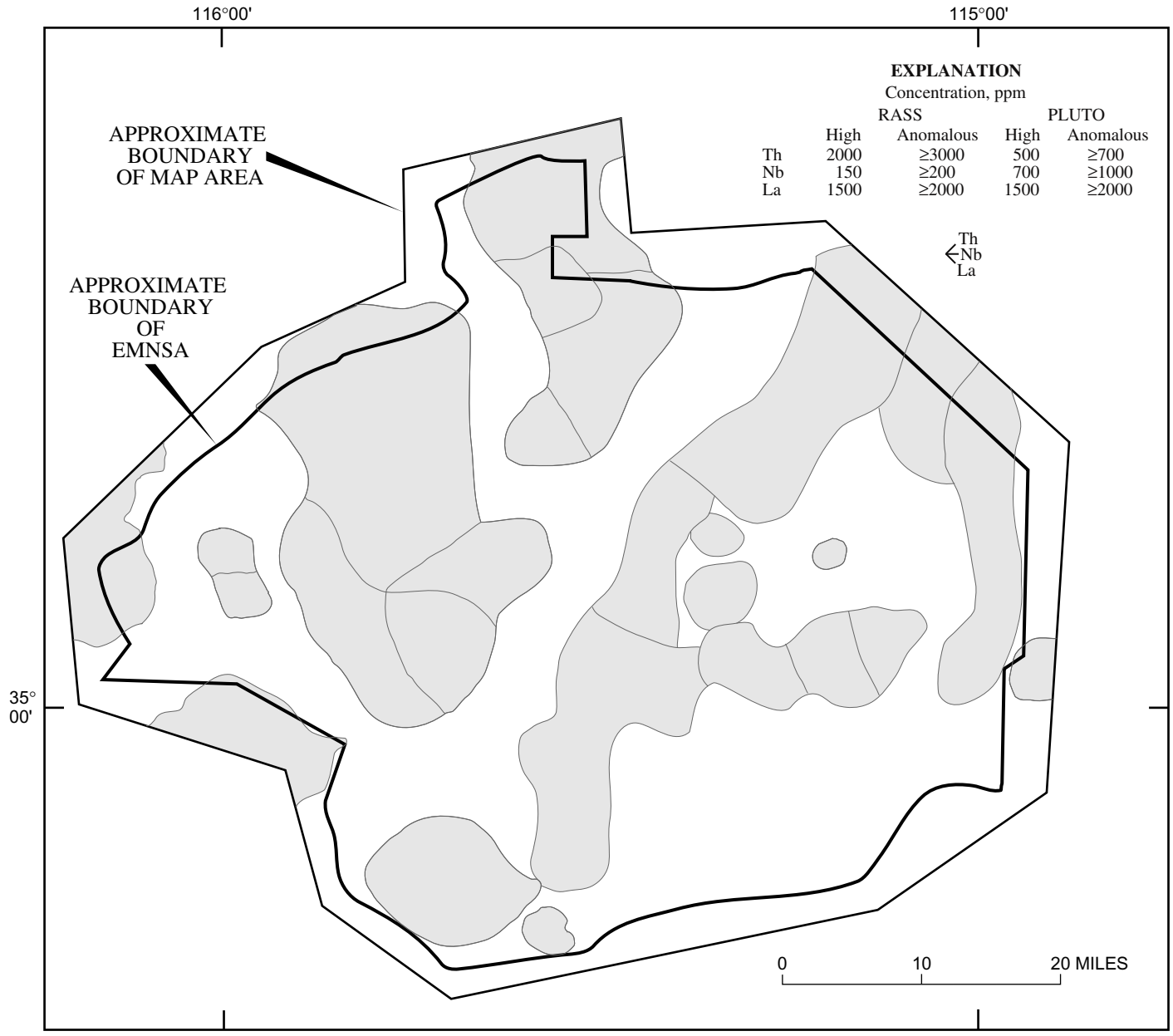

Figure 65. Distribution of anomalous and high concentrations, in parts per million, of Th, Nb, and La in Rock Analysis Storage System (RASS) and geochemical database for the United States (PLUTO) heavy-mineral-concentrate samples from East Mojave National Scenic Area (EMNSA), California, and surrounding area. For each locality, elements are shown by either horizontal or diagonal lines emanating from a common locality point (overlapping lines represent more than one locality). Longer lines indicate anomalous concentrations; shorter lines, high concentrations. Concentration values shown are defined as follows: anomalous, above threshold values given in table 13; high, selected ranges that include threshold values as upper limits. Percentiles for high concentrations in RASS samples are as follows: Th, 92 to 94; Nb, 93 to 96; La, 94 to 96. Percentiles for high concentrations in PLUTO samples are as follows: Th, 88 to 92; Nb, 95 to 96; La, 78 to 85. General outlines of geochemically evaluated areas (shaded) shown for reference; see figure 49 for location names. Statistical data given in table 13; summary of geochemical anomalies given in table 14; sample localities plotted on figure 51.

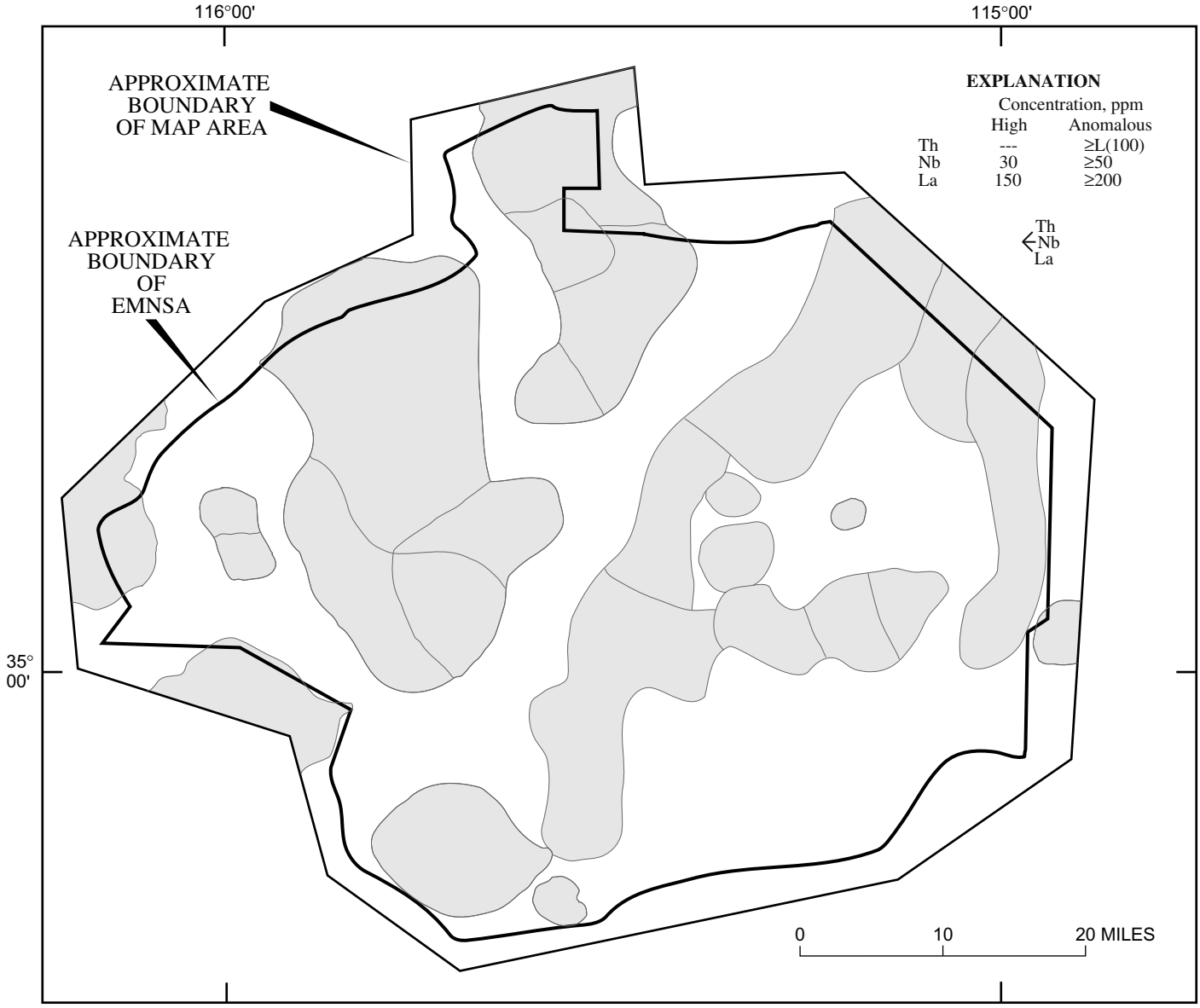

Figure 66. Distribution of anomalous and high concentrations, in parts per million, of Th, Nb, and La in Rock Analysis Storage System (RASS) and geochemical database for the United States (PLUTO) rock samples from East Mojave National Scenic Area (EMNSA), California, and surrounding area. For each locality, elements are shown by either horizontal or diagonal lines emanating from a common locality point (overlapping lines represent more than one locality). Longer lines indicate anomalous concentrations; shorter lines, high concentrations. Concentration values shown are defined as follows: anomalous, above threshold values given in table 13; high, selected ranges that include threshold values as upper limits; L, detected below lower limit of determination (given in parentheses); ---, no value (any detectable concentration is anomalous). Percentiles for high concentrations are as follows: Nb, 95 to 98; La, 94 to 97. General outlines of geochemically evaluated areas (shaded) shown for reference; see figure 49 for location names. Statistical data given in table 13; summary of geochemical anomalies given in table 14; sample localities plotted on figure 52.

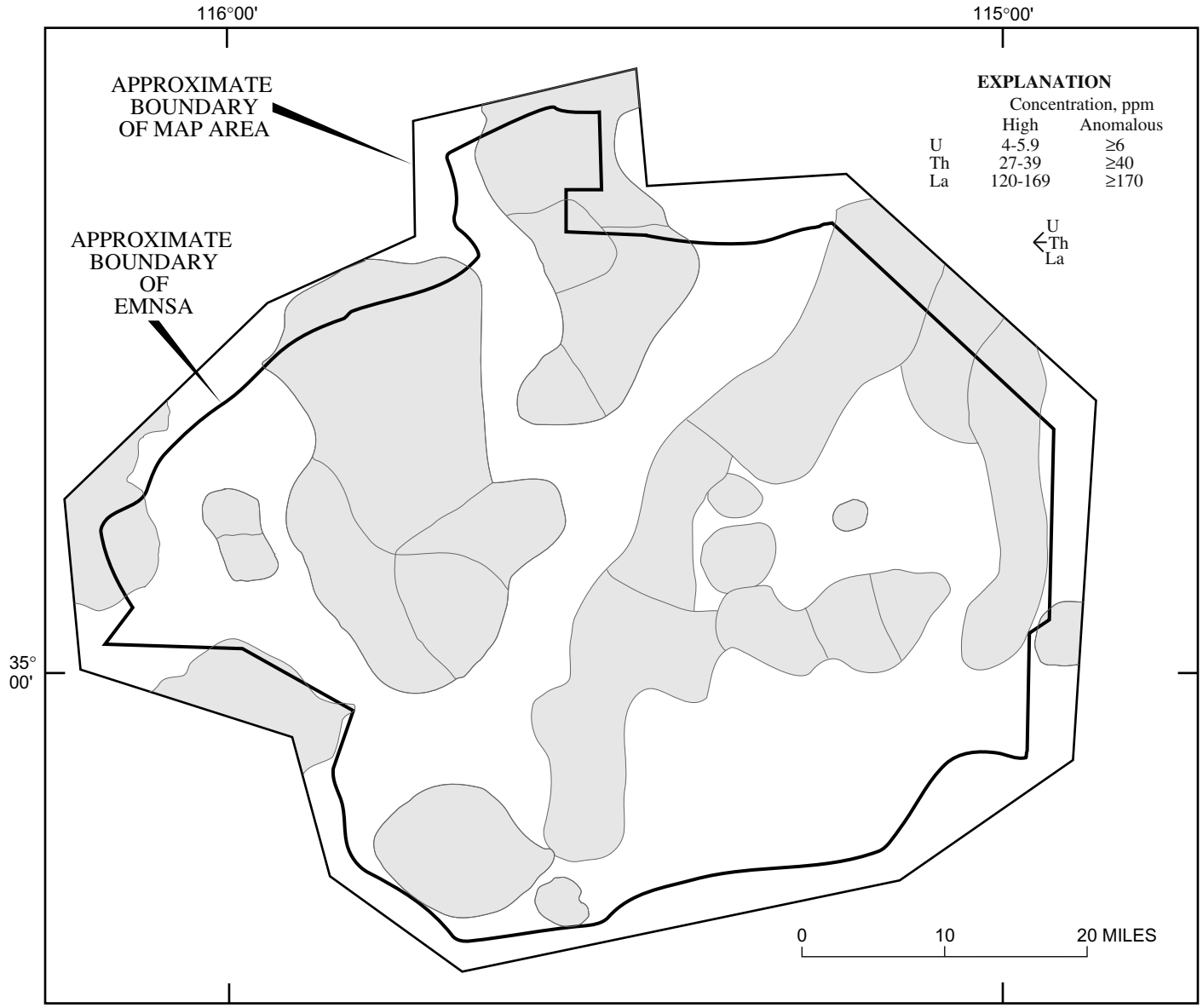

Figure 67. Distribution of anomalous and high concentrations, in parts per million, of U, Th, and La in National Uranium Resource Evaluation (NURE) stream-sediment and soil samples from East Mojave National Scenic Area (EMNSA), California, and surrounding area. For each locality, elements are shown by either vertical or diagonal lines emanating from a common locality point (overlapping lines represent more than one locality). Longer lines indicate anomalous concentrations; shorter lines, high concentrations. Concentration values shown are defined as follows: anomalous, above threshold values given in table 13; high, selected ranges that include threshold values as upper limits. Percentiles for high concentrations are as follows: U, 91 to 98; Th, 94 to 97; La, 97 to 98. General outlines of geochemically evaluated areas (shaded) shown for reference; see figure 49 for location names. Statistical data given in table 13; summary of geochemical anomalies given in table 14; sample localities plotted on figure 53.

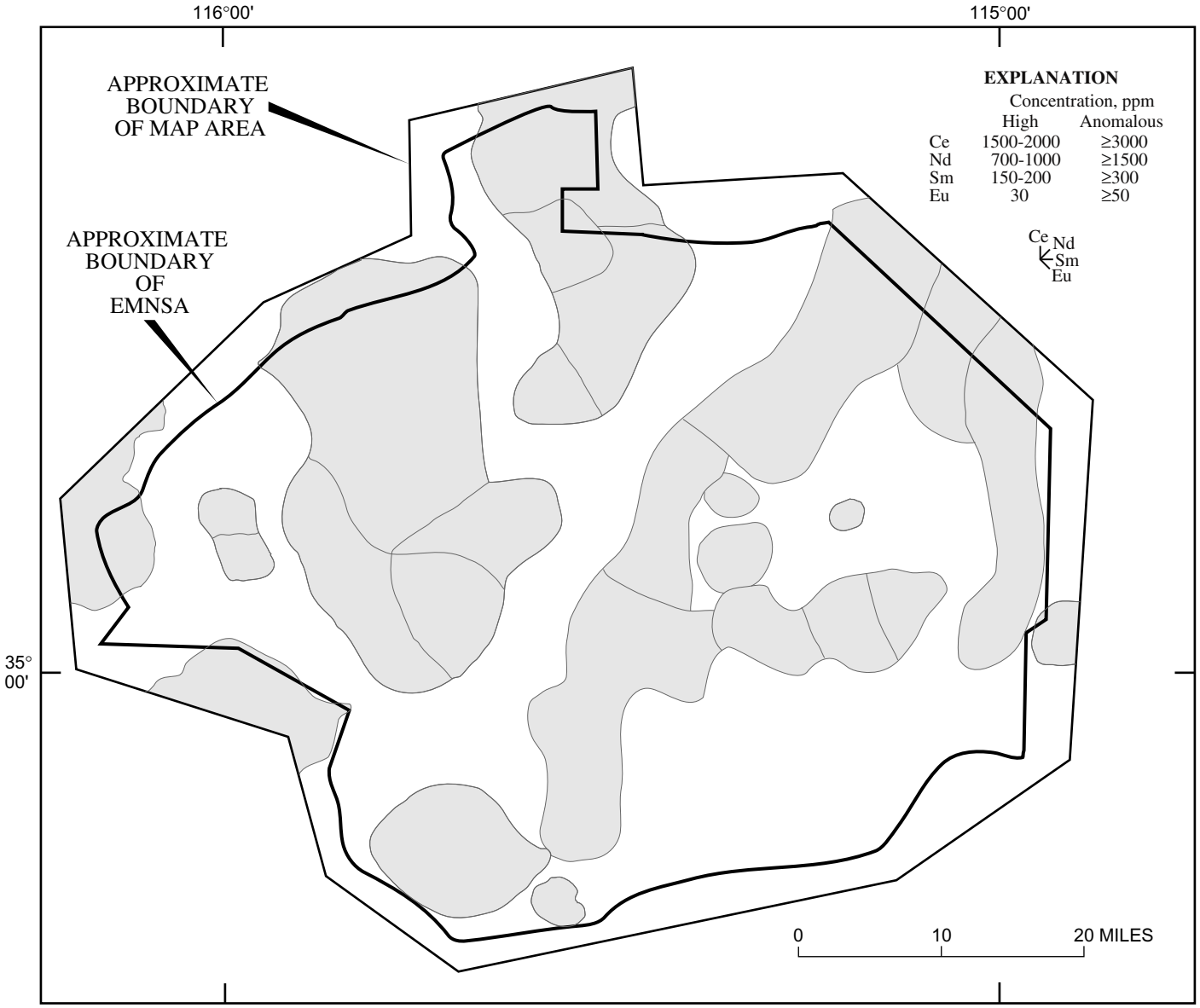

Figure 68. Distribution of anomalous and high concentrations, in parts per million, of Ce, Nd, Sm, and Eu in geochemical database for the United States (PLUTO) heavy-mineral-concentrate samples from East Mojave National Scenic Area (EMNSA), California, and surrounding area. For each locality, elements are shown by either vertical, horizontal, or diagonal lines emanating from a common locality point (overlapping lines represent more than one locality). Longer lines indicate anomalous concentrations; shorter lines, high concentrations. Concentration values shown are defined as follows: anomalous, above threshold values given in table 13; high, selected ranges that include threshold values as upper limits. Percentiles for high concentrations are as follows: Ce, 74 to 88; Nd, 73 to 90; Sm, 75 to 92; Eu, 87 to 96. General outlines of geochemically evaluated areas (shaded) shown for reference; see figure 49 for location names. Statistical data given in table 13; summary of geochemical anomalies given in table 14; sample localities plotted on figure 51.

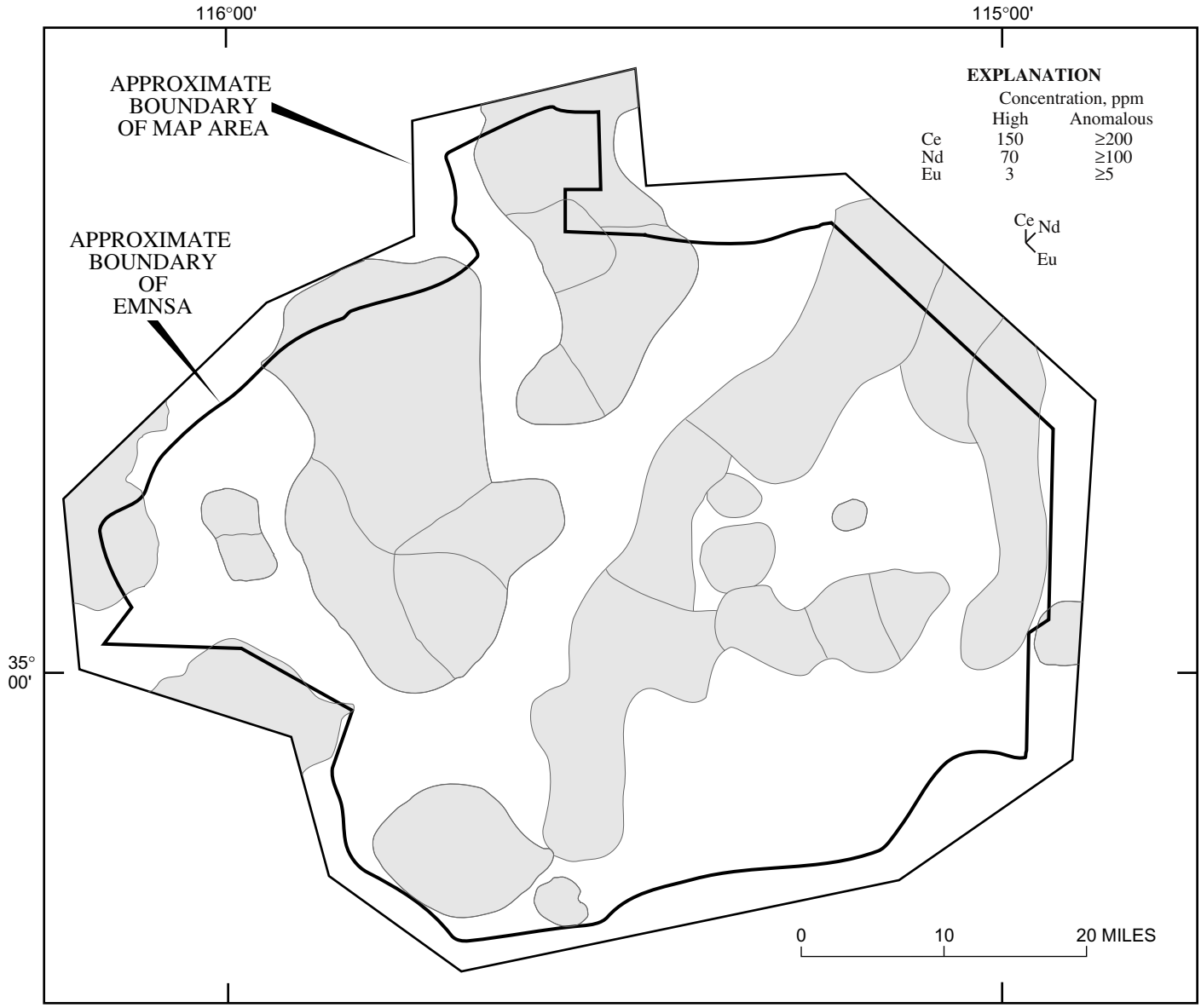

Figure 69. Distribution of anomalous and high concentrations, in parts per million, of Ce, Nd, and Eu in geochemical database for the United States (PLUTO) rock samples from East Mojave National Scenic Area (EMNSA), California, and surrounding area. For each locality, elements are shown by either vertical or diagonal lines emanating from a common locality point (overlapping lines represent more than one locality). Longer lines indicate anomalous concentrations; shorter lines, high concentrations. Concentration values shown are defined as follows: anomalous, above threshold values given in table 13; high, selected ranges that include threshold values as upper limits. Percentiles for high concentrations are as follows: Ce, 88 to 95; Nd, 73 to 91; Eu, 68 to 95. General outlines of geochemically evaluated areas (shaded) shown for reference; see figure 49 for location names. Statistical data given in table 13; summary of geochemical anomalies given in table 14; sample localities plotted on figure 52.

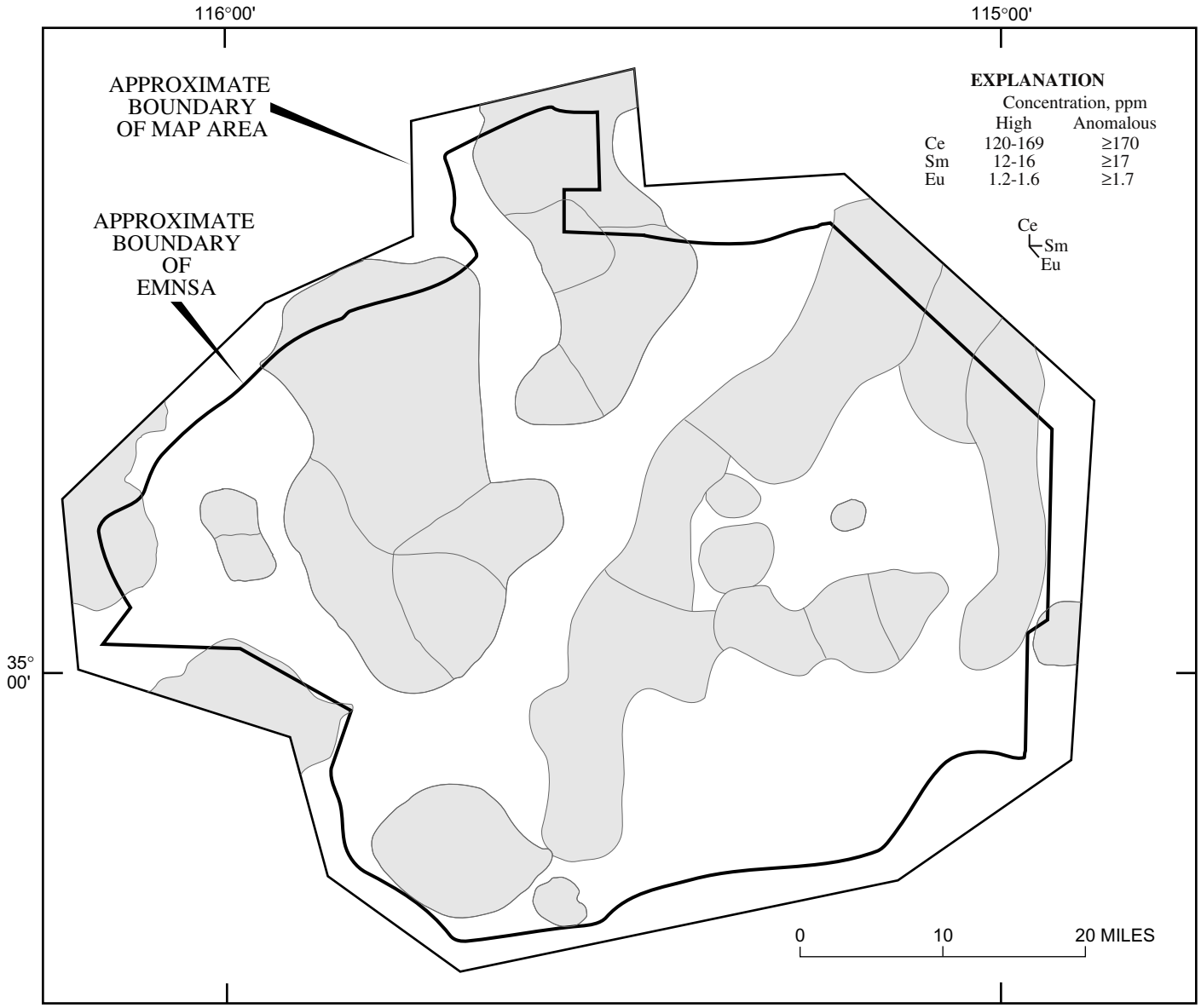

Figure 70. Distribution of anomalous and high concentrations, in parts per million, of Ce, Sm, and Eu in National Uranium Resource Evaluation (NURE) stream-sediment and soil samples from East Mojave National Scenic Area (EMNSA), California, and surrounding area. For each locality, elements are shown by either vertical, horizontal, or diagonal lines emanating from a common locality point (overlapping lines represent more than one locality). Longer lines indicate anomalous concentrations; shorter lines, high concentrations. Concentration values shown are defined as follows: anomalous, above threshold values given in table 13; high, selected ranges that include threshold values. Percentiles for high concentrations are as follows: Ce, 84 to 95; Sm, 89 to 95; Eu, 71 to 83. General outlines of geochemically evaluated areas (shaded) shown for reference; see figure 49 for location names. Statistical data given in table 13; summary of geochemical anomalies given in table 14; sample localities plotted on figure 53.

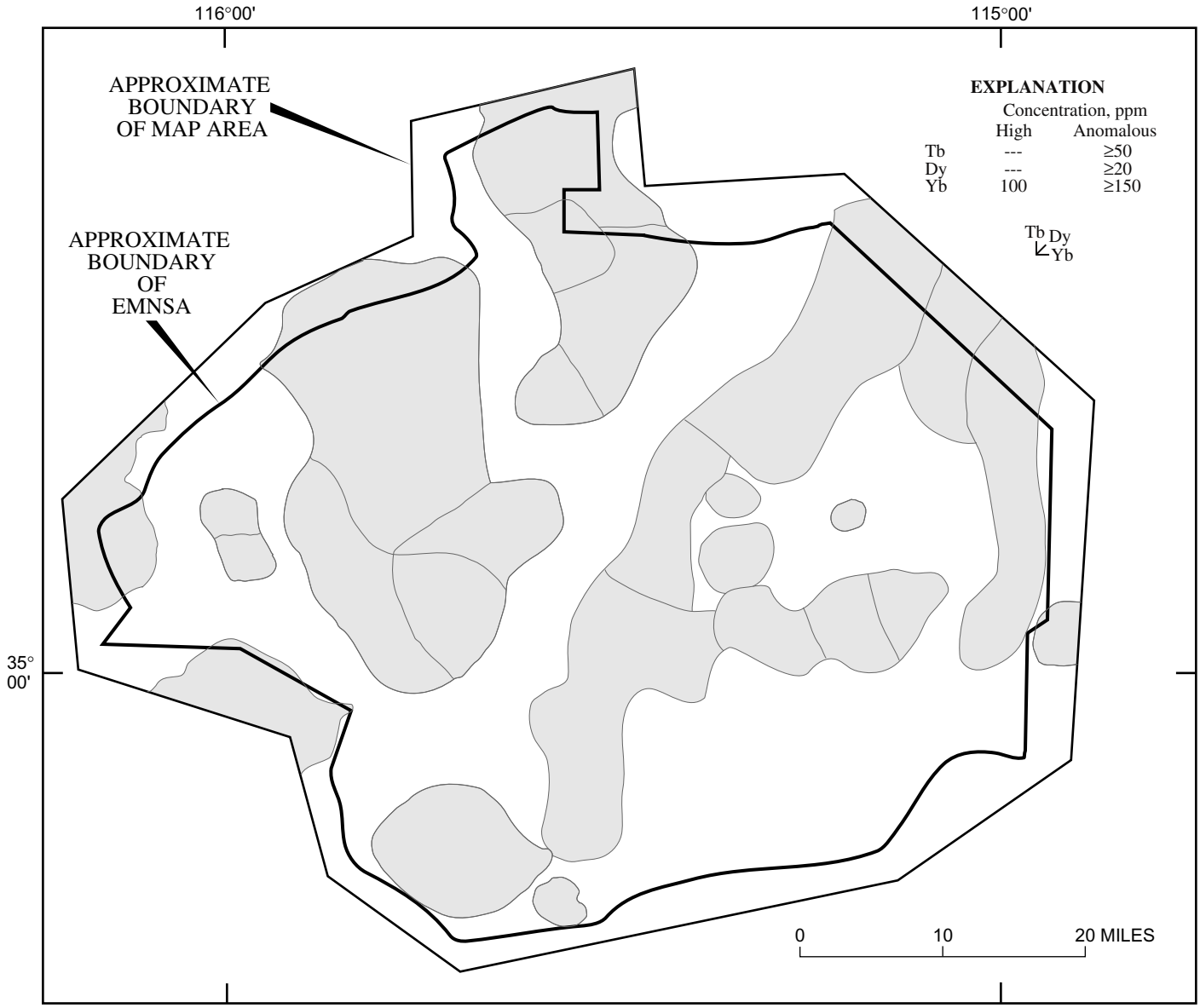

Figure 71. Distribution of anomalous and high concentrations, in parts per million, of Tb, Dy, and Yb in geochemical database for the United States (PLUTO) heavy-mineral-concentrate samples from East Mojave National Scenic Area (EMNSA), California, and surrounding area. For each locality, elements are shown by either vertical, horizontal, or diagonal lines emanating from a common locality point (overlapping lines represent more than one locality). Longer lines indicate anomalous concentrations; shorter lines, high concentrations. Concentration values shown are defined as follows: anomalous, above threshold values given in table 13; high, selected ranges that include threshold values; ---, no value (any detectable concentration is anomalous). Percentiles for high concentrations are as follows: Yb, 76 to 92. General outlines of geochemically evaluated areas (shaded) shown for reference; see figure 49 for location names. Statistical data given in table 13; summary of geochemical anomalies given in table 14; sample localities plotted on figure 51.

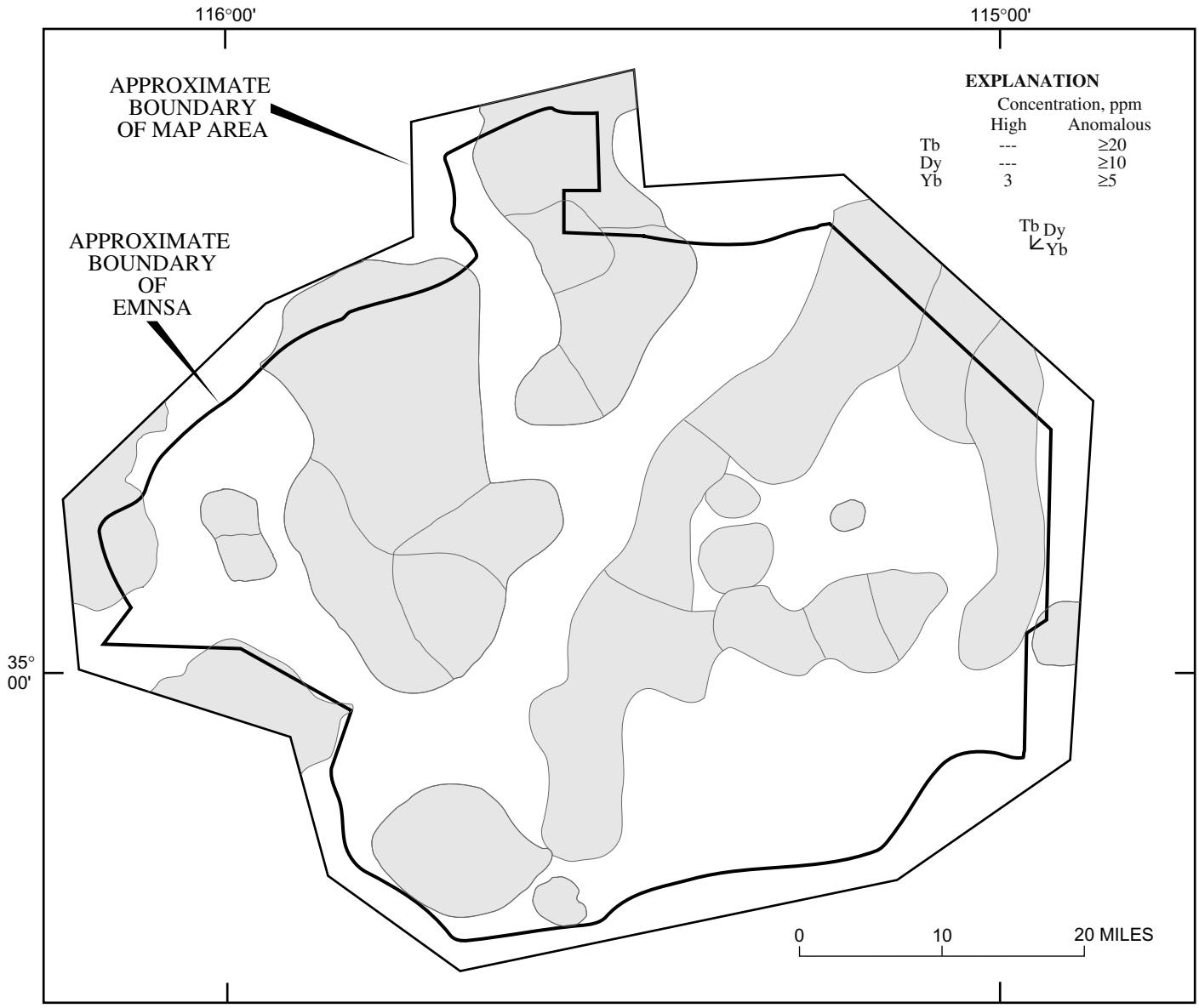

Figure 72. Distribution of anomalous and high concentrations, in parts per million, of Tb, Dy, and Yb in geochemical database for the United States (PLUTO) rock samples from East Mojave National Scenic Area (EMNSA), California, and surrounding area. For each locality, elements are shown by either vertical, horizontal, or diagonal lines emanating from a common locality point (overlapping lines represent more than one locality). Longer lines indicate anomalous concentrations; shorter lines, high concentrations. Concentration values shown are defined as follows: anomalous, above threshold values given in table 13; high, selected ranges that include threshold values; ---, no value (any detectable concentration is anomalous). Percentiles for high concentrations are as follows: Yb, 88 to 96. General outlines of geochemically evaluated areas (shaded) shown for reference; see figure 49 for location names. Statistical data given in table 13; summary of geochemical anomalies given in table 14; sample localities plotted on figure 52.

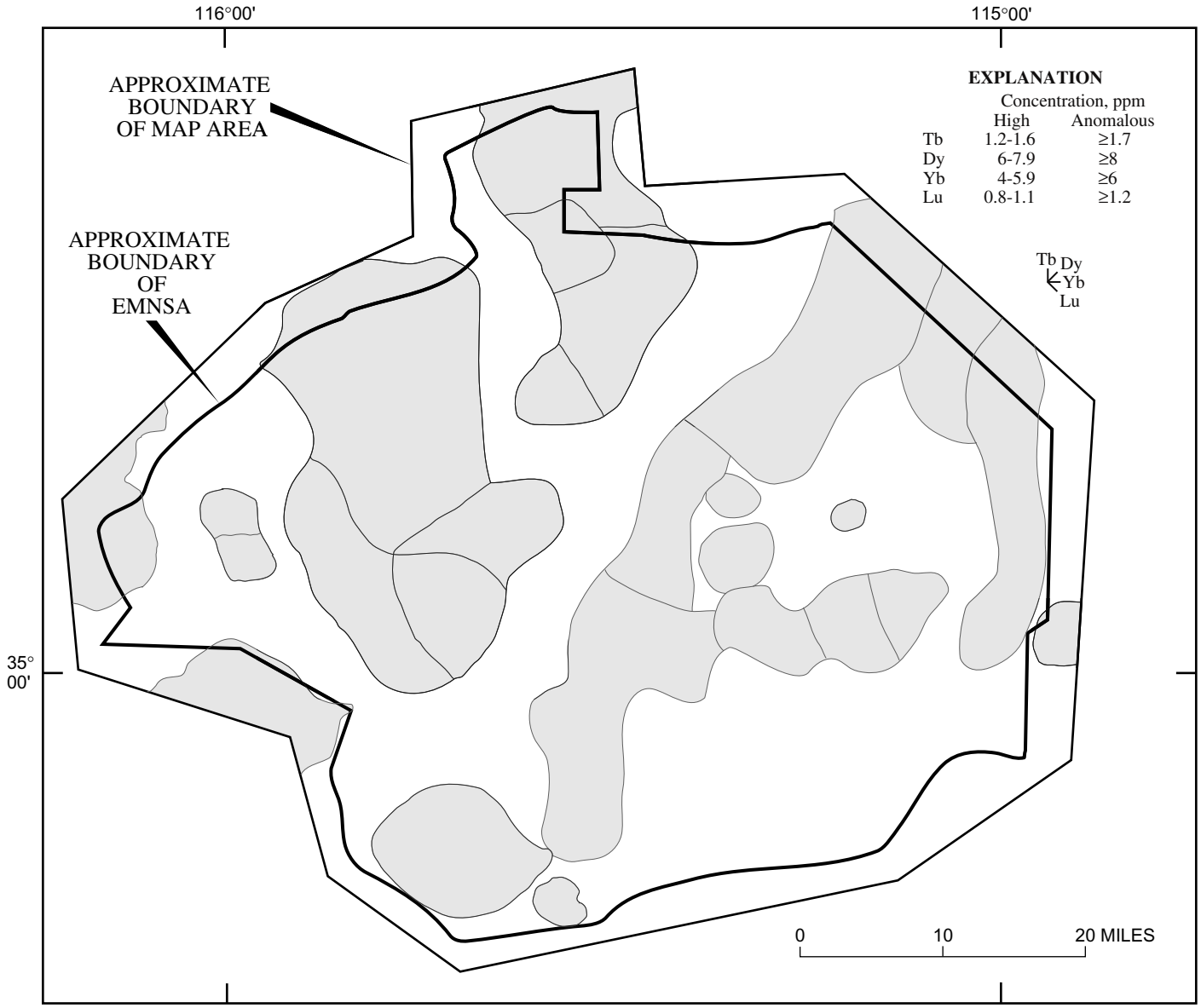

Figure 73. Distribution of anomalous and high concentrations, in parts per million, of Tb, Dy, Yb, and Lu in National Uranium Resource Evaluation (NURE) stream-sediment and soil samples from East Mojave National Scenic Area (EMNSA), California, and surrounding area. For each locality, elements are shown by either vertical, horizontal, or diagonal lines emanating from a common locality point (overlapping lines represent more than one locality). Longer lines indicate anomalous concentrations; shorter lines, high concentrations. Concentration values shown are defined as follows: anomalous, above threshold values given in table 13; high, selected ranges that include threshold values. Percentiles for high concentrations are as follows: Tb, 82 to 89; Dy, 82 to 91: Yb, 86 to 94; Lu, 87 to 96. General outlines of geochemically evaluated areas (shaded) shown for reference; see figure 49 for location names. Statistical data given in table 13; summary of geochemical anomalies given in table 14; sample localities plotted on figure 53.

Figure 74. Siderite brecciated along minor fault at El Lobo Mine, in Little Cowhole Mountain (fig. 49) near northwest boundary of East Mojave National Scenic Area, California; open spaces filled partly by quartz.

Figure 75. Iron and polymetallic skarn formed in general area of Mosaic Queen Mine, Cowhole Mountain (fig. 49), East Mojave National Scenic Area, California. View toward N. 50° W. along approximately 0.5-km-long zone of skarn. Note approximately 2-m-wide prospect pit near bottom of photograph.

Figure 76. Brecciated Early Proterozoic gneiss and granitoid rocks veined by quartz (white, at hammer point) at main workings of Paymaster Mine near Seventeenmile Point (fig. 49), west-central part of East Mojave National Scenic Area, California.

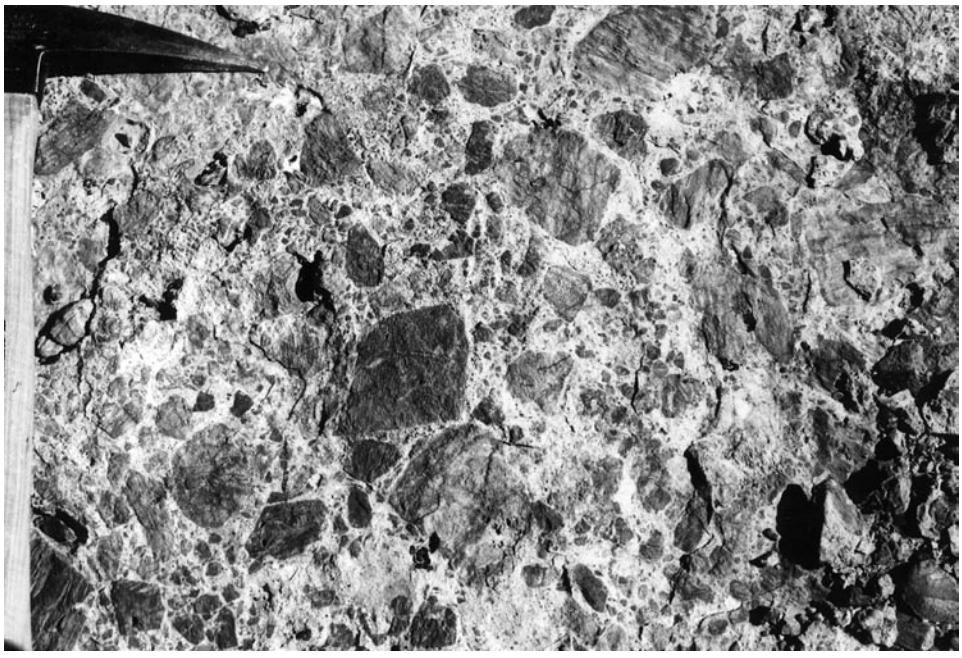

Figure 77. Brecciated Paleozoic limestone and dolomite in general area of Oro Fino Mine, approximately 3 km south of Seventeenmile Point (Old Dad Mountain, fig. 49), west-central part of East Mojave National Scenic Area, California.

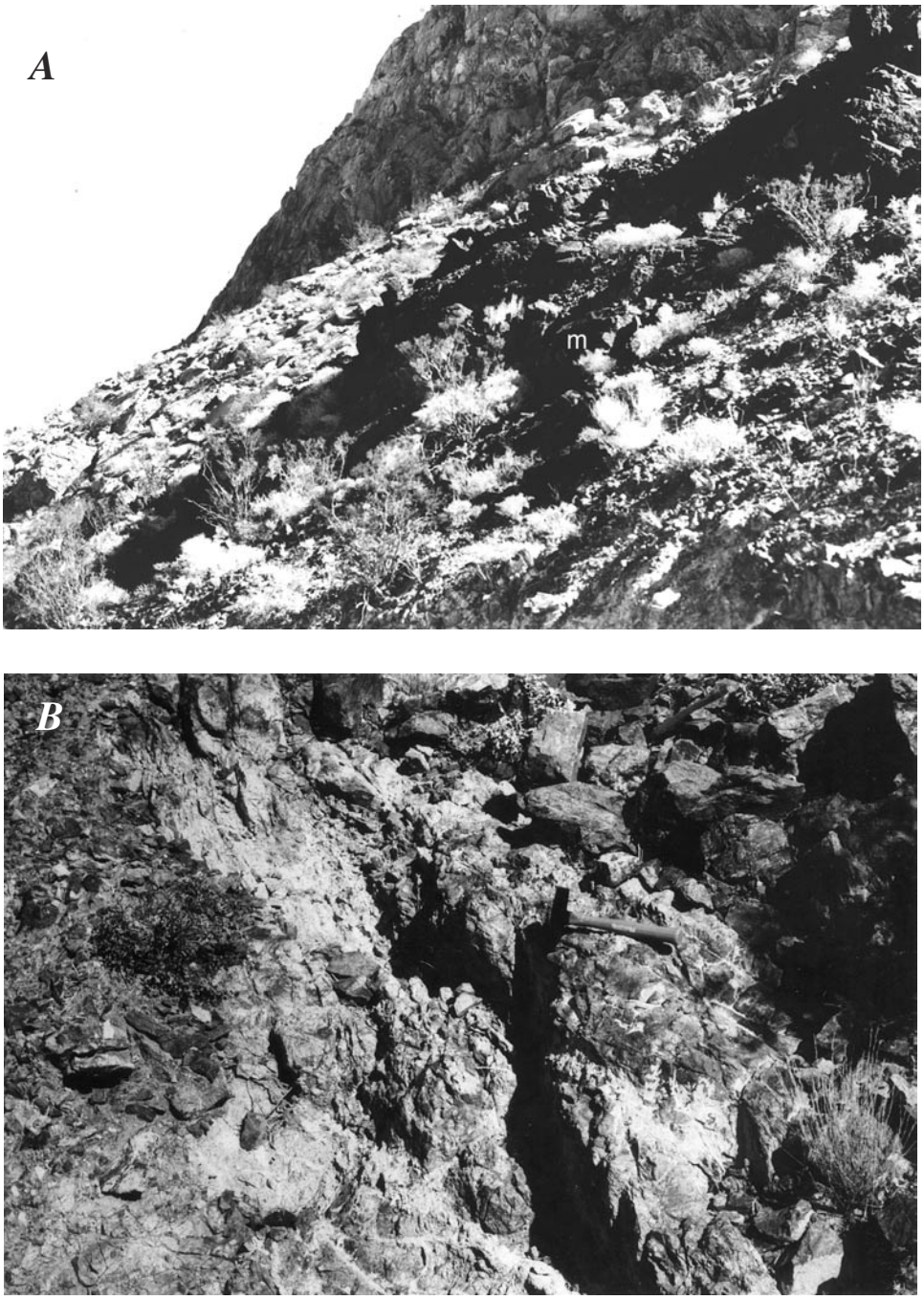

Figure 78. Mineral occurrences near Old Dad Mountain (fig. 49) in west-central part of East Mojave National Scenic Area, California. *A*, Massive magnetite (m) at Old Dad iron-skarn deposit, approximately10 m thick. In places, magnetite is associated with coarsely crystalline actinolite, which is present in clusters of radiating crystals. *B*, Shattered, sulfide mineral-impregnated silicic dike at Lucky (ODM) group of claims (NW1/4 sec. 11, T. 12 N., R. 10 E.); dike is probably associated genetically with nearby widespread alteration.

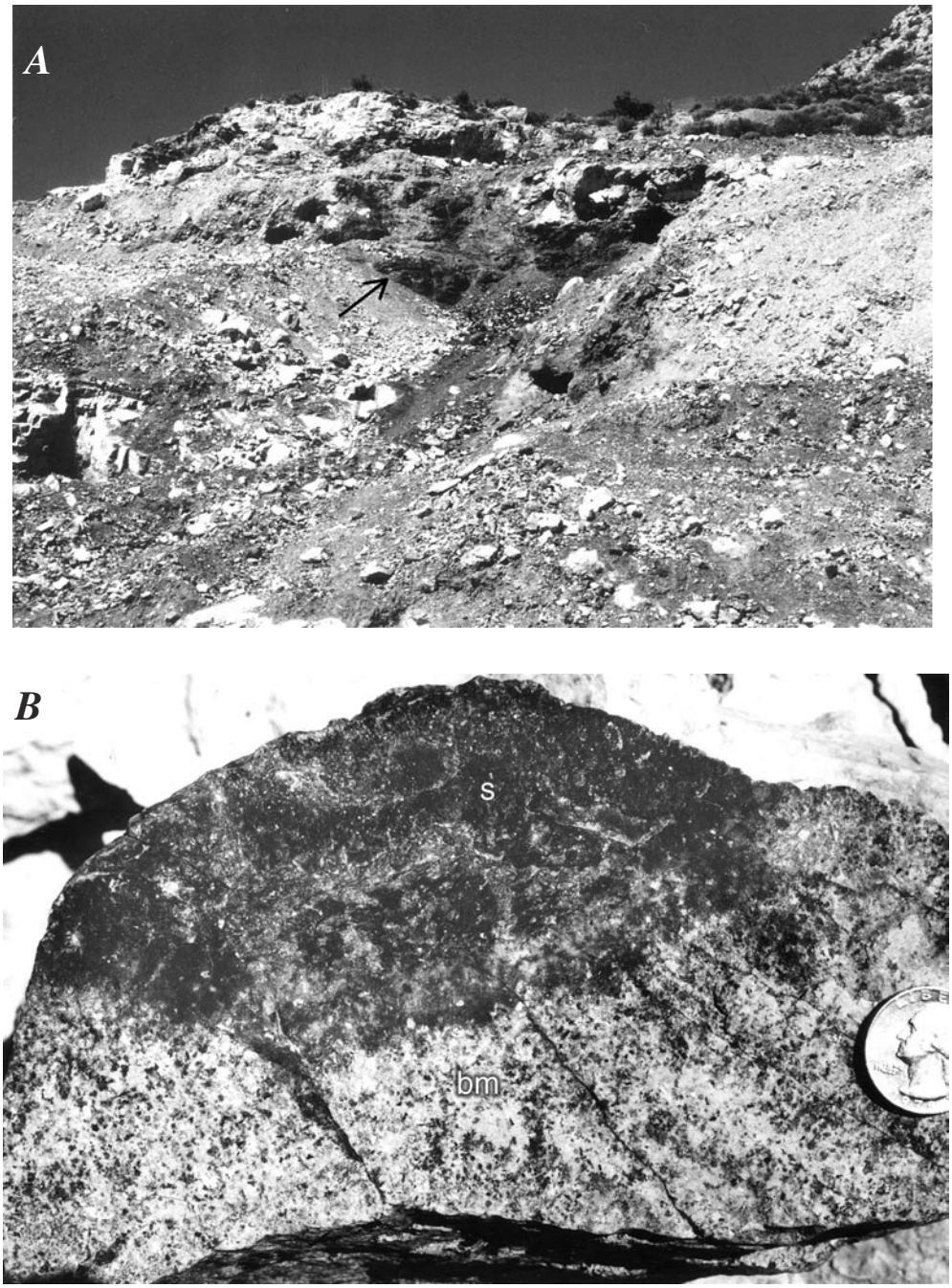

Figure 79. Skarn occurrences in north-central part of East Mojave National Scenic Area, California (fig. 49). *A*, Gossan (at head of arrow) formed in formerly iron-sulfide mineral-rich zones developed in layered marble and skarn adjacent to nonporphyritic hornblende diorite at Copper World Mine, south end of Clark Mountain Range. Dark area in center of photograph is approximately 30 m thick. *B*, Knife-edge contact between clay-altered biotite monzogranite (bm) and garnet-pyroxene skarn (s) at Mohawk Mine, near west end of Mohawk Hill at north end of Mescal Range. *C*, Massive epidote skarn (es) at Silverado-Tungstite Mine, showing sharp contact (at point of pick) with chloritic-altered hornblende diorite (hd) of Jurassic Striped Mountain pluton. *D*, Garnet-pyroxene skarn (s), possibly hedenbergitic, at Silvarado-Tungstite Mine, showing late-stage, open-cavity, and vein-type quartz (at head of arrow).

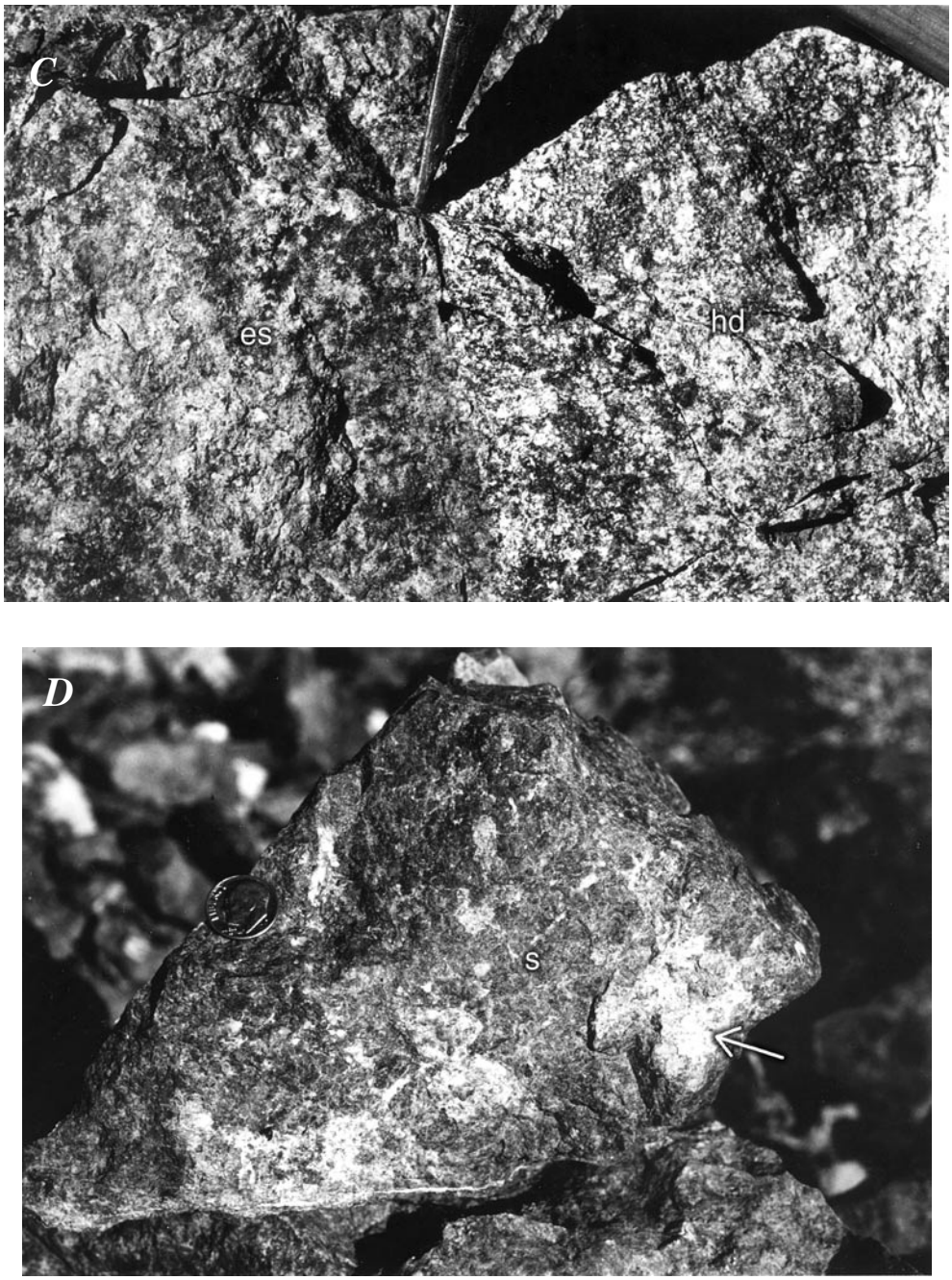

Figure 79. Skarn occurrences in north-central part of East Mojave National Scenic Area, California (fig. 49). *A*, Gossan (at head of arrow) formed in formerly iron-sulfide mineral-rich zones developed in layered marble and skarn adjacent to nonporphyritic hornblende diorite at Copper World Mine, south end of Clark Mountain Range. Dark area in center of photograph is approximately 30 m thick. *B*, Knife-edge contact between clay-altered biotite monzogranite (bm) and garnet-pyroxene skarn (s) at Mohawk Mine, near west end of Mohawk Hill at north end of Mescal Range. *C*, Massive epidote skarn (es) at Silverado-Tungstite Mine, showing sharp contact (at point of pick) with chloritic-altered hornblende diorite (hd) of Jurassic Striped Mountain pluton. *D*, Garnet-pyroxene skarn (s), possibly hedenbergitic, at Silverado-Tungstite Mine, showing late-stage, open-cavity, and vein-type quartz (at head of arrow).—Continued

Figure 80. Exposures of thin-bedded Paleozoic carbonate sequence at south end of Striped Mountain (fig. 49), East Mojave National Scenic Area, California. View to northeast.

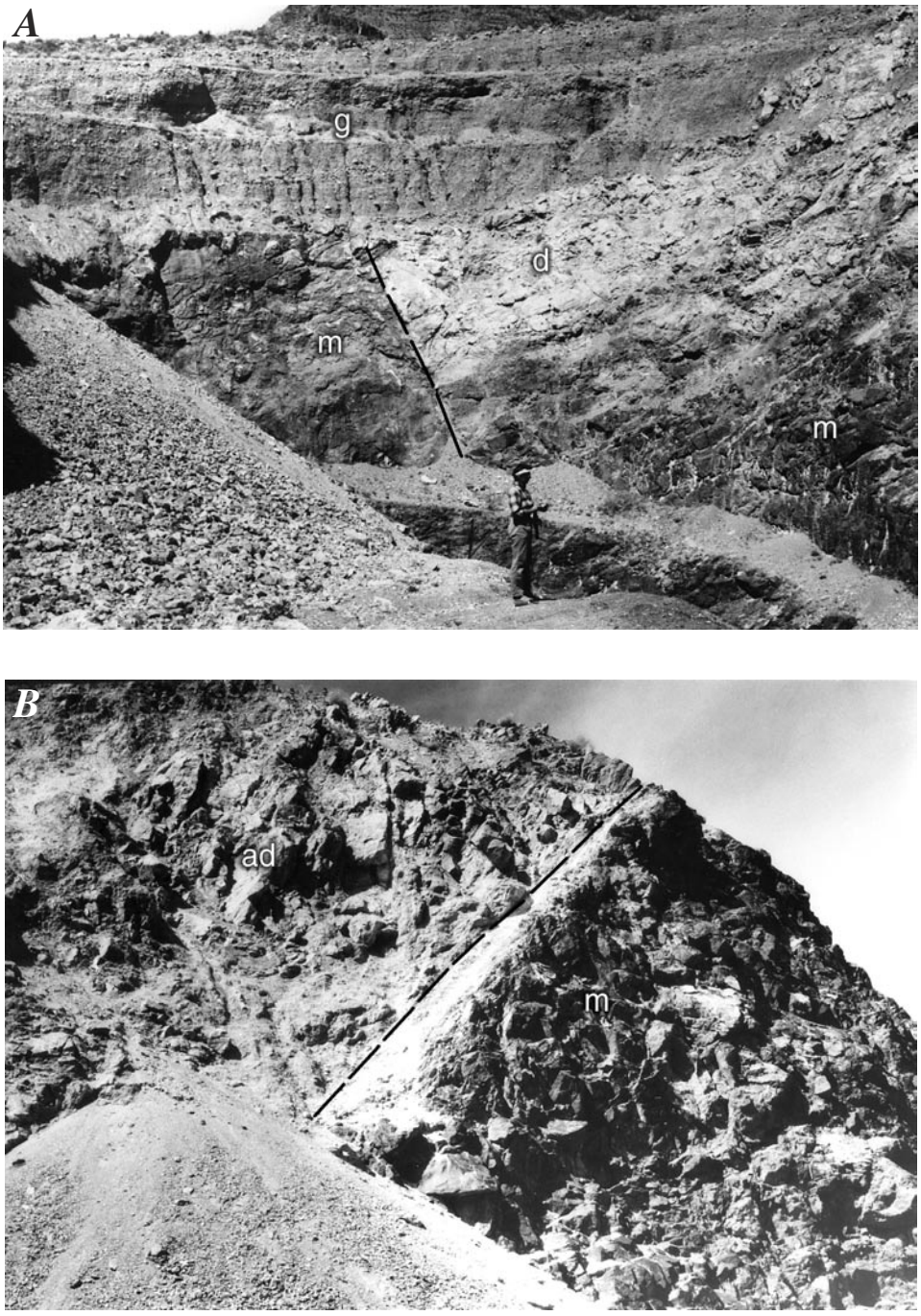

Figure 81. Exposures of magnetite skarn at Vulcan Iron Mine, Providence Mountains (fig. 49), East Mojave National Scenic Area, California. *A*, Main entrance to open cut at Vulcan iron skarn showing gravels (g) and dolomite (d; unit Ꞓd, pl. 1) overlying faulted (dashed line) magnetite-rich skarn (m). View to north. *B*, Fault (dashed) between Jurassic albitized diorite (ad) and magnetite skarn (m). View to N. 60° W. along strike of fault. Outcrop is approximately 20 m high.

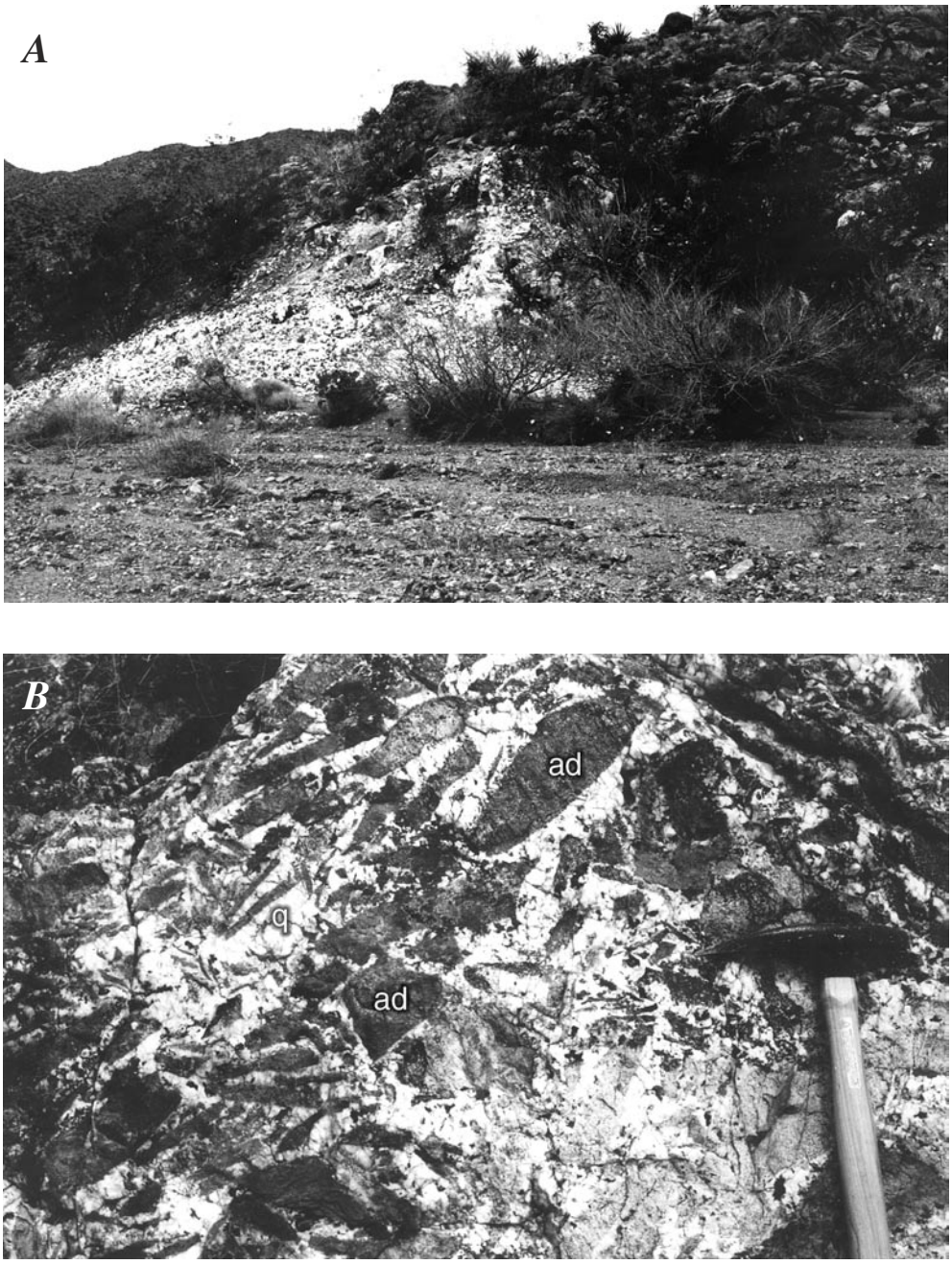

Figure 82. Massive quartz associated with molybdenite occurrence in Globe Wash, north-central Providence Mountains (fig. 49), East Mojave National Scenic Area, California. *A*, Exposure, approximately 30 m wide, of milky-white quartz in bottom of Globe Wash. View to north. *B*, Close-up view of 82*A* showing subangular fragments of leucogranite phase of informally named Cretaceous Mid Hills adamellite (ad) of Beckerman and others (1982) (unit Kmh, pl. 1) enclosed in massive quartz (q), which is characterized by widespread presence of brick-red iron oxide minerals.

Figure 83. Miocene ash-flow tuff (at head of arrow) at Pinto Mountain (fig. 49), East Mojave National Scenic Area, California. View to north.

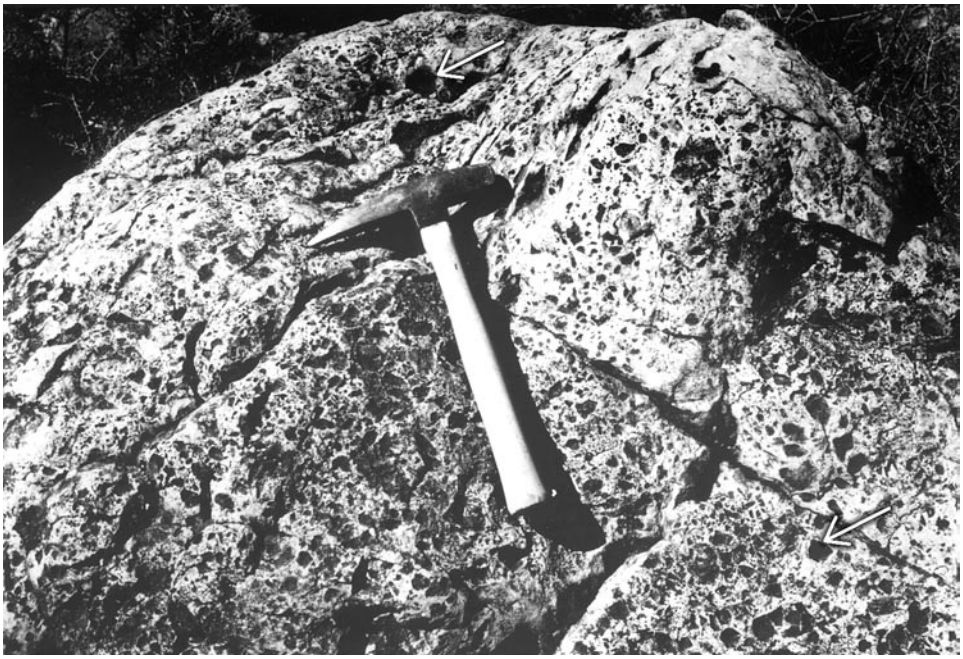

Figure 84. Exposure of vuggy-silica-altered Miocene rhyolite from Hart Mining District, Castle Mountains (fig. 49), East Mojave National Scenic Area, California. Vugs (at heads of arrows) result from acid leaching by meteoric fluids percolating through sulfur-enriched rocks.

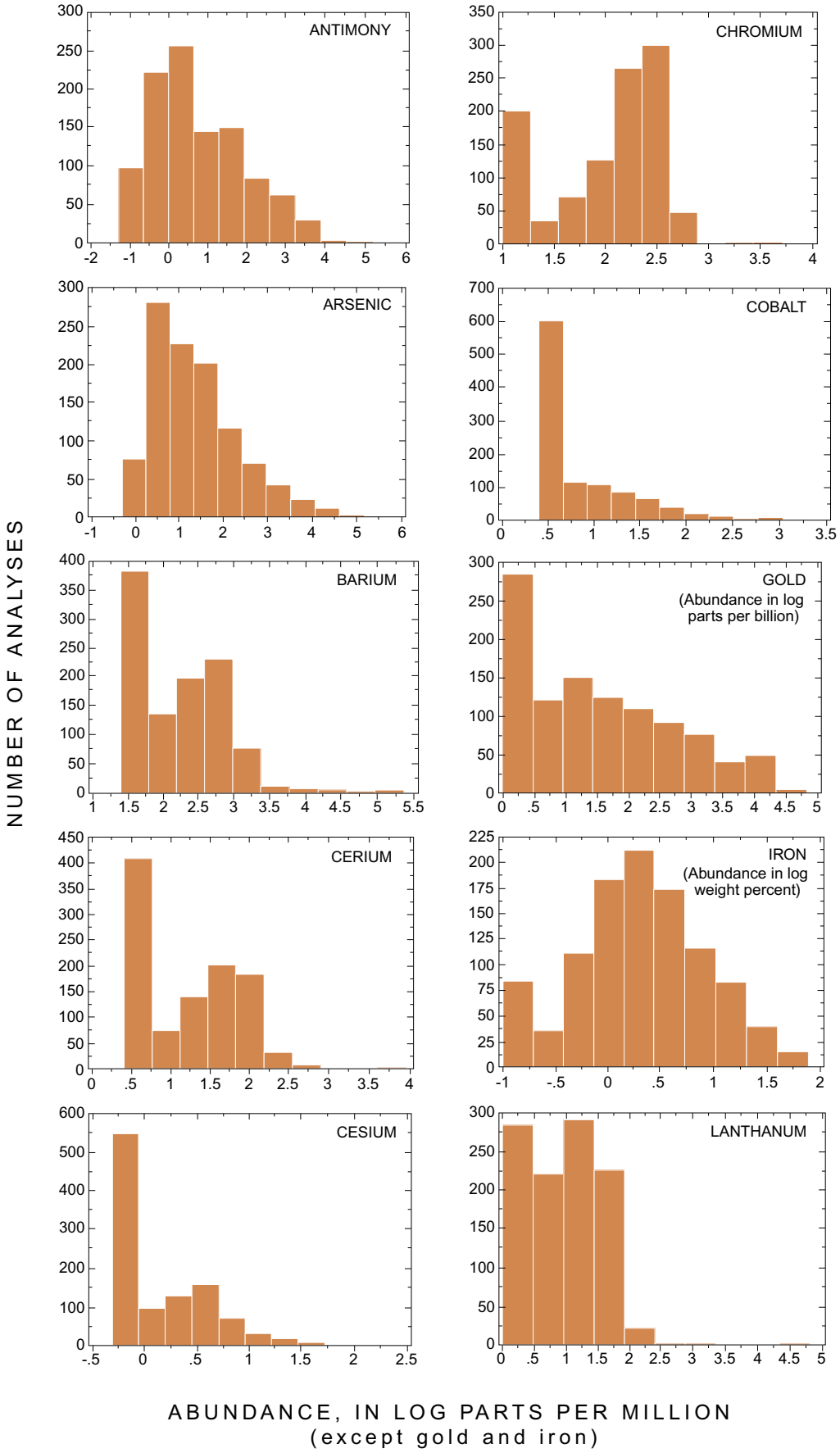

Figure 85. Frequency distribution of 20 elements in 1,050 rocks from East Mojave National Scenic Area, California. All abundances are in log parts per million, except gold, which are in log parts per billion, and iron, which are in log weight percent. Analyses by U.S. Bureau of Mines (1990a).

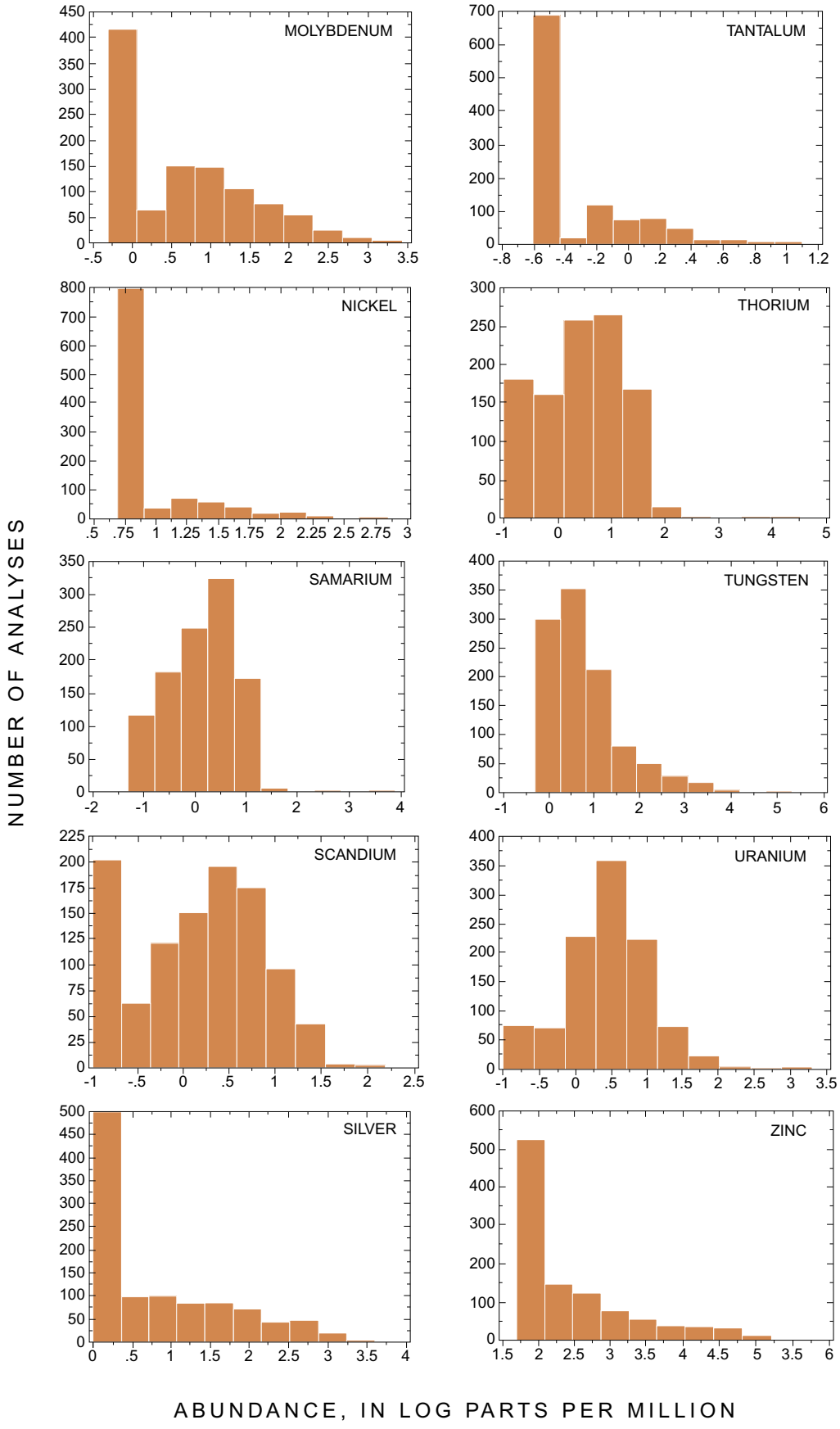

Figure 85. Frequency distribution of 20 elements in 1,050 rocks from East Mojave National Scenic Area, California. All abundances are in log parts per million, except gold, which are in log parts per billion, and iron, which are in log weight percent. Analyses by U.S. Bureau of Mines (1990a)—Continued.

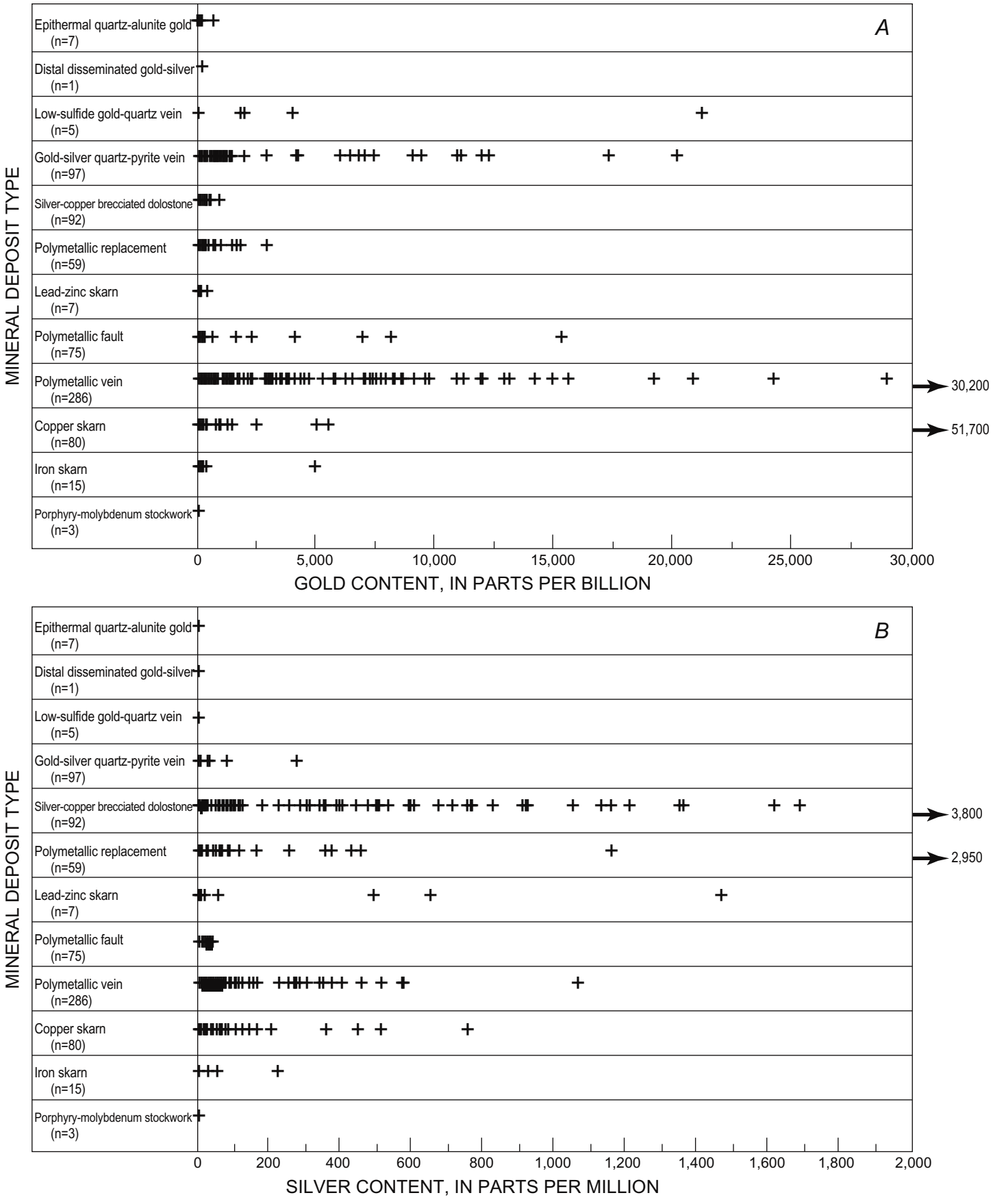

Figure 86. Plots showing detectable concentrations, grouped by deposit type, of four metals in mineralized rocks in East Mojave National Scenic Area, California. Analyses by U.S. Bureau of Mines (1990a); n, number of samples analyzed. *A*, Gold; *B*, Silver; *C*, Arsenic; *D*, Antimony.

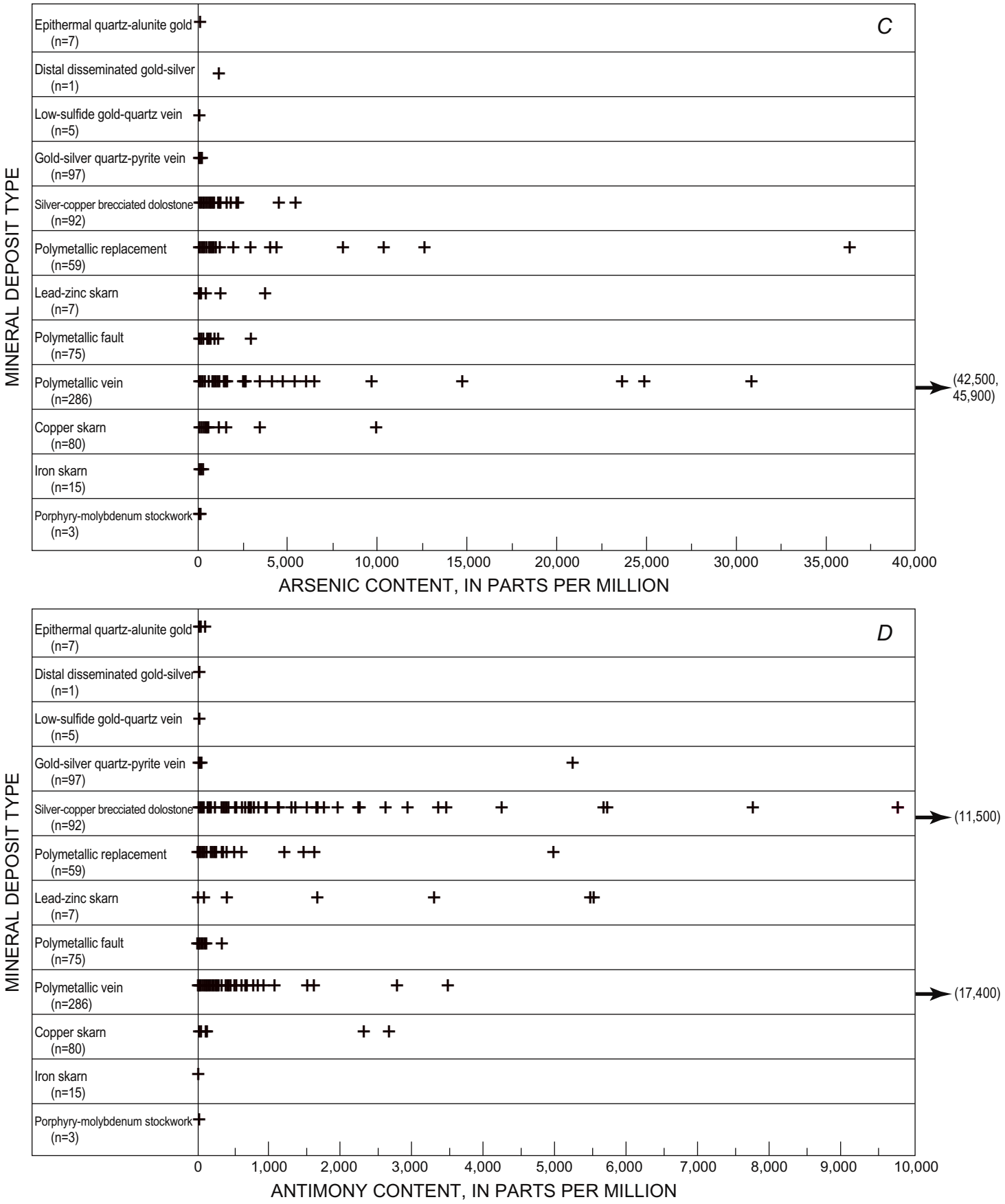

Figure 86. Plots showing detectable concentrations, grouped by deposit type, of four metals in mineralized rocks in East Mojave National Scenic Area, California. Analyses by U.S. Bureau of Mines (1990a); n, number of samples analyzed. *A*, Gold; *B*, Silver; *C*, Arsenic; *D*, Antimony—Continued.

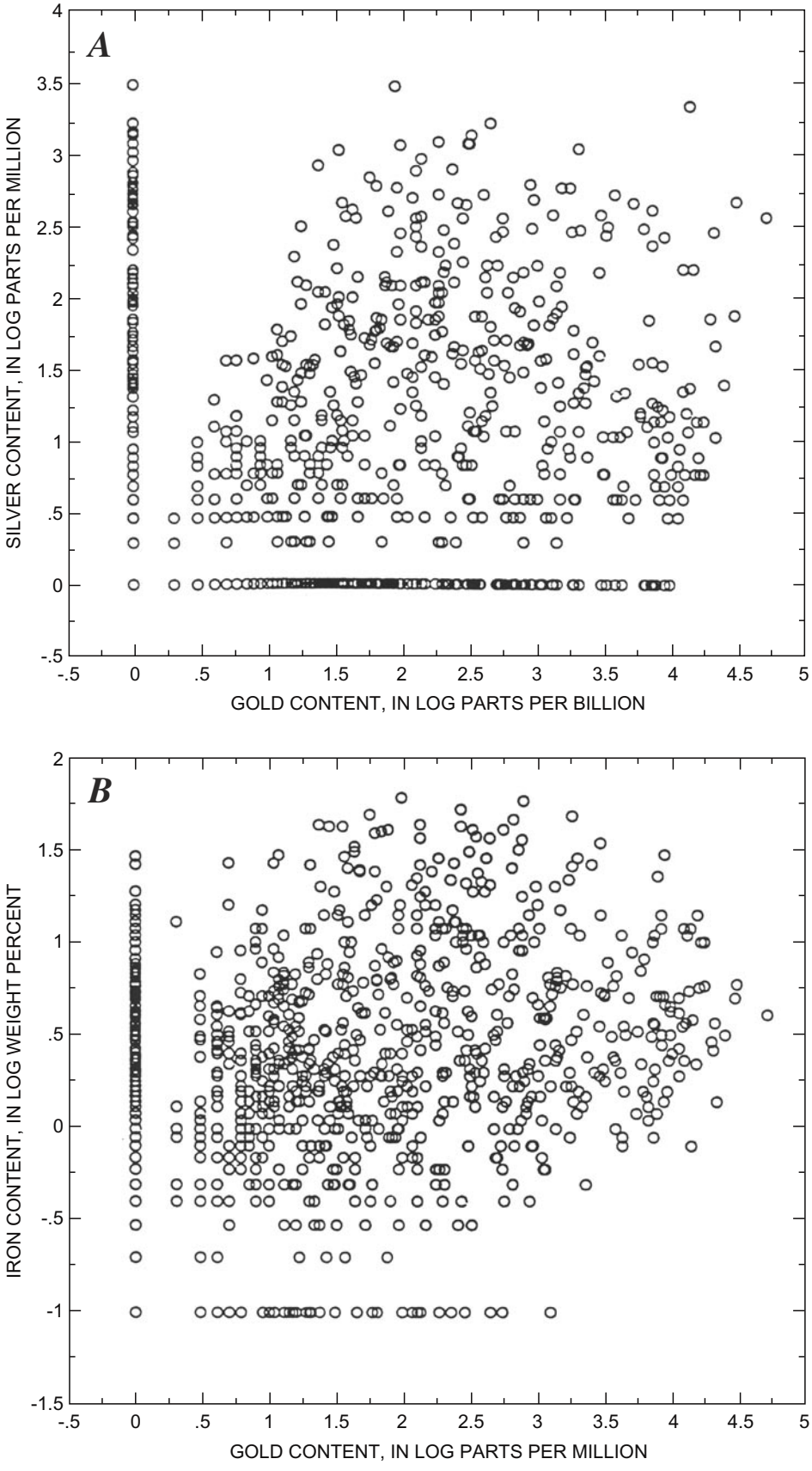

Figure 87. Chemical variation diagrams for 1,050 rocks from East Mojave National Scenic Area, California. Analyses by the U.S. Bureau of Mines (1990a). *A*, Silver versus gold content. *B*, Iron versus gold content. *C*, Samarium versus lanthanum content. *D*, Antimony versus silver content. *E*, Iron versus cobalt content. *F*, Barium versus uranium content.

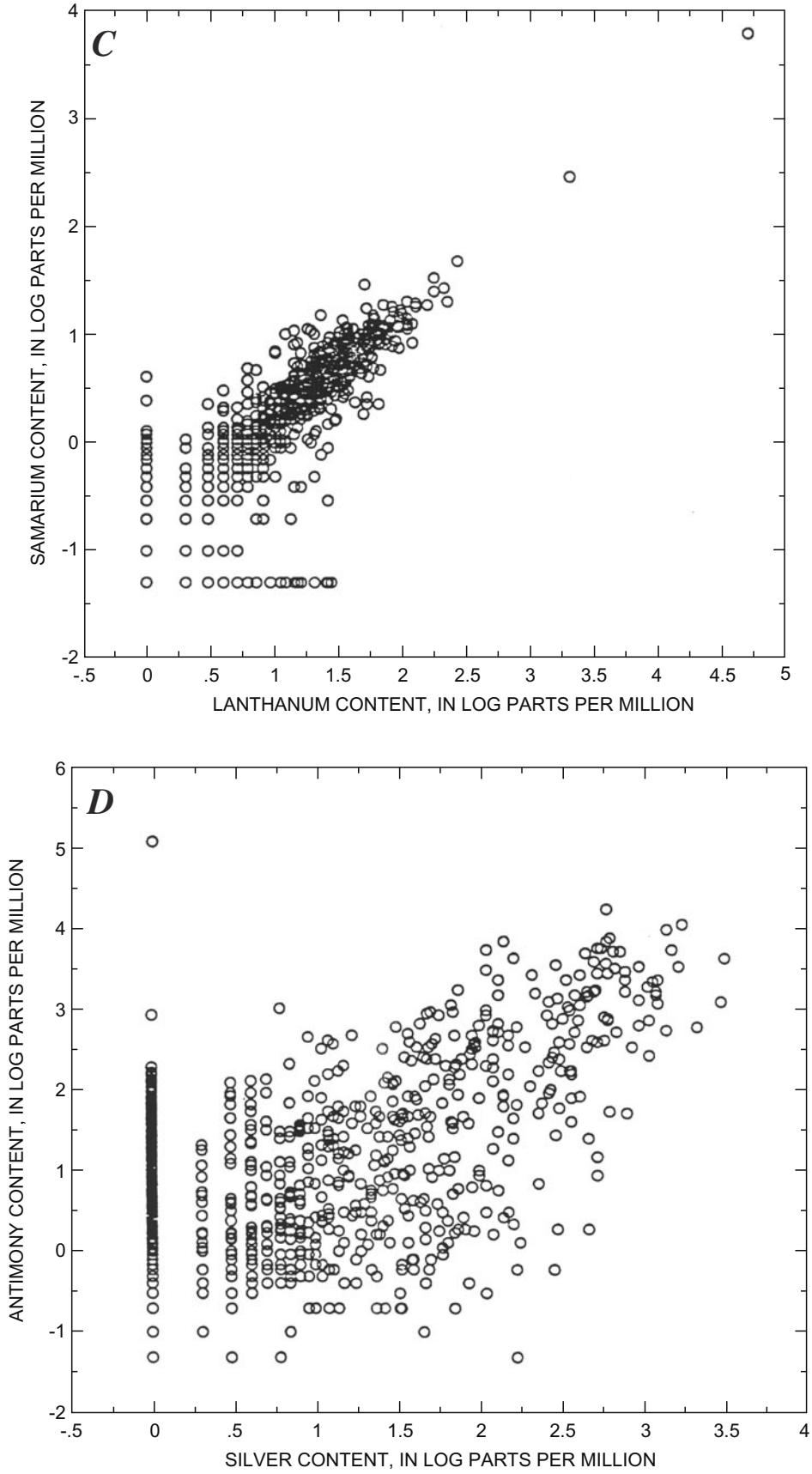

Figure 87. Chemical variation diagrams for 1,050 rocks from East Mojave National Scenic Area, California. Analyses by the U.S. Bureau of Mines (1990a). *A*, Silver versus gold content. *B*, Iron versus gold content. *C*, Samarium versus lanthanum content. *D*, Antimony versus silver content. *E*, Iron versus cobalt content. *F*, Barium versus uranium content—Continued.

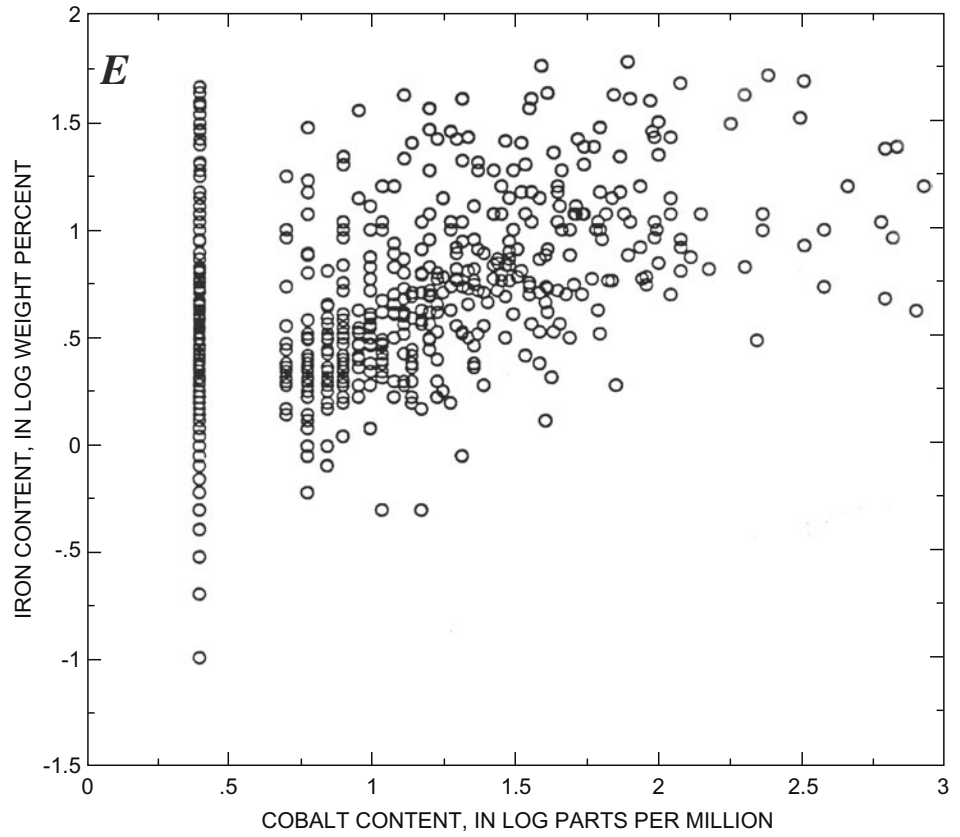

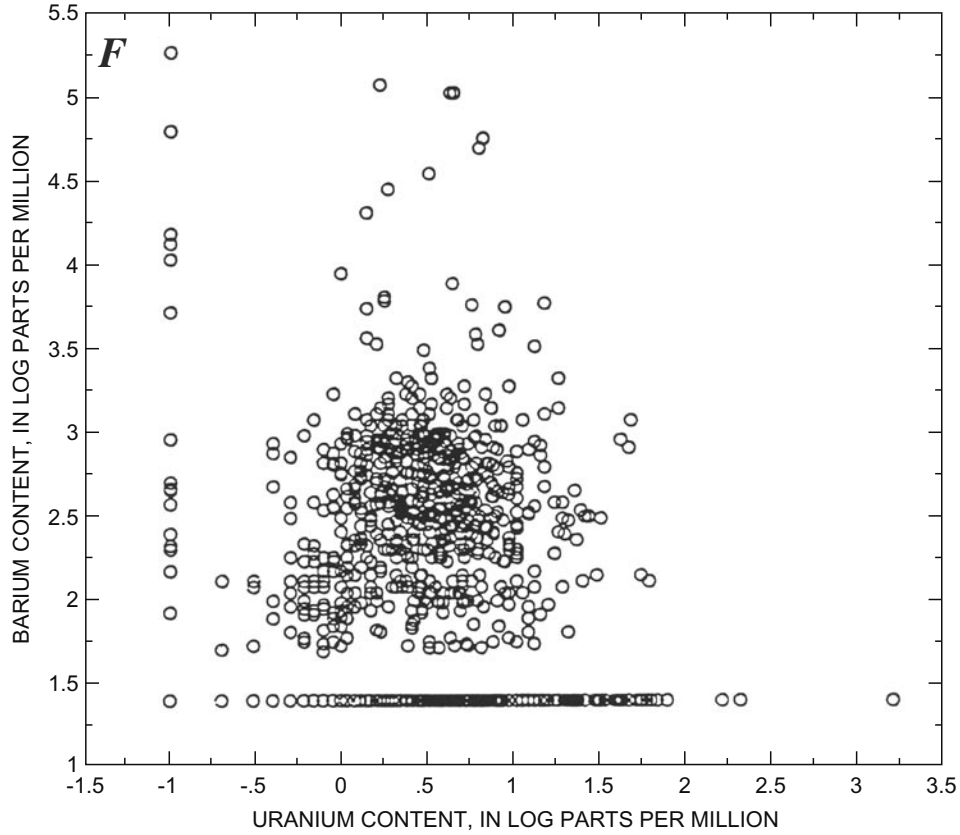

Figure 87. Chemical variation diagrams for 1,050 rocks from East Mojave National Scenic Area, California. Analyses by the U.S. Bureau of Mines (1990a). *A*, Silver versus gold content. *B*, Iron versus gold content. *C*, Samarium versus lanthanum content. *D*, Antimony versus silver content. *E*, Iron versus cobalt content. *F*, Barium versus uranium content—Continued.

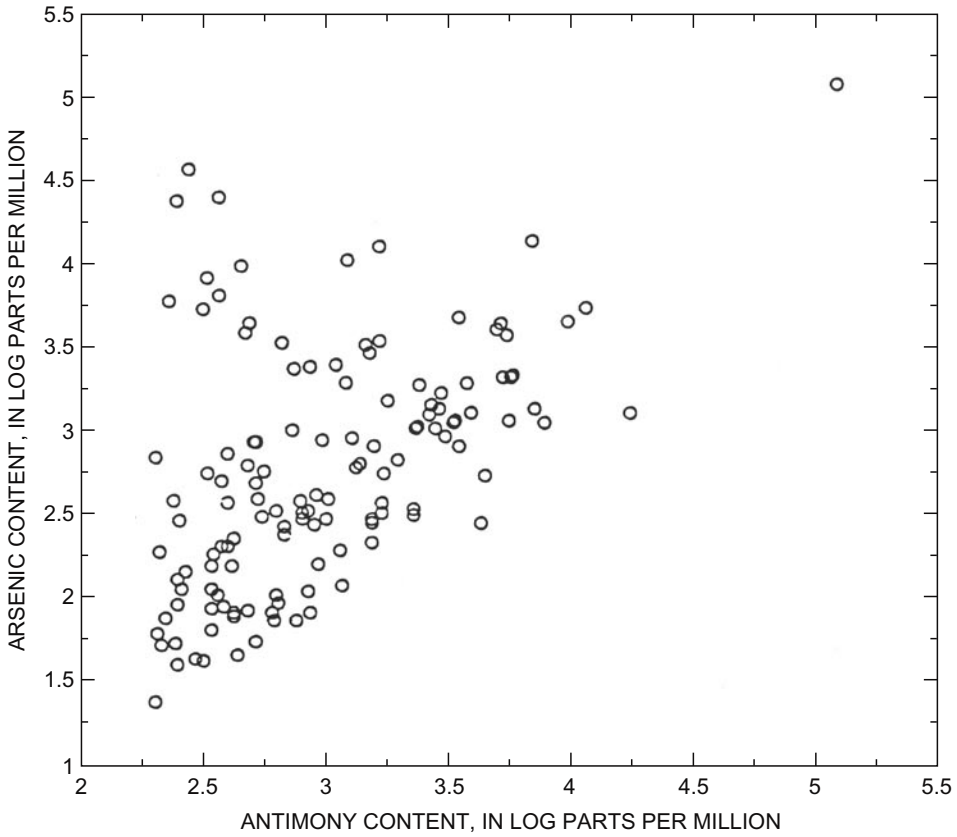

Figure 88. Plot showing arsenic versus antimony content in 131 samples that contain greater than 200 parts per million antimony, which have been selected from 1,050-rock database from East Mojave National Scenic Area, California. Analyses by U.S. Bureau of Mines (1990a).

Table 10. Areas in the East Mojave National Scenic Area, California, and their references to interpretive geochemical reports and (or) releases of raw geochemical data.

[--, no published report]

Area on figure 49	Interpretive report	Raw geochemical data
Soda Mountains	--	--
Little Cowhole Mountain	--	--
Cowhole Mountain	--	--
Cinder Cone area	Wilshire and others, 1987	Adrian and others, 1986b
Marl Mountains area	--	--
Old Dad Mountain	--	--
Kelso Mountains	--	--
Bristol Mountains	--	--
Clark Mountain Range	--	--
Mescal Range	--	--
Ivanpah Mountains	--	--
Cima Dome	--	--
New York Mountains	Miller and others, 1986	Adrian and others, 1986c
Mid Hills	--	--
Providence Mountains	Goldfarb and others, 1988	Folger and others, 1986
Do.	Miller and others, 1985	Detra and others, 1984
Granite Mountains	Howard and others, 1987	Detra and Kilburn, 1985
Do.	Yeend and others, 1984	--
Van Winkle Mountain	--	--
Grotto Hills	--	--
Pinto Mountain	--	--
Table Mountain	--	--
Woods Mountains	--	--
Hackberry Mountain	--	--
Vontrigger Hills	--	--
Piute Range	Nielson and others, 1987	Adrian and others, 1986a
Castle Mountains	--	--
Homer Mountain	--	--

Table 11. Analyses of select rock samples from some mineralized occurrences in the East Mojave National Scenic Area, California.

[Semiquantitative and quantitative optical spectroscopic analyses by inductively coupled plasma methods (Lichte and others, 1987; Motooka, 1988); analysts, D.L. Fey and J.M. Motooka; partial extraction of reported elements by selectively dissolving sulfides present in samples and analyzing contents of resulting solution. Looked for but not found, at detection levels shown in parentheses: Ho (4), Ta (40), and U (100). Precision for concentrations higher than 10 times detection limit is better than ±10 percent relative standard deviation; precision of scanning instrument is ±2 percent relative standard deviation. Chemical analyses are in parts per million except Au, which are in parts per billion: Au determined by combined graphite furnace and atomic-absorption spectroscopy; W determined colorimetrically; Hg determined by cold-vapor atomic-absorption; and As determined by hydride-generation atomic-absorption spectrometry (Wilson and others, 1987; Aruscavage and Crock, 1987); analysts, A.H. Love, E.P. Welsch, P.L. Hageman, and B.H. Roushey. --, not detected. See table 12 for sample locations and descriptions]

		Inductively coupled plasma atomic-emission spectroscopy (total)												
Analysis No.	Field No. 90TT	Ag	Ba	Be	Bi	Cd	Ce	Co	Cr	Cu	Eu	Ga	La	Li
1	015	99	28	<1	440	<2	8	7	12	30,100	<2	5	12	5
2	016	147	188	<1	1,140	<2	10	7	5	57,700	<2	<4	13	4
3	019	15	8	<1	70	7	<4	12	5	10,660	<2	6	4	11
4	020	3	13	1	50	3	<4	5	5	2,330	<2	9	7	11
5	027	9	7	2	20	3	6	58	118	13,500	<2	20	5	11
6	030	<2	4	<1	<10	4	4	227	1	151	<2	26	5	5
7	031	<2	3	<1	<10	<2	<4	2	<1	40	<2	<4	3	3
8	032	<2	347	3	<10	<2	117	1	<1	30	<2	15	56	3
9	035	<2	44	<1	<10	3	<4	126	5	224	<2	18	3	41
10	038	17	234	<1	220	<2	11	40	10	10,800	<2	4	7	6
11	040	<2	1,270	1	<10	<2	33	3	<1	16	<2	8	23	3
12	041	8	453	2	10	<2	13	4	4	637	<2	6	6	75
13	042	6	505	2	10	<2	34	5	3	1,510	<2	5	21	6
14	043	20	66	<1	70	<2	<4	1	<1	5,690	<2	<4	<2	5
15	045	6	356	<1	70	<2	34	9	10	464	<2	5	28	12
16	046	<2	673	2	<10	<2	88	3	<1	55	<2	14	58	2
17	047	<2	185	<1	<10	<2	<4	12	5	130	<2	<4	3	304
18	049	<2	338	3	<10	<2	120	1	<1	22	<2	14	57	3
19	050	<2	34	1	<10	<2	61	<1	<1	6	<2	14	33	<2
20	051	<2	262	1	40	<2	26	<1	<1	5	<2	9	16	3
21	052	<2	30	1	<10	<2	56	<1	<1	3	<2	14	33	2
22	053	<2	20	2	<10	<2	86	<1	<1	7	<2	15	50	2
23	054	<2	11	<1	<10	<2	24	<1	<1	2	<2	11	18	2
24	055	<2	494	1	10	<2	115	4	1	218	<2	13	66	3
25	056	6	220	1	30	<2	167	2	25	520	<2	17	78	6
26	058	<2	23	2	<10	2	99	<1	<1	15	<2	16	65	2
27	059	<2	371	3	<10	<2	152	<1	<1	6	<2	13	100	2
28	060	<2	27	2	<10	<2	115	<1	<1	23	<2	15	61	2
29	061	178	125	<1	<10	<2	11	<1	<1	411	<2	4	7	6
30	062	13	29	<1	<10	<2	<4	1	<1	2,120	<2	<4	<2	4
31	063	<2	485	2	<10	<2	137	2	<1	7	<2	14	76	4
32	065	<2	293	2	<10	<2	47	13	44	3	<2	12	28	18
33	066	150	101	<1	250	8	24	9	9	1,830	<2	6	14	12
34	067	<2	114	2	<10	<2	137	30	67	192	3	21	80	38
35	068	<2	690	2	<10	<2	101	13	28	62	2	19	55	27
36	069	25	54	<1	20	14	7	6	2	969	<2	<4	4	11
37	070	178	33	<1	140	3	6	<1	1	464	<2	5	4	22
38	071	103	29	<1	210	4	6	1	1	1,070	<2	6	4	19
39	072	4	86	1	<10	<2	44	12	20	65	<2	15	24	9
40	073	<2	757	2	<10	<2	132	<1	13	9	29	70	8	77
41	074	198	91	3	520	<2	13	23	73	96	2	<4	28	8
42	075	2	87	<1	<10	<2	42	4	<1	15	2	<4	18	34
43	076	<2	706	2	<10	<2	46	1	13	5	<2	37	28	13
44	077	<2	606	2	<10	<2	61	<1	13	6	<2	37	35	11
45	078	<2	445	1	<10	<2	49	<1	22	3	<2	24	26	5
46	079	<2	269	3	<10	<2	66	7	11	30	<2	14	57	39
47	080	9	46	1	<10	<2	<4	<1	<1	41	<2	<4	<2	88
48	081	4	65	2	<10	<2	14	1	2	101	<2	7	8	62
49	082	57	59	2	30	13	8	<1	<1	175	<2	7	5	68
50	083	385	282	<1	60	18	<4	<1	<1	2,560	<2	<4	<2	19
51	084	15	91	<1	<10	<2	<4	<1	<1	162	<2	<4	2	41
52	085	37	120	2	30	9	7	<1	1	289	<2	7	4	21
53	086	13	149	<1	<10	5	<4	<1	<1	99	<2	<4	<2	16
54	088	7	143	<1	20	4	5	1	1	632	<2	<4	3	9
55	089	7	115	2	140	<2	19	1	1	44	<2	16	10	8
56	090	<2	1,070	1	<10	2	8	2	<1	7	<2	5	9	3
57	091	<2	557	2	<10	<2	32	2	<1	5	<2	6	21	18
58	092	407	459	3	<10	85	<4	1	<1	4,690	<2	<4	3	112
59	093	7	393	6	200	<2	7	3	<1	20	<2	6	4	51
60	094	30	46	1	<10	<2	<4	<1	<1	98	<2	<4	<2	89

Table 11. Analyses of select rock samples from some mineralized occurrences in the East Mojave National Scenic Area, California—Continued.

Inductively coupled plasma atomic-emission spectroscopy (total)

Analysis No.	Field No. 90TT	Ag	Ba	Be	Bi	Cd	Ce	Co	Cr	Cu	Eu	Ga	La	Li
61	096	593	63	<1	490	13	<4	3	1	12,800	<2	<4	<2	12
62	100	<2	320	1	<10	<2	61	15	49	45	<2	9	30	16
63	101	<2	617	2	<10	<2	38	12	55	10	<2	16	24	18
64	102	7	1,010	1	10	<2	44	19	63	6,990	<2	12	21	18
65	103	3	746	1	<10	<2	30	20	44	851	<2	11	17	17
66	104	23	69	<1	<10	<2	<4	2	6	30	<2	<4	2	2
67	105	<2	1,370	1	<10	4	52	3	3	17	<2	10	29	5
68	106	<2	945	2	<10	5	219	24	6	22	3	15	97	18
69	107	<2	312	<1	<10	<2	74	<1	4	6	<2	7	41	9
70	108	14	409	2	170	<2	96	17	9	11	<2	14	48	29
71	109	<2	896	<1	<10	<2	46	1	6	3	<2	14	24	8
72	110	189	50	<1	20	75	<4	5	1	3,840	<2	<4	2	3
73	113	109	42	<1	<10	182	4	3	1	4,570	<2	<4	4	4
74	115	<2	104	1	<10	<2	23	5	15	124	<2	25	18	17
75	118	424	1,620	<1	190	46	<4	140	9	1,640	<2	<4	<2	2
76	128	2	76	<1	<10	<2	14	10	13	31	<2	6	8	13
77	130	20	246	<1	<10	297	7	3	6	305	<2	6	7	5
78	131	55	388	<1	<10	1,790	5	<1	7	360	<2	13	5	5

Inductively coupled plasma atomic-emission spectroscopy (total)

Analysis No.	Field No. 90TT	Mn	Mo	Nb	Nd	Ni	Pb	Sc	Sn	Sr	Th	V	Y	Yb	Zn
1	015	2,220	<2	7	18	<2	49	<2	130	24	<4	47	20	1	141
2	016	1,490	2	11	13	<2	86	<2	40	20	<4	39	14	<1	117
3	019	2,970	<2	<4	11	<2	15	<2	10	32	<4	13	10	<1	1,540
4	020	4,890	6	<4	13	3	10	<2	430	32	<4	15	15	<1	792
5	027	5,130	<2	5	4	18	18	<2	40	16	8	42	7	<1	378
6	030	465	<2	<4	<4	165	13	<2	<10	54	5	168	<2	<1	82
7	031	506	<2	<4	9	<2	5	<2	<10	61	<4	<2	<2	<1	6
8	032	99	<2	39	47	<2	8	3	<10	119	20	5	51	6	14
9	035	327	<2	<4	<4	36	7	<2	<10	64	<4	41	<2	<1	44
10	038	802	4	<4	7	15	58	2	<10	62	<4	22	4	<1	54
11	040	57	<2	10	11	<2	10	<2	<10	135	37	3	8	2	3
12	041	28	12	<4	6	4	18,600	2	<10	94	<4	32	3	<1	13
13	042	46	<2	<4	17	<2	66	2	<10	15	9	23	6	<1	16
14	043	7	2	<4	<4	<2	28	<2	<10	<10	<4	<2	<2	<1	9
15	045	553	4	<4	16	4	425	4	<10	<10	<4	50	5	<1	14
16	046	54	<2	20	37	2	10	2	<10	<10	31	5	25	3	8
17	047	21	17	<4	<4	10	5	<2	<10	<10	<4	115	<2	<1	24
18	049	98	<2	42	48	<2	10	3	<10	<10	29	5	55	6	12
19	050	19	<2	20	22	<2	<4	<2	<10	<10	24	3	9	2	3
20	051	31	5	6	10	<2	13	<2	<10	<10	4	12	<2	<1	9
21	052	15	3	13	19	<2	<4	<2	<10	<10	6	3	3	<1	<2
22	053	12	<2	11	29	<2	<4	2	<10	<10	39	3	13	2	<2
23	054	7	<2	5	13	<2	<4	<2	<10	<10	20	3	5	1	2
24	055	9	16	<4	44	<2	21	4	<10	<10	17	23	<2	<1	7
25	056	55	<2	7	72	<2	15	13	<10	<10	6	138	4	<1	5
26	058	11	2	<4	36	<2	6	<2	<10	<10	14	6	8	1	4
27	059	23	16	8	56	<2	10	2	<10	<10	25	4	27	3	5
28	060	21	4	13	42	<2	<4	3	<10	<10	19	7	15	2	9
29	061	44	17	<4	5	<2	6,060	<2	<10	<10	<4	5	<2	<1	51
30	062	64	66	<4	<4	<2	2,670	<2	<10	<10	<4	<2	<2	<1	9
31	063	80	<2	10	49	2	11	4	<10	<10	24	19	19	3	9
32	065	385	<2	<4	17	19	21	4	<10	<10	22	21	6	<1	45
33	066	55	<2	<4	11	<2	3,070	5	<10	<10	<4	16	3	<1	1,180
34	067	2,460	<2	11	61	37	55	16	<10	<10	13	105	26	2	385
35	068	1,040	<2	12	48	11	32	16	<10	<10	15	52	33	3	175
36	069	14	<2	<4	<4	<2	6,100	<2	<10	<10	<4	<2	<2	<1	1,910
37	070	48	26	<4	4	<2	3,010	<2	<10	<10	<4	9	<2	<1	495
38	071	49	4	<4	<4	<2	1,960	<2	<10	<10	<4	9	<2	<1	1,220
39	072	72	<2	4	19	7	177	10	<10	<10	9	39	5	<1	70
40	073	77	22	<4	64	<2	19	10	<10	28	29	47	16	<1	13
41	074	1,080	14	<4	36	36	5,810	7	<10	125	<4	44	29	2	328
42	075	132	2	<4	31	2	29	<2	<10	33	<4	3	121	9	13
43	076	104	69	4	21	3	8	10	<10	41	8	94	4	<1	8
44	077	72	24	4	25	<2	4	11	<10	64	7	104	5	<1	7
45	078	65	49	<4	23	<2	<4	9	<10	24	9	60	4	<1	6
46	079	102	664	<4	14	18	56	7	<10	849	9	155	8	1	64
47	080	16	15	<4	<4	4	65	<2	<10	10	<4	9	<2	<1	55
48	081	48	27	<4	7	<2	136	2	<10	24	5	26	<2	<1	162
49	082	260	126	<4	5	<2	3,730	<2	<10	17	<4	280	<2	<1	136
50	083	14	11	<4	<4	<2	4,800	<2	<10	15	<4	119	<2	<1	428

Table 11. Analyses of select rock samples from some mineralized occurrences in the East Mojave National Scenic Area, California—Continued.

		Inductively coupled plasma atomic-emission spectroscopy (total)													
Analysis No.	Field No. 90TT	Mn	Mo	Nb	Nd	Ni	Pb	Sc	Sn	Sr	Th	V	Y	Yb	Zn
51	084	18	5	<4	<4	<2	138	<2	<10	7	<4	11	<2	<1	15
52	085	455	7	<4	<4	<2	1,130	<2	<10	49	<4	52	<2	<1	232
53	086	4,820	<2	<4	<4	<2	324	<2	<10	14	<4	5	2	<1	232
54	088	2,620	<2	<4	<4	<2	60	<2	<10	19	<4	6	3	<1	284
55	089	23	12	<4	7	<2	178	<2	<10	39	<4	41	<2	<1	68
56	090	5,640	4	<4	20	<2	224	<2	<10	422	<4	20	36	3	26
57	091	3,480	2	<4	24	6	123	<2	<10	240	<4	16	24	2	18
58	092	57	112	<4	<4	<2	20,100	<2	<10	76	<4	760	4	<1	663
59	093	1,570	70	<4	<4	5	221	<2	<10	30	<4	11	5	<1	91
60	094	36	56	<4	<4	<2	539	<2	<10	9	<4	54	<2	<1	3,640
61	096	10	39	<4	<4	<2	12,500	<2	<10	196	<4	115	<2	<1	1,840
62	100	606	<2	<4	31	30	425	16	<10	303	<4	56	19	2	77
63	101	455	<2	<4	17	33	18	7	<10	660	<4	54	8	<1	48
64	102	471	<2	<4	19	34	119	7	<10	468	<4	65	10	1	60
65	103	721	<2	<4	13	26	215	4	<10	333	<4	58	6	<1	51
66	104	28	<2	<4	<4	4	271	<2	<10	<10	<4	17	<2	<1	9
67	105	144	<2	<4	24	3	130	4	<10	<10	11	13	17	2	73
68	106	2,650	6	<4	27	3	24	2	<10	<10	33	38	30	3	258
69	107	39	69	<4	27	3	24	2	<10	<10	21	8	5	<1	23
70	108	713	53	<4	51	10	120	6	<10	<10	9	44	26	2	116
71	109	29	8	<4	17	<2	29	3	<10	<10	45	11	3	<1	14
72	110	47	15	<4	<4	3	243,000	<2	20	<10	<4	4	<2	<1	9,940
73	113	878	<2	4	<4	<2	50,300	<2	<10	<10	<4	2	<2	<1	64,700
74	115	1,400	<2	<4	26	3	26	16	350	<10	9	109	22	3	85
75	118	46	33	<4	<4	<2	110	<2	<10	<10	5	4	<2	<1	6,840
76	128	153	<2	<4	7	23	76	2	<10	<10	<4	17	<2	<1	164
77	130	1,660	5	<4	9	2	19,400	<2	<10	<10	<4	7	4	<1	68,500
78	131	1,530	117	<4	6	3	39,000	<2	<10	<10	<4	9	<2	<1	257,000

		Inductively coupled plasma atomic-emission spectroscopy (partial)										Chemical Analyses			
Analysis No.	Field No. 90TT	Ag	As	Au	Bi	Cd	Cu	Mo	Pb	Sb	Zn	As	Hg	W	Au
1	015	87	--	--	360	--	25,000	--	72	--	28	16	0.38	--	450
2	016	130	--	--	920	--	45,000	--	88	46	15	7.8	0.14	--	400
3	019	14	46	--	73	7.7	10,000	--	14	7.9	1,300	37	0.04	2	50
4	020	2	52	--	51	3.1	2,400	1.3	--	--	720	39	--	--	26
5	027	0.86	--	--	--	0.8	7,300	--	--	--	--	31	0.04	2	24
6	030	--	22	--	--	--	170	--	1.1	--	1.6	26	--	--	<2
7	031	--	--	--	--	--	44.	--	--	--	1.6	2.1	--	--	150
8	032	--	--	--	--	--	28.	--	7.8	--	2.9	0.5	--	--	--
9	035	--	13	--	--	--	230	--	--	--	8.8	30	--	--	--
10	038	16	--	--	270	1.2	12,000	2.6	79	11	44	1.2	8.6	--	450
11	040	--	--	--	--	--	9.1	--	6.8	--	--	0.6	--	--	2
12	041	5.8	--	--	--	--	680	13	25,000	8.3	--	2.4	0.04	--	100
13	042	6.5	15	--	9.7	--	1,800	--	42	--	94	13	0.18	2	1,700
14	043	18	9.3	--	76	--	6,300	1.5	35	16	6.4	15	0.78	--	2,800
15	045	5.8	--	22	74	--	510	4.1	490	--	7.5	8	0.1	2	25,000
16	046	--	--	--	--	--	51	2	6	--	1.4	0.3	--	--	--
17	047	--	--	--	--	--	140	18	6.6	--	22	1.6	0.02	15	4
18	049	--	--	--	--	--	21	--	--	--	3.4	0.5	--	--	--
19	050	--	--	--	--	--	0.74	--	--	--	--	0.2	--	--	--
20	051	--	--	--	41	--	--	4.2	--	--	--	0.4	--	2	28
21	052	--	--	--	--	--	--	2.2	--	--	--	0.2	--	1	2
22	053	--	--	--	--	--	5.3	--	--	--	--	0.5	--	--	2
23	054	--	--	--	--	--	--	--	--	--	--	<0..2	--	--	--
24	055	--	--	--	6.4	--	210	15	7.8	--	--	1.8	0.04	--	4
25	056	6.7	--	--	--	--	510	1.2	--	--	--	0.8	0.16	7	6
26	058	--	--	--	--	--	8.8	1.6	--	--	--	<0.2	--	--	--
27	059	--	--	--	--	--	2.5	18	--	--	--	0.2	--	--	--
28	060	--	--	--	--	--	18.	3.4	--	--	--	0.3	--	--	--
29	061	200	--	1.7	--	1.9	490	18	8,100	--	40	1.5	0.28	--	3,600
30	062	10	--	--	--	0.81	2,300	58	3,300	--	4	<0.2	0.02	--	500

Table 11. Analyses of select rock samples from some mineralized occurrences in the East Mojave National Scenic Area, California—Continued.

		Inductively coupled plasma atomic-emission spectroscopy (partial)										Chemical Analyses			
Analysis No.	Field No. 90TT	Ag	As	Au	Bi	Cd	Cu	Mo	Pb	Sb	Zn	As	Hg	W	Au
31	063	--	--	--	--	--	0.92	--	11	--	5.6	0.7	--	--	--
32	065	--	--	--	--	--	--	1.7	22	--	41	1.1	--	--	2
33	066	190	--	5.6	290	9.7	2,100	--	4,400	--	1,000	14	0.34	--	7,600
34	067	--	--	--	--	1.6	210	--	41	--	390	2.5	--	1	6
35	068	--	--	--	--	--	73	--	20	--	180	0.6	--	2	--
36	069	26	--	--	18	17	1,100	--	8,100	--	1,800	3.2	0.08	--	450
37	070	210	--	7.1	160	3	540	29	4,100	--	370	5.2	0.28	--	5,100
38	071	110	11	2.3	240	5.2	1,200	3.7	2,600	--	1,200	13	0.32	--	3,150
39	072	4.4	--	--	--	--	72	1.4	240	--	31	4.1	0.02	--	100
40	073	--	--	--	--	--	0.38	24	12	--	6.3	4	0.02	4	2
41	074	250	68	--	620	0.78	110	16	9,600	--	300	50	0.06	3	45
42	075	0.55	6.7	--	--	--	13	2.7	21	--	6.8	6.6	0.02	--	800
43	076	--	--	--	--	--	2.8	66	--	--	--	0.4	--	4	--
44	077	--	--	--	--	--	1.4	19	--	--	--	0.5	--	4	--
45	078	--	--	--	--	--	--	53	--	--	--	0.5	--	3	--
46	079	--	22	--	--	--	32	730	63	--	70	23	0.02	4	6
47	080	2.4	96	--	--	--	37	13	83	--	52	78	0.36	--	300
48	081	2.4	140	--	--	--	110	30	180	14	160	100	0.32	4	150
49	082	71	260	--	42	11	190	160	5,500	760	120	260	9	38	50
50	083	520	360	--	260	23	3,000	11	7,100	1,800	440	270	17.1	12	1,450
51	084	12	--	--	--	1	160	4.5	160	160	8.9	13	1.2	3	4
52	085	42	150	--	22	5.1	340	8.7	1,500	790	240	190	10.5	56	100
53	086	12	77	--	--	1.1	110	2.7	430	220	46	86	1	1,700	30
54	088	5.7	68		13	3.4	710	2	90	190	310	66	3.9	1,080	4
55	089	2.1	27	--	130	--	44	8.8	220	110	65	26	1.2	13	12
56	090	--	--	--	--	2.7	4.7	3.6	310	--	23	9.9	0.12	67	2
57	091	--	--	--	--	1.5	3.8	2.5	170	--	14	8.7	0.02	85	4
58	092	500	760	1.9	41	96	5,400	180	29,000	4,700	530	490	>34	9	4,150
59	093	12	--	--	210	0.32	18	75	380	14	81	6.4	0.28	28	54
60	094	28	--	--	--	--	110	51	670	20	3,600	7.1	0.26	8	50
61	096	620	--	--	500	14	12,000	28	16,000	320	1,200	51	19.2	8	800
62	100	0.62	150	--	--	--	33	--	660	--	87	110	0.04	--	2
63	101	--	--	--	--	--	5.4	--	10	--	51	2	0.04	--	--
64	102	2.1	--	--	8.8	0.35	8,500	--	190	--	64	5.4	0.08	1	4,050
65	103	--	9.2	--	--	--	1,000	--	330	--	54	18	--	--	300
66	104	12	--	13	--	--	29	1	240	--	4.7	9.2	0.08	2	7,300
67	105	--	--	--	--	5.1	16	--	140	--	66	2.1	0.08	--	10
68	106	--	23	--	--	7.4	23	7.5	72	--	180	23	0.1	1	--
69	107	--	--	--	--	--	3.4	75	6.5	--	16	2	0.02	1	--
70	108	15	25	2.8	200	0.35	9.3	53	170	--	110	28	0.12	3	5,800
71	109	--	--	--	--	--	--	8.9	--	--	5.1	2.7	0.14	1	--
72	110	130	430	--	--	75	1,800	--	9,300	30	--	35,000	0.58	2	42
73	113	4.9	5,000	--	--	230	480	--	290	240	56	57,000	0.34	2	8
74	115	--	140	--	--	--	130	2.6	150	--	140	31	--	6	--
75	118	540	18	--	230	65	2,000	33	270	--	6,500	570	0.2	3	150
76	128	--	--	--	--	--	36	--	120	--	180	14	--	2	--
77	130	20	10	--	--	430	350	5.6	32,000	67	15,000	43	>34	1	20
78	131	57	10	--	--	2,400	390	110	53,000	240	110,000	61	>34	1	22

Table 12. Descriptions and locations of select rock samples collected from some mineralized occurrences in the East Mojave National Scenic Area, California.

[Mineral abbreviations: Gar, garnet; diop, diopside; trem, tremolite; mal, malachite; py, pyrite; px, pyroxene; hfs, hornfels; sph, sphalerite; qtz, quartz; cp, chalcopyrite; mag, magnetite; gn, galena; hb, hornblende; hm, hematite; cc, calcite; bx, breccia; cov, covellite; chrys, chrysocolla; bio, biotite; chl, chlorite; wm, white mica; pg, plagioclase; stib, stibiconite; wolf, wolframite; fl, fluorite; epi, epidote; fs, feldspar; kfs, K-feldspar; asp, arsenopyrite; zois, zoisite. See table 11 for analyses]

Analysis No.	Field No. (90TT...)	Location	Latitude	Longitude	Description
1	015	Evening Star Mine	35 21'39"	115 32'32"	Massive diop skarn retrograded to trem; two generations diop; mal and iron oxides after py.
2	016	do.	do.	do.	Do.
3	019	do.	do.	do.	Px hfs developed in sulfidized marble.
4	020	do.	do.	do.	Calc-silicate hfs, trem, and sph; replacement of marble.
5	027	Copper King Mine	35 21'06"	115 32'38"	Cp-mag skarn; includes retrograde chl and zois.
6	030	Vulcan Mine	34 55'23.91"	115 33'54.75"	Py-bearing, mag skarn.
7	031	do.	do.	do.	Marble; less than 0.5 m from skarn front.
8	032	do.	do.	do.	Py-bearing mag skarn.
9	035	do.	do.	do.	Mag skarn.
10	038	Big Horn Mine	34 50'28.7"	115 32'24.76"	Qtz-cp-py vein; late stage cc fills fractures.
11	040	do.	34 50'32.10"	115 32'23.47"	Rhyolite bx.
12	041	do.	do.	do.	Qtz-gn–cp veins; multiple qtz generations.
13	042	do.	34 48'28.66"	115 32'42.36"	Qtz-cp±hm veins; comb qtz, open-cavity fillings.
14	043	do.	34 48'32.5"	115 32'55.21"	Qtz-cp-base metal veins.
15	045	do.	34 48'41.71"	115 32'50.74"	Qtz-py (trace)-cc along fault; sparse wm.
16	046	Vic. Quail Spring Wash	34 49'46.92"	115 33'40.97"	
17	047	do.	34 49'55.33"	115 33'40.44"	Qtz-py veins associated with syenogranite of Quail Spring (Jqs, plate 1) (Miller and others, 1985).
18	049	do.	34 50'2.77"	115 33'31.91"	Syenogranite of Quail Spring (Jqs, plate 1).
19	050	do.	34 49'59.83"	115 33'24.36"	Do.
20	051	do.	34 49'50.09"	115 33'17.02"	Qtz-py vein; brick-red associated iron oxide(s).
21	052	do.	34 49'40.45"	115 33'19.18"	Py along east-west fractures in syenogranite of Quail Spring (Jqs, plate 1).
22	053	do.	54 49'38.12"	115 33'26.16"	Clay-altered syenogranite of Quail Spring (Jqs, plate 1).
23	054	do.	34 49'38.71"	115 33'30.97"	Syenogranite of Quail Spring (Jqs, plate 1).
24	055	do.	34 48'59.95"	115 33'11.59"	Fault bx; abundant gossan.
25	056	do.	do.	do.	Iron-oxide-stained metavolcanic rock.
26	058	do.	34 49'40.48"	115 33'54.7"	Porphyritic felsite dike.
27	059	do.	do.	do.	Hb-bio monzodiorite.
28	060	do.	do.	do.	Do.
29	061	Okaw Mine	35 2'45.22"	115 33'12.74"	Qtz-gn-cp-py vein; secondary cov.
30	062	do.	35 2'41.61"	115 33'5.21"	Qtz-gn-cp vein; secondary chrys.
31	063	do.	35 2'42.48"	115 33'1.13"	Porphyritic leucogranite dike; primary bio altered to chl; sparse wm alteration of pg.
32	065	Globe Canyon	35 3'6.75"	115 31'00"	Fault bx and gossan.
33	066	South Star Mine	35 3'5.42"	115 29'33.69"	Qtz-py vein; includes some wm.
34	067	do.	do.	do.	Qtz-cc veined and chl-altered dacite(?) dike.
35	068	do.	do.	do.	Qtz-py vein.
36	069	do.	35 3'6.65"	115 29'31.44"	Qtz-py-sph veins; brecciated, multiple generations of qtz.
37	070	S.S. nos. 17–19 , north	35 3'6.78"	115 29'46.97"	Fault bx; silicified.
38	071	do.	do.	do.	Gossan; along fault bx.
39	072	South Star Mine	35 3'12.89"	115 29'33.7"	Qtz vein; py-impregnated; abundant brick-red granitoid fragments.
40	073	SS. no.17	35 2'58.16"	115 29'55.04"	Qtz vein; massive outcrop; sericitically altered granitoid fragments.
41	074	Globe Mine	35 2'39.9"	115 29'8.23"	Gossan; reddish orange brown.
42	075	do.	do.	do.	Qtz-fl-py vein; abundant gossan.
43	076	S.S. no. 17	35 2'58.16"	115 29'55.04"	Qtz-wm-altered bio granite.
44	077	do.	do.	do.	Do.
45	078	do.	do.	do.	Ditto; heavily qtz veined and iron oxide stained.
46	079	do.	do.	do.	Gossan; brick red to brownish maroon.
47	080	Tungsten Flat	35 3'23.46"	115 2'50.74"	Qtz-py vein; moderate amounts fine-grained wm.
48	081	do.	do.	do.	Gossan; ochre.
49	082	do.	35 3'8.76"	115 2'50.41"	Qtz-py-stib (trace)-gn vein.
50	083	do.	35 3'8.76"	115 2'45.32"	Ditto; includes some secondary chrys.
51	084	do.	35 3'8.96"	115 2'37.23"	Qtz-py veins.
52	085	do.	35 2'53.85"	115 2'44.68"	Do.
53	086	do.	35 2'55.76"	115 2'49.63"	Qtz-wolf-gn (trace)-stib (trace)-py vein.
54	088	do.	35 2'47.19"	115 2'48.08"	Do.
55	089	do.	35 2'42.33"	115 2'31.1"	Qtz-py vein.
56	090	do.	35 2'30.43"	115 2'40.8"	Manganiferous cc vein; coarsely crystalline; streaked with iron oxide.
57	091	do.	do.	do.	Qtz-manganiferous cc vein.
58	092	do.	35 2'11.66"	115 2'47.39"	Qtz-chrys-gn-stib vein; coarsely
59	093	do.	35 2'7.33"	115 2'54.81"	Gossan; reddish brown.
60	094	do.	35 2'10.23"	115 2'55.87"	Qtz-sph vein; multiple generations qtz.
61	096	Leiser Ray Mine	35 1'33.22"	115 2'13.67"	Qtz-cp-gn-sph vein bx; multiple generations qtz.
62	100	True Blue Mine	35 5'2.04"	115 9'6.47"	Qtz vein; cuts chloritized gneissic granite; wm and epi alteration.
63	101	do.	do.	do.	Chloritized gneissic granite; relict bio; phyllonitic, strained fs porphyroclasts.
64	102	do.	35 4'54.14"	115 8'57.37"	Qtz-chrys veins; open-cavity fillings.
65	103	do.	do.	do.	Qtz-py-cp (trace) vein; some secondary Mn-bearing minerals.

Table 12. Descriptions and locations of select rock samples collected from some mineralized occurrences in the East Mojave National Scenic Area, California—Continued.

Analysis No.	Field No. (90TT...)	Location	Latitude	Longitude	Description
66	104	American Flag	35 4'35.89"	115 7'27.84"	Qtz-py-gn (trace) vein.
67	105	Rattlesnake Mine	35 6'7.72"	115 4'48.12"	Qtz-kfs±iron oxide (trace) vein; locally mylonitic fabric.
68	106	do.	35 5'50.12"	115 4'51.82"	Gossan; ochre to maroon; narrow seams in granite.
69	107	do.	35 5'40.93"	115 5'0.37"	Silicified fault zone.
70	108	do.	35 5'43.83"	115 5'7.71"	Qtz-py vein.
71	109	do.	35 5'39.74"	115 4'55.97"	Silicified granite; clay altered.
72	110	Mohawk Mine	35 28'43"	115 37'01"	Sulfidized (gn, asp, sph) shear zone; oxidized; some vein qtz.
73	113	do.	do.	do.	Oxidized gn, asp, and sph in vein qtz; some cp and py.
74	115	do.	do.	do.	Gar-px skarn; late stage wm and qtz.
75	118	Copper World Mine	35 30'20.49"	115 36'9.78"	Gossan.
76	128	Conquistador No. 2	35 31'23.8"	115 38'34.02"	Qtz-py (altered to buff-colored vein oxide) vein; chl- and wm-altered fragments
77	130	Emperor Mine	35 31'26.25"	115 37'51.45"	Gn-sph-cc along fault zone.
78	131	do.	do.	do.	Do.

Table 13. Geochemical statistics for analyses of selected elements in stream-sediment, heavy-mineral concentrate, rock, and soil samples from the East Mojave National Scenic Area and surrounding area, California and Nevada.

[Minimum, maximum, 50th (equal to 50th percentile; at least one-half of samples have concentrations equal to or less than value shown), 90th (equal to 90th percentile; at least 90 percent of samples have concentrations equal to or less than value shown), and threshold concentrations, as well as lower and upper limits of determination, are in parts per million (ppm). Concentrations in Rock Analysis Storage System (RASS) and PLUTO samples determined by emission-spectrographic methods; in National Uranium Resource Evaluation (NURE) samples, by neutron activation. Threshold (defined as highest background) concentrations for this study determined by visual and statistical examination of data, by observation of elemental concentrations near known mineralized areas, and by references to Goldfarb and others (1988) and Miller and others (1985); for PM (Providence Mountains Wilderness Study Area), determined by Goldfarb and others (1988, table 3); for SPM (South Providence Mountains Wilderness Study Area), determined by Miller and others (1985, tables 1, 2). Abbreviations: G, greater than upper limit of determination; L, detected below lower limit of determination; N, not detected at lower limit of determination; <, less than value shown; <<, threshold concentration is less than lower limit of determination (any concentration is anomalous); >, greater than value shown; --, unknown for lower or upper limits of determination, no data for PM and SPM. See table 14 for summary of geochemical anomalies]

	Limits of determination		Concentrations				Threshold concentrations			Number of analyzed samples	Number of anomalous samples
	Lower	Upper	Minimum	Maximum	50th	90th	This study	PM	SPM		
RASS and PLUTO stream-sediment samples[1, 2] (locations plotted in figure 50, data plotted in figures 54, 59, 62)											
Ag	0.5-1	5,000	N	>20	<0.5	0.5	0.7	--	<0.5	368	22
B	5-10	2,000	N	>100	10	50	50	--	--	368	16
Ba	20	5,000	70	5,000	700	1,000	1,500	--	--	368	11
Be	1-5	1,000	N	15	2	5	5	--	--	368	7
Co	1-5	2,000	L	100	10	30	30	--	--	368	30
Cu	2-5	20,000	<5	1,200	20	70	70	--	100	368	18
Mn	50	5,000	<50	7,000	700	2,000	2,000	--	--	368	17
Mo	1-5	2,000	N	100	3	15	10	--	--	368	54
Pb	5-10	20,000	N	5,000	20	70	70	--	--	368	22
Sn	2-10	1,000	N	30	<5	<5	<10	--	--	368	15
W	20-100	10,000	N	70	<50	<50	<50	--	--	368	5
Zn	5-200	10,000	N	7,000	50	150	N(200) or 100[5]	--	--	367	78
RASS nonmagnetic heavy-mineral-concentrate samples[1] (locations plotted in figure 51; data plotted in figures 55, 57, 60, 63, 65)											
Ag	1	10,000	N	1,000	N	3	3	L	3	498	69
As	500	20,000	N	3,000	N	N	N	N	--	498	3
Au	20	1,000	N	G	N	N	N	N	N	498	11
B	20	5,000	N	700	20	50	70	--	--	498	23
Ba	50	10,000	N	G	1,000	G	5,000	7,000	3,000	498	102
Be	2	2,000	N	200	L	3	3	--	--	498	28
Bi	20	2,000	N	G	N	N	N	N	30	498	34
Co	10-20	5,000	N	300	N	10	15	--	--	498	39
Cu	10	50,000	N	10,000	N	70	70	30	70	498	39
La	50-100	2,000	N	G	300	1,000	1,500	--	--	498	15
Mn	20	10,000	N	10,000	500	1,000	1,000	--	--	498	45
Mo	10	5,000	N	5,000	N	30	10	150	N	498	77
Nb	50	5,000	N	700	L	100	150	--	--	498	19
Pb	20	50,000	N	G	70	3,000	700	1,500	100	498	92
Sb	200	20,000	N	3,000	N	N	N	N	--	498	9
Sn	20	2,000	N	2,000	N	100	30	--	--	498	87
Th	200	5,000	N	G	L	1,500	2,000	--	--	480	26
W	50-100	20,000	N	10,000	N	500	300	--	--	498	83
Zn	500	20,000	N	G	N	N	N	N	--	498	19
PLUTO heavy-mineral-concentrate samples[3] (locations plotted in figure 51; data plotted in figures 55, 57, 60, 63, 65)											
Ag	1	--	<1	70	<1	2	1.5	--	--	262	58
Au	20	--	<10	20	<10	<10	10	--	--	262	3
B	20	--	<10	>200	50	100	100	--	--	262	18
Ba	2	--	100	>10,000	700	1,500	1,500	--	--	262	25
Be	1	--	<2	70	3	7	7	--	--	262	15
Bi	10	--	<20	200	<20	<20	<<	--	--	262	22
Co	5	--	3	200	50	100	70	--	--	262	33
Cu	1	--	3	7,000	70	200	100	--	--	262	51
La	20	--	20	>2,000	500	>2,000	1,500	--	--	262	39
Mn	2	--	200	>20,000	3,000	10,000	10,000	--	--	262	21
Mo	5	--	<2	300	15	50	20	--	--	262	63
Nb	10	--	5	3,000	150	500	700	--	--	262	9
Pb	10	--	<5	2,000	70	300	300	--	--	262	17
Sn	10	--	<5	>10,000	10	30	20	--	--	262	39
Th	200	--	<500	3,000	<500	500	500	--	--	262	19
W	100	--	<100	2,000	<100	<100	<<	--	--	262	9
Zn	200	--	30	5,000	200	700	300	--	--	262	53

Table 13. Geochemical statistics for analyses of selected elements in stream-sediment, heavy-mineral-concentrate, rock, and soil samples from the East Mojave National Scenic Area and surrounding area, California and Nevada—Continued.

	Limits of determination		Concentrations				Threshold concentrations			Number of analyzed samples	Number of anomalous samples
	Lower	Upper	Minimum	Maximum	50th	90th	This study	PM	SPM		
PLUTO heavy-mineral-concentrate samples[1] (locations plotted in figure 51; data plotted in figures 68, 71)											
Ce	200[3]	--	<200	10,000	700	3,000	3,000	--	--	262	29
Dy	50[3]	--	<20	1,000	<20	<20	<<	--	--	262	20
Eu	2-15[4]	--	<2	100	10	30	30	--	--	262	10
Nd	100[3]	--	<100	>2,000	300	1,000	1,000	--	--	262	26
Sm	100[3]	--	<100	1,000	100	200	200	--	--	262	21
Tb	50[4]	--	<50	300	<50	50	<50	--	--	262	35
Yb	5[3]	--	1.5	700	30	100	100	--	--	262	21
RASS and PLUTO rock samples[1, 2] (locations plotted in figure 52, data plotted in figures 56, 58, 61, 64, 66)											
Ag	0.5-1	5,000	N	1,000	<0.5	15	<0.5	--	--	943	249
As	100-500	10,000	N	G	<700	<200	<<	--	--	943	249
Au	5-10	500	N	150	<15	<5	<<	--	--	943	21
B	2-10	2,000	N	500	<10	30	20	--	--	937	111
Ba	2-30	5,000	N	G	300	1,500	1,500	--	--	943	80
Be	1-5	1,000	N	150	1	3	5	--	--	944	30
Bi	10-20	1,000	N	300	<10	<10	<<	--	--	944	107
Co	0.5-10	2,000	N	1,000	5	30	30	--	--	944	85
Cu	0.2-5	20,000	N	G	15	700	100	--	--	944	203
La	5-30	1,000	N	1,000	30	100	150	--	--	944	29
Mn	10	5,000	N	G	300	1,500	2,000	--	--	943	53
Mo	1-10	2,000	N	2,000	<5	10	7	--	--	942	125
Nb	5-20	2,000	N	100	<20	20	30	--	--	944	11
Pb	3-10	20,000	N	G	20	300	50	--	--	944	233
Sb	20-100	10,000	N	7,000	<100	<20	<<	--	--	944	27
Sn	5-10	1,000	N	G	<10	<5	<<	--	--	933	34
Th	100-500	2,000	N	300	<200	<300	<<	--	--	944	3
W	20-100	10,000	N	5,000	<50	<50	<<	--	--	944	46
Zn	5-200	10,000	N	G	500	500	N(200) or 100[5]	--	--	944	176
PLUTO rock samples[1] (locations plotted in figure 52; data plotted in figures 69, 72)											
Ce	200[3]	--	<20	300	70	100	150	--	--	155	8
Dy	50[3]	--	<10	20	<10	<20	<<	--	--	155	11
Eu	1-2[4]	--	<1	5	2	3	3	--	--	155	9
Nd	100[3]	--	<50	150	<100	70	70	--	--	155	14
Tb	20-50[4]	--	<20	30	<20	<50	<<	--	--	155	10
Yb	53	--	<0.5	10	1	3	3	--	--	155	6
NURE stream-sediment and soil samples[1, 4] (locations plotted in figure 53; data plotted in figures 67, 70, 73)											
Ce	10-20	--	<10	930	70	140	169	--	--	1,136	61
Dy	0.1-3.8	--	<1	45	2.7	7.7	7.9	--	--	911	85
Eu	0.1-3	--	<0.1	7.6	0.6	2.1	1.6	--	--	1,009	169
La	1-20	--	<1	1,900	36	77	169	--	--	1,157	108
Lu	0.1-0.6	--	<0.1	7.8	0.4	0.86	1.1	--	--	804	34
Sm	1-2	--	<1	130	6	12	16	--	--	963	48
Tb	--	--	0.13	2.3	0.9	1.8	1.6	--	--	28	3
Th	2	--	<2	320	13	24	39	--	--	1,153	67
U	--	--	0.10	30	2.4	3.9	5.9	--	--	1,259	42
Yb	1-2	--	<1	55	1.8	4.6	5.9	--	--	942	52

[1]Lower limits of determination are variable.
[2]Upper limits of determination for RASS samples are customary values.
[3]Lower limits of determination are from Myers and others (1961, table 2).
[4]Lower limits of determination are from the data.
[5]Lower limits of determination for Zn: RASS, 200 ppm; PLUTO, 5 ppm. Any detectable concentration in RASS samples and concentrations greater than 100 ppm in PLUTO samples are anomalous.

Table 14. Summary of geochemical anomalies in the East Mojave National Scenic Area, California.

[Geochemical anomalies are shown using the following notation: for each element, values indicate number of samples analyzed/ number of samples having high concentrations/number of samples having anomalous concentrations; na, no samples have high concentrations because any detectable concentration is considered anomalous; NS, no samples analyzed; NAH, concentrations of considered elements (see table 13) are neither anomalous nor high (the number of samples are in parentheses). Determination of whether or not area is geochemically anomalous with respect to a given element is based on (1) presence and proportion of samples having anomalous concentrations, (2) presence and proportion of samples having high but not necessarily anomalous concentrations, and (3) comparison of area with entire East Mojave National Scenic Area and its surrounding areas; see figure 49 for location of geographic areas. The absence of any notation for a specific sample type from an area means that samples of that type exist for the area but that none of the considered elements is present in either high or anomalous concentrations in those samples. Analyses of Rock Analyses Storage System (RASS) and and PLUTO samples determined by emission-spectrographic methods; of National Uranium Resource Evaluation (NURE) samples, by neutron activation; see table 13 for complete listing of geochemical statistics]

RASS and PLUTO Stream-sediment samples	RASS Heavy-mineral-concentrate samples	PLUTO Heavy-mineral-concentrate samples	RASS and PLUTO Rock samples	NURE Stream-sediment and soil samples
Soda Mountains				
B 8/0/1 Mo 8/0/1 Sn 8/01/1 Zn 8/1/1	NS	Ag 8/4/4 Au 8/na/1 B 8/01/1 Ba 8/0/1 Be 8/0/2 Bi 8/na/1 Co 8/0/1 Cu 8/1/2 Mn 8/2/1 Mo 8/1/2 Nb 8/0/1 Pb 8/3/1 Sn 8/3/2 Th 8/1/1 Zn 8/0/3 Ce 8/0/1 Dy 8/na/2 La 8/0/1 Tb 8/0/2 Yb 8/2/1	NS	Eu 4/0/2
Little Cowhole Mountain				
NAH (2)	NS	Be 2/1/1 Bi 2/na/1 Cu 2/1/1 Mo 2/0/1 Sn 2/0/1 Th 2/0/1 Tb 2/0/1	NS	NAH (0-4)
Cowhole Mountain				
NAH (1)	NS	NS	NS	NAH (0-1)
Cinder Cone Area				
Co 17/0/1 Mo 17/3/6 Zn 17/3/2	Be 28/1/1 Co 28/2/6 Mn 28/4/2 Nb 28/4/2 Sn 28/0/4 Th 28/4/9	Ag 17/4/4 Be 17/6/1 Bi 17/na/4 Cu 17/3/1 Mn 17/1/1 Mo 17/3/4 Sn 17/5/3 Tb 17/10/4 Th 17/2/2 Yb 17/3/1 Zn 17/2/1	Ag 18/1/9 As 18/na/1 B 18/1/2 Bi 18/na/4 Cu 18/2/7 Mn 18/0/2 Mo 17/2/2 Pb 18/3/9 Sb 18/na/1 W 18/na/3 Zn 18/0/5	Th 26/0/1 Ce 25/0/1 Eu 15/1/1

Table 14. Summary of geochemical anomalies in the East Mojave National Scenic Area, California—Continued.

RASS and PLUTO Stream-sediment samples	RASS Heavy-mineral-concentrate samples	PLUTO Heavy-mineral-concentrate samples	RASS and PLUTO Rock samples	NURE Stream-sediment and soil samples
Marl Mountains				
Ag 5/0/1 Mo 5/0/1 Pb 5/0/1 Zn 5/0/1	NS	Ag 5/1/1 Au 5/na/1 Bi 5/na/1 Ce 5/1/1 Cu 5/0/1 Dy 5/na/1 La 5/0/2 Mo 5/0/1 Nd 5/0/1 Sm 5/0/1 Tb 5/0/1 Th 5/0/1 Yb 5/0/1 Zn 5/0/1	NS	Dy 10/1/1 Th 10/0/1
Old Dad Mountain				
NAH (6)	Ag 3/0/2 Bi 3/na/1 Cu 3/0/1 Nb 3/0/1 Pb 3/0/2 Sn 3/1/2	Tb 6/0/1 Th 6/0/1	Ag 6/0/1 Au 6/na/1 B 6/0/1 Be 6/0/1 Bi 6/na/1 Co 6/0/1 Cu 6/0/1 Mo 6/1/1 Pb 6/1/1 Zn 6/0/1	NAH (0-22)
Kelso Mountains				
NAH (4)	NS	Ag 4/2/1 Au 4/na/1 Ce 4/0/1 Cu 4/0/1 Dy 4/na/1 La 4/0/1 Sn 4/3/0 Nd 4/1/1 Sm 4/0/1 Tb 4/0/1 W 4/na/1	NS	Dy 9/1/1 Eu 7/0/1
Bristol Mountains				
B 9/0/1 Mn 9/0/2 Mo 9/1/3 Pb 9/2/1 Sn 9/0/2 Zn 9/1/2	NS	Ag 8/3/1 Be 8/4/0 Cu 8/2/3 Dy 8/na/1 Eu 8/2/3 La 8/4/0 Mn 8/4/2 Mo 8/2/4 Nb 8/1/1 Nd 8/3/1 Sm 8/4/2 Sn 8/3/4 Yb 8/4/2 Zn 8/2/4	NS	Eu 6/0/1
Clark Mountain Range				
Ag 25/8/8 Be 25/1/1 Pb 25/3/3 Zn 25/4/1	Ag 15/0/8 As 15/na/2 B 15/0/14 Ba 15/5/2 Be 15/6/9 Bi 15/na/2 Cu 15/0/7 La 15/4/5 Mo 15/3/5 Nb 15/0/1 Pb 15/0/6 Sb 15/na/5 Sn 15/4/4 W 15/3/9 Zn 15/na/3	Ag 10/1/3 Ba 10/0/2 Be 10/1/2 Ce 10/1/2 Co 10/0/1 Cu 10/4/2 Eu 10/0/1 La 10/0/2 Nd 10/1/2 Pb 10/1/1 Tb 10/0/1 Th 10/0/1 W 10/na/1	Ag 3/0/2 Sn 3/0/1	Ce 19/2/2 Dy 20/1/4 Eu 11/1/2 La 24/0/2 Lu 14/2/2 Sm 13/1/2 Th 21/1/2 Yb 14/3/1

Table 14. Summary of geochemical anomalies in the East Mojave National Scenic Area, California—Continued.

RASS and PLUTO Stream-sediment samples	RASS Heavy-mineral-concentrate samples	PLUTO Heavy-mineral-concentrate samples	RASS and PLUTO Rock samples	NURE Stream-sediment and soil samples
Mescal Range				
NAH (3)	NS	Pb 3/0/1 Tb 3/0/1 Zn 3/0/1	NS	NAH (0-10)
Ivanpah Mountains				
Ag 26/2/1 Cu 26/5/5 Mo 26/2/1 Sn 26/0/7 W 26/na/3 Zn 26/4/19	Ag 15/0/1 Au 15/na/1 Bi 15/na/5 Co 15/0/11 Cu 15/12/3 Mn 15/6/8 Mo 15/0/12 Pb 15/2/7 Sb 15/na/1 Sn 15/0/14 Th 15/1/10 W 15/2/10	Ag 8/3/1 Be 8/2/1 Bi 8/na/1 Ce 8/3/2 Co 8/2/1 Cu 8/2/2 Dy 8/na/2 La 8/2/2 Mn 8/1/1 Mo 8/1/1 Nd 8/3/1 Pb 8/3/1 Sm 8/4/1 Tb 8/0/1 Th 8/0/1 W 8/na/1	Ag 26/1/12 As 26/na/4 B 26/2/8 Be 26/2/4 Bi 26/na/10 Co 26/3/7 Cu 26/3/12 Mn 26/3/13 Mo 26/0/4 Pb 26/4/3 Sn 26/1/16 W 26/na/16 Zn 26/0/23	Ce 19/1/1 Dy 20/3/5 Eu 12/3/2 La 20/0/1 Lu 13/4/3 Sm 15/0/1 Tb 1/0/1 Yb 15/3/1
Cima Dome				
NS	NS	NS	Tb 1/0/1	NS
New York Mountains				
Ag 18/1/1 B 18/0/1 Be 18/1/3 Co 18/3/1 Cu 18/1/2 Mn 18/2/1 Mo 18/3/1 Pb 18/1/1 W 18/na/1 Zn 18/3/7	Ba 59/4/4 La 59/0/4 Pb 59/1/1 W 59/6/4	Ag 18/6/4 B 18/2/4 Ba 18/0/3 Be 18/3/3 Bi 18/na/5 Ce 18/2/4 Co 18/2/2 Cu 18/9/6 Dy 18/na/2 Eu 18/3/2 La 18/0/7 Mn 18/6/1 Mo 18/1/6 Nd 18/3/5 Pb 18/7/2 Sm 18/3/5 Sn 18/7/3 Tb 18/0/1 Th 18/2/4 Yb 18/5/1 W 18/na/3 Zn 18/2/8	Ag 35/1/8 As 35/na/3 Au 35/na/3 B 35/0/2 Ba 35/5/1 Bi 35/na/4 Co 35/1/1 Cu 35/3/10 La 35/4/2 Mo 35/2/3 Pb 35/6/9 Sb 35/na/2 Zn 35/0/8	Ce 25/6/3 Dy 24/7/4 Eu 19/1/1 Lu 14/1/2 Th 26/2/2 Yb 15/1/2
Mid Hills				
B 8/0/1 Mo 8/1/2 Zn 8/3/1	Ba 6/1/2 Bi 6/na/2 Mn 6/0/5 Mo 6/0/1 Nb 6/0/1 W 6/1/2	Ag 7/3/1 Ba 7/0/1 Bi 7/na/3 Ce 7/1/1 Eu 7/4/0 La 7/2/1 Nd 7/3/1	Ag 10/0/3 Bi 10/na/1 Mn 10/0/1 Pb 10/2/2 Zn 10/0/1	Ce 12/4/1

Table 14. Summary of geochemical anomalies in the East Mojave National Scenic Area, California—Continued.

RASS and PLUTO Stream-sediment samples	RASS Heavy-mineral-concentrate samples	PLUTO Heavy-mineral-concentrate samples	RASS and PLUTO Rock samples	NURE Stream-sediment and soil samples
Providence Mountains				
Ag 82/3/5 Ba 85/6/3 Co 82/24/20 Cu 82/7/8 Mn 82/5/5 Mo 82/4/4 Pb 82/3/5 Sn 82/0/2 W 82/na/1 Zn 82/4/12	Ag 225/20/49 As 225/na/1 Au 225/na/8 B 225/7/7 Ba 225/73/81 Be 225/21/11 Bi 225/na/18 Co 225/6/17 Cu 225/53/17 La 225/0/5 Mn 225/59/23 Mo 225/2/50 Nb 225/10/14 Pb 225/22/66 Sb 225/na/2 Sn 225/8/55 Th 225/9/4 W 225/17/46 Zn 225/na/10	Ag 12/2/3 Bi 12/na/1 Ce 12/5/1 Co 12/4/2 Cu 12/6/1 Eu 12/2/1 La 12/2/3 Mo 12/1/3 Nd 12/4/1 Pb 12/4/2 Sm 12/4/1 Sn 12/6/2 Tb 12/0/3 Th 12/1/1 Zn 12/5/2	Ag 554/63/163 As 554/na/5 Au 554/na/13 B 554/40/57 Ba 554/24/52 Be 554/8/16 B i 554/na/64 Co 554/19/55 Cu 554/49/124 Eu 14/3/3 La 554/16/22 Mn 554/12/22 Mo 554/34/82 Nb 554/18/2 Nd 14/3/1 Pb 554/80/146 Sb 554/na/11 Sn 554/5/6 Th 554/na/1 W 554/na/8 Zn 554/0/93	Dy 20/2/2 Eu 21/4/1 La 25/0/1 Lu 20/1/1 Th 25/0/1 Yb 24/4/1
Granite Mountains				
NAH (7)	Ag 28/1/1 Ba 28/8/2 Bi 28/na/2 Co 28/0/2 Cu 28/2/3 La 28/1/1 Mn 28/11/2 Mo 28/0/4 Pb 28/1/2 Sn 28/0/4 Th 28/0/1 W 28/5/4 Zn 28/na/3	Ag 11/1/2 Ba 11/0/2 Be 11/1/1 Ce 11/1/1 Co 11/0/3 La 11/0/1 Mn 11/1/1 Mo 11/1/2 Nb 11/0/1 Nd 11/0/1 Pb 11/2/1 Sn 11/5/2 Tb 11/0/1 Yb 11/0/1 Zn 11/0/1	Ag 88/2/3 As 88/na/1 B 88/0/3 Ba 88/32/8 Bi 88/na/4 Ce 77/3/2 Co 88/1/4 Cu 88/4/5 Dy 77/na/4 La 88/0/1 Mo 88/1/2 Nd 77/15/16 Pb 88/11/3 Sn 88/1/1 Tb 77/0/6 Yb 77/5/1 Zn 88/7/10	Eu 19/2/4 La 19/0/1
Van Winkle Mountain				
NS	NS	NS	Nd 3/0/1	La 1/0/1
Grotto Hills				
Ag 1/0/1 Mo 1/0/1 Zn 1/0/1	NS	Co 1/0/1 Cu 1/0/1 Mn 1/0/1 Mo 1/0/1 Zn 1/0/1	NS	NAH (0-2)
Pinto Mountain				
NS	NS	NS	NS	NAH (0-3)
Table Mountain				
Co 2/0/1 Mo 2/0/1 Zn 2/0/1	NS	Ag 2/1/1	Ag 2/0/1 Cu 2/0/1 Eu 2/0/1 Mo 2/1/1 Pb 2/0/1 Sb 2/0/1 Sn 2/0/1	Ce 2/0/1 Dy 2/1/1 La 2/0/1 Th 2/0/1

Table 14. Summary of geochemical anomalies in the East Mojave National Scenic Area, California—Continued.

RASS and PLUTO Stream-sediment samples	RASS Heavy-mineral-concentrate samples	PLUTO Heavy-mineral-concentrate samples	RASS and PLUTO Rock samples	NURE Stream-sediment and soil samples
Homer Mountain				
Ag 1/0/1 Mo 1/0/1	NS	Mn 1/0/1	NAH (1)	Dy 4/1/1 Eu 4/1/1
Woods Mountains				
NAH (2)	NAH (1)	Ag 2/0/1 La 2/0/1	NS	Dy 2/0/2
Hackberry Mountain				
Ba 3/0/1	NS	Ag 3/0/1 Ba 3/0/1 Mn 3/0/1 Mo 3/0/1 Zn 3/0/1	NS	Ce 7/3/1 Dy 8/2/4 Eu 7/2/3 Yb 7/2/1
Vontrigger Hills				
NAH (1)	NS	Ag 1/0/1 Ba 1/0/1	Ag 15/0/4 As 15/na/1 B 15/1/8 Be 15/3/2 Bi 15/na/4 Cu 15/1/4 Mn 15/1/4 Mo 15/0/1 Nb 15/0/1 Pb 15/5/2 Zn 15/0/1	NAH (0-2)
Piute Range				
Be 6/0/1 Mo 6/0/1 Zn 6/0/1	Ag 29/0/1 B 29/3/1 Be 29/2/2 Bi 29/na/1 Cu 29/1/1 Mo 29/0/1 Pb 29/1/3 Sn 29/0/2 W 29/0/1 Zn 29/na/1	Ag 6/2/1 Ba 6/0/1 La 6/0/1 Sm 6/0/1 Tb 6/0/1 Zn 6/0/1	Ag 25/2/8 Au 25/na/1 B 25/0/1 Be 25/1/1 Bi 25/na/16 Cu 25/0/7 Mo 25/0/4 Pb 25/3/8 Sb 25/na/4 W 25/na/3 Zn 25/0/6	Ce 18/3/4 Dy 17/4/5 Eu 18/4/5 Lu 15/2/2 Sm 10/1/2 Yb 17/0/3
Castle Mountain				
B 4/0/1 Co 4/0/2 Mn 4/1/1 Mo 4/1/1	B 7/0/2	Ba 4/0/2 Bi 4/na/2 Ce 4/0/2 Co 4/0/1 Cu 4/0/2 Dy 4/na/2 Eu 4/1/1 La 4/0/2 Mn 4/1/1 Mo 4/1/1 Nd 4/0/2 Sm 4/0/2 Th 4/0/2 Yb 4/0/2 Zn 4/0/1	Ag 15/2/4 B 15/1/1 Ba 15/0/1 Eu 5/2/1 Mn 15/0/2 Mo 15/1/4 Nb 15/0/3 Pb 15/2/1 Sb 15/na/4 Tb 5/0/1	Dy 8/2/1 Eu 5/2/1

Table 15. Types of mineral deposits known in the East Mojave National Scenic Area, California, as of 1993.

[Abbreviations: C, amount of contained metal or ore before onset of mining; M, amount of metal or ore mined; --, not available]

Mineral-deposit model[1, 2]	Number identified in EMNSA[3]	Typical example of mineral deposit in EMNSA			
		Name	Principal commodities		Additional metals present
			Amount[4]	Type	
Carbonatite, rare-earth element (10)	5	Esperanza Group	--	Ce, La, Sm	U, Th
Polymetallic vein (22c)	206	Morningstar	480,000 oz Au (M)	Au	Ag, Pb, Zn, Cu
Low sulfide, Au-quartz vein (36a)	5	Conquistador No. 2	--	Au	--
Polymetallic replacement (19a)	23	Iron Horse	400 tons ore (M)	Pb, Zn	Fe, Cu, Au, Ag
Distal disseminated Au-Ag (--)	1	Unamed prospect	--	Au, Ag	Zn
Au breccia pipe (--)	2	Colosseum	10,500,000 tons ore (C)	Au, Ag	Cu, Pb, Zn
Ag-Cu brecciated dolostone (--)	25	Beatrice Mine	--	Ag, Cu	Au, V
Fluorite vein (--)	16	Pacific Fluorite	--	F	Sb, Ag, Pb, Zn
Tungsten vein (15a)	18	Mojave Tungsten	38,400 lb (M)	WO_3	Ba, F
Au-Ag, quartz-pyrite vein[5] (--)	80	Little Dove	--	Au, Ag	--
Polymetallic fault (--)	79	Billy Boy	--	Au	Zn, Cu, Ag
Polymetallic skarn (--)	18	Copper Commander	--	Cu, Pb, Zn	Au, Sb, As, Ag
Zn-Pb skarn (18c)	6	Mohawk Mine area	1,793,422 lb (M)	Zn	Cu, Pb, Ag, As
W skarn (14a)	3	Silverado-Tungsite	Small tonnage (M)	W	Au, Ag, Cu, Pb, Zn
Fe skarn (18d)	10	Vulcan	2,643,000 tons ore (M)	Fe	--
Sn (W) skarn (14b)	1	Evening Star Tin	3,200 lb (M)	Sn	W, Au, Ag, Zn, Cu
Cu Skarn (18b)	26	Copper World	5,321,184 lb (M)	Cu	Pb, Ag, Au, Zn
Vein barite (--)	6	Susan's Peak	--	Ba	--
Vein magnesite (--)	1	New Trail Magnesite	~300 tons ore (M)	Mg	--
Porphyry Mo, low F (21b)	3	Big Hunch	800,000,000 lbs MoS_2	Mo	Ag
Epithermal qtz-adularia (alunite) (Au) (25e)	11	Castle Mountains (Hart)	2,020,000 oz Au (C)	Au	Ag
Placer Au-PGE[6] (39a)	34	Terry	--	Au	--
Placer Fe±Ti (--)	2	Kelso Dunes	1,000 tons Fe_3O_4 (M)	Fe	Ti, Au

[1] Numbers in parentheses indicate model numbers as described by Cox and Singer (1986); other listed models from various sources in literature.

[2] Additional types of mineral deposits in EMNSA (and their number of occurrences) include sand and gravel (4), cinder (3), sandstone (1), marble (3), slate (1), limestone (6), dolomite (4), graphite (1), talc (1), mica (2), gemstone (1), decorative and dimension stone (5), pyrophyllite (1), clay (9), perlite (3), and pumice (2).

[3] Mineral-deposit models have been assigned provisionally in this report to 587 of 701 occurrences in EMNSA that were reported by U.S. Bureau of Mines (1990a, table 2). Small number of localities have been assigned to more than one deposit type.

[4] From U.S. Bureau of Mines (1990a, map no. 161).

[5] Deposits are mostly Mesozoic in age but also include some Tertiary gold-silver vein occurrences that are epithermal and apparently related to wrench-style tectonics, as exemplified by Telegraph Mine (Lange, 1988).

[6] Presence of PGE (platinum-group elements) has not been established in placers in EMNSA (U.S. Bureau of Mines, 1990a); however, model name has been retained to preserve terminology used by Cox and Singer (1986). Field examinations (U.S. Bureau of Mines, 1990a) indicate presence of visible gold at only nine placer locatlities in EMNSA, and nowwhere in EMNSA is placer-gold production occurring.

Table 16. Summary statistics for 20 elements in 1,050 samples of rock analyzed from the East Mojave National Scenic Area, California.

[All concentrations in parts per million except where noted; --, not applicable. Data from U.S. Bureau of Mines, 1990a, tables 2*A*,*B*]

	Number of undetermined concentrations	"Less than" concentrations		"Greater than" concentrations		Data matrix (including substituted values)							Log-transformed data	
		Number	Value substituted[1]	Number	Value substituted[2]	Minimum	Maximum	Mean	Geometric mean	50th percentile	Mode	Standard deviation	Kurtosis	Skewness
Ag	481	481	1	0	--	1	3,080	70.6	6.1	3	1	238	–0.0387	0.883
As	24	23	0.5	1	10,000	0.5	120,000	664	22.5	16	2	4,790	0.453	0.811
Au[3]	253	253	1	0	--	1.0	51,700	973	30.7	20.5	1.0	3,380	–0.778	0.456
Ba	369	369	25	0	--	25	184,000	1,150	151	170	25	8,900	0.478	0.598
Ce	402	402	2.5	0	--	2.5	7,200	51.3	14.4	17	2.5	268	–1.13	0.2
Co	642	642	2.5	0	--	2.5	859	20	6	2.5	2.5	66.8	1.28	1.36
Cr	209	209	10	0	--	10	3,990	181	99.5	160	10	2.8	–0.661	–0.74
Cs	549	549	0.5	0	--	0.5	138	2.6	1.2	0.5	0.5	6.2	0.113	1.01
Fe[4]	83	83	0.1	0	--	0.1	62	4.9	2	2	0.1	8	–0.185	–0.209
La	181	181	1	0	--	1	52,600	71.1	8.8	10	1	1,620	0.444	0.081
Mo	376	376	0.5	0	--	0.5	2,080	34.3	4	3	0.5	135	–0.618	0.589
Ni	801	801	5	0	--	5	560	15.7	7.8	5	5	39	3.63	2.04
Sb	18	18	0.05	0	--	0.05	122,000	346	5.9	3.2	0.2	3,890	–0.249	0.647
Sc	185	185	0.1	0	--	0.1	123	4.2	1.4	1.8	0.1	7.4	–0.875	–0.232
Sm	91	91	0.05	0	--	0.05	6,360	9.5	1.3	1.7	0.05	196	0.161	–0.355
Ta	687	687	0.25	0	--	0.25	10	0.6	0.42	0.25	0.25	0.9	0.887	1.34
Th	154	154	0.1	0	--	0.1	26,300	40.3	2.6	3.3	0.1	22	–0.054	–0.139
U	69	69	0.1	0	--	0.1	1,590	9.3	2.7	3.1	0.1	70	1.06	–0.286
W	256	256	0.5	0	--	0.5	165,000	93	5.2	4	0.5	6,050	1.74	1.16
Zn	477	477	50	0	--	50	325,000	4,080	254	130	50	17,400	0.608	1.22

[1]Substituted values are 50 percent of the minimum detection limit.
[2]Substituted value is concentration of maximum determination limit.
[3]Concentration values in parts per billion.
[4]Concentration values in weight percent.

Table 17. Array of Spearman correlation coefficients for 20 elements in 1,050 rock samples from the East Mojave National Scenic Area, California.

[See text. Calculated using data from U.S. Bureau of Mines (1990a); --, not applicable.]

	Log (Au)	Log (Ag)	Log (As)	Log (Ba)	Log (Ce)	Log (Co)	Log (Cr)	Log (Cs)	Log (Fe)	Log (La)	Log (Mo)	Log (Ni)	Log (Sb)	Log (Se)	Log (Sm)	Log (Ta)	Log (Th)	Log (U)	Log (W)	Log (Zn)
Log (Au)	1.0	--	--	--	--	--	--	--	--	--	--	--	--	--	--	--	--	--	--	--
Log (Ag)	.323	1.0	--	--	--	--	--	--	--	--	--	--	--	--	--	--	--	--	--	--
Log (As)	.136	.485	1.0	--	--	--	--	--	--	--	--	--	--	--	--	--	--	--	--	--
Log (Ba)	–.139	–.349	–.285	1.0	--	--	--	--	--	--	--	--	--	--	--	--	--	--	--	--
Log (Ce)	–.152	–.473	–.341	.614	1.0	--	--	--	--	--	--	--	--	--	--	--	--	--	--	--
Log (Co)	.241	.01	.046	.089	.108	1.0	--	--	--	--	--	--	--	--	--	--	--	--	--	--
Log (Cr)	.177	–.218	–.343	.222	.15	–.016	1.0	--	--	--	--	--	--	--	--	--	--	--	--	--
Log (Cs)	–.181	–.305	–.092	.519	.54	.156	–.012	1.0	--	--	--	--	--	--	--	--	--	--	--	--
Log (Fe)	.319	.013	.167	.133	.149	.691	.019	.14	1.0	--	--	--	--	--	--	--	--	--	--	--
Log (La)	–.101	–.345	–.221	.627	.883	.147	.085	.525	.22	1.0	--	--	--	--	--	--	--	--	--	--
Log (Mo)	.292	.367	.294	–.185	–.328	.053	.142	–.22	.166	–.271	1.0	--	--	--	--	--	--	--	--	--
Log (Ni)	.082	–.041	.077	.087	.089	.356	.042	.12	.313	.111	–.004	1.0	--	--	--	--	--	--	--	--
Log (Sb)	–.009	.552	.751	–.258	–.363	–.129	–.358	–.09	–.08	–.244	.248	.029	1.0	--	--	--	--	--	--	--
Log (Sc)	–.097	–.449	–.271	.579	.724	.417	.11	.555	.454	.714	–.279	.244	–.346	1.0	--	--	--	--	--	--
Log (Sm)	–.17	–.429	–.278	.621	.879	.177	.113	.554	.2	.896	–.341	.11	–.312	.777	1.0	--	--	--	--	--
Log (Ta)	–.184	–.349	–.3	.448	.649	.02	.054	.452	.07	.621	–.259	.034	–.278	–.535	.65	1.0	--	--	--	--
Log (Th)	–.091	–.459	–.334	.593	.838	.089	.206	.523	.182	.804	–.274	.053	–.387	.705	.813	.674	1.0	--	--	--
Log (U)	.24	.108	.205	.001	.166	.261	–.007	.149	.435	.216	.242	.102	.067	.177	.109	.184	.252	1.0	--	--
Log (W)	.165	.146	.163	.02	–.071	.19	.017	.147	.278	–.024	.316	.07	.141	.057	–.022	–.029	–.023	.204	1.0	--
Log (Zn)	.226	.559	.47	–.216	–.241	.217	–.322	–.049	.297	–.129	.289	.08	.442	–.13	–.199	–.17	–.233	.26	.196	1.0

Evaluation of Metallic Mineral Resources

By Ted G. Theodore

Introduction

Evaluation of metallic mineral resources primarily addresses known occurrences in the East Mojave National Scenic Area (EMNSA) but also includes some discussion of additional types of metallic-mineral deposits judged to be permissive in the various metallogenic terranes outlined for the EMNSA. Usage of the terms "occurrence" and "deposit" together with some other relevant expressions are defined in this section of the report below. Furthermore, some nonmetallic minerals (for example, fluorite, magnesite, and barite) also have been incorporated into some of the following discussions because of their intimate petrogenetic association with many metal-bearing systems. A total of approximately 15 person-weeks were spent during 1990 in the EMNSA by 10 geologists to gather information first hand for this report. Because of the short timeframe requested to the point of first release of our information concerning the EMNSA (U.S. Geological Survey, 1991) and the accompanying quantitative assessment (Hodges and Ludington, 1991), the conclusions in this report rely heavily on recently completed geologic investigations by others in the region (Miller and others, 1985, 1986; Goldfarb and others, 1988; Wooden and others, 1988; Wooden and Miller, 1990). In addition, studies by the U.S. Bureau of Mines (1990a; see also Schantz and others, 1990) and the California Division of Mines and Geology (for example, see Kohler, 1984) provided the major inventories of metallic minerals available to us for the EMNSA; this inventory was supplemented where appropriate by information contained in records of the Mineral Resources Data System (MRDS) of the U.S. Geological Survey and by data made available from the files of several major mining companies that have been active at various times in the EMNSA during the last 20 years. In addition, the U.S. Bureau of Land Management (1980) analyzed some 29 resource areas that total 7.59 million acres of the entire California Desert Conservation Area (CDCA) (and including all of the EMNSA), and they classified the land with respect to its potential for energy and mineral resources. As classified by them, the Clark Mountain Range, Mescal Range, Ivanpah Mountains, Hackberry Mountain, and Castle Mountains include areas favorable for future discovery of locatable mineral deposits. The New York Mountains, Mid Hills, Providence Mountains, Granite Mountains, and all ranges west of Kelso were classified as areas having unqualified or unknown potential.

Mineral evaluation in this report generally follows a methodology initially developed for the Alaska Mineral Resource Assessment Program (AMRAP) of the U.S. Geological Survey, which in effect is a methodology based on analogy (see Harris, 1984). This methodology in its entirety consists of (1) delineating areas or domains of coherent geology that are consistent with the geology associated with a particular type or types of metalliferous deposits elsewhere, (2) building grade-and-tonnage models that describe the types of deposits recognized, and (3) estimating the numbers of undiscovered deposits (Singer, 1975, 1990, 1993; Singer and Cox, 1988; Menzie and Singer, 1990; see also, Bultman and others, 1993, for an in-depth discussion of the methodology and Barton and others, 1995, for recommendations on procedures to follow during assessments). The U.S. Geological Survey (1992) recently completed an evaluation of selected metallic and nonmetallic resources in the West Mojave Management Area of the Bureau of Land Management, which is present just to the west of the EMNSA.

Mineral deposits and occurrences listed and described by the U.S. Bureau of Mines (1990a; see also Wetzel and others, 1992) in the EMNSA were classified into about 20 types of metallic-mineral occurrences after first examining a number of these occurrences in the field to (1) confirm their classification(s) and (2) ascertain any mining-district-wide characteristics pertinent to the overall evaluation (table 15). The types of models assigned to the occurrences in the EMNSA generally follow the models for ore deposits in Cox and Singer (1986) and several other deposit-specific supplemental reports (Rytuba and Cox, 1991; Orris and Bliss, 1991, 1992; Bliss, 1992a). The existence of fairly up-to-date compilations of grade-and-tonnage models (see for example, Cox and Singer, 1986; Singer, 1990, 1993; Bliss, 1992a) allows the foregoing of the second part of the evaluation and the comparing instead of the grades and tonnages of the various kinds of deposits in the EMNSA with similar deposits elsewhere. However, throughout the discussions below, the possibility of district-scale, petrogenetic

linkages among many individual types of metallic-mineral occurrences is emphasized (fig. 89). Many of these lithotectonic linkages are well established in a large number of mining districts elsewhere, and they are presented here in graphic form to emphasize that the presence of one type of mineral deposit or occurrence can be used potentially as an indicator of many other types of deposit or occurrence in a surrounding, geologically similar environment. However, the presence of one type of deposit or occurrence does not mean that some other sought-after occurrence will necessarily also be present. In addition, it is not implied that all examples of mineral occurrences from the EMNSA shown on figure 89 are linked temporally and genetically. For example, the Jurassic Vulcan iron-skarn deposit is not linked genetically to the apparently Cretaceous-age Big Hunch stockwork-molybdenum system. Instead, the presence of magnetite skarn in stockwork-molybdenum systems elsewhere suggests that the presence of a stockwork-molybdenum system in the EMNSA demonstrates an environment permissive for iron skarn, and, conversely, the presence of iron skarn in the EMNSA suggests that stockwork systems also are permissive.

Many well-documented genetic linkages exist among metal deposits. One of the best examples of linkages among deposits in a mining district in the North American Cordillera is at Bingham Canyon, Utah (Einaudi, 1982, fig. 7.14*A*). At Bingham Canyon, igneous rocks and their immediately surrounding sedimentary rocks in the core of the porphyry system contain two zones of disseminated metal, (1) copper plus molybdenum plus gold and (2) copper. In places, this proximal zone is followed outwards by copper plus gold skarn. Distal to these are the lead-zinc-silver ores (polymetallic-replacement deposits), which are as much as 3 km from the outcrops of the central body of middle Tertiary, genetically related monzogranite. By 1976, the Bingham Mining District yielded 1.18 billion tonnes of ore averaging 0.85 weight percent Cu (Einaudi, 1982). The mining district historically also has been a major producer of gold: by 1986, more than 19 million oz Au had been produced from lode and placer deposits, making the Bingham Mining District one of the largest producers of gold in the United States (Tooker, 1990). Most of the gold has been produced as a byproduct from the mining of porphyry-copper ore. Spatial linkages between skarn ores and disseminated, porphyry-hosted ores at Yerington, Nev., Christmas, Ariz., and Ely, Nev., also are depicted graphically by Einaudi (1982), and the zoning relation between precious metals and base metals is discussed by Einaudi (1990). At Ely, over 1 million oz Au have been discovered peripheral to the porphyry-copper ores (Benedetto and others, 1991). In addition, two sediment-hosted or distal disseminated-gold deposits (Mel-Co and Barney's Canyon) have fairly recently been discovered 5 and 8 km, respectively, from the outcrop of the central stock at Bingham Canyon (Sillitoe and Bonham, 1990). These two deposits also are inferred to be related genetically to emplacement of the central copper- and molybdenum-bearing ores in the core of the mining district, although the genetic connection can only be suggested at this time by the symmetry of the gold and arsenic patterns surrounding the porphyry center (Babcock, 1993). Minable-oxide reserves at the Barney's Canyon deposit are 10 million tonnes (t) (at an average grade of 1.44 g Au/t) and, at the Mel-Co deposit, they are 3.1 million tonnes (at an average grade of 2.19 g Au/t) (Gunter and others, 1990). Finally, the characteristics of gold skarn, another type of deposit that may be linked genetically to porphyry-type ores in these types of magmatic-hydrothermal systems is discussed by Theodore and others (1992). Another example of district-wide linkages is the zonation among various ore bodies and their Ag/Au ratios in the Leadville Mining District, Colo., as discussed in detail by Thompson (1990).

Emplacement of many of the individual epigenetic metallic occurrences and deposits in the EMNSA should not be viewed as isolated events in time and (or) space. The zonal arrangement of silver-copper brecciated dolostone, tungsten, and fluorite veins that surround a centrally located gold-bearing breccia pipe at the Colosseum Mine in the EMNSA provides an excellent example of such a linkage (Sharp, 1984; see section below entitled "Breccia Pipe and Related Deposits"). In addition, several other types of deposits that are not currently (1995) known to be present in the EMNSA may be found there at some time in the future because they are known elsewhere in geologic environments similar to those in the EMNSA. In 1980, new exploration techniques, concepts, and field investigations resulted in the recognition of several mineral environments in the CDCA that previously were not suspected (U.S. Bureau of Land Management, 1980). An attempt to estimate numbers of undiscovered metallic mineral deposits in the EMNSA, as has been done elsewhere (Richter and others, 1975; Singer and others, 1983; Peterson and others, 1983), is included in

the report by Hodges and Ludington (1991). Although model types have been assigned with variable degrees of certainty to 587 of the 701 mineral occurrences identified by the U.S. Bureau of Mines (1990a) in the EMNSA (table 15), only limited first-hand knowledge is known of, for example, (1) the character and intensity of alteration marginal to many of the occurrences, (2) the distribution of deposit-scale anomalous elements and elemental ratios, and (3) the intensity and preferred orientation(s) of fracture patterns that may or may not surround the identified deposits and occurrences. These types of data are critical for understanding the extent of penetration of epigenetic, mineralizing fluids into the rocks that surround any occurrence of metals and, as a corollary, whether or not that particular occurrence of metal is one part of a much larger system as described for the veins that surround the Colosseum Mine in the section below entitled "Breccia Pipe and Related Deposits."

The evaluation in this report assumes that many metalliferous concentrations cannot be treated as isolated occurrences exclusive of other types of deposits, as is presently recognized in much of the economic-geology literature. Indeed, many types of models listed by Cox and Singer (1986), as well as compendia of many others, can be linked genetically into a continuum of deposits whose sites of eventual deposition are controlled both laterally and vertically by various physicochemical processes, including depth below the paleosurface and separation of a vapor phase from the metal-bearing fluids. Furthermore, B.A. Berger (written commun., 1988) emphasized the dynamic nature of the evolution of many epithermal metalliferous systems: "We are using models [currently] as rigid static entities in combination with other geological variables in the assessment process. From my limited perspective, models of epithermal systems are not independent from dynamic geologic processes such as the tectonic evolution of a region, changes in climate through time, and evolving landscape.***we must look for ways to portray epithermal systems in a less rigid framework.***and to apply them in a more dynamic way." Lastly, we emphasize that (1) exploration methodologies are evolving continually (see for example, Bailly, 1981; Hutchinson and Grauch, 1991) and (2) quantitative, model-based assessments can be made only for those types of mineral deposits that are currently recognized and for which grade-tonnage distributions are available. Any assessment for Proterozoic, carbonatite-related rare earth element (REE) deposits made before the discovery of the deposits at Mountain Pass (just outside the EMNSA) would not have resulted in an accurate characterization of the geology of the EMNSA for these types of deposits. Such model-based, rather than target-based, numerical assessments of many geologic terranes that show signs of widespread mineralization and that are likely to be explored further at some future time would most likely yield estimates of metal endowment that would be lower than future actual endowment measured by physical exploration.

Several examples from north-central Nevada dramatically emphasize this potential for inadequate assessment. Before the discovery and recognition in the early 1960s of the sedimentary-rock-hosted gold-silver deposits near Carlin, Nev., no one could have properly assessed the surrounding geologic terranes as favorable or even permissive for the presence of large gold-silver deposits. Many of these sedimentary-rock-hosted gold-silver deposits are now known to be world class in size and grade (Bagby and Berger, 1985; Bagby and others, 1986; Berger, 1986b). The sedimentary-rock-hosted gold deposits at Getchell, Nev., were discovered in the 1940s (Joralemon, 1951), but the true nature of the deposits was not recognized until much later (see for example, Bagby and Cline, 1991). As pointed out by Roberts (1986), Roberts (1960) defined in one of his previous papers some mineral belts in north-central Nevada and noted that many of the then-known, apparently small mineral deposits, including gold in placers, are localized along traces of the margins of windows in the regionally extensive Roberts Mountains thrust fault. The spatial association between the trace of the Roberts Mountains thrust fault and the localized mineral deposits provided the geologic basis upon which private industry could then focus its exploration efforts. In another example, the Fortitude gold-skarn deposit in the Battle Mountain Mining District, Nev., was not discovered until 1981, some 115 years after the mining district was first organized (Roberts and Arnold, 1965; Wotruba and others, 1986). Before the start-up of mining operations in 1985, the Lower Fortitude gold-skarn orebody contained 5.1 million tonnes of ore at a grade of 10.45 g Au/t, 27.8 g Ag/t, and 0.2 weight percent Cu (Theodore and others, 1991). In fact, no skarns cropped out anywhere in the immediate area of the Fortitude deposit before its exposure during open-pit operations.

As with all applied-exploration methodologies, the discoveries of economic concentrations of metals that are actually brought to the stage of mining operation are substantially limited compared to the number of claim

groups commonly examined. Various estimates suggest that as many as 1,000 prospects are examined for every mine brought into production thus far (1993) in the 1990s. Peters (1978) introduced the concept of "teaser districts" as those areas that include an abundance of small mines and (or) prospects that draw an inordinate amount of exploration effort before eventual rejection by some exploration group. Two possibilities exist in such "teaser districts." On the one hand, the absence of some fundamental geologic condition from the ore-forming process apparently precludes accumulation of metals into an economic concentration; the process may never have attained that particular intensity required to affect a volume of rock sufficient for an orebody (Peters, 1978). On the other hand, the major orebody may still be there somewhere in the "teaser district," but it may be found only by a redirection of geologic concepts by the exploration team, a reassessment of economics in the district, or by the application of newly developed exploration tools and concepts.

An assessment of the EMNSA that is based on potential-exploration targets (Menzie and Singer, 1990) for a particular metal or groups of closely related metals can lead to the recognition of new models and, necessarily, to a delineation of geologic terranes that are permissive for those new models. However, the cost of implementing state-of-the-art geochemical and geophysical techniques in a program to determine potential-exploration targets in the 1.5 million acres of the EMNSA would be exorbitant, especially when one considers that geochemical expenditures higher than approximately $20,000 per 640 acres of bedrock are fairly commonplace in private industry.

Lode-metal mines apparently were first discovered in 1861 in the Clark Mountain Range, at Striped Mountain, and in the Ivanpah Mountains, a region that was subsequently included in the EMNSA (Hewett, 1956). Shortly thereafter, in 1865, these discoveries were followed by others in the Ivanpah Mountains, and, in that same year, the Clark Mountain Mining District was organized. The first shipments of ore from the Copper World Mine took place during 1869, and many small lode mines that have shown sporadic production in the intervening years were discovered between 1865 and 1892 (Hewett, 1956). Subsequently, the region was explored extensively for tungsten, zinc, and lead from 1915 to 1918 during World War I. However, many mines in the EMNSA ceased production at the end of World War I and apparently never produced again (fig. 90; data from U.S. Bureau of Mines, 1990a). Many other mines in the EMNSA, mostly gold producers, ceased production in 1941 and 1942, many with promulgation of U.S Government Limitation Order L–208 of October 8, 1942, which closed down domestic mining of most gold near the onset of World War II (see Shawe, 1988; Lucas, 1992).

Definitions

This section follows closely the overall organization of one prepared by John and others (1993) for the Reno $1° \times 2°$ quadrangle, Nev. and California, resource-evaluation study by the U.S. Geological Survey. In the present report, the definitions put forth by Cox and others (1986) for the terms "ore deposit," "mineral deposit," and "mineral occurrence" are adapted somewhat. Specifically, a "mineral occurrence" is "***a concentration of a mineral***that is considered valuable by someone somewhere or that is of scientific or technical interest." However, use of this definition does not imply endorsement of economic value by the U.S. Geological Survey for the mineral occurrences considered in this report. A "mineral deposit" is "***a mineral occurrence of sufficient size and grade that it might, under the most favorable of circumstances, be considered to have economic potential," a necessary corollary being that drilling has tested the system in the third dimension to the point that a grade and tonnage can be assigned to the volume of rock with some level of confidence. An "ore deposit" is "***a mineral deposit that has been tested and is known to be of sufficient size, grade, and accessibility to be producible to yield a profit." The inclusion of the concept of "profit" in this description put forth by Cox and others (1986) and many others is somewhat unfortunate in that it leads to contradictions when applied to estimates of speculative resources present in a given area (H.G. Wilshire and J.E. Nielson, written commun., 1991). We certainly can envision that national needs might require extraction of some metals under circumstances that do not yield a financial profit to society as a whole or even to some segment of society. If we were to attempt some estimate of the numbers of a particular type of deposit either present in a region or present in a favorable area for that deposit, then all existing occurrences, regardless of size and prior mining history, would have to be treated as unknowns if either the grade or the tonnage at the site were not available

to us. An ore deposit is the economic, measured and demonstrated, identified-resource part of the resource-reserve classification scheme adopted by the U.S. Bureau of Mines and U.S. Geological Survey (1980). Furthermore, the grade and tonnage of an ore deposit is not necessarily the same as the "geologic resource" of the deposit. The "geologic resource" is the grade or tonnage of the mineralized volume of rock that has not been constrained by economic-limiting factors such as topography or site location; the mineralized volume of rock is commonly broken down by variable grades and includes the ore deposit itself (see Peters, 1978). The "reserves," either measured or indicated, are the demonstrated economic portion of the identified resources in a mineralized system (U.S. Bureau of Mines and U.S. Geological Survey, 1980). Additional categories of reserves can be based on the economics and (or) probability of their presence. As pointed out by Bailly (1981), five major factors are generally involved in determining whether or not a deposit becomes an economic reserve: (1) existence of the deposit, (2) extractability of the elements of value from the deposit, (3) availability of energy and materials for extraction of the elements of value, (4) acceptable environmental requirements, and (5) favorable economics for a potential mining operation at the site of the deposit. In the EMNSA, recent exploration activities have resulted in discovery of several gold-silver deposits for which both grade and tonnage data have not been released and are considered proprietary by the holder of the claims.

Mineral occurrences, mineral deposits, and ore deposits are classified further into various types on the basis of descriptive mineral-deposit models contained primarily in Cox and Singer (1986), as described previously in this report, but additional references to particular types of other deposits that are not contained in Cox and Singer (1986) are included throughout various sections below. These include gold-bearing breccia pipe, gold skarn, gold-silver quartz-pyrite veins, and several others. The mineral-deposit models are based on groups of mineral deposits that have in common both a relatively wide variety and a large number of attributes, as well as formation in a common geologic environment. Table 15 lists mineral occurrences identified in the EMNSA by model type and the appropriate references to descriptive models for these deposit types. Some deposit types assigned to a given category include a small number of occurrences and deposits that diverge widely from the age and mode of emplacement of the rest of that particular category. For example, although most gold-silver quartz-pyrite veins presumably are Mesozoic in age and are related to the mesothermal batholithic environment in the EMNSA, some deposits of different age and origin, such as those at the Telegraph Mine, also are included under this same category. Mineralization at the Telegraph Mine apparently is Tertiary in age and seems to be associated with wrench-fault-related tectonism (Lange, 1988). This category of gold-silver quartz-pyrite veins is not subdivided further in this report because the age and tectonic environment for the 79 gold-silver quartz-pyrite veins other than those at the Telegraph Mine is not well understood.

Grade-and-tonnage frequency-distribution models contain data on the shape of curves for grades and tonnages for groups of mineral deposits from which grades and (or) tonnages at various percentiles may be extracted. They are useful in numerical resource assessments (Singer, 1990, 1992, 1993; see also, Drew and others, 1986; Singer and Cox, 1988; Root and others, 1992; Brew and others, 1991) by providing information about the potential metal content of undiscovered deposits within a tract of land permissive for a given type or model, and they are used in economic analyses of these resources, provided that (1) estimates may be made with some confidence concerning the number of individual deposits that may be present within that given tract of land and, further, that (2) any undiscovered deposits would show grade and tonnages that are within the limits of the grades and tonnages of the ore-deposit model under consideration. Grade-and-tonnage models typically are frequency cumulations; grade is based on average grades of each metal or mineral commodity for an individual deposit, and the associated tonnage is based on the total of past production, reserves, and resources at the lowest possible cutoff grade (Singer, 1990). However, appropriate care must be exercised in the accumulation of data for a grade-and-tonnage model because the strong possibility of a significant distortion of the grade and (or) tonnage curves exists if one mixes unlike data such as production data for one group of deposits and geologic-resource data from another group of deposits of the same deposit type. In addition, data from geologically mixed populations of deposits can result in distorted grade-and-tonnage distribution curves. Furthermore, prior production data may be influenced heavily by topography in the general area of a deposit that is being exploited presently or has been exploited completely in the past, as well as by price supports during times of national crisis. A "geologic" resource and not an "economic" one, ideally, should make up the individual

grade-and-tonnage data points along the entire distribution curve of a grade-and-tonnage model. However, such information may not be available in the geologic literature for many mined-out deposits.

Grade-and-tonnage distribution models currently are usually developed simultaneously by many workers as part of the descriptive aspects of the models (Cox and Singer, 1986). When sufficient grade-and-tonnage data are available to build a model, the grade-and-tonnage data can help refine descriptive mineral-deposit models (Singer, 1990, 1993). Singer (1990, 1993) discussed in detail the formulation of grade-and-tonnage models and some of the problems associated with their development and use. With regard to the EMNSA, one major shortcoming of present grade-and-tonnage models involves the bulk mineable, volcanic-hosted gold-silver deposits (John and others, 1993) such as those present in the Castle Mountains. A lack of sufficient grade-and-tonnage data for these types of deposits at one time resulted in retention by Cox and Singer (1986) of an artificial division of volcanic-hosted deposits into Comstock (adularia-sericite), quartz-alunite (acid-sulfate), and hot-spring types, and all bulk mineable, volcanic-hosted gold-silver deposits classified as hot-spring deposits (D.A. Singer, oral commun., 1990). However, grade-and-tonnage models for hot-spring gold-silver deposits were derived subsequently by Berger and Singer (1992). In a genetic sense, hot-spring deposits are shallow-level end members of adularia-sericite and quartz-alunite deposits as described by Berger and Henley (1989), and, with continued discoveries of adularia-sericite and quartz-alunite mineralized systems, hot-spring deposits will probably cease to have a separate grade-and-tonnage model (John and others, 1993; see also Albino, 1994).

Delineation of Areas Permissive and Favorable For Undiscovered Metalliferous Mineral Resources

Several subsections that follow present the characteristics of various metalliferous-mineral deposits in the EMNSA and, in addition, delineate those areas where the geology is permissive for as-yet-undiscovered mineral occurrences. For many mineral occurrences identified in the EMNSA, notable characteristics are described and cited, and many well-known deposits of that particular type in the EMNSA are described in detail. Criteria used to delineate areas that may contain undiscovered occurrences are described, as well as the geologic characteristics of these areas. Two types of areas that may contain undiscovered mineral occurrences, permissive terranes and favorable tracts (Menzie and Singer, 1990), are delineated for many model types.

"Permissive terranes" are areas that might contain a certain type of mineral occurrence. Any geologic terrane in the EMNSA that is geologically similar to another terrane containing mineralization that generally formed at the same time as that geologic terrane is considered permissive for the same type of mineralization, whether or not any signs of mineralization are present. Some permissive areas are very broadly outlined because their geologic environments that are conducive to the hosting of mineral occurrences in the EMNSA are wide ranging. For some types of mineral systems, we cannot demonstrate that a particular type of mineral occurrence actually is present within an area shown as permissive for that occurrence type.

"Favorable tracts" are domains within permissive terranes that are known to contain some positive indications either that a mineralized system, generally irrespective of overall size or grade, is present or that mineralizing processes have occurred. For example, the presence of some known mined deposits and some mineral occurrences, of hydrothermal alteration known to be restricted to a certain type of mineralized system, and of plutons of an age and chemical signature that are associated with known mineralized systems elsewhere are all considered characteristics for the potential presence of that type of mineralized system in an area. Because positive indications that some type of ore-forming processes have occurred are required to designate an area as favorable for a certain type of mineralized system or mineral-deposit model, favorable tracts are commonly much smaller in areal extent than permissive areas and are more likely, in the judgment of the persons making the mineral evaluation, to contain undiscovered mineral resources of that model type. In all likelihood, many areas judged to be favorable have already been considered as such by exploration geologists in private industry. The absence of any recent discoveries of major mineral occurrences in those areas designated as favorable may be interpreted to indicate a diminished likelihood for the presence of any future additional discoveries of the mineral-occurrence model in question. However, many ore-deposit models are not being sought as viable targets at all times, and the complete history of exploration for the favorable areas outlined

is not available. Thus, numerical judgments concerning probabilities of discoveries in favorable areas versus probabilities of discoveries in the enclosing permissive terrane cannot be made.

Nonetheless, some mineral occurrences in the EMNSA have been judged to constitute an exception to the above-stated rules for delineating a favorable tract within a permissive terrane for a given type of deposit. As has been described, the quartz-molybdenite-vein occurrence at Globe Wash has been judged not to merit classification as being within a surrounding tract that is favorable for the presence of a large stockwork-molybdenum system or systems at depth. By definition, permissive terranes must include all favorable tracts. Thus, these definitions of permissive terrane and favorable tract constitute a two-fold classification that also has been followed in a study currently in preparation that deals with metallic mineral resources of Nevada (Ludington and others, 1993). Refinement of the outlined permissive terranes by deleting parts that can be confidently described as barren of a particular type of mineral occurrence (see Menzie and Singer, 1990) have not been attempted primarily because the needed complete exploration histories and results of detailed studies in the various mountain ranges of the EMNSA are not available.

The permissive-and-favorable classification scheme of mineral resources is not the only one in use. As pointed out by Gair (1989b), an assessment of the mineral-resource potential of an area is an evaluation of the possibility or likelihood that such resources are present in an area; the assessment may or may not include some quantitative measures of the probability of the presence of a given type of mineral occurrence. Gair (1989b) and his associates attached a subjective classification scheme for various degrees of favorability, such as high, moderate, low, and nil categories, for the presence of mineral resources. The permissive terranes and favorable tracts outlined below in the EMNSA are not qualified further because the information needed to differentiate confidently among the above-listed categories is lacking.

It is worth emphasizing again, however, that all positive indications of mineral occurrences were not available, even for those mineral-occurrence types known to be present throughout the EMNSA, primarily because of inherent conditions that severely limited data gathering for the present investigation. Furthermore, the permissive terranes and favorable tracts are presented only for some of the currently recognized ore-deposit models. These include, on the one hand, those that are described formally in the economic-geologic literature together with their grade-and-tonnage distributions and, on the other hand, some additional models that either have not been formally described or are in the process of being described (for example, porphyry gold; see Rytuba and Cox, 1991). Yet, some categories of mineral-occurrence models can provide viable exploration targets in certain permissive terranes. Descriptions by Hewett (1931) of sericitized, unoxidized gold- and pyrite-bearing porphyry at the Red Cloud Mine in the Goodsprings Mining District, Nev., located east of the EMNSA about 13 km from the California-Nevada state line, indicate that a porphyry-gold type of mineralized system should at least be considered as being permissive in intrusive rocks of similar age in the EMNSA. The methodology outlined above, however, cannot consider any types of mineral occurrences that are currently unrecognized as constituting a separate deposit type.

The two-fold permissive-terrane and favorable-tract land-classification scheme used herein for the various types of metal-bearing mineral models is somewhat analogous to the scheme adopted recently by the State of California, as exemplified in its Mineral Land Classification Diagram (fig. 91; also, D.O. Shumway, written commun., 1991). As the term “permissive terrane” is used, it includes both of their sections that are entitled “Areas of Identified Mineral Resource Significance” and “Areas of Undetermined Mineral Resource Significance” of the Mineral Land Classification Diagram. “Favorable tract” is roughly equivalent to their “Areas of Identified Mineral Resource Significance” and “Known Mineral Occurrence “ (MRZ–3a, fig. 91).

Geophysical methods described above in the section entitled “Geophysics” that estimate depth to bedrock in those parts of the EMNSA that are covered by valley-fill deposits were used to place limits on extension of permissive terranes and favorable tracts from the mountain ranges into the valleys. A 500-m depth-to-bedrock limit was used to bound the permissive terranes and (or) favorable tracts in the valleys where the bedrock is covered by mostly unconsolidated Tertiary and (or) Quaternary deposits (pl. 3). This depth limit is somewhat arbitrary (for comparison, a recently completed 1:1,000,000-scale state-wide assessment for Nevada used a 1 km depth limit; see Blakely and Jachens, 1990, 1991), but it is believed that extrapolation of bedrock to depths greater than 500 m is subject to such uncertainties in the EMNSA as to have no scientific merit at the

publication scale of our assessment (1:125,000). Also, under present economic conditions, blind exploration for mineral deposits only very rarely exceeds a depth of 200 m, although exploration may extend to much greater depths than this in areas of known mineralization or altered rocks and in areas where specific geophysical targets are calculated to be at great depths.

For evaluation of deposits hosted by Mesozoic and older rocks, a map showing isopachs or depth contours to Mesozoic bedrock was constructed using procedures described by Jachens and Moring (1990) and using some of the data they acquired for partly contiguous regions in Nevada. This isopach map was then modified to reflect the detailed geology available in those areas where lack of gravity stations resulted in a spurious placement of the 500-m-depth contour line (pl. 3). As described by Jachens and Moring (1990), several uncertainties are associated with these contours showing depths to Mesozoic and older bedrock, and the 500-m isopach probably is less accurate than the 1-km isopach for the Cenozoic basin fill used in the study of the entire state of Nevada (R.C. Jachens, oral commun., 1990). Thus, the extent of permissive terranes and favorable tracts buried beneath Cenozoic, nonmagnetic (that is, nonvolcanic) sequences of rock shown on figures 92 and 93 should be viewed with extreme caution and regarded only as estimates subject to further refinement as additional information becomes available. Because of this uncertainty, we show permissive terranes and favorable tracts only at the relatively small scales of figures 92 and 93.

Thickness of nonmagnetic, late Cenozoic basin fill also was semiquantitatively estimated using aeromagnetic data collected by the National Uranium Resource Evaluation (NURE) program over the EMNSA. The NURE data were collected along east-west flightlines flown approximately 5 km apart and 120 m above the ground. These data were analyzed using both qualitative and quantitative techniques by J.D. Hendricks to produce a map showing areas of shallow magnetic sources (approximately <1 km depth to magnetic source) in the EMNSA. The map showing shallow magnetic sources, when combined with the available geologic map (pl. 1) and depths to mostly Mesozoic and older basement rocks, allows separation of areas of thick (>0.5–1.0 km), nonmagnetic Cenozoic deposits (valley-fill sediments) from areas of shallow basin fill. Areas are thus outlined to show the subsurface extent of shallow basin fill and may be considered to be within terranes permissive for the presence of certain types of mineral occurrence on the basis of extrapolation of permissive terranes from adjacent exposed bedrock (pl. 3).

In the following discussion, mineral occurrences are separated by age into three groups: occurrences that may have formed during the Proterozoic, those that may have formed during the Mesozoic, and those that may have formed during the Cenozoic. Some mineral-occurrence types may have formed during both the Mesozoic and Cenozoic (such as mineralized faults and polymetallic-vein deposits). Such deposit types are discussed in detail only with the age group with which they are most closely allied, generally the Mesozoic. This custom was followed even though the characteristics of known deposits elsewhere in the Mesozoic and Cenozoic, as well as the distribution of permissive terranes and favorable tracts for these deposits in the EMNSA, may be somewhat different. In addition, the Proterozoic rare earth element ore deposits at Mountain Pass, which are associated with carbonatite and alkalic intrusions just outside the EMNSA and are currently (1995) in production, were discussed in some detail in the section above entitled “Ultrapotassic Rocks, Carbonatite, and Rare Earth Element Deposit, Mountain Pass, Southern California” and so are not discussed in the sections to follow. Furthermore, also near Mountain Pass on the east flank of the Clark Mountain Range but inside the EMNSA, a breccia-pipe-related gold deposit that was in production during 1993 is present at the Colosseum Mine. This latter mineral deposit is associated genetically with felsic intrusions. Rocks that are similar in age to both of these mineralized systems, Mountain Pass and the Colosseum, also are present elsewhere in the EMNSA.

Proterozoic Deposits

Carbonatite-Related, Rare Earth Element Occurrences

Known Occurrences

Although four occurrences in the EMNSA are assigned provisionally to carbonatite-related, REE-type systems (U.S. Bureau of Mines, 1990a, map nos. 48, 156, 351, and 358, pl. 1), only one of these, the Esperanza

Group of claims (map no. 156), is known definitely to be associated with carbonatite or related types of rock. The other three may owe their reported elevated abundances of REE to Early Proterozoic quartz-bearing pegmatite, and so they may not have the resource implications ascribed to them. In the general area of the Esperanza Group of claims, which apparently straddle the boundary of the EMNSA near Mineral Spring in the northeastern Ivanpah Mountains, small bodies of scarce carbonatite and related ultrapotassic rocks crop out in an area of possibly as much as 5 to 6 km^2.

Permissive Terrane

The geologic terrane in the EMNSA that is permissive for Middle Proterozoic, carbonatite-related REE deposits and (or) occurrences includes all areas underlain, shallowly or otherwise, by rocks that are Early Proterozoic in age (pl. 1; see also fig. 92).

Favorable Tract

One tract favorable for the presence of additional discoveries of carbonatite-related REE deposits in and just outside the EMNSA is delineated (fig. 92). This tract is elongated and aligned in a northwest-southeast direction; it extends from the general area of the Mountain Pass REE deposit on the northwest to the general area of the Esperanza Group of claims on the southeast. Criteria used to delineate the favorable-tract boundaries (listed in table 18) primarily reflect the known presence of REE-bearing carbonatite and ultrapotassic rocks in numerous exposures of small bodies throughout the area delineated. According to the U.S. Bureau of Land Management (1982), drilling in the southeasternmost part of this outlined area that is favorable for REE deposits has resulted in discovery of "substantial resources of rare earth and thorium mineralization." Hodges and Ludington (1991) estimated that 0, 0, 1, 1, and 2 undiscovered carbonatite deposits remain to be discovered, at 90, 50, 10, 5, and 1 percent probability levels, respectively. However, in light of the conclusions of the section above entitled "Ultrapotassic Rocks, Carbonatites, and Rare Earth Element Deposit, Mountain Pass, Southern California," it is highly probable that the grade-and-tonnage distribution curves used by Hodges and Ludington (1991) to establish their numerical estimates are inappropriate for any REE-bearing carbonatite bodies that might be present in the EMNSA near Mountain Pass and that might be similar petrologically to the carbonatite bodies there.

Other Types of Proterozoic Deposits

By Clay M. Conway and Ted G. Theodore

Volcanogenic Massive Sulfide Deposits in Arizona and Nevada

Massive sulfide deposits are known in the Early Proterozoic rocks of Arizona (Anderson and Guilbert, 1979; Donnelly and Conway, 1988), including several in western Arizona (Stensrud and More, 1980; Conway, 1986; Conway and others, 1986, 1990) that are within the Mojave crustal province (Wooden and others, 1988; Wooden and Miller, 1990). The massive sulfide deposits in western Arizona range in size from small deposits of 1.45 thousand tonnes to as much as 1.5 million tonnes of copper-zinc-lead ore. The larger deposits, such as those located around Bagdad, Arizona, are comparable to a median-sized Cyprus-type massive sulfide deposit, on the basis of compiled grades and tonnages from throughout the world (Singer and Mosier, 1986). In central Arizona, the Early Proterozoic United Verde deposit at Jerome is a large deposit of similar grade and tonnage to some of the largest deposits in the world (Singer and Mosier, 1986). The deposit at Jerome, however, is associated with a sequence of Early Proterozoic rocks different in age and lithology from those found in western Arizona and in the EMNSA.

Massive sulfide deposits are mainly of three types: (1) Cyprus-type deposits, found in marine mafic-volcanic settings that also contain an ophiolite assemblage; (2) Besshi-type deposits, found in sedimentary sequences that consist of clastic terrigenous rocks and tholeiitic to andesitic tuff; and (3) Kuroko-type deposits, associated with marine rhyolite and dacite and subordinate basalt and sedimentary rocks (Cox and Singer, 1986; see also Sangster, 1980). Exhalative silica deposits and chloritized footwall rocks are associated with many of the deposits (Franklin and others, 1981). At high grades of metamorphism, the chloritized footwall rocks are converted to other assemblages, which include cordierite and anthophyllite.

Volcanogenic Massive Sulfide Deposits in the East Mojave National Scenic Area

Although no volcanogenic massive sulfide deposits are known in EMNSA, certain features that are characteristic of these deposits have been described in the Mojave crustal province, which includes the EMNSA. For example, massive sulfide deposits of varying size, as well as scattered chloritized rocks in the Early Proterozoic gneisses of the Mojave crustal province in western Arizona, suggest that the analogous Proterozoic terrane in the EMNSA may contain more deposits of this type. In addition, possible protoliths for bimodal felsic-gneiss-amphibolite sequences in the Providence Mountains include volcanic rocks (Wooden and Miller, 1990), although these sequences subsequently have been interpreted to have mostly plutonic protoliths (D.M. Miller, oral commun., 1991). Furthermore, cordierite-anthophyllite rocks are reported as small pods in Early Proterozoic gneiss in the Old Woman Mountains, 25 km to the south of the EMNSA (Stoddard and Miller, 1990). Other occurrences of somewhat similar rocks are known farther to the west in the Tranverse Ranges of California (Powell, 1981). Howard and others (1988) suggested the possibility of volcanogenic mineralization of Early Proterozoic age at the Virginia May Mine, 95 km south of EMNSA in the Turtle Mountains. Recent work confirms the volcanogenic character of the ore deposits at the Virginia May Mine (C.M. Conway, unpub. data, 1993). These deposits are likely to be of the Kuroko type. DeWitt and others (1989) recognized features in the McCullough Range, 10 to 20 km northeast of the EMNSA, which suggests the potential for Besshi-type, sedimentary-hosted massive sulfide deposits.

No permissive terranes or favorable tracts for these types of deposit are delineated in the EMNSA, but at least some possibility of volcanogenic massive sulfide occurrences exists in the EMNSA.

Granite-Related Uranium, Thorium, and Rare Earth Element Deposits in Alaska and Elsewhere

The predominant ore mineral in those granitic rocks favorable for the presence of uranium deposits is uraninite (UO_2). Ballhorn (1989) recognized three types of granite worldwide that have been shown to host uranium deposits: (1) metaluminous anorogenic granite of alaskitic composition, exemplified by those at Rossing, Namibia, whose ore is related primarily to magmatic differentiation; (2) peraluminous granite, exemplified by the Mississippian to Permian, mostly two-mica granites in the Central Massif, France; and (3) alkaline granite, exemplified by the Jurassic granite at Bokan Mountain, Alaska. Uranium-enriched rocks associated with the latter two types of granite apparently are related to circulation of mostly subsolidus fluids. Nokleberg and others (1987) designated uranium-bearing granites in Alaska to be included within a felsic-plutonic type of deposit, and they described this deposit type as follows. Felsic-plutonic uranium deposits in Alaska consist of uranium minerals, thorium minerals, and REE minerals in fissure veins and disseminated in alkaline granite dikes in or along the margins of alkalic and peralkaline granitic plutons or in granitic plutons. The ore-forming environment is mainly in or along the margins of epizonal to mesozonal granitic plutons. Ore minerals in the deposits include allanite, thorite, uraninite, bastnaesite, monazite, uranothorianite, and xenotime, sometimes with galena and fluorite. Notable examples are the Roy Creek (Mount Prindle) deposit in east-central Alaska and the Bokan Mountain deposits in southeastern Alaska.

Granite-Related Uranium, Thorium, and Rare Earth Element Deposits in the East Mojave National Scenic Area

Certain Early and Middle Proterozoic granitic rocks in the EMNSA are notably enriched in large-ion-lithophile elements (LILE) and high-field-strength elements (HSFE), and they also include somewhat elevated abundances of U, Th, and REE (Miller and others, 1986; Wooden and Miller, 1990). Despite this enrichment, mineral occurrences containing these elements are rare, with the exception of the carbonatite at Mountain Pass. However, allanite-bearing pegmatites that intrude Early Proterozoic gneiss in the New York Mountains have Th and REE concentrations that are anomalous for this region (Miller and others, 1986). Because of these occurrences and the general enrichment in U, Th, and REE in the EMNSA, the potential for deposits associated with the granitic rocks needs to be evaluated. Jurassic granitoids are enriched in LILE and HSFE (Fox and Miller, 1990), and some of the following discussion pertains to rocks of this age.

Geochemical studies at mining-district scale of the levels of overall enrichment(s) of U in rock associated with granite-related uranium deposits provide a basis to which we may compare apparent U concentrations

found in the EMNSA by airborne radiometric surveys described in the section above entitled "Aerial Gamma-Ray Surveys." Maximum concentrations of fairly widespread U detected in the EMNSA are slightly over 5 ppm (fig. 35*C*). Most areas showing these highest concentrations of U contain exposures of Proterozoic rocks and, locally, Jurassic rocks. In a comparative study of U concentrations in both uranium-mineralized and barren, peraluminous two-mica granitoids, Friedrich and Cuney (1989) found that 62 unaltered samples of coarse-grained granite in the massif of St. Sylvestre in France had an average U content of 22 ppm and that 45 fine-grained unaltered samples contained an average U content of approximately 17 ppm. The St. Sylvestre granitoid massif contains a proved resource of 38,000 tonnes U. In marked contrast, 90 unaltered peraluminous granitoid samples from the barren Manaslu massif in Tibet contain an average content of 9 ppm U. Therefore, the 5-ppm-maximum U contents over broad regions of the EMNSA suggest that this province is not likely to contain significant granite-related U deposits. Ballhorn (1989) noted that approximately 90 percent of the outcrops sampled within terranes judged to be favorable for the three types of granite-related uranium deposits that he recognized showed concentrations of approximately 10 to 20 ppm U. Such large volumes of uranium-enriched rocks provide the source(s) of the uranium that may be subsequently leached and concentrated by oxidizing as well as CO_2 enriched, subsolidus fluids (Friedrich and Cuney, 1989).

The conclusions above do not preclude the possibility of the existence of some small, high-grade occurrences of uranium in certain areas in the EMNSA. Figure 85 shows the distribution of U concentrations in 1,050 samples analyzed from the EMNSA (U.S. Bureau of Mines, 1990a). The two highest concentrations of U found during this sampling program are 1,570 and 1,590 ppm, the former of which is from the polymetallic vein at the Mammoth Mine (U.S. Bureau of Mines, 1990a, map no. 3, pl. 1) and the latter of which is from the Esperanza Group of claims (U.S. Bureau of Mines, 1990a, map no. 156, pl. 1), both of which are clustered in the general area of carbonatite-related REE occurrences near Mineral Spring in the Ivanpah Mountains. Both highly uranium enriched occurrences yield significant responses when examined by hand-held scintillometers, and both occurrences are in areas showing widespread outcrops of Early Proterozoic rocks. In addition, the Esperanza Group of claims is within the favorable tract we delimit above for the presence of carbonatite-related REE deposits that extends from northwest of the REE deposits at Mountain Pass to the trace of the 500-m depth-to-basement contour southeast of Mineral Spring (fig. 92).

No permissive terranes and favorable tracts for granite-related uranium, thorium, and REE deposits are delineated in the EMNSA, because all of the Early and Middle Proterozoic rocks make up a permissive terrane for these types of deposits.

Vein Deposits and Skarn Deposits in the East Mojave National Scenic Area

As discussed in the section above entitled "Proterozoic Rocks and Their Mineralization," Hewett (1956) suggested that certain base- and precious-metal vein deposits in the area of the EMNSA might be of Proterozoic age. Preliminary investigations in an area east of the Albermarle Mine in the New York Mountains suggests the possibility that polymetallic veins there predate or, more likely, are the same age as Middle Proterozoic diabase dikes. The time of emplacement of many veins examined by us in Early Proterozic rocks of the EMNSA can only be constrained to postdate deformation of the foliated host rocks. Thus the possibility remains that some vein deposits might be as old as Early Proterozoic. Nothing has been noted in the literature or discovered during our reconnaissance field investigations of the Early Proterozoic rocks to suggest that many veins predated deformation or were formed during either of the orogenic events. The presence of a ductilely deformed metamorphic fabric in some polymetallic veins in the general area of Mineral Spring, Ivanpah Mountains, can be used as evidence to support emplacement during the Proterozoic, possibly during the Middle Proterozoic. The REE signature of these veins is similar to the REE signature of Middle Proterozoic ultrapotassic rocks at Mountain Pass (T.G. Theodore, unpub. data, 1993). Furthermore, polymetallic skarn at the Butcher Knife Mine, in Butcher Knife Canyon in the New York Mountains, also may be Proterozoic in age (Ntiamoah-Agyakwa, 1987).

Tungsten veins of Early Proterozoic age are an additional type of vein deposit that may be found in EMNSA, although occurrences of these deposits are not presently known in the ENMSA. The possibility of veins of this type in the EMNSA is based on the association of tungsten-bearing veins with Early Proterozoic two-mica granite in the Hualapai Mountains, Ariz., located some 50 km to the southeast of EMNSA. Tungsten

is present there as wolframite in veins. The 1,680- to 1,690-Ma two-mica granite in the Hualapai Mountains is considered to be part of the widespread, postorogenic Early Proterozoic granites (Chamberlain and Bowring, 1990; Conway and others, 1990) that crop out in western Arizona and southern California. They are alkali-calcic in composition and have associated deposits or contain anomalous concentrations of W, Sn, Be, Nb, La, and Y (Conway, 1991). These granites are also found in the region of EMNSA (Bender and others, 1988; Miller and Wooden, 1988; Anderson and others, 1993).

Platinum-Group-Element Occurrences Associated With Ultramafic Rocks in Nevada and Arizona

Small exposures of ultramafic rocks are reported in Early Proterozoic rocks in the McCullough Range northwest of the EMNSA, the New York Mountains, and elsewhere in Nevada and Arizona. Some of these exposures are associated with somewhat elevated abundances of platinum-group elements. Ultramafic rocks are known in nearby Early Proterozoic sequences in the Gold Butte area of southern Nevada (Volborth, 1962; Dexter and others, 1983), Lost Basin in northwestern Arizona (Page and others, 1986; Theodore and others, 1987a), and near Bagdad, Ariz. (Floyd Gray, oral commun., 1988; C.M. Conway, unpub. data, 1990). Anomalous concentrations of Pt were reported by Lechler (1988) at the Gingerload prospect in the Crescent Peak Mining District, Nev., which is located outside the EMNSA at the north edge of the New York Mountains, approximately 11 km north of Castle Peaks. In the Crescent Peak Mining District, a silicified Early Proterozoic granitoid has probably been mineralized by Cretaceous granite (D.M. Miller, written commun., 1991). The Gingerload prospect is a Pb-Zn-Cu-Ag-Au polymetallic vein (Lechler, 1988).

Platinum-Group-Element Occurrences Associated With Ultramafic Rocks in the East Mojave National Scenic Area

No platinum-group mineral occurrences are known in the EMNSA. Some small exposures of metamorphosed Early Proterozoic ultramafic rocks in the Ivanpah Mountains in the EMNSA contain as much as 22 weight percent MgO (Wooden and Miller, 1990). However, no platinum-group analyses of these rocks are available. Some potential for copper, cobalt, chromium, and platinum-group elements may be associated with such rocks in the EMNSA in Alaskan platinum-group-element-type or zoned-ultramafic, chromium-platinum-type occurrences (Page and Gray, 1986). These Early Proterozoic ultramafic rocks in the EMNSA should be studied geochemically to evaluate this potential.

Mesozoic Deposits

Breccia Pipe and Related Deposits

By Carroll Ann Hodges

Gold Breccia Pipe

The Colosseum Mine, in the Clark Mountain Mining District north of Mountain Pass (pl. 2), at one time was the largest gold producer within the EMNSA and, from 1987 to 1992, was the largest metals mine in operation. It produced about 2,188 kg Au and 938 kg Ag per year during peak years of operation. The Clark Mountain Mining District includes the Mountain Pass REE deposit, just outside the EMNSA boundary, as well as numerous abandoned copper, fluorite, and tungsten mines and prospects.

The Colosseum gold deposit, investigated in detail by Sharp (1984), is in a breccia-pipe complex that consists of two connected felsite breccia pipes and outlying felsite dikes in a horst block of Proterozoic younger undivided granitoids (unit Xg, pl. 1). The ore is primarily free gold that is disseminated at the micrometer scale in auriferous pyrite. Surrounding related mineralized rock includes vein silver-copper in brecciated dolostone, tungsten, and fluorite, described in the following sections entitled "Silver-Copper Brecciated Dolostone," "Tungsten Veins," and "Fluorite Veins." Production, initially begun in 1929, was shut down in 1939, but the mine was reopened in 1987 as an open-pit operation. According to the U.S. Bureau of Mines (1990a), ore reserves in 1989 were estimated at 9.5 million tonnes (t), averaging 1.94 g Au/t. About 7 years of mine life were left as of February, 1990, at a production rate of about 219 kg/yr and a gold price of $400/oz. The following descriptive summary of the deposit largely is modified from Sharp (1984).

Breccia-pipe gold has not been defined formally as a deposit type (Cox and Singer, 1986), and so characteristics of the Colosseum orebody cannot readily be compared with those of other deposits assigned to this specific type, although descriptions of some individual breccia-pipe gold deposits are available (Baker and Andrew, 1991). Sillitoe (1991) included the Colosseum deposit with six other breccia-pipe-hosted gold deposits he described. The overall range in contained gold in those seven gold-bearing breccia pipes is 9 to 101 tonnes Au, and their mean content of Au is about 44 tonnes. Thus, the Colosseum Mine, which has been shown to contain about 20 tonnes Au, is one of the smaller of such systems known.

The Clark Mountain Mining District is in the southernmost tip of the 800-km-long Cordilleran fold and thrust belt, active tectonically from Permian through Cretaceous time. Three major northwest-striking thrust faults transect the region and, together, account for a total west-to-east displacement of 64 to 80 km (Burchfiel and Davis, 1971). Hewett (1956) estimated that 7,000 to 10,000 m of Paleozoic sedimentary rocks originally were thrust over the Proterozoic granitoids that now constitute the horst block in which the breccia pipes are found (fig. 94). Thrusting was followed by normal faulting along the high-angle Clark Mountain and Ivanpah faults, which offset the region during basin-and-range deformation. Only about 500 m of Paleozoic carbonate rocks are exposed presently in the downdropped block to the west. The mineralized breccia pipes, dated at approximately 100 Ma (Sharp, 1984), were intruded after thrusting but before the normal faulting that produced the basin-and-range horst-and-graben structures during the late Tertiary, as interpreted by Sharp (1984).

The breccia pipes and associated felsite dikes, which are exposed as resistant knobs enclosed within the Proterozoic gneisses, are each about 170 by 235 m wide at the surface, elongated to the northeast-southwest, and connected by a narrow dike. The pipes represent multiphase brecciation events, including significant collapse, and the lithologies within them indicate the composition of the overlying Paleozoic sedimentary rocks and the height of stoping during the development of the breccia. Overlying rocks included the Cambrian Tapeats Sandstone, Cambrian Bright Angel Shale, and Late Cambrian to Devonian dolomite units (included in units Ꞓd and PDl). The Colosseum orebody is in the western pipe, but both pipes are mineralized. Each pipe consists of early felsite that is disrupted by later igneous breccia; however, the western pipe also contains abundant clasts of the structurally higher Paleozoic rocks that had been thrust over the Proterozoic rocks before onset of breccia-pipe emplacement. The abundance of sedimentary rocks as clasts indicates that the western pipe stoped through the Tapeats Sandstone and Bright Angel Shale, well into the overlying dolomite, whereas the eastern pipe, predominantly containing basement rocks and felsite igneous breccia, did not invade the Paleozoic sedimentary rocks significantly. Height above the current surface that was subjected to stoping was at least 430 to 460 m. Gold is disseminated in breccia and associated closely with pyrite, commonly filling fractures in pyrite. Highest concentrations of gold are in the western pipe where pyrite has replaced carbonate-breccia fragments, greatly increasing the overall concentration of sulfide minerals.

Metal zoning in this part of the Clark Mountain Mining District (fig. 95) is apparently related spatially and genetically to breccia-pipe mineralization. The gold zone is restricted to a circular area around the breccia pipes, in addition to a crescent-shaped area west of and bounded by the Clark Mountain fault. Within the breccia pipes, gold is associated mainly with sulfide minerals, primarily pyrite, whereas outside the pipes, gold is a constituent of quartz-barite and quartz-pyrite veins and veinlets that form a complex network surrounding felsite dikes. Silver is present predominantly in a broadly concentric zone west of, and bounded by, the Keystone thrust fault; the veins make up the Ivanpah Mining District, which had significant production into the early part of the 20th century. Tungsten is found predominantly in a broad northwest-trending belt, which intersects a part of the gold zone and is bounded on the west by the Clark Mountain fault. Field inspection of the regional distribution of tungsten veins suggests that some of the tungsten veins in the Proterozoic granitoids to the south-southeast of the Colosseum Mine may not be related to the emplacement of the gold-bearing breccia pipe at the mine (pl. 2), inasmuch as known tungsten veins are present in Proterozoic granitoids as much as 6.5 km southeast of the mine. Nonetheless, felsite dikes related to the emplacement of the breccia pipes extend from Clark Mountain to Mountain Pass, a distance of 11 km (Sharp, 1984). Within the gold zone, tungsten is present as wolframite and scheelite in Proterozoic rocks. Fluorite is in veins and shear zones associated with the Keystone and Mesquite Pass thrust faults west of the silver zone.

Sharp (1984) attributed these spatial relations to development of a single hydrothermal system, which was initially stacked vertically but was subsequently displaced by gravity gliding (detachment faulting) on the then-extant Keystone thrust fault and by high-angle normal faulting on the Clark Mountain fault. Epithermal-vein silver, originally closest to the surface in the system, is now horizontally juxtaposed with the deeper gold-rich breccia-pipe complex. Thus, the district zoning from west to east represents the displaced slices of once-vertical zones, the vein silver in the silver-copper brecciated-dolostone occurrences being found at the top (fig. 95). As will be described later in this section, scanning electron microscope (SEM) studies have established the presence of tungsten in ore at the Colosseum Mine, and the presence of tungsten apparently in distal parts of the mineralized system here can only be attributed to mobility of tungsten in a hydrothermal environment, as was documented by Bateman (1965) in some of the retrograde parts of the Pine Creek, California, tungsten-skarn system. Alternatively, the Colosseum Mine may represent the superposition of a Cretaceous gold breccia pipe onto an environment already enriched in tungsten during a previous episode of tungsten mineralization.

Felsite, dated at 99.8±4 to 102±4 Ma, is the oldest rock in the breccia pipe (K-Ar dates by Geochron Laboratories, *as quoted* in Sharp, 1984) and consists of equal parts of quartz, K-feldspar, and sericite, plus secondary siderite; carbonate content is about 6 volume percent. The second phase of intrusion caused brecciation of the felsite, producing the igneous breccia that consists mainly of felsite matrix and minor quartzite, granite, gneiss, and andesite clasts. A third phase occurred in the western pipe, producing collapse-rubble breccia that is the most intensely mineralized rock type of the entire breccia-pipe complex. Dolomite breccia fragments are replaced by disseminated pyrite and are accompanied by sphalerite, siderite, and chalcopyrite that hosts gold and silver. As of 1984, commercial values of disseminated gold had been found as deep as 170 m below the surface.

The breccia pipes appear to have been emplaced by fluidization, carbon dioxide being the dominant fluidizing agent (Sharp, 1984). Carbonate content increases with each stage of fluidization and intrusion (6 volume percent in the felsite, 20 volume percent in the igneous breccia, and 30 volume percent in the rubble breccia), indicating that increasing amounts of carbonate rocks were assimilated by the intrusion and incorporated into the breccias as they reached progressively higher levels of stoping into the Late Cambrian to Devonian dolomites. Fluid-inclusion studies of a 751-m-deep drill hole into the breccia-pipe complex indicated that the lower 250 m of the drill hole is dominated by CO_2-rich fluids (Cook and others, 1992). These studies also suggested that the minimum lithostatic trapping pressures required to yield the observed fluid-inclusion relations range from 2.1 to 3.1 kilobars (kb). These pressures correspond to paleodepths of 7.9 to 11.7 km at the time of emplacement of the breccia-pipe complex, and they are remarkably consistent with the overburden estimated by Hewett (1956) at the time of breccia-pipe development.

Gold mineralization in the breccia pipes is present in an irregular vertical cylinder surrounding a barren core (Sharp, 1984). Depth of oxidation is about 100 m, and degree of oxidation is about 80 percent. Supergene enrichment, however, is of no mineralogic or economic importance. The barren core in the interior of the rubble-breccia pipe is devoid of gold but contains minor to major amounts of pyrite, zinc, and copper in well-silicified impervious rocks. Late gold-bearing fluids were unable to percolate through this impermeable unit to reach the favored sulfide sites for gold deposition. Gold content varies directly with depth, and gold is commonly alloyed with silver (as electrum) as fracture fillings in pyrite or along grain boundaries. According to Sharp (1984), Au/Ag ratios averaged 1.5 to 1, in marked contrast to the Au/Ag ratios found in the surrounding vein deposits (see following section entitled “Silver-Copper Brecciated Dolostone”). Gangue minerals, in order of decreasing abundance, are siderite, goethite, quartz, and sericite. Pyrite is the most susceptible host for precipitation of gold, apparently because of its ease of fracturing (Sharp, 1984).

The four principal vein types in the ore at the Colosseum Mine are quartz-pyrite, quartz-barite, calcite-barite, and calcite-dolomite, in addition to occasional veins of unknown source and genetic significance that contain lead, antimony, tungsten, and zinc, as well as minor silver. According to Sharp (1984), mineral paragenesis and sequence of events took place in the following stages: (1) early, coarse-grained, barren pyrite and minor quartz; (2) coarse-grained, second-stage pyrite that has gold, chalcopyrite, sphalerite, bornite(?), and pyrrhotite; (3) shattering and fracturing of coarse-grained pyrite; (4) major phase of gold mineralization, which filled fractures and interstices in pyrite, accompanied by apparently stable sphalerite, chalcopyrite, and galena;

(5) fine-grained, barren pyrite; (6) siderite replacement and flooding of the breccia matrix; and (7) localized veining by quartz and fine-grained pyrite. Gold is disseminated throughout the deposit; electrum mineralization was later paragenetically than the main-stage sulfide mineralization and its accompanying major amounts of gold.

Two examples of gold included in pyrite were identified in SEM micrographs, which were obtained from one polished thin section of felsite breccia from the Colosseum Mine (fig. 96*A*,*B*,*D*), and also were verified by an X-ray spectrogram (fig. 96*C*) . The largest grain of gold (about 7–8 μm; see fig. 96*B*) was clearly deposited along a fracture and possibly represents the major gold-mineralizing phase (stage 4) of Sharp's (1984) paragenetic sequence. The smaller grain (about 4 μm; see fig. 96*D*) may represent the second phase (Sharp's (1984) stage 2) of included gold associated with pyrrhotite. Examination by SEM also revealed grains of monazite and other rare earth element minerals that have been localized in cracks between euhedral pyrite crystals (figs. 96*E*,*F*). Additional minerals identified within pyrite include the following: small grains of wolframite (fig. 96*A*); bismuth and silver tellurides (fig. 96*G*); possibly resorbed chalcopyrite, pyrrhotite, and sphalerite (fig. 96*H*); and sphalerite that has small euhedral pyrite inclusions and conspicuous replacement rim of covellite surrounded by feldspar (fig. 96*I*). The relation shown in figure 96*A* seems to confirm the genetic gold-tungsten association in the ore-forming system at the Colosseum Mine.

Silver-Copper Brecciated Dolostone

Silver veins in the Clark Mountain Mining District are categorized as silver-copper brecciated dolostone; they are peripheral to the gold breccia pipes of the Colosseum orebody which was emplaced in Proterozoic rocks to the east of the silver veins (pl. 2). The veins are restricted to Late Cambrian to Devonian dolomite, which was downdropped to the west from its earlier overthrust position above the Proterozoic rocks (pl. 1).

According to the U.S. Bureau of Mines (1990a), the veins are present in fractured, sheared, and brecciated zones in gray-yellow dolostone. Ore mineralization is reported as stromeyerite (ideally, $(CuAg)_2S$) in pods and blebs that contain minor azurite and malachite, and a gangue of calcite-dolomite and quartz (Hewett, 1956). Most individual vein systems strike northwestward and dip steeply to the northeast. More than $4 million in silver was produced from the Clark Mountain Mining District in the late 1800s, primarily from the Beatrice, Monitor, Stonewall, and Lizzie Bullock Mines (Sharp, 1984); production from the Monitor Mine continued until 1942.

The U.S. Bureau of Mines (1990a) analyzed 92 samples from the silver-copper brecciated-dolostone deposits. Maximum Ag content was 3,080 ppm; maximum Au, 946 ppb. In 32 samples, Cu content was well over 1,000 ppm, and was greater than 10,000 ppm in 11 of them. Forty-seven samples contained more than 1 ppb Au and more than 1 ppm Ag; the average Ag/Au ratio was 4,660, which is notably high and contrasts with the Ag/Au ratio of approximately 0.67 at the Colosseum gold deposit. Zinc content was greater than 10,000 ppm in only three samples and greater than 1,000 ppm in 18 samples. Lead content was greater than 10,000 ppm in four samples and was 1,000 ppm or greater in 32 samples.

Sharp (1984) developed an intriguing hypothesis for the origin of the Ivanpah silver deposits, relating them genetically to the gold mineralization of the Colosseum breccia pipe. By this hypothesis, silver-bearing hydrothermal fluids accompanying the felsite breccias rose through the Proterozoic granitoid rocks, in which the gold orebodies are now present, into the overthrust Paleozoic sedimentary rocks. The fluids stoped upward well into the Cambrian to Devonian dolomite units; height of stoping is demonstrated by the presence of abundant carbonate fragments within the Colosseum breccia pipe. Mesothermal gold mineralization is richest in this pipe because of selective massive replacement of carbonate minerals by sulfide minerals. Epithermal-vein silver, however, emplaced in the overlying dolomite, was subsequently downdropped to the west along high-angle normal fault(s) and low-angle detachment fault(s) during a postmineralization extensional event localized along a preexisting thrust plane. Thus, the breccia pipe was effectively decapitated, juxtaposing the silver-copper occurrences in the dolomite on the west with the gold mineralization in lower parts of the pipe to the east (fig. 97). The mineral zoning and fault pattern as described by Sharp (1984) fit this explanation.

Although not exact analogues, the silver-copper deposits in the Ivanpah Mining District exhibit some characteristics of polymetallic-vein and polymetallic-replacement occurrences, which generally are related to

felsic igneous intrusions (Cox and Singer, 1986). They are particularly common in areas of high permeability, such as breccia veins and pipes, and may form replacement bodies in carbonate rocks. It seems unlikely that economic, large-tonnage deposits of a type similar to the silver veins of the Ivanpah Mining District will be discovered in the EMNSA.

Tungsten Veins

Tungsten is present in veins and skarns within the EMNSA. Veins are primarily in Proterozoic schist and gneiss and are localized in a northwest-trending belt south of and overlapping the gold and silver zones of the Colosseum breccia pipes (fig. 95*B*). Other small occurrences are present in presumed 70-Ma Cretaceous monzogranites, mostly in the Signal Hill Mining District near the south end of the Piute Range (area VI, fig. 92). Tungsten veins in the Signal Hill Mining District may be significantly younger than those associated with the ores at the Colosseum Mine. According to the U.S. Bureau of Mines (1990a), the Mojave Tungsten Mine, south of the Colosseum Mine, produced 29,090 kg of 60 percent WO_3 concentrates in 1915 and 1916; elsewhere, production has been minor or nil, although one sample (from the Old Boy prospect, lat 35°00′ N., long 115°02′ W.) analyzed by the U.S. Bureau of Mines (1990a) contains 2.59 weight percent W.

Tungsten veins in both the Ivanpah-Colosseum Mining District and the Cretaceous intrusive bodies farther south are in fault and shear zones that strike generally to the northwest. Tungsten mineralized rocks consist mainly of wolframite in vein quartz; scheelite is present in some veins. At the Mojave Mine, gold, silver, pyrite, azurite, and malachite, in a gangue of quartz and subsidiary calcite, are accessory to the iron-manganese and calcium tungstates. Limonite is common in some veins. Consistent detection of tungsten in veins within the Late Cambrian to Devonian dolomites, as well as in quartz veins of the Proterozoic granitoids, prompted extension of the tungsten zone around the Colosseum breccia pipes west of the Keystone thrust fault and Clark Mountain fault (fig. 95; Sharp, 1984).

Sharp (1984) concluded that the tungsten mineralization surrounding the Colosseum Mine was genetically related to the breccia-pipe complex. Tungsten was deposited in a zone both vertically and laterally intermediate between mesothermal gold and epithermal silver.

The descriptive model of tungsten veins by Cox and Bagby (1986) fits closely with characteristics of the tungsten veins in the EMNSA. Such deposits typically contain wolframite and base-metal sulfide minerals in quartz veins associated with granitoid rocks emplaced in sedimentary or metamorphic rocks. The deposits consist generally of swarms of parallel veins. Grade-and-tonnage models that are based on data from 16 deposits worldwide indicate that a 90 percent chance exists for any new discovery to contain at least 45,000 tonnes of ore, as well as a 90 percent chance that any newly discovered deposit will have a grade of as much as 0.6 percent WO_3, whereas only a 10 percent chance apparently exists for a new deposit to contain as much as 7,000,000 tonnes of ore (Jones and Menzie, 1986a).

Fluorite Veins

Fluorite veins are present at scattered localities in the EMNSA, most notably throughout the entire Clark Mountain Mining District (Sharp, 1984) where the mineralization is in low-angle shears and fractures parallel to the Keystone and Mesquite Pass thrust fault zones (fig. 95). In this northernmost part of the EMNSA, veins commonly contain varying amounts of pyrite, copper-carbonate minerals, silver, and tungsten, all of which are associated also with the Colosseum breccia-pipe gold mineralization. Because fluorite is much more broadly distributed than the mineralized zones adjacent to the breccia pipes, it is not clear that the fluorite is related genetically.

According to the U.S. Bureau of Mines (1990a), minor fluorite production occurred only at the Pacific and Juniper Mines, and no production has taken place since 1961. At the Pacific Mine, about 3.2 km southwest of the Colosseum orebody, fluorite is concentrated in zones as much as 2 m wide along low-angle, north-striking, west-dipping faults that crop out within Late Cambrian to Devonian dolomites. It also is present in high-angle shear zones together with quartz, sericite, limonite, stibnite, and copper minerals. Analyses of 11 samples showed metal contents as high as 122,000 ppm Sb, 367 ppm Mo, 592 ppm Ag, 190 ppm W, and 56,300 ppm Zn. One sample contained 3.07 weight percent Cu and 26.1 weight percent Pb; three others contained 3.68,

3.94, and 5.26 weight percent fluorine. The U.S. Bureau of Mines (1990a) concluded from these analyses that significant resources exist at the Pacific Mine. At the Juniper Mine, about 1.6 km south of the Pacific Mine, massive purple and green fluorite is present in sheared, brecciated zones 2 m thick or more within surrounding carbonate rocks. The zones are partly silicified, showing minor amounts of limonite and copper carbonate minerals. On the basis of sample analyses, the U.S. Bureau of Mines (1990a) estimated resources of approximately 272,000 tonnes (t) containing 20 to 30 weight percent fluorite, 3 weight percent Cu, and 312 g Ag/t. The fluorite veins at both the Pacific and Juniper Mines are associated with polymetallic veins, as are a number of fluorite prospects in the area. Scattered fluorite veins also are present in shear zones in Proterozoic granite gneiss near the Albemarle Mine in the northeast corner of the EMNSA in the Castle Peaks Wilderness Study Area (Miller and others, 1986). Production was insignificant from these veins, but 15 analyzed samples ranged from 1 to 5.9 weight percent fluorine (U.S. Bureau of Mines, 1990a). Miller and others (1986) did not identify any potential for resources in the general area of the Albemarle Mine. In addition, fluorite veins are present in dolomite near the contact with the informally named Mid Hills adamellite of Beckerman and others (1982), which is associated with the Big Hunch stockwork-molybdenum system in the southern New York Mountains (pl. 2). Select samples of mineralized Mid Hills adamellite in the general area of the Giant Ledge Mine (U.S. Bureau of Mines, 1990a, map no. 296, pl. 1) show flooding by fluorite to as much as 20 volume percent. Polymetallic veins that cut the Mid Hills adamellite at this locality in Caruthers Canyon also show assemblages of galena, chalcopyrite, quartz, pyrite, fluorite, and white mica. In the southern Providence Mountains, the Golden Nugget prospect includes blue and green fluorite veins in association with quartz and polymetallic veins in fault- and shear-breccia zones. Production from this prospect has been nil, but of 111 samples analyzed by the U.S. Bureau of Mines (1990a), 15 contained 100 to 620 ppm Pb, 25 contained 26 to 600 ppm Zn, 89 contained 20 to 990 ppm Cu, 56 contained 6 to 270 ppm Mo, 61 contained trace to 88 g Au/t, 59 contained trace to 44 g Ag/t, and 7 chip samples contained 0.08 to 25 weight percent fluorine. If the Golden Nugget prospect is developed for other metals, fluorite could be a possible by-product. However, most ore deposits of hydrothermal fluorspar veins and mantos contain more than 35 volume percent fluorite (Worl and others, 1973).

No descriptive or grade-and-tonnage model exists for fluorite veins (Cox and Singer, 1986). If, however, future production of fluorite in the EMNSA is contingent upon development of associated polymetallic veins, the probability is not high that large-tonnage economic orebodies of that type remain to be discovered in the EMNSA.

Known Occurrences

The only known occurrence of gold-bearing breccia pipes is at the Colosseum Mine. Silver-copper brecciated dolostone is present in a broad area, generally west of the orebodies at the Colosseum Mine, within Paleozoic rock sequences (pl. 1). The silver-copper brecciated-dolostone mineralization, which presumably developed at the same time as the orebodies at the Colosseum Mine were emplaced, forms a halo of petrogenetically linked deposits. Tungsten veins are present in Proterozoic granitoids in and around the general area of gold ores at the Colosseum Mine (pl. 2); most are presumably linked to the emplacement of the gold-bearing breccia pipe (Sharp, 1984) but some may not be related to the pipe development during the Cretaceous. In addition, scattered occurrences of tungsten veins are found elsewhere in the EMNSA, including widespread veins in the Signal Hill Mining District near the south end of the Piute Range (pl. 2) and minor occurrences hosted by the Mid Hills adamellite. Vein-type fluorite is associated with the Colosseum breccia pipes and is present in Paleozoic sequences of carbonate rocks west of the Colosseum Mine (pl. 2).

Permissive Terrane and Favorable Tract

A permissive terrane and a favorable tract for gold-bearing breccia pipes are largely coextensive and are defined in the northern part of the EMNSA by the outer limit of silver-copper brecciated-dolostone occurrences in Paleozoic rocks and the outer limit of tungsten veins in Proterozoic younger granitoids (pl. 2; see also fig. 92). The terrane outlined for gold-bearing breccia pipes also is shown as being both permissive and favorable for tungsten veins, as is another small area near the south end of the Piute Range (fig. 92). Hodges

and Ludington (1991) estimated that one tungsten-vein deposit, at a 1 percent probability level, remains to be discovered in the EMNSA at a size and grade comparable to the grade-and-tonnage model for these types of deposit.

No permissive terranes or favorable tracts specifically for silver-copper brecciated dolostones or fluorite veins are delineated in the EMNSA. Because silver-copper brecciated dolostones are probably related to Mesozoic magmatism, the common presence of Mesozoic igneous rocks in the EMNSA makes all carbonate sequences exposed there permissive hosts, which are largely coextensive with the permissive terranes discussed below for skarn.

Geologic factors controlling ore deposition at the Colosseum gold mine include the presence of Proterozoic crystalline host rocks overlain by reactive carbonate sequences at the time of emplacement of a CO_2-rich magmatic-hydrothermal system during the Cretaceous (fig. 97). Exposure of the mesothermal gold-bearing ores adjacent to the epithermal-silver veins was dependent on a complex sequence of tectonic and erosional events (Sharp, 1984). The vein silver is the downfaulted top of the Clark Mountain breccia-pipe system, emplaced adjacent to the Colosseum ore zone as a result of relative vertical uplift and tilting of the Proterozoic basement. This was then followed by detachment faulting that decapitated the breccia pipe and juxtaposed the vertically stacked precious-metal zones. The western breccia pipe was particularly favorable to ore mineralization because it stoped high into Late Cambrian to Devonian limestones and includes large volumes of carbonate fragments within the breccia. This reactive rock type was susceptible to replacement by pyrite, whose low strength and brittle character resulted in fracturing in response to continued brittle-style strain, thereby providing a receptive host for late gold-mineralizing fluids (Sharp, 1984).

Low-Fluorine Porphyry-Molybdenum Deposits

Classification of the Deposits

The Big Hunch stockwork-molybdenum system in the southwestern part of the New York Mountains in the EMNSA is one of a number of molybdenum deposits and molybdenum-enriched systems that are associated with Jurassic to Pliocene calc-alkaline magmatic arcs in the western North America Cordillera (this section of the report is modified from Theodore and others, 1992). In addition, several molybdenum-enriched porphyry systems of Paleozoic age (Schmidt, 1978) and presumed Paleozoic age (Ayuso and Shank, 1983) crop out in eastern North America and bear many similarities to the calc-alkaline ones in western North America. Such stockwork-molybdenum systems generally have low fluorine contents relative to deposits of the better known Climax-type molybdenum deposits in Colorado (Theodore and Menzie, 1984). The fluorine-deficient porphyry-molybdenum systems have been included in different ways in the several classifications of porphyry-molybdenum deposits (Woodcock and Hollister, 1978; Sillitoe, 1980; Mutschler and others, 1981; White and others, 1981; Cox and Singer, 1986; Carten and others, 1993). Guilbert and Park (1986) considered the low-fluorine stockwork-molybdenite deposits as a subset of porphyry base-metal systems. The one striking characteristic of all these systems is their minor-element signature, especially when compared to the better known stockwork-molybdenum systems exemplified by the one at Climax, Colo. (see for example, Westra and Keith, 1981; White and others, 1981; Carten and others, 1993). Thompson (1982b), in a further modification of the classification scheme for stockwork-molybdenum deposits, suggested that alkali-calcic and the alkali stockwork-molybdenum deposits of Westra and Keith (1981) be subdivided into a monzonite-syenite subtype and into a leucogranite subtype. The Climax-type systems are characterized by highly differentiated, high-silica rhyolite magmas that are enriched in F (locally as much as 2–3 weight percent), Nb, Rb, Mo, Sn, and W and are nearly depleted in Cu and Sr (Ludington, 1981). The Climax-type systems are present in rifted cratons, whereas the low-fluorine or quartz-monzonite type of systems are related to geologic processes associated with continental margins.

Fluorine-deficient porphyry-molybdenum systems generally show overall F contents of less than 0.1 weight percent, and many of these systems also include significant concentrations of Cu and Ag (Czehura, 1983); some include significant W and Au (Theodore and Menzie, 1984; Theodore and others, 1992). At Buckingham, Nev., gold skarns at the Surprise Mine and at the Carissa Mine probably are temporally and genetically related

to the Buckingham stockwork-molybdenum system (Schmidt and others, 1988). Westra and Keith (1981, fig. 9) showed a continuity of hypogene copper and molybdenum grades between porphyry-copper deposits and fluorine-deficient porphyry-molybdenum deposits.

Fluorine-deficient porphyry-molybdenum systems, which are widespread throughout the geologic provinces of the North American Cordillera, are present in magmatic arcs that generally parallel the Mesozoic batholiths. In the Basin and Range Province, several Late Cretaceous fluorine-deficient porphyry-molybdenum deposits in Nevada (for example, Buckingham or Hall) and many other prospects are related to small granitic bodies peripheral to the Sierra Nevada batholith. These prospects include the Magruder Mountain (Sylvania), Nev., and, in the EMNSA, the Big Hunch, California, systems, both of which may have been emplaced sometime in the Mesozoic.

Big Hunch Stockwork-Molybdenum System

The Big Hunch stockwork-molybdenum system is an extremely large system that at one time was inferred to encompass approximately 1.63 billion tonnes of mineralized rock that has an estimated grade of approximately 0.025 weight percent Mo (U.S. Bureau of Land Management, 1980; most of this section of the report is modified from Ntiamoah-Agyakwa, 1987). However, recently completed evaluations of this system suggest that the volume of significantly mineralized rock is about 43,000,000 tonnes (Wetzel and others, 1992). Nonetheless, mineralized rock at the surface here is widespread, and the main center of alteration associated with this system is the area of the Big Hunch Mine (pl. 2). A second center east of the Lighthouse Mine (also known as the Dorr Tungsten Mine; see also U.S. Bureau of Mines, 1990a, map no. 291, pl. 1) is much less strongly developed. The best developed alteration zones are silicic, phyllic (quartz-sericite), and argillic. No propylitic stage of alteration has been observed. A questionable potassic stage is poorly represented by an erratic, apparently relict, K-feldspar stable assemblage found in one vein. Intensity of silicification declines away from the core of the system, and concentrations of sericite and clay minerals increase successively. Ore mineralogy is simple, consisting chiefly of pyrite, chalcopyrite, sphalerite, galena, and molybdenite and minor amounts of magnetite, specularite, bornite, and wolframite-heubnerite. Two samples of diamond drill core from DDH York no. 9, which was drilled into the core of the Big Hunch system, were taken from depths of approximately 68 m below the surface and examined by SEM. The purpose of this examination was to determine the mineral phase(s) that hosts most of the silver in the system. Silver was not detected during any spot analyses of the polished surfaces. However, it was determined that many of the quartz-molybdenite veins in the Big Hunch system also contain tetrahedrite, as well as some minor amounts of galena as minute blebs in stout crystals of pyrite. None of the tetrahedrite was found to contain detectable silver, which is common in the tetrahedrite present in many low-fluorine stockwork-molybdenum systems elsewhere (Theodore and Menzie, 1984). In places, tetrahedrite seems to predate paragenetically the crystallization of minor amounts of sphalerite. In addition, some tetrahedrite in close proximity to chalcopyrite shows notable concentrations of As and some Zn. Growth zones of tetrahedrite against quartz suggest that some of the earliest crystallized tetrahedrite is more arsenian than the latest crystallized varieties. Fluorite is ubiquitous. Although the presence of fluorite in the Big Hunch system suggests highly elevated concentrations of fluorine during the metallogenesis here, the overall abundance of fluorine in these types of systems is still less than that found in the much higher grade, rift-related Climax-type systems (White and others, 1981; Westra and Keith, 1981; Theodore and Menzie, 1984; Carten and others, 1993).

The surficial and vertical extent of the Big Hunch system was established by Ntiamoah-Agyakwa (1987) from surface mapping on a scale of 1:4,800, as well as data from over 2,000 m of drill cores representing nine drill holes. All holes were drilled from the surface and went through the mineralized zones. The Big Hunch system is semielliptical, a hook-shaped (pseudoannular) compound system made up of two nested concentric patterns about 3.2 by 4 km. The larger outer system is incomplete, thought at one time by Ntiamoah-Agyakwa (1987) to be cut off on the west by the Cliff Canyon fault, but phyllic alteration associated with the Big Hunch system has since been determined to extend well beyond the trace of the Cliff Canyon fault (D.M. Miller, oral commun., 1993). On the north, the Big Hunch system appears to be bounded by an east-northeast-striking fault (pl. 1). The exposed vertical extent of the system is about 250 m, from 5,700 ft (1,737 m) to 6,500 ft (1,981 m) in elevation.

In the Big Hunch stockwork-molybdenum system, quartz-sericite or phyllic alteration is not only the most conspicuous but also the best developed alteration product in the informally named Mid Hills adamellite of Beckerman and others (1982) (unit Kmh, pl. 1), which hosts the system (Ntiamoah-Agyakwa, 1987). This type of alteration is characterized by a preponderance of quartz veins that have sericite selvages. Pyrite is not ubiquitous in this alteration; fluorite is commonly present. Muscovite is characteristically coarse grained. Development of the quartz-sericite veins apparently took place during three episodes, the second of which seems to have been the episode during which the bulk of the molybdenite was introduced. The second episode of quartz veining also involved intense hydroxyl metasomatism. Clay minerals and fine-grained hydrothermal quartz are replaced by quartz veins. This second-generation quartz is massive, compact, milky quartz. In most cases, veining is episodic, resulting in rhythmic bands of quartz and sulfide minerals and (or) oxide minerals. In its most advanced stage, silicification is the most destructive event, obliterating most of the earlier stages of alteration. In areas where development stages can be traced, such as at Lecyr Well, alteration proceeds from closely spaced fractures to quartz veins that have sericite selvages. Influx of altering fluids depended on either the extent of fracturing or permeability of the initially argillized host. Where extensive microfracturing preceeded fluid influx, the result is near complete silicification. Fluorite, molybdenite, or pyrite may accompany this second stage. Locally, sparse orthoclase-microcline veins developed, as is described later in this section.

Although the geochemistry of the Big Hunch stockwork-molybdenum system has been described by Ntiamoah-Agyakwa (1987) and the U.S. Bureau of Mines (1990a), additional analyses of 36 rocks in the general area of the system are included in this report (table 19). Analyses show the overall intensity of fluorine metasomatism (as fluorite and micas mostly in veins) and the sporadic intensity of molybdenum introduction. Furthermore, the large number of samples that show F abundances greater than 1,000 ppm, together with their locations throughout an area of approximately 5 km^2, emphasize that the emplacement of this system during the Late Cretaceous has affected significantly a very large volume of rocks.

Potassic alteration is either very weakly developed or absent throughout much of the Big Hunch system, in contrast to the extent of potassic alteration at other stockwork-molybdenum systems (Ntiamoah-Agyakwa, 1987). Secondary biotite was noted only in a 1-m-long section in one drill hole. Here, it is poorly developed at a depth of about 3 m as a thin vein about 0.1 mm wide. Pervasive argillic alteration is crosscut by 1- to 2-mm-wide sericite veinlets and 0.1-mm-wide, fine-grained, amorphous biotite microveins. Biotite in the original porphyritic to equigranular adamellite is in varying stages of degradation. Primary magmatic orthoclase is still preserved, however, which is suggestive of intermediate argillic-alteration assemblages.

No correlation has been made at the regional scale between density of deposits or nearby mineral occurrences and intensity or overall volume of metal introduced. As described above, the subeconomic (at 1994 market conditions) Big Hunch stockwork-molybdenum system hosts one of the largest concentrations of metal known to date (1995) in the EMNSA. However, the grade of this type of molybdenum system is the limiting factor that results in many of such systems in the western North American Cordillera being economically marginal. Nonetheless, some zoning of types of veins is present peripheral to the Big Hunch system. As pointed out by Ntiamoah-Agyakwa (1987), some of the more important polymetallic-vein occurrences in the general area of the Big Hunch System include Lighthouse (Dorr?) (copper-tungsten), Giant Ledge (lead-copper, with silver), and Sagamore (copper-lead, with zinc, silver, and tungsten); smaller prospects include Garvanza (copper-tungsten), Hard Cash (copper-zinc-fluorine, with tungsten?), Lecyr Well (copper, with zinc-molybdenum?), and Live Oak (copper-zinc, with tungsten). Thus, this area of the New York Mountains was classified by Ntiamoah-Agyakwa (1987) as a polymetallic molybdenum-copper-tungsten porphyry center that has varying amounts of silver, lead, and zinc in its surrounding veins.

Potassium-argon ages were obtained by Ntiamoah-Agyakwa (1987) on six samples spatially and (or) temporally associated with emplacement of the Big Hunch stockwork-molybdenum system. The six ages cluster into two groups, 67 to 71 Ma and 59 to 66 Ma; the short time interval between the two clusters suggested to Ntiamoah-Agyakwa (1987) that all dated samples are part of one continuous process during the Late Cretaceous magmatic event associated with emplacement of the Mid Hills adamellite. However, U-Pb data for zircons from the Mid Hills adamellite indicate that the rocks crystallized about 93 Ma (E. DeWitt, oral commun., 1985). The Late Cretaceous ages ascribed by Ntiamoah-Agyakwa (1987) to the alteration associated

with the Big Hunch system in the area of Fourth of July Canyon have been verified by others (69 to 88 Ma on biotite, Beckerman and others, 1982; 69 Ma on biotite in sericitized rocks, D.M. Miller, written commun., 1991). Thus, either the polyphase emplacement of the Mid Hills adamellite took place over approximately 25 m.y. or the alteration and emplacement of the Big Hunch system was related to a Late Cretaceous hydrothermal event that was discrete from emplacement and crystallization of the major part of the Mid Hills adamellite.

Known Occurrences

The presence of molybdenum in the general area of the New York Mountains has been known since the 1950s (Ntiamoah-Agyakwa, 1987), and, nearby, relatively small veins have achieved some production of note in the general area of the Big Hunch system. As indicated by the maps showing the classification of deposit types in the EMNSA (pl. 2), in fact only a small number of vein-type occurrences are known in the general area of the Big Hunch system. The petrogenetic linkage of polymetallic veins and other types of deposits to low-fluorine, porphyry-molybdenum systems is indicated schematically on figure 89. It cannot be precluded that linkages exist elsewhere in the EMNSA, but outside the general area of the Big Hunch system, such as between polymetallic veins and some buried porphyry-molybdenum system. A corollary from this schematic linkage is the fact that one does not need to observe enhanced abundances of Mo and F to indicate the possible presence of a porphyry-molybdenum system at depth, although F and Mo anomalies might be additional positive signatures. A number of samples analyzed from polymetallic veins in the EMNSA by the U.S. Bureau of Mines (1990a) were shown to include more than 500 ppm Mo. The pervasive character of veining, fractures, and alteration patterns, if present, are the diagnostic features that one must first consider before making a qualified judgment about the potential presence of a porphyry system, either a molybdenum or a copper-molybdenum one.

Permissive Terrane

One terrane is delineated as being permissive for stockwork-molybdenum systems in the EMNSA (fig. 92). This terrane follows generally the inferred and mapped outline of the informally named Mid Hills adamellite of Beckerman and others (1982). As such, the localities of possible stockwork-molybdenum mineralization at Globe Canyon, described above in the section entitled “Delineation of Areas Permissive and Favorable for Undiscovered Metalliferous Mineral Resources,” also are included within this permissive terrrane. The mineralization at Globe Canyon apparently is associated spatially with two small outliers of the Mid Hills adamellite that crop out approximately 0.5 km south of the main mass of the body (pl. 1). The mineralized rocks at Globe Canyon are categorized as being the possible site of a low-fluorine stockwork-molybdenum system (pl. 2). Jurassic plutonic rocks are excluded from the permissive terrane for stockwork-molybdenum systems primarily because most contain relatively reduced contents of silica relative to those stockwork-molybdenum systems known elsewhere in the western North American Cordillera. The Jurassic plutonic rocks in the EMNSA as a group are apparently not that highly evolved, and Westra and Keith (1981) showed that nearly all host intrusions for low-fluorine types of stockwork-molybdenum systems are apparently peraluminous, regardless of silica content. However, some of the least altered igneous rocks associated genetically with the Buckingham stockwork-molybdenum system, Nevada, are slightly metaluminous (Theodore and others, 1992). In addition, all Cretaceous plutons other than the Mid Hills adamellite are excluded because of either their low-silica chemical composition or the absence of a widespread composite mode of emplacement. The informally named Rock Spring monzodiorite of Beckerman and others (1982) (Krs) generally has an overall low silica content (54–64 weight percent) compared with igneous rocks that are associated with most of these types of molybdenum systems; the rocks are essentially porphyritic and compositionally variable, including mostly monzodiorite, quartz monzodiorite, and some quartz monzonite (pl. 1). Estimates of 0 to 3 kb pressures of emplacement for the Teutonia batholith by Anderson and others (1988, 1992) were obtained from the Kessler Springs adamellite (Kks), the Mid Hills adamellite, and the Rock Spring monzodiorite, all informally named units of Beckerman and others (1982). The 3-kb pressures of the Rock Spring monzodiorite suggest that its currently exposed levels may be well below those depths commonly ascribed to most porphyry systems, both molybdenum and copper-

molybdenum, in the Southwest, which are generally less than about 1.5 kb. The Kessler Springs adamellite is seemingly shallow seated (0–0.5 kb, Andersen and others, 1992), but it apparently shows minimal evidence of a wide-ranging, composite nature for its emplacement mode, as does the phase of the batholith represented by the informally named Teutonia adamellite of Beckerman and others (1982) (Kt) (D.M. Miller, oral commun., 1991).

Favorable Tract

A relatively small area in the general area of the Big Hunch system is delineated as being favorable for the presence of stockwork-molybdenum systems (fig. 92). The general area of Globe Canyon is not considered to be a favorable tract, which reflects the judgment that the occurrences there should not be ranked as equivalent to those at the Big Hunch system. Hodges and Ludington (1991) estimated that one low-fluorine porphyry-molybdenum system, at a probability level of 1 percent, remains to be discovered in the EMNSA.

Porphyry Copper and Skarn-Related Porphyry Copper

Known Occurrences

No known occurrences of porphyry-copper systems or skarn-related porphyry-copper systems, as defined by Cox and Singer (1986), are known in the EMNSA. In the exposed upper parts of many of these systems, the rocks commonly are intensely fractured and altered to various combinations of potassic, phyllic, intermediate-argillic, argillic, and advanced-argillic assemblages across widespread areas, sometimes as much as 20 to 30 km^2. Many systems include quartz-stockwork veins that also are commonly widespread, as well as distinctive pyritic halos, together with elevated abundances of many metals. Many of these features are shared with stockwork-molybdenum systems, and these features are present in the general area of the Big Hunch system. In addition, the porphyry-copper and the skarn-related porphyry-copper systems would show the same genetic relations to other types of mineral occurrences depicted for the stockwork-molybdenum systems (fig. 89). In the general region of the EMNSA, porphyry-copper systems have been inferred to be present in the area of Turquoise Mountain, 5 km north of the EMNSA, in the hills near Halloran Spring (Hall, 1972), as well as in the Crescent Peak Mining District, about 10 km northeast of the EMNSA in Nevada (D.M. Miller, oral commun., 1991). North of the Horse Hills, near the southern end of the Providence Mountains, Miller and others (1985) assigned a low potential for the presence of a gold-rich porphyry-copper system in iron-oxide-stained Jurassic igneous rocks. However, field examinations for the present report did not reveal the presence there of widespread altered and shattered rocks that are typical of the upper parts of many of these types of porphyry systems. In addition, the exposed iron oxide minerals appear to be related to mineralized dilational fractures that opened in response to displacements along the regionally extensive Bighorn fault about 3 km to the east. Finally, examination of about 10 thin-sectioned rocks from this area failed to show the presence of any alteration phenomena that are characteristic of these systems.

Permissive Terranes and Favorable Tract

All of the EMNSA that is underlain by Mesozoic igneous rocks is permissive for the presence of porphyry-copper systems. The areas where these igneous rocks are near or in contact with sequences of Paleozoic carbonate rocks also are permissive for the presence of skarn-related porphyry-copper systems. Excluding alteration associated with the Big Hunch system, the most likely porphyry-style alteration of igneous rocks noted during the study is in the general area of New Trail Canyon, in the northeastern part of the Ivanpah Mountains. Here, some outliers of the informally named Ivanpah granite of Beckerman and others (1982) (unit Ji, pl. 1), which crop out away from its major exposures farther south in the Ivanpah Mountains, are intensely fractured, iron stained, and hydrothermally altered across several square kilometers. The outlined favorable tract for porphyry-copper and skarn-related porphyry-copper systems (fig. 93) coincides with one of the tracts also classified as favorable for the occurrence of various other types of skarn and polymetallic replacement occurrences in the EMNSA. Hodges and Ludington (1991) estimated that one porphyry-copper deposit at each of the 5 and 1 percent probability levels remains to be discovered in the EMNSA.

Skarn

Smirnov (1976) suggested that classification of skarns be based on the composition of the original protolith of the skarn, either calcareous, magnesian, or silicate. However, the nongenetic definition of skarn proposed by Einaudi and others (1981) is followed in this report:

> *** replacement of carbonate [or other sedimentary or igneous rocks] by Ca-Fe-Mg-Mn silicates [resulting from] (1) metamorphic recrystallization of silica-carbonate rocks, (2) local exchange of components between unlike lithologies during high-grade regional or contact metamorphism, (3) local exchange at high temperatures of components between magmas and carbonate rocks, and (4) large-scale transfer of components over a broad temperature range between hydrothermal fluids *** and predominantly carbonate rocks.

Most metallized skarns owe their genesis to processes largely involving the fourth classification. Thus, we follow an overall classification of skarns that is based on their sought-after metal content (see also, Zharikov, 1970; Shimazaki, 1981).

Known Occurrences

Known metallized skarns in the EMNSA are classified into the following types, the number of each shown in parentheses: polymetallic (18), zinc-lead (6), tungsten (3), iron (10), tin-tungsten (1), and copper (26) (table 14). Almost all skarns apparently formed during emplacement of either Jurassic or Cretaceous magmas into the carbonate sequences of Paleozoic rocks that crop out in the EMNSA (pl. 1). A small number of relatively minor occurrences of skarn in the New York Mountains may be Proterozoic in age. Examination of the regional distribution of the types of skarn in the EMNSA suggests that no readily apparent clustering by type of skarn is evident in the immediate area of any particular type of granitoid body. Jurassic granitoids, however, seem to be associated preferentially with some of the largest and highest grade iron-skarn deposits in the EMNSA, such as those at the Vulcan Iron Mine (pl. 2). Skarns are distributed widely across most exposed carbonate sequences of rocks in the EMNSA (pl. 2). Some of the most conspicuous skarns in the EMNSA are at the following locations: (1) along the west flank of the Clark Mountain Range in the general area of the Mohawk and Copper World Mines, presumably Cretaceous in age; (2) in the Ivanpah Mountains in the general area of the Evening Star Mine and Standard Mine No. 2 and along the east edge of Striped Mountain, presumably Jurassic in age; (3) near the central Providence Mountains at the Vulcan Iron Mine, Jurassic in age; and (4) in the general area of Cowhole Mountain, Little Cowhole Mountain, and Old Dad Mountain (pl. 2).

Of the 197 rock samples analyzed by the U.S. Bureau of Mines (1990a) that contain greater than 500 ppb Au, 36 are from mineralized skarns of all types in the EMNSA. This particular database does not include rocks from the area of the Providence Mountains, which has been shown to host six skarn occurrences (pl. 2). Nonetheless, a small number of samples in the RASS and PLUTO heavy-mineral-concentrate and rocks databases obtained from the Providence Mountains show anomalous concentrations of Au (figs. 57, 58). All skarns, regardless of type, in the EMNSA can thus be characterized as being potential sites for the deposition of at least some gold, in significant concentrations in some places. The highest concentration of Au reported by the U.S. Bureau of Mines (1990a, map no. 163) is from copper skarn at the New Trail Mine (pl. 6) in the Ivanpah Mountains (51,700 ppb Au). In addition, our limited sample base collected during this study (tables 10, 11) includes a small number of samples from five occurrences of mineralized skarn in the EMNSA (Evening Star, Copper King, Vulcan Iron, Mohawk, and Copper World Mines). Four samples from the Evening Star Mine area show Au contents that range from 26 to 450 ppb (table 11, analysis nos. 1–4). The highest recorded Au content from the Mohawk Mine area is 42 ppb in four select samples (analysis no. 72) and from the Vulcan Iron Mine is 150 ppb (analysis no. 7). The highest content of Au found at the Vulcan Iron Mine is in marble less than 0.5 m beyond the magnetite front, suggesting a buildup of precious-metal content at the fringes of this iron-skarn system.

The geologic environments of gold-bearing skarn worldwide were examined by Ray and others (1990), Ray and Webster (1990), and Theodore and others (1992). Korobeinikov (1991) listed the following criteria for granitoid intrusions that are associated with productive gold-bearing skarns, mostly in the Soviet Union: (1) Na predominating over K by approximately 1 to 2 weight percent; (2) high Cl/F ratios in the evolved fluids; and (3)

wide-ranging gold-bearing contact zones in the surrounding hornfels, marbles, and magnesian skarns.

As recognized by Meinert (1983, 1988a,b, 1989, 1993), many deposits referred to as gold skarns in the literature have been classified, or could be classified, under skarn-deposit models as copper and iron skarns by their dominant base- or ferrous-metal contents. For these deposits, gold production may be considered a by-product of base- or ferrous-metal mining. Furthermore, gold-bearing skarn deposits commonly may be gradational into skarn that contains no gold but does contain significant other metal(s), including the silver-rich skarns as defined by Ray and others (1986), possibly sediment-hosted disseminated gold-silver deposits (also known as carbonate-hosted and Carlin-type), porphyry-copper or copper-molybdenum deposits, or polymetallic-replacement deposits (exemplified by the McCoy megasystem, Nevada), as well as other deposit types related to felsic- and (or) intermediate-composition plutonic emplacement or volcanic activity. Mineralized skarns show genetic linkages to a wide variety of deposit types, of which some linkages are well established by geologic relations in the EMNSA (fig. 89). The Cove deposit, McCoy Mining District, Nev., which has been shown to include proven and probable reserves of 48.7 million tonnes (t) with an average grade of 1.85 g Au/t and 87.1 g Ag/t (Kuyper and others, 1991), has been classified recently by Cox and Singer (1990) as a distal disseminated silver-gold deposit. Polymetallic veins, the most common type of deposit in the EMNSA, are another deposit type that may be present on the fringes of gold-bearing skarn deposits (pl. 2; see also table 12). Other commodities produced by gold-bearing skarns include silver, copper, zinc, iron, lead, arsenic, bismuth, tungsten, and tin, as principal or by-product commodities, and cobalt, cadmium, and sulfur, as by-products (Theodore and others, 1991).

Gold-bearing skarns are generally calcic exoskarns that have gold associated with intense retrograde hydrosilicate alteration, although gold-bearing magnesian skarns are known and in some areas are dominant. Some economically significant gold-bearing skarns, however, are partly in endoskarn (Knopf, 1913; Pardee and Schrader, 1933) (for example, Hedley, British Columbia, 2.986 million tonnes at 13.46 g Au/t, Theodore and others, 1991; Suian, South Korea, 0.53 million tonnes at 13.0 g Au/t, Theodore and others, 1991). Significant concentrations of gold-bearing endoskarn also are present at the Nambija, Ecuador, gold-skarn deposit (McKelvey and Hammarstrom, 1991). Gold-bearing skarns can show diverse geometric relations to genetically associated intrusive rocks and nearby premetallization structures (Theodore and others, 1992). Similar relations are present in some of the skarns in the EMNSA that have been shown to contain some gold.

Permissive Terranes and Favorable Tracts

Permissive terranes and favorable tracts for the presence of metallized skarn of all types, including gold-bearing skarn, are considered to be coextensive and to include all exposed areas of Paleozoic carbonate sequences in the EMNSA (fig. 93). In addition, some small parts of the Proterozoic rocks also may be permissive for the presence of mineralized skarn, especially in the New York Mountains, where a single favorable tract, mostly including Paleozoic carbonate strata, is shown. This favorable tract also is coextensive with the permissive terrane for metallized skarn in this area. On figure 93, a favorable tract for iron skarn is delineated, primarily on the basis of magnetic anomalies in the general area of the Vulcan Iron Mine in the Providence Mountains; in addition, the presence of magnetite-bearing skarn at two localities, the BC prospect and the Adams-Ikes Hope prospect, both in the Colton Hills, are categorized as being permissive for the presence of additional iron-skarn occurrences (Goldfarb and others, 1988). However, the amplitude of the magnetic anomaly in the general area of these latter two occurrences, about 2,000 nanoTeslas, is somewhat lower than that in the general area of the Vulcan Iron Mine, and Jurassic igneous rocks in the general area of the two prospects have a high magnetic susceptibility (Goldfarb and others, 1988). An extensive permissive terrane for iron skarn in the general area of Old Dad Mountain is delineated on the basis of wide-ranging positive magnetic anomalies that extend well into areas covered by unconsolidated gravels (fig. 93).

In established mining districts in the EMNSA that are zoned from mostly proximal, copper-dominant deposits to distal, precious-metal- and base-metal-dominant veins, all stratigraphic sequences favorable for development of skarn in the zone of precious-metal deposits should be considered as permissive hosts for development of gold-bearing skarn. One area in the EMNSA that seems to show some of these zonal relations between a copper-enriched part and a lead-zinc-enriched part is the general setting of the Mohawk and Copper

World Mines in the southwestern part of the Clark Mountain Range. In another area, a gold-copper-iron zone is distal to the iron skarn at the Vulcan Iron Mine in the Providence Mountains (Goldfarb and others, 1988). In addition, Ray (1990) and Ray and Webster (1990) included the Jurassic arc-related rocks in the EMNSA as being favorable hosts for the development of gold skarns.

Gold placers in regions permissive for the formation of skarn also may be suggestive of the presence of gold skarn (R.G. Russell, written commun., 1989), especially if the placer gold is intergrown with bismuth minerals, including bismuth oxides or bismuth tellurides (Theodore and others, 1987b; Theodore and others, 1989). However, only nine placer localities in the EMNSA show the presence of visible free gold (table 15). Even in some of the most heavily mineralized areas of the EMNSA, such as the northern parts of the Providence Mountains (pl. 2), only a small number of placer operations are developed in drainages whose upper reaches head in the heavily mineralized areas (Moyle and others, 1986).

Anomalous values of Bi, Te, As, Se, and Co, on the one hand, are useful geochemical signatures for some gold-bearing skarns (Brooks and Meinert, 1989). However, some economically important gold skarns are notably deficient in Bi, As, and Te (McKelvey and Hammarstrom, 1991).

Hodges and Ludington (1991) estimated that the following numbers of various types of skarn deposit remain to be discovered in the EMNSA at the ensuing probability levels (--, not determined):

Probability level-----90%	50%	10%	5%	1%
Deposit type	*Number of deposits*			
Copper skarn----------1	2	4	--	--
Lead-zinc skarn-------0	1	2	5	7
Iron skarn ----------0	0	1	3	5

Polymetallic Replacement, Distal Disseminated Gold-Silver, and Vein Magnesite

Known Occurrences

Twenty-three polymetallic-replacement deposits, one distal disseminated gold-silver occurrence, and one vein-magnesite occurrence are known in the EMNSA (table 15; see also pl. 2). Most polymetallic-replacement deposits are in the western part of the Clark Mountain Range where some are present distal to well-developed lead-zinc skarn at the Mohawk Mine. Another notable concentration of polymetallic-replacement deposits is near the south end of the Mescal Range, an area that was being evaluated for its mineral potential by private industry in 1991. Only one occurrence (U.S. Bureau of Mines, 1990a, map no. 161, pl. 1) in the Ivanpah Mountains has been classified tentatively as belonging to a distal-disseminated gold-silver type of occurrence, and it is described as a pyrite-bearing, iron-oxide-stained jasperoid developed in dolomite. The magnesite-vein occurrence is present in the New Trail Canyon area of the Ivanpah Mountains (fig. 98), near the copper and iron skarns at the New Trail Mine. These latter mineral occurrences are just to the north of a large mass of the informally named, Jurassic Ivanpah granite of Beckerman and others (1982) (unit Ji, pl. 1), which is a porphyritic monzogranite, and so mineralization is presumably Jurassic in age in the general area of New Trail Canyon.

Polymetallic-replacement deposits as classified and analyzed in Cox and Singer (1986) showed median tonnages of 1.8 million tonnes, and median grades of 5.2 weight percent Pb, 3.9 weight percent Zn, and approximately 0.1 weight percent Cu.

Permissive Terranes and Favorable Tracts

All areas of the EMNSA that are underlain by Paleozoic carbonate rocks are designated to be permissive for the presence of polymetallic-replacement deposits, distal-disseminated gold-silver occurrences, and magnesite-vein occurrences (fig. 93). As such, the areas so designated are coextensive with those that we consider to be permissive for the presence of various types of skarn. However, available data are not refined to the point that we can confidently discriminate favorable tracts for polymetallic replacement within the outlined permissive

terrane. Figure 89 depicts graphically the genetic linkages among all these deposits. Hodges and Ludington (1991) estimated that one polymetallic-replacement district remains to be discovered in the EMNSA at each of the 5 and 1 percent probability levels.

Polymetallic Vein, Polymetallic Fault, and Gold-Silver Quartz-Pyrite Vein

Known Occurrences

At least 206 polymetallic-vein occurrences, 79 polymetallic faults, and 80 occurrences classified as gold-silver quartz pyrite veins are known in the EMNSA (table 15; pl. 2). All three types of occurrences are essentially cogenetic. The major differences between the polymetallic-vein occurrences and the gold-silver quartz-pyrite veins are differences in the relative amounts of galena, sphalerite, and chalcopyrite. Polymetallic veins generally show high concentrations of all these minerals, even though they may have been exploited primarily for their precious metals. One of the most economically significant concentrations of polymetallic veins in the EMNSA apparently is at the Morning Star Mine (pl. 2; U.S. Bureau of Mines, 1990a, map no. 178, pl. 1). Mining operations at the Morning Star Mine were placed on standby during 1991, although gold continued to be produced from a 1.8-million-tonne heap-leach pad at the property (Keith Jones, Vanderbilt Gold Corp., oral commun., 1991). Some ore apparently was shipped in 1992 from polymetallic veins at the Golden Quail Mine (pl. 2; see also U.S. Bureau of Mines, 1990a, map no. 417, pl. 1), which was reported to contain 12,500 kg Au (Wetzel and others, 1992); operations at the Golden Quail Mine were suspended in 1993. As noted by Ausburn (1988) and Sheets and others (1989), proven reserves at the Morning Star Mine in 1988 included about 7.26 million tonnes (t) of ore at a grade of 1.88 g Au/t. The deposit is hosted by the informally named, Jurassic Ivanpah granite of Beckerman and others (1982) (unit Ji, pl. 1) and primarily is present along the hanging wall of a low-angle thrust fault related to the Mesozoic thrust belt (Burchfiel and Davis, 1971; Sheets and others, 1989). Early-stage quartz-carbonate veins in the deposit include pyrite, sericite, hematite, ilmenite, galena, electrum, chalcopyrite, sphalerite, and tetrahedrite (Sheets and others, 1988, 1989, 1990). According to these authors, mineralization at the Morning Star Mine appears to be associated spatially and genetically with metamorphic fluids. In addition, textural relations suggest that primary electrum was deposited and then remobilized by secondary supergene fluids (Sheets and others, 1995). The tonnage of the mineralized system at the Morning Star Mine is larger than any of the deposits used in the base-metal-silver category of polymetallic veins plotted by Bliss and Cox (1986). As pointed out by Bliss and Cox (1986), apparently two types of polymetallic veins are known: (1) base-metal-silver veins and (2) gold-silver polymetallic veins that contain significant concentrations of Cu, Pb, and Zn. The Morning Star deposit probably belongs to the latter of these two categories. Some major mining districts elsewhere that show significant production from gold-bearing polymetallic vein have been described by Morris (1990), Fisher (1990), Shawe (1990), and Thompson (1990).

The gold-silver quartz-pyrite veins in the EMNSA typically do not show visible presence of galena, sphalerite, or chalcopyrite, and, as such, they commonly have low contents of Pb, Zn, and Cu. The classification scheme adopted during study of the EMNSA for those occurrences that were not examined in the field and that do not report presence of galena, sphalerite, or chalcopyrite involved use of available analyses of mineralized rock reported by the U.S. Bureau of Mines (1990a). Those mineralized-vein samples reported to contain in excess of several hundred ppm Pb, Zn, or Cu were included with the polymetallic veins. Analyses are available for 97 mineralized rock samples from the sites of 47 gold-silver quartz-pyrite veins in the EMNSA (table 20). In these 97 rock samples, average contents are approximately 1,800 ppb Au, approximately 7 ppm Ag, 17 ppm As, 3 ppm Sb, and approximately 100 ppm Zn; Ag/Au ratios are approximately 4. The apparently low average contents of Sb in these veins probably are a reflection of emplacement of most of these veins in a mesothermal, base-metal-deficient environment, although Sb can be present in fairly large concentrations in some deep-seated geologic environments (Berger, 1993). The polymetallic veins seem generally to contain more As and Sb (fig. 86). The strongest elemental association of Au in these 97 rock samples is for Ag; calculation of Spearman's correlation coefficient yields a value of +0.4. Some gold-silver quartz-pyrite veins in the EMNSA may be Tertiary in age and epithermal rather than mesothermal (Lange, 1988). No grade-and-tonnage models are

available for gold-silver quartz-pyrite veins in the EMNSA. These types of veins in the EMNSA most likely are analogous to the gold-silver polymetallic veins of Bliss and Cox (1986). However, preliminary compilations by Bliss and Cox (1986) did not yield an adequate grade-and-tonnage sampling of gold-silver polymetallic veins, and they, therefore, present no plots showing their cumulative frequency distributions for grade and tonnage. Some gold-bearing quartz veins elsewhere bear some similarities to the gold-silver quartz-pyrite veins delineated in the EMNSA. Gair (1989a), in a comprehensive evaluation of the mineral resources of the Charlotte $1° \times 2°$ quadrangle, North Carolina and South Carolina, described some gold-quartz and gold-pyrite-quartz veins there that were important sources of gold from about 1825 to 1910. As pointed out by Gair (1989a), the gold-quartz and gold-pyrite-quartz veins he studied are epigenetic fissure fillings, many of which crosscut the foliation in the enclosing schists and gneisses. Many veins are in the upper parts of apparently subvolcanic intrusions, and some of the gold grades in the mined veins apparently were as much as 344 g Au/t, but probably grades of 9.4 to 15.6 g Au/t were more typical at some of the more significant deposits (Gair, 1989a).

Polymetallic faults are mostly brittle-type gouge and fracture zones along structures of variable regional importance. Such mineralized fault zones typically do not include a silicate-gangue mineralogy common to veins; quartz is not reported. Most of the brittle-type polymetallic faults in the EMNSA were exploited some time in the past primarily along their near-surface traces of gouge. Elsewhere, Wallace and Morris (1986) documented the highly variable geometric relations between gouge and the trace of the associated fault zones (fig. 99). Most importantly, however, these authors showed the complex geometry that some mineralized faults may attain at relatively great depths below the present erosion surface (fig. 100). Similar relations also may be found at some future time along the seemingly geometrically simple East Providence fault in the EMNSA (pl. 1). Some mineralized strands of the East Providence fault may be as complex at depth as those depicted in the Coeur d'Alene Mining District, Idaho, by Wallace and Morris (1986) and, in fact, to this date (1995) have not been deciphered properly to show the massive fluid-flow patterns suggested by the presence of many small mineral occurrences in the general area of the fault.

All three types of mineralized occurrences may be related spatially and genetically to mineralized skarn, polymetallic-replacement deposits, and any centers of porphyry-type mineralization. Distribution patterns of polymetallic veins and gold-silver quartz-pyrite veins were examined in the EMNSA to determine whether or not their distribution may, in places, have followed the proximal-to-distal copper-gold (silver)-lead (zinc) zonation recognized in many porphyry-type metallization centers elsewhere in the Southwest. However, the spatial relations between these two types of vein occurrence in the EMNSA seem to be highly erratic (pl. 2).

Permissive Terranes and Favorable Tracts

All areas of the EMNSA that mostly include outcrops of Proterozoic, Paleozoic, and Mesozoic rocks (including both igneous and sedimentary protoliths) are designated to be permissive for the presence of Mesozoic polymetallic veins, polymetallic faults, and gold-silver quartz-pyrite veins (pl. 1). Favorable tracts within the outlined permissive terranes could not be delineated on the basis of data available. Hodges and Ludington (1991) estimated that 3, 8, and 20 polymetallic-vein deposits, respectively, at 90, 50, and 10 percent probability levels, comparable to those in the published grade-and-tonnage curves (Bliss and Cox, 1986), remain to be discovered. No grade-and-tonnage models are available for the gold-silver quartz-pyrite vein or the polymetallic-fault occurrences.

Tertiary Deposits

By James J. Rytuba and Robert J. Miller

Volcanic-Hosted Epithermal-Gold Deposits

Known Occurrences

Tertiary volcanic rocks in the Castle Mountains, located near the California-Nevada border, hosted one of the largest mineable reserves of gold in southern California (pl. 2). These gold deposits are located in the easternmost part of the EMNSA and are economically the most important Tertiary deposits in the EMNSA. Development drilling in the Hart Mining District by Viceroy Gold Corporation from the mid-1980s

to the present (1993) delineated six individual orebodies in the southernmost part of the Castle Mountains (Linder, 1989). Total combined reserves were 34 million tonnes of ore containing more than 62,500 kg Au. Commercial production at Castle Mountains Mine by Viceroy began in April, 1992, and, in its first six months, approximately 1,600 kg Au had been produced (The Northern Miner, 1993, v. 79, p. 14). The volcanic-hosted gold deposits in the Hart Mining District are similar to other economically important volcanic-hosted deposits being mined in Nevada, such as Rawhide and Round Mountain; the latter, which has reserves of over 312,500 kg Au, is the largest volcanic-hosted deposit in the United States. The large tonnage and grade of these orebodies makes them amenable to open-pit and heap-leach methods, and this class of deposits constitutes a significant component of gold reserves in the United States. Gold was first located in the Hart Mining District in 1907 (Ausburn, 1991).

Similar-age middle Miocene volcanic rocks are present elsewhere in and west of the EMNSA, and, in the vicinity of the cities of Mojave and Lancaster, California, several rhyolite dome complexes host economically important gold deposits that were being mined in 1993. These deposits are characterized by widespread acid-sulfate and argillic alteration. Closely associated in time and space with these gold deposits is the largest borate deposit in North America at Boron, California, which formed from hot-spring systems that were active during volcanism. These hot springs vented into basins developed peripheral to the volcanic-dome field. On the basis of this association, a model for the gold deposits in the Hart Mining District must include the potential for B, as well as other lithophile elements (Li, Mo, F, U) peripheral to the gold deposits.

Tertiary volcanic rocks in the Castle Mountains are middle Miocene in age and range from 18.5 to 14 Ma (see section above entitled "Tertiary Rocks"). The volcanic rocks unconformably overlie a basement composed of Proterozoic metamorphic rocks covered by a thin sequence of Paleozoic carbonate rocks (Capps and Moore, 1990) and Miocene sedimentary rocks (pl. 1). Capps and Moore (1990) divided the volcanic rocks in the Castle Mountains into the following four informally named units (from oldest to youngest): (1) Castle Mountains tuff unit, rhyolitic ash-flow tuff; (2) Jacks Well unit, latite, basalt, and ash-flow tuff; (3) Linder Peak unit, rhyolite flow-dome complex; and (4) Hart Peak unit, basalt and intermediate-composition flows and volcaniclastic rocks (these four units are not shown on plate 1). The Linder Peak (rhyolite flow-dome) unit, which has an age of about 15.5 Ma, hosts the gold deposits that formed just after dome emplacement (Capps and Moore, 1990). North of the known orebodies, these rhyolitic rocks are present in a north-trending zone on the west side of the Castle Mountains, and they are potential hosts for volcanic-hosted gold deposits, in addition to those orebodies already delineated.

Gold mineralization is present in structurally controlled, silicified fracture zones and more permeable lithologies that have been silicified (Ausburn, 1991). Argillic alteration and local zones of advanced argillic alteration are associated with the orebodies, and adularia and pyrite are present in close association with the gold. The ore minerals are native gold and electrum. The geochemical suite associated with the ore consists of As, Sb, and Hg (Capps and Moore, 1990). Quartz-adularia alteration is associated with the main stage of gold mineralization.

Eleven specific localities in the EMNSA are shown as being volcanic-hosted epithermal gold occurrences (table 14; see also pl. 2), all of which are in the Castle Mountains. Although mineralized occurrences in the area of Hackberry Mountain have been classified as polymetallic-fault-related deposits, these occurrences are volcanic hosted and are directly analogous with those in the Castle Mountains. However, the mineralization at Hackberry Mountain may be confined to generally northeast striking fault zones.

Tertiary volcanic rocks of similar age to those hosting gold deposits in the Hart Mining District are present in a large area in the south-central part of the EMNSA and are associated with the Woods Mountains volcanic center (McCurry, 1988). These volcanic rocks consist of regionally extensive ash-flow tuffs and rhyolitic domes and flows. The ash-flow tuffs include the 15.8-Ma Wild Horse Mesa Tuff of McCurry (1988) (unit Tw, pl. 1), a compositionally zoned, metaluminous to mildly peralkaline tuff and the possibly younger Tortoise Shell Mountain Rhyolite of McCurry (1988) (Tts), which may be a lava flow. Large-amplitude, circular gravity (about –30 mGal) and magnetic (about –600 nT) anomalies are centered over the Woods Mountains volcanic center and reflect a caldera and associated, buried felsic stock about 9 km in diameter. McCurry (1985, 1988) suggested the presence of a trap-door style of collapse for a 10 km-diameter caldera, and the magnetic anomaly may reflect the outline of the caldera structure. However, the magnitude of the gravity anomaly and estimated depth to pre-Tertiary basement, about 7 km, indicate a symmetrical zone of subsidence that has a much larger component of collapse than previously postulated.

Similar-age volcanic rocks at Hackberry Mountain to the east of the Woods Mountains volcanic center consist of ash-flow tuffs, flows, and domes (pl. 1). These volcanic rocks are altered over a large area in the southern part of Hackberry Mountain. The alteration pattern is coincident with an east-west-trending magnetic-low anomaly, which probably reflects the oxidation or sulfidation of magnetic iron-oxide minerals during alteration. In the alteration zone, drilling indicated the presence of disseminated native gold, as much as 2.75 g Au/t, as well as stibnite and hematite in argillically altered and partly silicified ash-flow tuff that is cut by chalcedonic veinlets (Gottlieb and Friberg, 1984). Similar volcanic rocks are present around the north and west margins of the Woods Mountains volcanic center and have potential for volcanic-hosted gold deposits.

Volcanic-hosted gold deposits can be present in association with porphyry-type gold deposits (Rytuba and Cox, 1991). Most known porphyry-gold deposits are characterized by a stockwork of quartz and pyrite veins in subvolcanic intrusive rocks. These deposits form at greater depths and are lateral to volcanic-hosted gold deposits such as those in the Hart Mining District. The gold orebodies in porphyry-type gold deposits are generally low grade, 1.5 to 2.5 g Au/t, but are known to contain a very large tonnages of ore, as much as several hundred million tonnes. The subvolcanic intrusive rocks associated with the flow-dome complex in the Castle Mountains and the Woods Mountains volcanic center are permissive for porphyry-gold deposits, and those areas outlined below as being favorable for volcanic-hosted gold deposits also have potential for porphyry-gold deposits at depth.

Permissive Terranes

Three terranes in the EMNSA are delineated as permissive for Tertiary, volcanic-hosted epithermal-gold deposits of the quartz-alunite and (or) quartz-adularia variety (fig. 93). One is a north-northeast-trending terrane in the general area of the Castle Mountains. The northeast boundary of this terrane is based on the outermost limit of small numbers of rhyolite and (or) latite intrusions emplaced into Proterozoic basement rocks (pl. 1). The south boundary of the terrane is defined by our estimate of the southernmost extent of altered, demagnetized volcanic rocks under the overlying Quaternary gravels (fig. 93). The overall configuration of these apparently demagnetized rocks under the gravels is inferred from the available aeromagnetic data (pl. 5). The second of the two permissive terranes is a broadly ovoid one in the general area of Hackberry Mountain and the Woods Mountains, which includes the Miocene Hackberry Spring Volcanics of McCurry (1988) and Wild Horse Mesa Tuff of McCurry (1988) (units Ths and Tw, respectively) in the area of Hackberry Mountain and the mostly Miocene Tortoise Shell Mountain Rhyolite of McCurry (1988) (Tts) in the area of Woods Mountains. Relation of these rocks to a caldera is described above. The third terrane permissive for Tertiary, volcanic-hosted epithermal gold deposits is marked by sequences of ash-flow tuffs near the south-central edge of the EMNSA in the area of Van Winkle Mountain (fig. 93).

Favorable Tracts

A favorable tract for Tertiary, volcanic-hosted epithermal-gold deposits of the quartz-adularia or quartz-alunite type is delineated within each of the first two above-outlined permissive terranes (fig. 93). These favorable tracts are outlined using the presence of magnetic lows, mineralized occurrences, and alteration anomalies detected by Landsat Thematic Mapper. Within these zones, deposits of B and Li, F, and U also may be present. Hodges and Ludington (1991) estimated that 0, 1, 2, 3, and 3 hot-spring-gold deposits, at 90, 50, 10, 5, and 1 percent probability levels, respectively, remain to be discovered in the EMNSA using the tonnage and grade distributions for these types of deposits derived by Berger and Singer (1992). The tonnage and grade distributions of the hot-spring-gold type of Berger and Singer (1992) did not discriminate between the quartz-adularia and quartz-alunite subtypes of these systems that have been distinguished petrogenetically.

Speculative Associations

By Richard M. Tosdal and Ted G. Theodore

Some associations among known types of deposits in the EMNSA, as described above and as depicted schematically in figure 89, apparently have still not been utilized fully in the search for additional exploration targets. Recognition of linkages among some deposits, including gold skarn and the association of boron

and other lithophile elements with gold, might impact significantly exploration concepts in the Mesozoic and Tertiary magmatic-hydrothermal environments in the EMNSA. Application of an exploration concept based on linkages among deposit types is by no means a guarantee of an exploration success. Exploration failures far outnumber exploration successes. We recognize, furthermore, that no gold skarns, as defined by Theodore and others (1992), are currently known in the EMNSA. As compiled, 39 gold skarns show median tonnages worldwide of 213,000 tonnes (t) of ore and median grades worldwide of 8.6 g Au/t; these include the 13.2-million-tonne McCoy and the 5.1-million-tonne Fortitude deposits in Nevada. Domestic primary-gold production in 1989 was approximately 240 tonnes of contained gold (U.S. Bureau of Mines, 1990b).

Lastly, we examine two recently recognized deposit-type linkages as examples of how discoveries elsewhere can impact future concepts of exploration, which might be applied to the EMNSA. First, we will examine the possible linkage between distal sediment-hosted gold deposits and their presumed proximal variants, including skarn of all types and porphyry-stockwork systems, and, second, we will examine the possible association between some possibly wrench-fault-related Tertiary gold mineralization in the EMNSA and hot-spring-gold deposits similar to the Mesquite deposit in southern California.

Local mineralized Mesozoic skarn environments in the EMNSA should be examined from the perspective of (1) a location proximal to magma-equilibrated fluids exsolving from a progenitor intrusive complex and (2) a position interior to sediment-hosted gold systems in the surrounding sedimentary sequences. Sillitoe and Bonham (1990) proposed that most gold in many sediment-hosted gold deposits, in particular the distal-disseminated silver-gold type of deposit, originates in magma-derived fluids and may be deposited on the peripheries of base- and precious-metals mining districts as much as several kilometers from the mineralizing plutons. Gold-bearing skarns, of which several are known in the EMNSA, may be indicator occurrences for sediment-hosted gold deposits (Tingley and Bonham, 1986). The schematic model proposed by Sillitoe and Bonham (1990) that shows such linkages is applicable to some of the more shallow-seated magmatic-hydrothermal pulses associated with emplacement of the Teutonia batholith (fig. 101). As noted by Sillitoe and Bonham (1990), the fringes in most carbonate-rock sequences beyond many intrusion-centered base- and precious-metal districts have been minimally explored for gold. Such conclusions are probably applicable also to the EMNSA. The Navachab, Namibia, gold deposit may be an example of a type of mineralized system that might be present in the EMNSA. At Navachab, 9.5 million tonnes of gold ore with an average grade of 2.6 g Au/t is hosted by steeply dipping marbles that include mottled dolomitic marble, biotite hornfels, and calc-silicate marble (Wyllie, 1991). However, all of the above conclusions with regards to linkage between a porphyry-magmatic environment and the sediment-hosted gold environment are proposed on the basis of magmatic-hydrothermal fluids forming a significant component of the fluid regime in each environment during mineralization. This relation may not be true. Hofstra and others (1988, 1989) showed that nonmagmatic fluids, which are instead apparently equilibrated isotopically with deep-seated rocks, were heavily involved in generation of some of the largest sediment-hosted gold deposits in Nevada.

Gold-quartz veins at the Telegraph Mine in the north-central part of the EMNSA (pl. 2; Lange, 1988; U.S. Bureau of Mines, 1990a, map no. 121, pl. 1) apparently are related to wrench or strike-slip faults, suggesting that additional deposits of this type may be present elsewhere in the EMNSA. Mineralization at the Telegraph Mine is associated spatially with structures interpreted by Lange (1988) as Riedel shears (see Riedel, 1929; Tchalenko, 1970; Ramsay and Huber, 1987). These types of secondary shears are oriented generally at low angles to the general trace of a broad zone of shear. Prominent geomorphic and structural features trending N. 20° to 40° E. in the general area of the Telegraph Mine acted as open conduits or as breccia-filled high-permeability zones during mineralization, which has been dated by the K-Ar method at 10.3±0.4 Ma (Lange, 1988). This type of mineralization is particularly significant in terms of resource evaluation because of its geologic similarity to the world-class gold deposit at the Mesquite Mining District, California. No volcanism has been documented close to 10.3 Ma in the area of the Telegraph Mine; some andesite in the vicinity has been dated at 12.8 Ma, and the oldest alkaline basalts in the area are 7.5 Ma (H.G. Wilshire, written commun., 1991). Nonetheless, as Lange (1988) concluded, mineralization at the Telegraph Mine may be related to regional right-lateral, north-south-directed shortening strains that, in turn, resulted in the opening of low-angle, en echelon tension gashes oriented approximately northeasterly. These mineralized tension gashes at the Telegraph Mine

probably are related to post-20-Ma combined wrenching across the San Andreas, Death Valley, and Soda-Avawatz fault zones. Recent studies in the general area of the Telegraph Mine suggest that a regional wrench fault that strikes approximately N. 70° E. may pass through the general area of the mine (D.M. Miller, oral commun., 1995). Although we assigned mineralization at the Telegraph Mine to a gold-silver quartz-pyrite type of occurrence, the mineralization there seems to be an epithermal variety, showing relatively high Au/Ag ratios for the ores (Lange, 1988). Total production from the Telegraph Mine has been 1,976 tonnes of ore that included 68 kg Au, 169 kg Ag, and 227 kg Cu; 1948 was the last recorded year of production (U.S. Bureau of Mines, 1990a). Hewett (1956) showed production from the Telegraph Mine to include a total of 79 kg Au. Drilling in 1968, which was sponsored by the Office of Mineral Exploration of the U.S. Geological Survey, resulted in the blocking out of 66,016 tonnes at a grade of 15.6 g Au/t and 36.3 g Ag/t at the Telegraph Mine (U.S. Bureau of Mines, 1990a).

The Mesquite Mining District is located in southeastern California about 150 km south-southeast of the south border of the EMNSA and 60 km east of the Salton Sea. Large-scale gold production from the mining district began in 1985; announced reserves were 40.5 million tonnes at an average grade of 1.75 g Au/t (Lindquist, 1987). By 1988, the mining district had become one of the largest producers of gold in California (Burnett, 1990), and continued exploration through 1989 increased the known reserves to 52.3 million tonnes at an average grade of 1.34 g Au/t (Higgins, 1990).

Gold-bearing veins in the Mesquite Mining District formed in an epithermal setting within a few hundred meters of the surface (Willis and Holm, 1987; Manske and others, 1987; Willis, 1988; Manske and Einaudi, 1989; Manske, 1990; Willis and Tosdal, 1992). Gold-bearing quartz-adularia-sericite and ferroan-carbonate veins are the mineralized structures within the district (Willis, 1988; Manske, 1990). Quartz-cemented breccias are contemporaneous with the simple veins and are common in the parts of the deposit that have the highest economic grades. Younger, barren calcite veins and chalcedonic-quartz veins are present locally. Vein deposition occurred by episodic open-space filling, as indicated by vuggy and comb quartz and carbonate minerals, multiple banding of chalcedonic quartz, and clasts of silica-matrix breccia within other breccias. Veins vary from thin microcracks to breccias a meter or so thick. Little hydrothermal alteration of host lithologies accompanied mineralization (Manske and others, 1987; Willis, 1988). Weakly anomalous, sporadic concentrations of Au, Ag, As, Sb, Hg, W, Zn, and Te were found in surface-rock exposures before mining (Tosdal and Smith, 1987).

The veins are steeply dipping and are strongly controlled by right-lateral strike-slip faulting (Willis, 1988), as indicated by the vein geometry in complex dilational jogs (Sibson, 1990), by negative and positive flower structures (Harding, 1985), and by kinematic evidence for strike-slip faulting along the major mineralized faults (Willis and others, 1989; Willis and Tosdal, 1992). Mineralization in the mining district is hosted mostly by gneissic rocks that were metamorphosed at amphibolite grade and, to a lesser extent, by granite, pegmatite, and aplite that intrude the gneissic rocks (Willis, 1988). The ages of these rocks and their subsequent metamorphism have been established as Jurassic and Cretaceous, respectively (R.M. Tosdal, unpub. data, 1987–90). K-Ar and $^{40}Ar/^{39}Ar$ geochronologic studies indicate an Oligocene age of mineralization sometime between 37 and 27 Ma (Willis, 1988; see also D.L. Martin, *as quoted in* Shafiqullah and others, 1990), or a minimum of 60 m.y. after the host rocks were formed. The apparent age of the orebodies is, however, somewhat similar to the age of nearby volcanic and plutonic rocks in the Chocolate Mountains (Miller and Morton, 1977; Crowe and others, 1979). No Tertiary volcanic or plutonic rocks are known within the Mesquite Mining District, although they may have provided a heat source to drive the hydrothermal system (Manske, 1990).

The large gold deposit in the Mesquite Mining District is a typical epithermal precious-metal deposit similar to many of those hosted by volcanic rocks or by other rocks that are intruded by hypabyssal stocks elsewhere. Major distinctions between orebodies in the Mesquite Mining District and typical epithermal deposits include the gneissic host rocks, the large difference in age between the host rocks and the orebodies, and the lack of volcanic or plutonic rocks of the appropriate age within the district. The strike-slip environment is not unique, although it does provide a structural setting into which hydrothermal fluids could flow away from any associated heat source (Sibson, 1987).

Within the EMNSA, the Telegraph Mine appears to have an analogous setting to Mesquite. At this locality, gold-bearing epithermal veins and breccias, which consist of quartz-sericite-adularia-pyrite and quartz-carbonate, cut the informally named, Cretaceous Teutonia adamellite of Beckerman and others (1982) (unit Kt, pl. 1) (Lange, 1988). Veins in this mine are interpreted to have formed within a dextral strike-slip environment, the strike of which is now to the north-northeast, at a high angle to trends of regionally extensive strike-slip faults. A single K-Ar age on adularia implies that the main stage of mineralization occurred in the late Miocene, at about 10.3±0.4 Ma (Lange, 1988). No late Miocene volcanic rocks of this age are known in the immediate area of the Telegraph Mine (pl. 1), although Miocene felsic volcanism of similar age is present within the region, some 40 km to the east-southeast, and late Miocene to Pleistocene basaltic volcanism is present also in the Cima volcanic field to the immediate south (pl. 1). Some basaltic rocks elsewhere are known to host significant concentrations of gold. The Buckhorn deposit, the Mule Canyon deposit, and the Fire Creek occurrence, all in Nevada, apparently are hot-spring gold deposits in basaltic andesite above complexes of basaltic dikes associated with the middle Miocene northern Nevada rift. The Mule Canyon deposit initially was described as including a geologic resource of approximately 26.5 tonnes Au at an average grade of 3.75 g Au/t (Consolidated Gold Fields Defense Document Against Minorco, Sept. 1989); this was revised subsequently to 32.8 tonnes Au at a grade of 4.25 g Au/t (Bonham and Hess, 1993).

The question of mineral-resource potential for these types of gold-bearing epithermal deposits of Tertiary age within the EMNSA is difficult to address at this time. Information is inadequate for us to outline reasonably constrained permissive terranes, or favorable tracts, on the large pediments in the EMNSA. Select mineralized samples from gold-silver quartz-pyrite veins that show relatively high Au/Ag ratios might be one method that could be used to discriminate middle Miocene veins from older ones. Surface expressions of the orebodies at Mesquite on the pediment before exploration were small and consisted of local high-grade gold-quartz veins that had small amounts of reported production, as well as various small placer mines (Morton, 1977). In addition, weak and very limited geochemical expression, and no known geophysical expression, is associated with the orebodies. Only thorough exploration around these small occurrences in the Mesquite Mining District could define the large orebodies now identified there.

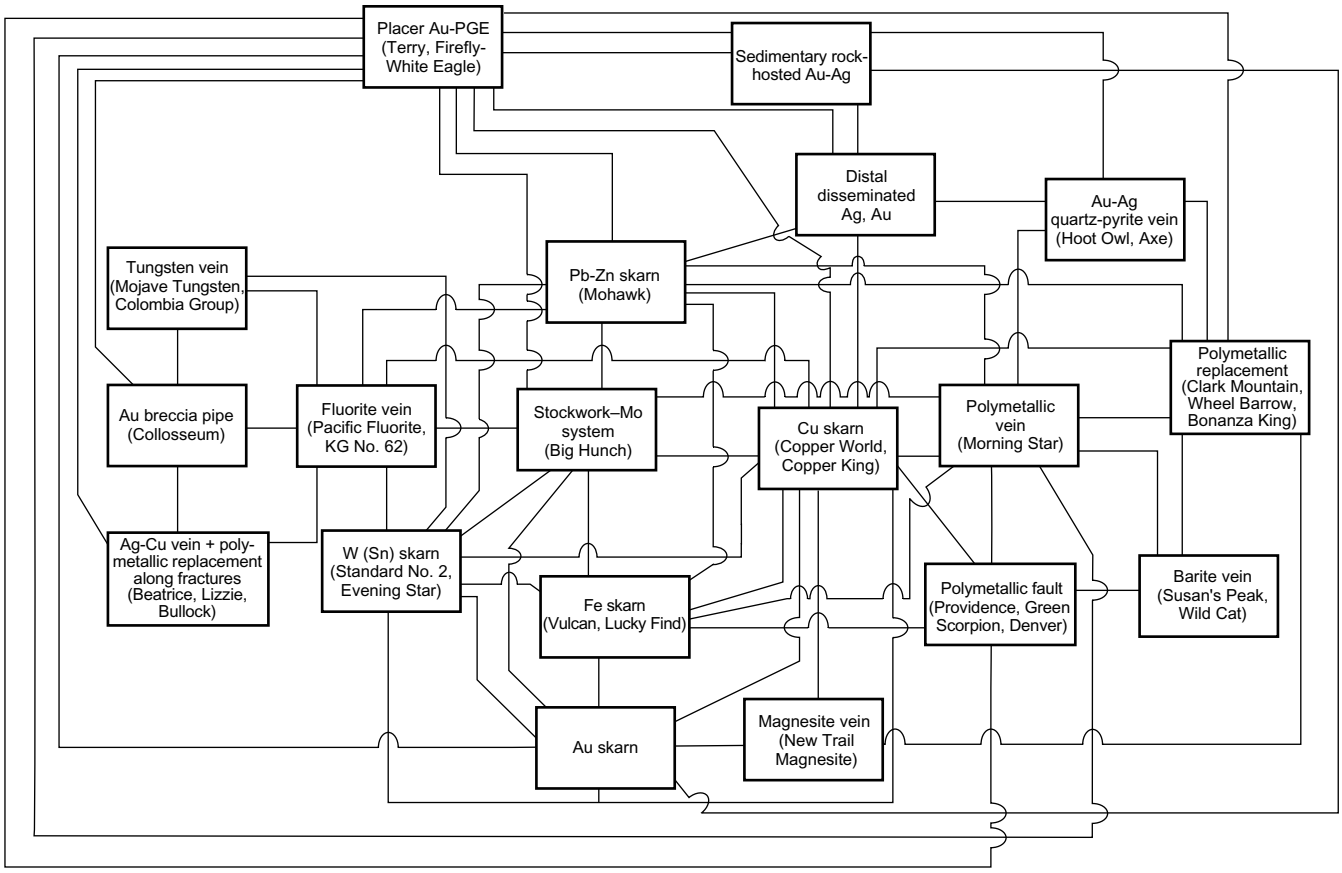

Figure 89. Possible linkages among some types of mineral occurrences that are associated with felsic intrusive rocks in the East Mojave National Scenic Area, California. Most linkages are inferred from mineral zonations established in mining districts elsewhere. Examples of mineral occurrences in East Mojave National Scenic Area are shown in parentheses.

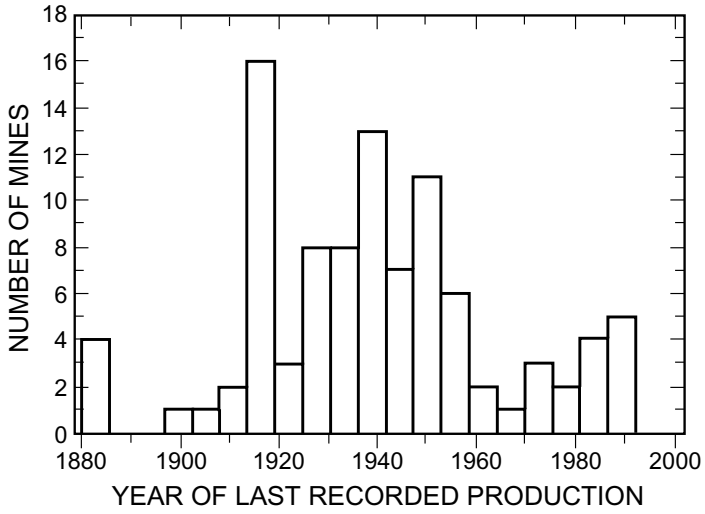

Figure 90. Plot showing number of formerly active mines in the East Mojave National Scenic Area, California, versus year of their last recorded production activity. Data for 97 mines from U.S. Bureau of Mines (1990a).

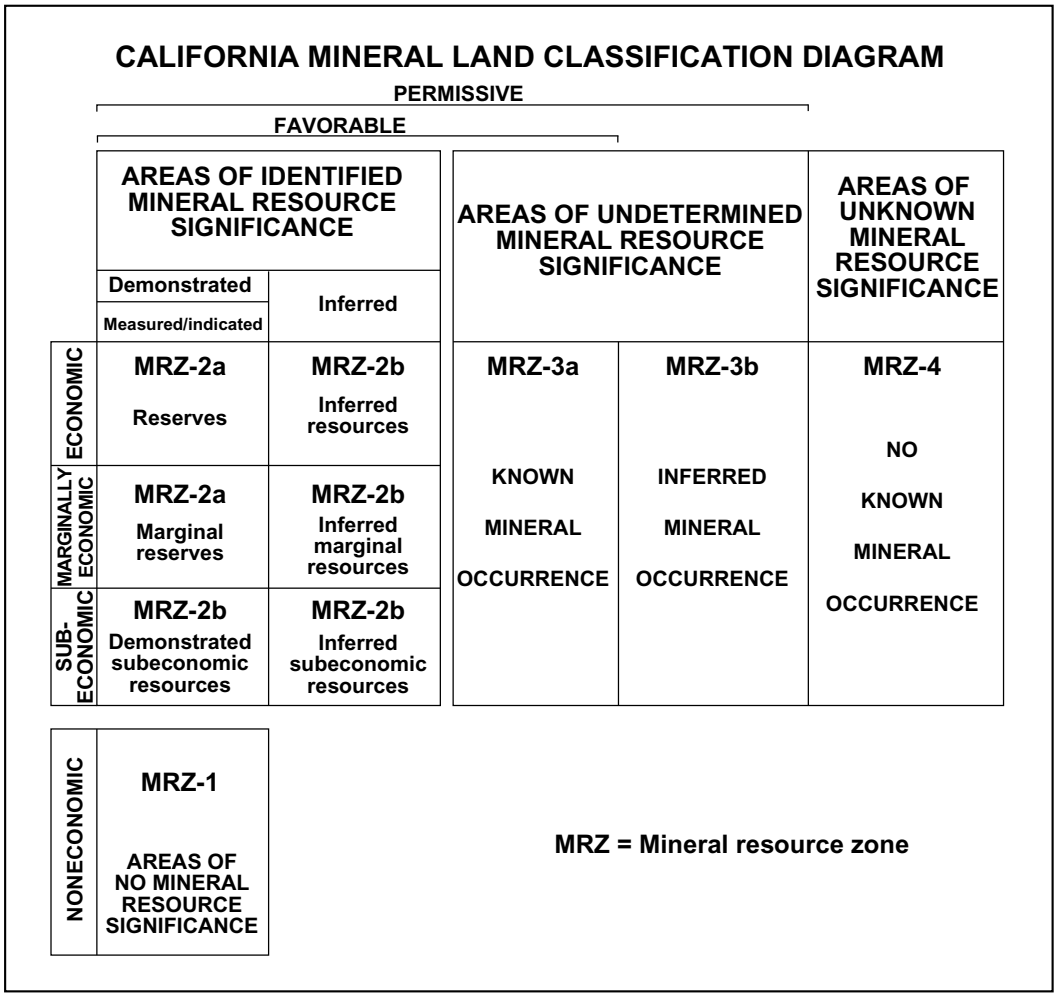

Figure 91. Mineral land-classification diagram adopted by State of California, showing diagrammatic relations of mineral-resource-zone categories to resource-reserve classification system. From D.O. Shumway (written commun., 1991). Major elements of mineral-resource classification modified from McKelvey (1972) and U.S. Bureau of Mines and U.S. Geological Survey (1980).

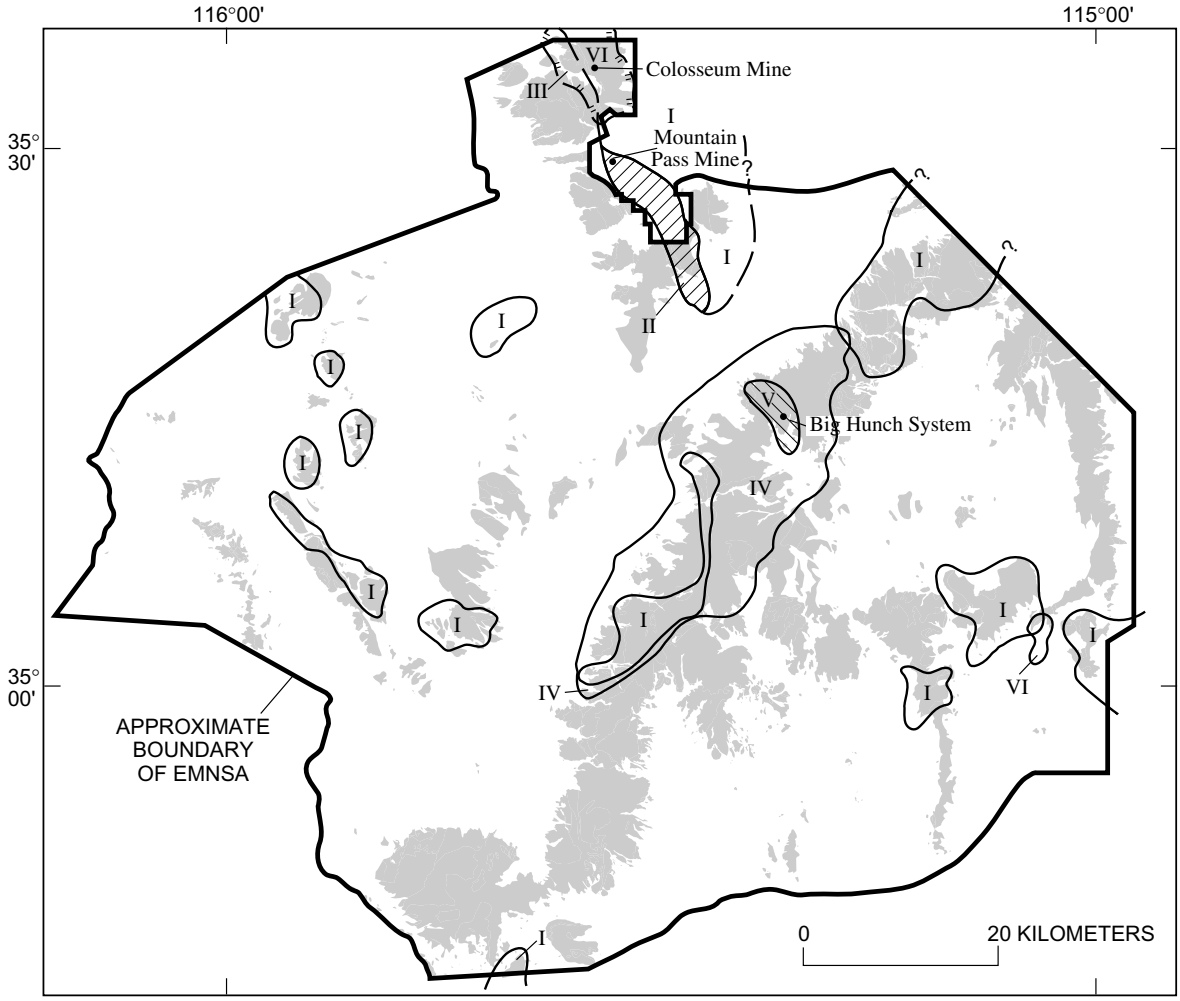

Figure 92. Map of East Mojave National Scenic Area (EMNSA), California, showing permissive terranes and favorable tracts for Proterozoic carbonatite-related rare earth element (REE) occurrences, Mesozoic gold-bearing breccia pipes, Mesozoic stockwork-molybdenum systems, and Mesozoic tungsten veins. Outlines of permissive terranes and favorable tracts established independently for specific mineral-occurrence models, and some terranes and (or) tracts may overlap or be nested within one another, because of the mineral-occurrence implications of the geology of the terranes and (or) tracts on that particular model. See figure 91 for explanation of terminology. Mountain areas shaded.

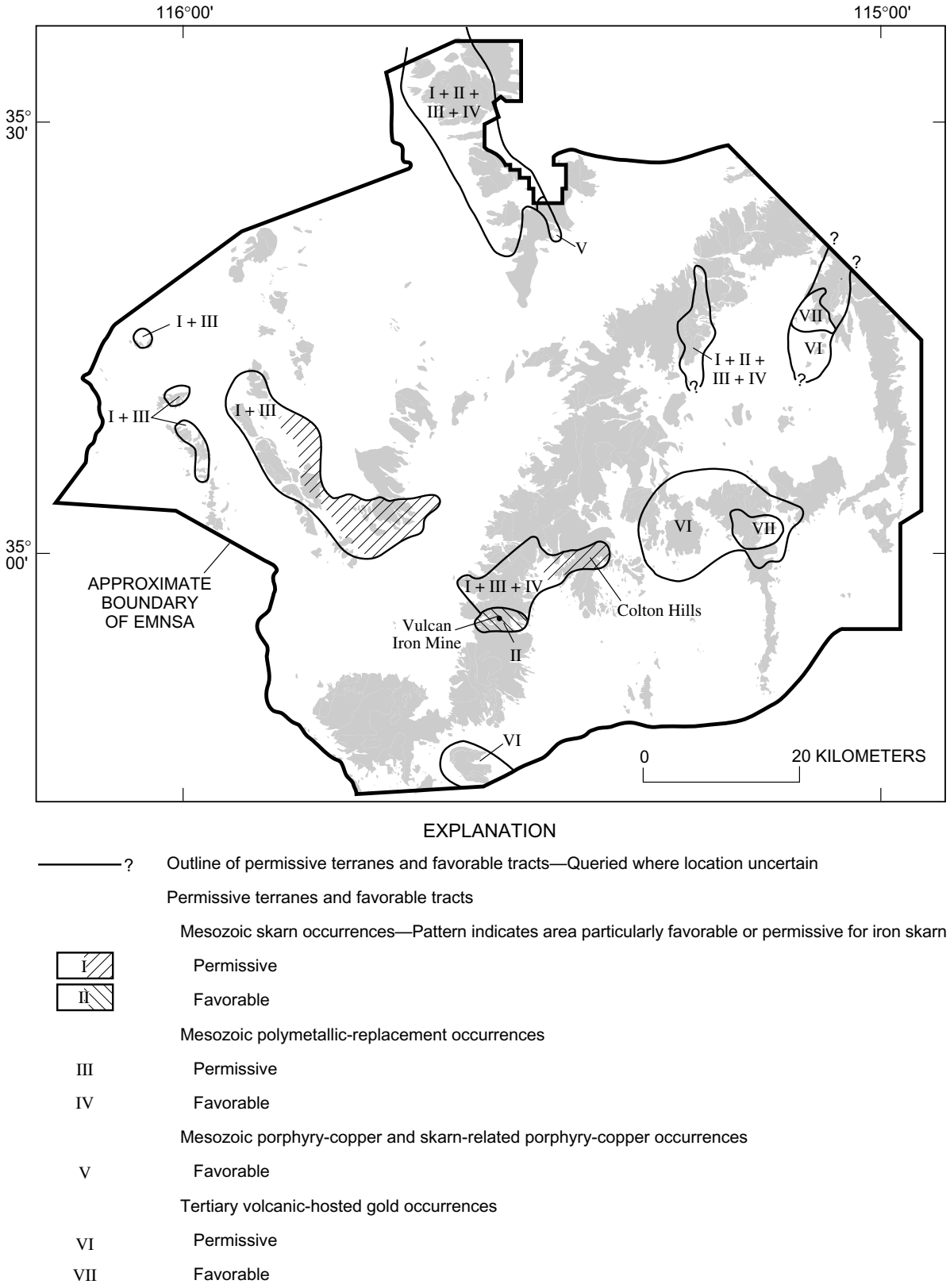

Figure 93. Map of East Mojave National Scenic Area (EMNSA), California, showing major permissive terranes and favorable tracts for Mesozoic mineralized skarns of all types and iron skarns in particular, Mesozoic skarn-related porphyry copper and porphyry copper systems, Mesozoic polymetallic-replacement occurrences, and Tertiary volcanic-hosted, gold-silver occurrences. See figure 91 for explanation of terminology.

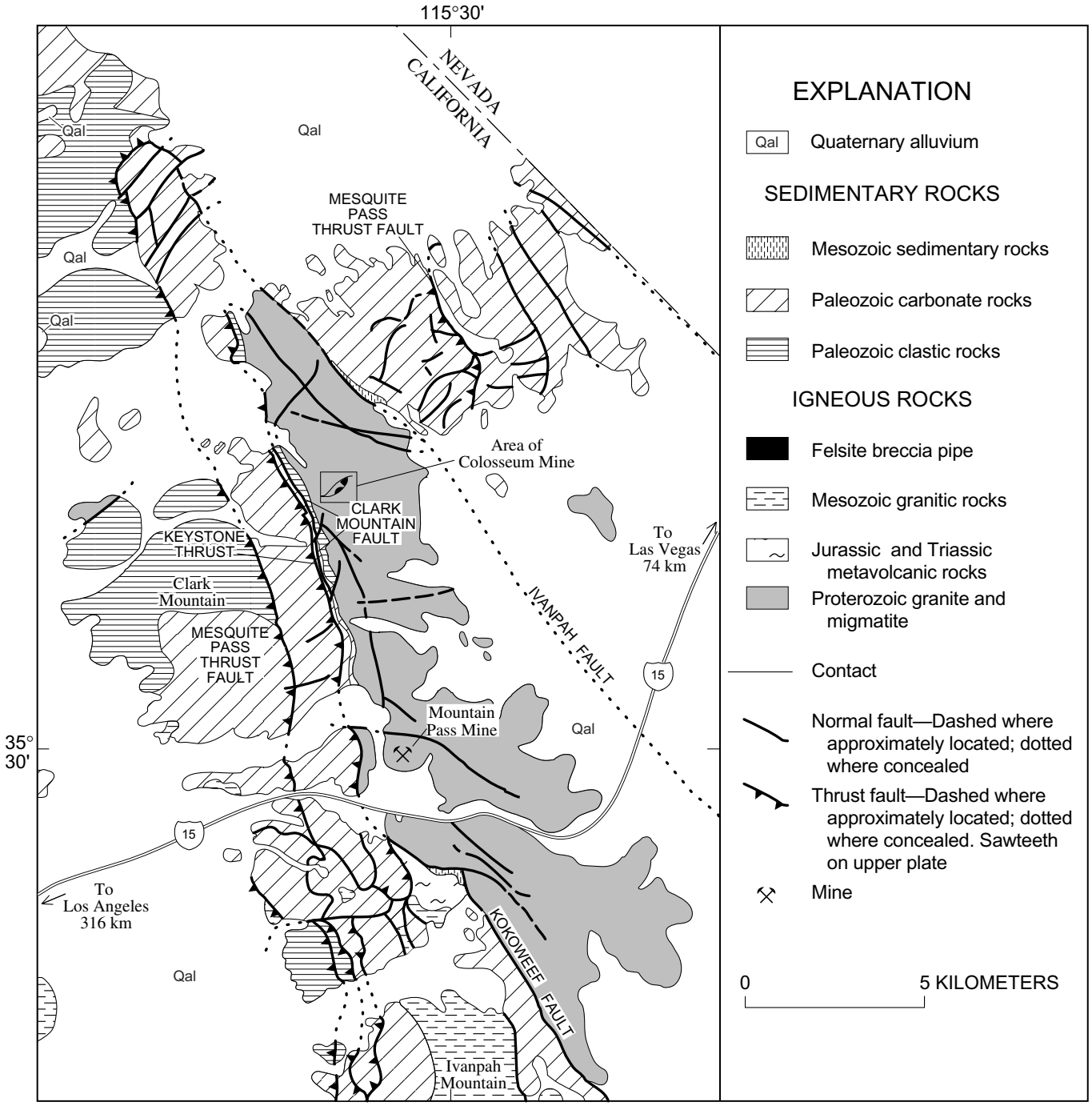

Figure 94. Geologic map of area surrounding Cretaceous gold-bearing breccia pipes at Colosseum Mine, in north-central part of East Mojave National Scenic Area, California. Modified from Sharp (1984).

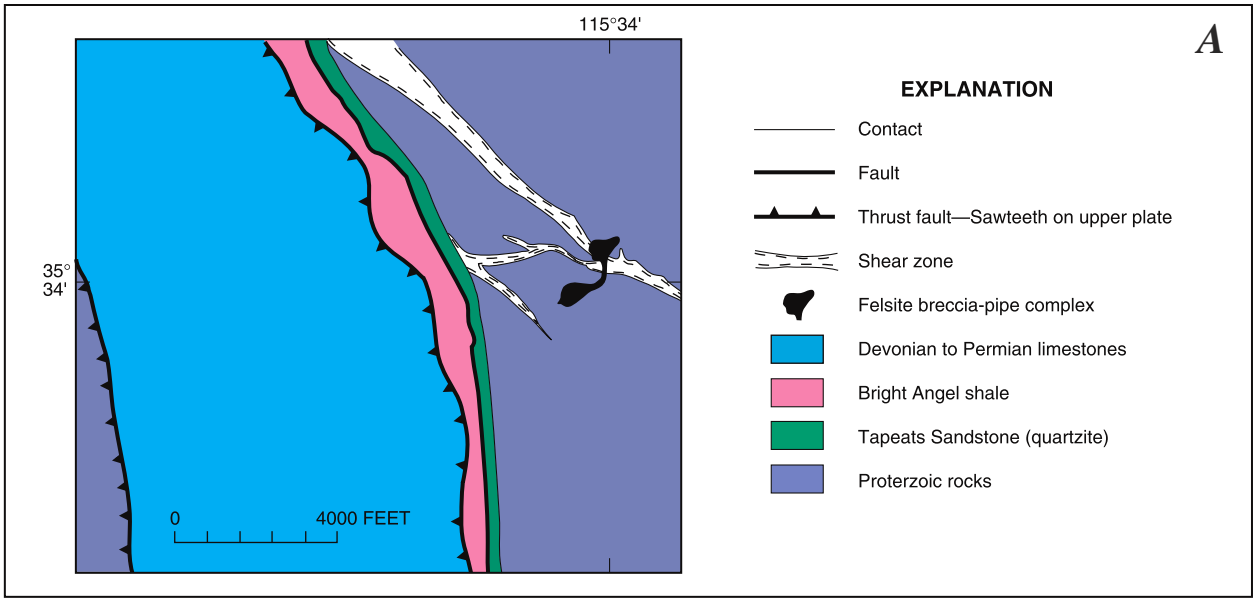

Figure 95. Northeastern part of Clark Mountain Mining District, north-central East Mojave National Scenic Area, California (see fig. 94 for location). *A*, Generalized geologic map of Clark Mountain Mining District. Some faults omitted for simplicity. Cambrian Bright Angel Shale, Cambrian Tapeats Sandstone, and Proterozoic rocks are included in unit €Zs (pl. 1); Devonian to Permian limestones are in unit PDl (pl.1). *B*, Map showing metal zoning in Clark Mountain Mining District (modified from Sharp, 1984).

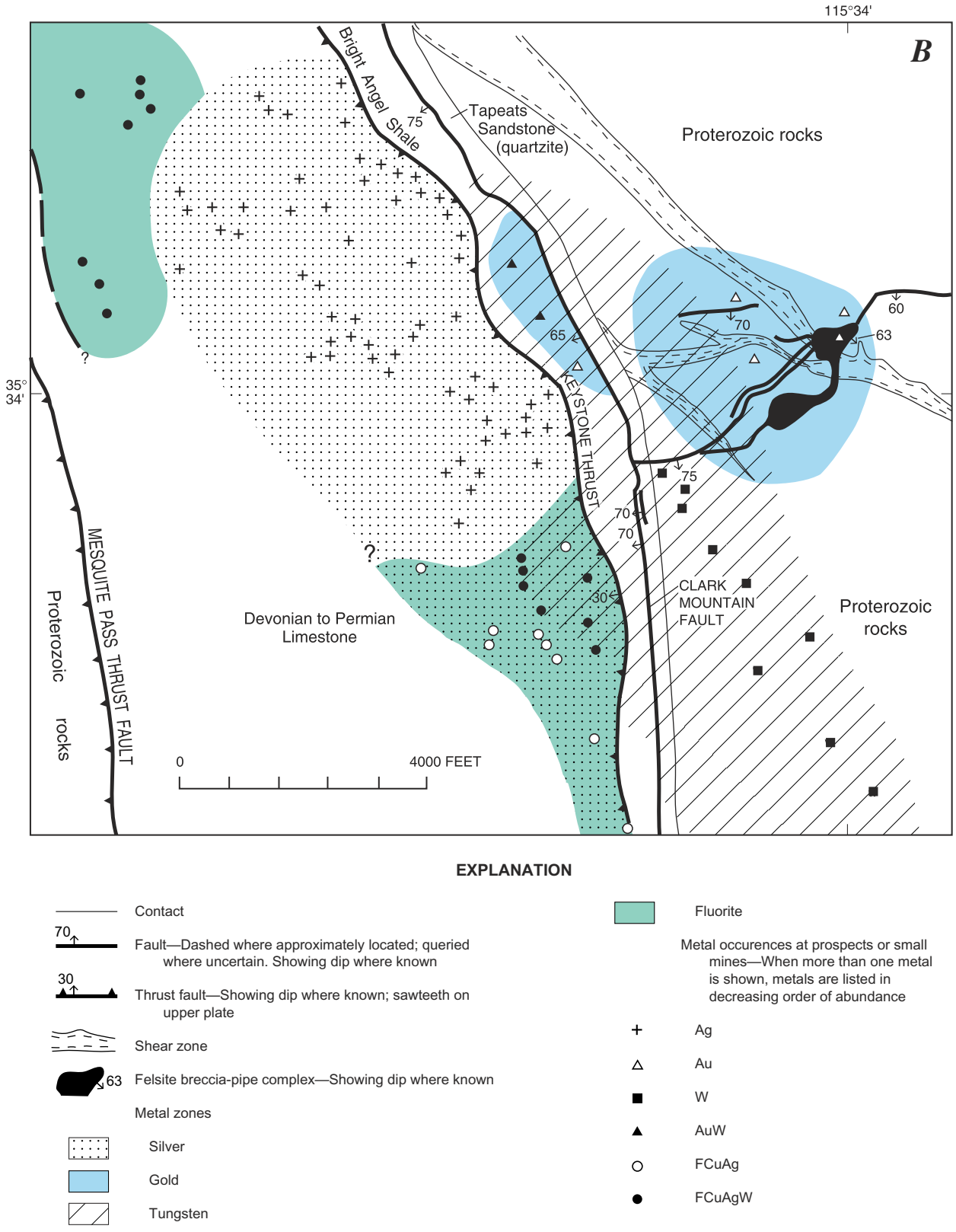

Figure 95. Northeastern part of Clark Mountain Mining District, north-central East Mojave National Scenic Area, California (see fig. 94 for location). *A*, Generalized geologic map of Clark Mountain Mining District. Some faults omitted for simplicity. Cambrian Bright Angel Shale, Cambrian Tapeats Sandstone, and Proterozoic rocks are included in unit €Zs (pl. 1). *B*, Map showing metal zoning in Clark Mountain Mining District (modified from Sharp, 1984)—Continued.

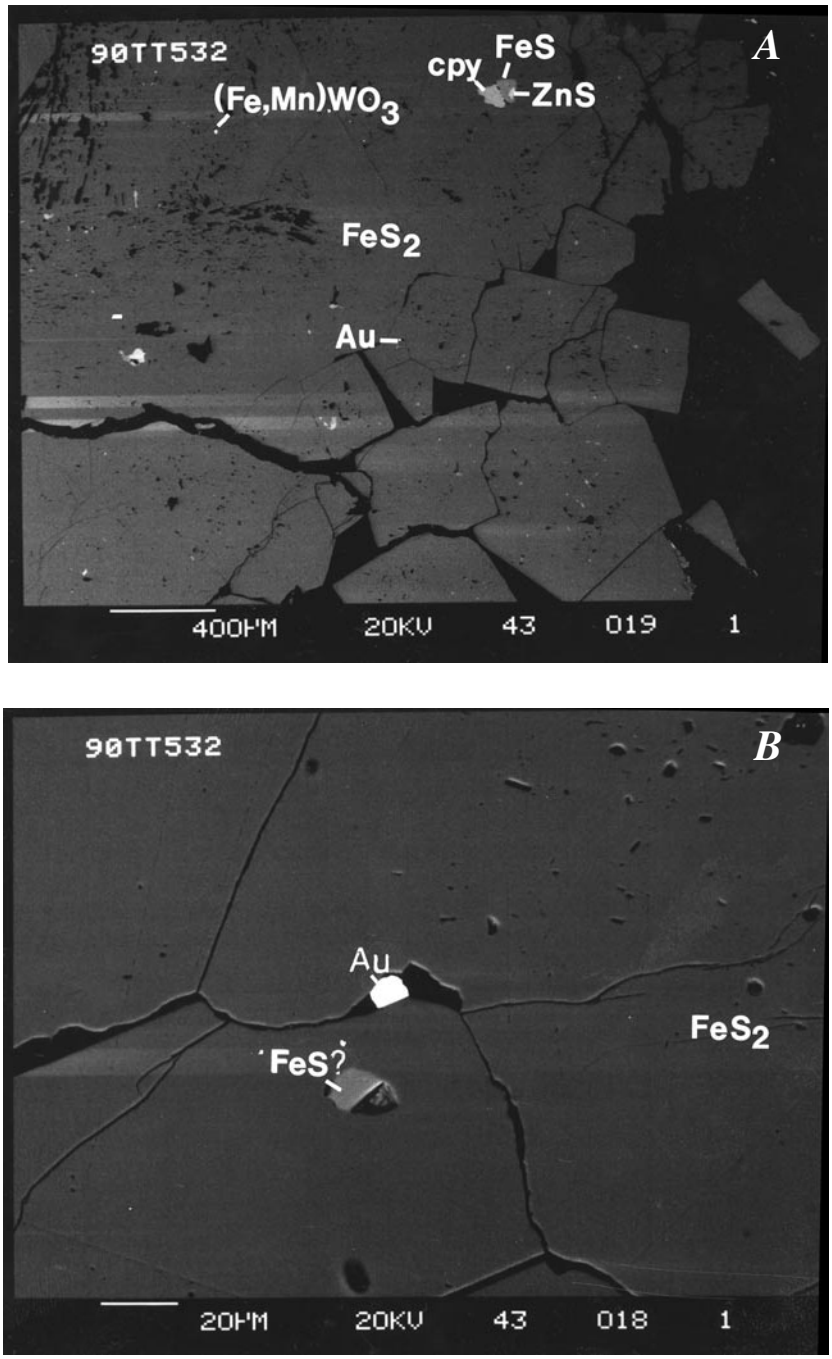

Figure 96. Scanning electron micrographs of gold-bearing breccia pipe at the Colosseum Mine, East Mojave National Scenic Area, California (fig. 94). Abbreviations: Ag, silver; AgTe, silver telluride; Au, gold; BiTe, bismuth tellurides; (Ce,La,Nd)PO_4, monazite; cpy, chalcopyrite; CuS, covellite; (Fe,Mn)WO_3, wolframite; FeS, pyrrhotite (queried where uncertain); FeS_2, pyrite; Kf, K-feldspar; Py, pyrite; SiO_2, quartz; ZnS, sphalerite. *A*, General morphology of pyrite hosting various minerals, including gold. *B*, Enlargement of part of 96*A*, showing argentiferous gold along microcrack in pyrite; some possible pyrrhotite also in the field of view. *C*, Energy-dispersive X-ray spectra of argentiferous gold grain in 96*B*. *D,* Gold associated with pyrrhotite in pyrite. *E*, Euhedral outlines of pyrite (py) crystals, common throughout sample. *F*, Enlargement of part of 96*E*, showing monazite crystals along margins between pyrite crystals. *G*, Silver tellurides and bismuth tellurides in pyrite. *H*, Enlargement of part of 96*A*, showing clot of chalcopyrite, pyrrhotite, and sphalerite in pyrite. *I*, Sphalerite surrounded by covellite in K-feldspar.

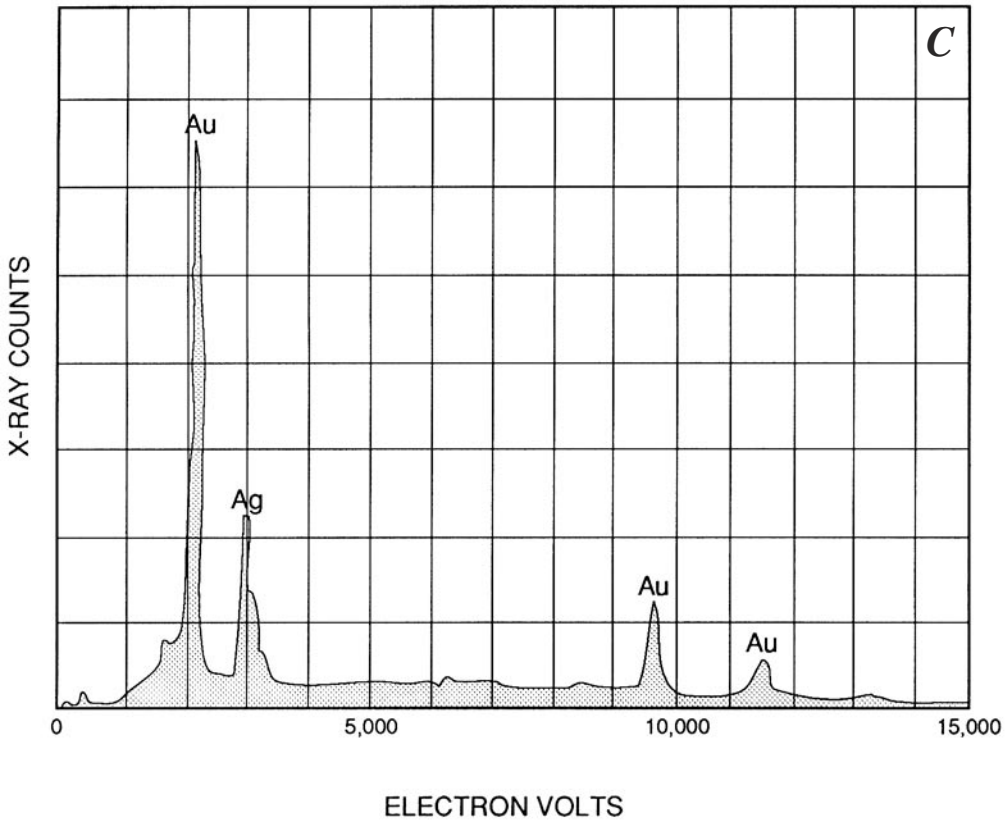

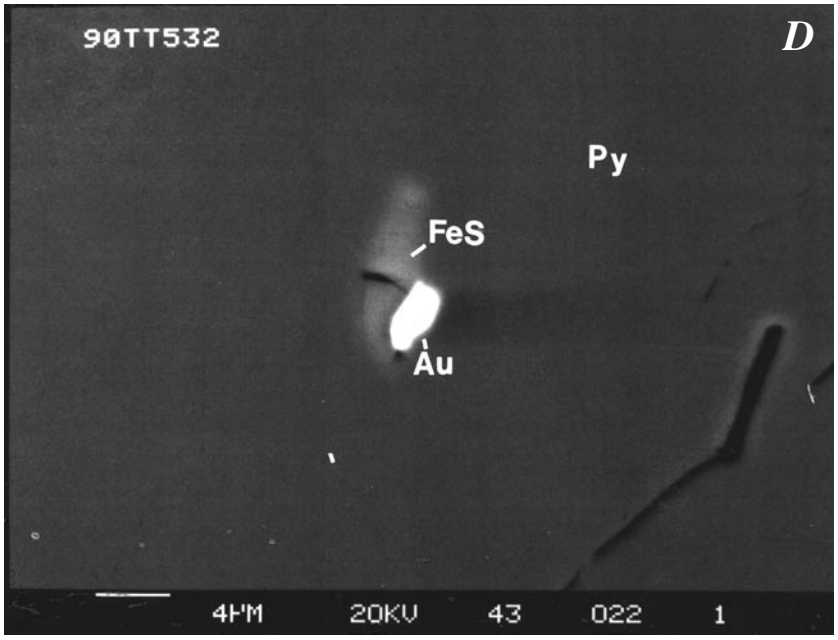

Figure 96. Scanning electron micrographs of gold-bearing breccia pipe at the Colosseum Mine, East Mojave National Scenic Area, California (fig. 94). Abbreviations: Ag, silver; AgTe, silver telluride; Au, gold; BiTe, bismuth tellurides; (Ce,La,Nd)PO_4, monazite; cpy, chalcopyrite; CuS, covellite; (Fe,Mn)WO_3, wolframite; FeS, pyrrhotite (queried where uncertain); FeS_2, pyrite; Kf, K-feldspar; Py, pyrite; SiO_2, quartz; ZnS, sphalerite. *A*, General morphology of pyrite hosting various minerals, including gold. *B*, Enlargement of part of 96*A*, showing argentiferous gold along microcrack in pyrite; some possible pyrrhotite also in the field of view. *C*, Energy-dispersive X-ray spectra of argentiferous gold grain in 96*B*. *D,* Gold associated with pyrrhotite in pyrite. *E*, Euhedral outlines of pyrite (py) crystals, common throughout sample. *F*, Enlargement of part of 96*E*, showing monazite crystals along margins between pyrite crystals. *G*, Silver tellurides and bismuth tellurides in pyrite. *H*, Enlargement of part of 96*A*, showing clot of chalcopyrite, pyrrhotite, and sphalerite in pyrite. *I*, Sphalerite surrounded by covellite in K-feldspar—Continued.

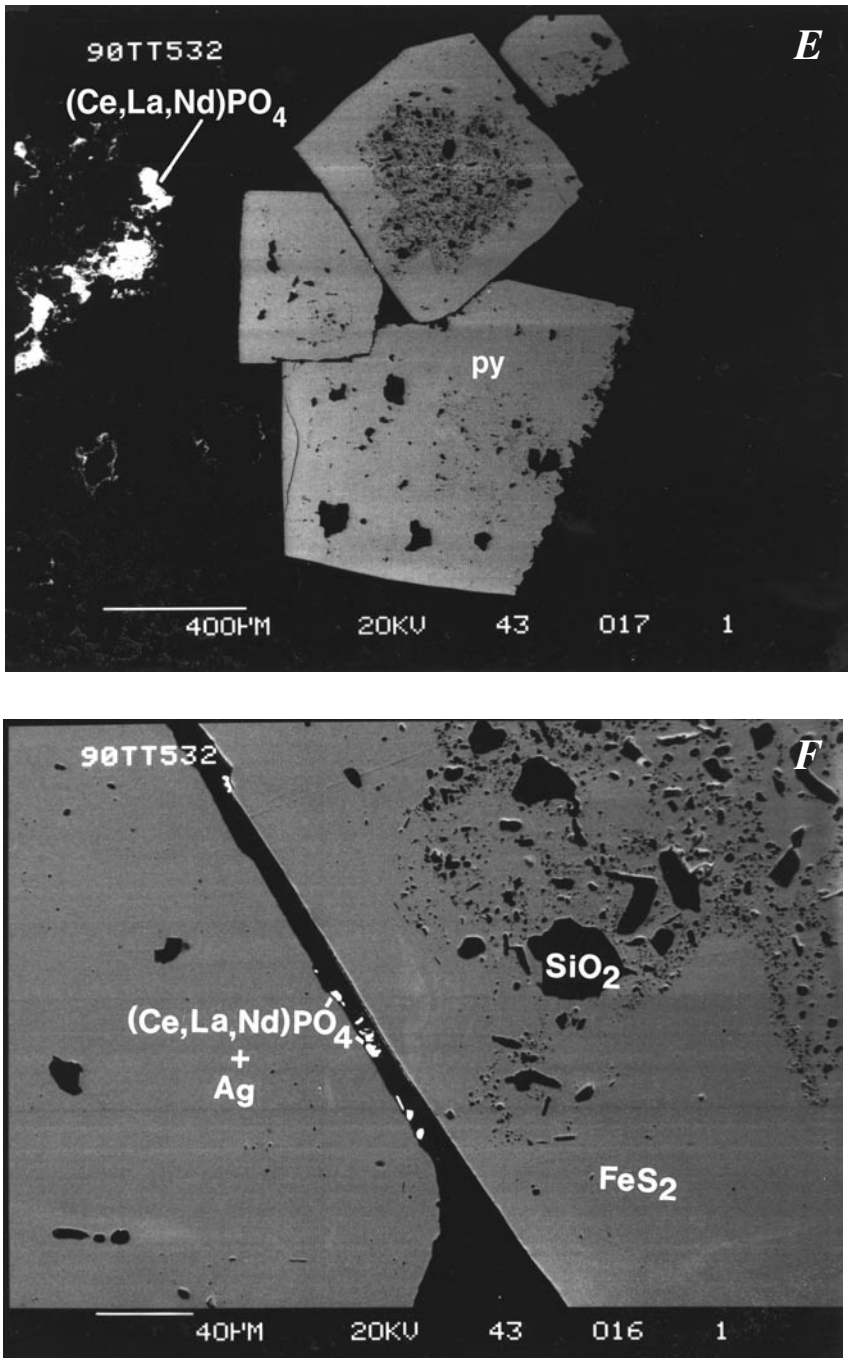

Figure 96. Scanning electron micrographs of gold-bearing breccia pipe at the Colosseum Mine, East Mojave National Scenic Area, California (fig. 94). Abbreviations: Ag, silver; AgTe, silver telluride; Au, gold; BiTe, bismuth tellurides; (Ce,La,Nd)PO_4, monazite; cpy, chalcopyrite; CuS, covellite; (Fe,Mn)WO_3, wolframite; FeS, pyrrhotite (queried where uncertain); FeS_2, pyrite; Kf, K-feldspar; Py, pyrite; SiO_2, quartz; ZnS, sphalerite. *A*, General morphology of pyrite hosting various minerals, including gold. *B*, Enlargement of part of 96*A*, showing argentiferous gold along microcrack in pyrite; some possible pyrrhotite also in the field of view. *C*, Energy-dispersive X-ray spectra of argentiferous gold grain in 96*B*. *D,* Gold associated with pyrrhotite in pyrite. *E*, Euhedral outlines of pyrite (py) crystals, common throughout sample. *F*, Enlargement of part of 96*E*, showing monazite crystals along margins between pyrite crystals. *G*, Silver tellurides and bismuth tellurides in pyrite. *H*, Enlargement of part of 96*A*, showing clot of chalcopyrite, pyrrhotite, and sphalerite in pyrite. *I*, Sphalerite surrounded by covellite in K-feldspar—Continued.

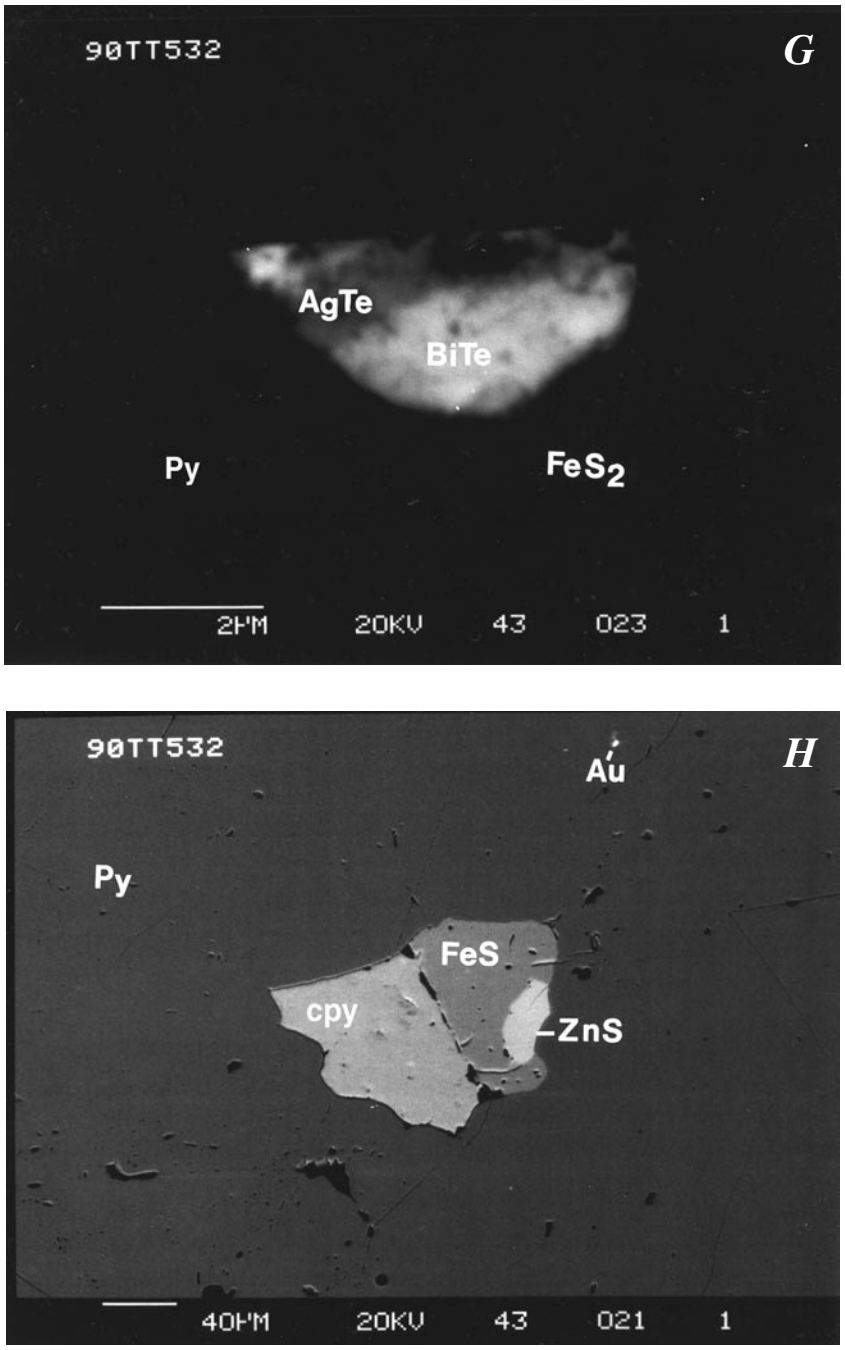

Figure 96. Scanning electron micrographs of gold-bearing breccia pipe at the Colosseum Mine, East Mojave National Scenic Area, California (fig. 94). Abbreviations: Ag, silver; AgTe, silver telluride; Au, gold; BiTe, bismuth tellurides; (Ce,La,Nd)PO_4, monazite; cpy, chalcopyrite; CuS, covellite; (Fe,Mn)WO_3, wolframite; FeS, pyrrhotite (queried where uncertain); FeS_2, pyrite; Kf, K-feldspar; Py, pyrite; SiO_2, quartz; ZnS, sphalerite. *A*, General morphology of pyrite hosting various minerals, including gold. *B*, Enlargement of part of 96*A*, showing argentiferous gold along microcrack in pyrite; some possible pyrrhotite also in the field of view. *C*, Energy-dispersive X-ray spectra of argentiferous gold grain in 96*B*. *D,* Gold associated with pyrrhotite in pyrite. *E*, Euhedral outlines of pyrite (py) crystals, common throughout sample. *F*, Enlargement of part of 96*E*, showing monazite crystals along margins between pyrite crystals. *G*, Silver tellurides and bismuth tellurides in pyrite. *H*, Enlargement of part of 96*A*, showing clot of chalcopyrite, pyrrhotite, and sphalerite in pyrite. *I*, Sphalerite surrounded by covellite in K-feldspar—Continued.

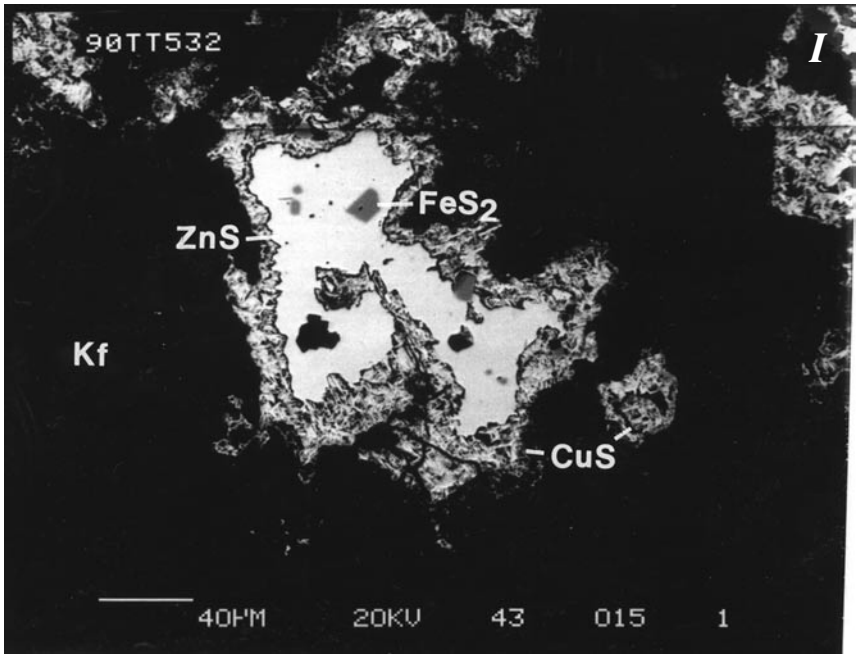

Figure 96. Scanning electron micrographs of gold-bearing breccia pipe at the Colosseum Mine, East Mojave National Scenic Area, California (fig. 94). Abbreviations: Ag, silver; AgTe, silver telluride; Au, gold; BiTe, bismuth tellurides; (Ce,La,Nd)PO_4, monazite; cpy, chalcopyrite; CuS, covellite; (Fe,Mn)WO_3, wolframite; FeS, pyrrhotite (queried where uncertain); FeS_2, pyrite; Kf, K-feldspar; Py, pyrite; SiO_2, quartz; ZnS, sphalerite. *A*, General morphology of pyrite hosting various minerals, including gold. *B*, Enlargement of part of 96*A*, showing argentiferous gold along microcrack in pyrite; some possible pyrrhotite also in the field of view. *C*, Energy-dispersive X-ray spectra of argentiferous gold grain in 96*B*. *D,* Gold associated with pyrrhotite in pyrite. *E*, Euhedral outlines of pyrite (py) crystals, common throughout sample. *F*, Enlargement of part of 96*E*, showing monazite crystals along margins between pyrite crystals. *G*, Silver tellurides and bismuth tellurides in pyrite. *H*, Enlargement of part of 96*A*, showing clot of chalcopyrite, pyrrhotite, and sphalerite in pyrite. *I*, Sphalerite surrounded by covellite in K-feldspar—Continued.

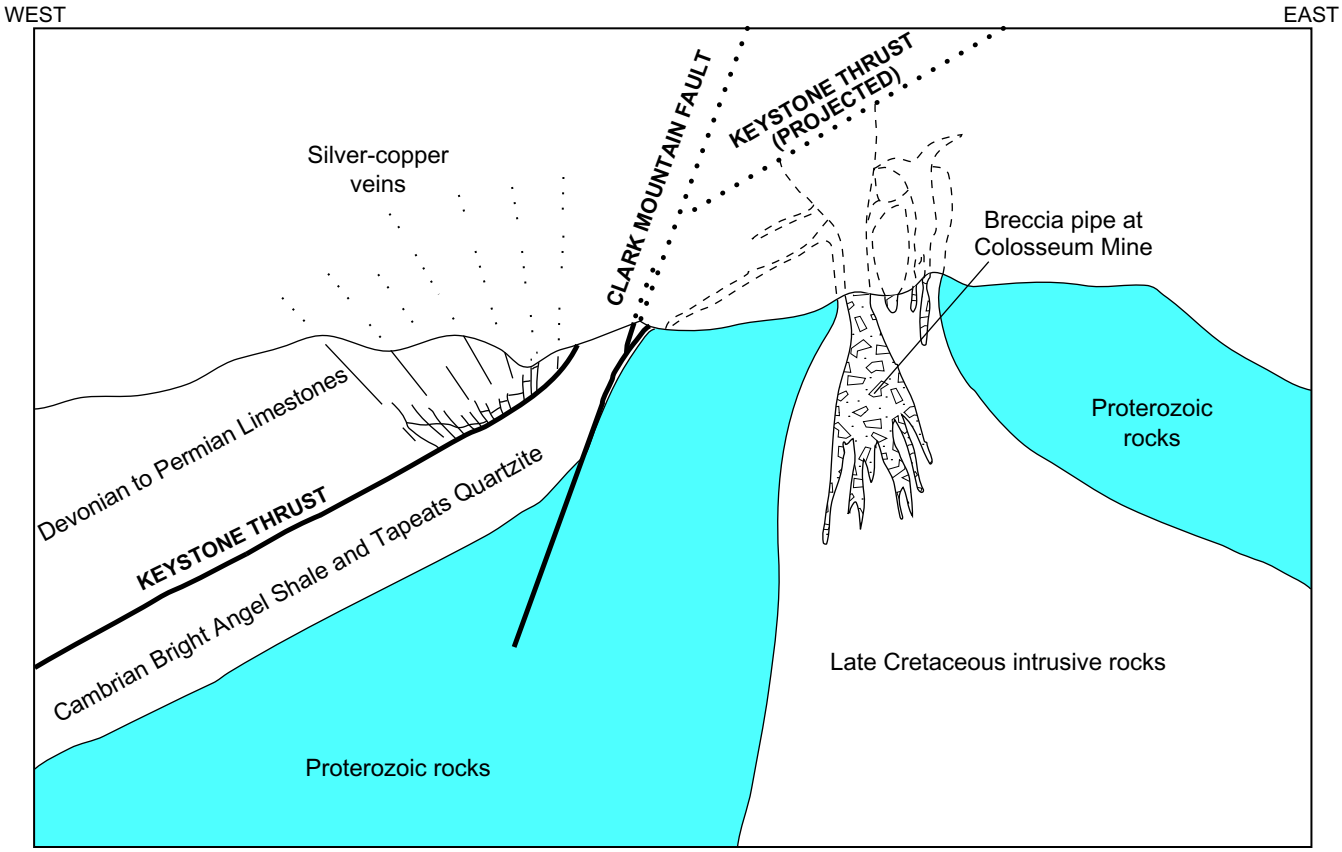

Figure 97. Schematic cross section showing displacement down to west along Clark Mountain fault (fig. 94) of silver-copper brecciated-dolostone vein-type occurrences from their initial positions at top of gold-bearing breccia pipes at Colosseum Mine, East Mojave National Scenic Area, California. Modified from Sharp (1984).

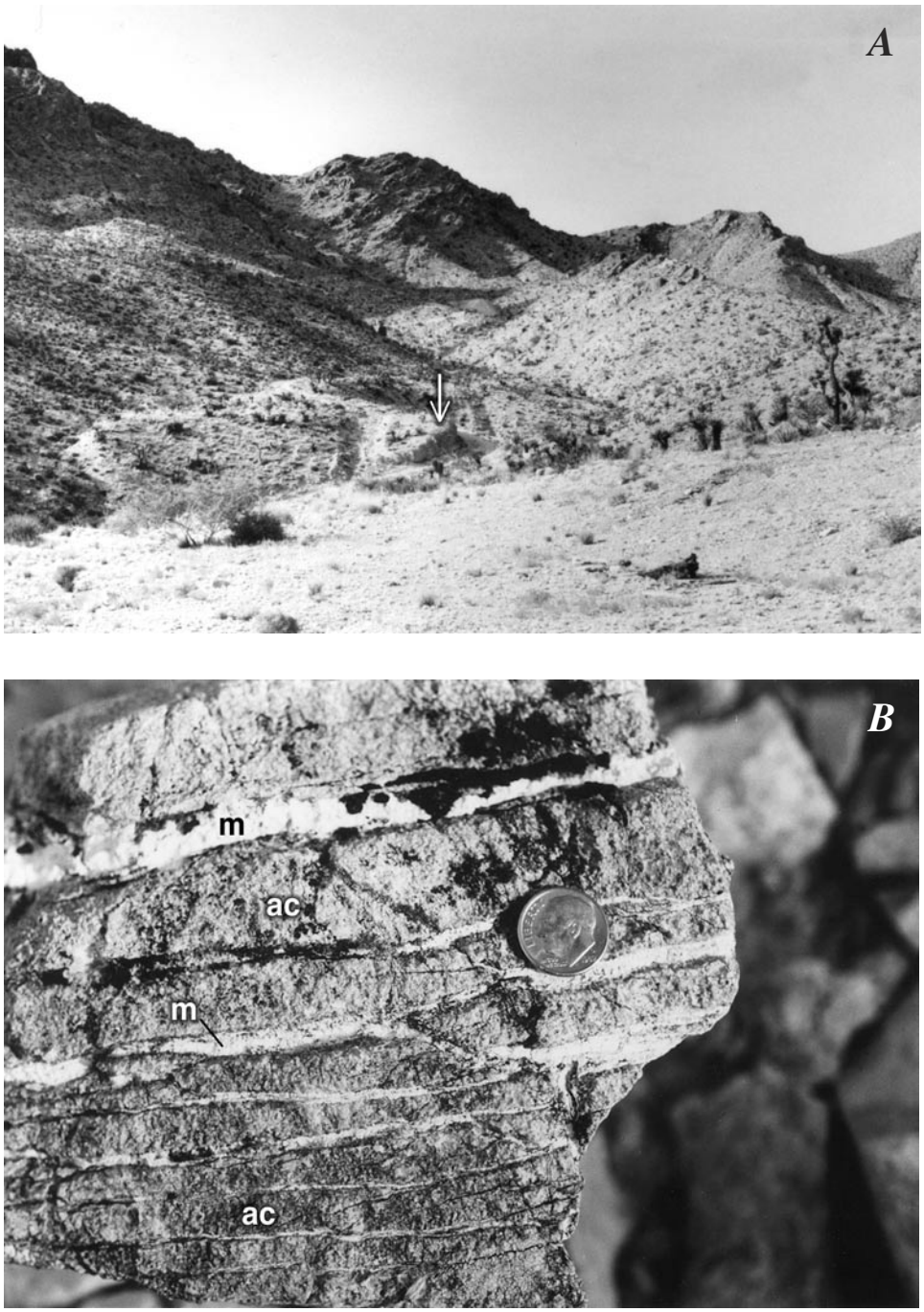

Figure 98. New Trail Canyon area, northern Ivanpah Mountains, East Mojave National Scenic Area, California (figs. 2, 26). *A*, Workings at New Trail Canyon Mine (at head of arrow), which explore copper and iron skarn. View to N. 40° W. from general area of Bullion Mine. *B*, Narrow veins of magnesite (m) cutting altered Paleozoic carbonate rocks (ac). Approximately 1 m from 1-m-wide main vein at New Trail Magnesite Mine, approximately 2.5 km southeast of the New Trail Mine.

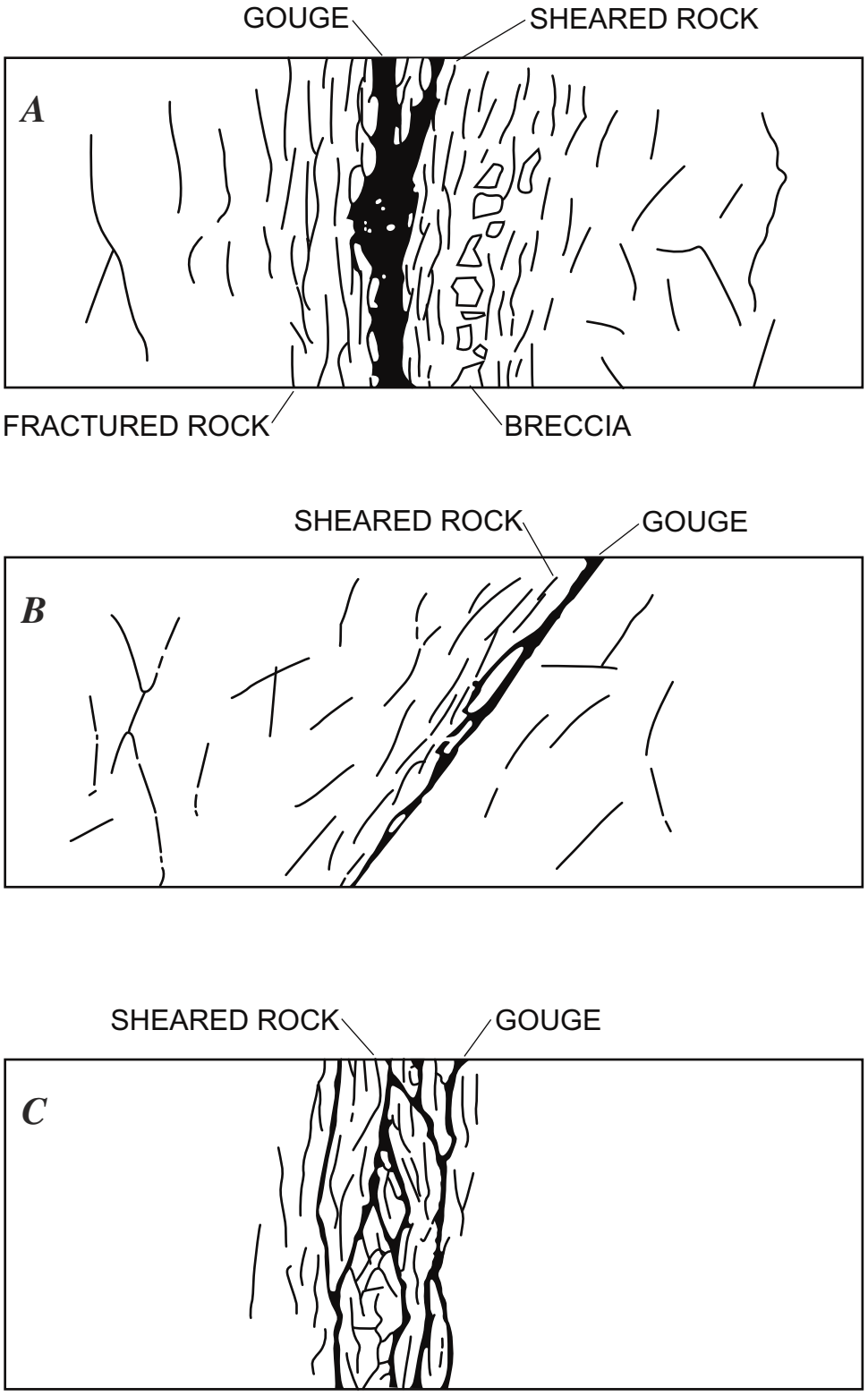

Figure 99. Schematic diagrams showing various relations of gouge within a fault zone (from Wallace and Morris, 1986). *A*, Gouge zone near center of trace of a fault zone. *B*, Gouge zone preferentially located near one boundary of a fault zone. *C*, Thin seams of gouge developed throughout zone of sheared rock that define overall width of a fault zone.

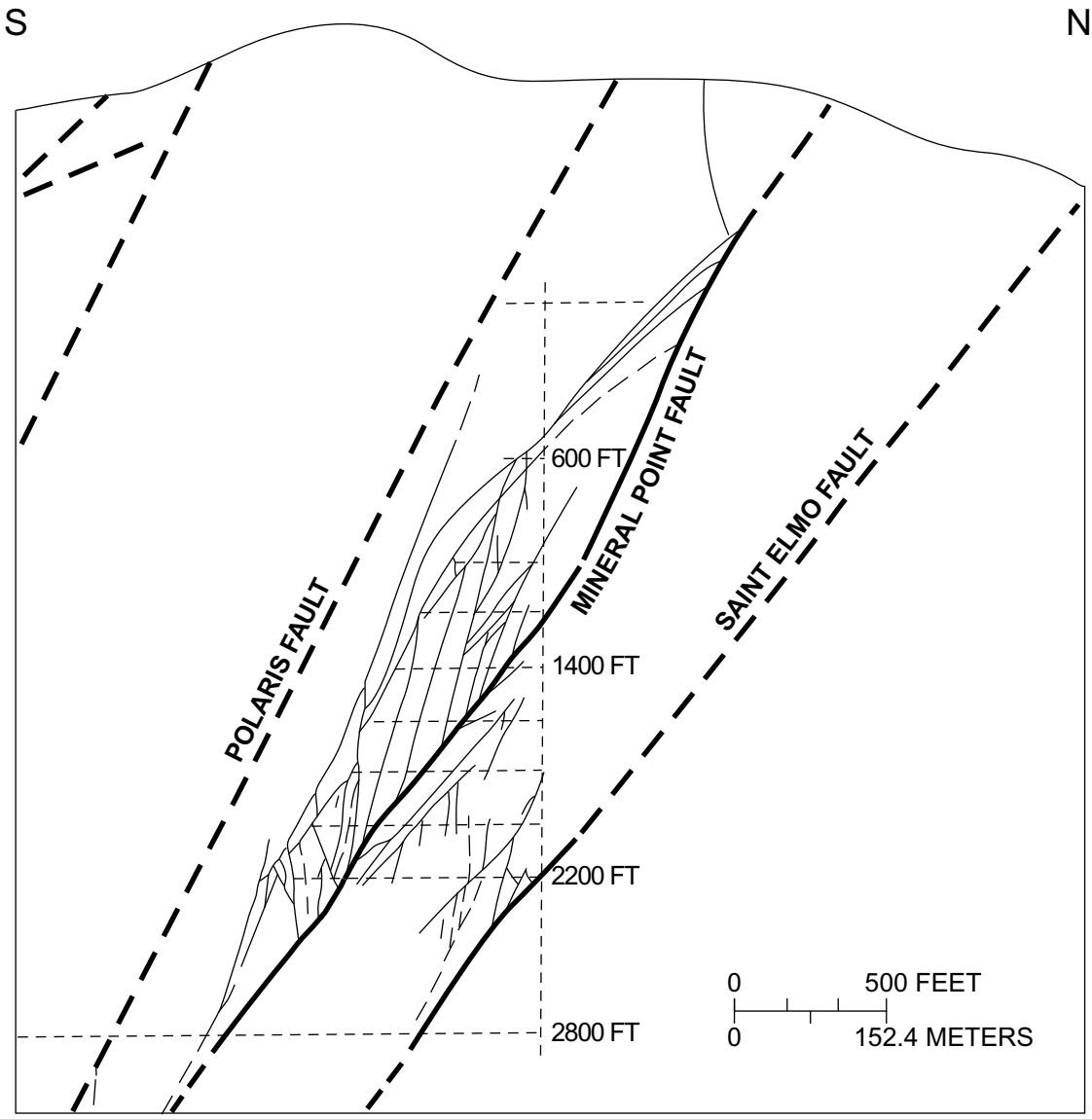

Figure 100. Cross section through Coeur d'Alene Mine, Idaho, showing complex anastomosing pattern of traces of fault found in approximately 70-m intervals of underground mine workings. Faults, dashed where approximately located; short-dashed lines, shaft and underground mine levels projected to plane of section. From Wallace and Morris (1986).

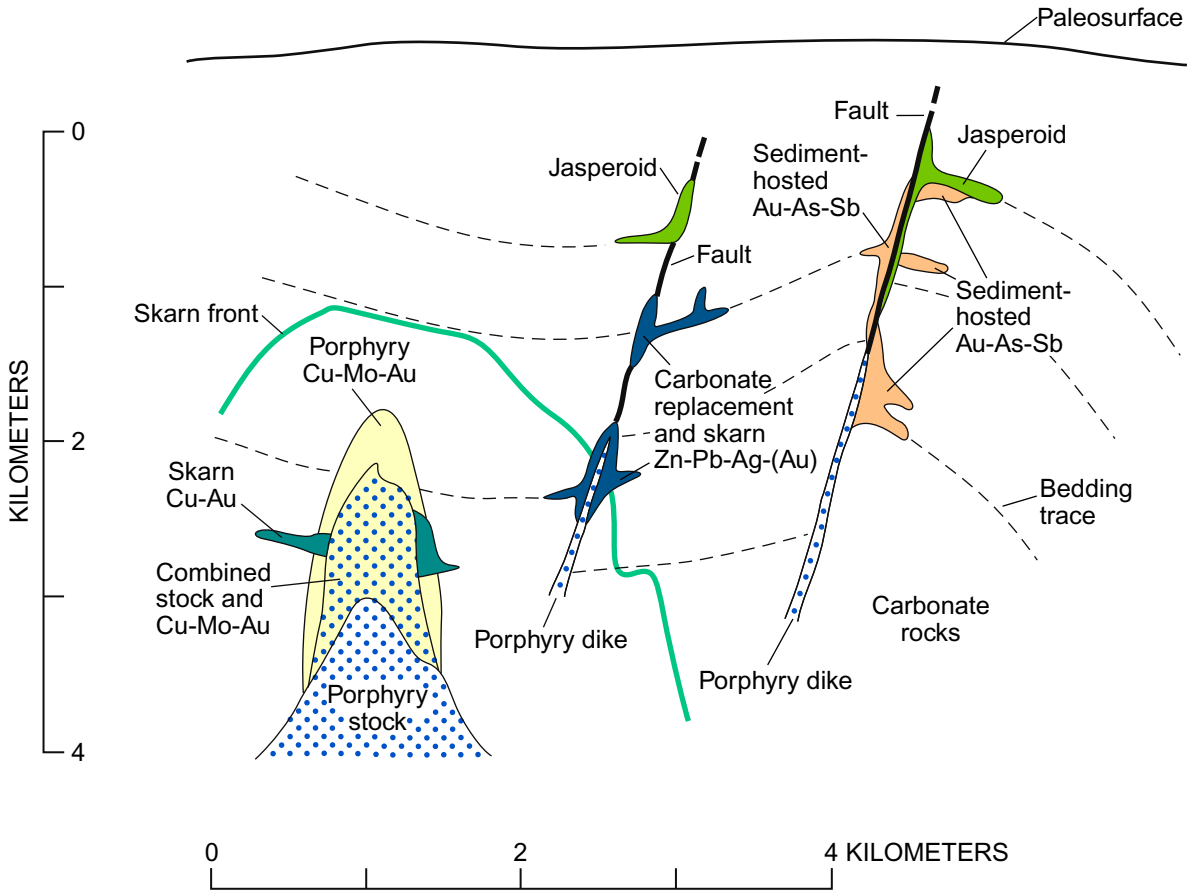

Figure 101. Schematic cross section showing inferred general relations of sediment-hosted gold deposits on fringes of base- and precious-metal mining districts. Porphyry Cu-Mo-Au deposits may include significant proportions of upper parts of associated stocks. Metals potentially present shown parenthetically. Short-dashed lines, schematic form lines of bedding in sedimentary strata. From Sillitoe and Bonham (1990).

Table 18. Characteristics of permissive terranes and favorable tracts for Proterozoic carbonatite-related, rare earth element (REE) deposits; Mesozoic gold-bearing breccia pipes; Mesozoic stockwork-molybdenum systems, and other types of deposits in the East Mojave National Scenic Area, California.

[------do.------, same as above; --, not available; n.a., possibly not applicable]

Deposit type	Permissive terrane	Favorable tract	Criteria used to delineate favorable tract[1]	Age	Worldwide Characteristics[2]	
					Median tonnage (million tonnes)	Median grade
Proterozoic						
Proterozoic carbonatite-related, REE deposit	All Early Proterozoic rocks	Belt of ultrapotassic rocks and carbonatite	1, 2, 3	1.4 Ga	60	[3]0.58 percent Nb_2O_5
Mesozoic						
Gold-bearing breccia pipe	Shallow-level magmatic hydrothermal environment	Area delinated by petrogenetically linked veins	1, 4, 5, 6, 9	~100 Ma	--	--
Stockwork molybdenum deposits	Area underlain by Mid Hills adamellite of Beckerman and others (1982)	Widespread alteration	1, 4, 5, 7, 8	~59–71 Ma	94	0.085 percent Mo
Copper skarn	Sequences of Paleozoic carbonate rocks[4]	Sequences of Paleozoic carbonate rocks[4]	1, 4, 5, 9, 10	Jurassic and Cretaceous	0.56	1.7 percent Cu
Lead-zinc skarn	------do.------	------do.------	------do.------	------do.------	1.4	5.9 percent Zn 2.8 percent Pb
Tungsten skarn	------do.------	------do.------	------do.------	------do.------	1.1	0.67 percent WO[3]
Tin (tungsten) skarn	------do.------	------do.------	------do.------	------do.------	[5]9.4	[5]0.31 percent Sn
Iron skarn	------do.------	------do.------	1, 4, 5, 9, 10, 11	------do.------	7.2	50 percent Fe
Gold skarn	------do.------	------do.------	4, 5, 9, 10	------do.------	[6]0.213	[6]8.6 g/tonne Au
Polymetallic replacement	------do.------	------do.------	1, 4, 5, 9, 10	------do.------	1.8	5.2 percent Pb 3.9 percent Zn
Polymetallic vein	All Mesozoic and older rocks	All Mesozoic and older rocks	1, 4, 5, 6, 12	------do.------	n.a.	n.a.
Tertiary						
Epithermal volcanic-hosted gold	Rhyolitic flow domes and caldera	Hydrothermally altered and demagnetized rocks	1, 4, 5, 7, 11, 12	15.5 Ma	[7]1.6	[7]8.4 g/tonne Au

[1]Criteria: 1, Presence of mines and prospects; 2, presence of ultrapotassic and carbonatite rocks; 3, anomalous concentrations of REE in rock geochemistry, concentrate samples, and National Uranium Resource Evaluation (NURE) samples; 4, geochemical anomalies of base and precious metals in various sample media; 5, presence of petrogenetically linked metal occurrences; 6, presence of major premineralization structure; 7, widespread hydrothermal alteration of host igneous phase; 8, widespread presence of quartz-sulfide stockworks; 9 presence of reactive, premineralization rocks; 10, skarn alteration in carbonate rocks together with widespread occurrences of polymetallic veins, polymetallic veins, polymetallic faults, and gold-silver quartz-pyrite veins; 11, aeromagnetic data; 12, widespread alteration detected using Thematic Mapper image.
[2]From Cox and Singer (1986), except as noted.
[3]World-class REE deposit at Mountain Pass, just outside EMNSA, includes sparse Nb and extraordinary contents of light rare earth elements.
[4]Includes copper, lead-zinc, iron, tungsten, tin (tungsten), and gold skarns in EMNSA.
[5]Based on only grade and tonnage information from four deposits.
[6]From Theodore and others (1991).
[7]From epithermal quartz-alunite vein deposit model in Cox and Singer (1986).

Table 19. Analyses of rocks in the general area of the Big Hunch stockwork-molybdenum system, New York Mountains, East Mojave National Scenic Area, California.

[Analyses in parts per million; --, not detected. Semiquantitative emission-spectrographic analyses by J. Harris and B. Spillare using methods of Grimes and Marranzino (1968). Results are reported with a relative standard deviation for each value of plus 50 percent and minus 33 percent. Looked for but not found, at part-per-million detection levels (shown in parantheses); As (150), Au (10), Cd (32), Dy (22), Er (10), Eu (2.2), Gd (15), Ge (1.5), Hf (15), Ho (6.8), In (6.8), Ir (15), Lu (15), Os (22), Pd (1), P (68), Pt (4.6), Re (10), Rh (2.2), Ru (2.2), Sb (32), Sm (10), Ta (460), Tb (32), Tm (4.6), U (320), W (10). Partial chemical analyses by E. Campbell and D. Kobilis using standard methods of Shapiro (1975)]

Analysis No.	Sample 81TT	Ag	B	Ba	Be	Ce	Co	Cr	Cu	Ga	La	Li	Mn	Mo	Nb	Nd	Ni	Pb	Sc	Sn	Sr
									Semiquantitative emission-spectrographic analyses												
1	40	--	--	860	--	--	--	--	19	10	--	--	33	13	--	--	--	6.9	1.7	--	310
2	41	--	9.6	320	2	--	--	--	32	13	24	75	95	84	7.5	--	--	--	4.6	4.5	410
3	42	0.096	--	1,000	3	--	--	--	70	25	25	--	130	190	4.9	--	--	24	4.1	8.3	340
4	43	1.3	--	600	--	--	--	--	8.6	29	29	--	77	4.3	--	41	--	9	3.1	3.1	300
5	44	--	5.7	320	2.3	--	--	--	32	10	10	--	110	1.2	10	--	--	18	4.4	--	300
6	45B	0.38	--	540	--	--	--	--	7.6	18	18	--	65	50	--	--	--	9.3	1.9	--	260
7	46	1.4	31	440	--	--	--	--	73	22	22	--	50	82	6.9	--	--	16	2.4	1.6	200
8	47	0.18	24	870	1.5	--	--	--	32	49	49	--	66	81	--	52	--	15	3	2.4	350
9	48	--	--	600	--	--	--	--	190	19	19	--	60	5.1	4.2	--	--	7.7	2.8	3.1	210
10	49	--	--	1,000	2.3	--	--	--	32	27	27	--	75	7	4.8	--	--	13	3.3	4.4	390
11	50	--	--	570	1.7	--	--	--	17	21	21	--	140	7.5	3.3	--	--	--	3.1	1.9	250
12	51	--	--	640	1.2	--	--	--	32	20	20	--	78	81	3.3	--	--	--	3.2	2.4	250
13	52	--	--	620	1.8	--	--	1.3	570	31	31	73	90	260	4.2	--	--	9.1	5.5	3	250
14	53	--	49	1,000	3.2	--	1.5	--	2,400	29	29	89	43	14	5.7	46	--	22	3.4	2.8	580
15	54	--	--	830	2.4	--	--	1.4	230	21	21	--	67	--	4.7	40	--	12	3.1	3.3	450
16	55	--	--	730	2.3	--	1.4	--	220	29	29	--	97	--	6.4	53	--	12	4	3.1	460
17	56	--	--	740	2.4	--	1.7	--	44	12	26	--	99	--	44	40	1.5	13	2.7	3.2	490
18	57	--	--	720	2.3	--	1.2	--	48	15	22	--	81	--	4.2	--	--	18	2.5	5.5	510
19	58	0.17	7.7	480	4.3	56	2	--	210	18	40	--	160	9.6	7.2	50	--	26	4.1	3.4	200
20	59	4.6	--	120	1.3	--	--	--	43	12	--	--	110	460	--	--	2.1	170	2.6	3.1	34
21	60	0.33	9.7	820	2.7	--	--	--	41	21	16	--	74	87	4.2	32	--	9.6	4	4	300
22	61	--	--	360	--	--	1.3	--	42	15	15	--	110	--	4.9	--	--	32	2.4	2.7	260
23	62	--	--	720	1.8	--	1.1	--	70	18	17	--	110	--	6	--	--	25	3	2.5	400
24	63	--	--	300	--	--	--	--	9.5	6.7	--	--	29	21	6.7	--	1.8	7.6	1.7	4.1	150
25	64	0.15	38	420	3.6	--	--	--	60	13	28	84	81	86	6	36	--	11	3.9	2.6	290
26	65	--	5.3	580	3	--	1.6	--	4,000	19	25	--	210	2.3	6.2	--	--	17	3.8	4	280
27	73	--	41.0	310	2.5	--	--	--	41	21	25	--	94	150	4.3	44	--	28	3.3	2.4	730
28	76	0.66	--	1,100	5.1	110	--	--	140	25	54	--	260	--	6.1	83	2	7.9	5.4	3	440
29	77	--	--	560	1.7	--	1.1	2.2	21	20	20	--	110	--	6.1	32	2.1	31	4	1.7	390
30	78	0.9	--	700	4.8	--	--	1.6	99	23	19	--	280	--	8	--	1.6	12	4.8	3.9	270
31	79	--	--	910	37	--	--	1.8	7	22	22	--	220	--	7.2	--	--	25	5	3.8	640
32	80	0.16	20	1,000	2.4	--	2.3	1.3	67	19	33	--	78	--	5.6	55	1.8	14	4.8	3.3	490
33	70	--	32	200	200	--	--	--	22	24	14	14	14	4.5	23	--	1.6	24	4.9	5.4	560
34	71	--	6.6	1,100	1,100	--	2.1	--	13	19	38	38	38	21	5.6	56	--	16	4.7	3.7	540
35	72	--	--	210	210	--	--	--	32	17	--	--	--	--	7.5	--	--	28	3.2	--	80
36	81	--	6.0	190	190	--	--	--	32	26	--	--	--	--	30	--	2	12	4.6	1.8	210

1-4 Variably quartz veined gneissic Mid Hills adamellite of Beckerman and others (1982).
5 Rhyodacite dike.
6-19 Variably quartz veined gneissic Mid Hills adamellite.
20-21 Variably quartz veined gneissic Mid Hills adamellite.
22 Teutonia adamellite of Beckerman and others (1982).
23-36 Variably quartz veined gneissic Mid Hills adamellite.
27-31 Variably altered, very weakly quartz veined, gneissic Mid Hills adamellite.
32 Surface grab sample; quartz veined, gneissic Mid Hills adamellite.
33 Drill core. Sericitically altered, porphyritic rhyodacite.
34 DDH York-5-110 ft. Potassic- and sericitically-altered Mid Hills adamellite.
35 DDH York-5-1,364 ft. Argillic-altered Mid Hills adamellite.
36 Surface grab sample; gneissic Mid Hills adamellite.

Table 19. Analyses of rocks in the general area of the Big Hunch stockwork-molybdenum system, New York Mountains, East Mojave National Scenic Area, California—Continued.

Analysis No.	Sample 81TT	V	Y	Yb	Zn	Zr	Cl	F	W
	Semiquantitative emission-spectrographic analyses						Chemical analyses		
1	40	5.7	3	0.32	--	41	22	700	2.7
2	41	14	6.8	0.5	23	88	13	2,500	7
3	42	20	4.3	0.54	--	71	13	2,200	7.9
4	43	12	4.6	0.51	18	34	13	1,000	4.6
5	44	5.9	7.9	0.92	--	23	17	1,000	2.8
6	45B	6.5	2.2	--	--	31	16	800	2.5
7	46	5.1	8.3	0.87	--	34	--	1,400	4.1
8	47	12	5.5	0.36	15	39	--	1,100	3.1
9	48	9.6	4.9	0.5	2	42	--	1,200	3.3
10	49	19	7.8	0.68	18	82	--	1,300	3.7
11	50	21	3.7	0.5	19	59	13	1,400	5.2
12	51	14	7.2	0.77	17	44	24	900	4.1
13	52	22	14	1.1	--	73	--	1,800	3
14	53	13	5.9	0.86	32	110	--	1,200	3.9
15	54	11	5.5	0.53	27	73	18	1,200	1.1
16	55	14	8.5	0.78	39	49	24	1,400	1.8
17	56	12	3.1	12	25	54	31	900	0.56
18	57	12	3.9	19	23	68	16	1,100	0.5
19	58	19	7.9	18	24	96	15	880	8.8
20	59	18	2.1	29	17	12	--	1,000	3.5
21	60	29	5.9	4.8	--	100	17	2,100	3.9
22	61	4.8	10	0.25	17	36	19	400	0.26
23	62	8.5	7.6	8.5	45	64	26	1,000	0.96
24	63	3.9	4.1	3.9	17	15	14	500	1.3
25	64	6.8	17	6.8	26	74	16	1,400	3.8
26	65	7.5	15	7.5	56	98	67	1,000	1.7
27	73	15	6.8	15	23	59	--	2,100	4
28	76	23	5.4	0.23	--	130	--	5,800	7.9
29	77	20	4.8	20	56	65	18	900	2.2
30	78	27	2.3	0.27	--	74	--	2,500	12
31	79	20	3	0.38	--	65	--	2,500	57
32	80	13	7.5	0.82	--	93	19	1,800	4
33	70	3.7	12	1.2	17	17	20	1,300	2.3
34	71	16	9.4	1	--	--	25	2,000	3.6
35	72	4.7	6.9	0.64	19	19	--	25	0.5
36	81	2.5	9.2	1.1	18	18	18	1,000	2.2

Table 20. Chemical analyses of 97 rocks from 47 mineralized sites designated as gold-silver quartz-pyrite veins in East Mojave National Scenic Area, California.

[All concentrations in parts per million except Au, which is in parts per billion; STD, standard deviation; MIN, minimum; MAX, maximum. Data from U.S Bureau of Mines, 1990a]

Sample No.	Au (ppb)	Ag	Au/Ag Ratio	As	Ba	Cd	Ce	Co	Cr	Cs	La	Lu	Mo	Ni	Sb	Sc	Sm	Ta	Th	U	W	Zn
CDC-10	701	1	0.701	2	190	2.5	56	7	300	1	23	0.4	0.5	5	0.2	2	3.4	0.7	14	2.4	1	100
CDC-11	483	37	0.013	14	130	2.5	47	6	210	4	20	0.6	12	5	25.4	5.2	4.4	0.25	3.6	5.2	13	480
CDC-12	5	1	0.005	2	460	2.5	120	2.5	190	5	54	0.9	0.5	5	0.4	11	10.2	1.1	13	2	3	140
CDC-148	3	1	0.003	7	560	2.5	53	8	340	3	25	0.1	1	5	2.4	2.4	3.8	0.25	11	3.1	6	130
CDC-159	11100	5	2.220	14	460	11	29	16	340	2	12	0.1	27	29	1.2	10	3.5	0.5	3.5	5.4	15	1500
CDC-160	635	5	0.127	4	120	2.5	6	15	390	0.5	5	0.1	7	13	0.4	1.1	0.8	0.25	1.9	2	4	50
CDC-166	298	1	0.298	3	140	2.5	68	2.5	300	2	22	1.4	5	5	0.3	3.4	6.8	2.2	31.3	2.9	3	50
CDC-167	794	2	0.397	3	100	2.5	45	13	250	2	17	1	5	5	0.4	3.1	5.4	1.9	12	2.7	4	50
CDC-168	12	1	0.012	1	110	2.5	91	2.5	340	3	26	1.3	0.5	5	0.4	4.1	8.6	2.4	58.8	3.4	3	50
CDC-169	1160	3	0.387	6	430	2.5	59	15	310	2	23	1.1	3	5	0.3	3	5.5	0.7	21.5	10	3	50
CDC-170	261	1	0.261	5	280	2.5	21	21	300	1	7	0.3	1	15	0.3	4.7	2.6	0.25	4.4	4.3	10	50
CEM-24	47	4	0.012	8	25	2.5	31	2.5	180	0.5	13	0.1	18	5	1.2	3.4	1.7	0.25	3.6	2.4	2	50
CEM-28	15	1	0.015	41	57	2.5	2.5	14	300	0.5	3	0.1	21	15	1	1	0.5	0.25	1.7	11	1	50
CJO-04	4350	5	0.870	7	160	2.5	11	14	490	0.5	5	0.2	2	5	1.7	1.1	0.8	0.25	1.2	2.6	0.5	50
CJO-05	885	4	0.221	25	52	2.5	10	5	450	0.5	6	0.8	16	5	4.7	0.4	1	0.25	1.8	6.8	0.5	50
CJO-06	6540	13	0.503	7	25	2.5	2.5	2.5	450	0.5	1	0.2	53	5	0.6	0.2	0.3	0.25	0.8	3.8	0.5	50
CJO-09	20300	288	0.070	17	330	2.5	2.5	2.5	240	2	7	0.1	15	5	0.6	0.1	0.9	0.25	2.6	13	3	280
CJO-11	1270	3	0.423	35	400	2.5	32	12	310	2	15	0.6	17	5	3.8	2	2.9	0.25	5.4	5.3	12	50
CJO-15	72	2	0.036	5	610	2.5	10	6	330	2	6	0.3	183	11	1.1	1.4	1	0.25	8.9	4.3	4	380
CJO-16	5	1	0.005	7	340	2.5	110	7	310	3	44	0.8	3	33	3.7	6.2	7.3	0.25	31.7	4.7	4	120
CJO-17	150	40	0.004	3	340	2.5	2.5	7	420	0.5	3	0.2	41	5	0.8	0.9	0.4	0.25	2	3.1	7	120
CJO-23	581	1	0.581	1	180	2.5	14	9	410	1	7	0.1	0.5	17	0.2	2	1.5	0.25	2.8	0.5	4	110
CJO-30	43	1	0.043	12	320	2.5	37	8	250	2	11	0.1	47	5	56.9	3.8	1	0.25	2.8	8.2	2	50
CJO-33	58	1	0.058	0.5	25	2.5	2.5	2.5	420	0.5	1	0.1	0.5	5	0.9	0.1	0.2	0.25	0.1	0.1	0.5	50
CMM-11-36	3	1	0.003	2	1300	2.5	94	2.5	200	0.5	42	0.05	0.5	12	0.2	3.8	6.2	1	19	1.6	4	50
CMM-11-44	1	1	0.001	1	130	2.5	20	2.5	240	0.5	8	0.1	0.5	5	0.05	0.7	1.3	0.25	3.6	0.2	3	50
CRM-07	1	1	0.001	5	110	2.5	2.5	2.5	280	0.5	1	0.2	5	5	0.3	0.3	0.2	0.25	1.5	4.9	2	50
CRM-14	3	1	0.003	6	250	2.5	16	2.5	350	0.5	8	0.1	0.5	5	0.5	1.1	1	0.6	8.7	1.9	0.5	50
CRM-18	8	1	0.008	23	1900	2.5	70	2.5	300	2	36	0.3	101	5	0.3	2.1	3.7	0.9	17	5.4	2	110
CRM-22	4	1	0.004	9	260	2.5	76	21	230	0.5	27	1.4	1	36	2.7	23.3	5.5	0.5	10	2.2	0.5	150
CRM-25	4	4	0.001	9	470	2.5	26	2.5	200	2	10	0.1	33	5	6.2	2.1	1.4	0.8	3.3	1.1	5	50
CRM-27	8	38	0.000	120	130	2.5	2.5	5	390	0.5	1	0.1	5	5	20.1	1.3	0.3	0.25	0.1	0.7	185	50
CRM-35	1	1	0.001	4	25	2.5	2.5	2.5	340	0.5	1	0.1	217	5	8.3	0.1	0.2	0.25	0.4	0.4	1	50
CRM-40	8	1	0.008	22	870	2.5	44	2.5	150	2	22	0.1	0.5	5	1.3	1.1	2.9	0.25	14	0.4	0.5	50
CRM-54	1	1	0.001	1	25	2.5	2.5	2.5	350	0.5	1	0.1	156	5	1.3	0.5	0.2	0.25	0.5	0.2	2	50
CRR-11	200	1	0.200	5	980	2.5	34	12	390	3	15	0.1	17	5	2.6	1.9	3.3	0.25	1.9	2.8	6	50
CRR-111	6090	1	6.090	3	120	2.5	2.5	2.5	580	0.5	4	0.1	4	5	0.3	0.6	0.5	0.25	3.1	0.7	2	50
CRR-112	674	1	0.674	16	1200	2.5	95	2.5	230	3	41	0.3	3	5	0.4	13	4.9	1.3	20.2	4.8	17	50
CRR-113	9540	1	9.540	8	25	2.5	2.5	2.5	400	0.5	1	0.1	2	5	0.4	0.2	0.05	0.25	0.5	4.4	2	50
CRR-114	1030	1	1.030	2	190	2.5	8	2.5	3250	0.5	8	0.1	1	5	0.4	0.6	0.6	0.25	2.9	0.7	17	50
CRR-115	549	1	0.549	6	120	2.5	8	2.5	360	0.5	4	0.1	3	5	0.6	0.7	0.6	0.25	2.3	0.3	2	50
CRR-116	13	1	0.013	4	250	2.5	13	2.5	320	0.5	6	0.1	3	5	0.4	1.2	1	0.25	5.1	1.6	1	50
CRR-12	9	1	0.009	7	440	2.5	54	6	430	0.5	22	0.1	15	5	3.2	1.2	4.6	0.25	1.1	3	1	50
CRR-13	27	1	0.027	4	300	2.5	48	8	250	1	21	0.1	14	5	2.4	4.6	3.7	0.25	5.5	5.6	4	50
CRR-14	9	1	0.009	8	200	2.5	120	10	330	1	54	0.1	12	5	1.5	5.8	4.2	0.25	4.5	3.8	6	50
CRR-41	804	1	0.804	211	25	2.5	2.5	2.5	240	0.5	3	0.1	46	5	3.7	2.2	0.05	1.4	13	16	11	260
CRR-55	89	1	0.089	5	180	2.5	13	2.5	380	0.5	7	0.1	0.5	5	0.2	0.9	1.3	0.25	4.7	1.4	2	50
CRR-57	224	1	0.224	96	620	2.5	110	36	61	9	37	0.3	3	26	1.3	20	11.3	0.25	8.2	16	8	140
CRR-58	2970	1	2.970	84	680	2.5	77	42	140	3	27	0.3	15	29	0.7	15	9.4	0.5	7.4	9.5	4	110
CRR-59	130	1	0.130	4	120	2.5	16	2.5	420	0.5	9	0.1	3	5	0.3	1	0.7	0.25	6.9	0.8	0.5	50
CRR-60	10	1	0.010	19	1400	2.5	240	2.5	140	2	110	0.1	0.5	5	0.4	6	12.5	1	328	7.7	2	50
CRR-61	516	1	0.516	2	25	2.5	5	2.5	430	0.5	3	0.1	1	5	0.2	0.6	0.4	0.25	2.7	0.8	0.5	50
CRR-62	13	3	0.004	16	380	2.5	60	2.5	310	1	36	0.5	6	12	1	13	3.8	1.2	36.3	4.8	0.5	50
CRR-63	991	4	0.248	74	120	2.5	2.5	63	270	0.5	3	0.1	29	5	1	1.7	0.8	0.25	1.8	14	4	410
CRR-64	84	1	0.084	2	55	2.5	7	15	250	0.5	4	0.1	9	5	0.1	0.5	0.7	0.25	1.3	0.8	3	50
CRR-65	3	1	0.003	7	340	2.5	2.5	2.5	140	2	3	0.1	0.5	5	0.4	15	0.6	2	8.5	5.3	0.5	50
CRR-66	7	1	0.007	2	1200	2.5	88	25	150	2	37	0.4	0.5	44	0.5	19	8.7	1.2	10	2.3	2	150
CRR-67	11200	3	3.733	12	230	2.5	18	13	410	0.5	8	0.1	7	5	0.5	1.5	1.1	0.25	6	1.7	4	50
CRR-68	256	2	0.128	86	25	2.5	9	2.5	200	1	7	0.1	49	5	1.6	1.6	1.2	0.25	2.4	11	10	430
CRR-69	9210	3	3.070	8	89	2.5	2.5	7	350	0.5	3	0.1	8	5	0.3	0.8	0.4	0.25	1.6	3	2	50
CRR-70	12100	4	3.025	31	120	2.5	2.5	5	360	0.5	4	0.1	16	5	0.3	1	0.5	0.25	3.4	1	5	50

Table 20. Chemical analyses of 97 rocks from 47 mineralized sites designated as gold-silver quartz-pyrite veins in East Mojave National Scenic Area, California—Continued

Sample No.	Au (ppb)	Ag	Au/Ag Ratio	As	Ba	Cd	Ce	Co	Cr	Cs	La	Lu	Mo	Ni	Sb	Sc	Sm	Ta	Th	U	W	Zn
CRR-75	522	1	0.522	8	620	2.5	110	8	340	1	47	0.3	0.5	21	0.7	10	7.1	1	20	4.7	10	50
CRR-76	496	1	0.496	7	300	2.5	21	10	320	0.5	13	0.1	17	15	0.2	2.2	1.7	0.25	5.6	2.7	4	50
CRR-77	1390	1	1.390	2	380	2.5	25	7	400	0.5	14	0.1	2	5	0.1	1	2	0.25	8.4	1.2	3	50
CRR-78	1250	1	1.250	7	410	2.5	52	2.5	360	0.5	25	0.1	33	12	0.2	1.9	3.3	0.25	10	1.2	2	50
CRR-79	6900	1	6.900	8	180	2.5	25	2.5	370	0.5	15	0.1	7	5	0.2	1	2.2	0.25	6.9	2.6	1	50
CRR-80	7530	1	7.530	3	310	2.5	21	10	290	0.5	7	0.1	2	5	0.1	0.5	1.4	0.25	3.4	1	3	50
CRR-81	4270	1	4.270	3	460	2.5	19	2.5	270	1	14	0.1	1	5	0.2	1.2	2.6	0.25	8	1.2	4	50
CRR-82	45	1	0.045	0.5	210	2.5	15	2.5	270	0.5	8	0.1	1	5	0.05	1	1.4	0.25	10	1.1	3	50
CRR-84	1450	6	0.242	95	25	2.5	6	8	290	0.5	4	0.1	13	5	3.4	1.5	0.8	0.25	2.7	2.1	6	50
CRR-85	17400	6	2.900	103	180	2.5	2.5	32	220	0.5	6	0.1	23	5	3.3	4.5	1.3	0.25	1.1	11	12	50
CRR-86	899	1	0.899	6	82	2.5	7	11	330	0.5	3	0.1	4	11	0.5	0.3	0.6	0.25	2.6	0.7	0.5	50
CRR-87	1390	2	0.695	20	120	2.5	2.5	14	410	0.5	1	0.1	8	5	0.6	0.3	0.3	0.25	1	0.6	1	50
CRR-88	20	1	0.020	5	960	2.5	77	6	190	3	34	0.4	5	20	0.4	11	5.6	1.8	15	4.4	3	50
CRR-89	1	1	0.001	12	25	2.5	2.5	19	61	0.5	3	0.1	0.5	5	0.05	1.4	2.3	0.25	0.7	2.6	28	50
CRR-90	98	1	0.098	9	82	2.5	32	460	250	5	20	0.1	23	57	0.3	1.9	3.1	0.25	5.3	15	22	50
CRR-91	333	1	0.333	5	140	2.5	7	13	300	0.5	4	0.1	48	5	0.2	1.3	0.7	0.25	3.4	1.1	3	50
CRR-92	28	1	0.028	16	320	2.5	67	6	150	0.5	22	0.1	15	23	0.9	17	5.7	0.8	6.9	28.9	6	50
CRR-93	85	1	0.085	2	130	2.5	2.5	2.5	340	0.5	1	0.1	3	12	0.1	0.8	0.2	0.25	1	0.6	0.5	50
CRR-94	7140	1	7.140	4	25	2.5	2.5	2.5	450	0.5	1	0.1	3	5	0.2	0.4	0.2	0.25	0.1	0.8	1	50
CRR-97	268	8	0.034	4	110	2.5	20	2.5	310	0.5	11	0.1	2	5	1.7	1.5	1.5	0.25	18	1.6	3	50
CRR-98	5	1	0.005	17	98	2.5	18	799	350	0.5	13	0.1	5	49	0.2	0.8	0.9	0.25	1.1	5.2	2	50
CTN-54	1	1	0.001	11	180	2.5	2.5	2.5	280	0.5	2	0.1	116	5	1.6	0.1	0.3	0.25	0.5	8.1	0.5	50
CTN-55	8	6	0.001	20	25	2.5	2.5	2.5	310	0.5	1	0.1	10	5	0.05	0.2	0.1	0.25	0.9	5.6	1	50
CTP-031	352	12	0.029	25	1000	2.5	43	6	330	3	22	0.5	32	5	24.6	3.7	3	0.7	17	4.1	4	330
CTP-033	1110	7	0.159	13	590	2.5	28	2.5	250	3	14	0.3	9	5	11.4	1.9	2	1.1	20.5	3.2	2	50
CTP-118	1	1	0.001	2	530	2.5	62	7	170	2	34	0.1	0.5	5	0.1	3.7	2.7	1.6	37.8	6.4	0.5	50
CTP-119	1	1	0.001	2	79	2.5	5	2.5	440	0.5	2	0.1	0.5	5	0.4	0.5	0.4	0.25	2.6	0.4	0.5	50
CTP-120	693	86	0.008	4	370	2.5	57	51	280	3	25	0.1	21	5	0.4	7	4.4	1	9.3	14	21	50
CTP-121	2010	12	0.168	11	130	2.5	32	2.5	170	2	18	0.1	0.5	11	7.8	2.2	1.9	0.25	12	4.6	3	50
CTP-122	263	89	0.033	7	170	2.5	9	2.5	170	0.5	3	0.1	1	5	33.3	0.4	0.4	0.25	1.7	0.9	0.5	50
CWC-28	822	1	0.822	25	82	2.5	2.5	2.5	390	0.5	5	0.3	0.5	22	1.2	5.4	1.1	0.25	1.3	0.6	6	50
CWC-42	82	1	0.082	33	25	2.5	14	9	280	0.5	7	0.1	2	5	1.2	2.8	1.1	0.25	0.8	2.4	2	50
CWC-45	13	1	0.013	10	65	2.5	18	92	290	2	11	0.1	3	5	0.6	3.7	1.3	0.25	1.9	1.7	4	50
CWC-47	36	4	0.009	5	750	2.5	230	2.5	210	1	100	0.5	0.5	5	1.4	4.1	15.6	0.6	89	5.1	0.5	50
CWC-48	7	1	0.007	1	320	2.5	33	2.5	240	0.5	15	0.3	1	5	0.2	0.4	2.5	0.25	11	3	0.5	50
CWC-51	12400	6	2.067	26	370	2.5	62	2.5	250	2	28	0.3	9	11	9	1.2	4	0.25	19	1.9	4	50
AVERAGE:	1813.16	7.21		17.37	315.47	2.59	34.99	22.03	329.71	1.30	15.91	0.24	17.42	9.44	2.90	3.48	2.68	0.49	12.00	4.17	6.15	96.39
STD:	3836.02	30.59		30.87	343.28	0.86	43.01	92.39	312.58	1.32	18.31	0.29	35.69	9.91	7.68	4.74	2.98	0.48	34.60	4.53	18.93	166.92
MIN:	1	1		0.5	25	2.5	2.5	2.5	61	0.5	1	0.1	0.5	5	0.05	0.1	0.05	0.25	0.1	0.1	0.5	50
MAX:	20300	288		211	1900	11	240	799	3250	9	110	1.4	217	57	56.9	23.3	15.6	2.4	328	28.9	185	1500

Summary

From our evaluations that largely used model-based criteria, we conclude that much of the East Mojave National Scenic Area (EMNSA) contains significant indications of epigenetic mineralization of various types. Economically significant concentrations of many metals may possibly remain to be discovered in many parts of the EMNSA (see also Wetzel and others, 1992). We have discussed specific types of metallic deposits that are known to be present in the EMNSA. Some mountain ranges that have widespread occurrences are the Providence Mountains, Clark Mountain Range, Ivanpah Mountains, and New York Mountains; the area of Hackberry Mountain is included in a tract that is judged to be favorable for the discovery of epithermal, volcanic-hosted gold deposits (pl. 2). These ranges make up a broad, roughly north-south-trending region in the central part of the EMNSA. Much less endowed with known occurrences of all of the various types of deposits considered above are the Granite Mountains, the central parts of the Piute Range, the Fenner Valley area, the general area of Cima Dome, the Cima volcanic field, and areas west to Soda Lake. We have attempted to make some judgments concerning the gravel-covered areas in the EMNSA (pl. 3), including the areal extent of bedrock apparently covered only by thin veneers of gravel. But few data are available to us for the overwhelming bulk of the covered areas. The presence of any mineralization, the type of mineralization, and the extent and intensity of mineralization in the covered areas is essentially unknown. The likelihood is high, however, that those areas in the EMNSA covered only by a thin cap of gravels could host mineralization similar to that known in the adjoining mountain ranges. Most buried epigenetic-mineral deposits do not respond to standard geophysical methods, particularly at the coarse spacing of the data-collection points available for our evaluation.

Restricting judgments concerning the presence of undiscovered metal resources in the EMNSA only to currently known types of deposits and to regionally representative tonnages for such deposits would undoubtedly yield small estimates for volumes of many metals that might be exploited.

Metals from most newly discovered, base- and ferrous-metal deposits of the types presently known in the EMNSA probably would be insignificant from the standpoint of national needs. For example, copper from a newly discovered skarn deposit in the EMNSA would have roughly a 25 percent chance of being in excess of approximately 10,000 tonnes contained Cu, if the grade-and-tonnage distribution curves of Jones and Menzie (1986b) for copper skarns are applicable to copper skarn in the EMNSA. Most copper in the United States is produced in the Southwest from much larger open-pit operations than those associated with the typical copper skarn; the former operations exploit large-tonnage porphyry-type systems. Historically, the EMNSA has been the site of minor production of many metals from a large number of sites. Since 1985, however, a small number of sites in the EMNSA whose gold production and reserves are much greater than that of the preceding discoveries have been developed (see U.S. Bureau of Mines, 1990a).

Nonetheless, widespread distribution of numerous types of deposits (including copper skarn, lead-zinc skarn, tin-tungsten skarn, polymetallic vein, gold-silver quartz-pyrite vein, low-fluorine porphyry molybdenum, gold breccia pipe, and volcanic-hosted gold) that are petrogenetically associated with igneous rock in many parts of the EMNSA is indicative of a metallogenic environment that may be the site of future discoveries of mineral-deposit types that are not now recognized by the exploration community. The science, art, and, yes, even luck of exploration procedures continually evolve, and this evolution is one of the most important aspects of currently employed methods of exploration (Bailly, 1981; Hutchinson and Grauch, 1991).

References Cited

Adrian, B.M., Frisken, J.G., Briggs, P.H., Bradley, L.A., and Crock, J.G., 1986a, Analytical results and sample locality map of heavy-mineral-concentrate and rock samples from the Fort Piute Wilderness Study Area (CDCA–267), San Bernardino County, California: U.S. Geological Survey Open-File Report 86–584, 15 p.

Adrian, B.M., Frisken, J.G., Malcolm, M.J., and Briggs, P.H., 1986b, Analytical results and sample locality map of heavy-mineral-concentrate and rock samples from the Cinder Cones Wilderness Study Area (CDCA–239), San Bernardino County, California: U.S. Geological Survey Open-File Report 86–403, 13 p.

Adrian, B.M., Frisken, J.G., Malcolm, M.J., and Crock, J.G., 1986c, Analytical results and sample locality map of heavy-mineral-concentrate and rock samples from the Castle Peaks Wilderness Study Area (CDCA–266), San Bernardino County, California: U.S. Geological Survey Open-File Report 86–416, 18 p.

Albin, A.L., and Karlstrom, K.E., 1991, Orthogonal Proterozoic fabrics in northwestern Arizona—Multiple orogenic events or progressive deformation during continental assembly, *in* Karlstrom, K.E., ed., Proterozoic geology and ore deposits of Arizona: Arizona Geological Society Digest 19, p. 67–84.

Albino, G.V., 1994, Time-pH-f_{O_2} paths of hydrothermal fluids and the origin of quartz-alunite-gold deposits, *in* Berger, B.R., ed., Advances in research on mineral resources, 1994: U.S. Geological Survey Bulletin 2081, p. 33–42.

Anderson, J.L., 1989, Proterozoic anorogenic granites of the southwestern United States, *in* Jenney, J.P., and Reynolds, S.J., eds., Geologic evolution of Arizona: Arizona Geological Society Digest 17, p. 211–238.

Anderson, J.L., Barth, A.P., Young, E.D., Davis, M.J., Farber, D., Hayes, E.M., and Johnson, K.A., 1988, Contrasting depth of emplacement across the Tujunga-North America terrane boundary [abs.]: Geological Society of America Abstracts with Programs, v. 20, no. 3, p. 139.

———1992, Plutonism across the Tujunga-North American terrane boundary—A middle to upper crustal view of two juxtaposed arcs, *in* Bartholomew, M.J., Hyndman, D.W., Mogk, D.W., and Mason, R., eds., Characterization and comparison of ancient and Mesozoic continental margins: Dordrecht, Netherlands, Kluwer Academic Publishers, Proceedings of the 8th International Conference on Basement Tectonics, p. 205–230.

Anderson, J.L., and Bender, E.E., 1989, Nature and origin of Proterozoic A–type magmatism in the southwestern United States of America: Lithos, v. 23, no. 1/2, p. 19–52.

Anderson, J.L., Wooden, J.L., and Bender, E.E., 1993, Mojave province of southern California and vicinity, *in* Van Schmus, W.R., and Bickford, M.E., eds., Transcontinental Proterozoic provinces, *in* Reed, J.C., Jr., and others, eds., Precambrian—Conterminous U.S.: Geological Society of America Decade of North American Geology Volume C–2, p. 176–188.

Anderson, J.L., Young, E.D., Barth, A.P., Wooden, J.L., Tosdal, R.M., and Morrison, Jean, 1991, Mesozoic batholiths of the Mojave [abs.]: Geological Society of America Abstracts with Programs, v. 23, no. 2, p. 3.

Anderson, J.L., Young, E.D., Clarke, H.S., Orrell, S.E., and Winn, M., 1985, The geology of the McCullough Range Wilderness area, Clark County, Nevada: Los Angeles, University of Southern California, Final Technical Report to the U.S. Geological Survey, 26 p., scale 1:24,000.

Anderson, P., and Guilbert, J.M., 1979, The Precambrian massive sulfide deposits of Arizona—A distinct metallogenic epoch and province: Nevada Bureau of Mines and Geology Report 33, Papers on mineral deposits of western North America, International Association on the Genesis of Ore Deposits, Fifth Quadrennial Symposium, v. 11, p. 39–48.

Aronsson, Bertil, Lundström, Torsten, and Rundqvist, Stig, 1965, Borides, silicides, and phosphides—A critical review of their preparation, properties, and crystal chemistry: London, Methuen and Co., 120 p.

Arth, J.G., 1976, Behavior of trace elements during magmatic processes—A summary of theoretical models and their applications: U.S. Geological Survey Journal of Research, v. 4, p. 41–47.

Aruscavage, P.J., and Crock, J.G., 1987, Atomic absorption methods, *in* Baedecker, P.A., ed., Methods for geochemical analysis: U.S. Geological Survey Bulletin 1770, p. C1–C6.

Ausburn, K.E., 1988, Tertiary volcanic hosted epithermal Au-mineralization at the Hart Mining District, Castle Mountains, northeastern San Bernardino County, California [abs.]: Geological Society of America Abstracts

with Programs, v. 20, no. 3, p. 140.
———1991, Ore-petrogenesis of Tertiary volcanic hosted epithermal gold mineralization at the Hart Mining District, Castle Mountains, northeastern San Bernardino County, California, *in* Raines, G.L., Lisle, R.E., Schafer, R.W., and Wilkinson, W.H., eds., Geology and ore deposits of the Great Basin: Reno, Nev., Geological Society of Nevada, Symposium Proceedings, p. 1,147–1,188.
Ayuso, R.A., and Shank, S.G., 1983, Quartz-molybdenite veins in the Priestly Lake granodiorite, north-central Maine: U.S. Geological Survey Open-File Report 83–800, 10 p.
Babcock, R.C., 1993, A summary of the geology of the Bingham district, Utah [abs.]: Reno, Nev., Society of Mining Engineers and Society of Economic Geology, Annual Meeting, Program and Abstracts, p. 148.
Baedecker, P.A., 1987, Methods for geochemical analysis: U.S. Geological Survey Bulletin 1770, 132 p.
Bagby, W.C., and Berger, B.R., 1985, Geologic characteristics of sediment-hosted, disseminated precious-metal deposits in the western United States, *in* Berger, B.R., and Bethke, P.M., eds., Geology and geochemistry of epithermal systems: Society of Economic Geologists Reviews in Economic Geology, v. 2, p. 169–202.
Bagby, W.C., and Cline, J.S., 1991, Constraints on the pressure of formation of the Getchell gold deposit, Humboldt County, as interpreted from secondary-fluid-inclusion data, *in* Raines, G.L., Lisle, R.E., Schafer, R.W., and Wilkinson, W.H., eds., Geology and ore deposits of the Great Basin: Reno, Nev., Geological Society of Nevada, Symposium Proceedings, p. 793–804.
Bagby, W.C., Menzie, W.D., Mosier, D.I., and Singer, D.A., 1986, Grade and tonnage model carbonate-hosted Au–Ag, *in* Cox, D.P., and Singer, D.A., eds., Mineral deposit models: U.S. Geological Survey Bulletin 1693, p. 175–177.
Bailly, P.A., 1981, Today's resource status, tomorrow's resource problems—The need for research on mineral deposits, *in* National Research Council, Mineral Resources—Genetic understanding for practical applications: Washington, D.C., National Academy Press, p. 21–32.
Baker, E.M., and Andrew, A.S., 1991, Geologic, fluid inclusion, and stable isotope studies of the gold-bearing breccia pipe at Kidston, Queensland, Australia: Economic Geology, v. 86, no. 4, p. 810–830.
Ballhorn, R.K., 1989, Ore deposit genesis and characterization, *in* International Atomic Energy Agency, ed., Uranium deposits in magmatic and metamorphic rocks: Vienna, International Atomic Energy Agency Proceedings, Salamanca, 29 Sept.–30 Oct., 1986, p. 239–243.
Barnum, E.C., 1989, Lanthology—Applications of lanthanides and the development of Molycorp's Mountain Pass operations, *in* The California desert mineral symposium, Compendium: Sacramento, California, U.S. Bureau of Land Management, p. 245–249.
Barth, A.P., Tosdal, R.M., and Wooden, J.L., 1990, A petrologic comparison of Triassic plutonism in the San Gabriel and Mule Mountains, southern California: Journal of Geophysical Research, v. 95, no. B112, p. 20,075–20,096.
Barton, P.B., 1986, Commodity/geochemical index, *in* Cox, D.P., and Singer, D.A., eds., Mineral deposit models: U.S. Geological Survey Bulletin 1693, p. 303–317.
Barton, P.B., Brew, D.A., Ludington, Steve, Lindsey, D.A., Ayuso, R.A., Force, E.R., Gamble, B.M., Goldfarb, R.J., John, D.A., and Johnson, K.M., 1995, Recommendations for assessments of undiscovered resources: U.S. Geological Survey Open-File Report 95–82, 90 p.
Bateman, P.C., 1965, Geology and tungsten mineralization of the Bishop district, California, *with a section on* Gravity study of Owens Valley, by L.C. Pakiser and M.F. Kane, *and a section on* Seismic profile, by L.C. Pakiser: U.S. Geological Survey Professional Paper 470, 208 p.
Battles, D.A., 1991, Hydrothermal alteration within the tilted Shamrock Batholith, Yerington district, Nevada, *in* Raines, G.L., Lisle, R.E., Schafer, R.W., and Wilkinson, W.H., eds., Geology and ore deposits of the Great Basin: Reno, Nev., Geological Society of Nevada, Symposium Proceedings, p. 351–353.
Beard, R.D., 1987, Geology and geochemistry of the central part of the Gold Hill mining district, Hidalgo and Grant Counties, New Mexico: Albuquerque, University of New Mexico, M.S. thesis, 110 p.
Beckerman, G.M., Robinson, J.P., and Anderson, J.L., 1982, The Teutonia batholith—A large intrusive complex of Jurassic and Cretaceous age in the eastern Mojave Desert, California, *in* Frost, E.G., and Martin, D.M., eds., Mesozoic-Cenozoic tectonic evolution of the Colorado River region, California, Arizona, and Nevada:

San Diego, California, Cordilleran Publishers, p. 205–220.
Bender, E.E., Anderson, J.L., Wooden, J.L., Howard, K.W., and Miller, C.F., 1988, Correlation of 1.7 Ga granitoid plutonism in the lower Colorado River region [abs.]: Geological Society of America Abstracts with Programs, v. 20, p. 142.
Benedetto, K.M.F., Dean, D.A., and Durgin, D.C., 1991, Roadside geology and precious-metal mineralization along US 50, Reno to Ely, Nevada, *in* Buffa, R.H., and Coyner, A.R., eds., Geology and ore deposits of the Great Basin: Reno, Nev., Geological Society of Nevada, Fieldtrip Guidebook Compendium, v. 2, p. 1,124–1,140
Bennett, V.C., and DePaolo, D.J., 1984, The definition of crustal provinces in the southern Rocky Mountain region using Sm-Nd isotopic characteristics [abs.]: Geological Society of America Abstracts with Programs, v. 16, p. 214.
———1987, Proterozoic crustal history of the western United States as determined by neodymium isotopic mapping: Geological Society of America Bulletin, v. 99, p. 674–685.
Berger, B.R., 1986a, Descriptive model of low-sulfide Au-quartz veins, *in* Cox, D.P., and Singer, D.A., eds., Mineral deposit models: U.S. Geological Survey Bulletin 1693, p. 239.
———1986b, Descriptive model of carbonate-hosted Au-Ag, *in* Cox, D.P., and Singer, D.A., eds., Mineral deposit models: U.S. Geological Survey Bulletin 1693, p. 175.
Berger, B.R., and Henley, R.W., 1989, Advances in the understanding of epithermal gold-silver deposits, with special reference to the western United States, *in* Keays, R.R., Ramsay, W.R.H., and Groves, D.I., eds., The geology of gold deposits—The perspective in 1988: Economic Geology Monograph 6, p. 405–423.
Berger, B.R., and Singer, D.A., 1992, Grade and tonnage model of hot-spring Au-Ag, *in* Bliss, J.D., ed., 1992, Developments in mineral deposit modeling: U.S. Geological Survey Bulletin 2004, p. 23–25.
Berger, V.I., 1993, Descriptive and grade-tonnage model for gold-antimony deposits: U.S. Geological Survey Open-File Report 93–194, 24 p.
Bergman, S.C., 1987, Lamproites and other potassium-rich rocks—A review of their occurrence, mineralogy, and geochemistry, *in* Fitton, J.G., and Upton, B.G.J., eds., Alkaline igneous rocks: Geological Society of London, Special Publication 30, p. 103–190.
Bingler, E.C., and Bonham, H.F., Jr., 1972, Reconnaissance geologic map of the McCullough Range and adjacent areas, Clark County, Nevada: Nevada Bureau of Mines and Geology Map 45, scale 1:125,000.
Bishop, C.C., comp., 1963, Geologic map of California, Needles sheet: California Division of Mines and Geology, scale 1:250,000.
Blakely, R.J., and Jachens, R.C., 1990, Concealed mineral deposits in Nevada—Insights from three-dimensional analysis of gravity and magnetic anomalies [abs.]: Geological Society of Nevada, Geology and Ore Deposits of the Great Basin, Program with Abstracts, p. 52–53.
———1991, Regional study of mineral resources in Nevada—Insights from three-dimensional analysis of gravity and magnetic anomalies: Geological Society of America Bulletin, v. 103, no. 6, p. 795–803.
Blanchard, Roland, 1968, Interpretation of leached outcrops: Nevada Bureau of Mines Bulletin 66, 196 p.
Bliss, J.D., ed., 1992a, Developments in mineral deposit modeling: U.S. Geological Survey Bulletin 2004, 168 p.
———1992b, Grade and tonnage model of Chugach-type low-sulfide Au-quartz veins, *in* Bliss, J.D., ed., Developments in mineral deposit modeling: U.S. Geological Survey Bulletin 2004, p. 44–46.
Bliss, J.D., and Cox, D.P., 1986, Grade and tonnage model of polymetallic veins, *in* Cox, D.P., and Singer, D.A., eds., Mineral deposit models: U.S. Geological Survey Bulletin 1693, p. 125–129.
Bonham, H.F., Jr., and Hess, R.H., 1993, Major precious-metal deposits, *in* The Nevada mineral industry—1992: Nevada Bureau of Mines and Geology Special Publication MI–1992, p. 18–27.
Bonura, C.J., 1984, Geology, stratigraphy, and origin of the Miocene volcanolacustrine rocks of Hackberry Mountain and Vontrigger Hills in the eastern Mojave desert, San Bernardino County, California: Los Angeles, California State University, M.S. thesis, 164 p.
Brew, D.A., Drew, L.J., Schmidt, J.M., Root, D.H., and Huber, D.F., 1991, Undiscovered locatable mineral resources of the Tongass National Forest and adjacent lands, southeastern Alaska: U.S. Geological Survey Open-File Report 91–10, 370 p.
Brooks, J.W., and Meinert, L.D., 1989, Mineralogy and petrology of the McCoy gold skarn, Lander County,

Nev. [abs]: Geological Society of America Abstracts with Programs, v. 21, no. 5, p. 59–60.
Brown, H.J., 1986, Detailed geologic map of the eastern New York Mountains, San Bernardino County, California [abs.]: Geological Society of America Abstracts with Programs, v. 18, no. 2, p. 89.
Brown, P.H., Rathjen, A.H., Graham, R.D., and Tribe, D.E., 1990, Rare earth elements in biological systems, *in* Gschneidner, K.A., and Eyring, L., eds., Handbook on the physics and chemistry of rare earths: Amsterdam, Elsevier, v. 13, chap. 92, p. 423–452.
Bryant, B., 1992a, Geologic map of the Poachie Range, Mohave and Yavapai Counties, Arizona: U.S. Geological Survey Miscellaneous Investigations Series Map I–2198, scale 1:25,000.
———1992b, Preliminary geologic map of the Alamo Lake 30' × 60' qaudrangle, west-central Arizona: U.S. Geological Survey Open-File Report 92–311, scale 1:100,000.
Bultman, M.W., Force, E.R., Gettings, M.E., and Fisher, F.S., 1993, Comments on the "three-step" method for quantification of undiscovered mineral resources: U.S. Geological Survey Open-File Report 93–23, 59 p.
Burchfiel, B.C., and Davis, G.A., 1971, Clark Mountain thrust complex in the Cordillera of southeastern California—Geologic summary and field trip guide, *in* Elders, W.A., ed., Geological excursions in southern California: Riverside, University of California, Campus Museum Contributions Number 1, p. 1–28.
———1977, Geology of the Sagamore Canyon-Slaughterhouse Spring area, New York Mountains, California: Geological Society of America Bulletin, v. 88, no. 11, p. 1,623–1,640.
———1981, Mojave Desert and environs, *in* Ernst, W.G., ed., The geotectonic development of California (Rubey Vol. I): Englewood Cliffs, N.J., Prentice-Hall, p. 217–252.
———1988, Mesozoic thrust faults and Cenozoic low-angle normal faults, eastern Spring Mountains, Nevada, and Clark Mountains thrust complex, California, *in* Weide, D.L., and Faber, M.L., eds., This extended land—Geological journeys in the southern Basin and Range: Geological Society of America Field Trip Guidebook, p. 87–106.
Burnett, J.L., 1990, California mining review: California Geology, v. 43, no. 10, p. 219–224.
Busby-Spera, C.J., 1988, Speculative tectonic model for the early Mesozoic arc of the southwest Cordilleran United States: Geology, v. 16, no. 12, p. 1,121–1,125.
Busby-Spera, C.J., Schermer, E.R., and Mattinson, J., 1989, Volcano-tectonic controls on sedimentation in an extensional continental arc—A Jurassic example from the eastern Mohave Desert, California [abs.], *in* Continental magmatism abstracts, International Association of Volcanology and Chemistry of the Earth's Interior, General Assembly, Santa Fe: New Mexico Bureau of Mines and Mineral Resources Bulletin 131, p. 34.
Calzia, J.P., Crowley, J.A., Dockter, R.D., Simoni, T.R., and Server, G.T., 1979, Leasable mineral resources of the California Desert Conservation Area: U.S. Geological Survey Administrative Report, two appendices, 183 p.
Capps, R.C., and Moore, J.A., 1990, Geologic setting of mid-Miocene gold deposits in the Castle Mountains, San Bernardino County, California, and Clark County, Nevada [abs.]: Geological Society of Nevada and U.S. Geological Survey Great Basin Symposium, Geology and ore deposits of the Great Basin, Program with Abstracts, p. 128.
———1991, Geologic setting of mid-Miocene gold deposits in the Castle Mountains, San Bernardino County, California, and Clark County, Nevada, *in* Raines, G.L., Lisle, R.E., Schafer, R.W., and Wilkinson, W.H., eds., Geology and ore deposits of the Great Basin: Reno, Nevada, Geological Society of Nevada, Symposium Proceedings, p. 1,195–1,219.
Carlisle, D.L., Luyendyk, B.P., and McPherron, R.L., 1980, Geophysical survey in the Ivanpah Valley and vicinity eastern Mojave Desert, California, *in* Fife, D.E., and Brown, A.R., eds., Geology and mineral wealth of the California desert: Santa Ana, California, South Coast Geological Society, p. 485–494.
Carten, R.B., White, W.H., and Stein, H.J., 1993, High-grade granite-related molybdenum systems—Classification and origin, *in* Kirkham, R.V., Sinclair, W.D., Thorpe, R.I., and Duke, J.M., eds., Mineral deposit modeling: Geological Association of Canada Special Paper 40, p. 521–554.
Castor, S.B., 1990, Rare earth resources—Comparisons of the geology of existing and potential resources, *in* Geitgey, R.P., and Vogt, B.F., eds., Industrial rocks and minerals of the Pacific northwest: Oregon Department of Geology and Mineral Industries Special Paper 23, p. 73–78.
———1991, Rare earth deposits in the southern Great Basin, *in* Raines, G.L., Lisle, R.E., Schafer, R.W., and Wilkinson, W.H., eds., Geology and ore deposits of the Great Basin: Reno, Nevada, Geological Society of

Nevada, Symposium Proceedings, p. 523–528.
Castor, S.B., and Gleason, J.D., 1989, Proterozoic ultrapotassic intrusive rocks in southeastern California [abs.]: Geological Society of America Abstracts with Programs, v. 21, no. 5, p. 64.
Chaffee, M.A., 1976, The zonal distribution of selected elements above the Kalamazoo porphyry copper deposit, San Manuel district, Pima County, Arizona: Journal of Geochemical Exploration, v. 5, p. 145–165.
Chamberlain, K.R., and Bowring, S.A., 1990, Proterozoic geochronologic and isotopic boundary in northwestern Arizona: Journal of Geology, v. 20, p. 149.
Chen, J.H., and Moore, J.G., 1979, Late Jurassic Independence dike swarm in eastern California: Geology, v. 7, p. 129–133.
Clark, A.M., 1984, Mineralogy of the rare earth elements, *in* Henderson, P., ed., Rare earth element geochemistry: Amsterdam, Elsevier, p. 33–61.
Clary, M.R., 1967, Geology of the eastern part of the Clark Mountain Range, San Bernardino County, California: California Division of Mines and Geology Map Sheet 6.
Conway, C.M., 1986, Field guide to Early Proterozoic strata that host massive sulfide deposits at Bagdad, Arizona, *in* Nations, J.D., Conway, C.M., and Swann, G.A., eds., Geology of central and northern Arizona, Geological Society of America, Rocky Mountain Section, field trip guidebook: Flagstaff, Northern Arizona University, p. 140–157.
———1991, Tectonomagmatic settings of Proterozoic metallogenic provinces in the southwestern United States [abs.], *in* Goode, E.E., Slack, J.E., and Kotra, R.K., eds., USGS Research on Mineral Resources—1991 Program and Abstracts: U.S. Geological Survey Circular 1062, Seventh Annual McKelvey Forum on Mineral and Energy Resources, p. 9–10.
———1994, Precambrian massive sulfide deposits in amphibolite- and granulite-facies rocks, western Arizona and southeastern California [abs.], *in* Carter, L.M.H., Toth, M.I., and Day, W.C., eds., USGS research on mineral resources—1994 Program and Abstracts: U.S. Geological Survey Circular 1103–A, p. 18.
Conway, C.M., Connelley, T.J., and Robison, L.C., 1986, An Early Proterozoic volcanic-hydrothermal-exhalative system at Bagdad, Arizona: Arizona Geological Society Digest, v. 16, p. 24–34.
Conway, C.M., Elston, D.P., and Wrucke, C.T., 1993, southwestern U.S. diabase province—A 1.1–Ga intrusion event of middle Grenville and middle Keweenawan age [abs.]: Geological Society of America Abstracts with Programs, v. 25, no. 1, p. 7.
Conway, C.M., Hassemer, J.R., Knepper, D.H., Jr., Pitkin, J.A., Jachens, R.C., and Chatman, M.L., 1990, Mineral resources of the Wabayuma Peak Wilderness Study Area, Mohave County, Arizona: U.S. Geological Survey Bulletin 1737–E, 52 p.
Cook, J.R., and Fay, W.M., 1982, Data report, western United States, hydrogeochemical and stream sediment reconnaissance—National Uranium Resource Evaluation Program, Savannah River from the Bristol/Granite Mountains (CDCA–256) Wilderness Study Area, San Bernardino County, California: U.S. Geological Survey Open-File Report 85–510, 8 p.
Cook, J.R., McKibben, M.A., and Williams, A.E., 1992, Fluid inclusion constraints on breccia pipe petrogenesis at the Colosseum gold deposit, southeastern California [abs.]: Pan-American Current Research on Fluid Inclusions IV, Program and Abstracts, p. 27–28.
Cox, D.P., and Bagby, W.C., 1986, Descriptive model of W veins, *in* Cox, D.P., and Singer, D.A., eds., Mineral deposit models: U.S. Geological Survey Bulletin 1693, p. 64.
Cox, D.P., Barton, P.B., and Singer, D.A., 1986, Introduction, *in* Cox, D.P., and Singer, D.A., eds., Mineral deposit models: U.S. Geological Survey Bulletin 1693, p. 1–10.
Cox, D.P., and Singer, D.A., eds., 1986, Mineral deposit models: U.S. Geological Survey Bulletin 1693, 379 p.
Cox, D.P., and Singer, D.A., 1990, Descriptive and grade-tonnage models for distal disseminated Ag-Au deposits—A supplement to U.S. Geological Survey Bulletin 1693: U.S. Geological Survey Open-File Report 90–282, 7 p.
Crow, H.C., 1984, Geochemistry of shonkinites, syenites, and granites associated with the Sulfide Queen carbonatite body, Mountain Pass, California: Las Vegas, University of Nevada, M.S. thesis, 56 p.
Crowe, B.M., Crowell, J.C., and Krummenacher, D., 1979, Regional stratigraphy, K-Ar ages and tectonic

implications of Cenozoic volcanic rocks, southeastern California: American Journal of Science, v. 279, no. 2, p. 186–216.
Cullers, R.L., and Graf, J.L., 1984, Rare earth elements in igneous rocks of the continental crust—Predominantly basic and ultrabasic rocks, *in* Henderson, P. ed., Rare earth element geochemistry: Amsterdam, Elsevier, p. 237–274.
Cullers, R.L., Ramakrishnan, S., Berendsen, P., and Griffin, T., 1985, Geochemistry and petrogenesis of lamproites, Late Cretaceous age, Woodson County, Kansas, U.S.A.: Geochimica et Cosmochimica Acta, v. 49, p. 1,383–1,402.
Czehura, S.J., 1983, Vein paragenesis at Nevada Moly Hall deposit [abs.]: Geological Society of America Abstracts with Programs, v. 15, no. 5, p. 276.
Davis, J.C., 1986, Statistics and data analysis in geology: New York, John Wiley, 646 p.
Davis, W.M., 1933, Granitic domes of the Mohave Desert, California: San Diego Society Natural History Transactions, v. 7, p. 211–258.
Deines, P., 1989, Stable isotope variations in carbonatites, *in* Bell, K., ed., Carbonatites, genesis and evolution: London, Unwin Hyman, p. 301–359.
DePaolo, D.J., and Wasserburg, G.J., 1976, Inferences about magma sources and mantle structure from variations of $^{143}Nd/^{144}Nd$: Geophysical Research Letters, v. 3, p. 743–746.
Detra, D.E., and Kilburn, J.E., 1985, Analytical results and sample locality map of heavy-mineral-concentrate samples from the Bristol/Granite Mountains (CDCA–256) Wilderness Study Area, San Bernardino County, California: U.S. Geological Survey Open-File Report 85–510, scale 1:62,500, 8 p.
Detra, D.E., Meier, A.L., Goldfarb, R.J., and Weaver, S.L., 1984, Analytical results and sample locality map of stream-sediment, panned-concentrate, and rock samples from the South Providence Mountains Wilderness Study Area, San Bernardino County, California: U.S. Geological Survey Open-File Report 84–118, 26 p.
DeWitt, E., 1987, Proterozoic ore deposits of the southwestern U.S.: Society of Economic Geologists Guidebook Series, v. 1, 189 p.
DeWitt, E., Anderson, J.L., Barton, H.N., Jachens, R.C., Podwysocki, M.H., Brickey, D.W., and Close, T.J., 1989, Mineral resources of the South McCullough Mountains Wilderness Study Area, Clark County, Nevada: U.S. Geological Survey Bulletin 1730, 24 p.
DeWitt, E., Armstrong, E.L., Sutter, J.F., and Zartman, R.E., 1984, U-Th-Pb, Rb-Sr, and Ar-Ar mineral and whole-rock isotope systematics in a metamorphosed granitic terrane, southeastern California: Geological Society of America Bulletin, v. 95, no. 6, p. 723–739.
DeWitt, E., Kwak, L.M., and Zartman, R.E., 1987, U-Th-Pb and $^{40}Ar/^{39}Ar$ dating of the Mountain Pass carbonatite and alkalic igneous rocks, southeastern California: Geological Society of America Abstracts with Programs, v. 19, no. 7, p. 642.
Dexter, J.J., Goodknight, C.S., Dayvault, R.D., and Dickson, R.E., 1983, Mineral evaluation of part of the Gold Butte district, Clark County, Nevada: U.S. Department of Energy Open-File Report GJBX–18, 31 p.
Dohrenwend, J.C., 1987, Basin and Range, *in* Graf, W.L., ed., Geomorphic systems of North America: Boulder, Colo., Geological Society of America, Centennial Special Volume 2, p. 303–342.
———1988, Age of formation and evolution of pediment domes in the area of the Cima volcanic field, Mojave Desert, California, *in* Weide, D.L., and Faber, M.L., eds., This extended land—Geological journeys in the southern Basin and Range: Las Vegas, Nevada, Geological Society of America, Cordilleran Section, Field Trip Guidebook, p. 214–217.
Dohrenwend, J.C., McFadden, L.D., Turrin, B.D., and Wells, S.G, 1984, K-Ar dating of the Cima volcanic field, eastern Mojave Desert, California—Late Cenozoic volcanic history and landscape evolution: Geology, v. 12, no. 3, p. 163–167.
Dohrenwend, J.C., Wells, S.G., McFadden, L.D., and Turrin, B.D., 1987, Pediment dome evolution in the eastern Mojave Desert, California, *in* Gardiner, V., ed., International Geomorphology 1986, Part II: London, John Wiley & Sons, p. 1,047–1,062.
Donnelly, M.E., and Conway, C.M., 1988, Metallogenic map of volcanogenic massive-sulfide occurrences in Arizona, *in* Earhart, R.L., ed., Volcanogenic massive-sulfide map series: U.S. Geological Survey

Miscellaneous Field Studies Map MF–1853–B, scale 1:100,000.
Drew, L.J., Bliss, J.D., Bowen, R.W., Bridges, N.J., Cox, D.P., DeYoung, J.H., Jr., Houghton, J.C., Ludington, S.D., Menzie, W.D., Page, N.J, Root, D.H., and Singer, D.A., 1986, Quantitative estimation of undiscovered mineral resources—A case study of U.S. Forest Service wilderness tracts in the Pacific Mountain system: Economic Geology, v. 81, no. 1, p. 80–88.
Drew, L.J., Qingrun, M., and Weijun, Sun, 1990, The Bayan Obo iron–rare-earth–niobium deposit, Inner Mongolia, China: Lithos, v. 26, no. 1/2, p. 43–65.
Dunne, G.C., 1972, Geology of the Devil's Playground area, eastern Mojave Desert, California: Houston, Tex., Rice University, Ph.D. dissertation, 79 p.
———1977, Geology and structural evolution of Old Dad Mountain, Mojave Desert, California: Geological Society of America Bulletin, v. 88, no. 6, p. 737–748.
Duval, J.S., Cook, Beverly, and Adams, J.A.S., 1971, A study of the circle of investigation of an airborne gamma-ray spectrometer: Journal of Geophysical Research, v. 76, no. 35, p. 8,466–8,470.
Duval, J.S., Jones, W.J., Riggle, F.R., and Pitkin, J.A., 1989, Equivalent uranium map of conterminous United States: U.S. Geological Survey Open-File Report 89–478, 10 p., scale 1:2,500,000.
———1990, Potassium and thorium maps of the conterminous United States: U.S. Geological Survey Open-File Report 90–338, 17 p., scale 1:2,500,000.
Eaton, G.P., 1984, The Miocene Great Basin of western North America as an extending back-arc region: Tectonophysics, v. 102, p. 275–295.
Einaudi, M.T., 1982, Skarns associated with porphyry copper plutons—I. Descriptions of deposits, southwestern U.S.; II. General features and origin, *in* Titley, S.R., ed., Advances in the geology of the porphyry copper deposits, southwestern United States: Tucson, University of Arizona Press, p. 139–209.
———1990, Zoning of gold and silver in central portions of porphyry copper districts [abs.]: Reno, Nev., Great Basin Symposium, Program with Abstracts, April 1–5, p. 59–60.
Einaudi, M.T., Meinert, L.D., and Newberry, R.J., 1981, Skarn deposits, *in* Skinner, B.J., ed., Seventy-fifth anniversary volume, 1905–1980, Economic Geology: New Haven, Conn., Economic Geology Publishing Company, p. 317–391.
Evans, J.R., 1964, Xenotime mineralization in the southern Music Valley area, Riverside County, California: California Division of Mines and Geology Special Report 79, 24 p.
———1966, California's Mountain Pass mine now producing europium oxide: California Division of Mines and Geology, Mineral Information Service, v. 19, no. 1, p. 23–32.
Farmer, G.L., Wilshire, H.G., Wooden, J.L., Glazner, A.F., and Katz, Marvin, 1991, Temporal variations in the sources of alkali basalts at the Cima volcanic field, southeastern California [abs.]: Geological Society of America Abstracts with Programs, v. 23, no. 2, p. 23.
Fisher, F.S., 1990, Gold deposits in the Sneffels-Telluride and Camp Bird Mining District, San Juan Mountains, Colo., *in* Shawe, D.R., Ashley, R.P., and Carter, L.M.H., eds., Gold-bearing polymetallic veins and replacement deposits—Part II: U.S. Geological Survey Bulletin 1857–F, p. F12–F18.
Fleck, R.J., Mattinson, J.M., Busby, C.J., Carr, M.D., Davis, G.A., and Burchfiel, B.C., 1994, Isotopic complexities and the age of the Delfonte volcanic rocks, eastern Mescal Range, southeastern California—Stratigraphic and tectonic implications: Geological Society of America Bulletin, v. 106, no. 10, p. 1,242–1,253.
Foley, S.F., 1992, Petrological characterization of the source components of potassic magmas: geochemical and experimental constraints: Lithos, v. 28, no. 3–6, p. 187–204.
Foley, S.F., Venturelli, G., Green, D.H., and Toscani, L., 1987, The ultrapotassic rocks—Characteristics, classification, and constraints for petrogenetic models: Earth-Science Reviews, v. 24, p. 81–134.
Foley, S.F., and Wheller, G.E., 1990, Parallels in the origin of the geochemical signatures of island arc volcanics and the continental potassic igneous rocks—The role of residual titanites: Chemical Geology, v. 85, p. 1–18.

Folger, P.F., Detra, D.E., Goldfarb, R.J., Crock, J.G., Briggs, P.H., and Bradley, L.A., 1986, Analytical results and sample locality map of heavy-mineral-concentrate and rock samples from the Providence Mountains Wilderness Study Area (CDCA–263), San Bernardino County, California: U.S. Geological Survey Open-File Report 86–512, 58 p.

Fox, L.K., 1989, Albitization of Jurassic plutons in the southern Bristol Mountains, east-central Mojave Desert, southeastern California: Santa Barbara, California, University of California, Ph.D. dissertation, 324 p.

Fox, L.K., and Miller, D.M., 1990, Jurassic granitoids and related rocks of the southern Bristol Mountains, southern Providence Mountains, and Colton Hills, Mojave Desert, California: Geological Society of America Memoir 174, p. 111–132.

Franklin, J.M., Sangster, D.M., and Lydon, J.W., 1981, Volcanic-associated massive sulfide deposits, *in* Skinner, B.J., ed., Economic Geology seventy-fifth Anniversary Volume: New Haven, Conn., Economic Geology Publishing Company, p. 485–627.

Friedrich, M.H., and Cuney, M., 1989, Uranium enrichment processes in peraluminous magmatism, *in* International Atomic Energy Agency, ed., Uranium deposits in magmatic and metamorphic rocks: Vienna, International Atomic Energy Agency, Proceedings Salamanca, 29 Sept.–3 Oct., 1986, p. 11–35.

Gair, J.E., 1989a, Gold-quartz, and gold-pyrite-quartz veins, *in* Gair, J.E., ed., Mineral resources of the Charlotte 1° × 2° quadrangle, North Carolina and South Carolina: U.S. Geological Survey Professional Paper 1462, p. 61–64.

———1989b, Criteria for assessment of mineral-resource potential, *in* Gair, J.E., ed., Mineral resources of the Charlotte 1° × 2° quadrangle, North Carolina and South Carolina: U.S. Geological Survey Professional Paper 1462, p. 51–55.

Geodata International, Inc., 1977, Lake Mead dynamic test range for calibration of airborne gamma radiation measuring systems: U.S. Departmemt of Energy Open-File Report GJBX–46(77), 83 p.

Gerber, M.E., Miller, C.F., Wooden, J.L., and Foster, D.A., 1991, Plutonism at the eastern edge of the Cordilleran Jurassic magmatic belt, Mojave Desert, California [abs.]: Geological Society of America Abstracts with Programs, v. 23, no. 5, p. 249.

Gittins, J., 1989, The origin and evolution of carbonatite magmas, *in* Bell, K., ed., Carbonatites, genesis and evolution: London, Unwin Hyman, p. 580–600.

Glass, J.J., Evans, H.T., Carron, M.K., and Hildebrand, F.A., 1958, Cerite from Mountain Pass, San Bernardino County, California: American Mineralogist, v. 43, p. 460–475.

Glazner, A.F., Bartley, J.M., and Walker, J.D., 1989, Magnitude and significance of Miocene crustal extension in the central Mojave Desert, California: Geology, v. 17, no. 1, p. 50–53.

Glazner, A.F., Nielson, J.E., Howard, K.A., and Miller, D.J., 1986, Correlation of the Peach Springs Tuff, a large-volume Miocene ignimbrite sheet in California and Arizona: Geology, v. 14, no. 10, p. 840–843.

Glazner, A.F., and O'Neil, J.R., 1989, Crustal structure of the Mojave Desert, California—Inferences from Sr and O isotope studies of Miocene volcanic rocks: Journal of Geophysical Research, v. 94, no. B6, p. 7,861–7,870.

Gleason, J.D., 1988, Petrology and geochemistry of the Barrel Spring pluton and related potassic rocks, Old Woman-Piute Range, southeastern California: Nashville, Tenn., Vanderbilt University, M.S. thesis, 263 p.

Gleason, J.D., Miller, C.F., and Wooden, J.L., 1988, Barrel Spring alkalic complex—1.4 Ga anorogenic plutonism in the Old Woman-Piute Range, eastern Mojave Desert, California [abs.]: Geological Society of America Abstracts With Programs, v. 20, no. 3, p. 164.

Goldfarb, R.J., Miller, D.M., Simpson, R.W., Hoover, D.B., Moyle, P.R., Olson, J.E., and Gaps, R.S., 1988, Mineral resources of the Providence Mountains Wilderness Study Area, San Bernardino County, California: U.S. Geological Survey Bulletin 1712 , chap. D, 70 p.

Gottfried, D., Jaffe, H.W., and Senftle, F.E., 1959, Evaluation of the lead-alpha (Larsen) method for determining ages of igneous rocks: U.S. Geological Survey Bulletin 1097–A, 63 p.

Gottlieb, O.J., and Friberg, L.M., 1984, The geology and geochemistry of the Hackberry Mountain gold prospect, San Bernardino Co., California [abs.]: Geological Society of America Abstracts with Programs, v. 16, no. 6, p. 522.

Grasty, R.L., and Darnley, A.G., 1971, The calibration of gamma-ray spectrometers for ground and airborne use: Geological Survey of Canada Paper 71–17, 27 p.
Greenwood, N.N., and Earnshaw, A., 1984, Chemistry of the elements: Oxford, Pergamon Press, 1,542 p.
Grimes, D.J., and Marranzino, A.P., 1968, Direct-current arc and alternating-current spark emission spectrographic field methods for the semiquantative analysis of geologic materials: U.S. Geological Survey Circular 591, 6 p.
Grose, L.T., 1959, Structure and petrology of the northeast part of the Soda Mountains, San Bernardino County, California: Bulletin of the Geological Society of America, v. 70, p. 1,509–1,548.
Guilbert, J.M., and Park, C.F., Jr., 1986, The geology of ore deposits: New York, W.H. Freeman, 985 p.
Gunter, W.L., Hammitt, J.W., and Babcock, R.C., 1990, Geology of the Barneys Canyon gold deposit, Bingham Canyon, Utah [abs.]: Salt Lake City, Utah, 119th American Institute of Mining, Metallurgical, and Petroleum Engineers (AIME) Annual Meeting, February, 1990, Abstracts with Programs, p. 38.
Guo, J., and Green, T.H., 1990, Experimental study of barium partioning between phlogopite and silicate liquid at upper-mantle pressure and temperature: Lithos, v. 24, no. 2, p. 83–95.
Gusa, Sharon, Howard, K.A., and Nielson, J.E., 1987, Heavy-mineral suites confirm the wide extent of the Peach Springs Tuff in California and Arizona, U.S.A.: Journal of Volcanology and Geothermal Research, v. 33, no. 4, p. 343–347.
Hall, A., 1987, Igneous petrology, chap. 4, *in* Nephelinites and carbonatites: Essex, England, Longman Scientific & Technical, p. 439–453.
Hall, D.K., 1972, Hydrothermal alteration and mineralization in the East Camp of the Turquoise District, San Bernardino County, California: Tucson, Ariz., University of Arizona, M.S. thesis, 137 p.
Hamilton, D.L., Bedson, P., and Esson, J., 1989, The behaviour of trace elements in the evolution of carbonatites, *in* Bell, K., ed., Carbonatites, genesis and evolution: London, Unwin Hyman, p. 405–427.
Hammond, J.G., 1990, Middle Proterozoic diabase intrusions in the southwestern U.S.A. as indicators of limited extensional tectonism, *in* Gower, C.F., Rivers, T., and Ryan, B., eds., Mid-Proterozoic Laurentia-Baltica: Geological Association of Canada Special Paper 38, p. 517–531.
Harding, T.P., 1985, Seismic characteristics and identification of negative flower structures, positive flower structures, and positive structural inversion: American Association of Petroleum Geologists Bulletin, v. 69, p. 582–600.
Harland, W.B., Armstrong, R.L., Cox, A.V., Craig, L.E., Smith, A.G., and Smith, D.G., 1989, A geologic time scale 1989: Cambridge, Cambridge University Press, 247 p.
Harrah, H.W., 1967, Rare earth concentration at Molybdenum Corporation of America—Solvent extraction plant: Deco Trefoil, v. 31, p. 9–16.
Harris, D.P., 1984, Mineral resource appraisal: Oxford, Clarendon Press, 445 p.
Hawkesworth, C.J., Gallagher, K., Hergt, J.M., and McDermott, F., 1993, Trace element fractionation processes in the generation of island arc basalts: Philosophical Transactions of the Royal Society of London, v. A342, p. 179–191.
Haxel, G.B., Hedrick, J.B., and Orris, G.J., 2002, Rare earth elements—Critical resources for high technology: U.S. Geological Survey Fact Sheet 087–02, 4 p.
Haxel, G.B., Smith, D.B., Whittington, C.L., Griscom, A., Diveley-White, D.V., Powell, R.E., and Kreidler, T.J., 1988, Mineral resources of the Orocopia Mountains Wilderness Study Area, Riverside County, California: U.S. Geological Survey Bulletin 1710, chap. E, 18 p.
Hazzard, J.C., 1954, Rocks and structures of the northern Providence Mountains, San Bernardino County, California, *in* Jahns, R.H., ed., Geology of southern California: California Division of Mines Bulletin 170, chap. 4, p. 27–35.
Heaman, L.M., and Grotzinger, J.P., 1992, 1.08 Ga diabase sills in the Pahrump Group, California—Implications for development of the Cordilleran miogeocline: Geology, v. 20, no. 7, p. 637–640.

Hedrick, J.B., 1995, Rare earths: U.S. Bureau of Mines Mineral Commodity Summaries, January 1995, p. 134–135.
Heinrich, E.W., 1960, Some rare-earth mineral deposits in Mojave County, Arizona: Arizona Bureau of Mines Bulletin 167, 22 p.
———1966, The geology of carbonatites: Chicago, Rand McNally, 555 p.
Henderson, P., 1982, Inorganic geochemistry: Oxford, Pergamon Press, 353 p.
Herbst, J.F., 1993, Permanent magnets: American Scientist, v. 81, p. 252–260.
Hewett, D.F., 1931, Geology and ore deposits of the Goodsprings quadrangle, Nevada: U.S. Geological Survey Professional Paper 162, 172 p.
———1956, Geology and mineral resources of the Ivanpah quadrangle, California and Nevada: U.S. Geological Survey Professional Paper 275, 172 p.
Hewitt, C.H., 1959, Geology and mineral deposits of the northern Big Burro Mountains-Redrock area, Grant County, New Mexico: New Mexico Bureau of Mines and Mineral Resources Bulletin 60, 150 p.
Higgins, C.T., 1990, Mesquite Mine, a modern example of the quest for gold: California Geology, v. 43, no. 3, p. 51–56.
Hileman, G.E., Miller, C.F., and Knoll, M.A., 1990, Mid-Tertiary structural evolution of the Old Woman Mountains area—Implications for crustal extension across southeastern California: Journal of Geophysical Research, v. 95, no. B1, p. 581–599.
Hodges, C.A., and Ludington, Steve, eds., 1991, Quantitative assessment of undiscovered metallic mineral resources in the East Mojave National Scenic Area, southern California: U.S. Geological Survey Open-File Report 91–551, 18 p.
Hodgson, S.F., ed., 1980, Oil and gas prospect wells drilled in California through 1980: California Division of Oil and Gas Publication TRO 1, 258 p.
Hoffman, D.C., Lawrence, F.O., Mewherter, J.L., and Rourke, F.M., 1971, Detection of plutonium–244 in nature: Nature, v. 234, p. 132–134.
Hofstra, A.H., Landis, G.P., Rye, R.O., Birak, D.J., Dahl, A.R., Daly, W.E., and Jones, M.B., 1989, Geology and origin of the Jerritt Canyon sediment-hosted disseminated gold deposits, Nevada [abs.], *in* Schindler, K.S., ed., USGS Research on Mineral Resources—1989 Programs and Abstracts: U.S. Geological Survey Circular 1035, p. 30–31.
Hofstra, A.H., Northrop, H.R., Rye, R.O., Landis, G.P., and Birak, D.J., 1988, Origin of sediment-hosted disseminated gold deposits by fluid mixing—evidence from jasperoids in the Jerritt Canyon gold district, Nevada, U.S.A. [extended abs.], *in* Goode, A.D.T., and Bosma, L.I., eds., Bicentennial Gold 88, Extended Abstracts, Oral Programme: Geological Society of Australia, Abstract Series no. 22, p. 284–289.
Hopson, C.A., 1988, Independence dike swarm—Origin and tectonic significance: EOS, American Geophysical Union, Transactions, v. 69, no. 44, p. 1,479.
Howard, K.A., 1991, Intrusion of horizontal dikes—Tectonic significance of Middle Proterozoic diabase sheets widespread in the upper crust of the southwestern United States: Journal of Geophysical Research, v. 96, no. B7, p. 12,461–12,478.
Howard, K.A., Kilburn, J.E., Simpson, R.W., Fitzgibbon, T.T., Detra, D.E., Raines, G.L., and Sabine, C., 1987, Mineral resources of the Bristol/Granite Mountains Wilderness Study Area, San Bernardino County, California: U.S. Geological Survey Bulletin 1712–C, 18 p.
Howard, K.A., Miller, C.F., and Stone, P., 1980, Mesozoic thrusting in the eastern Mojave Desert, California [abs.]: Geological Society of America Abstracts with Programs, v. 12, no. 3, p. 112.
Howard, K.A., Nielson, J.E., Simpson, R.W., Hazlett, R.W., Alminas, H.V., Nakata, J.K., and McDonnell, J.R., Jr., 1988, Mineral resources of the Turtle Mountains Wilderness Study Area, San Bernardino County, California: U.S. Geological Survey Bulletin 1713, 28 p.
Hughes, C.J., and Hussey, E.M., 1976, M and Mg values in igneous rocks—Proposed usage and a comment on currently employed Fe_2O_3 corrections: Geochemica et Cosmochimica Acta, v. 40, p. 485–486.
Hutchinson, R.W., and Grauch, R.I., eds., 1991, Historical perspectives of genetic concepts and case histories

of famous discoveries: New Haven, Conn., The Economic Geology Publishing Co., Economic Geology Monograph 8, 359 p.
Irving, A.J., and Frey, F.A., 1984, Trace element abundances in megacrysts and their host basalts—Constraints on partition coefficients and megacryst genesis: Geochimica et Cosmochimica Acta, v. 48, p. 1,201–1,221.
Jachens, R.C., and Griscom, Andrew, 1982, An isostatic residual gravity map of California—A residual map for interpretation of anomalies from intracrustal sources: Dallas, Tex., Society of Exploration Geophysicists, Technical Program Abstracts and Biographies, Fifty-Second Annual International Meeting and Exposition, October 17–21, 1982, p. 299–301.
Jachens, R.C., and Moring, B.C., 1990, Maps of the thickness of Cenozoic deposits and the isostatic residual gravity over basement for Nevada: U.S. Geological Survey Open-File Report 90–404, 15 p.
Jaffe, H.W., 1955, Precambrian monazite and zircon from the Mountain Pass rare-earth district, San Bernardino County, California: Geological Society of America Bulletin, v. 66, p. 1,247–1,256.
Jaffe, H.W., Meyrowitz, R., and Evans, H.T., Jr., 1953, Sahamalite, a new rare earth carbonate mineral: American Mineralogist, v. 38, p. 741–754.
Jahns, R.H., 1952, Pegmatite deposits of the White Picacho district, Maricopa and Yavapai Counties, Arizona: Arizona Bureau of Mines Bulletin, v. 162, 105 p.
James, E.W., 1989, Southern extension of the Independence dike swarm of eastern California: Geology, v. 17, no. 7, p. 587–590.
Jenner, G.A., Foley, S.F., Jackson, S.E., Green, T.H., Fryer, B.J., and Longerich, H.P., 1994, Determination of partition coefficients for trace elements in high pressure-temperature experimental run products by laser ablation microprobe-inductively coupled plasma mass spectrometry (LAM–ICP–MS): Geochimica et Cosmochimica Acta, v. 58, p. 5,099–5,103.
Jennings, C.W., 1961, Geologic map of California, Kingman sheet: California Division of Mines and Geology, scale 1:250,000.
Jochum, K.P., Seufert, H.M., Spettel, B., and Palme, H., 1986, The solar-system abundances of Nb, Ta, and Y, and the relative abundances of refractory lithophile elements in differentiated planetary bodies: Geochimica et Cosmochimica Acta, v. 50, p. 1,173–1,183.
John, D.A., Stewart, J.H., Kilburn, J.E., Silberling, N.J., and Rowan, L.C., 1993, Geology and mineral resources of the Reno 1° × 2° quadrangle, Nevada and California: U.S. Geological Survey Bulletin 2019, 65 p.
Johnson, N.L., 1966, Rare earth concentration at Molybdenum Corporation of America: Deco Trefoil, v. 30, p .9–16.
Jennings, C.W., comp., 1961, Geologic map of California, Kingman sheet: California Division of Mines and Geology, scale 1:250,000.
Jones, A.P., and Wyllie, P.J., 1983, Low-temperature glass quenched from a synthetic, rare-earth carbonatite—Implications for the origin of the Mountain Pass deposit, California: Economic Geology, v. 78, p. 1,721–1,723.
Jones, G.M., and Menzie, W.D., 1986a, Grade and tonnage model of W veins, *in* Cox, D.P., and Singer, D.A., eds., Mineral deposit models: U.S. Geological Survey Bulletin 1693, p. 65–66.
———1986b, Grade and tonnage model of Cu skarn deposits, *in* Cox, D.P., and Singer, D.A., eds., Mineral deposit models: U.S. Geological Survey Bulletin 1693, p. 86–89.
Joralemon, Peter, 1951, The occurrence of gold at the Getchell mine: Economic Geology, v. 46, no. 3, p. 267–310.
Kaiser, H.F., 1970, A second generation little jiffy: Psychometrika, v. 35, p. 401–415.
Karish, C.R., Miller, E.L., and Sutter, J.F., 1987, Mesozoic tectonic and magmatic history of the central Mojave Desert, *in* Dickinson, W.R., and Klute, M.A., eds., Mesozoic rocks of southern Arizona and adjacent areas: Arizona Geological Society Digest, v. 18, p. 15–32.
Kjarsgaard, B.A., and Hamilton, D.L., 1989, The genesis of carbonatites by immiscibility, *in* Bell, K., ed., Carbonatites, genesis and evolution: London, Unwin Hyman, p. 388–404.
Klovan, J.E., 1968, Selection of target areas by factor analysis: Vancouver, B.C., Proceedings, Symposium on decision-making in exploration, January 26, 1968, 9 p.
Knepper, D.H., Jr., and Simpson, S.L., 1992, Remote sensing, *in* U.S. Geological Survey and Servicio

Geologico de Bolivia, Geology and mineral resources of the Altiplano and Cordillera Occidental, Bolivia: U.S. Geological Survey Bulletin 1975, p. 47–55.
Knopf, Adolph, 1913, Ore deposits of the Helena mining region, Montana: U.S. Geological Survey Bulletin 527, 143 p.
Kohler, S.L., 1984, Mineral land classification of the Lanfair Valley, Homer Mountain, and Davis Dam quadrangles, San Bernardino County, California: California Division of Mines and Geology Open-File Report 84–30 SAC, 68 p.
Korobeinikov, A.F., 1991, Gold conduct in the contact-metasomatic processes of intrusions, *in* Aksyuk, A.M., Collins, L.G., Dobrovolskaya, M., Lun-Chi, Hu, Lowell, G.R., van Marcke de Lummen, G., Shimazaki, H., Liren, Wu, Zarikov, V.A., and Augustithis, S.S., eds., Skarns—Their genesis and metallogeny: Athens, Theophrastus Publications, S.A., p. 203–226.
Kruesi, P.R., and Duker, George, 1965, Production of rare earth chloride from bastnaesite: Journal of Metals, v. 17, p. 847–849.
Krumbein, W.C., and Graybill, F.A., 1965, An introduction to statistical models in geology: New York, McGraw-Hill, 475 p.
Kuyper, B.A., Mach, L.E., Streiff, R.E., and Brown, W.A., 1991, Geology of the Cove gold-silver deposit: Society for Mining, Metallurgy, and Exploration, Inc., preprint no. 91–125, 20 p.
Lange, P.C., 1988, Geology of the Telegraph Mine tectono-hydrothermal breccias, San Bernardino County, California: Fort Collins, Colo., Colorado State University, M.S. thesis, 190 p.
Lanphere, M.A., 1964, Geochronologic studies in the eastern Mohave Desert, California: Journal of Geology, v. 72, p. 381–399.
Le Bas, M.J., 1987, Nephelinites and carbonatites, *in* Fitton, J.G., and Upton, B.G.J., eds., Alkaline igneous rocks: Geological Society of London, Special Publication 30, p. 53–83.
Le Bas, M.J., LeMaitre, R.W., Streckeisen, A., and Zanettin, B., 1986, A chemical classification of volcanic rocks based upon the total alkali-silica diagram: Journal of Petrology, v. 27, p. 745–750.
Lechler, P.J., 1988, A new platinum-group-element discovery at Crescent Peak, Clark County, Nevada: Nevada Bureau of Mines and Geology Open-File Report 88–1, 5 p.
Levinson, A.A., 1980, Exploration Geochemistry, 2d ed.: Wilmette, Ill., Applied Publishing, 924 p.
Lichte, F.E., Golightly, D.W., and Lamothe, P.J., 1987, Inductively coupled plasma—Atomic emission spectrometry, *in* Baedecker, P.A., ed., Methods for geochemical analysis: U.S. Geological Survey Bulletin 1770, p. B1–B10.
Linder, Harold, 1988, Geology of the Castle Mountains gold deposit, *in* Weide, D.L., and Faber, M.L., eds., This extended land—Geological journeys in the southern Basin and Range: Las Vegas, Nev., Geological Society of America, Field Trip Guidebook, Cordilleran Section Meeting, p. 78–80.
———1989, Castle Mountains gold deposit, Hart Mining District: California Geology, v. 42, no. 6, p. 134–140.
Lindquist, W.F., 1987, Discovery of the Mesquite gold deposit, Imperial County, California [abs.]: Abstracts American Institute of Mining Engineers, 116 Annual Meeting, p. 84.
Lister, B., and Cogger, N., 1986, The preparation and evaluation of bastnäsite reference materials IGS 40 and 41: Geostandards Newsletter, v. 10, p. 33–59.
Lucas, J.M., 1992, Gold: U. S. Bureau of Mines, Annual Report 1991, 43 p.
Ludington, S.D., 1981, Granite molybdenite systems, *in* Erickson, R.L., ed., Characteristics of mineral deposit occurrences: U.S. Geological Survey Open-File Report 82–795, p. 43–46.
Ludington, S.D., Cox, D.P., Singer, D.A., Sherlock, M.G., Berger, B.R., and Tingley, J.V., 1993, Spatial and temporal analysis of precious-metal deposits for a mineral-resource assessment of Nevada, *in* Kirkham, R.V., Sinclair, W.D., Thorpe, R.I., and Duke, J.M., eds., Mineral deposit modeling: Geological Association of Canada Special Paper 40, p. 31–40.
Manske, S.L., 1990, The relative timing and phase assemblages of vein controlled hypogene mineralization and alteration in the Mesquite deposit, Imperial County, California [abs.]: Geological Society of America Abstracts with Programs, v. 22, no. 3, p. 63.
Manske, S.L., and Einaudi, M.T., 1989, Relations of structure and rock fabric to alteration and mineralization

in the Big Chief pit, Mesquite gold deposits, Imperial County, California, and implications for ore genesis [abs.]: Geological Society of America Abstracts with Programs, v. 21, no. 6, p. A295.
Manske, S.L., Matlack, W.F., Springett, M.W., Strakele, A.E., Jr., Watowich, S.N., Yeomans, B., and Yeomans, E., 1987, Geology of the Mesquite deposit, Imperial County, California: Society of Mining Engineers, no. 87–107, 9 p.
Mariano, A.N., 1989a, Nature of economic mineralization in carbonatites and related rocks, *in* Bell, K., ed., Carbonatites, genesis and evolution: London, Unwin Hyman, p. 149–176.
———1989b, Economic geology of rare earth elements, *in* Lipin, B.R., and McKay, G.A., eds., Geochemistry and mineralogy of rare earth elements: Mineralogical Society of America, Reviews in Mineralogy, v. 21, p. 309–337.
Mariano, John, and Grauch, V.J.S., 1988, Aeromagnetic maps of the Colorado River region including the Kingman, Needles, Salton Sea, and El Centro 1° x 2° quadrangles, California, Arizona, and Nevada: U.S. Geological Survey Miscellaneous Field Studies Map MF-2023, scale 1:250,000.
Mariano, John, Helferty, M.G., and Gage, T.B., 1986, Bouger and isostatic residual gravity maps of the Colorado River region, including the Kingman, Needles, Salton Sea, and El Centro quadrangles: U.S. Geological Survey Open-File Report 86–347, scales 1:750,000 and 1:250,000.
Marzolf, J.E., 1983, Early Mesozoic eolian transition from cratonal margin to orogenic-volcanic arc, *in* Gurgel, K.D., ed., Geologic excursions in stratigraphy and tectonics—From southeastern Idaho to the southern Inyo Mountains, California, via Canyonlands and Arches National Parks, Utah, Guidebook, Part II: Utah Geological and Mineral Survey Special Studies 60, p. 39–46.
———1988, Reconstruction of Late Triassic and Early and Middle Jurassic sedimentary basins—Southwestern Colorado Plateau to the eastern Mojave Desert, *in* Weide, D.L., and Faber, M.L., eds., This extended land—Geological journeys in the southern Basin and Range: Las Vegas, Nev., Geological Society of America, Field Trip Guidebook, Cordilleran Section Meeting, p. 177–200.
———1991, Lower Jurassic unconformity (J–O) from the Colorado Plateau to the eastern Mojave Desert: evidence of a major tectonic event at the close of the Triassic: Geology, v. 19, no. 4, p. 320–323.
McColl, J.R., and Palilla, F.C., 1981, Use of rare earths in television and cathode ray phosphors, *in* Gschneidner, K.A., ed., Industrial applications of the rare earth elements: Washington, D.C., American Chemical Society Symposium Series 164, p. 177–193.
McCulloh, T.H., 1954, Problems of the metamorphic and igneous rocks of the Mojave desert, California, *in* Jahns, R.H., ed., Geology of Southern California: California Division of Mines Bulletin 170, chap. 7, p.
McCurry, M.O., 1985, The petrology of the Woods Mountains volcanic center, San Bernardino County, California: Los Angeles, University of California, Ph.D. dissertation, 403 p.
———1988, Geology and petrology of the Woods Mountains volcanic center, southeastern California—Implications for the genesis of peralkaline rhyolite ash flow tuffs: Journal of Geophysical Research, v. 93, no. B12, p. 14,835–14,855.
McCurry, M.O., and Hensel, G., 1988, Structural, petrological, and geophysical constraints on the Miocene—Recent crustal evolution of the eastern Mojave Desert [abs.]: Geological Society of America Abstracts with Programs, v. 20, no. 3, p. 212.
McGetchin, T.R., and Nikhanj, Y.S., 1973, Carbonatite-kimberlite relations in the Cane Valley diatreme, San Juan County, Utah: Journal of Geophysical Research, v. 78, p. 1,854–1,869.
McKelvey, G.E., and Hammarstrom, G.M., 1991, A reconnaissance study of gold mineralization associated with garnet skarn at Namija, Zamora Province, Ecuador [abs.], *in* Good, E.E., Slack, J.F., and Kotra, R.K., eds., USGS Research on mineral resources—1991 Program and Abstracts: U.S. Geological Survey Circular 1062, p. 55.
McKelvey, V.E., 1972, Mineral resource estimates and public policy: American Scientist, v. 60, p. 32–40.
McKenzie, D., 1985, Some remarks on the movement of small melt fractions in the mantle: Earth and Planetary Science Letters, v. 95, no. 1–2, p. 53–72.

McKenzie, D., and O'Nions, R.K., 1991, Partial melt distributions from inversion of rare earth element concentrations: Journal of Petrology, v. 32, p. 1,021–1,091.
McKie, D., 1966, Fenitization, *in* Tuttle, O.F., and Gittins, J., eds., Carbonatites: Interscience, p. 262–294.
Meinert, L.D., 1983, Variability of skarn deposits—Guides to exploration, *in* Boardman, S.J., ed., Revolution in the Earth Sciences: Dubuque, Iowa, Kendall-Hunt Publishing Co., p. 301–316.
———1988a, Gold in skarn deposits—A preliminary overview, *in* Zachrisson, E., ed., Proceedings of the Symposium of the 7th Quadrennial International Association of the Geochemistry of Ore Deposits: Stuttgart, E. Schweizerbart'sche, p. 363–374.
———1988b, Gold and silver in skarn deposits, *in* Goode, A.D.T., Smyth, E.L., Birch, W.D., and Bosma, L.I., comps., Bicentennial Gold 88, Extended Abstracts, Poster Programme, v. 2: Geological Society of Australia, p. 614–616.
———1989, Gold skarn deposits—Geology and exploration criteria, *in* Keays, Reid, Ramsay, Ross, and Groves, David, eds., The geology of gold deposits—The perspective in 1988: Economic Geology Monograph, 6 p.
———1993, Igneous petrogenesis and skarn deposits, *in* Kirkham, R.V., Sinclair, W.D., Thorpe, R.I., and Duke, J.M., eds., Mineral deposit modeling: Geological Association of Canada Special Paper 40, p. 569–583.
Menges, C.M., and McFadden, L.D., 1981, Evidence for a latest Miocene to Pliocene transition from Basin-Range to post-tectonic landscape evolution in southeastern Arizona: Arizona Geological Society Digest, v. 13, p. 151–160.
Menzie, W.D., and Singer, D.A., 1990, A course on mineral resource assessment *in* Proceedings of International Symposium on Mineral Exploration, Tokyo, Japan, The Use of Artificial Intelligence, p. 172–182.
Menzies, M.A., 1987, Alkaline rocks and their inclusions—A window on the Earth's interior, *in* Fitton, J.G., and Upton, B.G.J., eds., Alkaline igneous rocks: Geological Society of London, Special Publication 30, p. 15–27.
Menzies, M.A., and Hawkesworth, C.J., eds., 1987, Mantle metasomatism: London, Academic Press, 472 p.
Menzies, M.A., Rogers, N., Tindle, A., and Hawkesworth, C.J., 1987, Metasomatic and enrichment processes in lithospheric periodotites, an effect of asthenosphere-lithosphere interaction, *in* Menzies, M.A., and Hawkesworth, C.J., eds., Mantle metasomatism: London, Academic Press, p. 313–361.
Miller, C.F., 1978, An early Mesozoic alkalic magmatic belt in western North America, *in* Howell, D.G., and McDougall, K.A., eds., Mesozoic Paleogeography of the Western United States: Pacific Section, Society Economic Paleontologists and Mineralogists, Pacific Coast Paleogeography Symposium 2, p. 163–187.
Miller, C.F., and Barton, M.D., 1990, Phanerozoic plutonism in the Cordilleran interior, U.S.A. *in* Kay, S.M., and Rapela, C.W., eds., Plutonism from Anarctica to Alaska: Geological Society of America Special Paper 241, p. 213–231.
Miller, D.M., Frisken, J.G., Jachens, R.C., and Gese, D.D., 1986, Mineral resources of the Castle Peaks Wilderness Study Area, San Bernardino County, California: U.S. Geological Survey Bulletin 1713–A, 17 p.
Miller, D.M., Glick, L.L., Goldfarb, R., Simpson, R.W., Hoover, D.B., Detra, D.E., Dohrenwend, J.C., and Munts, S.T., 1985, Mineral resources and resource potential map of the South Providence Mountains Wilderness Study Area, San Bernardino County, California: U.S. Geological Survey Miscellaneous Field Studies Map MF–1780–A, scale 1:62,500.
Miller, D.M., Howard, K.A., and John, B.E., 1982, Preliminary geology of the Bristol Lake region, Mojave Desert, California, *in* Cooper, J.D., comp., Geologic excursions in the California desert (Geological Society of America Cordilleran Section meeting guidebook): Shoshone, California, Death Valley Publishing Company, p. 91–100.
Miller, D.M., Miller, R.J., Nielson, J.E., Wilshire, H.G., Howard, K.A., and Stone, Paul, comps., 1991, Preliminary geologic map of the East Mojave National Scenic Area, California: U.S. Geological Survey Open-File Report 91–435, 8 p.
Miller, D.M., and Wooden, J.L., 1988, An Early Proterozoic batholithic belt in the northern New York Mountains area, California and Nevada [abs.]: Geological Society of America Abstracts with Programs, v. 20, no. 3, p. 215–216.

———1993, Geologic map of the New York Mountains area, California and Nevada: U.S. Geological Survey Open-File Report 93–198, 10 p., scale 1:50,000.
———1994, Field guide to Proterozoic geology of the New York, Ivanpah, and Providence Mountains, California: U.S. Geological Survey Open-File Report 94–674, 40 p.
Miller, F.K., and Morton, D.M., 1977, Comparison of granitic intrusions in the Pelona and Orocopia Schists, southern California: U.S. Geological Survey Journal of Research, v. 5, no. 5, p. 643–649.
Miller, W.J., 1946, Crystalline rocks of southern California: Geological Society of America Bulletin, v. 57, no. 5, p. 457–542.
Mitchell, R.H., 1973, Isotopic composition of lead in galena from the Mountain Pass carbonatite, California: Nature Physical Science, v. 241, p. 17–18.
Mitchell, R.H., and Bergman, S.C., 1991, Petrology of lamproites: New York, Plenum Publishing Corporation, 447 p.
Mitchell, R.H., and Krouse, H.R., 1971, Isotopic composition of sulphur in carbonatite at Mountain Pass, California: Nature Physical Science, v. 231, p. 182.
———1975, Sulphur isotope geochemistry of carbonatites: Geochemica et Cosmochimica Acta, v. 39, p. 1,505–1,513.
Mitchell, R.H., Platt, R.G., and Downey, M., 1987, Petrology of lamproites from Smoky Butte, Montana: Journal of Petrology, v. 28, p. 645–677.
Mittlefehldt, D.W., and Miller, C.F., 1983, Geochemistry of the Sweetwater Wash pluton, California—Implications for "anomalous" trace element behavior during differentiation of felsic magmas: Geochimica et Cosmochimica Acta, v. 47, p. 109–124.
Möller, P., 1989, Rare earth mineral deposits and their industrial importance, *in* Möller, P., Cerny, P., and Saupé, F., eds., Lanthanides, tantalum, and niobium: Berlin, Springer-Verlag, p. 171–188.
Morris, H.T., 1990, Gold in the Tintic Mining District, Utah, *in* Shawe, D.R., Ashley, R.P., and Carter, L.M.H., eds., Gold-bearing polymetallic veins and replacement deposits—Part II: U.S. Geological Survey Bulletin 1857–F, p. F1–F11.
Morton, P.K., 1977, Geology and mineral resources of Imperial County, California: California Division of Mines and Geology County Report 7, 104 p.
Mosier, D.L., Sato, Takeo, Page, N.J, Singer, D.A., and Berger, B.R., 1986, Descriptive model of Creede epithermal veins, *in* Cox, D.P., and Singer, D.A., eds., Mineral deposit models: U.S. Geological Survey Bulletin 1693, p. 145.
Motooka, J.M., 1988, An exploration geochemical technique for the determination of preconcentrated organometallic halides by ICP–AES—Applied Spectroscopy, v. 42, no. 7, p. 1,293–1,296.
Motooka, J.M., and Grimes, D.J., 1976, Analytical precision of one-sixth order semiquantitative spectrographic analysis: U.S. Geological Survey Circular 738, 25 p.
Moyle, P.R., Olson, J.E., and Gaps, R.S., 1986, Mineral resources of the Providence Mountains study area, San Bernardino County, California: U.S. Bureau of Mines Open-File Report MLA 47–86, 306 p.
Muecke, G.K., and Möller, P., 1988, The not-so-rare earths: Scientific American, v. 258, p. 72–77.
Mueller, P.A., Ragland, P.C., Ranson, W.A., and Burchfiel, B.C., 1979, High–K calc-alkaline plutonic rocks from southeastern California: The Mountain Geologist, v. 16, p. 105–115.
Mutschler, F.E., Wright, E.G., Ludington, Steve, and Abbott, J.T., 1981, Granite molybdenite systems: Economic Geology, v. 76, no. 4, p. 874–897.
Myers, A.T., Havens, R.G., and Dunton, P.J., 1961, A spectrochemical method for the semiquantitative analysis of rocks, minerals and ores: U.S. Geological Survey Bulletin 1084, p. 207–229.
Nakamura, N., 1974, Determination of REE, Ba, Mg, Na, and K in carbonaceous and ordinary chondrites: Geochemica et Cosmochimica Acta, v. 38, p. 757–775.
Neary, C.R., and Highley, D.E., 1984, The economic importance of the rare earth elements, *in* Henderson, P., ed., Rare earth element geochemistry: Amsterdam, Elsevier, p. 423–466.
Nielson, J.E., Frisken, J.G., Jachens, R.C., and McDonnell, J.R., Jr., 1987, Mineral resources of the Fort Piute Wilderness Study Area, San Bernardino County, California: U.S. Geological Survey Bulletin 1713–C, 12 p.
Nielson, J.E., Lux, D.R., Dalyrmple, G.B., and Glazner, A.F., 1990, Age of the Peach Springs Tuff, southeastern

California and western Arizona: Journal of Geophysical Research, v. 95, no. B1, p. 571–581.
Nielson, J.E., and Nakata, J.K., 1993, Tertiary stratigraphy and structure of the Piute Range, California and Nevada, in Sherrod, D.R., and Nielson, J.E., eds., Tertiary stratigraphy of highly extended terranes, California, Nevada, and Arizona: U.S. Geological Survey Bulletin 2053, p. 51–53.
Nielson, J.E., Turner, R.D., and Glazner, A.F., 1993, Tertiary stratigraphy and structure of the Castle Mountains and Castle Peaks, California and Nevada, *in* Sherrod, D.R., and Nielson, J.E., eds., Tertiary stratigraphy of highly extended terranes, California, Nevada, and Arizona: U.S. Geological Survey Bulletin 2053, p. 45–49.
Nokleberg, W.J., Bundtzen, T.K., Berg, H.C., Brew, D.A., Grybeck, Donald, Robinson, M.S., Smith, T.E., and Yeend, Warren, 1987, Significant metalliferous lode deposits and placer districts of Alaska: U.S. Geological Survey Bulletin 1786, 104 p.
Novitsky-Evans, J.M., 1978, Geology of the Cowhole Mountains, southeastern California: Houston, Tex., Rice University, Ph.D. dissertation, 100 p.
Ntiamoah-Agyakwa, Yaw, 1987, Geology, hydrothermal mineralization, and geochemical exploration: New York Mountains and northern Mid Hills, San Bernardino County, California: Los Angeles, California, University of California, Ph.D. dissertation, 262 p.
Oberlander, T.M., 1974, Landscape inheritance and the pediment problem in the Mojave Desert of southern California: American Journal of Science, v. 274, no. 8, p. 849–875.
O'Driscoll, M., 1988, Rare earths—Enter the dragon: Industrial Minerals, no. 254, p. 21–55.
———1990, Minerals in the US south-west—Breaking rocks in the hot sun: Industrial Minerals, no. 272, p. 52–87.
Oliver, H.W., Churchel, B.A., and Saltus, R.W., 1986, Aeromagnetic map of Nevada, Kingman sheet: Nevada Bureau of Mines and Geology, scale 1:250,000.
Olson, J.E., and Pray, L.C., 1954, The Mountain Pass rare-earth deposits, *in* Mineral deposits and mineral industry, chap. 8 *of* Jahns, R.H., ed., Geology of southern California: California Division of Mines Bulletin 170, p. 23–39.
Olson, J.E., Shawe, D.R., Pray, L.C., and Sharp, W.N., 1954, Rare-earth mineral deposits of the Mountain Pass district, San Bernardino County, California: U.S. Geological Survey Professional Paper 261, 75 p.
Orris, G.J., and Bliss, J.D., eds., 1991, Industrial mineral deposit models—Descriptive deposit models: U.S. Geological Survey Open-File Report 91–11A, 73 p.
———1992, Industrial mineral deposit models—Grade and tonnage models: U.S. Geological Survey Open-File Report 92–437, 84 p.
Otton, J.K., Glanzman, R.K., and Brenner, E., 1980, Uranium, rare-earth, and thorium mineralization at the Hope mine, eastern Bristol Mountains, San Bernardino County, California: U.S. Geological Survey Open-File Report 80–821, 18 p.
Page, N.J, and Gray, Floyd, 1986, Descriptive model of Alaskan PGE, *in* Cox, D.P., and Singer, D.A., eds., Mineral deposit models: U.S. Geological Survey Bulletin 1693, p. 49.
Page, N.J, Theodore, T.G., and Bradley, L.A., 1986, Discussion of ultramafic and mafic rocks and platinum-group element analyses from the Lost Basin mining district, northwestern Arizona: U.S. Geological Survey Open-File Report 86–33, 13 p.
Pardee, J.T., and Schrader, F.C., 1933, Metalliferous deposits of the greater Helena mining region, Montana: U.S. Geological Survey Bulletin 842, 318 p.
Peccerillo, A., 1992, Potassic and ultrapotassic rocks—Compositional characteristics, petrogenesis, and geologic significance: Episodes, v. 15, p. 243–251.
Peters, W.C., 1978, Exploration and mining geology: New York, John Wiley & Sons, 696 p.
Peterson, F., and Pipiringos, G.N., 1979, Stratigraphic relations of the Navajo Sandstone to Middle Jurassic Formations, southern Utah and northern Arizona: U.S. Geological Survey Professional Paper 1035–B, 43 p.
Peterson, J.A., Cox, D.P., and Gray, Floyd, 1983, Mineral resource assessment of the Ajo and Lukeville $1° \times 2°$ quadrangles, Arizona: U.S. Geological Survey Miscellaneous Field Studies Map MF–1834–B, scale 1:250,000.
Pollard, P.J., 1989a, Geologic characteristics and genetic problems associated with the development of granite-hosted deposits of tantalum and niobium, *in* Möller, P., Cerny, P., and Saupé, F., eds., Lanthanides, tantalum, and niobium: Berlin, Springer-Verlag, p. 240–256.

———1989b, Geochemistry of granites associated with tantalum and niobium mineralization, *in* Möller, P., Cerny, P., and Saupé, F., eds., Lanthanides, tantalum, and niobium: Berlin, Springer-Verlag, p. 143–168.
Powell, J.L., Hurley, P.M., and Fairbain, H.W., 1966, The strontium isotopic composition and origin of carbonatites, *in* Tuttle, O.F., and Gittins, J., eds., Carbonatites: Interscience, p. 365–378.
Powell, R.E., 1981, Geology of the crystalline basement complex, eastern Transverse Ranges, southern California: constraints on regional tectonic interpretations: Pasadena, California Institute of Technology, Ph.D. dissertation, 441 p.
Preinfalk, C., and Morteani, G., 1989, Industrial applications of the rare earth elements, *in* Möller, P., Cerny, P., and Saupé, F., eds., Lanthanides, tantalum, and niobium: Berlin, Springer-Verlag, p. 359–370.
Ramsay, J.G., and Huber, M.I., 1987, The techniques of modern structural geology—Volume 2, folds and fractures: London, Academic Press Inc., Ltd., p. 309–700.
Ray, G.E., 1990, Precious metal enriched skarns of British Columbia: The Gangue, no. 30 (January), p. 2–4.
Ray, G.E., Ettlinger, A.D., and Meinert, L.D., 1990, Gold skarns—Their distribution, characteristics and problems in classification: British Columbia Ministry of Energy, Mines, and Petroleum Resources, Geological Fieldwork 1989, Paper 1990–1, p. 237–246.
Ray, G.E., McClintock, J., and Roberts, W., 1986, A comparison between the geochemistry of the gold-rich and silver-rich skarns in the Tillicum Mountain area, *in* Geological fieldwork, 1985: British Columbia Ministry of Energy, Mines and Petroleum Resources Paper 1986–1, p. 37–44.
Ray, G.E., and Webster, I.C.L., 1990, An overview of skarn deposits: Vancouver, B.C., Geological Association of Canada, Short Course Notes, p. 7–1 to 7–55.
Reynolds, R.E., 1983, Jurassic trackways in the Mescal Range, San Bernardino County, California, *in* Gurgel, K.D., ed., Geologic excursions in stratigraphy and tectonics—From southeastern Idaho to the southern Inyo Mountains, California, via Canyonlands and Arches National Parks, Utah, Guidebook—Part II: Utah Geological and Mineral Survey Special Studies 60, p. 46–48.
———1993, Erosion, deposition, and detachment—The Halloran Hills area, California, *in* Sherrod, D.R., and Nielson, J.E., eds., Tertiary stratigraphy of highly extended terranes, California, Nevada, and Arizona: U.S. Geological Survey Bulletin 2053, p. 21–24.
Reynolds, R.E., and Nance, M.A., 1988, Shadow Valley Basin—Late Tertiary deposition and gravity slides from the Mescal Range, *in* Weide, D.L., and Faber, M.L., eds., This extended land—Geological Journeys in the southern Basin and Range: Las Vegas, Nev., Geological Society of America, Field Trip Guidebook, Cordilleran Section Meeting, p. 207–209.
Richter, D.H., Singer, D.A., and Cox, D.P., 1975, Mineral resources map of the Nabesna quadrangle, Alaska: U.S. Geological Survey Miscellaneous Field Studies Map MF–655–K, scale 1:250,000.
Riedel, W., 1929, Zur Mechanik geologischer Brucherscheinangen: Neues Jahrbuch fur Mineralogie, Geologie und Palaontologie, Monatschefte, v. 1929 B, p. 354–368.
Roberts, R.J., 1960, Alinements of mining districts in north-central, Nevada: U.S. Geological Survey Professional Paper 400–B, p. B17–B19.
———1986, The Carlin story, *in* Tingley, J.V., and Bonham, H.F., Jr., eds., Sediment-hosted precious-metal deposits of northern Nevada: Nevada Bureau of Mines and Geology Report 40, p. 71–80.
Roberts, R.J., and Arnold, D.C., 1965, Ore deposits of the Antler Peak quadrangle, Humboldt and Lander Counties, Nevada: U.S. Geological Survey Professional Paper 459–B, 94 p.
Rock, N.M.S., 1987, The nature and origin of lamprophyres—An overview, *in* Fitton, J.G., and Upton, B.G.J., eds., Alkaline igneous rocks: Geological Society of London, Special Publication 30, p. 191–226.
———1991, Lamprophyres: Glasgow, Blackie; New York, Van Nostrand Reinhold, 285 p.
Rock, N.M.S., Gaskarth, J.W., and Rundle, C.C., 1986, Late Caledonian dyke-swarms in southern Scotland—A regional zone of primitive K-rich lamprophyres and associated vents: Journal of Geology, v. 94, p. 505–522.
Rock, N.M.S., Griffin, B.J., Edgar, A.D., Paul, D.K., and Hergt, J.M., 1992, A spectrum of potentially diamondiferous lamproites and minettes from the Jharia coalfield, eastern India: Journal of Volcanology and Geothermal Research, v. 50, p. 55–83.

Root, D.H., Menzie, W.D., and Scott, W.A., 1992, Computer Monte Carlo simulation in quantitative resource estimation: Nonrenewable Natural Resources, v. 1, p.125–138.
Rose, A.W., Hawkes, H.E., and Webb, J.S., 1979, Geochemistry in mineral exploration, 2d ed.: New York, Academic Press, 657 p.
Rytuba, J.J., and Cox, D.P., 1991, Porphyry gold—A supplement to U.S. Geological Survey Bulletin 1693: U.S. Geological Survey Open-File Report 91–116, 7 p.
Sangster, D.F., 1980, Distribution and origin of Precambrian massive sulphide deposits of North America, *in* Strangway, D.W., ed., The continental crust and its mineral deposits: Geological Association of Canada Special Paper 20, p. 723–739.
Saunders, I., and Young, A., 1983, Rates of surface processes on slopes, slope retreat, and denudation: Earth Surface Processes and Landforms, v. 8, p. 473–501.
Schantz, Radford, Wetzel, Nicholas, Adams, Robert, and Raney, R.G., 1990, Minerals in the East Mojave National Scenic Area, California—An economic analysis, volume II: U.S. Bureau of Mines Open-File Report MLA 6–90, 52 p.
Schmidt, K.W., Wotruba, P.R., and Johnson, S.D., 1988, Gold-copper skarn and related mineralization at Copper Basin, Nevada: Geological Society of Nevada Fieldtrip Guidebook, 6 p.
Schmidt, R.G., 1978, The potential for porphyry copper-molybdenum deposits in the Eastern United States: U.S. Geological Survey Professional Paper 907–E, p. E1–E31.
Shafiqullah, Muhammad, Frost, E.G., Frost, D.L., and Damon, P.E., 1990, Regional extension and gold mineralization in the southern Chocolate Mountains, southeastern California—K-Ar constraints from fault rocks [abs.]: Geological Society of America Abstracts with Programs, v. 22, no. 3, p. 82.
Shapiro, Leonard, 1975, Rapid analysis of silicate, carbonate, and phosphate rocks (revised edition): U.S. Geological Survey Bulletin 1401, 76 p.
Sharp, J.E., 1984, A gold mineralized breccia pipe complex in the Clark Mountains, San Bernardino County, California, *in* Wilkins, Joe, Jr., ed., Gold and silver deposits of the Basin and Range province, western U.S.A.: Arizona Geological Society Digest, v. 15, p. 119–139.
Sharp, R.E., 1957, Geomorphology of Cima Dome, Mojave Desert, California: Geological Society of America Bulletin, v. 68, p. 273–290.
Shastri, L.L., Chamberlain, K.R., and Bowring, S.A., 1991, Inherited zircon from ca. 1.1 Ga mafic dikes, northwestern Arizona [abs.]: Geological Society of America Abstracts with Programs, v. 23, no. 4, p. 93.
Shaw, V.E., 1959, Extraction of rare-earth elements from bastnaesite concentrate: U.S. Bureau of Mines Report of Investigations 5474, 12 p.
Shawe, D.R., 1988, The case for gold—An introduction to geology and resources of gold in the United States, *in* Shawe, D.R., Ashley, R.P., and Carter, L.M.H., eds., Introduction to geology and resources of gold and geochemistry of gold: U.S. Geological Survey Bulletin 1857–A, p. A1–A8.
———1990, Gold in the Alma Mining District, Colorado, *in* Shawe, D.R., Ashley, R.P., and Carter, L.M.H., eds., Gold-bearing polymetallic veins and replacement deposits—Part II: U.S. Geological Survey Bulletin 1857–F, p. F19–F31.
Sheets, R.W., Ausburn, Kent, Bodnar, R.J., and Craig, J.R., 1990, Fault-related gold mineralization—Ore petrology and geochemistry of the Morning Star Deposit, California [abs.], *in* Geology and ore deposits of the Great Basin, Great Basin Symposium, Program with Abstracts: Reno, Nev., Geological Society of Nevada and U.S. Geological Survey (April), p. 109–110.
Sheets, R.W., Ausburn, Kent, Bodnar, R.J., Craig, J.R., and Law, R.D., 1989, Geology and precious metal mineralization at the Morning Star deposit, San Bernardino County, California: U.S. Bureau of Land Management Compendium, The California Desert Mineral Symposium (March), p. 219–231.
Sheets, R.W., Bodnar, R.J., Craig, J.R., and Ausburn, K.E., 1988, Precious-metal mineralization at the Morning Star deposit, San Bernardino County, California [abs.]: Geological Society of America Abstracts with Programs, v. 20, no. 7, p. A142.
Sheets, R.W., Craig, J.R., and Bodnar, R.J., 1995, Composition and occurrence of electrum at the Morning Star deposit, San Bernardino County, California—Evidence for remobilization of gold and silver: The Canadian

Mineralogist, v. 33, pt. 1, p. 137–151.
Shimazaki, Hideiko, 1981, Skarn deposits and related acid igneous activities: Hermosillo State of Sonora [Mexico] Special Publication, Director of Minerals, Geology, and Energy, 50 p.
Sibson, R.H., 1987, Earthquake rupturing as a mineralizing agent in hydrothermal systems: Geology, v. 15, no. 8, p. 701–704.
———1990, Faulting and fluid flow, *in* Nesbitt, B.E., ed., Fluids in tectonically active regimes of the continental crust: Mineralogical Association of Canada Short Course, v. 18, p. 93–132.
Silberman, M.L., and Wenrich, K.J., 1993, Mineralized quartz veins along the Grand Wash Cliffs in the Music Mountains, northwestern Arizona [abs.]: Geological Society of America Abstracts with Programs, v. 25, no. 5, p. 147.
Sillitoe, R.H., 1979, Some thoughts on gold-rich porphyry copper deposits: Mineralium Deposita, v. 14, p. 161–174.
———1980, Types of porphyry molybdenum deposits: Mining Magazine, v. 142, p. 550–551, 553.
———1991, Intrusion-related gold deposits, *in* Foster, R.P., ed., Gold metallogeny and exploration: Glasgow and London, Blackie and Son Ltd., p. 165–209.
Sillitoe, R.H., and Bonham, H.F., Jr., 1990, Sediment-hosted gold deposits—Distal products of magmatic-hydrothermal systems: Geology, v. 18, no. 2, p. 157–161.
Silver, L.T., McKinney, C.R., and Wright, L.A., 1961, Some Precambrian ages in the Panamint Range, Death Valley, California [abs.]: Geological Society of America Special Paper 68, p. 55.
Singer, D.A., 1975, Mineral resource models and the Alaskan mineral resource assessment program, *in* Vogley, W.A., ed., Mineral materials modeling—A state-of-the-art review: Baltimore, Md., The Johns Hopkins University Press, p. 370–382.
———1990, Development of grade and tonnage models for different deposit types [abs.]: Toronto, 8th International Association on the Genesis of Ore Deposits (IAGOD) Symposium, Program with Abstracts, p. A99–A100.
———1992, Some basic concepts used in three-part quantitative assessments of undiscovered mineral resources [abs.]: Tokyo, Japan, International Symposium on Mineral Exploration, September, 1992, p. 4–5.
———1993, Development of grade and tonnage models for different deposit types, *in* Kirkham, R.V., Sinclair, W.D., Thorpe, R.I., and Duke, J.M., eds., Mineral deposit modeling: Geological Association of Canada Special Paper 40, p. 21–30.
Singer, D.A., and Cox, D.P., 1988, Applications of mineral deposit models to resource assessment: U.S. Geological Survey Yearbook 1987, p. 55–57.
Singer, D.A., and Mosier, D.L., 1986, Grade and tonnage model of Cyprus massive sulfide, *in* Cox, D.P., and Singer, D.A., eds., Mineral deposit models: U.S. Geological Survey Bulletin 1693, p. 131–135.
Singer, D.A., Page, N.J, Smith, J.G., Blakely, R.J., and Johnson, M.G., 1983, Mineral resource assessment maps of the Medford 1° by 2° quadrangle, Oregon-California: U.S. Geological Survey Miscellaneous Field Studies Map MF–1383–C, scale 1:250,000.
Smirnov, V.I., 1976, Geology of mineral deposits: Moscow, Mir Publishers, 520 p.
Snoke, A.W., and Miller, D.M., 1988, Metamorphic and tectonic history of the northeastern Great Basin, *in* Ernst, W.G., ed., Metamophism and crustal evolution of the western United States (Rubey vol. 7): Englewood Cliffs, N.J., Prentice-Hall, p. 606–648.
Snyder, D.G., Roberts, C.W., Saltus, R.W., and Sikora, R.F., 1982, A magnetic tape containing the principal facts of 64,026 gravity stations in the state of California: U.S. Geological Survey NTIS PB–82–168287 [available from U.S. Department of Commerce, National Technical Information Service, Springfield, Va., 22152].
Spencer, J.E., 1985, Miocene low-angle normal faulting and dike emplacement, Homer Mountain and surrounding areas, southeastern California and southernmost Nevada: Geological Society of America Bulletin, v. 96, p. 1,140–1,155.
Spencer, J.E., and Turner, R.D., 1985, Geologic map of Homer Mountain and the southern Piute Range, southeastern California: U.S. Geological Survey Miscellaneous Field Studies Map MF–1709, scale 1:24,000.

Stensrud, H.L., and More, S., 1980, Precambrian geology and massive sulfide environments of the west-central Hualapai Mountains, Mohave County, Arizona—A preliminary report, *in* Jenney, J.P., ed., Studies in western Arizona: Arizona Geological Digest, v. 12, p. 155–164.

Stewart, J.H., 1970, Upper Precambrian and Lower Cambrian strata in the southern Great Basin, California and Nevada: U.S. Geological Survey Professional Paper 620, 206 p.

Stewart, J.H., and Poole, F.G., 1975, Extension of the Cordilleran miogeosynclinal belt to the San Andreas fault, southern California: Geological Society of America Bulletin, v. 86, p. 205–212.

Stoddard, E.F., and Miller, C.F., 1990, Chemistry and phase petrology of amphiboles and orthoamphibolite-cordierite rocks, Old Woman Mountains, southeastern California, U.S.A.: Mineralogical Magazine, v. 54, p. 393–406.

Stone, Paul, Howard, K.A., and Hamilton, W., 1983, Correlation of metamorphosed Paleozoic strata of the southeastern Mojave Desert region, California and Arizona: Geological Society of America Bulletin, v. 94, no. 10, p. 1,135–1,147.

Streckeisen, A., 1976, To each plutonic rock its proper name: Earth-Science Reviews, v. 12, p. 1–33.

Sun, S.-S., 1980, Lead isotopic study of young volcanic rocks from mid-ocean ridges, ocean islands, and island arcs: Philosophical Transaction of the Royal Society of London, v. A297, p. 409–445.

Sun, S.-S., and McDonough, W.F., 1989, Chemical and isotopic systematics of oceanic basalts—Implications for mantle compositions and processes, *in* Saunders, A.D., and Norry, M.J., eds., Magmatism in the ocean basins: Geological Society [London] Special Publication 42, p. 313–345.

Sutter, J.F., 1968, Geochronology of major thrusts, southern Great Basin, California: Houston, Tex., Rice University, M.S. thesis, 32 p.

Tainton, K.M., and McKenzie, D., 1994, The generation of kimberlites, lamproites, and their source rocks: Journal of Petrology, v. 35, p. 787–817.

Taylor, S.R., and McLennan, S.M., 1985, The continental crust—Its composition and evolution: Oxford, Blackwell Scientific Publications, 312 p.

Tchalenko, J.S., 1970, Similarities between shear zones of different magnitudes: Geological Society of America Bulletin, v. 81, no. 6, p. 1,625–1,640.

Theodore, T.G., Blair, W.N., and Nash, J.T., 1987a, Geology and gold mineralization of the Gold Basin-Lost Basin mining districts, Mohave County, Arizona: U.S. Geological Survey Professional Paper 1361, 167 p.

Theodore, T.G., Blake, D.W., Loucks, T.A., and Johnson, C.A., 1992, Geology of the Buckingham stockwork molybdenum deposit and surrounding area, Lander County, Nevada, *with a section on* Potassium-argon and $^{40}Ar/^{39}Ar$ geochronology of selected plutons in the Buckingham area, by E.H. McKee, *and a section on* Economic geology, by T.A. Loucks and C.A. Johnson, *and a section on* Supergene copper deposits at Copper Basin, by D.W. Blake, *and a section on* Mineral chemistry of Late Cretaceous and Tertiary skarns, by J.M. Hammarstrom: U.S. Geological Survey Professional Paper 798–D, 307 p.

Theodore, T.G., Czamanske, G.K., and Keith, T.E.C., 1987b, Sillenite and other bismuth minerals associated with placer gold, Battle Mountain mining district, Nevada [abs.]: Geological Society of America Abstracts with Programs, v. 20, no. 3, p. 237.

Theodore, T.G., Czamanske, G.K., Keith, T.E.C., and Oscarson, R.L., 1989, Bismuth minerals associated with placer gold, Battle Mountain Mining District, Nevada [abs.], *in* Shindler, K.S., ed., USGS Research on Mineral Resources—1989 Program and Abstracts: U.S. Geological Survey Circular 1035, p. 72–74.

Theodore, T.G., and Menzie, W.D., 1984, Fluorine-deficient porphyry molybdenum deposits in the cordillera of western North America, *in* Janelidze, T.V., and Tvalchrelidze, A.G., eds., Proceedings of the Sixth Quadrennial International Association on the Genesis of Ore Deposits (IAGOD) Symposium, Tbilisi, U.S.S.R., September 6–12, 1982, v. 1: Stuttgart, E. Schweizerbart'sche Verlagsbuchhandlung, p. 463–470.

Theodore, T.G., Orris, G.M., Hammarstrom, J.M., and Bliss, J.D., 1991, Gold-bearing skarns: U.S. Geological Survey Bulletin 1930, 61 p.

Thomas, W.M., Clarke, H.S., Young, E.D., Orrell, S.E., and Anderson, J.L., 1988, Proterozoic high-grade metamorphism in the Colorado River region, Nevada, Arizona, and California, *in* Ernst, W.G., ed., Metamorphism and crustal evolution of the western United States (Rubey Vol. VII): Englewood Cliffs, N.J., Prentice-Hall, p. 526–537.

Thompson, R.N., 1982a, Magmatism of the British Tertiary volcanic province: Scottish Journal of Geology, v. 18, p. 49–107.
Thompson, T.B., 1982b, Classification and genesis of stockwork molybdenum deposits—Discussion: Economic Geology, v. 77, no. 3, p. 709–710.
———1990, Precious metals in the Leadville Mining District, Colorado, *in* Shawe, D.R., Ashley, R.P., and Carter, L.M.H., eds., Gold-bearing polymetallic veins and replacement deposits—Part II: U.S. Geological Survey Bulletin 1857–F, p. F32–F49.
Tingley, J.V., and Bonham, H.F., Jr., eds., 1986, Sediment-hosted precious-metal deposits of northern Nevada: Nevada Bureau of Mines and Geology Report 40, 103 p.
Tooker, E.W., 1990, Gold in the Bingham District, Utah, *in* Shawe, D.R., Ashley, R.P., and Carter, L.M.H., eds., Geology and resources of gold in the United States: U.S. Geological Survey Bulletin 1857–E, p. E1–E16.
Tosdal, R.M., Haxel, G.B., and Wright, J.E., 1989, Jurassic geology of the Sonoran Desert region, southern Arizona, southeastern California, and northernmost Sonora—Construction of a continental-margin magmatic arc, *in* Jenney, J.P., and Reynolds, S.J., eds., Geologic evolution of Arizona: Arizona Geological Society Digest 17, p. 397–434.
Tosdal, R.M., and Smith, D.B., 1987, Some characteristics of gneiss-hosted gold deposits of southeastern California [abs.]: U.S. Geological Survey Circular 995, p. 71.
Turner, R.D., 1985, Magma mixing and fractional crystallization of Miocene volcanic rocks in the Castle Mountains, northeastern Mojave desert [abs.]: Geological Society of America Abstracts with Programs, v. 17, no. 6, p. 414.
Turner, R.D., and Glazner, A.F., 1990, Miocene volcanism, folding, and faulting in the Castle Mountains, southern Nevada and eastern California, *in* Wernicke, B.P., ed., Cenozoic tectonics of the Basin and Range Province at the latitude of Las Vegas: Geological Society of America Memoir 176, p. 23–35.
Turner, R.D., Huntoon, J.E., and Spencer, J.E., 1983, Miocene volcanism, sedimentation and folding in the northeastern Castle Mountains, California and Nevada [abs]: Geological Society of America Abstracts with Programs, v. 15, no. 5, p. 433.
Turrin, B.D., Dohrenwend, J.C., Drake, R.E., and Curtis, G.H., 1985, K-Ar ages from the Cima volcanic field, eastern Mojave Desert, California: Isochron/West, no. 44, p. 9–16.
Turrin, B.D., Dohrenwend, J.C., Wells, S.G., and McFadden, L.D., 1984, Geochronology and eruptive history of the Cima volcanic field, eastern Mojave desert, California, *in* Dohrenwend, J.C., ed., Surficial geology of the eastern Mojave Desert, California: Reno, Nev., Geological Society of America 1984 Annual Meeting Guidebook, p. 88–100.
Twyman, J.D., and Gittins, J., 1987, Alkalic carbonatite magmas—Parental or derivative, *in* Fitton, J.G., and Upton, B.G.J., eds., Alkaline igneous rocks: Geological Society of London, Special Publication 30, p. 85–94.
U.S. Bureau of Land Management, 1980, The California desert conservation area plan: U.S. Bureau of Land Management, 173 p.
———1982, Final environmental impact statement and proposed plan California Desert Conservation Area, Appendix 14, volume G (revised), Geology-Energy-Minerals: U.S. Bureau of Land Management, p. 1–202.
———1988, East Mojave National Scenic Area Final Management Plan: Needles, Calif., Department of Interior, Bureau of Land Management, Needles Resource Area, May 1988.
U.S. Bureau of Mines, 1990a, Minerals in the East Mojave National Scenic Area, California—A minerals investigation, v. 1: U.S. Bureau of Mines Open-File Report MLA 6–90, 356 p.
———1990b, Copper, gold: U.S. Bureau of Mines Mineral Commodity Summaries, 1990, p. 52–53, 70–71.
U.S. Bureau of Mines and U.S. Geological Survey, 1980, Principles of a resource/reserve classification for minerals: U.S. Geological Survey Circular 831, 5 p.
U.S. Department of Energy, 1979a, Aerial radiometric and magnetic survey, Trona National Topographic Map, California: U.S. Department of Energy Open-File Report GJBX–65 (79), 204 p.
———1979b, Airborne gamma-ray spectrometer and magnetometer survey, Las Vegas quadrangle (Arizona, California, Nevada), William quadrangle (Arizona), Prescott quadrangle (Arizona), and Kingman quadrangle (Arizona, California, Nevada): U.S. Department of Energy Open-File Report GJBX–59(79), 993 p.

———1979c, Aerial radiometric and magnetic survey, Needles National Topographic Map, California and Nevada: U.S. Department of Energy Open-File Report GJBX–114(79), v. I, 189 p., v. II, 88 p.
———1980, Airborne gamma-ray spectrometer and magnetic survey, Los Angeles quadrangle, San Bernardino quadrangle, Santa Ana quadrangle, California: U.S. Department of Energy Open-File Report GJBX–214(80), 5 v., 640 p.
U.S. Geological Survey, 1981, Aeromagnetic map of the Needles 1° 2° quadrangle, California and Arizona: U.S. Geological Survey Open-File Report 81–85, scale 1:250,000.
——— 1983, Aeromagnetic map of the Kingman-Trona area, California: U.S. Geological Survey Open-File Report 83–663, scale 1:250,000.
———1991, Evaluation of metallic mineral resources and their geologic controls in the East Mojave National Scenic Area, San Bernardino County, California: U.S. Geological Survey Open-File Report 91–427, 278 p.
———1992, Evaluation of selected metallic and nonmetallic mineral resources, West Mojave Management Area, southern California: U.S. Geological Survey Open-File Report 92–595, 89 p.
VanTrump, George, Jr., and Miesch, A.T., 1977, The U.S. Geological Survey RASS–STATPAC system for management and statistical reduction of geochemical data: Computers and Geosciences, v. 3, p. 475–488.
Vijayan, S., Melnyk, A.J., Singh, R.D., and Nuttall, K., 1989, Rare earths—Their mining, processing, and growing industrial usage: Mining Engineering, v. 41, p. 13–18.
Villemant, B., Jaffrezic, H., Joron, J.-L., and Treuil, M., 1981, Distribution coefficients of major and trace elements—Fractional crystallization in the alkali basalt series of Chaîne de Puys (Massif Central, France): Geochimica et Cosmochimica Acta, v. 45, p. 1,997–2,016.
Volborth, A., 1962, Allanite pegmatites, Red Rock, Nevada, compared with allanite pegmatites in southern Nevada and California: Economic Geology, v. 57, p. 209–216.
Walker, J.D., 1987, Permian to Middle Triassic rocks of the Mojave Desert, *in* Dickinson, W.R., and Klute, M.A., eds., Mesozoic rocks of southern Arizona and adjacent areas: Arizona Geological Society Digest, v. 18, p. 1–14.
Wallace, R.E., 1978, Geometry and rates of change of fault-generated range fronts, north-central Nevada: U.S. Geological Survey Journal of Research, v. 6, p. 637–650.
Wallace, R.E., and Morris, H.T., 1986, Characteristics of faults and shear zones in deep mines: Pure and Applied Geophysics, v. 124, no. 1–2, p. 107–125.
Ward, D.L., 1978, Construction of calibration pads facility, Walker Field, Grand Junction, Colorado: U.S. Department of Energy Open-File Report GJBX–37(78), 57 p.
Warhol, W.N., 1980, Molycorp's Mountain Pass operations, *in* Fife, D.L., and Brown, A.R., eds., Geology and mineral wealth of the California desert: Santa Ana, California, South Coast Geological Society, p. 359–366.
Warnke, D.A., 1969, Pediment evolution in the Halloran Hills, central Mojave Desert, California: Zeitschrift fur Geomorphologie, v. 13, p. 357–389.
Wasserburg, G.J., Wetherill, G.W., and Wright, L.A., 1959, Ages in the Precambrian terrane of Death Valley, California: Journal of Geology, v. 67, p. 702–708.
Watson, K.D., Morton, D.M., and Baird, A.K., 1974, Shonkinite-syenite plutons, Mountain Pass, San Bernardino County, California [abs.]: Geological Society of America Abstracts with Programs, v. 6, no. 3, p. 273.
Weldin, R.D., 1991, The California Desert—Protect it or develop it?: U.S. Bureau of Mines, Minerals Today (January), p. 12–17.
Wenrich, K.J., and Silberman, M.L., 1993, Au-Ag polymetallic mineralization within tectonically weak zones along the southwestern edge of the Colorado Plateau [abs.]: Geological Society of America Abstracts with Programs, v. 25, no. 5, p. 162.
Westra, Gerhard, and Keith, S.B., 1981, Classification and genesis of stockwork molybdenum deposits: Economic Geology, v. 76, no. 4, p. 844–873.
Wetzel, Nicholas, Benjamin, David, Blackman, Leonard, and Schantz, Radford, 1992, Economic analysis of the minerals potential of the East Mojave National Scenic Area, California: U.S. Bureau of Mines Open-File Report 56–92, 43 p. [attachments, 44 p.].
White, W.H., Bookstrom, A.A., Kamilli, R.J., Ganster, M.W., Smith, R.P., Ranta, D.E., and Steininger, R.C., 1981, Character and origin of Climax-type molybdenum deposits, *in* Skinner, B.J., ed., Economic Geology, 75th anniversary volume, 1905–1980: New Haven, Conn., Economic Geology Publishing Co., p. 270–316.

Willis, G.F., 1988, Geology and mineralization of the Mesquite open pit gold mine, *in* Schafer, R.W., Cooper, J.J., and Vikre, P.G., eds., Bulk mineable precious metal deposits of the Western United States: Geological Society of Nevada, Symposium Proceedings, 1987, p. 473–486.

Willis, G.F., and Holm, V.T., 1987, Geology and mineralization of the Mesquite open pit gold mine, *in* Johnson, J.L., ed., Bulk mineable, Guidebook for field trips: Geological Society of Nevada, Symposium, 1987, p. 52–56.

Willis, G.F., and Tosdal, R.M., 1992, Formation of gold veins and breccias during dextral strike-slip faulting in the Mesquite Mining District, southeastern California: Economic Geology, v. 87, p. 2,002–2,022.

Willis, G.F., Tosdal, R.M., and Manske, S.L., 1989, Structural control on epithermal gold veins and breccias in the Mesquite district, southeastern California [abs.]: U.S. Geological Survey Circular 1035, p. 78.

Wilshire, H.G., 1987, Multistage generation of alkalic basalt in the mantle—The Cima volcanic field, California [abs.]: Geological Society of America Abstracts with Programs, v. 19, no. 7, p. 892.

———1988, Geology of the Cima volcanic field, San Bernardino County, California, *in* Weide, D.L., and Faber, M.L., eds., This extended land—Geological journeys in the southern Basin and Range: Las Vegas, Nev., Geological Society of America, Field Trip Guidebook, Cordilleran Section Meeting, p. 210–213.

Wilshire, H.G., Frisken, J.G., Jachens, R.C., Prose, D.V., Rumsey, C.M., and McMahan, A.B., 1987, Mineral resources of the Cinder Cones Wilderness Study Area, San Bernardino County, California: U.S. Geological Survey Bulletin 1712–B, 13 p.

Wilshire, H.G., Meyer, C.E., Nakata, J.K., Calk, L.C., Shervais, J.W., Nielson, J.E., and Schwarzman, E.C., 1988, Mafic and ultramafic xenoliths from volcanic rocks of the western United States: U.S. Geological Survey Professional Paper 1443, 179 p.

Wilson, M., 1989, Igneous petrogenesis: London, Unwin Hyman, 466 p.

Wilson, S.A., Kane, J.S., Crock, J.G., and Hatfield, D.B., 1987, Chemical methods of separation for optical emission, atomic absorption spectrometry, and colorimetry, *in* Baedecker, P.A., ed., Methods for geochemical analysis: U.S. Geological Survey Bulletin 1770, p. D1–D14.

Woodcock, J.R., and Hollister, V.F., 1978, Porphyry molybdenite deposits of the North American Cordilleran: Minerals, Science, and Engineering (Johannesburg), v. 10, p. 3–18.

Wooden, J.L., and DeWitt, E., 1991, Pb isotopic evidence for the boundary between the Early Proterozoic Mojave and central Arizona crustal provinces in western Arizona, *in* Karlstrom, K.E., ed., Proterozoic geology and ore deposits of Arizona: Arizona Geological Society Digest 19, p. 27–50.

Wooden, J.L., and Miller, D.M., 1990, Chronologic and isotopic framework for Early Proterozoic crustal evolution in the eastern Mojave Desert region, southeastern California: Journal of Geophysical Research, v. 95, no. B12, p. 20,133–20,146.

Wooden, J.L., Stacey, J.S., Howard, K.A., Doe, B.R., and Miller, D.M., 1988, Pb isotopic evidence for the formation of Proterozoic crust in the southwestern United States, *in* Ernst, W.G., ed., Metamorphism and crustal evolution of the western United States (Rubey vol. VII): Englewood Cliffs, N.J., Prentice-Hall, p. 69–86.

Woolley, A.R., 1987, Alkaline rocks and carbonatites of the world, part 1—North and South America: Austin, University of Texas Press, 216 p.

Woolley, A.R., and Kempe, D.R.C., 1989, Carbonatites—Nomenclature, average chemical composition, and element distribution, *in* Bell, K., ed., Carbonatites, genesis and evolution: London, Unwin Hyman, p. 1–14.

Worl, R.G., Van Alstine, R.E., and Shawe, D.R., 1973, Fluorine, *in* Brobst, D.A., and Pratt, W.P., eds., United States mineral resources: U.S. Geological Survey Professional Paper 820, p. 223–235.

Wotruba, P.R., Benson, R.G., and Schmidt, K.W., 1986, Battle Mountain describes the geology of its Fortitude gold-silver deposit at Copper Canyon: Mining Engineering, v. 38, no. 7, p. 495–499.

Woyski, M.S., 1980, Petrology of the Mountain Pass carbonatite complex—A review, *in* Fife, D.L., and Brown, A.R., eds., Geology and mineral wealth of the California desert: Santa Ana, California, South Coast Geological Society, p. 367–378.

Wright, L.A., 1968, Talc deposits of the southern Death Valley-Kingston Range region, California: California Division of Mines and Geology Special Report 95, 79 p.

Wright, L.A., Troxel, B.W., Williams, E.G., Roberts, M.T., and Diehl, P.E., 1976, Precambrian sedimentary environments of the Death Valley region, eastern California: California Division of Mines and Geology Special Report 106, p. 7–15.

Wrucke, C.T., Otton, J.K., and Desborough, G.A., 1986, Summary and origin of the mineral commodities in the Middle Proterozoic Apache Group in central Arizona, *in* Beatty, B., and Wilkinson, P.A.K., eds., Frontiers in geology and ore deposits of Arizona and the southwest: Arizona Geological Society Digest, v. 16, p. 12–17.

Wyllie, P.J., 1989, Origin of carbonatites—Evidence from phase equilibrium studies, *in* Bell, K., ed., Carbonatites, genesis and evolution: London, Unwin Hyman, p. 500–545.

Wyllie, R.J.M., 1991, Navachab, Namibia's new mine: Engineering and Mining Journal (January), p. 28–31.

Yeend, Warren, Dohrenwend, J.C., Smith, R.S.U., Goldfarb, R.J., Simpson, R.W., Jr., and Munts, S.R., 1984, Mineral resources and mineral resource potential of the Kelso Dunes Wilderness Study Area (CDCA–250), San Bernardino County, California: U.S. Geological Survey Open-File Report 84–647, 19 p.

Young, E.D., 1989, Petrology of biotite-cordierite-garnet gneiss of the McCullough Range, Nevada II. *P–T–*a_{H_2O} path and growth of cordierite during late stages of low-*P* granulite-grade metamorphism: Journal of Petrology, v. 30, pt. 1, p. 61–78.

Young, E.D., Anderson, J.L., Clarke, H.S., and Thomas, W.M., 1989, Petrology of biotite-cordierite-garnet gneiss of the McCullough Range, Nevada I. Evidence for Proterozoic low-pressure fluid-absent granulite-grade metamorphism in the southern Cordillera: Journal of Petrology, v. 30, pt. 1, p. 39–60.

Young, E.D., Wooden, J.L., Shieh, Y.-N., and Farber, D., 1992, Geochemical evolution of Jurassic diorites from the Bristol Lake region, California, U.S.A. and the role of assimilation: Contributions to Mineralogy and Petrology, v. 110, p. 68–86.

Young, R.A., and Brennan, W.J., 1974, Peach Springs Tuff—Its bearing on structural evolution of the Colorado Plateau and development of Cenozoic drainage in Mohave County, Arizona: Geological Society of America Bulletin, v. 85, no. 1, p. 83–90.

Zharikov, V.A., 1970, Skarns: International Geology Review, v. 12, p. 541–559, 619–647, 760–775.